सरदार वल्लभभाई राष्ट्रीय प्रौद्योगिकी संस्थान, सुरत
Sardar Vallabhbhai National Institute of Technology, Surat

TECHNICAL PROJECT REPORT

IMPACT OF CLIMATE CHANGE ON WATER RESOURCES OF TAPI BASIN

Submitted to

MINISTRY OF JAL SHAKTI,
DEPARTMENT OF WATER RESOURCES, RIVER DEVELOPMENT & GANGA REJUVENATION,
GOVERNMENT OF INDIA.

PRINCIPAL INVESTIGATOR
Dr. P. L. PATEL
DEPARTMENT OF CIVIL ENGINEERING
SVNIT-SURAT

CO-PRINCIPAL INVESTIGATOR
Dr. ROHIT GOYAL (MNIT-JAIPUR)
Dr. VISHNU PRASAD (MANIT-BHOPAL)
Dr. P. V. TIMBADIYA (SVNIT-SURAT)

DEPARTMENT OF CIVIL ENGINEERING
SARDAR VALLABHBHAI NATIONAL INSTITUTE OF TECHNOLOGY (SVNIT)
SURAT-395007, GUJARAT, INDIA

This is Draft Report and yet to be accepted by Competent Authority

CERTIFICATE

Subject: "Impact of Climate Change on Water Resources of Tapi Basin."

It is to certify that the current research project, **"Impact of Climate Change on Water Resources of Tapi Basin,"** includes the findings as per the terms of reference (ToR) conveyed vide administrative approval letter no. 16/22/2016-R&D/3059-3076 dated November 07, 2016.

The current study has investigated the spatio-temporal variability of hydroclimate variables, like temperature, precipitation, and streamflow indices for the baseline period. The hydrological models are also developed to assess the response of the Tapi basin to the changing climatic variables in the future. The hydrologic modeling of Purna sub-catchment and Lower Tapi basin is carried out by SVNIT-Surat, Burhanpur sub-catchment by MNIT-Jaipur, and Middle Tapi basin by MANIT-Bhopal. Also, the impact on irrigation water demands in the command area of Ukai and Girna reservoirs are investigated. The temporal variability of hydroclimatic variables, i.e., precipitation and temperature, and drought parameters, for future are also included in the study. A 2D hydrodynamic model has been developed for the Lower Tapi basin (LTB), which is used for simulating the flooding conditions in Surat city in future. This report includes objectives and scope of work; a brief theoretical background and literature review; description of the Tapi basin and data sources; methodology; data analysis and model development; climate change impact analysis and discussions; and conclusions and adaptation measures.

The impacts of climate change reported in the current report are based on data provided by the statistical downscaling team of IIT Bombay and observed data from other data disseminating agencies. The funding agency, data sharing agencies, and those who supported the completion of this research project are duly acknowledged.

Dr. P. L. Patel,
PI, Lead Institute,
Professor, Department of Civil Engineering,
SVNIT Surat.

EXECUTIVE SUMMARY

In the research project "**Impact of Climate Change on Water Resources of Tapi Basin**", the hydroclimatic variability in the temperature, rainfall, and streamflow for entire Tapi River basin (TRB) using the station data in the basin has been investigated. The gridded temperature and rainfall data are used to assess the meteorological droughts in the TRB. The SWAT hydrological models are developed and calibrated/validated individually for the Purna sub-catchment, Burhanpur sub-catchment, and Middle Tapi basin. The MIKE-SHE hydrological and 2D hydrodynamic flood models are developed for the Lower Tapi basin (LTB). In addition, the irrigation water demands are also calculated for the Ukai-Kakrapar and Girna command areas for the baseline and future periods. The Kernel Regression-based statistically downscaled (KRSD) precipitation and bias corrected temperature data received from downscaling team at IIT Bombay, are used to assess the impacts of climate change on various aspects discussed above.

The Burhanpur sub-catchment in the Upper Tapi basin (UTB) experienced increasing rainfall extremes with decreasing annual rainfall. The Purna sub-catchment, in the UTB, showed significant rise in the daily rainfall intensity. The total annual rainfall, daily rainfall intensity, frequency and magnitude of rainfall extremes are found to increase in the LTB for the baseline period. The persistence of the dry spells is uniformly observed over the entire TRB. The UTB and LTB have observed prominent rise in daily maximum temperature and daily minimum temperature respectively. The temporal assessment of annual runoff in TRB indicated that the MTB is prone to significant reduction in the water availability. Invariably, the annual runoff is decreasing across TRB, except at Hatnur and Burhanpur gauging stations.

The KRSD data states that the UTB would get improved rainfall conditions in future with rising total annual rainfall, no. of rainy days, decreasing dry spells under RCP 4.5 scenario. However, under RCP 8.5 scenario aforesaid parameters are likely to increase for near- and mid-future and decrease in far-future period. While in the MTB, the total annual rainfall magnitude, rainy days, magnitude and intensity of rainfall extremes are likely to increase under RCP 4.5 for near-future to far-future. These observations are likely to be more intensified under the RCP 8.5 scenario. The moderate rainfall days (and rainfall extremes) would likely to increase (decrease) considerably under the RCP 8.5 scenario, particularly in the far-future period, in the LTB. The noteworthy observation in the temperature data indicated that the no. of days exceeding 37 ºC would rise, on average, by 48.8% (and 131.3%) by the end of the 21st century under the RCP 4.5 (8.5) scenario in the basin.

The temporal trend in the annual drought indices showed that the part of the UTB and MTB is prone to short-term drought conditions compared to moderate-and long-term droughts while the LTB showed decreasing drought conditions during the baseline period. A small portion of the UTB can experience moderate- and long-term droughts in far-future under RCP 8.5 while the LTB can experience short-, moderate-, and long-term droughts in the mid-future under RCP 4.5.

The statistical performance assessment of the developed hydrologic models, i.e., SWAT for the UTB and MTB; and MIKE-SHE for the LTB, showed that the developed models are fairly simulating the catchment scale hydrology with overall water balance error within ±5%. The simulated response of the TRB, particularly the UTB and MTB, for the future climate scenarios shows that the extreme flows (Q_{10}) are likely to decrease in the basin while median flows (Q_{50}) are likely to increase under RCP 4.5 and 8.5 scenarios for all the GCMs in the TRB.

The bivariate approach been used to develop the flood risk maps with distinct contribution of flood hazard and socio-economic vulnerability of the Surat city. For 100-years return period flood, the north zone and larger area of west zone is under high flood risk which is due to equal contribution of flood hazard and socio-economic vulnerability.

The gross irrigation water requirements are likely to increase (decrease), particularly for January, March, April, May, and December months (August, October, and November months) months with reference to the base line period in Ukai-Kakrapar command area for future periods.

The significant increasing trends of minimum temperature in future in the basin may likely to have negative impacts on the paddy crop in the TRB. On the other hand, significant increase in temperature beyond 37^{o}C, may likely to cause heat stress condition in the TRB. The increasing trend in temperature in the basin are likely to increase the evapotranspiration in the basin. This may result in increasing water demand in future. Thus, rainwater harvest measures are recommended to be adopted in the basin to cope with the increasing water demand in the future. As per the mandate of the project, a workshop was held with stake holders including the personnel from Central Water Commission, Surat Municipal Corporation, Tapi Irrigation Development Corporation, project advisors from IISc Bangalore and IIT Bombay, Member Secretary (INCCC-NIH), and Co-PI from partnering institutes, i.e., MANIT Bhopal and MNIT Jaipur. The suggestions received from the participants were incorporated in the report. The minutes of the workshop is included at Annexure-B.

Dr. P. L. Patel

ACKNOWLEDGEMENT

The Project team thankfully acknowledges the support provided by the Sardar Vallabhbhai National Institute of Technology (SVNIT) Surat, Malviya National Institute of Technology (MNIT) Jaipur, and Maulana Azad National Institute of Technology (MANIT) Bhopal for permitting the team to take up the project and help towards carrying out the relevant procurement and computational work. We are thankful to the Directorate, Indian National Committee on Climate Change (INCCC), Ministry of Jal Shakti, Department of Water Resources, River Development & Ganga Rejuvenation, Government of India (GoI) for funding the research project entitled **"Impact of Climate Change on Water Resources of Tapi Basin"** to SVNIT Surat, as a leading institute, and MNIT Jaipur and MANIT Bhopal, as partnering institutes. We express our heartfelt gratitude to the INCCC for their timely evaluation and suggestions in the meeting. Special thanks to Dr. R P Pandey, Scientist 'G', National Institute of Hydrology, Roorkee, and Member Secretary, INCCC, and his team for excellent suggestions and quick administrative support.

We are also thankful to India Meteorological Department (IMD), Pune; Central Water Commission (CWC) Tapi division Surat; State Water Data Center (SWDC) Gandhinagar; Ukai Civil Circle, Ukai; Surat Irrigation Circle (SIC), Surat; Tapi Irrigation Development Corporation (TIDC) Jalgaon; Girna Irrigation Division (GID), Jalgaon; Surat Municipal Corporation (SMC), Surat; National Remote Sensing Centre (NRSC) Hyderabad; National Bureau of Soil Survey and Land Use Planning (NBSS&LUP) Nagpur; Statistical downscaling team from IIT Bombay, and USGS Earth-Explorer portal for providing the required data for the present study. We are also thankful to the Head of the Department of Civil Engineering, Dean (R&C), and Directors of SVNIT Surat, MANIT Bhopal, and MNIT Jaipur for quick administrative assistance.

The assistance rendered by the project staff, Mr. Shubham M. Jibhakate, Mr. Lalit Kumar Gehlot, and Mr. Kalpesh B. Baladaniya from SVNIT Surat; Mr. Ankur Sharma from MANIT Bhopal; and Dr. Priyamitra Munoth from MNIT Jaipur are deeply appreciated. Also, the technical assistance provided by Dr. Priyank J. Sharma (Assistant Prof. IIT, Indore), Ms. Prajakta P. Surkar (PG Research Scholar, MANIT Bhopal) is highly appreciated. The help received from Ms. Alka Sharma and Ms. Vineela Nandam, Research Scholars (SVNIT), and Ms. Meenal Dave, (Technician) under Centre of Excellence (CoE) on "Water Resources and Flood Management", Department of Civil Engineering, SVNIT Surat in drafting the report is highly acknowledged.

We show a deep sense of gratitude to all those who helped us directly or indirectly in completing this project.

Dr. P. L. Patel,
PI, Lead Institute,
Professor, Department of Civil Engineering, SVNIT Surat.

TABLE OF CONTENTS

LIST OF FIGURES

LIST OF TABLES

CHAPTER 1
INTRODUCTION

1.1 GENERAL

Hydrological cycle is combination of different complex hydrological processes treating all phases of earth's water (Chow et al. 1988). Water movement in the hydrological cycle is the largest movement of matter in the earth's system. As the water is essential entity for existence of life on planet earth, it is necessary to study the impact of ongoing and future projected climate change on water resources and its availability. Water on earth and climate are closely connected. The large-scale exchange of water mass and heat between land, ocean and atmosphere influence the climate, also get influence by climate. The change in the climatic condition induce change in water system and vice versa (Kundzewicz 2008). Climate change resulted into regional changes in precipitation pattern, water availability, evaporative crop water demand, ground water recharge, events of floods and droughts, water quality, saltwater intrusion in coastal regions and other related processes (Mondal and Mujumdar 2015b). The changes in various hydroclimatic variables at large spatial scale are attributed to increase in emission of greenhouse gases and aerosols.

The primary characteristics of changing climate are change in temperature and precipitation. Global warming caused by the consistent rise in greenhouse gases is estimated through long term changes in mean temperature of earth's surface (Vinnarasi et al. 2017). The continuous increase in temperature is observed from second half of 20^{th} century. The 0.88 ºC rise in global ocean and land surface temperature is recorded between 1985-2020. The rise in global average atmospheric carbon dioxide during 1980s (1.58 ppm/year) was larger than the 1990s (1.49 ppm/year) majorly due to increase in usage of fossil fuel compared to earlier decades (Canadell et al. 2007). Therefore, 1980 was considered as major change point beyond which an accelerating change in climate trends was observed (Lobell et al. 2011). The change in air temperature have significant impact on hydrologic, environmental, and socio-economic factors. The rise in temperature and associated decrease in rainfall affect the crop water availability leads to reduction in agricultural production (Riha et al. 1996). As per the Clausius-Clapeyron relation, one degree surface warming can increase 6-7% water vapour concentration (Trenberth 2011) leading to the increase in frequency and magnitude of extreme precipitation. The compilation of various regional studies by IPCC's fifth assessment report (AR5) suggested the increasing warm temperature extremes and decrease in cold temperature extremes across many parts of the world (Stocker et al. 2013). In India, the increase in frequency and intensity

of warm extremes representing daily minimum temperature and decrease in cold extremes is observed during 1971-2005 (Panda et al. 2014). Also, Kumar et al. (2017) found increasing summer hot days with decrease in winter cold nights in many parts of India. The change in extreme rainfall pattern due to extreme urbanization (Vittal et al. 2013) with 50 % increase in rainstorm and 80% increase in duration of rainstorm was observed in India (Guhathakurta et al. 2017) after 1950.

The recent decade also experienced significant rise in flood events which can be attributed to increasing trend in extreme precipitation, glaciers melt, rising sea levels as effect of climate change (Alfonso et al. 2016). The year 2020 recorded 201 disastrous flood events (23 % more) compared to 163 events averaged over last two decades 2000-2019; It also records 18 % more deaths i.e., 6171 compared to previous average of 5233 across the globe. In Indian context, in the year 2020, country lost 1,922 people and nearly 7.5 billion US dollars against 11 major floods in different part of the country (CREDD and UNDRR 2021). In order to minimize the losses, various structural flood mitigation measures were adopted by government by investing the millions of dollars. On the other hand, the non-structural measures such as flood warning, flood hazard and risk mapping can provide adoptable solution in cost-effective way. The flood modeling using hydrodynamic model approach (Timbadiya et al. 2014b; Patel et al. 2017) and flood hazard maps using the flood model output (depth, velocity) (Mani et al. 2014; Mohanty et al. 2020; Ghosh et al. 2021) was widely put into the practice. The flood risk mapping with integration of flood hazard, vulnerability and exposure can be the primary step toward flood management in flood prone region.

The effects of historic climatic variability and expected future climate change on hydrologic processes and water resources may vary greatly in space and time. The runoff, soil moisture, evapotranspiration within a watershed can vary to the greater extent and affect the dynamics associated with the streamflow generation (Faramarzi et al. 2013). Recently the efforts have been taken to understand the climate change impact on water resources at various spatial scales. However, the regional scale studies can provide the better understanding of various impacts associated with climate change and their socioeconomic implications. Here, we propose to evaluate impacts of climate variability and climate change in the Tapi River basin using the downscaled climate projections from multiple models and the physically based hydrologic modeling system.

1.2 PROJECT SUMMARY

The Prime Minister of India launched the National Water Mission (NWM) on June 30, 2008, under the National Action Plan for climate change. The national water mission has prior agenda of prediction of climate change and its impact on water resources of Indian river basins. Also, the depleting condition of water resources in the country and its vulnerability against the changing climate was discussed by Prime Minister in India Water week on April 10, 2012. The 20 river basins in the country have been identified for the detailed study on effect of climate change and its impact on water resources of respective basins under NWM. The information on future climate scenarios will help in adapting to the effect of climate change and its mitigation from the adverse impact of flood, droughts, heat wave etc.

The project Proposal was submitted on "Impact of Climate Change on Water Resources of Tapi Basin" by SVNIT as a lead institute and MNIT Jaipur and MANIT Bhopal as partnering institute. The Indian National Committee on Climate Change (INCCC), Ministry of water resources, River Development & Ganga Rejuvenation (MoWR, RD & GR), (now Ministry of Jal Shakti) Government of India had accorded the administrative approval vide letter no. 16/22/2016-R&D/3059-3076 dated November 7, 2016. The financial approval was received vide letter no. 28/4/2016-R&D/246-265 dated February 9, 2018. Subsequently, the research activities of the project were started from July 2018 in SVNIT Surat, January 2019 in MNIT Jaipur and April 2019 in MANIT Bhopal after the recruitment of research staff in respective institute.

1.3 MOTIVATION OF THE STUDY

The Tapi River is the second largest west flowing interstate river in India after Narmada River. The Tapi basin is spread over 65,145 km^2 area, covering nearly 2% of the total geographic area of the country. The 66.19 % area of the basins is under agriculture with around 4.29 Mha. as a culturable area. There are 13 Major and 68 Medium projects completed within the Tapi basin in the past including two multipurpose reservoir Hathnur Reservoir and Ukai reservoir along the main Tapi River act as primary source of irrigation and plays major role in agrarian economy of Maharashtra and Gujarat states apart from feeding several domestic water supply schemes, industries, and hydropower in its catchment. At present, the agrarian economy suffers from the uneven incidence of rainfall, therefore there is strong demand for the development of water resources of the basin. Apart from benefits from Tapi river, major historical floods had occurred in the past in the coastal urban flood plain of the Tapi River in the Surat city. The

flood of year 2006 alone had caused a loss of Rs.21,000/- Crores and the economy of the country was severely affected for several months after the flood. Based on the analysis of annual peak flow, Timbadiya et al. (2013) reported the increasing trend in flood in Tapi basin. Keeping in view the aggravating situation of the climate change across the globe, in general, and, for the Tapi basin, in particular, hydrological and hydraulic analyses are required to predict the water yield in the basin and status of flood and drought for different future RCP scenarios using downscaled climatic variables like precipitation, temperature (Min., Max., and Mean), solar radiation, wind velocity, relative humidity and sunshine hours at basin levels.

The project consists of detection of spatio-temporal trend in hydro-meteorological variables for Tapi basin to understand the climate variability across the basin. Development of rainfall-runoff model to understand the hydrological processes and water balance model at the different sub-catchments. Assessment of crop water requirement for the cropping pattern in the Ukai and Girna reservoir command area for existing and projected climatic conditions. Calibration of the hydraulic model for the flood prediction in Lower Tapi basin including coastal urban flood plain of Surat city. And the flood hazard-risk assessment of all the cases for the future RCP scenarios for the changing climatic condition.

1.4 PROJECT OBJECTIVES

The key objective of the proposed project can be described as below:

i. Collection of base line data of Tapi basin which would include stream gauge data, topography, soil, land use/land cover, ground water levels, reservoir and its utilities, cropping pattern of Ukai command area, past floods and tidal levels, vegetation, land management practices, sediment etc.
ii. Development of Hydrological (SWAT/MIKE SHE) and hydraulic models (MIKE FLOOD) and their calibration from past observed data.
iii. Parametric and non-parametric tests for trend detection for hydro-meteorological and hydrological variables in the basin.
iv. Quantification of impact of climate change on irrigation water demand in Ukai-Kakrapar and Girna command area.
v. Using the output from dynamic/statistical downscaling, prediction of flood situation downstream of Ukai dam in lower Tapi River under changing climatic conditions and preparation of flood risk maps of the Surat city under changing climatic conditions.

vi. Organize Workshops during the project duration as capacity building measures and awareness for the stakeholders in the river basin and academic institutions involved in such activities.

These objectives for Tapi River basin have been divided into various sub-groups based on sub-catchments, as shown in Fig. 1.1

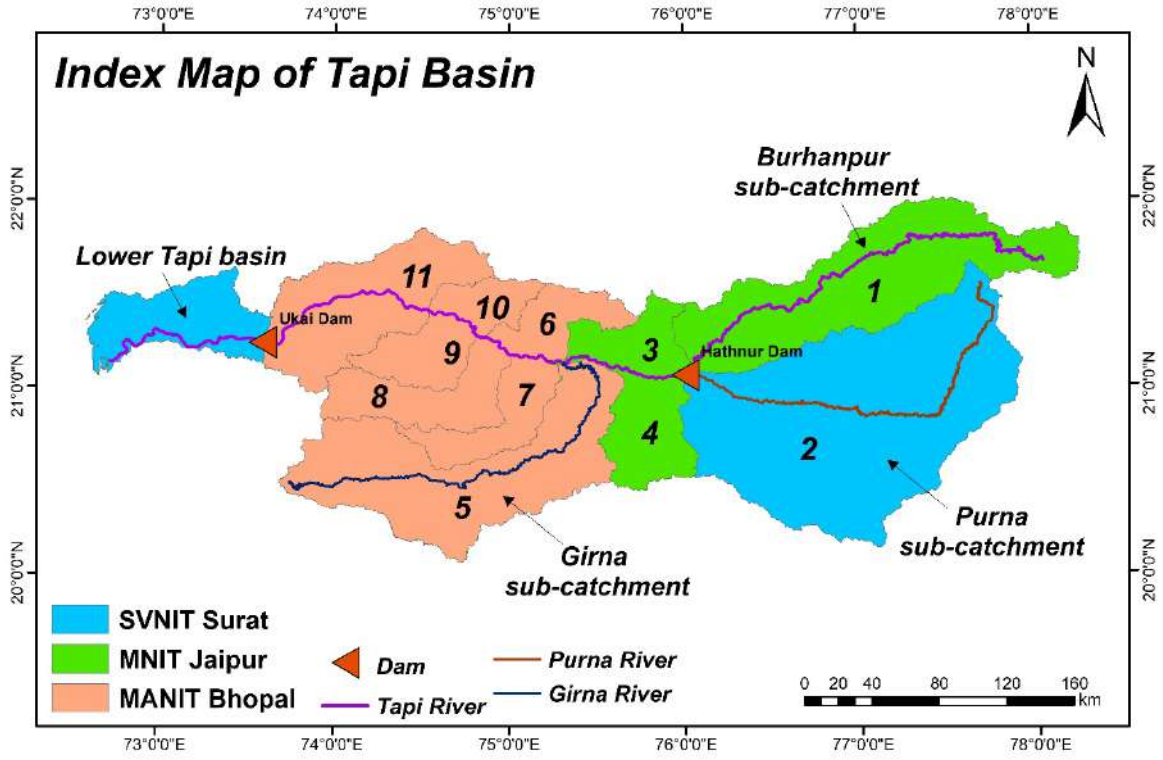

Fig. 1.1 Index map showing description of sub-catchments

1.5 PROJECT DELIVERABLES

The key deliverables of the current research project are as following:

i. Base line data, information, and past studies,

ii. Results of parametric/non-parametric tests for trend detection for hydro-meteorological and hydrological variables,

iii. Calibrated and validated hydrological model(s),

iv. Impacts on water availability at various gauging sites within the basin (in terms of change in flow duration curves),

v. Impacts on irrigation water demands,

vi. Identification of hydrological extremes based on the base line data,

vii. Impacts on meteorological/hydrologic droughts (in terms of change in frequencies of occurrence), Analysis of uncertainties in the impacts. The impacts and the associated uncertainties must be assessed for near-future (2015-2040) and for distant future (2040-2100),

viii. Generation of flood scenarios in lower Tapi river and Surat city, preparation of flood maps and risk analysis for observed and future scenarios, synthesis of the model output for observed and future scenarios,

ix. Recommendations for adaptation measures/options,

x. Organization of Workshop for Stakeholders and research partners.

1.6 OUTLINE OF REPORT

The proposed report entitled "Impact of Climate Change on Water Resources of Tapi Basin" has been divided into seven chapters, and the summary of each is presented in following paragraphs:

Chapter 1 includes a brief introductory summary of the project, motivation of the study, objectives of the project, scope of the work for partnering institute and the outline of the progress report.

Chapter 2 consists of the theoretical background and literature review undertaken during the project with reference to the assessment hydroclimatic variability, hydrologic models i.e., semi-distributed hydrologic model (SWAT), fully distributed physical based integrated hydrological model (MIKE-SHE/MIKE 11), flood risk assessment using 2D hydrodynamic modeling (MIKE 21) approach, irrigation water demand and drought assessment.

Chapter 3 consists of the description of study area with details of each sub-catchment and reservoir command area. It also includes the list of data along with sources, used in achieving the objectives of the project.

Chapter 4 consists of detailed methodology adopted in attaining the objectives related to hydroclimatic variability, hydrological and hydraulic models, flood risk assessment and irrigation water demand of Ukai-Kakrapar command area and Girna command area. It also explains the analysis of future projected downscaled rainfall received from IIT Bombay.

Chapter 5 describes the development of hydrological model for Upper, Middle, and Lower Tapi basin including their calibration and validation processes. The chapter also describes the development of 2D HD model, its performance evaluation and flood risk assessment of coastal urban flood plain of Surat city.

Chapter 6 describes results of spatio-temporal variability of hydro-climatic variables for baseline as well as future climate scenarios. The chapter discusses the impact of climate change on water availability, drought, crop water demand and flooding situation in the Surat city for various climatic scenarios.

Chapter 7 consists of the conclusions derived from the various analysis performed in the present study. It also includes the possible recommendation and adaptation measures and future scope of the current study.

CHAPTER 2
THEORETICAL BACKGROUND & LITERATURE REVIEW

2.1 GENERAL

The assessment of hydroclimatic variability holds due importance in the field of water resources engineering for better management of the asset, i.e., water. Apart from the variability, understanding of the basin scale hydrology aids impacts of local scale phenomenon, i.e., anthropogenic changes in the basin etc. on water availability. Though, mathematical simulation of the real time hydrology is very complex task, but with certain assumptions, realistic results can be obtained through hydrologic models. The mismanagement of the incoming water turns out to havoc, through floods and droughts. Therefore, the current study emphasises on ascertaining the impact of climate change on various aspects of basin scale hydrology and its associated impacts on the socio-ecological aspects. The present chapter includes brief theoretical descriptions of the statistical methods used for assessment of hydroclimatic variability, governing equations of hydrologic and hydrodynamic models, drought assessment and estimation of gross irrigation water requirement etc. The brief review of the recent advancements in the described themes have also been included in this chapter.

2.2 NON-PARAMETRIC TREND DETECTION METHODS

The outcomes of the study primarily depend upon the quality of the data used (Yuan et al. 2019). The observed hydrometeorological datasets may have missing observation values. The inferences derived based on analysis of such datasets, where more than 5% of the records are missing, can be misleading. Thus, infilling of missing observations in such datasets, using suitable statistical techniques, is a preliminary step. The stations having more than 5% missing data can be discarded from the analysis. The missing observations in the rainfall and temperature data, wherever reported, are computed using inverse distance weighing method (IDW). The IDW method has gained more popularity because of its ease in implementation and fair accuracy. According to Chen and Liu (2012) the missing values can be calculated as (see Eq. 2.1):

$$P_o = \frac{\sum_{i=1}^{n} \frac{R_i}{d_i^2}}{\sum_{i=1}^{n} \frac{1}{d_i^2}} \tag{2.1}$$

Here, P_o is the missing precipitation value at a rain gauge station (mm), R_i is the known precipitation value at nearby/surrounding i^{th} rain gauge station (mm) and d_i is the distance

between the nearby/surrounding i^{th} rain gauge station and the station at which the precipitation value is missing (km).

The assessment of homogeneity in the data is also having significance as homogeneous and continuous data accurately characterizes the local climatic conditions. The homogeneity of the can be assessed using the widely accepted tests, i.e., Pettitt's test (Pettitt 1979), standard normal homogeneity test (SNHT) (Alexandersson 1986), Buishand range test (Buishand 1982) and von Neumann ratio test (von Neumann 1941) etc. The Pettitt's test, SNHT and Buishand range tests can detect break point(s) in the continuous time series, while von Neumann ratio test fails to do so.

2.2.1 Modified Mann-Kendall (MMK) Test

The widely used non-parametric Mann-Kendall (MK, Mann 1945; Kendall 1955) test is used for exploring the presence of monotonic trend in a time series. However, it cannot be used when the times series have serial correlation. The basic statistic S of Mann-Kendall test is calculated by comparing individual value with subsequent values as (see Eq. 2.2):

$$S = \sum_{k=1}^{n-1} \sum_{j=k+1}^{n} sgn(x_j - x_k) \tag{2.2}$$

where, $sgn(x)$ = +1 if $x > 0$; = –1 if $x < 0$; and = 0 if $x = 0$. The statistic S is approximately Gaussian when $n \geq 18$, and the mean and variance of S is given by Eq. 2.3.

$$E(S) = 0 \quad \text{and} \quad Var(S) = \frac{n(n-1)(2n+5) - \sum_{i=1}^{m} t_i(t_i-1)(2t_i+5)}{18} \tag{2.3}$$

where, n and m are the number of data and ties respectively. Each tie represents a set of similar subsequent data in a time series and the data count in each of them is t. The test statistic Z, is computed by Eq. 2.4.

$$Z = \begin{cases} \dfrac{S-1}{\sqrt{Var(S)}} & if\ S > 0 \\ 0 & if\ S = 0 \\ \dfrac{S+1}{\sqrt{Var(S)}} & if\ S < 0 \end{cases} \tag{2.4}$$

Hamed and Rao (1998) stated that presence of serial correlation/dependency in a time series does not falsify either mean of the MK test statistic S or the asymptotic normality, but the variance $Var(S)$ changes. Hence, correction factors are proposed to take care of the serial correlation present among the time. The presence of either of positive or negative serial

correlation may result in increase or decrease in the variance of MK test statistic Z. Hence, MMK with variance correction approach was proposed by Hamed and Rao (1998). The modified variance $Var\ (S)_*$ (see Eq. 2.5-2.6) for computing the test statistic (Z) is given by:

$$Var\ (S)_* = CF \times Var\ (S) \tag{2.5}$$

where, *CF* is the correction factor, which is given as:

$$CF = 1 + \frac{2}{n(n-1)(n-2)} \sum_{k=1}^{n-1} (n-k)\ (n-k-1) \times (n-k-2) r_k^R \tag{2.6}$$

where, r_k^R = ranks of data, and n = total length of the time series.

2.2.2 Sen's Slope Estimator Test

The non-parametric robust estimate for quantifying, magnitude of, monotonic trend in time series was given by Hirsch et al. (1982) as (see Eq. 2.7):

$$\beta = Median\left(\frac{X_j - X_i}{(j-i)}\right) \qquad \forall\ i < j \tag{2.7}$$

where, β = slope between the data points X_i and X_j; and X_i and X_j are data points at time i and j respectively. A positive (negative) value of β is an indicator of an increasing (decreasing) trend in the time series. The percentage change can be estimate by assuming β a linear trend (see Eq. 2.8) and can be expressed

$$\text{Percentage Change (\%)} = \left(\frac{\beta\ \times \text{length of data years}}{\text{mean of time series}}\right) \times 100 \tag{2.8}$$

2.3 HYDROLOGIC & HYDRAULIC MODELING

The key concept behind hydrologic and/or hydraulic modeling, in one or other way, is to establish a relationship between the inputs to the system, i.e., a watershed or a basin etc., and the outputs from the system, i.e., streamflow, water levels, groundwater recharge, flow velocity etc. The well-developed, calibrated, and validated models can be used for real-time flood forecasting and taking appropriate mitigation measures to minimize the losses. In the present study two different hydrologic models have been used, i.e., Soil Water Assessment tool (SWAT) and MIKE SHE (Système Hydrologic Europeèn) for establishing the rainfall-runoff relationships for different sub-basins of TRB. The study also uses the MIKE-1D (one-dimensional) and -2D (two dimensional) hydrodynamic modeling in the lower reach of TRB for flood modeling. The brief descriptions of the aforesaid hydrologic and hydrodynamic models are presented in the succeeding sub-sections.

2.3.1 Rainfall-Runoff Modeling using SWAT

- **Soil Water Assessment Tool (SWAT)**

The SWAT is a semi-distributed, continuous-time watershed simulation model which operates at a daily/sub-daily time step and can simulate hydrologic and water quality processes at the basin level (Arnold et al. 1998). It was developed to predict the impact of land management practices on water, sediment, and agricultural chemical yields in large complex watersheds with varying soils, land use and management conditions over long periods of time. The model divides a basin into a smaller unit called sub-basins or watersheds, which are further sub-divided into hydrologic response unit (HRU). The HRUs are the percentage of the area of sub-basin in which unique combinations of land cover, soil, slope, and management practices are lumped. The major advantage of the model is that unlike the other conventional conceptual simulation models it does not require much calibration and therefore can be used on ungauged watersheds also.

The SWAT model is based on the water balance equation in soil profile, where the simulated processes include precipitation, infiltration, surface runoff, evapotranspiration, lateral flow, and percolation (Fan and Shibata 2015) (see Fig. 2.1). In SWAT, the hydrology of watershed is simulated in two phases: the land phase, which controls the amount of water, sediment, nutrient/pesticide, and bacterial loading to the main channels in each sub-basin and the water or routing phase, which controls the movement of water, sediments, and nutrients/pesticides to the outlet through the channel network of the watershed. For the Land phase, the hydrologic cycle is based on the water balance equation:

$$SW_t = SW_0 + \sum_{i=1}^{t} (R_{day} - Q_{surf} - E_a - W_{seep} - Q_{gw})_i \quad (2.9)$$

where SW_t is the final soil water content (mm), SW_0 is the initial soil water content (mm), t is the time (days), R_{day} is the amount of precipitation per day (mm), Q_{surf} is the amount of surface runoff per day (mm), E_a is the amount of evapotranspiration per day (mm), W_{seep} is the amount of percolation and bypass flow exiting in the soil profile bottom per day (mm), and Q_{gw} is the amount of return flow/base flow per day (mm).

The routing phase consists of defining the movement of water, sediments etc. through channel network of the watershed. For routing phase, the flow is routed through the channel using a variable storage coefficient method (default method in SWAT; developed by Williams 1969)

or the Muskingum routing method. Manning's equation for uniform flow in a channel is used to calculate the rate and velocity of flow in a reach segment for a given time step. The surface runoff from HRUs, are estimated using soil conservation service (SCS) curve number (CN) method from daily rainfall (USDA-SCS 1972). The equation of SCS-CN is given in Eq. (2.10)

$$Q = \frac{(P - I_a)^2}{(P - I_a) + S} \tag{2.10}$$

where Q = Runoff depth, P = Rainfall, I_a = initial abstraction of water, S = maximum potential retention, all in units of millimetre (mm). The initial abstraction of water (I_a) is the function of maximum potential retention (S) and given as follows in Eq. (2.11).

$$I_a = \lambda S \tag{2.11}$$

where λ = constant and based on several measurements λ = 0.2 is adopted as standard value. Therefore,

$$I_a = 0.2\, S \tag{2.12}$$

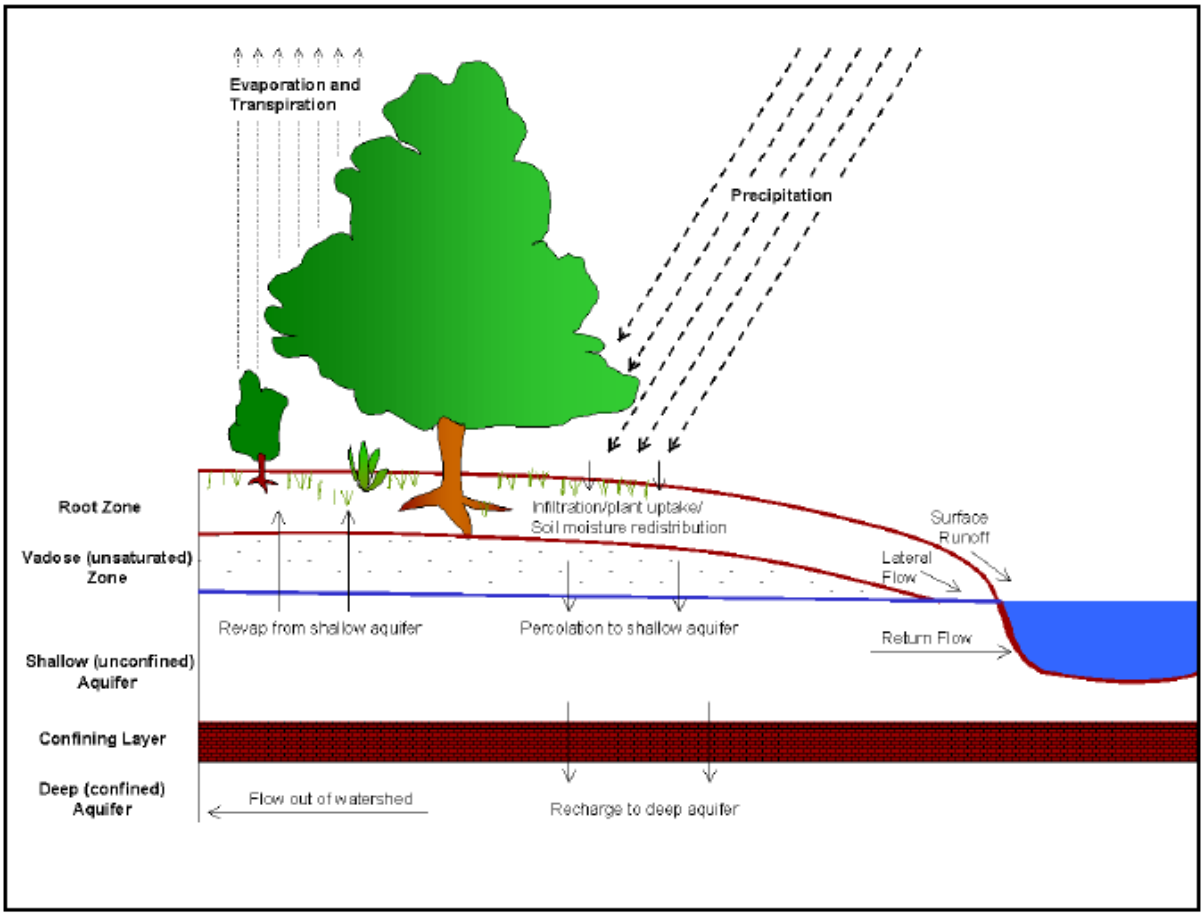

Fig. 2.1 Representation of Hydrological Cycle in SWAT (Neitsch et al. 2011)

By combining Eq. (2.10) and (2.12) the Runoff (Q) is given as follows in Eq. (2.13).

$$Q = \frac{(P - 0.2S)^2}{(P + 0.8S)} \tag{2.13}$$

The occurrence of runoff happens when $P > 0.2\ S$. The parameter S Depends upon soil types, topography, slope, land use and the antecedent soil moisture condition in the catchment. Therefore, the maximum potential retention (S) is correlated with dimensionless parameter curve number (CN) expressed in the Eq. (2.14).

$$S = \left(\frac{25400}{CN}\right) - 254 \tag{2.14}$$

The constant 254 is used to denote S in mm. From the above Eq. (2.14). The curve no. (CN) can be related to S as

$$CN = \frac{25400}{S + 254} \tag{2.15}$$

The range of CN is $100 \geq CN \geq 0$. The CN value of 100 represents the condition of zero potential retention, i.e., impervious catchment and $CN = 0$ shows an infinitely abstracting catchment with $S = \infty$ (Subramanya 2013).

In addition, SWAT also computes sediment loads using Modified Universal Soil Loss Equation (MUSLE) generated from the watershed based on soil loss equation developed by Williams and Berndt (1977) as given in Eq. (2.16)

$$Sed = 11.8\left(Q_{surf} \times q_{peak} \times area_{hru}\right)^{0.56} \times K_U \times C_U \times P_U \times LS_U \times C_{FRG} \tag{2.16}$$

where Sed is the sediment yield (tones), Q_{surf} is the surface runoff volume (mm), q_{peak} is the peak runoff rate (m^3/s), $area_{hru}$ is the area of a HRU (km^2), K_U is the soil erosion factor, C_U is the land cover and management factor, P_U is the conservation measures factor, LS_U is the topographic factor, and C_{FRG} is the coarse fragment factor (Zhang et al. 2014). The Universal Soil Loss Equation (USLE) model uses rainfall as the erosion energy factor and the MUSLE model replaces it with runoff (Neitsch et al. 2011). This replacement can improve the prediction accuracy, reduce the requirement of using a sediment transport ratio and allows the estimation of the sediment yield of a single rainstorm.

- **SWAT-CUP (Calibration and Uncertainty Program)**

SWAT-CUP was developed by the Swiss Federal Institute of Aquatic Science and Technology (EAWAG) for automating calibration and uncertainty analysis with five algorithms

Generalized Likelihood Uncertainty Estimation (GLUE), Parameter Solution (ParaSol), Sequential Uncertainty Fitting algorithm (SUFI-2), Markov Chain Monte Carlo (MCMC) and Particle Swarm Optimisation (PSO) (Abbaspour 2011). SUFI-2 is the most popularly used algorithm to calibrate the SWAT model for streamflow. SUFI-2 algorithm considers all uncertainty in sources including model input, structure, parameter, and observed data and use Latin Hypercube Sampling. The model performance is assessed by using statistical indicators like coefficient of determination (R^2), Nash–Sutcliffe model efficiency (*NSE*), Modified Nash-Sutcliffe model efficiency (*MNS*), root mean square error (*RMSE*), Kling-Gupta efficiency (*KGE*), and percentage bias (*PBIAS*) by comparing the model simulated output with the observed data. The R^2, *NSE*, *KGE*, *PBIAS* and *RMSE* can be computed using Eq. (2.17) to (2.21) respectively.

$$R^2 = \frac{[\sum_i (Q_{m,i} - \overline{Q_m}) * (Q_{s,i} - \overline{Q_s})]^2}{\sum_i (Q_{m,i} - \overline{Q_m})^2 * \sum_i (Q_{s,i} - \overline{Q_s})^2} \quad (2.17)$$

$$NSE = 1 - \frac{\sum_i (Q_m - Q_s)_i^2}{\sum_i (Q_{m,j} - \overline{Q_m})_i^2} \quad (2.18)$$

$$KGE = 1 - \sqrt{(r-1)^2 + (\propto -1)^2 + (\beta - 1)^2} \quad (2.19)$$

$$PBIAS = \frac{\sum_{i=1}^{n} (Q_m - Q_s)_i}{\sum_i^n Q_{m,j}} \times 100\% \quad (2.20)$$

$$RMSE = \sqrt{\frac{\sum_i (Q_m - Q_s)_i^2}{n}} \quad (2.21)$$

Where Q_m , Q_s , $\overline{Q_m}$, $\overline{Q_s}$ represents measured, simulated, average of measured and simulated discharge respectively; $\propto = \frac{\sigma_s}{\sigma_m}$, $\beta = \frac{\mu_s}{\mu_m}$, r is the linear regression coefficient, μ_s (μ_m) , σ_s (σ_m) are mean and standard deviation of simulated (measured) variables; and *n* is the length of data. The low absolute value of *PBIAS* indicates overall better performance of the model and its optimum value is zero. The *NSE* is the fraction of the variance in the observation explained by the model; a high value indicates an accurate model. The *MNS* is more sensitive to the high flows and considers the effect of low flows also by adjusting the power, *a*. The *KGE* considers the linear regression fitting as well as the distribution parameters. The *RMSE* is most widely use statistical parameter to compare two data sets and it is a measure of error between observed and predicted data sets. The Table 2.1 gives the general performance criteria of the SWAT model.

Table 2.1 Performance ratings for the monthly time step model (Moriasi et al. 2007)

Performance Rating	R^2	NSE	PBIAS (%)	
			Stream Flow	Sediment
Very Good	$R^2 > 0.7$	$0.75 < NSE \leq 1.00$	PBIAS < ±10	PBIAS < ±15
Good	$0.60 < R^2 \leq 0.70$	$0.65 < NSE \leq 0.75$	±10 ≤ PBIAS ≤ ± 15	±15 < PBIAS < ±30
Satisfactory	$0.50 < R^2 \leq 0.60$	$0.50 < NSE \leq 0.65$	±15 ≤ PBIAS ≤ ± 25	±30 < PBIAS < ±55
Unsatisfactory	$R^2 \leq 0.50$	NSE ≤ 0.50	PBIAS ≥ ± 25	PBIAS > ±55

2.3.2 Distributed Rainfall-Runoff Modeling using Integrated MIKE-SHE/MIKE 11

- **MIKE SHE Model Description**

MIKE SHE (Système Hydrologic Europeèn) is fully distributed, physically based, deterministic hydrological model which is capable of both continuous and event-based analysis (DHI 2017a). The model structure for the hydrologic processes in the MIKE SHE is shown in Fig. 2.2. The process starts with the user defined input precipitation, a portion of which is intercepted by the vegetation and tall buildings before it reaches to the ground surface. The intercepted precipitation is stored and later evaporate back into the atmosphere. The remaining amount of precipitation falling on the soil surface either undergo infiltration or generate the overland flow depending on the soil characteristics of the area. As infiltration continues, the unsaturated zone turns saturated and, after all surface storage areas are filled up, overland flow Starts flowing from one cell to another cell based on the topographic condition of the watershed. As this process continue the moister from the unsaturated zone is transferred into the saturated zone at a rate depending on soil properties. The MIKE SHE consists of two main modules. i.e., water movement (WM) and water quality (WQ), of which water movement module used in the present study. The WM module further consist of many sub-modules, the mathematical description of hydrological processes in MIKE SHE is shown in Fig. 2.3. MIKE SHE uses the finite difference approach to solve the partial difference equation which describes the process of overland flow (2D Saint Venant equation), unsaturated (2-layer water balance method), saturated flows (3D Darcy's equation) and channel flow (1D kinematic wave approximation of Saint Venant equation). The analytical solutions are used to describe the hydrological process like interception and evapotranspiration (DHI 2017a).

Governing Hydrological Processes in MIKE SHE

In the present study simulation has been carried out for the hydrological process within the catchment including precipitation, evapotranspiration, overland flow, stream flow and

unsaturated flow. The input data included the spatial data on topography, drainage network, land use, soil type, geology, temporal precipitation, and potential evapotranspiration.

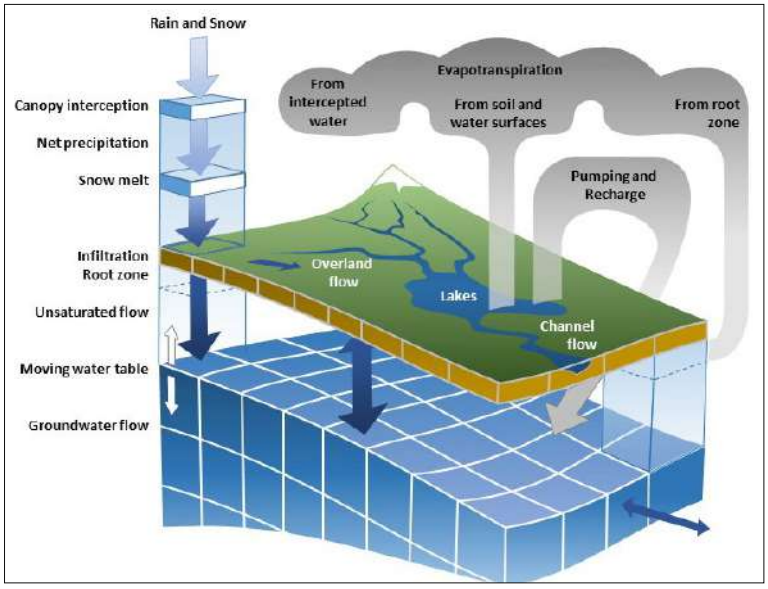

Fig. 2.2 Schematic diagram of model structure for hydrological processes in MIKE SHE (DHI 2017a)

Precipitation

Precipitation is a major input parameter in MIKE SHE models. The rainfall data can be imported in the model as uniform over the catchment, station-based input using the Thiessen polygon approach or fully distributed (spatially gridded) rainfall. The precipitation is required to be represented for each grid within the distributed model for predefined grid pattern within the model domain. Interception of the rainfall in the MIKE SHE depends on vegetation type and stages of development, which is characterized by the leaf area index (LAI), where more than 60-70% of intercepted rainfall return to the atmosphere by evapotranspiration process. In the present study station-based Thiessen polygon approach is used to for rainfall as input.

Evapotranspiration (ET)

In MIKE SHE the evapotranspiration will be modelled in the order as (a) fraction of rainfall evaporates after intercepted by the vegetation canopy; (b) remaining rainfall water reaches to the soil surface, generates surface runoff or percolating to the unsaturated zone; (c) part of infiltrated water gets evaporate from upper part of the soil or transpired by the plant roots; and (d) remaining part of infiltrated water reaches ground water table in saturated zone.

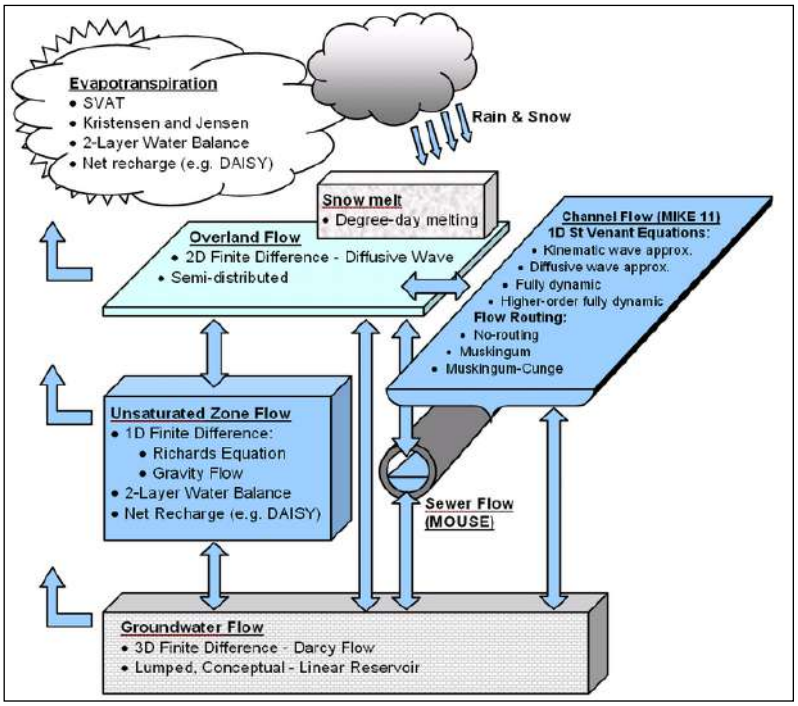

Fig. 2.3 Mathematical Schematic diagram for hydrological processes in MIKE SHE (DHI 2017a)

Leaf area index (LAI) and Root depth (RD)

The leaf area index (LAI) and root depth (RD) define the vegetation properties for the model. LAI is the area of leaves over the unit area of ground surface. The meteorological condition from year to year requires to decide the LAI value (varies between 0-7). The root depth is defined as the average depth of active roots in vegetated area. Deciduous forest areas are having the constant value of RD whereas, for agricultural and fallow land it begins with the low value reaches to the peak when crop fully grown and drops down when the crop get harvested. The temporal variation during growing season can also be specified in MIKE SHE. The LAI and RD values for vegetation area in the present study were derived from the literature (Foster and Allen 2015; Loliyana and Patel 2020). Coefficient for interception storage (C_{int} in mm) is a calibration parameter based on interception by vegetation.

Unsaturated Zone

The Unsaturated zone is one of the central processes (MIKE SHE), solved using 2-layer water balance method. The unsaturated zone is usually characterized by the cyclic fluctuation in the soil moisture as water is replenished by the rainfall and removed by the evapotranspiration and recharge to the groundwater storage. Unsaturated zone is primarily vertical since, gravity plays the important role during the infiltration, hence calculated only vertical in one-dimension in

MIKE SHE. The iterative coupling process between unsaturated zone and saturated zone is used to compute the correct soil moisture and water table dynamics in the lower part of the soil profile. The soil water content at saturation (θ_s) the maximum water content in the soil which may be taken as porosity of the soil, Soil water content at field capacity (θ_{fc}) the soil water content at which infiltration becomes negligible, Soil water content at wilting point(θ_{wp}) the minimum water content that plant can extract water from the soil, and saturated hydraulic conductivity (K_s) the maximum rate of infiltration in the soil. These are all the calibrated parameters of the flow in the unsaturated zone.

The 2-Layer water balance method

The Two-later UZ/ET model divides the unsaturated zone into root zone from which ET can occur and the zone where ET does not occur (Yan and Smith 1994). The main purpose was to provide an estimation of actual evapotranspiration and the amount of water that recharges the saturated zone. It is suitable for the area where water table is shallow. The method includes the process of interception, ponding and evapotranspiration while considering the entire unsaturated zone. The output is the estimate of actual evapotranspiration, and amount of water recharges the saturated zone.

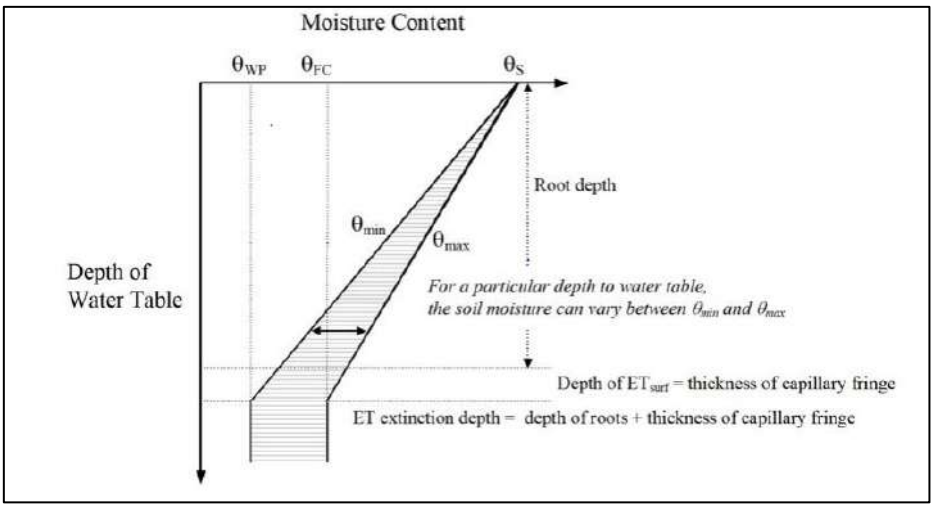

Fig. 2.4 Deception of the 2-Layer water balance ET/UT method (DHI 2017a)

ET extinction depth

It is the maximum depth (Capillary fringe) where ET can remove water from the saturated zone through roots i.e., root depth + ET depth (Thickness of Capillary fringe). If the capillary fringe reaches the bottom of root zone, then water removed from the root zone through

evapotranspiration will be replaced by water drawn by capillary action. In 2-layer water balance method, the unsaturated zone consists of one or two layers shown in Fig. 2.4.

(a) The upper layer extends from ground surface to the ET extinction depth. If the water table is at ground surface, then the thickness of the upper layer is zero.

(b) If the water table is below the Et extinction depth, then a second layer is added that extends from the bottom of first layer to the water table. If the water table is above the ET extinction depth, the thickness of the lower layer is zero.

The ET surface depth is calibration parameter, typical values is 0.5 or more.

Overland Flow

As the net rainfall exceeds the infiltration capacity of the soil, water is ponded on the ground surface. The water available as the surface runoff is to be routed downstream towards the river system. The routed flow is determined by using topography, flow resistance as well as losses occurred due to the evaporation and infiltration along the flow path. The overland flow is routed by using the diffusive wave approximation of Saint-Venant equations or using the semi distributed approach based on the Manning's equation. In the present study diffusive wave approximation is used.

Diffusive wave approximation

A two-dimensional form of Saint Venant equation is described using diffusive wave approximation as:

Conservation of mass equation,

$$\frac{\partial h}{\partial t} + \frac{\partial}{\partial x}(uh) + \frac{\partial}{\partial y}(vh) = i \tag{2.22}$$

Momentum equation,

$$S_{f_x} = S_{O_x} - \frac{\partial h}{\partial x} - \frac{u}{g}\frac{\partial u}{\partial x} - \frac{1}{g}\frac{\partial u}{\partial t} - \frac{qu}{gh} \tag{2.23}$$

$$S_{f_y} = S_{O_y} - \frac{\partial h}{\partial y} - \frac{v}{g}\frac{\partial v}{\partial y} - \frac{1}{g}\frac{\partial v}{\partial t} - \frac{qu}{gh} \tag{2.24}$$

Here, horizontal plane is represent in rectangular cartesian (x, y) coordinate system, where h(x, y) represent the water depth; u(x, y) and v(x, y) respectively represent flow velocities in x and y directions; let I is the net input to the overland flow (net rainfall minus infiltration). The S_f and S_O is friction slope in x- and y- directions respectively. The dynamic solution of two-dimensional St. Venant equation is numerically challenging. Therefore, it is common to reduce the complexity of the problem by dropping the last three terms of momentum equation.

Thereby, we are ignoring the momentum losses due to local and convective acceleration and lateral inflow perpendicular to the flow direction. The equation is known as the diffusive wave approximation which is implemented in MIKE SHE.

$$S_{f_x} = S_{O_x} - \frac{\partial h}{\partial x} \tag{2.25}$$

$$S_{f_y} = S_{O_y} - \frac{\partial h}{\partial y} \tag{2.26}$$

The Sticklers law for the friction slope is used, where K_x and K_y are Stickler's coefficients in two different x and y direction. The stickler roughness coefficient is equivalent to Manning's M which is inverse of manning's 'n'. The value of n is typically in the range of 0.01 (smooth channels) 0.1 (thickly vegetated channels) which correspond to values of M in between 100 to 10 respectively.

$$S_{f_x} = \frac{u^2}{K_x^2 h^{4/3}} \tag{2.27}$$

$$S_{f_y} = \frac{v^2}{K_y^2 h^{4/3}} \tag{2.28}$$

Substituting equation (2.24) and (2.25) into equation (2.26) and (2.27) result in simplified form as

$$uh = K_x \left(-\frac{\partial z}{\partial x}\right)^{1/2} h^{5/3} \tag{2.29}$$

$$vh = K_y \left(-\frac{\partial z}{\partial y}\right)^{1/2} h^{5/3} \tag{2.30}$$

uh and vh represent discharge per unit length along the cell boundary in x and Y- direction respectively.

Channel Flow

Water can enter and can be exchanged within the river either from overland flow with the help of MIKE 11, a one-dimensional hydraulic model based on the digitized points (chainage location) and calculation nodes (cross-section points) with hydrologic components of MIKE SHE. The coupling of MIKE SHE grid and MIKE 11 (see in Fig. 2.5) H points (water level points). As the exchange occurred along the edge of the grid it is important to note that the more highly resolve the grid the more accurate representation of river network it would be. Location of MIKE SHE river links are automatically determines with reference to coordinates of MIKE 11 river points that define the branch of hydraulic model.

The governing equation of one-dimensional unsteady flow, represented by saint-venant equation in conservative form of continuity and momentum equation as:

Continuity equation,

$$\frac{\partial h}{\partial t} + \frac{\partial}{\partial x}(uh) = i \tag{2.31}$$

Momentum equation,

$$S_{f_x} = S_{O_x} \tag{2.32}$$

Here, h is flow depth above the ground surface, t is time in (s) u is the flow velocity, i is the net input in the overland flow, S_f is the friction slope, S_o is the slope of the ground surface and uh represent the discharge. The transformation of saint-venant equations, to a set of implicit finite difference equation is performed in computational grid consisting of alternating Q and h-point, i.e., discharge and the water level points respectively. The Q point is always placed in between two h-points whereas the distance between the two-neighboring h-points may get differ. The discharge be defined as positive in the positive x-direction (increasing chainage). The six-point implicit finite difference Abbott-Ionescu scheme is used for solution of 1D kinematic wave approximation of saint venant equation (Abbott and Ionescu 1967).

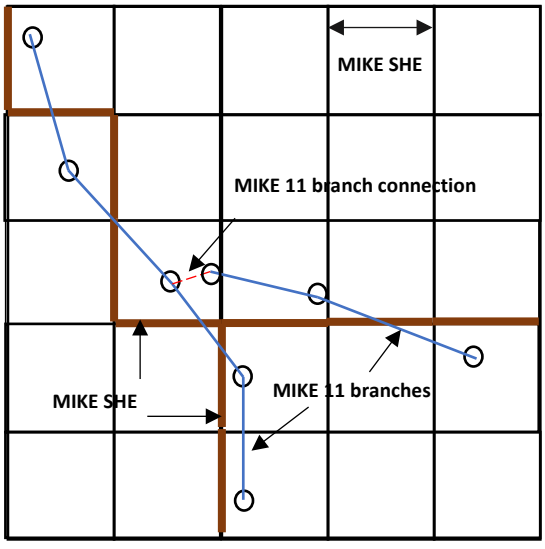

Fig. 2.5 Coupling of MIKE SHE and MIKE 11 (DHI 2017b)

2.3.3 Flood Modeling using MIKE-21

MIKE 21 is a professional engineering software which is capable of comprehensive modeling of two-dimensional (2D) free-surface flows. It can simulate hydraulic and environmental phenomenon in lakes, estuaries, bays, coastal region, and sea (DHI 2017c). The MIKE 21

simulate the 2D free-surface flows using numerical solution approach based on depth-average Navier Stokes equations which describes the conservation of mass and momentum in two horizontal dimensions (DHI 2017c). The water depth and flow computations are performed in rectangular (2D) grid for a complex floodplain. The simplified equations are given as follows:

$$\frac{\partial \zeta}{\partial t} + \frac{\partial p}{\partial x} + \frac{\partial q}{\partial y} = \frac{\partial d}{\partial t} \tag{2.33}$$

$$\frac{\partial p}{\partial t} + \frac{\partial}{\partial x}\left(\frac{p^2}{h}\right) + \frac{\partial}{\partial y}\left(\frac{pq}{h}\right) + gh\,\frac{\partial \zeta}{\partial x} + \frac{gp\sqrt{p^2+q^2}}{C^2.h^2} - \frac{1}{\rho_w} + \left[\frac{\partial}{\partial x}(h\tau_{xx}) + \frac{\partial}{\partial y}(h\tau_{xy})\right] - \Omega q - fVV_x +$$

$$\frac{h}{\rho w}\frac{\partial}{\partial x}(p_a) = 0 \tag{2.34}$$

$$\frac{\partial q}{\partial t} + \frac{\partial}{\partial y}\left(\frac{q^2}{h}\right) + \frac{\partial}{\partial x}\left(\frac{pq}{h}\right) + gh\,\frac{\partial \zeta}{\partial y} + \frac{gq\sqrt{p^2+q^2}}{C^2.h^2} - \frac{1}{\rho_w} + \left[\frac{\partial}{\partial y}(h\tau_{yy}) + \frac{\partial}{\partial x}(h\tau_{xy})\right] + \Omega q - fVV_y +$$

$$\frac{h}{\rho w}\frac{\partial}{\partial y}(p_a) = 0 \tag{2.35}$$

Here,

h = water depth, d = time varying depth (m), ζ = surface elevation (m), p, q = flux densities in x and y direction ($m^3/s/m$), C = Chezy's constant ($m^{1/2}/s$), g = acceleration due to gravity (m/s^2), f = wind friction factor, V, Vx, Vy = wind speed and its component in x and y direction (m/s), Ω = Coriolis parameter, latitude dependent (s^{-1}), Pa = atmospheric pressure ($kg/m/s^2$), ρw = density of water (kg/m^3), t = time (s), τ_{xx}, τ_{xy}, τ_{yy} = component of effective stress (N/m^2).

- **MIKE 21 HD Model Description**

Basic Parameters

Module Selection -The MIKE 21 Flow Model used in the current study, consist of different modules which can be adopted based on the applications. The hydrodynamic (HD) module is basic module in MIKE 21 flow Model which simulate water level variation and flows with respect to forcing (boundaries) in lakes, estuaries, and coastal regions. The HD module uses Alternating Direction Implicit (ADI) technique to integrate the equation on mass and momentum conservation in space-time domain. The equation matrix resulted in each direction and each individual grid line are solved by using Double Sweep (DS) algorithm (DH1 2017c). For detailed description please refer scientific documentation on MIKE 21 Flow Model HD module.

Bathymetry - Bathymetry of the model domain or area is the primary requirement in the flood simulation. In MIKE 21 Flow Model HD a separate bathymetry editor is provided. However, it can also be generated from the Digital Elevation Model (DEM) of the study area using any GIS tool and MIKE 21 Grid Editor.

Boundary location - The MIKE 21 Flow Model requires either the surface elevation or flux at all open boundary points. However, the source and sink provisions are made to define the internal boundaries. The locations of boundaries are either program detected, or user define in special cases.
In case of area with tidal flats, model is enables with flooding and drying facility. It computes the flow in area which sometimes dries out and sometimes flooded.

Hydrodynamic Parameters
Initial Condition - The information about initial (water) surface level needs to be provided in the simulation. It can be specified in two ways as (a) constant value over the entire domain and (b) fully distributed for each grid (for single time step). In case of hot-start simulation, the initial conditions are read from the hot-file (previous simulation).

Boundary Specification – The open boundary can be either level or flux. The values of level or flux can be specified in five different ways viz. (a) constant value, (b) sine series, (c) time series, (d) line series, (e) transfer data and, (f) rating curve.
The flow directions are assumed to be perpendicular to open boundary. However, in special case the direction can be specified.

Infiltration - The effect of infiltration and leakage of the surface may be important in certain flooding scenario. The infiltration of the area can be included in two ways-

(a) Net infiltration – it can be specified as constant value (both time and space); constant in time and varying in space; varying in both time and space.
(b) Constant infiltration capacity – for this type of infiltration zone must be define by depth or level. The initial water volume (0 - 100 %) or porosity (0 - 1) in infiltration zone must be defined.

Bed Resistance – The bed resistance can be defined by Manning's number, Chezy's number or wave induces resistance. The bed resistance described by Manning's and Chezy's number

can be specified either a constant value over the entire domain or spatially distributed grid map containing value for individual grid in bathymetry. In case of Manning's number, the values in the range of 20-40 $m^{1/3}/s$ are suggested. However, the actual values can be based on the land use land cover of the certain area. It is the calibration parameter in MIKE 21 Flow Model HD.

Structures – MIKE 21 implement the structure as a one-dimensional. Therefore, flow across the structure is calculated as discharge for the whole structure. There are three types of structures are available viz. (a) weir, (b) culvert and (c) dikes. The composite (combining two or more) structure can also be defined in the simulation.

2.4 IRRIGATION WATER DEMAND

The amount of water required for irrigation or the prediction of irrigation demand for a command area is critical for the design and operation of an irrigation project. The water need, also known as the irrigation requirement, is most frequently described as the total quantity of water required by the crops in the command area from the time of their initial watering to the time of harvesting or last watering (base period) (Garg 2005). The Gross Irrigation Requirements are dependent on Net Irrigation Requirements (NIR) of crops. NIR is a function of Reference Evapotranspiration, Crop Evapotranspiration or Crop Water Requirement (CWR) and Effective Rainfall (Peff). The calculation procedure is explained in further sections.

- **Reference Evapotranspiration (ETo)**

The reference evapotranspiration was estimated using a modified Hargreaves approach (Samani 2000) to estimate solar radiation and crop evapotranspiration with use minimum climatological data.

- **Hargreaves Method**

The difference between maximum and minimum air temperatures is proportional to the amount of cloud cover in a certain region. Clear-sky circumstances result in high temperatures during the day (Tmax) because the atmosphere is transparent to incoming solar radiation and low temperatures at night (Tmin) because the atmosphere absorbs less outgoing longwave radiation. Tmax is less under overcast situations because a considerable portion of the incoming solar energy never reaches the earth's surface and is absorbed and reflected by the clouds. Similarly, Tmin will be substantially greater because cloud cover acts as a blanket, reducing net outgoing longwave radiation. As a result, the difference between maximum and minimum

air temperatures (Tmax - Tmin) may be used to estimate the proportion of extra-terrestrial radiation that reaches the earth's surface. Hargreaves and Samani (1985) used this concept to produce estimations of ETo using only air temperature data. Furthered modified by (Samani 2000) minimizes the error associated with estimating solar radiation, thus improving the estimation of reference evapotranspiration. For the computation of Evapotranspiration (ET_o), the Samani (2000) Method explained in Eq. (2.36).

$$ET_o = 0.0135 * KT * R_a * (T_{mean} + 17.8) * (T_{max} - T_{min})\text{^}0.5 \qquad (2.36)$$
$$KT = 0.00185 * (T_{max} - T_{min})^{0.5} - 0.0433 * (T_{max} - T_{min}) + 0.4023$$

where Radiation (R_a) (mm/day) = 0.408 * radiation (MJ/m^{2}day) is extra-terrestrial radiation (MJ/m^{2}day), T_{max} is maximum air temperature (°C), T_{max} is minimum air temperature (°C), T_{mean} is mean air temperature (°C), ET_o is evapotranspiration (mm/day).

- **Crop Water Requirement (CWR)**

Consumptive usage of a crop, also known as crop evapotranspiration, is the total quantity of water consumed by the plant in transpiration (building of plant tissues) plus evaporation from neighbouring soils and plant leaves. This number varies for various crops and can also vary for the same crop at different locations and times. This is also known as crop water requirement (CWR), which may be determined using Eq. (2.37)

$$CWR = ET_c = K_c \times ET_o \qquad (2.37)$$

ETc denotes crop evapotranspiration (mm), *Kc* denotes crop coefficient at a certain development stage (dimensionless), and *ETo* denotes reference evapotranspiration (mm).

- **Effective Precipitation (P_{eff})**

Effective rainfall is the precipitation that falls during crop growth and is available to supply the crop evapotranspiration demands, eliminating precipitation lost through deep percolation below the root zone and surface drainage. The Soil Conservation Service (SCS) Method, as defined in Equation (2.38) below, was used to determine effective rainfall.

$$P_{eff_t} = \frac{P_t}{125} * (125 - 0.2 * P_t) \qquad P_t \leq 250\ mm$$
$$P_{eff_t} = 125 + 0.1 * P_t \qquad P_t > 250\ mm \qquad (2.38)$$

Where, P_{eff_t}=effective rainfall in tth month; and P_t=rainfall in tth month.

- **Net Irrigation Requirement (NIR)**

Net irrigation need is the amount of irrigation water required to fulfil a crop's evapotranspiration demand as well as additional needs such as leaching (Special needs), as expressed in Eq. (2.39).

$$NIR = CWR - P_{eff} + Special\ needs \tag{2.39}$$

Filed irrigation requirement (*FIR*) and Gross irrigation water requirement are calculated as per Equation (2.40) and Equation (2.41)

$$FIR = \frac{NIR}{n_a} \tag{2.40}$$

$$GIWR = \frac{FIR}{n_c} \tag{2.41}$$

where, *NIR*=Net Irrigation Requirement; *FIR* = Field irrigation requirement; *GIWR*= Gross irrigation water requirement; n_a= Application efficiency (60% for flood irrigation); and n_c=Conveyance efficiency (70% considered for present study).

2.5 DROUGHT ANALYSIS

A clear and universal definition of what a drought can be labelled as, have not been achieved yet. Drought is neither aridity nor water scarcity, and it is not a permanent climatic feature. Palmer (1965) stated "Drought means various things to various people depending on their specific interest".

Some of the commonly used definitions are:

- The World Meteorological Organization (WMO; WMO 1986) defines drought as "a sustained, extended deficiency in precipitation."
- The UN Convention to Combat Drought and Desertification (UN Secretariat General 1994) defines "drought means the naturally occurring phenomenon that exists when precipitation has been significantly below normal recorded levels, causing serious hydrological imbalances that adversely affect land resource production systems."
- The Food and Agriculture Organization (FAO 1983) of the United Nations defines a drought as "the percentage of years when crops fail from the lack of moisture."
- The encyclopaedia of climate and weather (Schneider et al. 1996) defined a drought as "an extended period - a season, a year, or several years - of deficient rainfall relative to the statistical multi-year mean for a region."

2.5.1 Types of droughts and their advancement

Droughts can be classified into four types based on the climatological parameter that is being used as data to quantify a drought.

Meteorological drought

A drought is said to be a meteorological drought when there is lack of precipitation over a sustained period over the region of interest. The precipitation is most widely used meteorological parameter to assess drought. Other meteorological parameters such as temperature and evapotranspiration are also considered for assessment of meteorological droughts.

Hydrological drought

A hydrological drought persists whenever there is an inadequate amount of surface and sub-surface water flow to the streams, reservoirs, and ground waters of an area. Streamflows and geology of an area highly affect the drought persistence in that area.

Agricultural drought

This drought occurs whenever the root zone soil moisture content of crops declines over a period. In other words, an agricultural drought is said to be identified whenever there is a crop failure resulting in huge reduction of crop production. This drought is a consequence of deviation of rainfall and streamflow values from their normal value. In countries like India which are majorly dependent on agricultural sector, this type of drought declaration is used.

Socioeconomic drought

The socio-economic drought is the failure of water resources systems to meet the water demands of an area. The economic standard of that area also declines due to the socio-economic drought.

Advancement of drought

The drought initiates due to deficit of rainfall and the impact of drought are revealed in different hydrological systems at different time periods. For example, the deficit of rainfall has immediate effect on soil moisture, whereas this impact is revealed in stream flows with a lag of 2-3 months. Hence the propagation of drought is also to be considered in the analysis.

Usually, the drought propagates from meteorological to agricultural. Then it advances from hydrological towards groundwater.

- **Characteristics of droughts**

Beginning and End

It is crucial to determine the beginning and end of a drought. The beginning of a drought can be identified whenever the drought indices are persistently decreasing below a threshold level. Similarly, the end of a drought can be identified whenever the drought indices are nearing the threshold level and increases beyond it.

Duration of drought

It is the time between beginning and end of a drought and during this duration the drought indices are continuously below the critical level. The duration of drought depends upon the region and can vary from weeks to few years and is expressed as weeks/months/years.

Drought severity

The degree or magnitude of the cumulative deficit of drought parameter below the threshold level indicates the drought severity of an area. It can also be defined as the degree of impacts due to deficit.

Drought intensity

It is the average value of drought parameter below the critical level and can be measured by dividing the drought severity with duration.

2.5.2 Drought Indices

- **Standardized Precipitation Index (SPI)**

The SPI is a popular meteorological drought index developed by McKee et al. (1993) that is calculated solely on long-term precipitation records for the desired period. The data is first fitted to the gamma probability distribution, then transformed to a standard normal distribution. The probabilistic modeling can be done using parametric or empirical probability distribution fittings. The SPI can be calculated either monthly or weekly. In 2010, WMO designated the SPI as a key meteorological drought indicator to be produced operationally by meteorological services. The SPI is calculated over a wide range of time scales. The time scale depicts the

effect of drought on the availability of various water resources. The significance of each time scale and the classifications of the drought classes are shown in Table 2.2 and 2.3 respectively. The classification of the drought classes is used invariably for other standardized drought indices also.

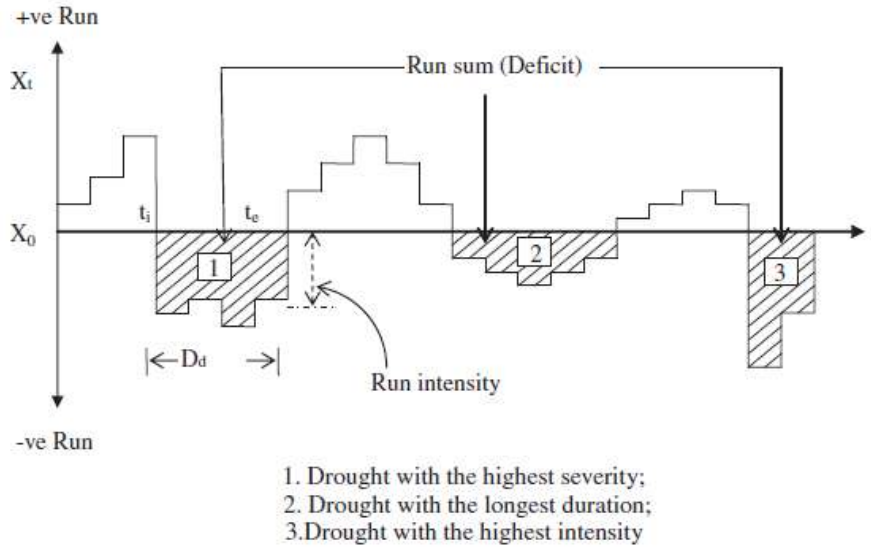

Fig. 2.6 Drought characteristics (Mishra and Singh 2010)

Table 2.2 significance of each time scale of SPI

Time scale	Significance
SPI_1	Short term soil moisture, crop stress
SPI_3	Estimation of seasonal precipitation
SPI_6	Precipitation of distinct seasons
SPI_9	Impacts on agriculture
SPI_{12}	Reservoir levels, groundwater levels

Table 2.3 Classification of drought classes based on SPI

SPI value	Drought Category
>2	Extremely wet
1.5 to 1.99	Very wet
1 to 1.49	Moderately wet
-0.99 to 0.99	Near normal
-1.49 to -1	Moderately dry
-1.99 to -1.5	Severely dry
< -2	Extremely dry

- **Standardized Precipitation Evapotranspiration Index (SPEI)**

Vicente-Serrano et al. (2010) proposed the SPEI as one of meteorological drought indices. It is intended to account for the effects of both precipitation and potential evapotranspiration (PET) while determining drought. It is particularly well suited for examining the impact of global warming on the intensity, duration, and size of droughts. The SPEI is used by High-

Resolution South Asia Drought Monitor to assess the drought trigger (Sahana et al. 2021). It is computed similarly to SPI by replacing the precipitation data with the climatic water balance. Climatic water balance is the difference of precipitation and potential evapotranspiration. The data is then fitted to a suitable distribution, preferably log-logistic distribution (Vicente-Serrano et al. 2010).

- **Standardized Streamflow Index (SSFI)**

The SSFI is a hydrological drought index which is used to get spatial and temporal variation of streamflow (Vicente-Serrano et al. 2012). It is computed like SPI by putting streamflow data series instead of precipitation series.

- **Standardized Soil Moisture Index (SSI)**

The SSI is similar in methodology to that of the SPI. The soil moisture data, particularly the root-zone soil moisture, at monthly scales is used for estimation of SSI. The SSI is widely used as a measure of agricultural drought assessment.

- **Multivariate Standardized Drought Index (MSDI)**

The assessment of drought considering only one drought indicator may not be enough because drought is an event affected by many indicators (For e.g., Precipitation, soil moisture, streamflow, temperature, etc.) (Hao and AghaKouchak 2013). Depending upon the importance of study different drought variables can be combined, for e.g., Kao and Govindaraju (2010) considered precipitation and streamflow in copula-based joint index with Kendall distribution for drought analysis. Several data aggregation techniques such as linear combination techniques, principal component analysis, copulas, etc. can be used for analysis of drought using multiple variables (Hao and Singh 2015). These multivariate drought factors are known to detect the onset and termination of droughts more precisely (Hao and AghaKouchak 2013; Shah and Mishra 2020).

2.6 LITERATURE REVIEW

2.6.1 Hydroclimatic Variability

Kannan and Ghosh (2011) acknowledged inability of the conventional statistical downscaling techniques to capture multisite correlation, thus, poor prediction of multi-site rainfall. They

developed a model to predict future rainfall states using *K*-means clustering coupled with CART (Classification and Regression Tree) model. The relationship between optimum rainfall clusters identified, i.e., daily rainfall states, and NCEP/NCAR (National Centers for Environmental Prediction/National Center for Atmospheric Research) climate datasets were established for training CART model. The developed relationships were used to predict the future rainfall states, due to global warming, using the large-scale global climate models for the Mahanadi River basin.

Duhan and Pandey (2013) investigated the spatiotemporal variability in annual and seasonal total precipitation of the 45 districts of the Madhya Pradesh, India for the period of 1901-2002. Trend detection was carried out using Mann-Kendall test, and Sen's slope estimator along with percentage change; and change point was detected using Pettit-Mann-Whitney test, and cumulative deviations. Significant decreasing trend in monsoon seasons was observed at Balaghat and Dindori; with an additional station Shahdol in annual precipitation series. The mean percentage change in annual and seasonal precipitation over the entire state was found to be decreasing with rate of -2.59% and -12.9% respectively.

Kannan and Ghosh (2013) developed an algorithm to predict the future rainfall amounts using nonparametric kernel regression (KR) using the rainfall states obtained from *K*-means clustering and CART model for the Mahanadi River basin. The developed model was found to outperform conditional random field based and multi-site downscaling models. The analysis of future rainfall scenarios states conservable change in the rainfall intensity and dry as well as wet spell durations in the Mahanadi River basin with dimetric changes across upper and lower part of the basin.

Salvi et al. (2013) attempted for statistical downscaling of course resolution GCM rainfall data to 0.5-degree spatial resolution for entire India using CART model and non-parametric KR technique for the first time. The study found that the developed model is capable to capture the individual station mean, standard deviation, cross-correlation, and effect of orography, particularly along the Western Ghats and northeast India.

Sonali and Kumar (2013) reviewed the various approaches (rank, slope based) to identify short term, long term, gradual, abrupt changes, changes in trend and change of trend over the time. The result of the study shows that there is significant trend in minimum temperature at

all the seven homogeneous regions of the country at annual, monthly, and seasonal level. The outcome of sequential MK test shows that most of the minimum or maximum temperature begins after the 1970 for all the seasons.

Vittal et al. (2013) analysed the long-term rainfall extremes, obtained from 1-degree resolution data for the duration 1901-2004, using extreme value theory in terms of intensity, duration, frequency, and volume of extreme rainfall events using peak over threshold approach using 95% rainfall values as threshold. Majority of the grids in India were found have diametrically opposite trends in pre-1950 and post-1950 periods, while majority of the urbanised areas have a change point in post-1975 period.

Han et al. (2014) performed extensive analyses of trends in precipitation and streamflows in Xiangxi watershed, China, and diagnosed the presence of heterogeneous trends in precipitation and streamflow due to significant influence of anthropogenic activities in the watershed.

Lacombe and McCartney (2014) extensively studied the trends in monthly and seasonal cumulative precipitation depth, maximum precipitation, and number of rainy days, peak, and onset and retrieval of monsoon in India over the second half of the 20^{th} century using gridded rainfall data of IMD. The onset of monsoon in Northern India is 5% field significant delay.

Pingale et al. (2014) studied the spatiotemporal trend in the mean, extreme precipitation events and temperature over the 33 districts of Rajasthan, India using IMD gridded daily rainfall and temperature data at spatial resolution of $0.5° \times 0.5°$ and $1° \times 1°$ respectively. The urban centres on eastern part of the Aravalli range reported significantly decreasing trends in monsoon and annual precipitation. The northeast (southeast) part of the state showed decreasing (increasing) trends in the extreme precipitation events. Significant increasing trends were observed in the daily minimum and maximum temperature for major part of the state.

Mondal and Mujumdar (2015a) assessed the changes in extreme rainfall characteristics, intensity, duration, and frequency, over India using high resolution daily gridded data with the help of recent advancements in extreme value theory. The nonstationary distributions, with covariates as El-Nino, global mean temperature, and local temperature, were used to model

these characteristics and it was found that the intensity and frequency (duration) and local changes in mean temperature depicted non-stationarity (stationarity) at most of the locations.

Abeysingha et al. (2016) analysed the streamflow trends in Gomti River basin of North India for a period from 1982-2012 using MK and Sen's slope tests. The declining streamflows in the Gomti River were partially attributed to the increase in water withdrawal from the river, increase in air temperature, population escalation and partially due to significant reduction in post-monsoon rainfall in the downstream sub-catchment.

Deshpande et al. (2016) examined the temporal variations in the frequency, spatial coverage and intensity of the precipitation and temperature extremes over the major Indian river basins using the IMD gridded daily data at spatial resolution of 0.25° × 0.25° (rainfall) and 1° × 1° (temperature) for the period of 1951-2014 and 1951-2013 respectively. They reported decreasing trend in the southwest monsoon seasonal rainfall for all the river basins, except for the Krishna and the Peninsular River basins. Further, increase in the number of grids experiencing heavy rainfall events was noticed in all the river basins, with significant increase observed for the river basins located in the central part of India, viz., the Ganga, Narmada-Tapi and Godavari River basins.

Ghosh et al. (2016) observed significant contradicting behaviour in trend of the spatial variability of extreme and mean ISMR. The decreasing spatial variability of total monsoon precipitation detected in response to decreasing precipitation over surplus water river basins demands reconsideration for the river interlinking. The study also contradicts with the assertion that wet (dry) regions are getting wetter (drier) over India. The significant spatial variability in ISMR extremes were accounted due to dominating convective precipitations.

Singh et al. (2016) projected future rainfall states using the Kernel regression based statistical downscaling, with and without conditioning on rainfall states, for five GCM models with two RCP scenarios at 0.25-degree resolution for Tapi River basin. The study concludes that the KR model with conditioning outperformed one without conditioning. The study also reported decreasing (increasing) frequency of heavy/extreme (medium) rainfall events in the future.

Guhathakurta et al. (2017) highlighted increasing trends in frequency of dry days in monsoon, winter, and pre-monsoon seasons during the period of 1901-2010 over most of the part of India. The study of station data and gridded rainfall data revealed a significant increasing trend in very heavy to extremely heavy rainfall over the Indian river basins. The variation in the sea surface temperature over oceans were reported responsible for the significant decadal variation in extreme rainfall events over Central India.

Bisht et al. (2018) investigated the rainfall trend over the major river basins of India, using high resolution (0.25° × 0.25°) gridded daily rainfall data of IMD, from 1901-2015. This study comprises of long-term trend (1901-2015), pre-urbanisation trend (1901-1970) and post-urbanisation trend (1971-2015) analysis of annual and seasonal rainfall, rainfall extremes (R95p and R99p), maximum cumulative rainfall of 1-, 2-, 3- and 5-days. Majority of Indian river basins showed profound decreasing trends in annual and monsoonal rainfall during post-urbanisation period; significantly increasing trend in rainfall extremes; and increasing trend in 1-, 2-, 3- and 5-days cumulative rainfall. Their study also emphasised the importance of rainfall variability analysis at sub-basin level over basin level to consider the spatial heterogeneity of rainfall.

2.6.2 Hydrological Modeling using SWAT

Abbaspour et al. (2007) tested the performance of SWAT and its feasibility to use this model for simulating flow and transport processes in Thur River basin. They concluded that with good data quality, availability and relatively small model uncertainty, SWAT is efficient in simulating flow and transport processes.

Gassman et al. (2007) presented a brief review of the applications of SWAT model, explaining the component of SWAT and studies in which SWAT has been used. The summary of various applications was categorized into calibration, sensitivity analysis, and hydrologic analysis, impact analysis of climate change on hydrology and pollutant load simulation. The strengths and limitation of SWAT model were also discussed along with future scope of research.

Yang et al. (2008) carried out a comparative study of five philosophically different uncertainty analysis procedures, viz., Generalized Likelihood Uncertainty Estimation (GLUE), Parameter Solution (ParaSol), Sequential Uncertainty Fitting algorithm (SUFI-2) and a Bayesian

framework using Markov Chain Monte Carlo (MCMC). These techniques were implemented to the Chaohe Basin in China in SWAT model. These methods were evaluated on basis of their performance with respect to the best estimates, prediction uncertainty, implementation difficulty, conceptual basis, and computational efficiency. It was inferred that Bayesian-based approach was found to be most efficient amongst the aforesaid techniques.

Ghaffari et al. (2010) used the SWAT model to simulate the water balance and investigate the impacts of land-use changes on the hydrology of Zanjanroob Basin, Iran. SUFI-2 was employed to carry out calibration and uncertainty analysis. The model was calibrated for monthly streamflow with correlation coefficient and Nash-Sutcliffe coefficient as 0.86 and 0.79 respectively for calibration period and 0.80 and 0.79 respectively for validation period.

Gong et al. (2010) assessed the impact of threshold drainage area (TDA) for watershed delineation and hence on hydrologic model, for simulation of streamflow and sediment erosion, and parametric uncertainty over the Upper Daning River Watershed, China. The investigation states that the model does not perform good at finest (TDA of 2,000 ha) nor at coarsest (20,000 ha) delineation schemes. The best model performance for the aforesaid study area was obtained at TDA of 5,000 ha. Also, the 95% prediction uncertainties (assessed P-factor and R-factor) in the developed model were reported to be least at TDA of 5,000 ha.

Gosain et al. (2011) undertook a study to quantify the possible impacts of climate change on hydrology of river basins in India using SWAT model. The study evaluated the severity of droughts and floods, and thus, identified the most vulnerable hotspots across the country under the climate change scenarios.

Mango et al. (2011) investigated the impact of projected climate change and continued land use changes on the hydrology of Mara River using SWAT. In their study, satellite data was used as input, which improved the performance of the model. The results show that reduction in dry season flows and increase in peak flows were observed because of the conversion of forests to agriculture and grassland, which caused water scarcity in the catchment.

Zhang et al. (2012) assessed the impact of climate change and human activates on the runoff in Huifa River Basin, Northeast China using SWAT. The SWAT model was calibrated and validated for the baseline period of 1956-1964 and the runoff driven by climate forcing only

was simulated for the period of 1965-2005. As a result, the decrease in the observed runoff was found due to both climate and human activities. During wet years, the decrease in runoff was observed to be dominated by the impact of human activities such as regulatory and water storage projects.

Chandra et al. (2014) estimated sediment yield for Burhanpur sub-catchment in Upper Tapi basin using SWAT. The model was calibrated and validated to achieve average values for NSE and RSR (ration of RMSE and standard deviation) for sediment yield up to 0.85 and 0.36 respectively. This shows the capability of SWAT in simulating the sediment yield in a catchment where large variations terms of topography, physiography, and land use/land cover are observed.

Abbaspour et al. (2015) developed and calibrated SWAT for Europe and addressed the issue regarding data availability and calibration procedure for large-scale distributed hydrologic model. Many flows measuring stations, nitrate concentrations of rivers, and yields of wheat, maize and barely were calibrated. The study also presented a calibration protocol for large-scale models with reference to sensitivity of the parameters to calibration output. Overall, a significant information of availability of freshwater at continent-scale and water quality at sub-basin level, at monthly time step, was derived.

Chandra et al. (2016) in his study calibrated and validated observed runoff and sediment yield in Upper Tapi basin, India for a period of 12 years using SWAT. The difference in the topographical, land cover, soil, and climate characteristics were observed to be the reason of such contrasting behaviour. In the study results, Burhanpur sub-catchment was observed to be significantly prone to soil erosion compared to Purna sub-catchment, since the former contributed to about 80% of the sedimentation in Hathnur reservoir. Further, the watersheds most prone to soil erosion were identified and suitable BMPs were suggested as a measure to control the soil erosion form the sub-basin.

Kamali et al. (2017) attempted to address the uncertainty in identification of the input data sources leading to least source of uncertainty in hydrological model simulations. The study used four climate databases and two land use maps and showed that their results estimated significantly different WRC (Water resource components). The study concludes that non-negligible level of uncertainty are introduces from different sources of input data sets.

Worku et al. (2017) studied the impact of land use and land cover change on the streamflow and sediment using SWAT in the Beressa watershed. The continuous change in the land use and land cover between 1984 to 2015 had substantial impact on the streamflow and sediment yield. The increased farmland and settlements and considerable deforestation led to the increase in surface runoff and sediment yield leading to loss of fertile soil and hence food shortage to the local farmers.

Gashaw et al. (2018) analysed the hydrological impact of land use and land cover change and predict its impact on the hydrological status of future in Andassa watershed. The future land use prediction was carried out using the Cellular-Automata Markov (CA-Markov) algorithm and hydrological response were simulated by SWAT. The change in the hydrological components were attributed to the significant transition from vegetation to non-vegetation cover in the watershed.

Narsimlu et al. (2018) studied the impact climate change on water availability in Sindh River basin, India, using semi-distributed hydrologic model SWAT. The mean monthly streamflow operations at three gauging stations were used for calibration and validation of the model. The model performance estimators showed very good prediction during validation period and the values of R^2 ranged from 0.83-0.92, NSE from 0.81-0.89 and PBIAS from -12.08 to -24.19.

Wang et al. (2018) emphasised on the hydrological response to the spatiotemporal land use and land cover change in Yangtze River Delta region, China using an integrated approach involving SWAT and GWR (geographical weighted regression) models. The study also established a positive correlation of La (land use intensification index) with water yield and surface runoff, and negative correlation with percolation, evapotranspiration and baseflow for the study region. The rural regions were identified to be severely affected by the land use and land cover change.

Nilawar and Waikar (2019) studied the impact of climate change on streamflow and sediment concentration considering three regional circulation models (RCMs) with two representative concentration pathways (RCP) 4.5 and 8.5 for Purna sub-catchment of Godavari basin. The SWAT model was prepared on monthly scale for base period (1980-2005) with calibration period (1980-1994) and validation period (1995-2005). The projected precipitation and temperature data showed significant increasing trend with respect to base period. The average

monthly streamflow and sediment concentration rose from 24.47 - 115.94 m^3/s and 32.58 - 162.96 mg/l respectively under RCP 4.5 and 8.5, particularly from June to September months.

Munoth and Goyal (2019) assessed the effect of DEM sources, its spatial resolution and drainage area threshold values (ATV) using SWAT for the Upper Tapi River sub-basin, India. The ASTER, CARTOSAT and SRTM DEM were resampled at 30, 90 and 180 m spatial resolutions and six different ATVs were used to assess their impact on the simulation of flow and erosion in the catchment. They concluded from their study that appropriate ATV for Upper Tapi River Sub-basin is between 100 km^2 to 300 km^2.

Triana et al. (2019) argued the inability of the hydrological models, dominantly working on single-domain modeling approach, to closely represent the hydrological system of the study region. The application of the unsupervised calibration algorithms may result satisfactory/good/very good model performance, estimated using NSE/R^2/PBIAS etc, however, may lead to distorted parameters set. The model calibration accounting for equifinality, model inadequacy and constraint inadequacy are likely to better represent the circulation of the water within the hydrological system of the area.

Moazami Goudarzi et al. (2020) used two GCMs (MICROC5 and HadGEM2-ES) to process climate data over the future period under RCP scenarios (RCP 4.5 and RCP 8.5) and compared temperature changes and precipitation to the base period of 23 years and future scenario of 20 years each. The model's correctness was assessed using statistical indices (R^2 and NSE), both were satisfactory at 3 different stations. Precipitation changes appear in several manners. The arid seasons alter more than the rainy seasons. Under two alternative scenarios, the SWAT model anticipated runoff response in the future. Runoff will increase in the spring.

Rani and Sreekesh (2020) analysed the effect of climate and land cover changes on the discharge of the Upper Beas River basin. They used climate, soil, land use/land cover, and elevation data in SWAT to estimate the discharge. The result suggest that watershed hydrology is more sensitive to climate change with rise of mean annual discharge between 0.31% - 9.65%, while it may decline by 9% under land cover change scenarios by the mid-21st century. They suggested that seasonal changes would be beneficial in the short run but may adversely affect the water availability in the long run.

Sahana and Timbadiya (2020) quantified spatiotemporal variability of the water availability for semi-arid Upper Girna basin, India using SWAT model. The application of predicted future rainfall and temperature from CMIP-5, for two RCP 4.5 and 8.5, with SWAT found that the late century (2071-2100) flow indices exhibit large variability as compared to early (2011-2040) and mid (2041-2070) century. The study undertakes the impact of climate change on hydrology of the Upper Girna basin without considering the anthropogenic changes over the period.

Sinha et al. (2020) investigated the impacts of land use/land cover (LULC) and climate change on the streamflows and sediment yield using SWAT. They used land change modeller to derive the future LULC, using transition matrix method, and GCMs data for two RCP scenarios, i.e., RCP 4.5 (moderate emission) and RCP 8.5 (high emission). The results showed that decrease in forests and grasslands and increase in plantation, agricultural, and urban areas would lead to an increase in the mean streamflow (11.23%) and sediment yield (17.41%). Under RCP 4.5, climate change would decrease the streamflow by 2.38% in 2030. However, under RCP 8.5, climate change would increase the streamflow by 0.12% in 2030.

Tan et al. (2020) extensively reviewed the application of the SWAT model for assessment of hydro-climatic extremes, i.e., floods and droughts, under the climate change. In addition, the model has extensive applications in streamflow and sediment yield modeling, water quality and nutrients transport modeling and agricultural yield estimation etc. The research also highlighted the current research gaps in modeling the extremes using the SWAT for historical as well as future climate scenarios.

Das et al. (2021) used the SWAT model for CC assessment for 4 different GCMs viz. MIROC-ESM, MIROC_MIROC5, MOHC_HADGEM2_ES and MIROC-ESM-CHEM. The NSE and R^2 values obtained during the calibration and validation time periods were very much satisfactory. According to the sensitivity analysis, the most sensitive parameter is the SCS runoff curve number (CN2), then soil hydraulic conductivity (SOL K), and Soil water content (SOL AWC). CC is having a negative effect on the Gomti River basin and its environment. In this region, a warmer temperature will quicken the hydrologic cycle, altering precipitation quantities and runoff. Due to a decrease in precipitation and a rise in temperature, the stream flow decreased.

Nkhonjera et al. (2021) used the SWAT model in conjunction with regional climate downscaled data from the CORDEX (Africa project) to examine local seasonal precipitation variability in the Olifants River basin's upper middle catchment (UMC). They found greater monthly and seasonal precipitation variability based on two scenarios (RCP4.5 and RCP8.5). Their research also found a significant drop in future seasonal precipitation, mainly in the mid-term timeframe (2021–2050). Drought conditions and streamflow reductions of the major river (Olifants) and its tributaries were increased by the general decrease in future seasonal precipitation.

Thomas et al. (2021) studied the potential impacts of climate change for optimal utilization of available water resources in Narmada basin. They incorporated the existing dams in the river basin into SWAT model for simulating the future developmental scenarios under projected climate change. The study incorporated Coordinated Regional Climate Downscaling Experiment datasets for South-Asia (CORDEX-SA) at 0.5◦ × 0.5◦ resolution for four-time periods, viz., 1970–2005 (historical), 2006–2040 (near-term), 2041–2070 (mid-term) and 2071–2099 (end-term) under two RCP scenarios, RCP 4.5, and RCP 8.5 to investigate the changes in the future climate and simulation of future streamflow. The findings show that the simulation–optimization framework based integrated reservoir operation of four reservoirs had led to better reservoir performance with substantial reduction in the number of irrigation and hydropower failures. In addition, there were no failures in meeting the domestic water supply and environment flow demands.

2.6.3 Distributed hydrological modeling using MIKE-SHE

Refsgaard et al. (1997) developed MIKE SHE/MIKE 11 integrated hydrological model for environmental assessment in the Danubian Lowland between Slovakia and Hungary. The developed integrated MIKE SHE model include the river and the river branches (1D flow in MIKE 11), reservoir (2D flow) the ground water (3D flow), agricultural aspects (crop yield, irrigation, nitrogen modeling) and flood plain condition. The integration between different models provides the complex description of various processes. The validation was carried on the individual model as well as on integrated model. The result of integrated model shows the less uncertainty against the result of individual model components.

Stisen et al. (2008) developed the remote sensing driven distributed hydrological model for the Senegal river basin of 350000 km^2 in West Africa. They considered the 6 × 6 km horizontal

grid resolution for simulating the model during 1998-2005 for six different sub-catchments. They utilized the historical meteorological data only to calibrate the remote sensing algorithms. The model shows better performance well with satisfactory range. The simulated and actual evapotranspiration was compared to the measurement at the point scale and found good agreement for both event and seasonal scale. The predicted discharge and average AET were found at the same order as observed data, however, considerable spatial variation was observed in the catchment.

Huang et al. (2010) developed the integrated MIKE SHE/MIKE 11 model for the Tarim river basin in China (19000 km^2) to study the water resources management with the application of remote sensing (RS) and GIS. The model was developed with the grid resolution of 1 x 1 km^2. The MIKE SHE/MIKE 11 considered the lumped parameter over the catchment for the calibration and validation of the model during 1998-1999 and 2000-2001 respectively. The model was simulated for the RS data against the gauged data where RS data shows the better performance in the simulation of actual evapotranspiration for the catchment.

Shu et al. (2012) developed fully distributed physics based hydrological model for the Hebei province (7230 km^2) in China using MIKE SHE and MIKE 11 with the grid resolution of 500 m x 500 m. The model parameters for overland flow parameters, vegetation characteristics and groundwater flow were lumped over the catchment. The model was calibrated for the groundwater with observed wells and ET with agricultural stations data for the catchment for 1996-2002. The calibrated model provides acceptable results for seasonal dynamics of both the parameters whereas the declining trend in the ground water level were observed. The investigation shows that the declining ground water trend can be controlled with different water management and distribution techniques.

Foster and Allen (2015) developed the MIKE SHE/MIKE 11 model for the interaction of groundwater and surface water in a mountain to coast watershed of Cowichan (area 930 km^2) in Canada, also included the effect of climate change and human activities. They studied the seasonal and spatial interaction of groundwater and surface water in the catchment, whereas the total water balance demonstrated for the period of 1998-2012 using the remote sensing data. The results of water balance show that decrease in amount of recharge and precipitation with increasing evapotranspiration compared to the average condition in the catchment. Also, found that channel and aquifer within the catchment were affected by ground water pumping.

Loliyana and Patel (2018) developed the physics based hydrologic model in MIKE SHE integrated with MIKE 11 for the Yerli sub-catchment (area 15,881 km^2) of Upper Tapi basin in India. The model was calibrated using the multi-objective approach for period of 1991-1998. The local sensitivity of the model parameter was performed and found the saturation water content, filed capacity and horizontal hydraulic conductivity of saturated porous media are the most sensitive parameters. The calibrated model was validated or the year 1999-2004, the simulation results shows the applicability of the model to simulate the hydrograph satisfactorily for the Yerli sub-catchment at daily and monthly time scale. The results of the study for the water balance shows the 78% of the water lost from the system via evapotranspiration, out of which about 3.5% contributed from the groundwater zone.

Shu et al. (2018) developed the distributed hydrological model by using MIKE SHE codes for Haihe Plain, China to study the importance of modeling ET and groundwater process using remote sensing data. Prior to calibration the sensitivity analysis was carried out to find the most sensitive groundwater parameter. The model has been calibrated for the year 1996-2002 and validated for the year 2003-2004 using the groundwater heads in the selected observation wells using parameter estimation software PEST. From the study they have concluded the spatial structure of the input of remotely sense data plays an important role in the model output such as accurate spatial and temporal ET patten are important in the groundwater resources assessment which determines the recharge to the saturated zone.

Loliyana and Patel (2019) developed integrated MIKE SHE/MIKE 11 model for the Gopalkheda sub-catchment India, to simulate the soil moisture content within top 90 cm vertical soil profile. The lumped model parameters were calibrated for the period of 1991-1998 and validate for the year 1999-2004 for simulation of streamflow and soil moisture content at the sub-catchment outlet using station-based rainfall vis-à-vis gridded rainfall data. The result obtained from the model indicates that the performance of the model is highly dependent on the nature of rainfall input and concluded that the gridded rainfall data is more promising in prediction of streamflow and soil moisture within study area.

Loliyana and Patel (2020) developed integrated physics based distributed hydrological model in MIKE SHE/ MIKE 11 for Yerli sub-catchment of Upper Tapi basin India. The model is calibrated for the period of 1991-1998 using multi-objective calibration approach for minimizing the error in the prediction of streamflow and ground water levels within study reach

and validate for year 1999-2004. They found that distributed Manning's roughness co-efficient, vegetation, soil and geologic parameters improves the performance of model significantly in the prediction of streamflow as well as ground water level. The model also satisfactorily simulates the soil moisture for the plain area. They also analysed the water balance for different period which revels the capability of integrated hydrological model to simulate the dynamics of hydrological processes in with changing land use, ground water draft and irrigation practices across the region.

Ramteke et al. (2020) developed the physics based distributed hydrological model in MIKE she to study the impact of conservation measure on watershed hydrology for under changing climate scenario. The detailed estimation of water balance for individual year from 1979 to 2009 revels the reduction in surface runoff (10.06 %) and increase in groundwater recharge (11.33 %). The consistent reduction and enhancement in surface runoff and recharge were also observed for RCP 4.5 and RCP 8.5 scenario of RegCM4 regional climate model.

2.6.4 Flood Inundation and Risk Assessment

Mani et al. (2014) developed 1D-2D coupled hydrodynamic model for the proposed industrial plant area. The two scenarios viz. flooding due to probable maximum flood (PMF) and probable maximum precipitation (PMP) at the plant site in addition with PMF are considered in the analysis. The model output flood depth, cross product of depth, velocity and duration have been used to calculate flood hazard. The flood hazard assessment considering the PMF and PMP assistance in determining the plinth level for the plant site and helps in identifying the flood protection measure.

Sahoo and Sreeja (2015) demonstrated the flood inundation modeling as an effective tool in managing the flooding in urban catchment of northeast India. They find out the inundation pattern for peak rainfall intensities corresponds to different return period. The flood hazard ranks were developed in interaction vulnerability parameters such as flood depth, inundation area, affected land use, population and road. They also identified the flood risk zones based on hazard ranks.

Sherly et al. (2015) proposed the framework to assess the vulnerability of densely populated coastal urban area by considering both population and assets at the risk. The social, socio-economic, infrastructure, critical facility and adaptive capacity indicators are identified to

assess the individual vulnerability of the city using GIS at 1-km grid scale spatial scale. The principal component analysis (PCA) was performed to decorrelate the data and Data Envelopment Analysis (DEA) is used to find the efficiency of the indicator. The analysis performed over twenty-four ward of Mumbai city found that, city is most vulnerable mainly due to increase in population and marginal worker ratio. The reduction in social vulnerability was observed and positive improvement in literacy and main worker ration.

Pasquier et al. (2019) developed 1D-2D coupled hydrodynamic model in HEC-RAS for eastern coast of UK. The Peaks-Over-Threshold method was adopted for defining the extreme scenarios. The model was simulated for sea-level rise up to year 2100 and found detailed inundation in the coastal urban area. The model was also combined with fluvial source of flooding. They found that, the sea level rise as primary source of flooding and it increases 5-40 % with average depth increase of 10-32 % when combine with other source of flooding.

Sahoo and Bhaskaran (2018) developed the coastal vulnerability index (CVI) for Odisha coast which is highly prone to cyclones. They attempt to investigate the physical environmental, social and economic impact on coastal vulnerability. They also investigate the coastal vulnerability under changing climate scenarios. Eight fair weather parameters including storm surge height and onshore inundation to quantify the physical vulnerability index (PVI). The PVI along with social, environmental and economic vulnerability used to calculate overall CVI with GIS application. They believe the comprehensive study will be benefit to coastal zone management authority.

Jha and Gundimeda (2019) assessed the vulnerability of flood affected district with integration of indictors for exposure, sensitivity and, adaptive capacity into composite index using principal component analysis (PCA). They found that, Bihar is highly vulnerable to floods specifically north Bihar due to recurring flooding and strong pattern among the vulnerable districts. They also found that, the biophysical and social factors are dominant in determining the degree of vulnerability among the district of Bihar.

Mohanty et al. (2020) reviewed the status and future challenges in flood management in India. They identified the region-specific flood problems in India and discuss the initiatives undertaken by major Indian flood management agencies with emphasis on the current ongoing flood management practices. They also discussed the long-term effectiveness and gap between

these practices. Finally, provide the recommendation to stakeholder and policymakers in formulating the sustainable flood management plan for improving flood resilience.

Mohanty et al (2020) quantify the flood risk through compound contribution of flood hazard and flood vulnerability at the finest administrative scale of village-level over Jagatsingpur district in Mahanadi River basin, Odisha. The study focuses on four key aspects in calculating the flood risk includes (i) regionalize design rainfall (ii) flood hazard mapping using the hydrodynamic modeling, socio-economic vulnerability analysis and (iv) quantifying the bivariate flood risk through risk classifier. The analysis performed on two-time frames 1970-2011 and 1970-2001 found villages are more prone to compound effect of hazard and vulnerability during 1970-2011 whereas, more vulnerable during 1970-2001.

Gusain et al. (2020) develop the new approach for translation of flood hazard information in the form of decision priority maps which derived from the combination of physical and statistical model for Mahanadi basin India. They also identified the impact of climate change for 1 in 100-year return period flood under future conditions. They analyse the change in flood hazard classes or future climate change scenarios for prioritizing areas under great hazard. The model result found that, the changes from low to high flood hazard category in agriculture dominated area. They also found that, the flood hazard is increasing significantly under RCP4.5 and RCP8.5 scenario with 12.5% and 27.35% respectively.

Ghosh et al. (2021) proposed the novel, comprehensive hydrodynamic flood modeling framework over Mithi River watershed in Mumbai, India to decrease the inundation extent by incorporating different inland hydraulic scenarios. They developed three-way coupled flood model including river, overland flow and stormwater is developed in MIKE FLOOD platform. It was followed by flood hazard maps flood for various inland hydraulic scenario with feasible cross-section and lining material. The flood hazard maps were developed for 10-, 50- and 200-year flood with possible flood reducing scenario. They found that, trapezoidal river cross section with concrete lining relatively maximizes the reduction in flood extent.

2.6.5 Impacts on Irrigation Water Demand

Hargreaves and Samani (1985) The authors introduced a method that was used to estimate ETo values for various sites using eight years of daily lysimeter data from Davis, California. Comparisons with other methods using measured cool season grass evapotranspiration in New

Jersey, California, Australia, Aspendale, Seabrook and Lompoc; lysimeter data from Haiti, Damin: and the modified Penman for various locations in Bangladesh confirmed that the method does not typically require local calibration and that the estimated values are likely to be as reliable and usable as those from the other estimating methods used for comparison. The proposed technique is able for usage when there is a scarcity of climatic data, as well as for better irrigation planning and management.

Samani (2000) The author presented a method for estimating solar radiation and then referencing crop evapotranspiration using minimal climatological data. The study provides a modification to an original equation that estimates solar radiation and crop evapotranspiration using maximum and maximum temperature. The suggested improvement allows for the correction of inaccuracies caused by indirect climatological factors that impact the local temperature range. The suggested adjustment also enhances the accuracy of temperature-based estimations of solar radiation.

Tukimat et al. (2017) The purpose of this work was to explore the changes in irrigation water demand in a heavily irrigated area of Malaysia under a climate change scenario. To estimate future changes in rainfall and temperature at the local scale, the outputs of global circulation models (GCMs) are downscaled using a statistical downscaling model (SDSM). The CROPWAT irrigation water demand estimating model is calibrated and verified using historical data before being used to forecast future changes in irrigation demand under SDSM anticipated climatic conditions. Climate change will lower agricultural water consumption in the area by 0.9 percent every decade.

Yirga (2019) Author has calculated ETo values using a combination Penman–Monteith model and to develop a model for predicting reference evapotranspiration in the Megecha watershed. The potential of a multiple linear regression model using least squares is studied in this work while modeling mean monthly reference evapotranspiration calculated using the standard FAO-56 Penman–Monteith equation. Multiple correlation analysis revealed that solar hour, wind speed, and maximum temperature all had a high positive association with ETO (r=0.82, 0.71, and 0.78, respectively), although relative humidity had a modestly negative link (r=0.604). For the meteorological station under consideration, the multiple linear regression model yielded residual errors of 0.26 mm/day and a co-efficient of determination of 0.92.

Yadeta et al. (2020) This research assesses potential evapotranspiration (PET) estimation methods, model potential evapotranspiration, and project potential evapotranspiration under various climatic scenarios. The modified Hargreaves–Samani, Thornthwait, and Blaney–Criddle models were compared to the FAO 56 Penman–Monteith technique in terms of relative error (Re), normalised root-mean-squared error, and Pearson correlation (r). A PET estimating model based on six climatic characteristics was created using the multiple linear regression approach (maximum and minimum temperatures, relative humidity, solar radiation, wind speed and sun hours). To anticipate future PET, the outputs of 17 global climate model ensembles were employed for RCP 4.5 and 8.5 emission scenarios. The modified Hargreaves–Samani equation outperformed others at both the Shola Gebeya and Aleltu Agriculture stations, according to the model evaluation.

Sunil et al. (2021) The downscaled future climatic data from the General Circulation Model (GCM), CanESM2, was used in this work to assess the monthly agricultural water demand of the key crops farmed in the Jayakwadi command area, Maharashtra, India. The statistical downscaling model was used for statistical downscaling, while the CROPWAT model was used to anticipate future irrigation demands. The CanESM2 GCM model was statistically downscaled, and future temperature and precipitation predictions were made for two typical concentration pathways (RCP) scenarios, RCP 4.5 and RCP 8.5. The data showed a rise in temperature and precipitation across time periods. The average annual irrigation demand was reduced by 14.07 percent and 14.72 percent for the RCP 4.5 and RCP 8.5 scenarios, respectively.

2.6.6 Drought Analysis

Mishra and Singh (2010) attempted to provide a review of fundamental concepts of drought, classification of droughts, drought indices, historical droughts using paleoclimatic studies, and the relation between droughts and large-scale climate indices.

Hao and AghaKouchak (2013) proposed a new multivariate standardized drought index (MSDI) combining Standardized Precipitation Index (SPI) and the Standardized Soil Moisture Index (SSI) for complex drought analysis. The study area for the analysis includes two climatic divisions in California and three climatic divisions in North Carolina. Monthly precipitation and soil moisture data for the period (1932–2009) were obtained from the Climate Prediction Centre (CPC). Frank copula function was used to derive the joint distribution of the two

variables. Results revealed that multivariate standardized drought index (MSDI) showed similarity with onset determination of drought as similar to Standardized Precipitation Index (SPI) and persistence as similar to the Standardized Soil Moisture Index (SSI) and about the severity it showed lower of that as shown by Standardized Precipitation Index (SPI) and the Standardized Soil Moisture Index (SSI), also the multivariate standardized drought index (MSDI) indicated drought when neither precipitation nor soil moisture indicated drought.

Hao and AghaKouchak (2014) studied a multivariate multi-index drought monitoring framework, namely, the multivariate standardized drought index (MSDI), for describing droughts based on the states of precipitation and soil moisture. The MSDI was evaluated against U.S. Drought Monitor (USDM) data as well as the commonly used standardized indices for drought monitoring, including detecting drought onset, persistence, and spatial extent across the continental United States. The results indicated that MSDI includes attractive properties, such as higher probability of drought detection, compared to individual precipitation and soil moisture–based drought indices. The study showed that the MSDI leads to drought information generally consistent with the USDM and provides additional information and insights into drought monitoring.

Farahmand and AghaKouchak (2015) calculated probability of variables using the empirical Gringorten equation and then transformed into Standardized Index (SI). Parametric method for calculating indices give inconsistent output as variables have the different probability distribution for various climatic conditions. Empirical nonparametric distributions are based on the ranks of data points instead of their actual values and does not require to calculate distribution specific parameters and goodness of fit value.

Hao and Singh (2015) have reviewed various methods for computation of multivariate drought index which includes Blending objective and subjective indicators (e.g., USDM), water balance model (e.g., Palmer Drought severity index (PDSI)), Latent variable (e.g., Reconnaissance Drought Index (RDI) and Standardized Precipitation Evapotranspiration Index (SPEI)), Linear Combination (e.g., Optimal Blended NLDAS Drought Index (OBNDI), Joint distribution (e.g., Multivariate standardized drought index (MSDI)), Principal component analysis (e.g., Aggregate Drought Index(ADI)) together with their advantages and limitations. To identify the overall utility of drought indices to aid the selection several criteria are reviewed by authors

which includes robustness, tractability, transparency, sophistication, extendibility, and dimensionality.

Joshi et al. (2016) studied seasonal trends as well as dominant and significant periods of variability of drought variables for 30 rainfall subdivisions in India over 141 years (1871–2012). Standardized precipitation index (SPI) was used as a meteorological drought indicator, and various drought variables (monsoon SPI, non-monsoon SPI, yearly SPI, annual drought duration, annual drought severity and annual drought peak) were analysed. Discrete wavelet transform was used in conjunction with the Mann-Kendall test to analyse trends and dominant periodicities associated with the drought variables. Furthermore, continuous wavelet transforms (CWT) based global wavelet spectrum was used to analyse significant periods of variability associated with the drought variables. The trend analysis showed that over the second half of the 20^{th} century, drought occurrences increased significantly in subdivisions of Northeast and Central India.

Mishra et al. (2019) has tried to establish the linkage between famines and droughts in India. They have taken study period for a long duration, of over a decade from 1870-2016. In India, millions of people died due to crop failure which is a consequence of famine and drought in the nineteenth century, during which irrigation facilities were sparse. In this study, the authors have reconstructed the soil moisture drought using the gridded precipitation data, station observations and have used the Variable Infiltration Capacity (VIC) model to reconstruct soil moisture. Firstly, they have identified the drought years by using (Severity area duration corves) SAD analysis. Later they have identified the famines from the year 1870 to 2016. Now the overlapping years of famines and soil moisture droughts have been found out. They have concluded that out of seven major droughts and six major famines in India, five of the famines were linked to drought and one was not. They have also concluded that the three most deadly droughts were linked with the positive phase of El Niño–Southern Oscillation.

Sharma and Goyal (2020) presented an analysis of trends in six drought variables at 566 stations across India over the period 1901–2002. Six drought variables were computed using standardized precipitation index (SPI). The Mann-Kendall (MK) trend test and Sen's slope estimator were used for trend analysis of drought variables. Discrete wavelets transform (DWT) was used to identify the dominant periodic components in trends, whereas the significance of periodic components was examined using continuous wavelet transform (CWT)

based global wavelet spectrum (GWS). The findings show an increasing trend in droughts in eastern, northeastern and extreme southern regions, and a decreasing trend in the northern and southern regions of the country. The periodic component influencing the trend was 2–4 years in south, 4–8 years in west, east and northeast, 8–64 years in central parts and 32–128 years in the north; however, most of the periodic components were not statistically significant.

Sahana et al. (2021) has studied the drought risk and vulnerability in India using different aggregation techniques. Most of the studies conducted on drought risk have been region-specific, So, employing a multivariate framework and accurate drought risk indicators with exposure, sensitivity, and adaptive capacity, a thorough, country-wide assessment was carried out in this study. In the vulnerability assessment, comprehensive aggregation techniques like the Analytical Hierarchy Process (AHP) + ENTROPY and TOPSIS methods have been used. First, the Drought hazard index has been calculated using the multi-Variate standardized index (MSDI), then the drought vulnerability index is found out using the aggregation techniques. The final drought risk assessment is computed by multiplying these two indices. From a multivariate drought hazard and TOPSIS-based vulnerability assessment, bivariate choropleth drought risk maps were created. These maps become the aid for long-term drought risk assessment and help the decision-makers of government bodies to build drought resilience.

Singh et al. (2021) proposed a new drought index—the Standardized Net-Precipitation Distribution Index (SNEPI), which incorporates the distribution characteristics of the daily net-precipitation variable. The applicability of SNEPI was critically evaluated using synthetically generated and observed precipitation series over six diverse climatic locations of India, at 1-, 3-, 6-, and 12-month time scales. The utility of SNEPI was more profound for longer time scales, understandably due to the enhanced emphasis imparted on the distribution of rainfall spells by the longer periods. Standardized Net-Precipitation Distribution Index proved to be efficient in capturing the present scenario of increasing dryness (wetness) in wet (dry) regions when compared with the traditional Standardized Precipitation Evapotranspiration Index.

2.7 CLOSURE

From the literature review, it was found that basin-scale studies are important for better understanding of the regional phenomenon governing the hydroclimatic variability leading to sustainable water resources development and management. The assessment of trend in hydroclimatic variables provides necessary indication of the spatio-temporal

changes/variability over the period. Additionally, the hydrologic and hydrodynamic modeling helps understanding the basin-scale variability in hydrological cycle and quantifying changes in various components of basin-scale hydrology. Temperature based method is adopted to estimate crop water requirement with minimal climatological data. These models also provide meaningful information related to the identification of critical regions prone to soil erosion, water stress conditions, droughts, floods etc. Further, scenario-based modeling can also be undertaken to assess the impact of specific conditions on basin hydrology. In addition to the assessment of spatio-temporal variability and hydrologic and hydrodynamic modeling, estimation of the irrigation water demands is also important for integrated watershed management practices.

3.1 GENERAL

The current chapter describes the study area including its topographical, hydrometeorological characteristics, and climatology of the basin, in brief. The chapter also enlists the data used, along with their sources, for assessment of hydroclimatic variability, development of hydrologic and hydrodynamic model, estimation of crop water requirement etc. The GCM models used for the impact assessment due to climate change are also briefly introduced.

3.2 STUDY AREA

The Tapi River is the sixth largest river of Indian Peninsula and second largest westward flowing river draining into the Arabian Sea. The Tapi River basin (TRB), situated in west central India drains 65,145 km^2 which is about 2% of the geographical area of India. The Tapi River emerges near Multai in Betul district of Madhya Pradesh at an elevation of 752 m and covers a total distance of 724 km flowing through three different states viz., Madhya Pradesh (282 km), Maharashtra (228 km), and Gujarat (214 km) before falling into Gulf of Khambhat near Surat city. The basin is elongated in shape with maximum north to south width of 210 km and maximum east to west length of 687 km. The entire basin is divided into three sub-basins viz. Upper Tapi basin (UTB), from origin of Tapi River to Hatnur dam (29,430 km^2); Middle Tapi basin (MTB), from Hatnur dam to Ukai dam (32,925 km^2) and Lower Tapi basin (LTB), from Ukai dam to the Arabian sea (2,790 km^2). Furthermore, the major tributaries of the Tapi River are Purna (length = 379 km) and Girna (length = 346 km) Rivers draining an area of 18,490 km^2 and 10,061 km^2 respectively. Almost 80% of the basin lies in Maharashtra covering the Vidarbha and Khandesh regions. The major land use land cover type in the basin assessed during year 2005-06 comprised of agricultural land (66.19%) followed by forest cover (24.41%), wasteland (5.16%), waterbodies (2.99%) and built-up land (1.26%) (CWC 2014). The major urban centres in the TRB, having population more than 2.5 lakh, as per Census of India, 2011 (http://www.censusindia.gov.in accessed on March 05, 2019), are Akola, Amaravati, Bhusaval, Burhanpur, Dhule, Jalgaon, Malegaon and Surat.

The topographical variations in the TRB, shown in Fig. 3.1 (background), are represented by extracting information from Shuttle Radar Topography Mission (SRTM) Digital Elevation Model (DEM). From Fig. 3.1, it is seen that the TRB is surrounded by hill ranges on three sides, namely, Satpura ranges in the north, Mahadeo hills in the east and Ajanta-Satmala ranges

in the south along with the Western Ghats in the south-west side. The narrow western part of the LTB is adjacent to large water mass, viz., the Arabian Sea. The physiographic cross-sections (marked in Fig. 3.1), derived from SRTM DEM, are shown in Fig. 3.2. The transverse section A-A (see Fig. 3.2), passing through UTB, clearly shows that Burhanpur and Purna sub-catchments are separated by the ridge line of Gwaligarh hills. It can be observed that Burhanpur sub-catchment lies between Satpura ranges and Gwaligarh hills, resulting into steep topography as compared to the Purna sub-catchment lying between Gwaligarh hills and Ajanta-Satmala ranges. Another transverse section B-B through MTB shows that basin is bounded between Satpura ranges and Satmala hills, The MTB has additional tributaries like Girna, Bori and Panjhara Rivers, which originates at higher elevation of Ajanta-Satmala ranges and travel northwards to meet the Tapi River. The transverse section C-C, through coastal plains of LTB, shows much flatter terrain compared to cross-sections, wherein, the local hillocks separate the area discharging into Kim and Tapi Rivers. The longitudinal section D-D, passing through UTB and MTB, portrays the rain shadow region of the Western Ghats which extends up to Jalgaon Plateau having an average elevation of 350 m. It is noted that topographic variations in the TRB play an important role in governing the climatic pattern in the basin.

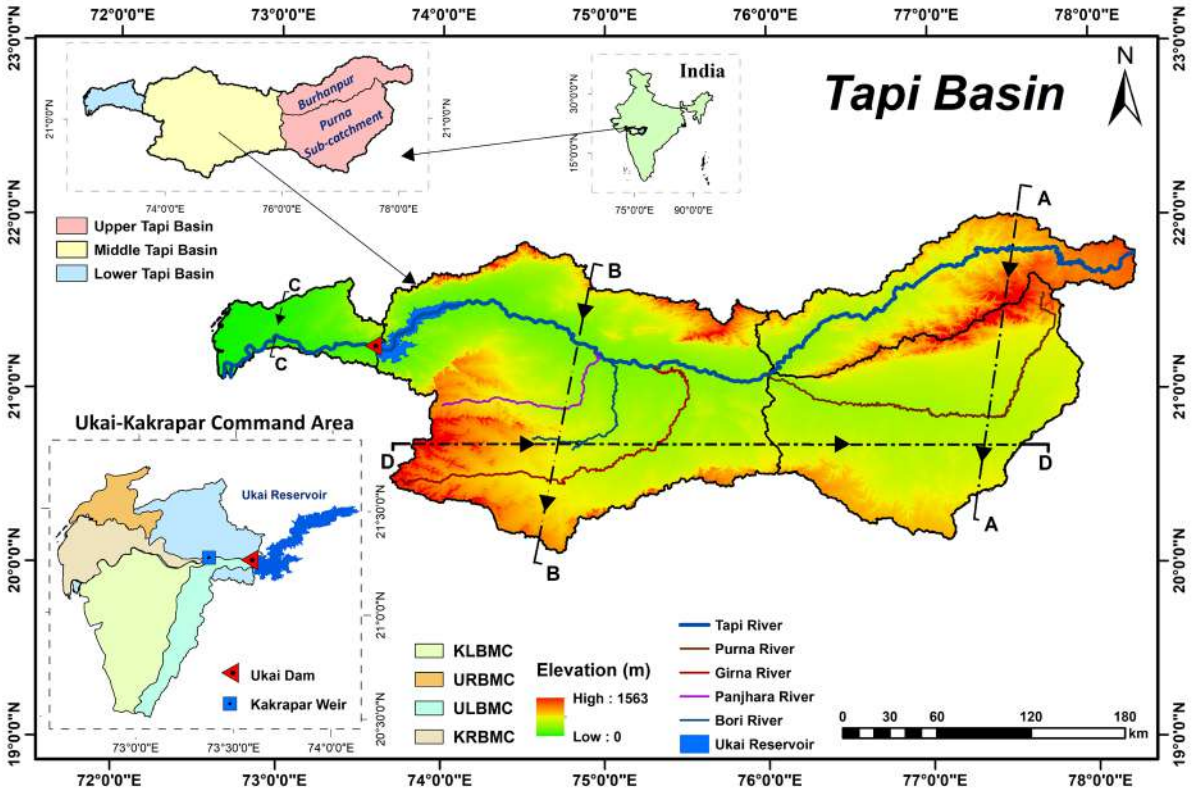

Fig. 3.1 Index map of Tapi River basin

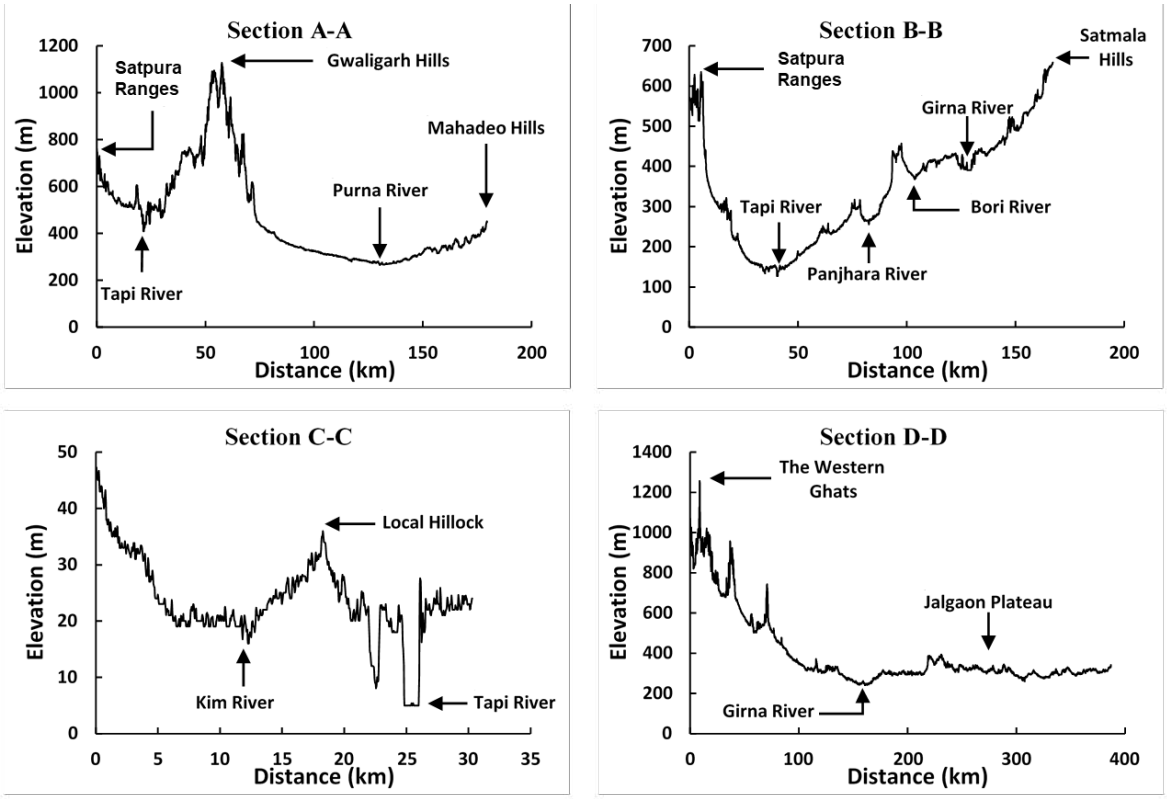

Fig. 3.2 Physiographic cross-sections across Tapi basin (marked in Fig. 3.1).

(a) Upper Tapi basin (UTB)

The Upper Tapi basin extends over two states, i.e., Maharashtra and Madhya Pradesh, wherein Maharashtra covers major portion of the Purna sub-catchment while Madhya Pradesh covers major portion of the Burhanpur sub-catchment. The Tapi River, from its origin at Multai, travels 350 km till the Hatnur dam/reservoir. The Purna River is the major tributary of the Tapi River having confluence with Tapi River around eight km upstream of the Hatnur Dam. The Burhanpur sub-catchment is surrounded by Satpura ranges in north and Gwaligarh hills in south, thus, having a narrow steep topography. The Purna sub-catchment is situated between Gwaligarh hills in north, the Ajanta and Satmala ranges in south, and the Mahadeo hills in east. The Burhanpur and Purna sub-catchments are having catchment area of 10,600 km^2 and 18,490 km^2 respectively, up to their confluence point. The major tributaries of Purna River are Pedhi, Kate Purna, Chandrabhaga, Mohali, Morna, Mun, Wan, Ghan, Biswa, and Wagar Rivers. The Burhanpur sub-catchment is covered with Deccan trap lava flows while Purna sub-catchment, from geological point of view, comprises of predominately impermeable and very poorly permeable Deccan basalts and permeable quaternary alluvial deposits. The Upper Tapi basin consists of shallow and black soil having medium to fine texture with moderately low productiveness to highly productiveness.

(b) Middle Tapi basin (MTB)

The Middle Tapi basin is has most of its drainage area in Maharashtra state with small fraction of its area fall in Madhya Pradesh and Gujarat states. The MTB having basaltic hills in peripheral part and alluvial plains in central region. There is total nine major tributaries on both banks having a length more than 50 km. The Girna river (largest), Waghur, Bori, Panjhra, Buray lies in left bank while Aner, Arunavati, and Gomai lies in the right bank of the Tapi river. Hatnur dam, a massive earthen dam in Maharashtra, is the inlet point for MTB, located around 15 km downstream of the confluence of Tapi and Purna Rivers, while Ukai dam, Gujarat's second largest earth-cum-masonry dam, serves the outlet point for MTB, located 300 km downstream of the Hatnur dam. The Hatnur reservoir is a medium sized hydraulic structure having a gross (live) storage capacity of 388.0 (255.0) MCM (million cubic meter), whereas the Ukai reservoir is a multipurpose large reservoir with a gross (live) storage capacity of 7414.29 (6730.0) MCM at FRL (Sharma et al. 2019). The Girna reservoir, one of the major reservoirs across Girna River with gross (live) storage and live storage capacity of 608.4 (523.6) MCM. In addition, there are total 225 reservoir, 6 barrage and 7 weirs constructed across various tributaries for irrigation purpose (https://indiawris.gov.in/wris). The dominant soil classes in the region varies from very gentle sloping to moderate and level surface. Soil texture range from loamy to clayey and dep black soil.

(c) Lower Tapi basin (LTB)

The entire Lower Tapi basin falls within administrative boundary of Gujarat state. The topography of the LTB consists of narrow valley along with gentle sloping ground. The LTB comprise terrain variability such as hilly terrain (highest elevation of 360 m) above mean sea level (amsl) with mostly forest area near the Ukai dam, the middle part of the basin consists of rural and agricultural field whereas the lower part of LTB (nearly 100 km downstream of Ukai dam) has coastal urban floodplain where Surat-Hazira twin city is located. The lower part of LTB is having flat topography where surface elevation ranges from -10 m to +20 m above mean sea level. The clay is dominant soil class across the LTB. The urban settlement i.e., Surat city is one of the most prominent urban centres and highly populated city located on the bank of lower Tapi River and in coastal plain of Arabian sea. Surat is an eighth largest city, a centre for diamond cutting, polishing, biggest textile hub in the country and the administrative capital of the Gujarat. The entire city divided into seven different zones viz. Southwest, South, Southeast, Central, Northwest, and East. The total area of Surat city is 462.15 km^2 with

population of 46,45,384 (https://www.suratmunicipal.gov.in as per census 2011) and average population density 10,052 persons/km^2.

(d) Ukai-Kakrapar Command Area

The Ukai-Kakrapar Irrigation Project on the Tapi River is second largest multipurpose project of Gujarat state, wherein the Kakrapar weir (latitude 21°16'9.72"N and longitude 73°21'54.66"E) lies 24 km downstream of the Ukai Dam (latitude 21°15'12.21"N and longitude 73°35'35.49"E). The Ukai reservoir serves as multipurpose reservoir, like irrigation, hydropower, domestic and industrial sectors, and hydropower. The current study considers the Ukai left bank command area (ULBCA), Ukai right bank command area (URBCA), Kakrapar left bank command area (KLBCA) and Kakrapar right bank command area (KRBCA) (see Fig. 3.1). The gross command area (GCA, in ha) of ULBCA, URBCA, KLBCA and KRBCA are 1,21,458; 84,686; 2,47,000; and 1,18,838 respectively; and culturable command area (CCA, in ha) are 66,168; 48,117; 1,45,335; and 71,937 respectively.

3.3 CLIMATOLOGY OF TAPI RIVER BASIN

The Indian Summer Monsoon Rainfall (ISMR) primarily governs the availability of fresh water across major portion of India. The average onset of the south-west monsoon begins in the basin by mid-June and withdraws by the first week of October. The average annual rainfall of TRB is 815.7 mm, seasonal distribution is 90.0%, 7.0%, 1.4% and 1.6% during monsoon (JJAS), post-monsoon (ON), winter (DJF) and pre-monsoon (MAM) seasons respectively. The rainfall received during June, July, August, and September months is 16.4%, 29.0%, 26.5% and 18.1% of total annual rainfall respectively. Apart from temporal variability, TRB exhibits large-scale spatial variability on the rainfall. From Fig. 3.3, it is seen that Songadh (in LTB) and Chikhalda (in UTB) stations receive maximum rainfall in the basin due to strong orographic effects, with the former being situated on the foothills of the Western Ghats, while the latter is situated on the Gwaligarh hill range. The Western Ghats (having elevation > 1000 m) block major portion of the south-west monsoon winds from the Arabian Sea and, thereby, forms a rain shadow region in the southwest of the basin resulting in scanty rainfall at Dhule, Malegaon, Nandgaon, Sakri and Sindkheda stations in MTB.

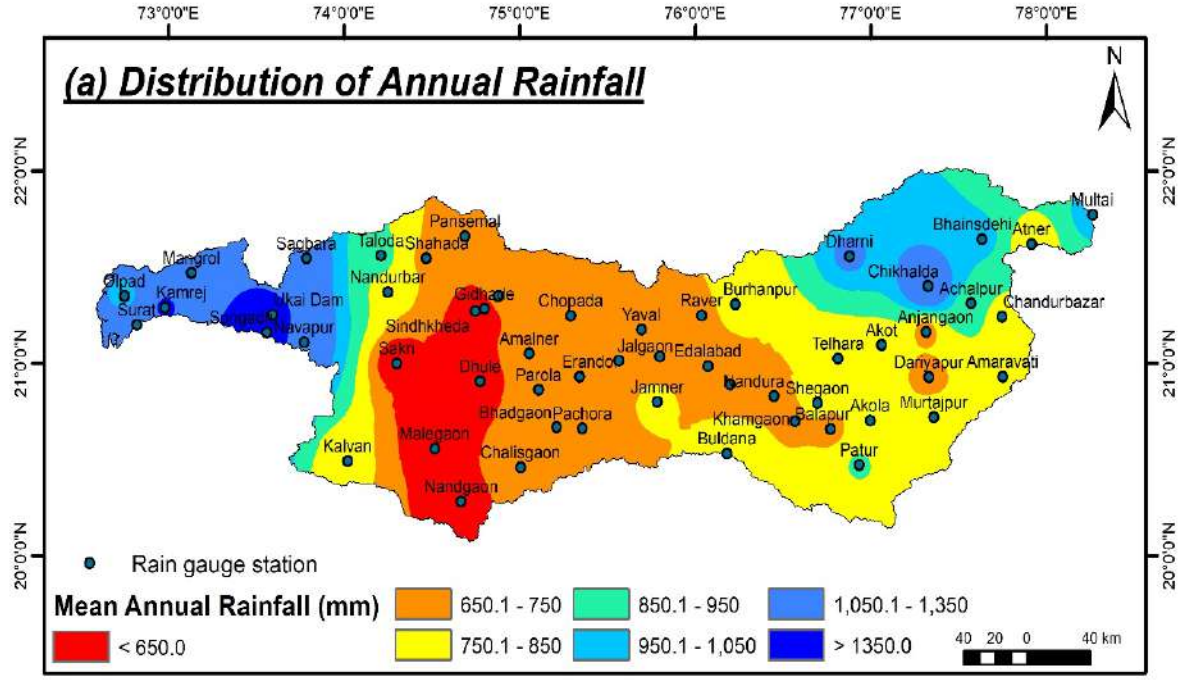

Fig. 3.3 Rainfall variability across Tapi basin (Sharma 2021)

From the global maps of the Köppen-Geiger climate classification (Rubel and Kottek 2010) at spatial resolution of 0.5° × 0.5° for the period 1976-2000, it is found that the coastal plains of LTB exhibit tropical wet savanna climate (Aw), whereas major portions of UTB and MTB experience tropical dry savanna (As) and hot semi-arid (BSh) climate respectively. The approximate areas under Aw, As and BSh climate types in TRB are estimated to be 15.2%, 47.1% and 37.7% respectively. The TRB experiences high intra-annual temperature variations, with May being the hottest month and January being the coldest month. Regionally, the LTB (27.1 °C) exhibits highest mean temperature compared to MTB (26.4 °C) and UTB (26.3 °C), while relatively lower daily/seasonal fluctuations in the temperature range were observed in LTB due to its proximity to the Arabian Sea. The semi-arid regions of MTB and Purna sub-catchment (in UTB) having Plateau type topography records intensely high temperatures (around 45 °C) during the summer months. Heat wave conditions are predominant during April and May months over Jalgaon, Amravati and Akola regions. It is observed that Jalgaon station has highest recorded temperature of 48.4 °C in the year 1988, while Betul station has lowest recorded temperature of -0.2 °C in year 1977. The physiographical and meteorological characteristics of Upper, Middle, and Lower Tapi basin are summarised in Table 3.1.

Table 3.1 Physiographical and meteorological characteristics of Upper, Middle, and Lower Tapi basin.

Characteristics	Upper Tapi basin (UTB)	Middle Tapi basin (MTB)	Lower Tapi basin (LTB)
Geographical Area	29,430 km^2	32,925 km^2	2,790 km^2
Areal extent	Origin (Multai) to Hatnur Dam	Hatnur dam to Ukai dam	Ukai Dam to the Arabian Sea
Terrain details	Hilly (Burhanpur sub-catchment) and river plains (Purna sub-catchment)	Mostly plain except south-west part near the Western Ghats	Coastal-urban plains near the Arabian Sea
Average annual rainfall	839.2 mm	742.9 mm	1,284.6 mm
Normal rainfall variation (*Cv*)	22.6%	21.6%	37.0%
Annual rainy days (averaged)	44.5	41.2	49.4
Mean Climate type [#]	Tropical dry savanna (As)	Hot semi-arid (Bsh)	Tropical wet savanna climate (Aw)
Mean Annual temperature	26.3 ºC	26.4 ºC	27.1 ºC
Mean Temperature Variation (*Cv*)	2.04 %	0.89 %	0.88 %

[#] As per Köppen–Geiger climate classification (Rubel and Kottek 2010).

The streamflows in TRB have been found to exhibit larger variability as compared to rainfall. The observed annual runoff in the main Tapi River has been found to be significantly higher than its major gauged tributaries, see Fig. 3.4. There is total fifteen stream gauging stations in the TRB with fair length of streamflow records. Out of these, eight stream gauging stations are across the main Tapi River, while remaining seven stations are on the tributaries such as Purna, Girna, Bori and Panjhara Rivers. From Fig. 3.4, it is seen that stream gauging stations in the MTB, viz., Savkheda, Gidhade and Sarangkheda stations, recorded considerable higher annual runoff (i.e., > 6,000 Mm^3), which predominantly contribute towards inflows into the Ukai reservoir (present gross storage capacity ≈ 7,414.29 Mm^3). On other hand, the annual runoff contributions from Girna, Bori and Panjhara Rivers to the Tapi River are reported to be meagre (i.e., < 500 Mm^3). It is also found that the contribution of two major tributaries, i.e., Girna and Purna Rivers, to the Tapi River is much less (i.e., around 27%), given that they drain almost 45% of the basin area. Thus, widespread variability in runoff characteristics is evidently observed in the TRB.

- **Surat city and History of Floods**

The Tapi river was frequently flooded and caused the disastrous situation generally in the lower reaches of the river including Surat city. The Surat city had experienced highest flood with magnitude of 43,891.1 m^3/s in august 1968. After the flood event, to prevent the city flood

embankment were constructed along both bank of the lower Tapi river from Nehru bridge to Amroli Bridge. The Ukai dam was constructed in 1972 with gross storage of 7414.29 Mm^3 (revised) provide partial flood control to the Surat city. Flood forecasting in Surat city is based upon the level at Nehru Bridge. The warning and danger level at Nehru Bridge are 8.5 m and 9.5 m above mean sea level respectively. The major flood events occurred in 20th and recently in 21st century after the construction of Ukai dam is given in Table 3.2. The flood of year 2006 alone costs the loss of Rs. 21,000/- crore and 300 lives (Patel and Srivastava 2013).

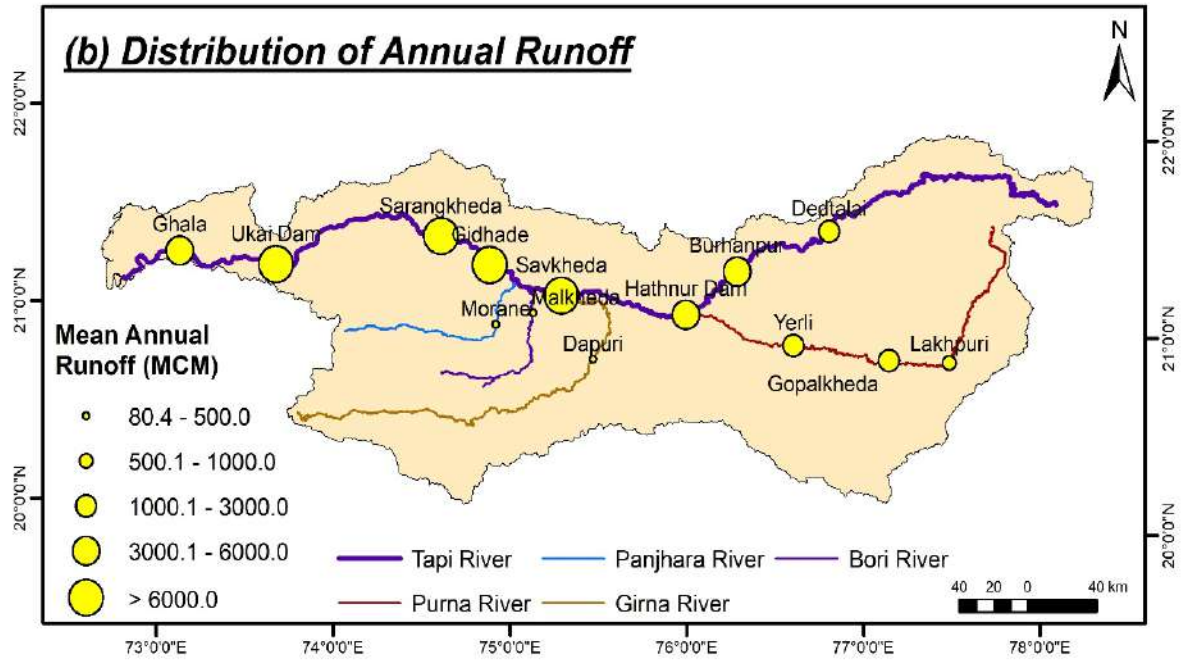

Fig. 3.4 Variation in mean annual runoff across Tapi basin (Sharma 2021)

Table 3.2 Historic floods and corresponding water level at Surat city

Sr. No	Date	Peak Inflow into Reservoir (m^3/s)	Peak Flood discharge (m^3/s)	Corresponding water level at Nehru Bridge (m)
1	31st Aug 1978	25,145	12,459	8.59
2	12th Aug 1979	24,296	9,345	8.22
3	8th Sept 1994	25,117	14,866	10.10
4	16th Sept 1998	29,817	19,057	11.40
5	7th Aug 2006	34,122	25,768	12.40
6	23rd Sept 2013	20,673	12,257	9.70

Jain et al. (2007) found out the reduction in safe carrying capacity of Tapi River at Surat city from design discharge of 24,070 m^3/s at the time of construction of Ukai dam (1972) to just 11,320 m^3/s at present. Additionally, the water level at Nehru bridge shows huge variation, i.e., 12.08 m for peak discharge of 43,891 m^3/s in 1968 whereas, 12.40 m for lower peak of 25,768

m^3/sec in 2006. The reduction in carrying capacity of river is attributed to extensive urbanization in floodplain, siltation in the riverbed due to afflux from construction of Singanpur weir in 1995 (Vora et al. 2018).

3.4 DATA USED

The data used for various aspects of the current study are summarised below in Table 3.3 with their sources.

Table 3.3 Data used in current study and their sources

Data	Frequency/ Resolution	Period of data used	Source
Spatio-temporal variability of Rainfall, Temperature and Streamflow: TRB			
Rainfall	Daily (Station)	1944 - 2013	India Meteorological Department (IMD), Pune
Temperature	Daily (0.5º×0.5º)	1951 - 2016	
Streamflow	Daily (Station)	1973 - 2013	Central Water Commission (CWC), Surat Division
Drought Analysis: TRB			
Rainfall	Monthly (0.25º×0.25º)	1951 - 2020	IMD, Pune
Temperature		1951 - 2020	
Hydrologic Modeling (SWAT): Burhanpur & Purna sub-catchments; and MTB			
SRTM DEM	30 m	2000	USGS (https://earthexplorer.usgs.gov)
LULC Map	56 m	2005-06	National Remote Sensing Centre (NRSC), Hyderabad
Soil Map	1:2,50,000	-	National Bureau of Soil Survey & Land Use Planning (NBSS&LUP), Nagpur
Rainfall	Daily (Station)	1994-2013	IMD Pune
Temperature	Daily (0.5º×0.5º)		
Streamflow	Daily (Station)		CWC, Surat Division
Inflow and Outflow@Hatnur	Daily		Tapi Irrigation Development Corporation (TIDC), Jalgaon
Inflow @Ukai	Daily		Ukai Civil Circle, Ukai, Government of Gujarat.
Hydrologic Modeling (MIKE-SHE): LTB			
DEM (Composite DEM; SoI+SMC+SRTM)	30 m	1970-1972	Survey of India (SoI) Toposheet Contours
		2007	Surat Municipal Corporation (SMC), Surat (Physically surveyed contour of lower Tapi River, Surat city and its outskirt area)
		2000	SRTM-DEM
River cross-section	-	2007	SMC, Surat
LULC	30 m	2000	Landsat-7; USGS (https://earthexplorer.usgs.gov)
Soil Map	1:2,50,000	-	NBSS&LUP, Nagpur
Rainfall	Daily (0.25º×0.25º)	1980-2004	IMD, Pune
Temperature			
Streamflow	Daily (Station)		CWC, Surat Division
			State Water Data Centre (SWDC), Gandhinagar
Inflow and outflow@ Ukai	Daily	1980-2016	Ukai Civil Circle, Ukai, Government of Gujarat.
Tidal level	Hourly	Dec. 6, 2009 – Jan. 5, 2010	Surat Irrigation Circle (SIC), Surat

Data	Frequency/ Resolution	Period of data used	Source
Ground water levels	-	1980-2018	Central Ground Water Board (CGWB), Ahmedabad Geohydrologist Ground Water Unit – 1, (SWDC)
Hydrodynamic Modeling (MIKE 21): LTB			
DEM	30 m	-	Same as DEM used for MIKE-SHE model
LULC Map	56 m	2006-07	NRSC, Hyderabad
Inflow and outflow@ Ukai	Hourly	2006	Ukai Civil Circle, Ukai, Government of Gujarat.
Water levels	Hourly	1991-2013	Nodal Officer, Flood Control Cell, SIC Surat
Tidal level	Hourly	Dec 6, 2009 – Jan 5, 2010	SIC, Surat
Distributed maximum water level (Surat city)	-	2006	SMC, Surat
Impact on Irrigation Water Demands: Ukai-Kakrapar and Girna Command Area			
Crop wise irrigation area in Ukai-Kakrapar command area	Rabi, Kharif and Hot seasons	2010-2018	SIC, Surat Ukai Civil Circle, Ukai, Government of Gujarat
Crop wise irrigation area in Girna command areas	Rabi, Kharif and Hot seasons	2019	Girna Irrigation Division (GID), Jalgaon.
Meteorological data	Daily	1951-2020	IMD, Pune
Crop Coefficient	Crop Period	-	Navsari Agricultural University, Navsari, Gujarat; Food and Agriculture Organization of the United States (FAO).

- **Statistically Downscaled Data using Kernel Regression**

The daily precipitation data of five GCM models RCP 4.5 and RCP 8.5 (see Table 3.4) statistically downscaled using the kernel regression based statistical downscaling (KRSD) method (Kannan and Ghosh 2013; Salvi et al. 2013) has been used in the current study. The downscaled data at the spatial resolution of 0.25º×0.25º has been obtained from the research project "Statistical Downscaling for Hydro-climatic projections with CMIP5 simulations to assess Impact of Climate Change" funded by the Indian National Committee on Climate Change (INCCC), Ministry of Jal Shakti, Department of Water Resources, River Development & Ganga Rejuvenation, Government of India. In addition, the bias-corrected temperature data (Tmax and Tmin) at spatial resolution of 1.0º×1.0º has also been obtained from the same project. The aforesaid data has been obtained for historical period (1951-2005) and future period (2006-2100) for two RCP scenarios, i.e., RCP 4.5 and RCP 8.5. The future period is further divided in to subperiods of 30 years, i.e., near-future (2011-2040), mid-future (2041-2070) and far-future (2071-2100).

Table 3.4 Global Climate Models used in the present study

Modeling Centre	GCM Model*	Resolution	Details
BNU	BNU ESM	2.8º×2.8º	Beijing Normal University Earth System Model, China
CCCma	CanESM2	2.8º×2.8º	Canadian Centre for Climate Modeling and Analysis-Second generation Canadian Earth System Model, Canada
CNRM-CERFACS	CNRM CM5	1.4º×1.4º	Centre National de Recherches Meteorologiques, France
MPI-M	MPI ESM LR	1.9º×1.9º	Max Planck Institute for Meteorology (Germany) Earth System Model running on low resolution grid
MPI-M	MPI ESM MR	1.9º×1.9º	MPI ESM running on mixed resolution grid

*The GCM models are denoted/cited/named as BNU, CCCma, CM5, MPI-LR and MPI-MR hence forth throughout this report.

3.5 CLOSURE

The TRB is found to exhibit heterogeneous climatic behavior as reflected in the hydroclimatic variability observed across the basin. It is also learnt that the LTB is prone to recurrent flooding, whereas MTB is prone to water scarce conditions. Also, large scale annual as well as intra-annual variability in the streamflow is observed, resulting into the major tributaries being dry for most of the time in a year. Nearly 2/3rd of the basin is used for agriculture which is primarily dependent on ISMR and ground water. Therefore, the understanding of the assessment of hydroclimatic variability under the impact of climate change are required for sustainable planning of the available water potential of the basin. Under this context, the spatio-temporal assessment of hydroclimatic variables; hydrologic and hydrodynamic modeling; and impact of climate change on water availability and crop water requirements are ascertained in the successive chapters of this report.

CHAPTER 4
METHODOLOGY AND DATA ANALYSIS

4.1 GENERAL

The current study considers various aspects of the climate change impact at basin scale. The impact of climate change on variability (spatial and temporal) of hydroclimatic variables, basin scale hydrology, availability of water, magnitude, and frequency of hydroclimatic extremes, crop water demands etc. are a few important aspects covered in the current study. The present chapter includes the methodology framework adopted for addressing the aforesaid issues. Along with this, the data processing required to achieve the deliverable of the current research project is also included in brief.

4.2 METHODOLOGY

The methodology adopted to ascertain the impact of climate change on hydroclimatic variability, availability of the water at various gauging sites, hydrological extremes, i.e., droughts and floods, and crop water demands are described with the help of the flow charts in the following sub-sections.

4.2.1 Assessment of Hydroclimatic variability

The detailed methodology adopted in the spatio-temporal variability of hydroclimatic variables, i.e., rainfall, temperature and streamflow are shown in Fig. 4.1. The stations with more than 5% of the missing observations were discarded from the current analysis. The remaining missing values were calculated using the IDW considering the nearby station within 50km radius. The data homogeneity is also ascertained using various homogeneity tests, i.e., Pettitt's test, SNHT test, Buishand range test, and von Neumann ratio test. Finally, the rainfall/temperature/streamflow indices describing magnitude, frequency and duration of the mean, extremes and their variability were derived on annual scale. To identify the variability in extreme rainfall and temperature, the Expert Team on Climate Change Detection and Indices (ETCCDI) recommended extreme climatic indices. In the current investigation of climate variability of Tapi basin, a total of 23 indicators have been used. The indicators were widely used in the past studies (Panda et al. 2016; Sharma et al. 2018; Dash and Maity 2019; Zhu and Troy 2018; and Kumar et al. 2020). A total of 12 rainfall and 11 temperature indices have been used in the current study. Apart from the two variables, the streamflow indices are also derived

in line with the aforesaid extreme indices. The definition and description of the selected indices is given in Table 4.1.

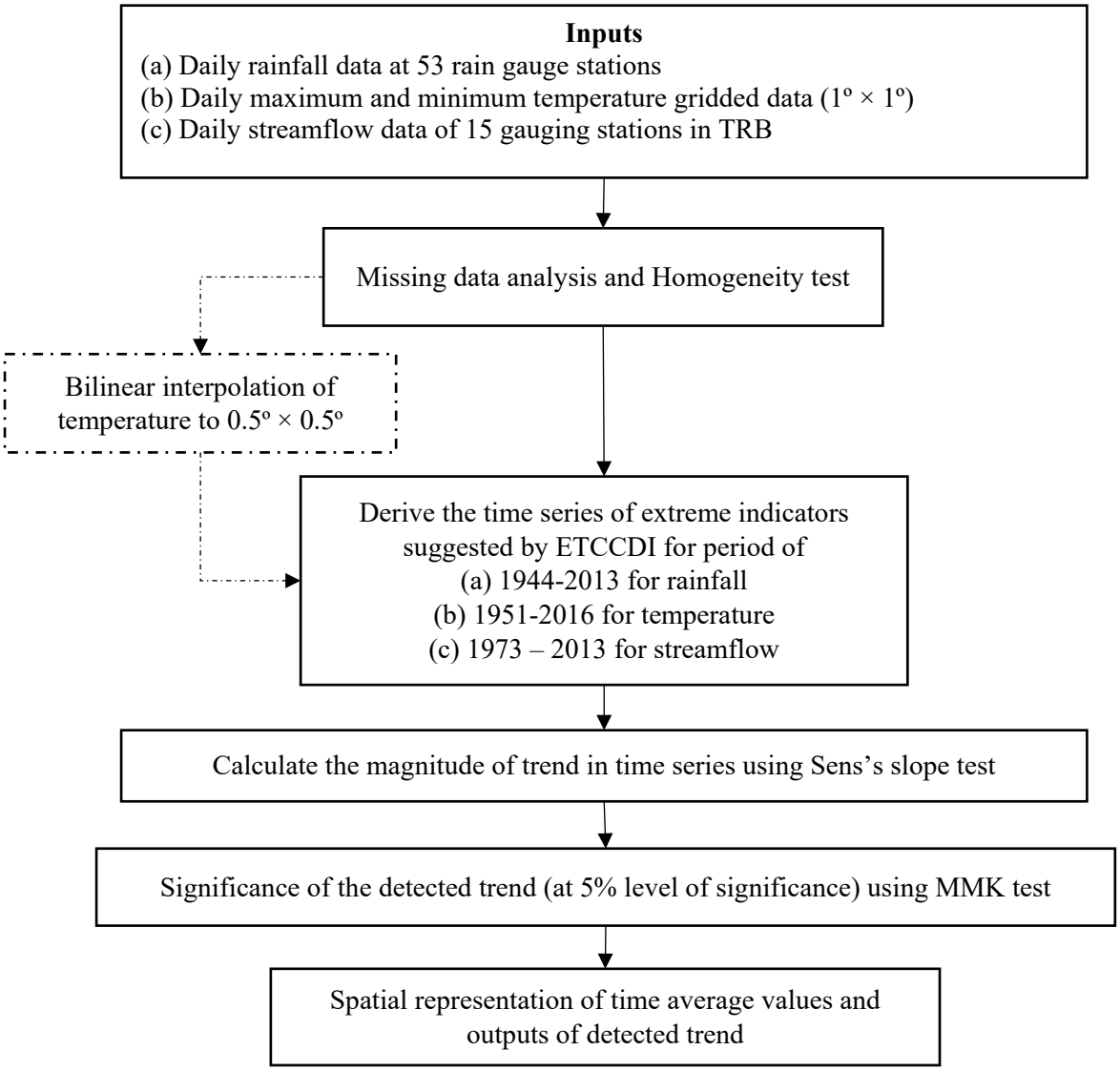

Fig. 4.1 Methodology adopted for spatio-temporal investigation of hydroclimatic variability

Table 4.1 Rainfall, temperature and streamflow indices used in present study

Indicator		Indicator name	Indicator definitions	Units
Rainfall Indices				
PRCPTOT	**Absolute based**	Annual total rainfall	Annual total rainfall from days ≥2.5 mm	mm
RD		Rainy days	Number of days when rainfall ≥2.5 mm	days
SDII		Simple daily intensity index	The rate of annual total rainfall to the number of rainy days	mm/ day
Rx1day	**Threshold based**	Maximum 1-day rainfall amount	Annual maximum 1-day rainfall	mm
Rx5day		Maximum 5-day rainfall amount	Annual maximum consecutive 5-day rainfall	mm
R99p		Extremely wet days	Annual total rainfall from days >99th percentile	mm

Indicator		Indicator name	Indicator definitions	Units
R95p		Very wet days	Annual total rainfall from days >95th percentile	mm
R5TOT		Rainfall extreme proportion	Proportion of annual rainfall from top 5 events in the year	%
Rmod	Count based	Number of moderate rainfall days	Number of days when rainfall ≥7.5 mm <64.5 mm	days
Rheavy		Number of heavy rainfall days	Number of days when rainfall ≥64.5 mm <124.5 mm	days
CDD		Consecutive dry days	Maximum Number of consecutive days when rainfall <2.5 mm	days
CWD		Consecutive wet days	Maximum Number of consecutive days when rainfall ≥ 2.5 mm	days
Temperature Indices				
TXx	Extreme Temperature based	Hottest day	Highest values of daily maximum temperature in the year	^{o}C
TXn		Coldest day	Lowest values of daily maximum temperature in the year	^{o}C
TNx		Warmest night	Highest values of daily minimum temperature in the year	^{o}C
TNn		Coldest night	Lowest values of daily minimum temperature in the year	^{o}C
DTR		Diurnal Temperature Range	Annual mean difference between daily maximum and minimum temperature	^{o}C
ITR		Intra-annual Extreme Temperature Range	Difference between the highest Tmax and lowest Tmin in the year	^{o}C
HSpC	Count and Duration Based	Hot spell count	Annual count of consecutive five days with maximum temperature more than 90th percentile	Nos.
HSpMax		Longest duration of hot spell	No of days in the longest hot spell duration with maximum temperature more than 90th percentile	days
CSpC		Cold spell count	Annual count of consecutive five days with minimum temperature less than 10th percentile	Nos.
CSpMax		Longest duration of cold spell	No of days in the longest cold spell duration with minimum temperature less than 10th percentile	days
Tx37*		-	No of days in year where in daily maximum temperature Tx > 37 ^{o}C	days
Streamflow Indices				
Qx1day	Absolute, percentile-, and frequency based	Maximum 1-day flow magnitude	Annual maximum 1-day streamflow	m^3/s
Qx5day		Maximum 5-day flow magnitude	Annual maximum consecutive 5-day streamflow	m^3/s
Q99p		Extremely high flow days	Annual total streamflow from days >99th percentile	m^3/s
Q95p		High flow days	Annual total streamflow from days >95th percentile	m^3/s
LFD		Low flow days	Maximum number of consecutive days when streamflow <10th percentile	days

* As per Disaster Management Report daily maximum temperature > 37 ^{o}C is uncomfortable to the human

4.2.2 Hydrologic Modeling using SWAT

The hydrologic model for Purna sub-catchment, Burhanpur sub-catchment of UTB and MTB are developed using the SWAT model. These catchments being climatically as well as

topographically heterogenous, the models are developed separately for each of sub-catchment. The basic methodology used for model development is shown below in Fig. 4.2. The models developed for baseline scenarios, including calibration and validation, were used for simulating the response of sub-catchments for the future scenarios. The Purna river being the first major tributary of the Tapi River is modelled first. The outputs of Purna sub-catchment were given as inputs to Upper Tapi river for inflow prediction into the Hatnur reservoir. The Hatnur reservoir was operated using SWAT with the existing rule curve conditions and the simulated outputs were used as input for hydrologic model of MTB, to predict the inflow into the Ukai reservoir. The model so developed was used to simulate the response of catchment for future climate data and the water availability was quantified in terms of flow duration curves as well as long-term mean during near-, mid-, and far-future scenarios.

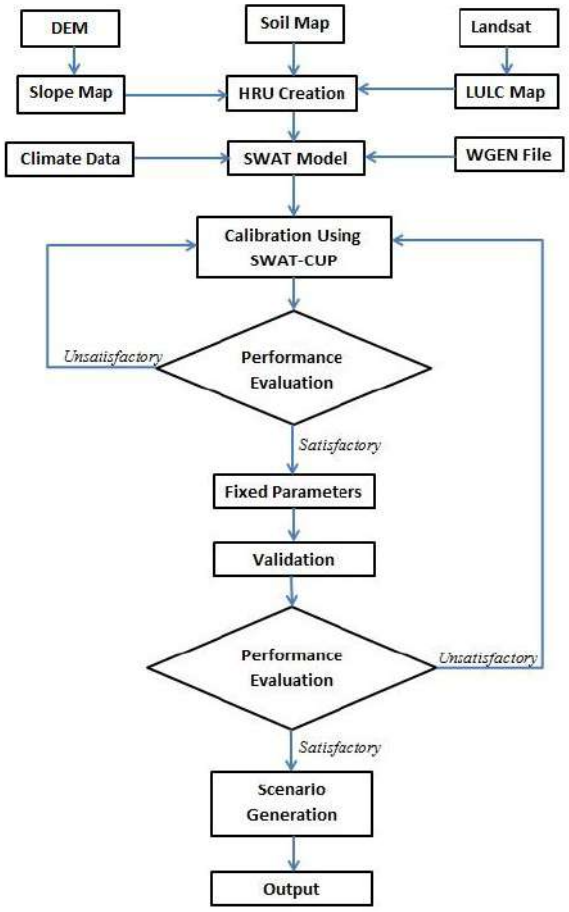

Fig. 4.2 Methodology adopted for hydrologic modeling using SWAT

4.2.3 Distributed Physics Based Hydrological Model (MIKE SHE/ MIKE 11) for LTB

The methodology in the development of physics based hydrological model for LTB (See Fig. 4.3) is broadly divided into (i) development of MIKE SHE and MIKE 11 model with input,

boundary conditions for different hydrological processes and their integration, (ii) calibration and validation of developed model including its performance evaluation, (iii) estimation of total water balance within LTB using the calibrated model.

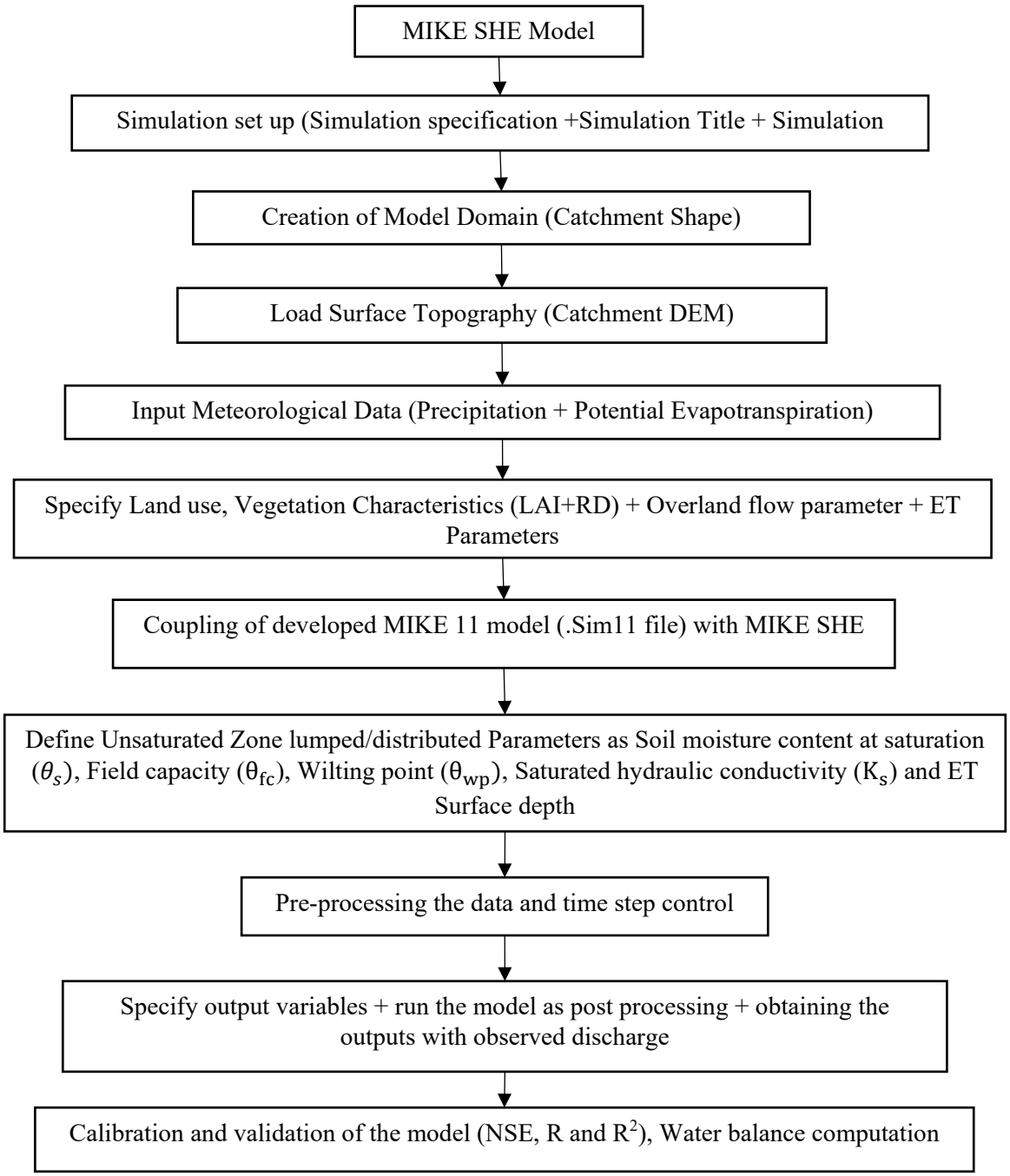

Fig. 4.3 Methodology adopted for development of distributed physics based hydrological model

4.2.4 Drought Analysis

The methodology used for calculation of the drought indices, i.e., standardized precipitation index (SPI), standardized precipitation evapotranspiration index (SPEI), and multivariate

standardized drought index (MSDI) and temporal assessment of drought indices is discussed below in Fig. 4.4. The drought indices for baseline period, i.e., 1951-2005 have been calculated using IMD datasets, i.e., monthly rainfall and PET. The similar assessment for future periods is applied for temporal assessment of drought parameters like annual drought duration (ADD), annual drought peak (ADP), and annual drought severity (ADS).

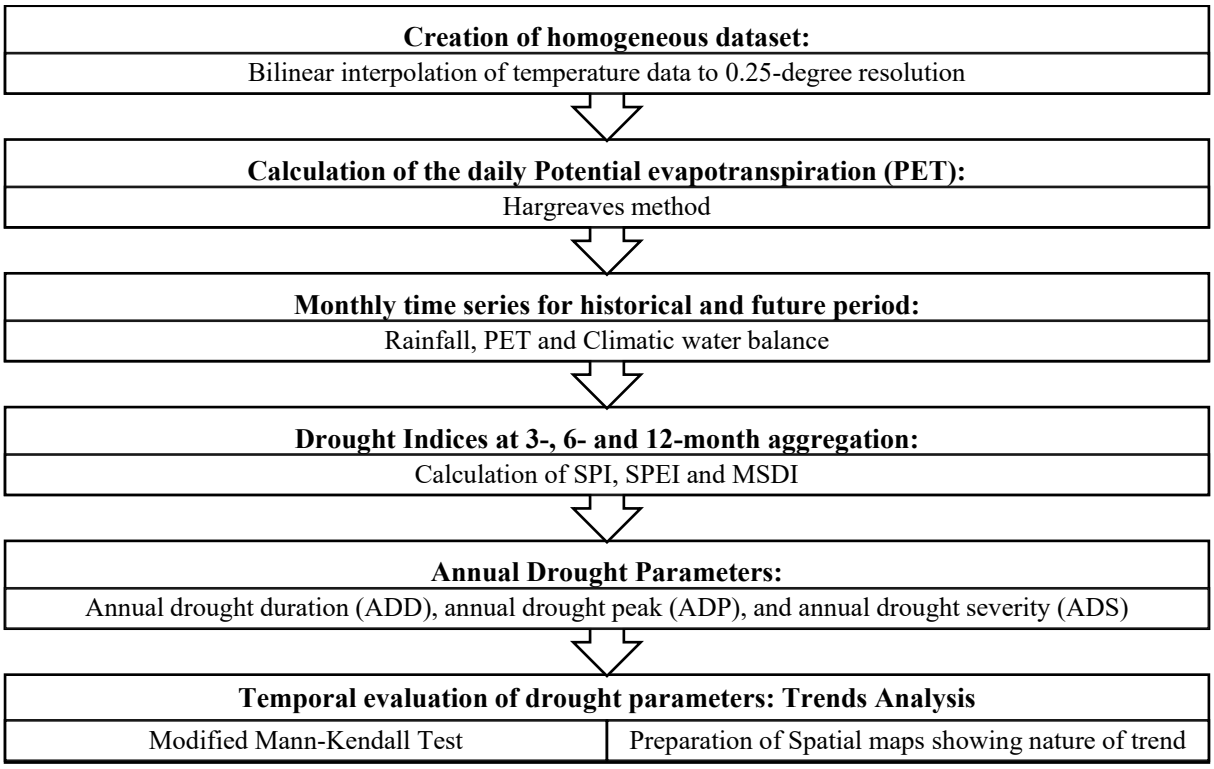

Fig. 4.4 Methodology adopted for drought analysis

4.2.5 Flood Inundation and Risk Assessment using 2D Hydrodynamic Model for LTB

The methodology of flood inundation and risk assessment for LTB (See Fig. 4.5) consist of (i) development of 2D HD model for LTB with distributed flood plain roughness and its performance evaluation (ii) flood frequency analysis for the inflow into Ukai reservoir to estimate the flood of different magnitude (iii) development of flood hazard maps for different return period flood using the results of 2D HD model, (iv) computation of socio-economic vulnerability of population in Surat city using census based data, (v) development of flood risk maps for densely populated Surat city with integration of flood hazard and Socio-economic vulnerability.

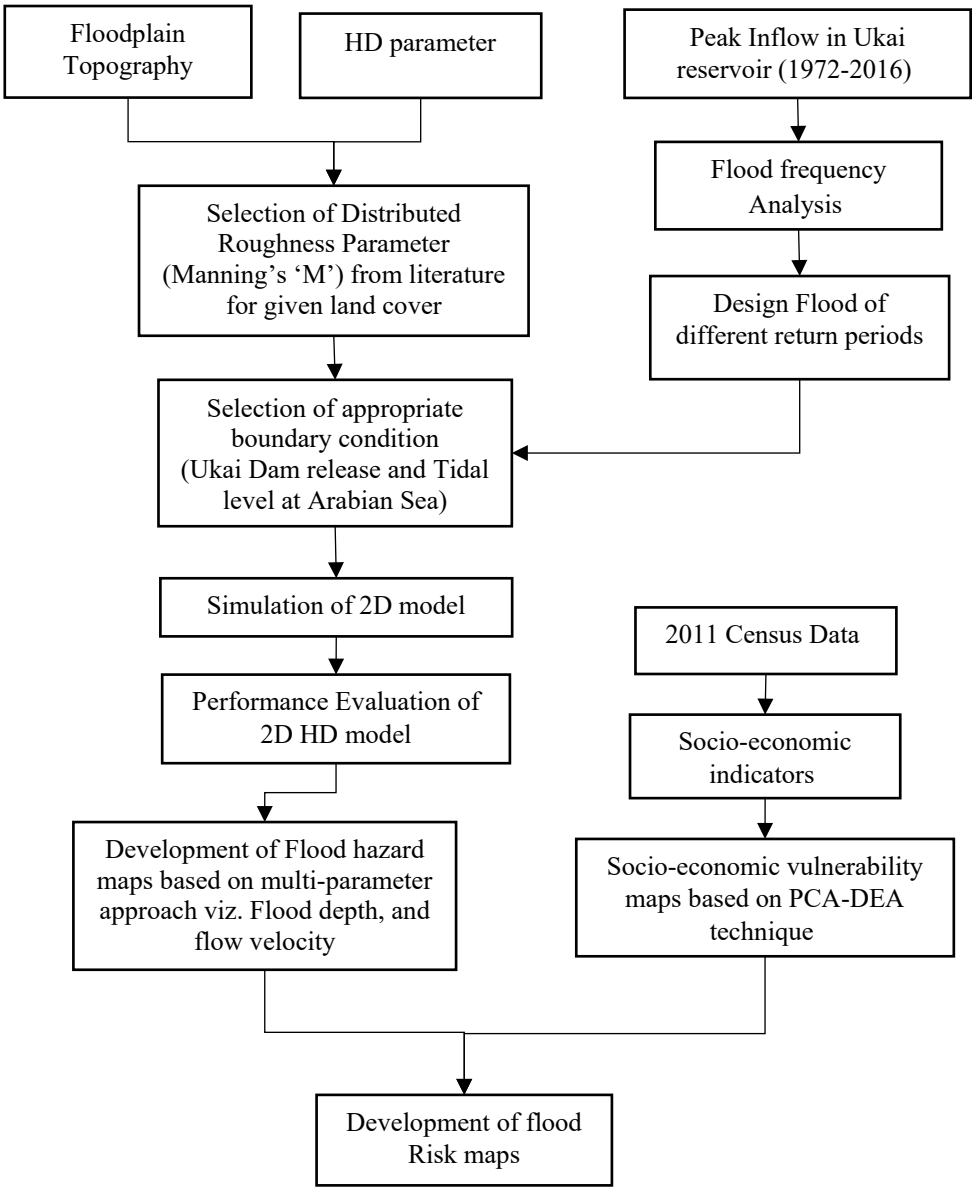

Fig. 4.5 Methodology adopted in the flood risk assessment of Surat city using 2D HD model

- **Flood Frequency Analysis**

The regional flood frequency analysis is used to predict the design flood of different return period into Ukai reservoir. These design floods are useful in detailed investigation of flood prone area of respective region. The maximum flood (inflow) into Ukai reservoir from 1973-2016 (44 years) is fitted with 2-parameter log-normal (LN), Gumbel distribution and 3-parameter generalize extreme value (GEV), generalize Pareto (GPA), log-normal III (LN-III) and log-Pearson type-III distribution. The fitted distribution is validated with goodness-of-fit (GOF) tests i.e., Kolmogorov-Smirnov, Anderson-Darling and Chi-square test using EasyFit 5.6 software. It resulted into LN-III is the best fit distribution for the inflow into Ukai reservoir

and used to compute peak flood magnitude for different return periods with flood frequency curve as shown in Fig. 4.6.

The observed flood hydrograph of year 2006 (See Fig. 4.7 (a)) divided by maximum observed peak discharge (34110.0 m^3/s) to obtain the non-dimensional flood hydrograph (See Fig. 4.7 (b)). The design flood hydrographs of different return periods shown in Fig. 4.7 (c), are obtained by multiplying the ordinates of non-dimensional hydrograph with design discharge magnitude obtained from flood frequency analysis. The similar methodology was adopted by Farooq et al. (2019) and Tansar et al. (2020).

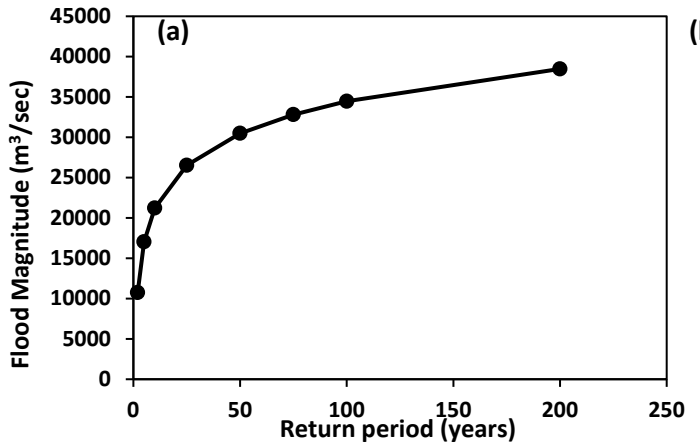

(b)

Return Period (-Year)	Ukai reservoir inflow (m^3/s)
2	10736.4
5	17030.2
10	21216.8
25	26521.1
50	30484.3
75	32806.0
100	34459.4
200	38475.3

Fig. 4.6 (a) Flood frequency curve based on log-normal III distribution and **(b)** flood magnitude of different return period into Ukai reservoir

- **Flood Hazard Classification**

The flood hazard act as an indicator for the likely threat due to flooding. Flood hazard represents the probability of occurrence of certain magnitude flood for specific location (Domeneghetti et al. 2013). The results of well calibrated hydrodynamic flood model (flood depth, flow velocity) can be converted into flood hazard maps for the flood of various exceedance probabilities. The past investigators developed the flood hazard maps using flood depth (Russo et al. 2013) as the damage increases with increasing the flood depth. The depth alone fails to incorporate the important aspect of physical damage. The low depth with high velocity flow significantly affects the stability of standing humans as well as foundation of the structures. To account the importance of flow velocity, the momentum of flood water i.e., product of depth and velocity (Mani et al. 2014 and Mohanty et al. 2020), is considered in the

present investigation of flood hazard computation. The flood hazard classification based on product of depth and velocity given in Table 4.2.

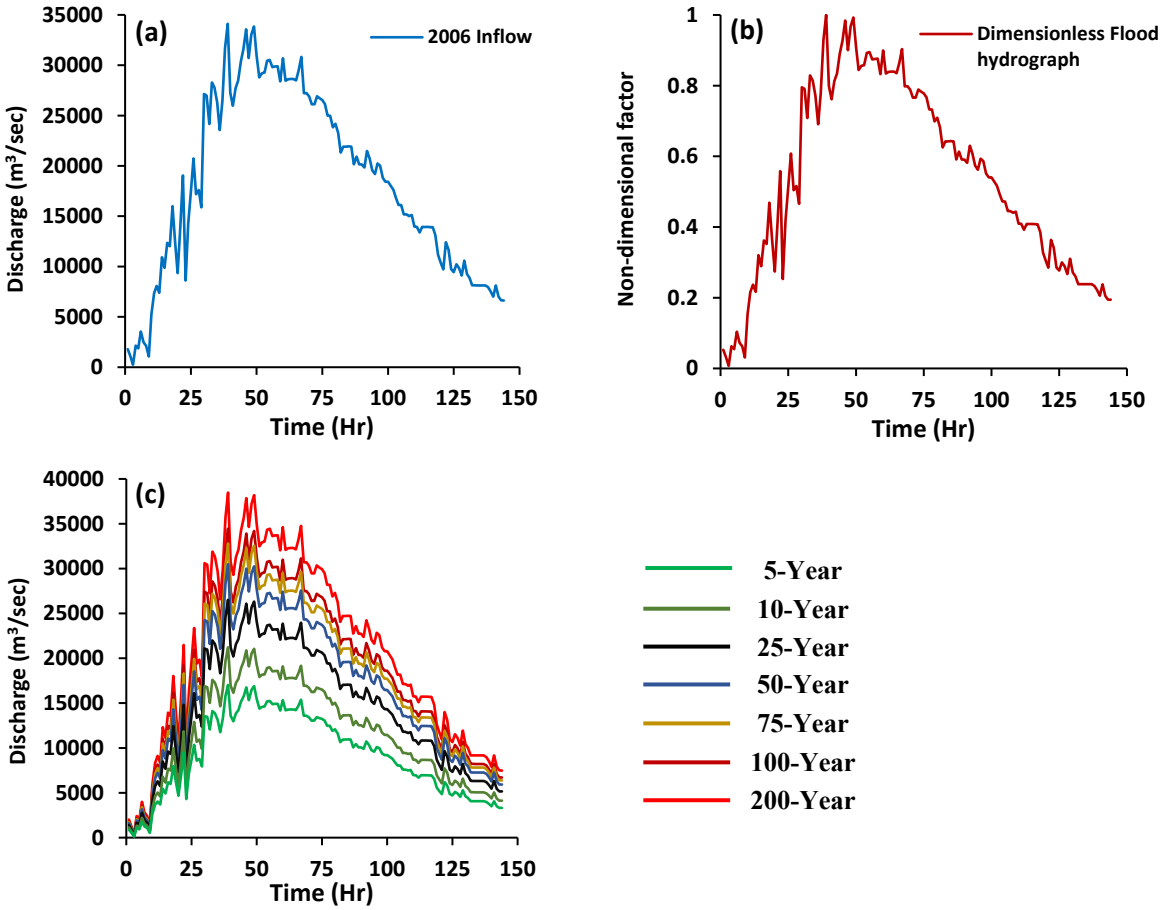

Fig. 4.7 (a) Maximum observed inflow flood of year 2006, (b) dimensionless flood hydrograph, (c) design flood hydrograph of different return period.

Table 4.2 Flood Hazard classifications for individual flooding parameters (Mani et al. 2014)

Flood water depth (m)	Depth x Flow velocity (m^2/s)	Hazard classification
0.0-0.2	0.0-0.3	Very Low
0.2-0.6	0.3-0.7	Low
0.6-1.5	0.7-1.2	Medium
1.5-3.5	1.2-1.6	High
>3.5	>1.6	Very High

- **Socio-Economic Vulnerability Assessment of Surat City**

The area under very high flood hazard category is not necessary under any risk until the area is vulnerable to damage. Vulnerability of an area, community can be defined as the measure of susceptibility of certain region against the hazard and its lack of ability to adapt or react the situation (Zachos et al. 2016; Eini et al. 2020). The socio-economic vulnerability related to the

capability of community or population of a region along with economic aspects. The socio-economic vulnerability of Surat city is evaluated using ward level demographic and economic data based on Census of India, 2011 report. Total 20 feasible indicators based on 2011 census data representing the social and economic status (Sherly et al. 2015; Vittal et al. 2020) were identified for the Surat city. The indicators were further categorized into two types as positive (increase the vulnerability) and negative (decreases the vulnerability) indicators. In the current study, the analysis is performed for each ward, which is considered as the Decision making unit (DMU). The list of selected indicators along with corresponding justification is given in Table 4.3 The standardization of indicator with different units (Karmakar et al. 2010) is performed as shown in Eq. (4.1).

$$A_i^{std} = \frac{A^{max} - A_i}{A^{max} - A^{min}} \text{ for positive indicators} \quad (4.1)$$

$$A_i^{std} = \frac{A_i - A^{min}}{A^{max} - A^{min}} \text{ for negative indicators}$$

Here, A_i^{std} = standardize vulnerability indicator for i^{th} ward

A_i = vulnerability indicator for i^{th} ward

A^{max} = Maximum value of vulnerability indicator amongst all the ward

A^{min} = Minimum value of vulnerability indicator amongst all the ward

There are different approaches for computation of vulnerability including simple averaging to various complex methods. The Data Envelopment Analysis (DEA) method (Sherly et al. 2015; Mohanty et al. 2020; Vittal et al. 2020) is a non-parametric aggregation technique widely accepted for evaluating the relative efficiency amongst DMUs. It does not require the weight assignment, hence reduce the subjectivity. Therefore, in the present study the popular BCC (Banker-Charnes-Cooper) model of DEA has been used to aggregate the standardized indicators. For the detailed stepwise explanation of DEA, readers can refer Sahana et al. (2021). In case of implementing DEA model efficiently, the indicators should not have high co-relation. To decorrelate the indicators, the Principal Component Analysis (PCA) is performed. The PCA is a statistical tool used to decorrelate and dimensional reduction of the standardize dataset. The PCA converts the correlated indicators into uncorrelated set of components, called Principal Components (PCs). The number of PCs explaining more than (>) 75 % of variance are used as input to DEA. In the current investigation, 2 PCs are given as input to DEA. DEA computes the efficiency of DMUs by assigning the rank, lower is the efficiency higher would be the vulnerability.

Table 4.3 List of socio-economic indicators for each ward of Surat city

Indicators	Influence on the socio-economic vulnerability	Justification
No of households	Positive	More no of household having more habitats and economic dependence hence increases the vulnerability during flood
Total Population	Positive	Larger population leads to increase exposure to flood hazard
Total Female population	Positive	Majority of the female population devoted to household activities and less exposure to educational and social activities
Population in the age group < 6 year	Positive	Required special attention during evacuation and depends on the adults for their care and needs during disaster
Population SC+ST	Positive	It is the weaker economic section of the society categorized under backward community.
Population SC+ST Female	Positive	Backward community and women tend to have more responsivity in taking care of the family.
Population Illiterate	Positive	Tend to have less employable skill and less access to the information regarding the hazard or risk during flood
Population illiterate Female	Positive	They find more difficult to follow the evacuation warning or guidelines during taking care of their family during disaster
Slum households	Positive	House conditions are depleted (kaccha house), leaving in unsensitized area and more susceptible against the flood
Slum Populations	Positive	Already susceptible category will lead to more exposure of the people
Marginal Workers Population	Positive	They are having temporary jobs, mostly landless labours (low financial stability)
Non-workers population	Positive	These population will depend on the other adult family member and more susceptible against copping the disaster effect
Location of drinking water source (Away) (%)	Positive	The away source of drinking water has huge impact during the flood or other disaster
Number of households without latrine and drainage facility (%)	Positive	No latrine and drainage facility increase the possibility of spread of diseases during the flood
Total Workers Population	Negative	Higher working population will have higher resilience against the flood
Total Workers Population Female	Negative	The resiliency of the family increases with the more working female population
Population literate	Negative	Higher literacy tends to enhance the knowledge of the society pertaining to cop up with the flood
Population literate Female	Negative	Increases the resiliency of the family due to access to the knowledge and warnings during to flood
Household with good house condition (%)	Negative	The impact of the flood will be less on good house condition
Drinking water from treated source (%)	Negative	Availability of drinking water from treated source will help families to cope with (diseases) during flood.

- **Computation of Bivariate Flood Risk**

A new bivariate method suggested by Mohanty et al. (2020), has been adopted for quantifying the flood risk of the Surat city. In case of new bivariate method, the risk is identified by the distinct contribution of flood hazard and socio-economic vulnerability. It has also been used to calculate the hydroclimatic risk over India by Vittal et al. (2020). The bivariate risk from flood hazard and socio-economic vulnerability is calculated as shown in Eq. (4.2).

$$Risk: Hazard * Vulnerability = M^{a \times b} \quad (4.2)$$

where, a *and* b are the cardinality of *Hazard* and *Vulnerability and* * is cartesian product of *Hazard* and *Vulnerability*.

The graphical representation of $M^{a \times b}$is demonstrated via 5 × 5 bivariate choropleths shown in Fig. 4.8. The upper triangular blocks with blue colour and lower triangular block with red colour shows dominant contribution of vulnerability and hazard respectively in the computation of risk. Whereas the diagonal blocks show the equal contribution.

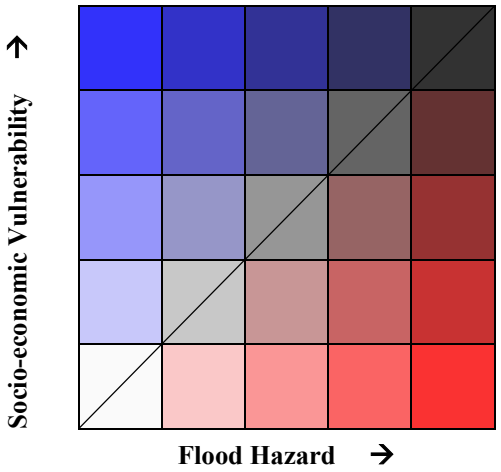

Fig. 4.8 A 5 × 5 bivariate choropleths representation used in the current study

4.2.6 Irrigation water demand

The methodology adopted for prediction of irrigation demand in the command area is shown in the Fig. 4.9. The input data includes the climatic parameters like maximum, minimum temperature and rainfall which were obtained from the statistically downscaled data of Ukai Kakrapar command area. The extra-terrestrial radiations were estimated as per the FAO approach. The cropping patterns for calculation of irrigation demand for base line and future were taken as per Table **A1 (in Annexure)**. The reference evapotranspiration was calculated

using (Samani 2000), effective precipitation P_{eff} was calculated using Soil Conservation Service (SCS) method. The output obtained was estimated as gross irrigation water demand (GIWD) as shown in Fig. 4.9. For detailed methodology for estimation of GIR please refer Subsection 2.4.

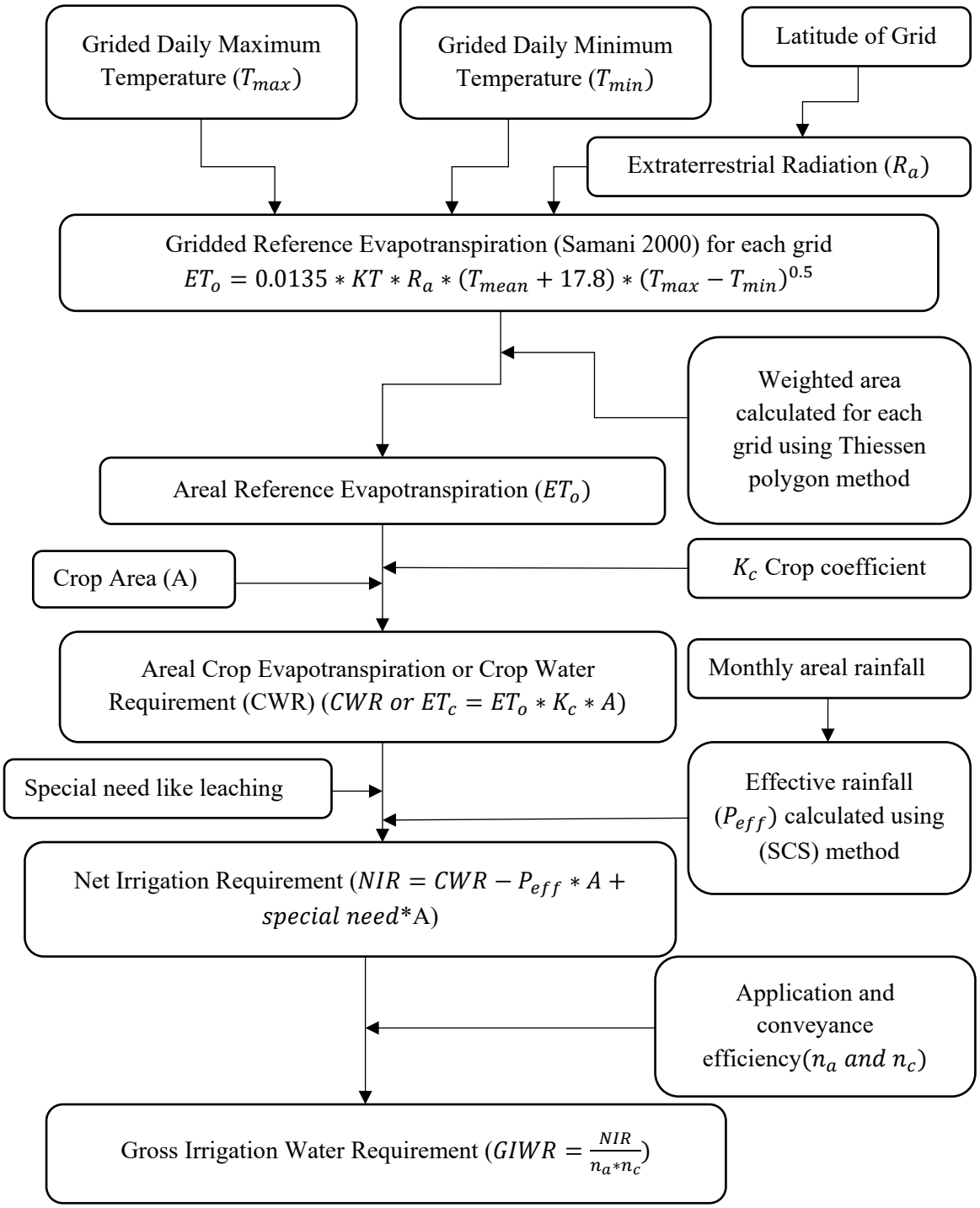

Fig. 4.9 Methodology adopted for estimation of irrigation water demand

4.3 ANALYSIS OF KRSD DOWNSCALED PRECIPITATION

The coarser scale GCM data for the five GCM models, statistically downscaled using Kernel regression, is used for its performance assessment with reference to the Indian Summer Monsoon Rainfall (ISMR) over the TRB for baseline period (1951-2005). The characteristics of ISMR, i.e., magnitude, duration, frequency, and extremes, have been used to quantify the performance of KRSD rainfall data w.r.t. IMD gridded rainfall data. The six indices representing different characteristics of ISMR, used in the current study are PRCPTOT, RD, Rx1Day, Rx5Day, R95p and CWD. The percentage deviations index, obtained from GCM data, has been estimated as $\frac{I_{IMD}-I_{GCM}}{I_{IMD}} * 100$ where I_{IMD} and I_{GCM} represent the index value calculated using IMD data and KRSD rainfall data respectively. Since the water availability in TRB is monsoon driven, the percentage deviations in the aforesaid rainfall characteristics have been estimated for June, July, August, and September months including annual estimates.

The normal PRCPTOT of TRB ranges from 519 – 1460 mm with large scale spatial variability. The historical simulations of rainfall obtained from five GCM models, downscaled to 0.25º spatial resolution are analyzed and their percentage deviations are shown in Fig. 4.10. From Fig. 4.10, it is apparent that the PRCPTOT for June month is underestimated by all the GCM models. The average (and variability range) error (%) over TRB for June month is 18.8 (40.2 - -19.2) for BNU, 47.1 (64.7 – 17.7) for CCCma, 55.7 (78.9 – 24) for CM5, 18.7 (45.5 - -12.9) for MPI-LR and 33.3 (53.6 – 4.7) for MPI-MR GCM models. The respective error (%) estimates for July, August and September month for aforesaid models are 19.6 (41.5 - -9.7), 41.6 (73 – 23.4), 33.0 (54.5 - -2.6), 19.4 (45.3 - -0.1) and 19.8 (41.9 - -6.8); 21.0 (51.3 - -17.8), 14.6 (35.7 - -18.4), 28 (61.4 - -44.9), 24.7 (43.0 – 10.5) and 20.6 (37.8 - -25.0); and 31.2 (61.9 - -6.0), -4.8 (49.3 - -64.2), -5.5 (35.7 - -65.2), 17.6 (57.6 - -9.3) and 9.1 (52.3 - -42.7) respectively. However, on annual scale the percentage error (%) estimates for aforesaid GCM models are 23.1 (44.3 – 0.9); 23.1 (50.8 - -33.1), 28.4 (50.5 - -12.9), 21.7 (37.6 – 7.8) and 22.7 (38.5 – 3.5) respectively. It can also be seen that the GCM precipitation estimates are higher in LTB particularly during August and September months. From the error estimates during monsoon months and annual time scale, it can be stated that the monsoonal rainfall has been underestimated while the non-monsoonal rainfall has been overestimated (see **Fig. A1a-b, in Annexure**). In other words, the monsoon/seasonal cycles of ISMR over TRB has not been simulated well. Overall, based on the error estimates the MPI-LR model can be considered better that the remaining GCM models.

The number of days having precipitation more than 2.5 mm, are defined as a rainy day (RD), can be considered important from the hydrological perspective in conjunction to the prevailing wet soil conditions in the area. The number of RDs obtained from KRSD rainfall data and their relative deviations w.r.t. IMD data are shown in Fig. 4.11. The mean (variability range) RDs for TRB ranges from 36 to 74.5 days (8.0 – 14.6 days) with maximum RDs in headwater regions of TRB. The error estimates for GCM RDs with reference to IMD (see Fig. 4.11) show that all the GCMs have overestimated the RD for the historical period, except a few instances in the leeward side of the Western Ghats in MTB, where underestimation is observed during June and July months. The mean percentage deviations (%) in RD during the monsoon months (JJAS) for BNU, CCCma, CM5, MPI-LR and MPI-MR models are -57.4, -33.0, -36.5 and -62.5; -8.8, -3.5, -46.3 and -130.0; 0.4, -12.1, -20.2 and -99.6; -46.1, -25.1, -21.8 and -82.3; and -20.0, -25.1, -29.8 and -99.8 respectively. The mean (and variability range) percentage deviation at annual scale for aforesaid GCM models are -41.5 (-14.7 - -76.0), -42.2 (-11.3 - -85.5), -28.5 (4.1 - -70.3), -36.8 (-15.9 - -65.9) and -36.9 (-17.1 - -67.1) respectively. The RD in September month is poorly simulated by all the GCM models with many folds overestimation. The CM5 model seems to simulate RDs fairly with the least mean error, probably due to simultaneous over/underestimation at various grids. The overestimation of the RDs and underestimated PRCPTOT, in general, reduces the expected simple daily intensity of the rainfall.

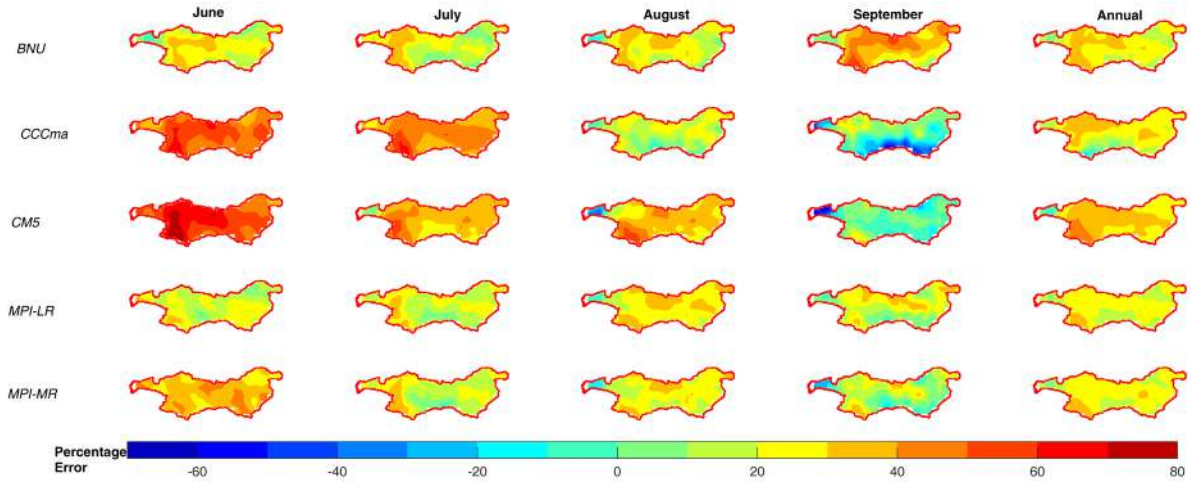

Fig. 4.10 Percentage error in PRCPTOT derived from KRSD-Historical period rainfall

The one-day and five-day maximum rainfall (Rx1Day and Rx5Day) are significantly important for pluvial flooding and erosion point of view. The mean Rx1Day and Rx5Day over TRB range

from 57.0 to 159.3 mm and 113.0 to 348.8 mm, respectively. The estimated errors in Rx1Day show that the GCM simulated one-day maximum rainfall during monsoon months (JJAS) is underestimated by 50% (on average). The percentage deviation (%) range during JJAS for BNU, CCCma, CM5, MPI-LR and MPI-MR models is 45.5 – 57.2, 48.1 – 58.6, 39.9 – 64.1, 41.6 – 51.6 and 40.5 – 51.8 respectively, while their respective mean (and variability range) percentage deviations at annual scale are 52.7 (64.1 – 29.2), 50.0 (64.3 - -23.8), 46.4 (62.4 – 16.4), 47.8 (62.4 – 25.5) and 48.6 (62.8 – 21.2) (see Fig. 4.12). Similarly, the corresponding results for Rx5D during JJAS months for aforesaid GCM models are 35.0 – 46.3, 34.6 – 51.8, 27.1 – 57.4, 31.2 – 39.9 and 30.8 – 39.6 respectively with their annual estimates of mean percentage deviation (variability range) by 44.1 (56.4 – 23.3), 41.4 (54.5 - -73.6), 41.5 (55.9 – 7.1), 41.6 (53.7 – 27.2) and 41.8 (54.3 – 27.6) respectively (see Fig. 4.13). The MPI-LR can be considered to performs better than remaining models for June, July, and August months while CNRM CMS has considerably performed better for September month with minor overestimation of Rx1Day and Rx5Day for the LTB region. The annual estimates show that MPI-LR and CM5 have shown relatively better estimation of Rx5Day and Rx1Day across the Tapi basin for the historic period. The underestimation of such extreme events by GCM models may lead to a false representation of reduced chances of pluvial flooding, erosion, and other damages in the study region.

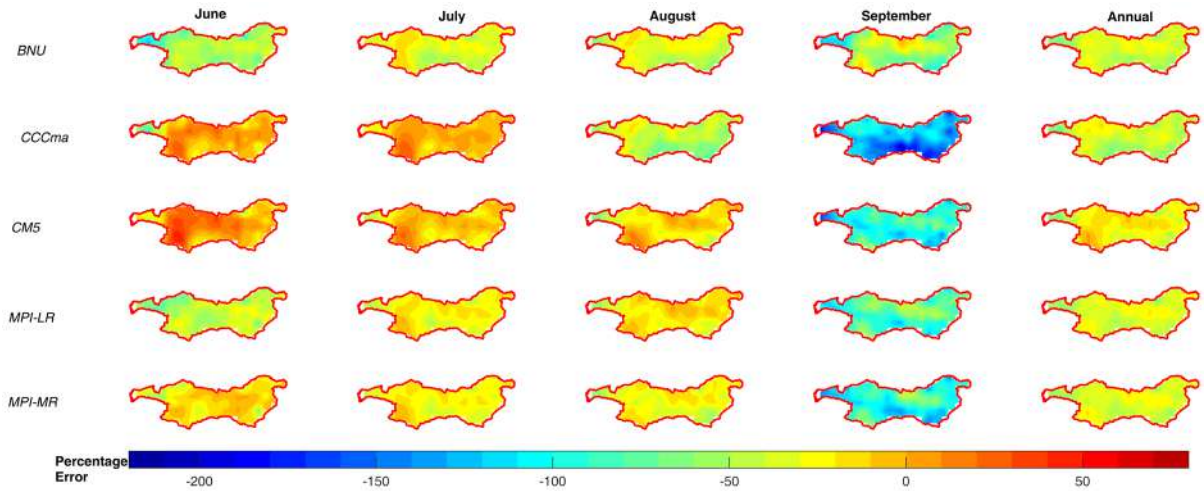

Fig. 4.11 Percentage error in RD derived from KRSD-Historical period rainfall

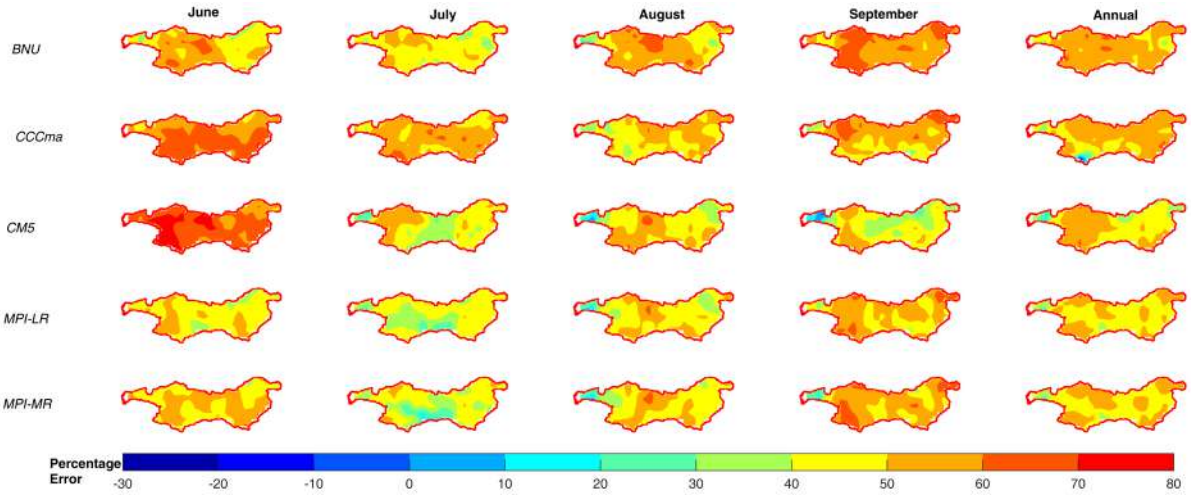

Fig. 4.12 Percentage error in Rx1Day derived from KRSD-Historical period rainfall

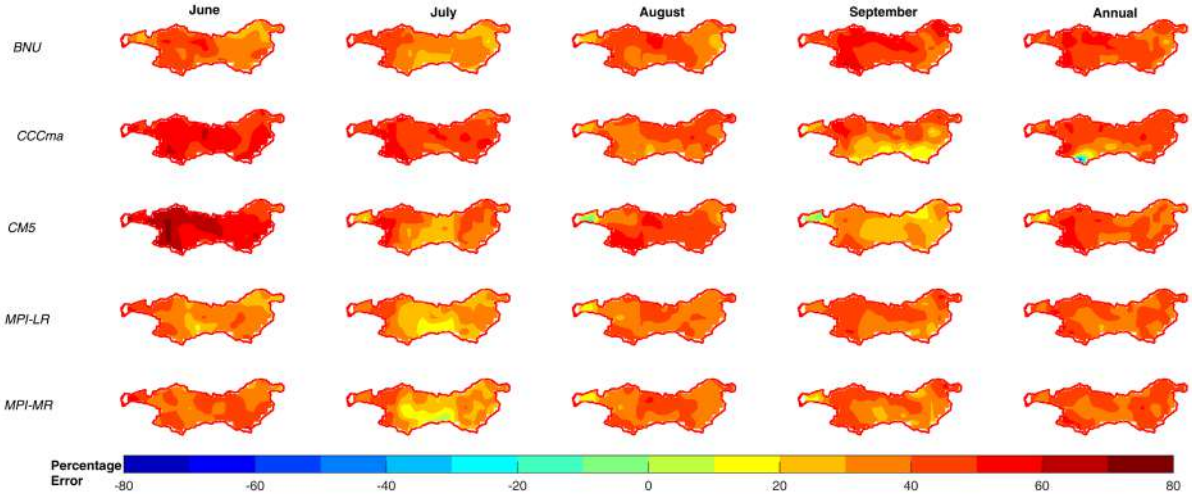

Fig. 4.13 Percentage error in Rx5Day derived from KRSD-Historical period rainfall

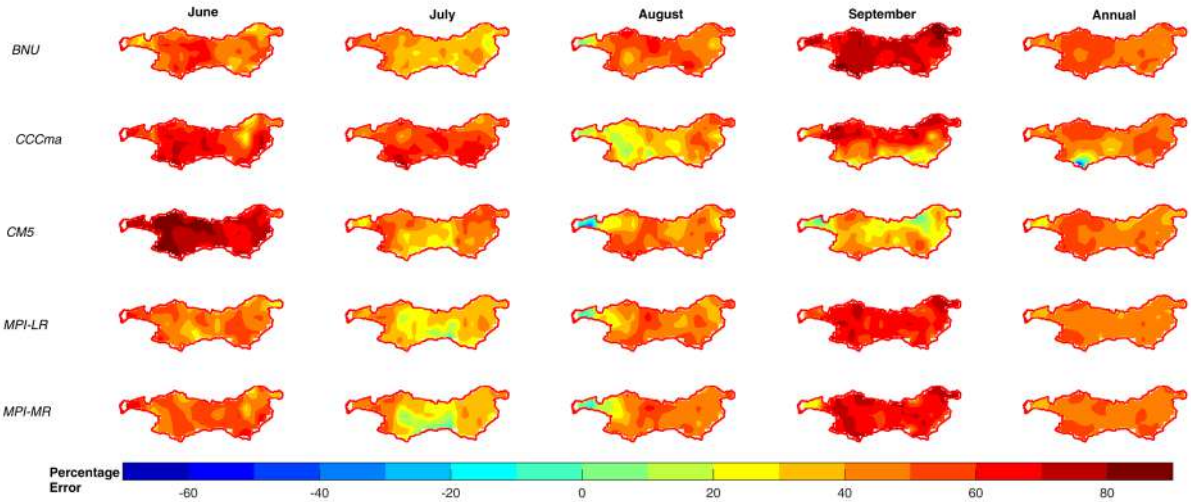

Fig. 4.14 Percentage error in R95p derived from KRSD-Historical period rainfall

The rainfall amount of more than 95% threshold (R95) plays a crucial role in hydrologic assessments and designs. The mean (spatial variability range) R95p for TRB ranges from 245.0 to 646.9 mm (103.0 – 458.6 mm). The estimated errors in R95p show that the GCMs simulated very wet days during monsoon months (JJAS) are underestimated by 48.1% (on average). The percentage deviation (%) range during JJAS for BNU, CCCma, CM5, MPI-LR and MPI-MR models is 37.5 – 71.6, 34.5 – 59.1, 29.9 – 73.6, 34.1 – 63.0 and 33.4 – 63.6 respectively, while their respective mean (and spatial variability range) percentage deviations are 48.8 (59.7 – 33.5), 45.0 (60.8 - -71.1), 45.2 (61.5 – 15.7), 45.2 (57.2 – 32.6) and 46.8 (59.5 – 26.3) (see Fig. 4.14). MPI-LR, MPI-MR, CCCma, and CM5 reasonably simulated R95p for June and Annual scale; July; August; and September respectively during the historical period.

The consecutive spell of rainy days (CWD) significantly affects the predictability of hydrological variables in the river basin. The mean (variation) RD for the Tapi basin ranges from 5.0 to 19.7 days (1.0 – 9.7 days). The large-scale overestimation of the CWD has been seen during the monsoon months with mean overestimation of 75.6% and ranging from 13.8 to 238.3% (see Fig. 4.15). The percentage overestimation during September month is four to seven-fold larger than June, July, and August months. The MPI-LR has been found to reasonably simulate the longest consecutive spells over the Tapi basin.

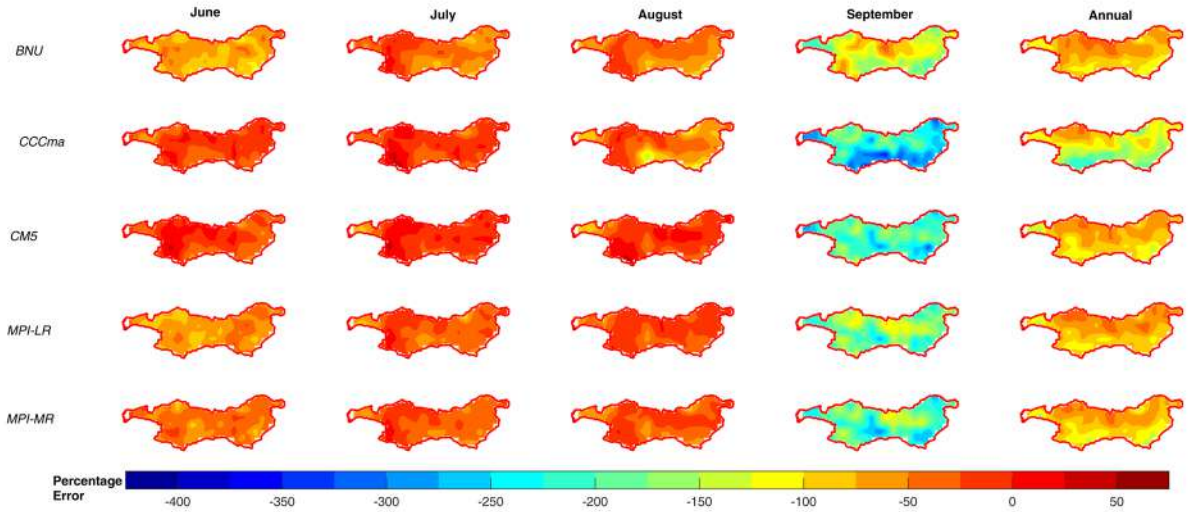

Fig. 4.15 Percentage error in CWD derived from KRSD-Historical period rainfall

- **Sub-basin wise Rainfall Distribution**

The spatial distribution of rainfall varies significantly due to its geographical setting. The presence of the Western Ghats and the large water mass (the Arabian Sea) are the reasons for the highest magnitude of rainfall in the LTB. On the other hand, the region on the leeward side

of the Western Ghats receives the least rainfall in the basin. The narrow valley of UTB, i.e., Burhanpur sub-catchment between Satpura hills and Gwaligarh hills, also receives rainfall above the average rainfall of TRB. The empirical cumulative distribution functions (eCDF) of observed daily rainfall over three sub-basins of TRB are compared with KRSD rainfall data. The rainfall events are further sub-divided into three categories, i.e., high, medium, and low rainfall depths with their respective exceedance probability ranging above 95%, between 95 – 70%, and below 70%., as shown in Fig. 4.16. The low rainfall depths are generally overestimated by all the GCM models, particularly for LTB. For UTB and MTB, the low rainfall depths are reasonably overestimated due to mixed behavior. Similar patterns are also evident in the simulation of RD (see Fig. 4.11) in TRB. The large-scale overestimation of RD is mainly due to poor simulation of the low rainfall depth over TRB.

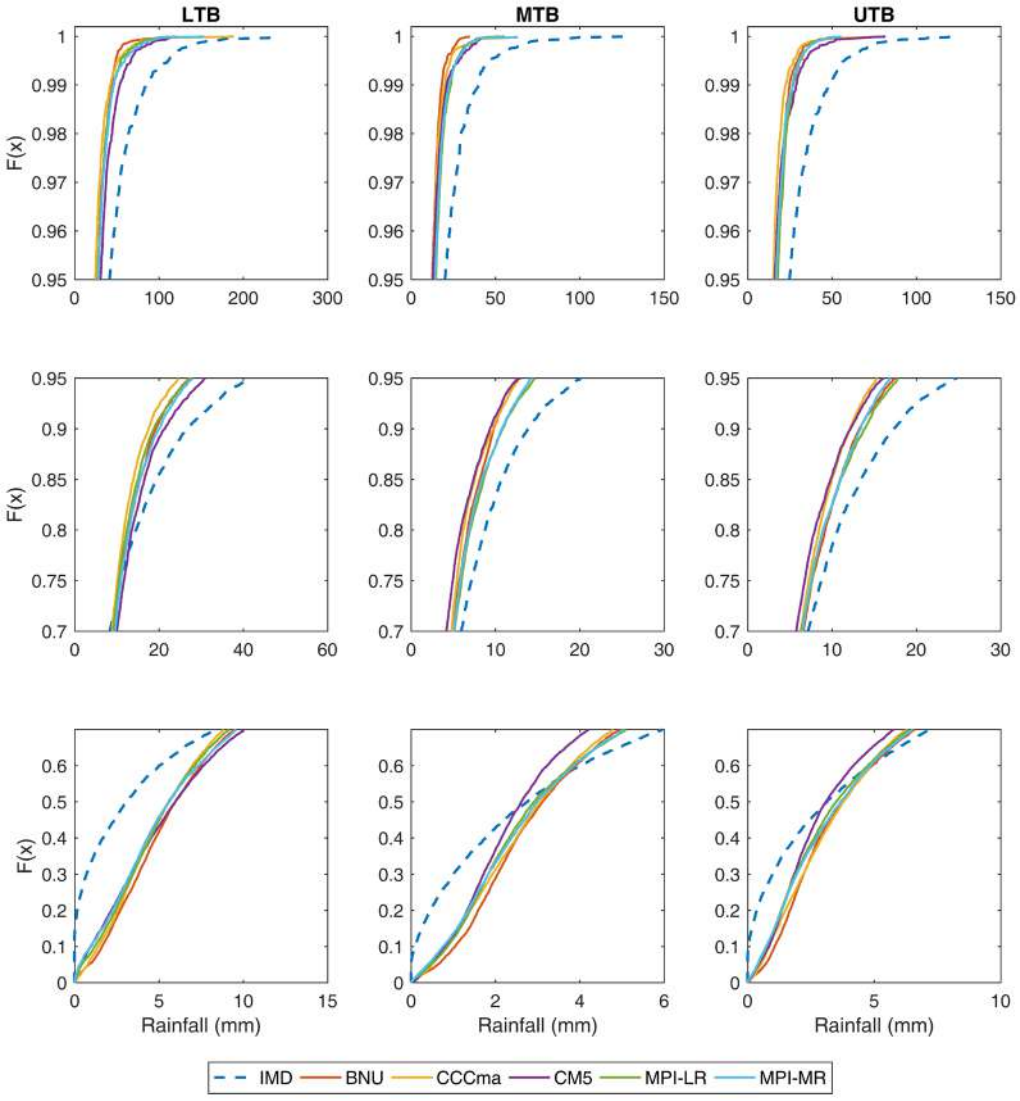

Fig. 4.16 Empirical cumulative distribution function of daily precipitation for LTB, MTB and UTB.

Similarly, the KRSD rainfall underestimates moderate and large rainfall depths, as seen from Fig. 4.16. However, the deviation in medium rainfall depths is highest in UTB, while the MTB received the least one-day maximum rainfall from KRSD data. Similar evidence can be seen in the spatial variation of the one-day maximum rainfall depth simulation over TRB, see Fig. 4.12. Overall, underestimation of the Rx1D rainfall seems to be the primary factor responsible for the general underestimation of mean/total rainfall in TRB. The variation in the simulation of various rainfall depths over TRB, in general, and three sub-basins, are the indicators that the GCM models and, thus, KRSD models are not able to account for the seasonality of the ISMR and therefore the future simulations are required to be interpreted accordingly.

- **Frequency Analysis**

The annual maximum rainfall series for the observed/historical period as well as near-, mid-, and far-future period under RCP 4.5 and RCP 8.5 were extracted. The observed/historical time series were derived using the data for the period 1951-2005 while 2011-2040, 2041-2070, and 2071-2100 time periods were used for future. The return period analysis was done using Gumbel extreme value type-I distribution (Chow et al. 1988) for various return periods, i.e., 2-, 5-, 10-, 50-, and 100-year. The spatial variation of return levels corresponding to 2-, 5-, and 100-year return period are shown Fig. 4.17 and remaining are shown in Fig. **A1c-d** (**in Annexure**). The spatial maps shows that the LTB region received the highest rainfall in the entire basin with 2-year return level rainfall ranging from 84.9 mm to 148.6 mm, while UTB and MTB has range of 59.3 mm to 113.8 mm and 49.4 mm to 129.9 mm respectively for historical period. The mean of observed return levels (in mm) for LTB, MTB and UTB is found to be 116.8, 72.1, and 82.1 respectively, while the same calculations using GCM for historical data is 68.7, 35.8, and 41.8 respectively. The mean values of extreme rainfall (in mm) for 5-years return period, calculated using observed (and GCM historical data) for LTB, MTB, and UTB are 167.1 (97.4), 103.7 (50.6), and 117.9 (57.9) respectively. The corresponding values of extreme rainfall (in mm) for 100-year return period are 304.6 (175.7), 189.9 (91.1) and 215.9 (101.8) respectively. In general, it is observed that the extreme rainfall estimated using GCM historical data are underestimated, on average for all return periods, by 41% in LTB, 51% in MTB, and 52% in UTB.

The simple ensembled average values of extreme rainfall (in mm) corresponding to 100-years return period in near-, mid-, and far-future under RCP 4.5 (and RCP 8.5) scenarios for LTB are 193.2 (196.0), 184.6 (170.5), and 184.7 (146.4) respectively; for MTB are 104.7 (104.1), 102.5

(104.8), and 100.6 (96.0) respectively; and for UTB are 104.6 (108.0), 107.2 (107.8), and 110.7 (99.8) respectively. The corresponding extreme rainfall (in mm) for 5-year return period over LTB are 112.9 (115.0), 109.5 (102.4), and 109.5 (86.5) respectively; over MTB are 59.1 (59.8), 61.2 (63.9), and 61.8 (60.3) respectively; and over UTB are 61.3 (62.5), 64.5 (64.3), and 65.1 (59.1) respectively. It is also observed that under RCP 8.5 scenario, the extreme rainfall is decreasing in LTB towards the end of 21st century; and in MTB and UTB region the extreme rainfall is increasing till mid-future and then decrease in far-future. On other hand, under RCP 4.5 scenario, the return levels are increasing in UTB by the end of 21st century, however, the change is not significant as compared to RCP 8.5 scenario. There is distinct pattern/indication of significant change under RCP 4.5 scenarios over all the three sub-basins of TRB.

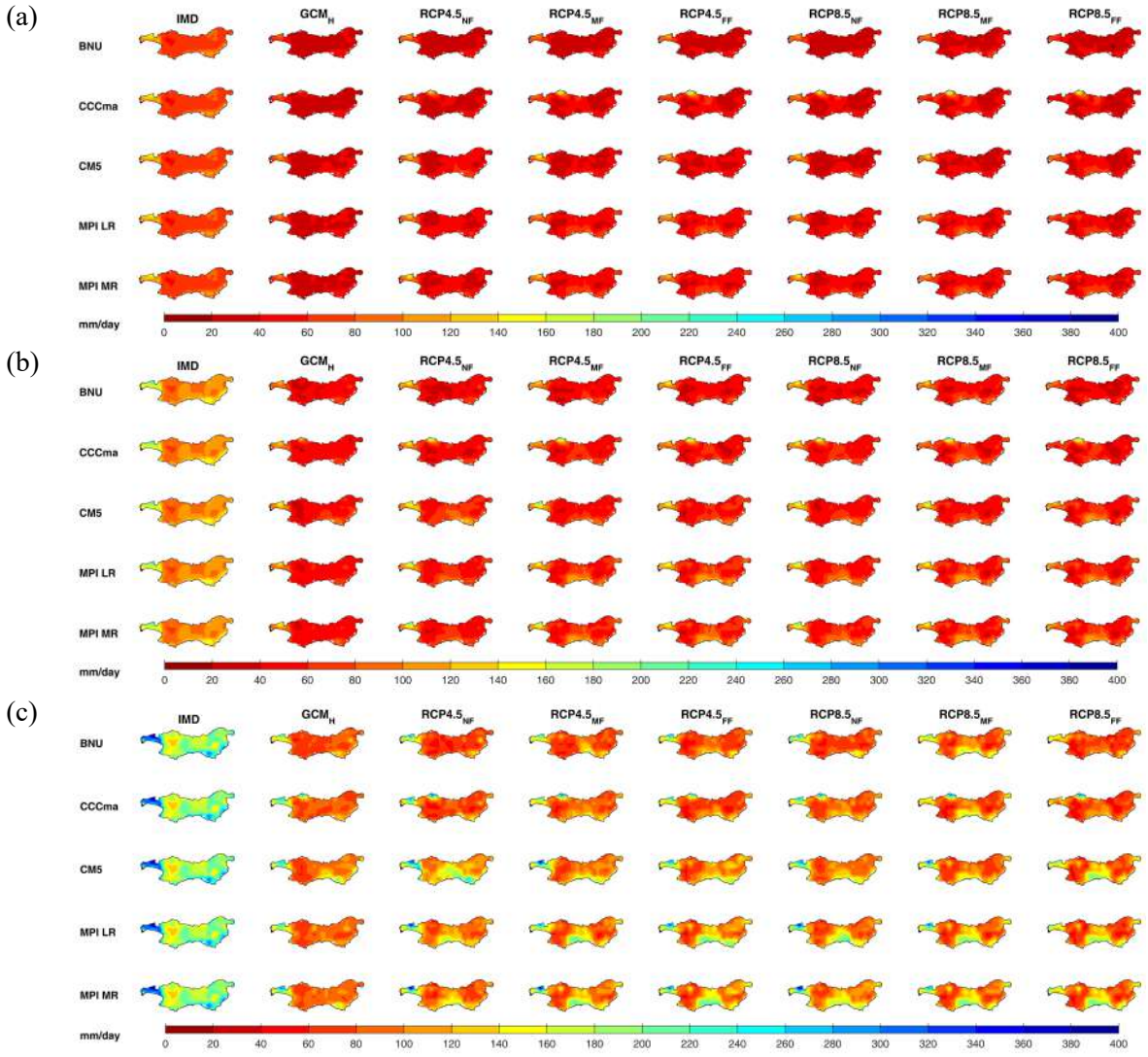

Fig. 4.17 Return levels of annual maximum rainfall for (a) 2-, (b) 5-, and (c) 100-year return periods.

4.4 CLOSURE

The methodological frameworks discussed in this chapter were adopted based on literature for various aspects of the current project. The key interest of the project is to ascertain the climate change impact on hydrologic phenomenon at basin scale. The KRSD data of five GCM models have been used for the aforesaid purposes. The precipitation being the major variable, has been analyzed in detail and adequacy of KRSD data has been assessed with reference to observed IMD data for historical period (1951-2005). Also, frequency analysis of the rainfall for the historical and future period has been accomplished.

The annual rainfall (PRCPTOT) estimated by the GCM are found to be underestimated by 21.7 – 28.4 % (on average), with respect to observed IMD dataset, on annual scale with random over/under estimations over the space. The MPI ESM LR is found to perform better than other GCM models in case of PRCPTOT. A large-scale overestimation has been observed in the number of rainy days (RD) and maximum spell of consecutive rainy days (CWD) with overestimation for September month being four to seven-fold as compared to June, July and August. The mean over estimation for both the indices ranges from 28.5% to 42.2% and 77.2% - 128.4% wherein CNRM CM5 and MPI ESM LR simulated well these two rainfall indices respectively. The extreme indices Rx1D, Rx5D and R95, on annual scale, showed the percentage errors ranging from 46.4% - 52.7%, 41.4% - 44.1% and 45.0% - 48.8% respectively. MPI ESM LR and CNRM CM5 has been found to fairly simulate Rx5D and R95; and Rx1D during the historical period at annual scale. The hydrologic implications of the GCM climate projections have been described in the succeeding chapters.

CHAPTER 5
DATA ANALYSIS & MODEL DEVELOPMENT

5.1 GENERAL

The current chapter described the development of hydrological model of the Upper, Middle, and Lower Tapi basin, including calibration and validation processes. Further, this chapter also discusses the hydrodynamic modeling of the lower Tapi basin while taking the release from Ukai reservoir and tidal level at the Arabian Sea as an upstream and downstream boundary conditions respectively. The flood risk maps of Surat city are also prepared by taking the input from hydrodynamic model for computation of flood hazard, and census based socio-economic vulnerability.

5.2 HYDROLOGICAL MODELING OF UPPER TAPI BASIN

The UTB having large scale topographical, morphological and hydroclimatic heterogeneity, the hydrologic models for Burhanpur and Purna sub-catchments are developed separately. The Upper Tapi River extends up to Hatnur reservoir and the Purna River merges in it around eight km upstream of the reservoir. Thus, the Burhanpur sub-catchment model is extended up to Hatnur reservoir to predict the inflows in to the Hatnur reservoir with provision of inlet point at the confluence, where the contribution of Purna sub-catchment, being modeled separately, is added to the Upper Tapi River (See Fig. 5.1). The key details of the hydrologic model development for these two sub-catchments are discussed in subsequent sections.

5.2.1 Rainfall-Runoff Modeling of Purna sub-catchment

The Purna sub-catchment, having catchment area of 18,490 km^2, has three gauging stations of CWC, namely: Lakhpuri, Gopalkheda and Yerli. The streamflow measurement at Lakhpuri station is not available since 2005 while measurements are available for other two stream gauging sites. The hydrological model developed for Purna sub-catchment is calibrated at Yerli, Gopalkheda and Lakhpuri stream gauging sites and validated at former two sites only. The area downstream of Yerli stream gauging station is an ungauged area. Since the topographical and hydroclimatic variations in the Purna sub-catchment are mostly homogeneous, the calibrated parameters are applied uniformly over the entire Purna sub-catchment to estimate the contribution of the Purna River into the Upper Tapi River. The index map showing DEM and location of rain gauge stations, weather stations and stream gauging stations, is shown in Fig. 5.1. The DEM is SRTM DEM having a spatial resolution of 30 m. The Purna River originates from the Gwaligarh hills, in Betul district of Madhya Pradesh at an

elevation of 783 m (amsl), traverses through the plains of Deccan Plateau and meets with main Tapi River at an elevation of 189 m (amsl). The total delineated area draining into the Purna River up to Yerli sub-catchment is 15,933 km^2. The major soil type in the region is gently to very gently sloping deep loamy to clayey and nearly level to gently sloping deep black soils. The UTB consists of shallow and black soil having medium to fine texture with moderately low productiveness to highly productiveness (CWC 2014). The Purna sub-catchment, from geological point of view, comprises of predominately impermeable and very poorly permeable Deccan basalts and permeable quaternary alluvial deposits.

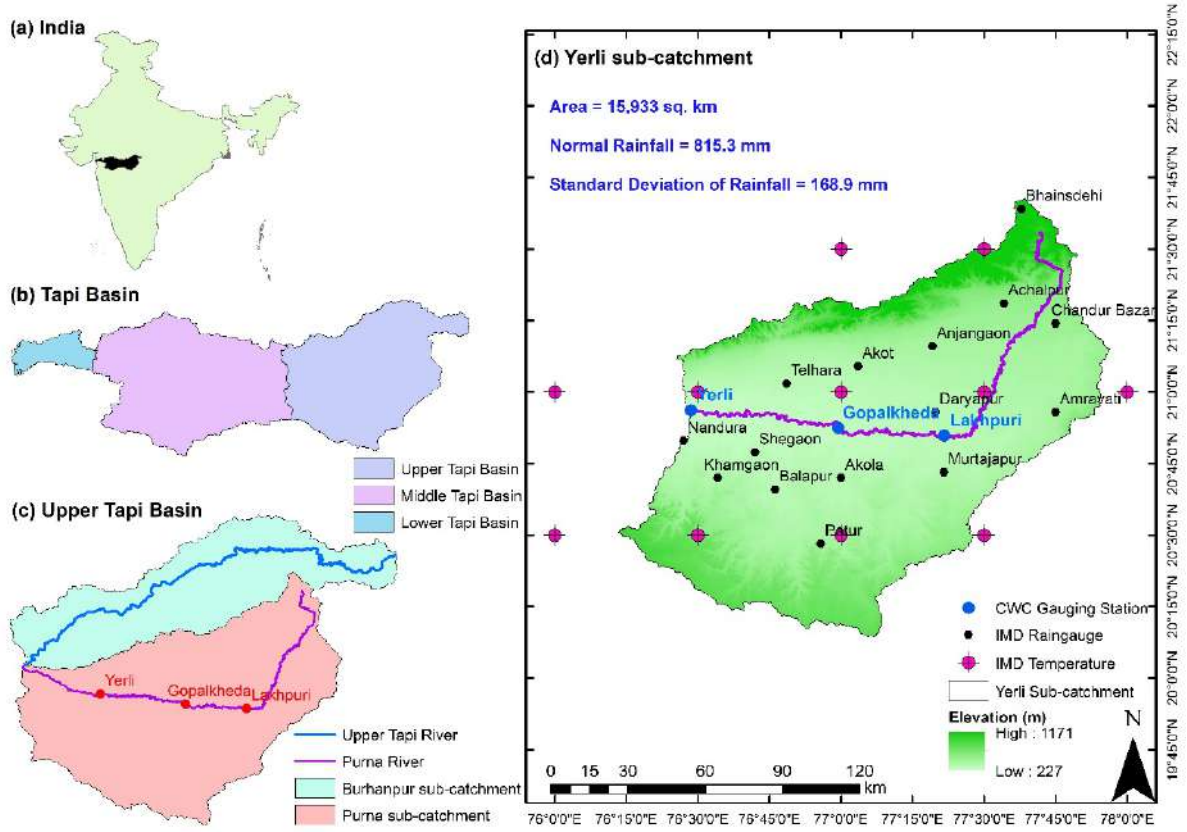

Fig. 5.1 Index map of Yerli sub-catchment

- **Data used and their sources**

The development of hydrological model requires topographical, hydrologic and climate data. The various data sets used for development of hydrologic model are enlisted in Table 3.3. The remaining weather parameters, i.e., solar radiation, wind speed and relative humidity, have been generated by the model using the monthly weather generator statistics derived from the long term daily weather data of IMD and was obtained from SWAT website (https://swat.tamu.edu/data/india-dataset/ last visited in July, 2019). The locations of rain gauging stations and their elevation (amsl) are shown in Table 5.1.

- **Development of SWAT model**

The sole purpose of any model is to better represent the complex processes and their interconnection in simplified manner with the help of set of mathematical equations. Also, the degree of accuracy of the model prediction/performance depends on the quality and spatio-temporal resolution of the database, i.e., topographical, land use and land cover, and hydroclimatic data etc. The present study undertakes use of SRTM DEM having horizonal and vertical resolution/accuracy of ± 30 m and ± 16 m respectively. The resolution and resampling technique used for development of DEMs have significant impact on the uncertainty in the simulated flow, erosion, and nutrients from the catchments (Kumar et al. 2017). The purpose of DEM in SWAT model is to generate the streamflow network, corresponding to certain stream area threshold, using the principle of accumulation of the flow and direction of flow from higher elevation to lower elevation. The stream network threshold required to generate the stream network in the basin also plays significant role in defining the number of sub-watersheds in the basin and uncertainty in the model predictions. In the present study, the stream network has been generated using arbitrary threshold value of 200 km^2 resulting in to the 55 watersheds in the Purna sub-catchments. The smaller sub watersheds were further merged to nearby sub watershed and thereby the number of sub watershed reduced to 38 (see Fig. 5.2a). The locations of the Purna sub-catchment outlet, Yerli, Gopalkheda and Lakhpuri are at watershed no. 02, 07, 23, and 27 respectively (see Fig. 5.2a).

Table 5.1 Characteristics of rain gauge and stream gauging stations in Purna sub-catchment

Sr. No.	Stations	Latitude	Longitude	Elevation (m)	Period of data availability
			Rain gauge stations		
1	Achalpur	21° 18' N	77° 34' E	377	1944-2013
2	Akola	20° 42' N	77° 00' E	285	1944-2013
3	Akot	21° 05' N	77° 04' E	314	1951-2013
4	Amravati	20° 55' N	77° 45' E	366	1944-2013
5	Anjangaon	21° 09' N	77° 19' E	339	1944-2013
6	Atner	21° 37' N	77° 56' E	665	1944-2013
7	Bhainsdehi	21° 38' N	77° 38' E	767	1944-2013
8	Chandur bazar	21° 14' N	77° 44' E	373	1944-2013
9	Chikhalda	21° 24' N	77° 19' E	1084	1976-2013
10	Daryapur	20° 55' N	77° 20' E	285	1976-2013
11	Murtajapur	20° 43' N	77° 22' E	307	1944-2013
12	Patur	20° 27' N	76° 56' E	348	1944-2013
13	Telhara	21° 02' N	76° 49' E	286	1944-2013
14	Nandura	20° 50' N	76° 27' E	271	1944-2013
15	Shegaon	20° 47' N	76° 49' E	286	1944-2013

Sr. No.	Stations	Latitude	Longitude	Elevation (m)	Period of data availability
Temperature grids					
11 grids in the Purna sub-catchment having data from 1951-2017					
Stream gauging stations					
1	Yerli	20° 56' N	76° 28' E	213	1979-2013
2	Gopalkheda	20° 52' N	76° 59' E	236	1979-2013
3	Lakhpuri	20° 50' N	77° 21' E	259	1979-2005

The level-I classification has been adopted for the LULC map of the Purna sub-catchment as shown in Fig. 5.2b. It can be seen from Fig. 5.2b that Purna sub-catchment is agriculture dominated catchment (AGRL, 66.0%) followed by deciduous forest (FRSD, 14.6%), located at foothills of the Gwaligarh and Ajanta-Satmala Ranges, and range land or fallow land (RNGB, 11.5%). There were 37 soil polygons (see Fig. 5.2c) having different soil textures and properties, classified by NBSS&LUP, have been used as soil map input for the present study. The soil texture of the Purna sub-catchment has major proportion of clay, followed by clay-loam, sandy-loam, and sandy clay loam. Most of the soils were classified as D, followed by C type hydrological soil group, indicating the presence of the high organic content and low drainage capacity. The three land slope classes (see Fig. 5.2d), viz., 0-2.5%, 2.5-5% and >5%, have been used such that all the classes have uniform fraction of the basin area with their respective representative area of 34%, 30% and 36%. The curve numbers (CN) defined in the SWAT database are expected to work well for the slope up to 5% only. The CN has been found sensitive to the land slope and needs to be updated when the land slope is greater than 5%. The unique feature group identified from overlapping sub-watershed, LULC, soil and slope layers lead to definition of the hydrological response unit (HRUs). The HRUs so formed were further redefined using the land use, soil, and slope thresholds of 5%, 10% and 10% respectively, wherein the HRUs having area less than the defined thresholds were equally distributed to the nearby large HRUs. The total number of HRUs so formed were 1054 in number. Apart from the physiographic data, hydroclimatic data such as precipitation, temperature, wind speed, solar radiation and relative humidity are also required to generate the response of the catchment against these variables. Along with these, weather generator database consisting of monthly statistical parameters (mean, standard deviation etc.) of the aforesaid hydroclimatic variables are required to simulate the missing values in the data set, if any. The present study incorporates the use of readily available weather generator database developed from IMD daily gridded data of 85 years at spatial resolution of 1° × 1° (accessible on https://swat.tamu.edu/software/india-dataset).

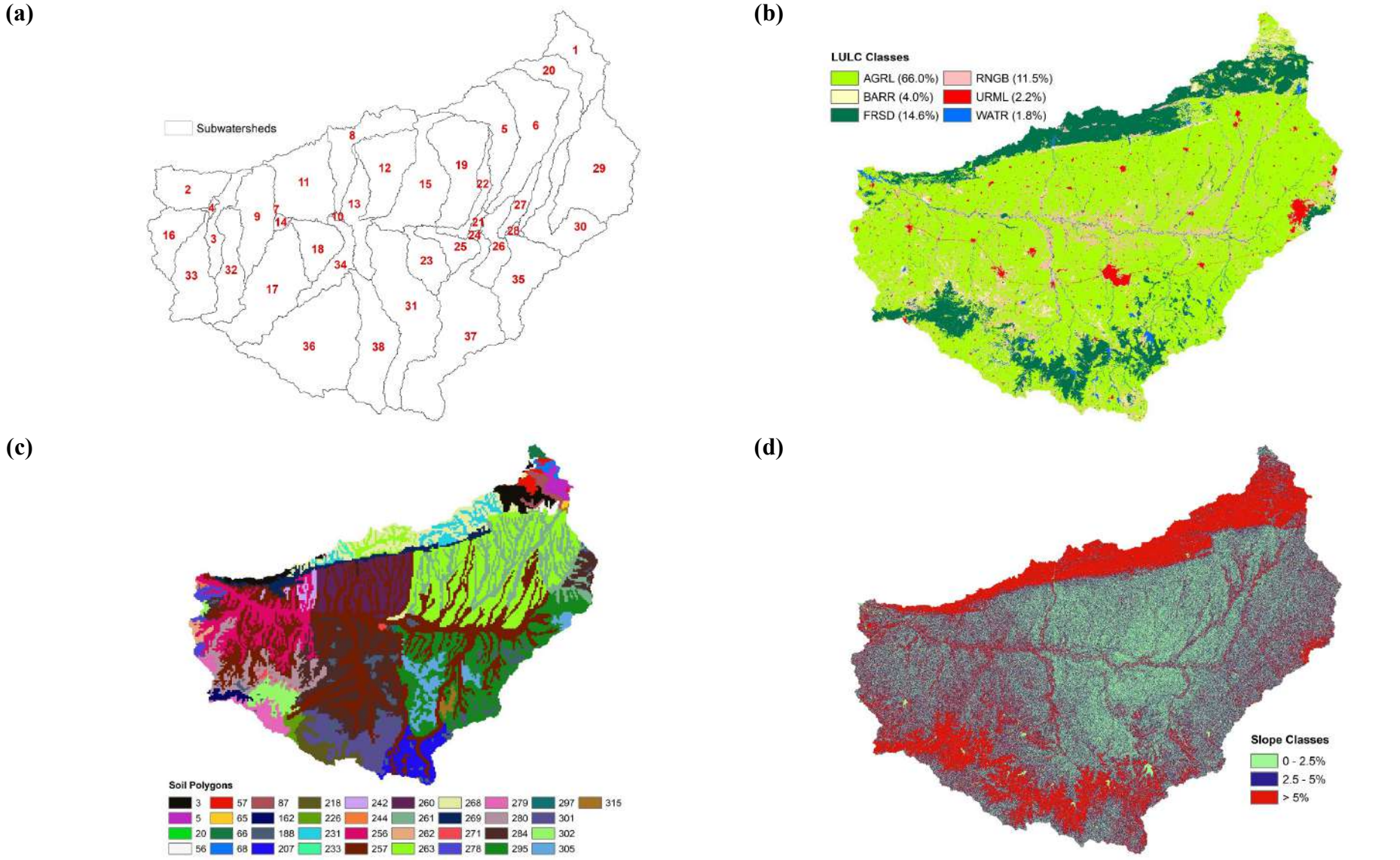

Fig. 5.2 (a) Sub watersheds delineated, (b) LULC classes, (c) NBSS&LUP soil polygons, and (d) slope classes in Purna sub-catchment

- **SWAT simulation**

The calibration and validation period of the continuous hydrological model must be such that both the periods include wet, normal, and dry years. Also, the statistical parameters calculated for both the periods must not have large scale deviations among them. The developed model in the present study has been calibrated and validated for the period 1998 – 2007 and 2008 – 2013 respectively such that both the periods include high as well as low rainfall years. The basic statistical parameters of the observed streamflow at Yerli during calibration and validation periods are presented in Table 5.2. It is evident from the Table that there is no significant variation in the flow statistics during the calibration and validation periods.

Table 5.2 Daily streamflow statistics of Yerli sub-catchment during calibration and validation period

Statistical Parameter	Calibration Period (1998 – 2007)			Validation Period (2008 – 2013)	
	Yerli	**Gopalkheda**	**Lakhpuri**	**Yerli**	**Gopalkheda**
Average (m^3/s)	60.27	35.29	12.12	52.04	33.74
Standard deviation (m^3/s)	297.27	188.58	64.90	173.10	156.96
Peak discharge (m^3/s)	8358.85	4124.0	1580.06	2701.16	3235.11

The present model has been used to simulate the streamflow for the duration Jan. 1998 to Dec. 2013 excluding four years of hot start period, of which initial ten years were used for calibration while later six years were used for validation of the model. The NYSKIP/hot start period is used to stabilise the initial conditions of the model and plays crucial role in model performance. The simulated streamflow has been initially checked for coefficient of determination (R^2), wherein, $R^2 < 0.5$ indicates that the developed model needs to be re-evaluated. Such model is not going to perform well even after extensive calibration. However, the model R^2 value obtained before calibration was found to be more than 0.5 for current study, thus, it is expected that the model performance can be improved with calibration. The SUFI-2 in SWAT-CUP has been used for the calibration, sensitivity, and uncertainty analyse, followed by the validation after the model performance was found satisfactory as per Moriasi et al. (2015) criterion (See Table 5.5). Apart from the mathematical performance assessment, it is needed to ensure that the model is having close representation of the water circulation by means of water balance studies. During calibration due care must be taken that the model does not violate the water balance and the absolute physical ranges of the parameters used for the calibration.

- **Parametric uncertainty and Sensitivity analysis**

The real-time representation of the hydrologic cycle with the help of suitable model consists of many parameters which makes modeling very complex. However, with certain assumptions, the realistic answer to the real-life problems can be derived using hydrologic modeling. To make any model realistic, large number of hydrological variables are required to be measured over the space and time, which is not feasible. Thus, hydrological models are required to be calibrated based on the observed data such as streamflow, sediment yield, nutrients load, evapotranspiration, ground water levels etc. For realistic calibration, it is required for a modeler to have knowledge about the watershed characteristics, hydrology, and the feasible range of the selected parameters. The uncertainty associated with the input datasets and the multicollinearity of the hydrological processes and parameters leads to the equifinality conditions. Thus, multi-metric performance assessment of the model is required to deal with the equifinality conditions. The multi-metric approach includes multivariate, multisite and multiparameter calibration, assessed with the help of multiple indices. The present study undertakes the multisite calibration of the hydrological model at Yerli, Gopalkheda and Lakhpuri sub-catchments. However, the parameters were varied uniformly over the entire Purna sub-catchment. Also, the model performance has been ascertained for single site calibration as well as multisite calibration and their comparative performance assessment has also been presented accordingly.

The sensitivity analysis helps in identifying the parameters largely affecting the output/objective function, thus, modeler can focus more on the sensitive parameters for effective calibration of the model. The SWAT-CUP programme facilitates one-at-a-time and global sensitivity analysis, however, later is adopted for the present study as it takes care of the simultaneous variation of all the set of parameters within the range. The SUFI-2 algorithms of the SWAT-CUP has been used to ascertain parametric sensitivity and uncertainty analysis. The SUFI-2 algorithm uses Latin hypercube sampling (LHS) to cover the entire range of the parameter samples such that none of the sample combination is repeated. The linear combination of central values of each parameter, obtained from LHS for corresponding simulation number, is fitted to the model and the relative change in the objective functions due to change in parameters values is assessed. The either of the three methods, i.e., relative (*r__*), absolute (*a__*) or replace (*v__*) can be adopted for fitting the central values of the LHS bands. The aforesaid method must be selected based on the nature of the parameter, i.e., the parameter which are likely to vary spatially (e.g., curve number) must be varied relatively (*r__*). During

the sensitivity analysis, the few of the parameters were parameterised as per their LULC to preserve the spatial heterogeneity of their properties. It has been observed that after parameterisation, the parameter may turn out to be insensitive depending upon the spatial extent of the basis on which parameterisation has been done. The objective function plays a critical role in sensitivity analysis as well as the performance of the model, however, uncertainty in the predicted model is independent of the objective function defined. Furthermore, the KGE was used in the present study as objective function for the calibration purpose, keeping in view the other performance indices also. Two different approaches for calibration have been employed, i.e., single-site calibration (SSC) and multi-site calibration (MSC). In SSC, the parameters were varied and fitted keeping in view the farthest point of measurement, i.e., Yerli gauging station. On other hand, in MSC the parameters were varied and fitted with respect to all three gauging sites simultaneously.

To calibrate the model initial set of parameters were identified based on the literature/previous studies (see Table 5.3, with their description and absolute range). The parameters tabulated in Table 5.3 are related to the basic processes of water circulation in the hydrological cycle, viz. ground water (.gw), land management (.mgt), soil (.sol), main channel (.rte), hydrological response units (.hru), tributary channels (.sub) and basin parameters (.bsn). The default/initial range, calibrated range, fitted parameter, t-stat, p-value, and parameter sensitivity rank corresponding to multisite calibration have been presented in Table 5.4. The top five sensitive parameters corresponding to the SSC are *GWQMN.gw, GW_REVAP.gw, CN2.mgt, RCHRG_DP.gw* and *CNCOEF.bsn* while the same during MSC are *GW_REVAP.gw, SOL_BD.sol, CN2.mgt, CNCOEF.bsn* and *CH_N2.rte*. It can be observed that during SSC the most sensitive parameters are concentrated to the ground water parameters while MSC considers the other aspects also, viz., soil and main channel related parameters also, while the *CN2* and *CNCOEF* were common. Thus, it can be inferred that MSC is more rigorous and advantageous over SSC.

The uncertainty assessment has been carried out in the present study using SUFI-2 which estimates *P-factor* and *R-factor*. The algorithm estimates the 95% prediction uncertainty (PPU) as the difference between the 97.5% and 2.5% prediction bands in the simulated outputs. The parametric uncertainty in the model is governed by the best estimation range, wider the band, more is the uncertainty in the model prediction. The *P-factor* is the percentage of the observed data bracketed by the *95PPU* band. This index is a measure of the capability of the model to

capture the uncertainties in the model. The *R-factor*, on other hand, is the measure of the quality of the model calibration and estimated as the ratio of the thickness of the 95PPU band to the standard deviation in the observed data. The ideal calibration is the one which encapsulates the maximum observed values at minimum uncertainty band thickness. The ideal values of the *P-factor* and *R-factor* are 1 and 0 respectively, however, uncertainties are always introduced in the model due to uncertainty in the observed hydroclimatic data, spatial input, and the model itself. It is recommended that maximum observations must be encapsulated by the model keeping *R-factor* less than 1. The *P-factor* and *R-factor* during MSC (SSC) at Yerli were found to be 0.39 (0.38) and 0.39 (0.62) respectively, thus, indicating that the MSC has been found to perform better than SSC.

Table 5.3 Input parameters for sensitivity analysis and calibration

Parameter	Description	Absolute Range
v__ALPHA_BF.gw	Baseflow alpha factor (days)	0 – 1
v__GW_DELAY.gw	Groundwater delay (days)	0 – 500
v__GWQMN.gw	Threshold depth of water in the shallow aquifer required for return flow to occur (mm)	0 – 5000
v__GW_REVAP.gw	Groundwater "revap" coefficient	0.02 – 0.2
v__REVAPMN.gw	Threshold depth of water in the shallow aquifer for "revap" to occur (mm)	0 – 500
v__RCHRG_DP.gw	Deep aquifer percolation fraction	0 – 1
r__CN2.mgt	SCS runoff curve number	35 – 98
r__SOL_AWC().sol	Available water capacity of the soil layer	0 – 1
r__SOL_K().sol	Saturated hydraulic conductivity (mm/hr)	0 – 2000
r__SOL_BD().sol	Moist bulk density (gm/cc)	0.9 – 2.5
v__SOL_ZMX.sol	Maximum rooting depth of soil profile (mm)	0 - 3500
r__SOL_ALB().sol	Moist soil albedo	0 – 0.25
v__CH_N2.rte	Manning's "n" value for the main channel	0.01 – 0.3
v__CH_K2.rte	Effective hydraulic conductivity in main channel (mm/hr)	0 – 300
r__CH_S2.rte	Average slope of main channel	0.001 – 10
v__ALPHA_BNK.rte	Baseflow alpha factor for bank storage	0 – 1
v__ESCO.hru	Soil evaporation compensation factor	0 – 1
v__EPCO.hru	Plant uptake compensation factor	0 – 1
v__CANMX.hru	Maximum canopy storage (mm)	0 – 100
v__OV_N.hru	Manning's "n" value for overland flow	0.01 – 30
r__HRU_SLP.hru	Average slope steepness	0 – 1
v__CH_N1.sub	Manning's "n" value for the tributary channels	0.01 – 0.3
v__CH_K1.sub	Effective hydraulic conductivity in tributary channel alluvium	0 – 300
r__CH_S1.sub	Average slope of tributary channels	0.001 – 10
v__SURLAG.bsn	Surface runoff lag time factor	0.05 – 24
v__EVRCH.bsn	Reach evaporation adjustment factor	0.5 – 1
v__CNCOEF.bsn	Plant ET curve number coefficient	0.5 – 2

- **Performance evaluation of SSC vs MSC**

The MSC has been found to outperform SSC in capturing the effect of various processes involved in basin hydrology including uncertainty in model inputs and parameters. In SSC, the model is calibrated with respect to streamflow at Yerli station for monthly scale and the flow at other two stations have been simulated using the calibrated parameters. On the other hand, MSC simultaneously considers the flow variable at all three stream gauging sites and estimates the best parameters within the uncertainty range provided. However, the parametric variations were spatially uniform.

Table 5.4 Calibrated model parameter values, uncertainty range and sensitivity rank for Multisite calibration

Parameter	Initial Range	Calibrated Range	Fitted Value	t-Stat	p-value	Rank*
v__ALPHA_BF.gw	0.048	0.438 - 0.514	0.459	1.422	0.166	8(24)
v__GW_DELAY.gw	31	2.602 - 32.602	9.852	0.602	0.552	16(29)
v__GWQMN.gw	1000	1217 - 1658	1375.140	-0.899	0.376	12(1)
v__GW_REVAP.gw	0.02	0.141 - 0.207	0.202	8.811	0.000	1(2)
v__REVAPMN.gw	750	300.99 - 354.0	337.660	0.589	0.561	20(30)
v__RCHRG_DP.gw	0.05	0.025 - 0.066	0.056	0.752	0.458	14(4)
r__CN2.mgt	72-94	-0.128 - -0.089	-0.100	-1.910	0.066	3(3)
r__SOL_AWC().sol	0.06-0.16	0.134 - 0.204	0.155	-0.069	0.946	28(11)
r__SOL_K().sol	0.72-7.5	-0.054 - 0.039	0.004	0.594	0.557	18(9)
r__SOL_BD().sol	1.27-1.6	-0.383 - -0.144	-0.301	-2.790	0.009	2(6)
v__SOL_ZMX.sol	1200	1380 - 1794.9	1411.143	-1.535	0.136	7(23)
r__SOL_ALB().sol	0.0484	-0.244 - -0.181	-0.193	0.590	0.560	19(18)
v__CH_N2.rte	0.014	0.029 - 0.03	0.030	-1.611	0.118	5(27)
v__CH_K2.rte	0	-23.62 - 42.38	25.333	-0.432	0.669	24(12)
r__CH_S2.rte (x10^4)	1.93-234	-0.032 - 0.105	0.083	0.526	0.603	22(22)
v__ALPHA_BNK.rte	0	0.266 - 0.322	0.279	0.671	0.507	15(21)
v__ESCO.hru	0.95	0.191 - 0.274	0.248	0.042	0.967	30(8)
v__EPCO.hru	1	0.553 - 0.678	0.600	-0.598	0.555	17(13)
v__CANMX.hru	0	12.767 - 18.4	14.504	0.893	0.379	13(26)
v__OV_N.hru^{1,2}	0.1	0.143 - 0.168	0.143	-1.582	0.124	6(17)
v__OV_N.hru^{3,4}	0.14	0.035 - 0.038	0.036	-0.442	0.662	23(15)
v__OV_N.hru^{5}	0.15	0.04 - 0.044	0.041	0.091	0.928	27(7)
v__OV_N.hru^{6}	0.01	0.028 - 0.03	0.030	-0.283	0.779	25(28)
r__HRU_SLP.hru	0.006-0.33	0.11 - 0.137	0.112	0.044	0.965	29(25)
v__CH_N1.sub	0.014	0.03 - 0.032	0.031	-0.264	0.794	26(10)
v__CH_K1.sub	0	73.2 - 84.466	78.927	0.968	0.341	11(16)
r__CH_S1.sub (x10^4)	1.93-234	-0.007 - 0.079	0.034	-1.299	0.204	9(20)
v__SURLAG.bsn	4	1.906 - 4.644	4.576	0.974	0.338	10(19)
v__EVRCH.bsn	1	0.744 - 0.831	0.796	0.542	0.592	21(14)
v__CNCOEF.bsn	1	0.548 - 0.647	0.567	-1.680	0.104	4(5)

1,2,3,4,5 and 6 indicates URML, FRSD, AGRL, BARR, RNGB and WATR respectively.

* The bracketed values correspond to the parametric sensitivity rank during single site calibration.

The statistical and graphical comparison of the model performance during SSC and MSC have been carried out to determine the most suitable and efficient method for calibration of hydrological model for Purna sub-catchment. The Fig. 5.3 shows the comparison of the observed flow with respect to the simulated flows for MSC at Yerli gauging station in Purna sub-catchment for monthly and daily time scale. The model simulated high flows better during MSC as compared to SSC, while the intermediate flows were consistently overpredicted. It can also be noticed that both calibration methods overpredicted the lean /non monsoon flows at both the gauging sites during simulation period. It can be observed that the runoff coefficient in the sub-catchment is very high during August to October due to high antecedent moisture contain in the ground profile.

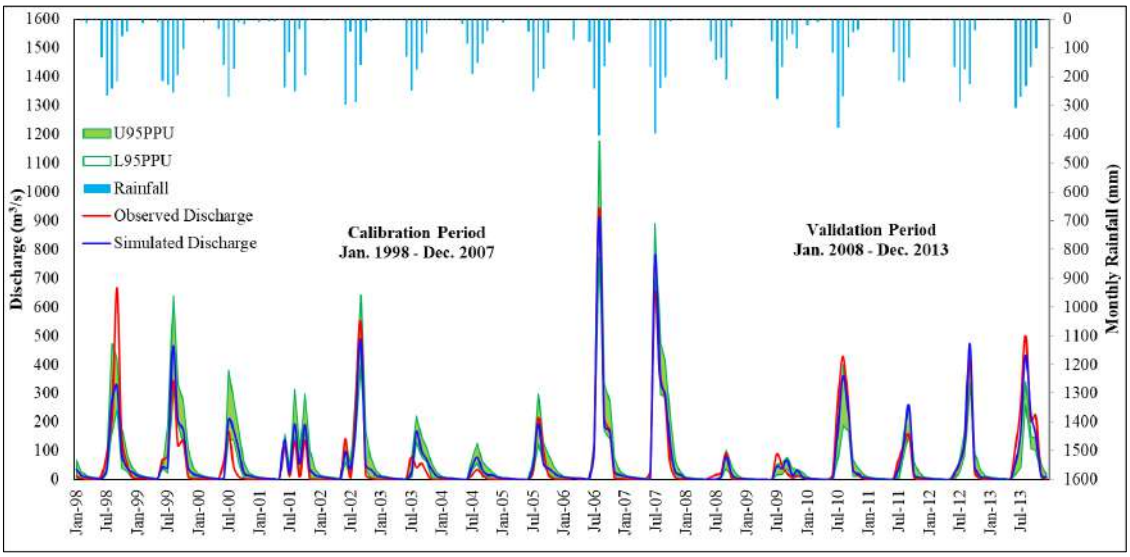

(a)

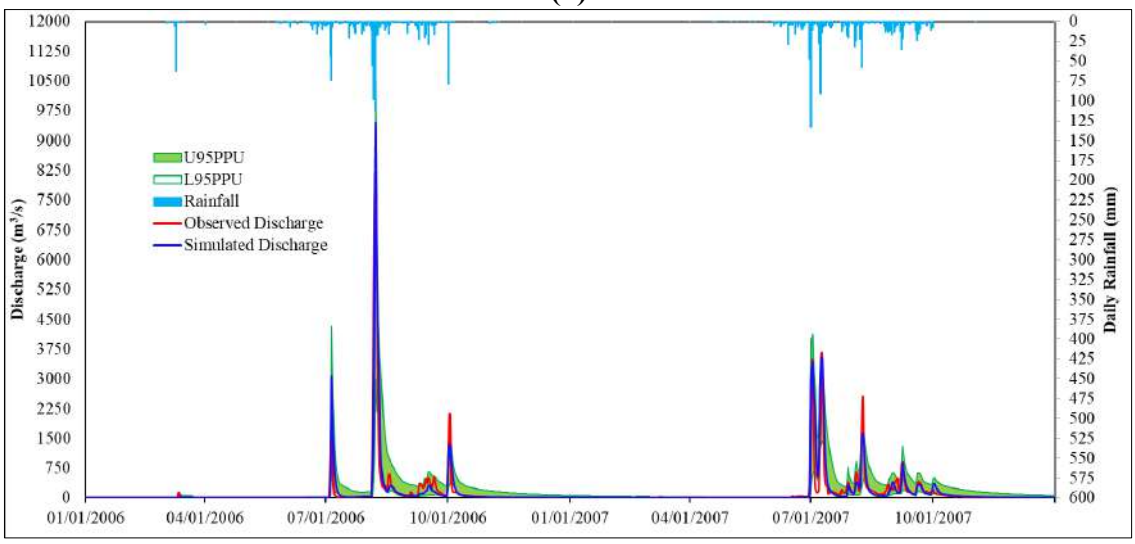

(b)

Fig. 5.3 Time series of observed and simulated discharge (a) at Monthly Scale and (b) Daily Scale (for year 2006 and 2007) for Multisite calibration at Yerli gauging station

The scatter plot of the observed v/s simulated flow for all three gauging sites are shown in Fig. 5.4. It is seen that the linear regression coefficient and coefficient of determination of the MSC are close to 1, showing better performance indicator of MSC as compared to SSC. The statistical indices used for the assessment of the model performance are *P-factor*, *R-factor, R^2, bR^2, NSE*, *PBIAS*, *MNS, RSR* and *RMSE* (see Table 5.5).

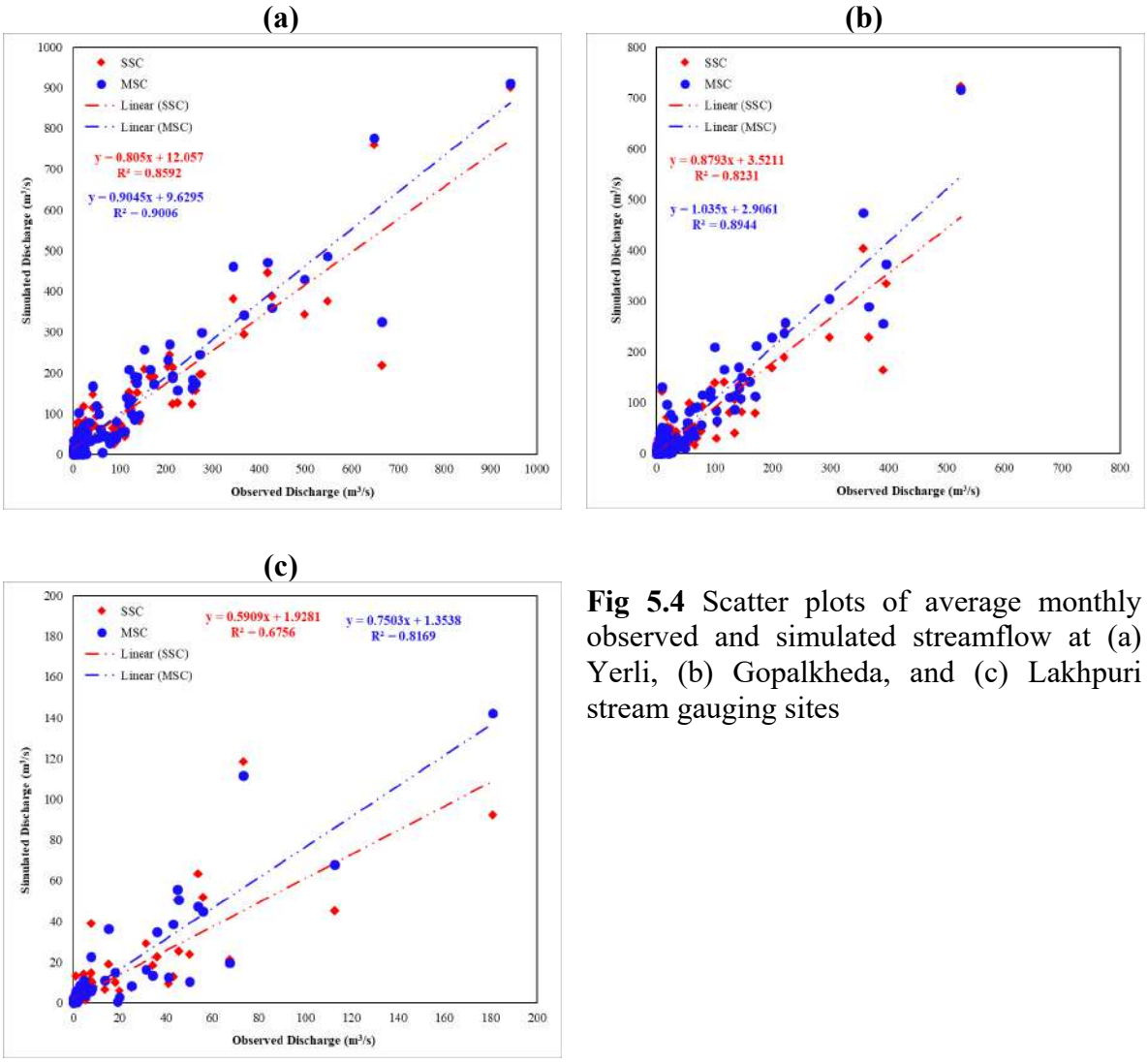

Fig 5.4 Scatter plots of average monthly observed and simulated streamflow at (a) Yerli, (b) Gopalkheda, and (c) Lakhpuri stream gauging sites

The *P-factor* and *R-factor* address the model capability to account for all possible sources of uncertainty, R^2 and bR^2 addresses the similarity in the pattern of observed and simulated flows, *NSE (MNS)* and *RSR* attributes how well the peak (low) flows are simulated and *PBIAS* represents the percentage error in the observed and simulated mean flows. The more details of the performance indicators given in Table 5.5, can be found in Abbaspour (2011) and Moriasi et al. (2015). The statistical indicators in Table 5.5, shows that MSC has resulted into R^2 >0.80, bR^2 > 0.80, *NSE* >0.85, *MNS* > 0.65 and *RSR* <0.5 at the most of the instances, except at

Lakhpuri. According to Moriasi et al. (2015) the model performance can be rated as good to very good in simulating the monthly streamflows. However, the systematic overprediction can has been reported by the model during MSC during the calibration, indicated by the *PBIAS* < -15%, however, the same is not the case during the validation period. The probable reason could be the dominance of high flood magnitudes and number of flood events during the calibration period as compared to the validation period where dry/normal/wet years were uniform in number. Also, the model does not incorporate the impacts of check dams and other detention structures which affects the flows in the stream. Thus, from the sensitivity and uncertainty analysis, graphical and statistical assessment of the MSC and SSC techniques employed in the present study, it can be stated that the MSC technique is expected to account for the hydrological variations over the space and hence leading to better measures for calibration of a hydrological model. For brevity, the detailed, results, and performance assessment of daily scale hydrologic model are included in Table **A2** and Fig. **A2 (in Annexure)**.

Table 5.5 Performance evaluation of multisite calibration and validation

Performance Indicators[$]	**Calibration Period (1998 – 2007)**			**Validation Period (2008 – 2013)**	
	Yerli*	***Gopalkheda***	***Lakhpuri***[#]	***Yerli***	***Gopalkheda***
P-factor	0.39 (0.38)	0.38	0.42	0.32	0.32
R-factor	0.39 (0.62)	0.34	0.32	0.48	0.36
R^2	0.89 (0.86)	0.90 (0.82)	0.82 (0.68)	0.93 (0.87)	0.92 (0.87)
NSE	0.89 (0.85)	0.85 (0.80)	0.81 (0.65)	0.93 (0.86)	0.92 (0.86)
RSR	0.33 (0.38)	0.39 (0.44)	0.44 (0.59)	0.26 (0.37)	0.29 (0.38)
MNS	0.69 (0.69)	0.65 (0.62)	0.66 (0.61)	0.79 (0.65)	0.77 (0.65)
PBIAS (%)	-14.3 (-3.0)	-18.9 (0.91)	13.8 (24.9)	5.8 (0.79)	0.2 (3.53)
bR^2	0.81 (0.70)	0.82 (0.78)	0.61 (0.40)	0.82 (0.67)	0.83 (0.65)

 # Data was available up to May 2005.
** The bracketed values correspond to the single site calibration with respect to Yerli.*
$The reference values of the performance indicators, as specified in Moriasi et al. (2007), are included in Table 2.1.

5.2.2 Rainfall-Runoff Modeling of Burhanpur sub-catchment

The study area covers the part of UTB from Multai (Madhya Pradesh), the origin of Tapi River, up to Hatnur Reservoir (Maharashtra). The Upper Tapi River, travels about 350 km till it drains into the Hatnur reservoir from Multai. The catchment area of the Burhanpur sub-catchment is around 10,600 km^2. The region is bounded by Satpura and Mahadeo hills ranges on northern and southern side respectively, while west side is bounded by Khandesh Plains (CWPC 1952). The part of sub-basin lies in Maharashtra (Amravati District), is full of cuts and valleys,

whereas the parts lie in Madhya Pradesh (Betul and Burhanpur Districts), is covered with Deccan trap lava flows (CWC 2014). The climatic condition of the Burhanpur sub-catchment is sub-tropical to temperate and receives heaviest rainfall during the months of June to September (Resmi et al. 2018). The hydrological parameters like gauge, discharge, and sediment concentration are monitored at Burhanpur gauge station as shown in Fig. 5.5.

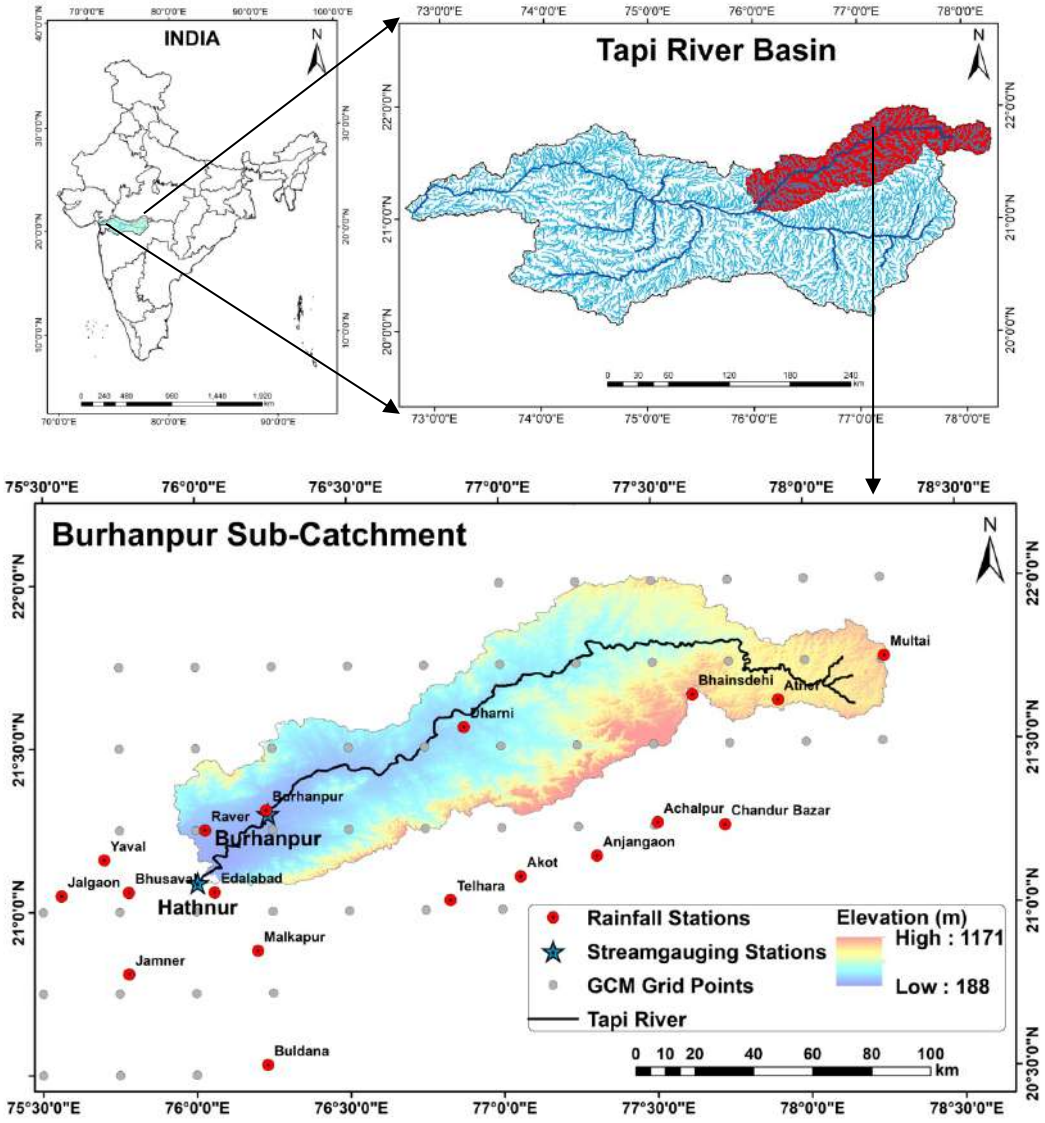

Fig. 5.5 Index Map of Burhanpur sub-catchment

- **Data used and their sources**

The raster datasets such as Digital Elevation Model (DEM), land use land cover (LULC), hydrological soil group map and datasets such as precipitation, temperature, and observed stream flow data were required for the generation of water balance parameters. The input data used for hydrological modeling of Burhanpur sub-catchment have been shown in Table 3.3. The locations of rain gauging stations and their elevation (amsl) are shown in Table 5.6.

- **Development of SWAT model**

The SWAT program was used for the hydrological modeling of Burhanpur sub-catchment in this study. The SWAT program requires mainly four inputs i.e., DEM, LULC, soil properties and climate data of the study area. The slope classes, stream network and the catchment boundary are generated using the DEM of the study area. The DEM used in this study was made from SRTM1 void filled data of resolution 1 arc-second (30m) (Table 3.3). The elevation of study area ranges from 188m to 1171m above the mean sea level. Average elevation of study area is 486.04m (Fig. 5.5). This program divides the watershed into multiple sub-watersheds, which are further sub divided into units of unique soil, land-use and slope characteristics known as hydrologic response unit (HRU). The hydrology of the watershed is computed at the HRU level by using the climate data. The weather generator (WGEN) file is used to simulate the missing climate data values. The Burhanpur sub-catchment is delineated in QSWAT model, and the drainage pattern is delineated with a drainage threshold area of 300km^2. The Burhanpur sub-catchment has been further sub-divided into 15 sub watersheds (Fig. 5.6a). The land use map, soil map and slope map (derived from DEMs) were used to create HRUs within each sub-basin. Three slope classes 0-5%, 5-10% and >10% were used with 2% threshold of land use, soil, and slope band for removing small HRUs and total 155 HRUs are formed. The minimum slope extracted from DEM is 0°, while the maximum slope is 32° near to the hilly region of the study area (Fig. 5.6b). The main land use types in the Burhanpur sub-catchment are agriculture, forest, and rangeland (Fig. 5.6c). LULC for the year 2005-06 shows forest area was 54.71%, agriculture land with 31.91% area, 5.60% area with rangeland, 5.82% area was covered with barren land and area of water bodies was 1.26% and 0.71% by urban area of the total sub-basin area. Agriculture is the largest economic activity in the sub-basin, and it is largely dependent on rainfall. In Madhya Pradesh, kharif is the main cropping season.

Cotton is the main crop, followed by the sorghum in Khandwa and Khargaon districts. Groundnut is also widely grown in the study area. In Bethi district, sorghum, wheat, and paddy are major crops. Pulses are widely cultivated as Rabi crops in all the three districts of Madhya Pradesh. In Maharashtra, the major crops grown are cotton and groundnut apart from sorghum and pearl millet. In this study, the land use land cover dataset was procured from National Remote Sensing Centre (NRSC) India at 56m resolution for the year 2005 (Fig. 5.6c; Table 3.3). The Burhanpur Sub-Catchment covers the districts of Madhya Pradesh and Maharashtra State, which consists of shallow & black soils. The dominant soil, in the region, are gentle to very gently sloping deep loamy to clayey and deep black soils The soil analogue maps

(1:2,50,000 scale) of the study area was obtained from National Bureau of Soil Survey and Land Use Planning (NBSS & LUP) Nagpur and for further classification into various soil groups this was converted in digital form in GIS platform (Fig. 5.6d; Table 3.3).

Table 5.6 Characteristics of rain gauge and stream gauging stations in Burhanpur sub-catchment

Sr. No.	Stations	Latitude	Longitude	Elevation (m)	Period of data availability
			Rain gauge stations		
1	Achalpur	21° 18' N	77° 34' E	377	1944-2013
2	Akot	21° 05' N	77° 04' E	314	1951-2013
3	Anjangaon	21° 09' N	77° 19' E	339	1944-2013
4	Atner	21° 37' N	77° 56' E	665	1944-2013
5	Bhainsdehi	21° 38' N	77° 38' E	767	1944-2013
6	Burhanpur	21° 31' N	76° 23' E	253	1945-2016
7	Chandur bazar	21° 14' N	77° 44' E	373	1944-2013
8	Chikhalda	21° 24' N	77° 19' E	1084	1976-2013
9	Dharni	21° 56' N	76° 88' E	318	1937-2016
10	Edalabad	21° 06' N	76° 06' E	225	1950-2016
11	Mulkapur	20° 88' N	76° 20' E	254	1940-2016
12	Multai	21° 76' N	78° 26' E	746	1930-2015
13	Raver	21° 25' N	76° 03' E	254	1950-2016
14	Telhara	21° 02' N	76° 49' E	286	1944-2013
			Temperature grids		
	19 grids in the Purna sub-catchment having data from 1951-2017				
			Stream gauging stations		
1	Burhanpur	21° 31' N	76° 23' E	253	1979-2013
2	Hatnur	21° 07' N	75° 94' E	216	1994-2013

- **SWAT Simulations**

The base model was run with 33 years (1981 to 2013) period climate data with 4 years warm-up period. The flow was calibrated for the period of 1998 to 2007 and validated from 2008 to 2013 with observed stream flow data. The basic statistical parameters of the observed stream flow at Burhanpur and Hatnur during calibration and validation period are presented in Table 5.7. First the baseline model was calibrated and then the future scenarios have been simulated using all the five GCMs with the calibrated parameters of the baseline model.

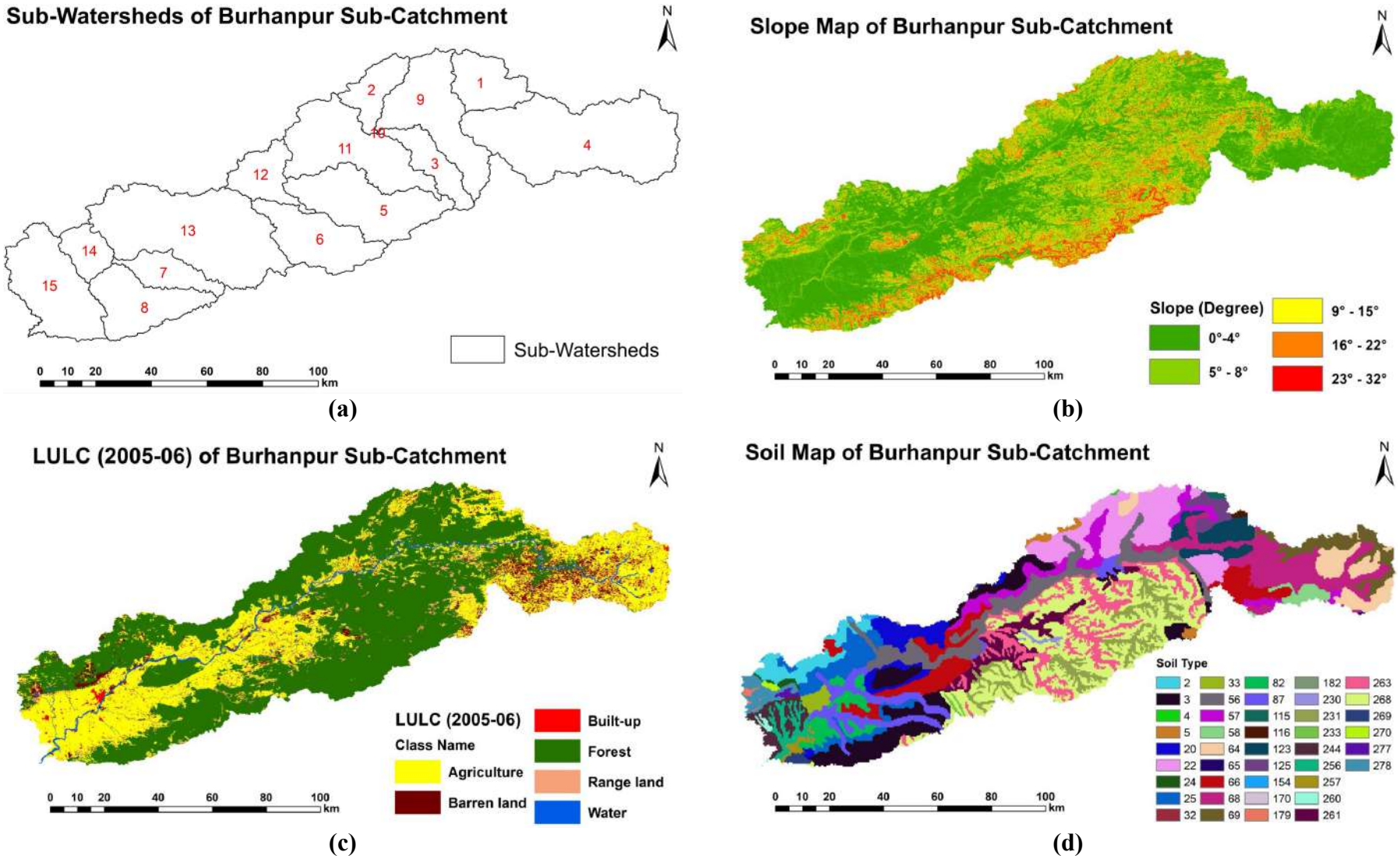

Fig. 5.6 (a) Sub-watersheds (b) Slope classes, (c) LULC classes, and (d) NBSS&LUP soil polygons, in Burhanpur sub-catchment

- **Parametric uncertainty and Sensitivity analysis**

The developed models were calibrated in SWAT-CUP in this study. The SUFI-2 algorithm was used to calibrate the simulated model for stream flow in this study. The output uncertainty of the model was quantified by the 95% prediction uncertainty band (95PPU) calculated at the 2.5% and 97.5% levels of the cumulative distribution function of the output variables. The output uncertainty in the model results is measured by P-factor and R-factor. All sources of uncertainty were mapped to a set of parameter ranges. The sensitivity analysis can also be carried out using SWAT-CUP.

Table 5.7 Daily stream flow statistics of Burhanpur sub-catchment during calibration and validation period

Statistical Parameter	Calibration Period (1998 – 2007)		Validation Period (2008 – 2013)	
	Burhanpur	**Hatnur**	**Burhanpur**	**Hatnur**
Average (m^3/s)	143.85	172.23	159.93	194.88
Standard deviation (m^3/s)	878.96	764..02	515.04	672.99
Peak discharge (m^3/s)	32686.0	15673.31	8612.79	13497.0

Sensitivity analysis is a process to identify a few individual parameters which play an important role in the hydrological modeling (Sandu and Virsta 2015). The hydrological processes are represented by parameters, and sensitivity analysis provides information on the most important processes in hydrological study. Also, the sensitivity analysis eliminated the non-sensitive parameters, and decreases the number of parameters in the calibration process. The most used types of sensitivity analysis are one-at-a-time or local sensitivity analysis, and all-at-a-time or global sensitivity analysis. In one at a time sensitivity analysis, only one parameter changes at a time, while all other parameters are kept constant to identify its effect on model output or objective function (Khalid et al. 2016; Abbaspour et al. 2017). In this case, less number (3–5) of model runs are sufficient. In global sensitivity analysis, all parameters are changing simultaneously; therefore, large number of models runs (500–1000 or more, depending on the number of parameters and procedure) are required, to see the impact of each parameter on the objective functions. Both the methods have limitations and advantages. Limitation of one at a time is that sensitivity of one parameter is dependent on the values of other parameters, which are all fixed to values whose accuracy is not known. The limitation of global sensitivity analysis is that parameter ranges and the number of runs affects the relative sensitivity of the parameters. The advantage is that global sensitivity analysis produces more reliable results (Abbaspour et al. 2017).

In global sensitivity analysis parameter sensitivities are determined by calculating the multiple regression equations and the sensitivities can be estimated by measuring average changes in the objective function resulting from changes in each parameter. This gives relative sensitivity based on the linear approximations and two statistical parameters (t-test and p-value) were computed. The t-stat (student's t distribution) uses to identify the relative significance of each parameter. The p-value is used to measure the sensitivity of the parameter as per 95% confidence. The larger absolute value of t-stat and p-value of <0.05 is generally accepted as sensitive parameter (Abbaspour 2011). The twelve parameters were selected for calibration viz. CN2, ALPHA_BF, GW_DELAY, GWQMN, GW_REVAP, ESCO, Sol_AWC, OV_N, SLSUBBSN, HRU_SLP, SLSOIL, RCHRG_DP (see Table 5.3 for parameter description) based on the sensitivity analysis and protocol given in Arnold et al. (2012) and Abbaspour et al. (2015). Table 5.8 shows the sensitive parameters with their t-stat and P-values along with values used in calibration with their minimum maximum and fitted values. The parameters of QSWAT model have been calibrated for stream flow within their defined ranges.

- **Performance evaluation**

The Table 5.9 shows the performance indices of the developed model at Burhanpur and Hatnur Reservoir. The R^2 and NSE values for discharge were 0.70, 0.65 during calibration and 0.70 and 0.70 during validation at Burhanpur. Table 5.9 also shows the P-factor and R-factor values of the developed model for streamflow. Fig. 5.7a and 5.7b shows best fit between observed and simulated values of discharge for calibration and validation periods for Burhanpur and shows that the observed and simulated data have similar trends.

Table 5.8 Parameters used in calibration and their calibrated values

S. No.	Parameter	Minimum Value	Maximum Value	Fitted Value	t-stat	P-value	Rank
1.	CN2	-0.2	0.2	-0.17	41.66	0	1
2.	ALPHA_BF	0	1	0.73	0.04	0.963	12
3.	GW_DELAY	0	50	40.5	0.49	0.624	9
4.	GWQMN	0	5000	2000	-22.94	0	2
5.	GW_REVAP	0	0.2	0.17	-21.96	0	3
6.	ESCO	0	1	0.64	1.43	0.05	7
7.	Sol_AWC	0.02	0.2	0.19	11.15	0	4
8.	OV_N	0.01	1	0.30	0.12	0.459	11
9.	SLSUBBSN	0	10	2.35	1.87	0.059	6
10.	HRU_SLP	0	1	0.06	0.35	0.888	10
11.	SLSOIL	0	150	90	9.27	0	5
12.	RCHRG_DP	0	1	0.40	0.85	0.391	8

5.2.3 Prediction of Inflows into Hatnur Reservoir and outflow simulation

The flow of Purna and Burhanpur sub-catchments were added at the Hatnur Reservoir and the performance indices mentioned above (R^2, NSE and PBIAS) were used to evaluate the performance of the simulated SWAT model at Hatnur reservoir. The performance of the simulated model was evaluated at daily scale as shown in Fig. 5.7c and 5.7d. The R^2 and NSE values during the calibration period (1998-2007) have been found to be 0.71, 0.67 and 0.72, 0.71 for validation period (2008-2013). The PBIAS values for calibration and validation were -8.7 and -6.2 (see Table 5.9).

The Hathnur reservoir is one of the major reservoirs of Tapi Basin. The Hathnur dam is the outlet of Upper Tapi sub-basin, constructed 7-8 km downstream of confluence of the Tapi and Purna Rivers. The Hathnur reservoir is a medium-sized reservoir having gross storage capacity of 388 Mm^3 and live storage capacity of 255 Mm^3. The Hathnur dam was completed in 1982 and commissioned in 1983. The full reservoir level in Hathnur reservoir is at RL 214m, which corresponds to a water storage of 388 Mm^3. The maximum height of the masonry dam above the riverbed is 25.5m. The revised operating policy of the Hathnur reservoir suggests non impoundment of water in the reservoir till 21st August, with a minimum lake level of RL 209.5m, against a storage capacity of 180 Mm^3. After this period, the dam gates are gradually closed for filling up the reservoir up to FRL of 214m till 15th October, to achieve the storage volume of 388 Mm^3 (WRD 2015). In present study, the inflows into the Hathnur reservoir are considered as combined flows of the Purna and Upper Tapi Rivers observed at Yerli and Burhanpur stations, respectively.

For the safety of dam structures, it is necessary to understand the hydrology of reservoirs. The water balance for reservoirs includes inflow, outflow, rainfall on the surface, evaporation, seepage from the reservoir bottom and diversions. The SWAT model offers three alternatives for estimating outflow from the reservoir. The first option allows the user to input measured outflow. The second option, designed for small, uncontrolled reservoirs, requires the users to specify a water release rate. When the reservoir volume exceeds the principal storage, the extra water is released at the specified rate. Volume exceeding the emergency spillway is released within one day. The third option, designed for larger, managed reservoirs, has the user specify monthly target volumes for the reservoir. The reservoir module of SWAT model has been used to simulate the Hathnur reservoir using the Target-Storage method. The inflow of Burhanpur and Purna sub-catchments were added to compute the total inflow in Hathnur dam. The monthly target storage for monsoon months (June-October) were provided based on existing rule curve of the reservoir, while the target storage of FRL was used for remaining months to

maximise the reservoir storage. The different parameters used for simulating the reservoir are shown in Table **A3 (in Annexure)**. The simulated outflows from Hatnur reservoir using the target-storage method during the calibration and validation are shown in Fig. 5.7e-f and the performance statistics are shown in Table 5.9. The performance metrics shows that the target-storage approach used for simulation of Hatnur reservoir is capable to simulate the reservoirs based on the existing rule-curve policy. The similar parameters were employed for simulation of the reservoir during the future period also.

(a)

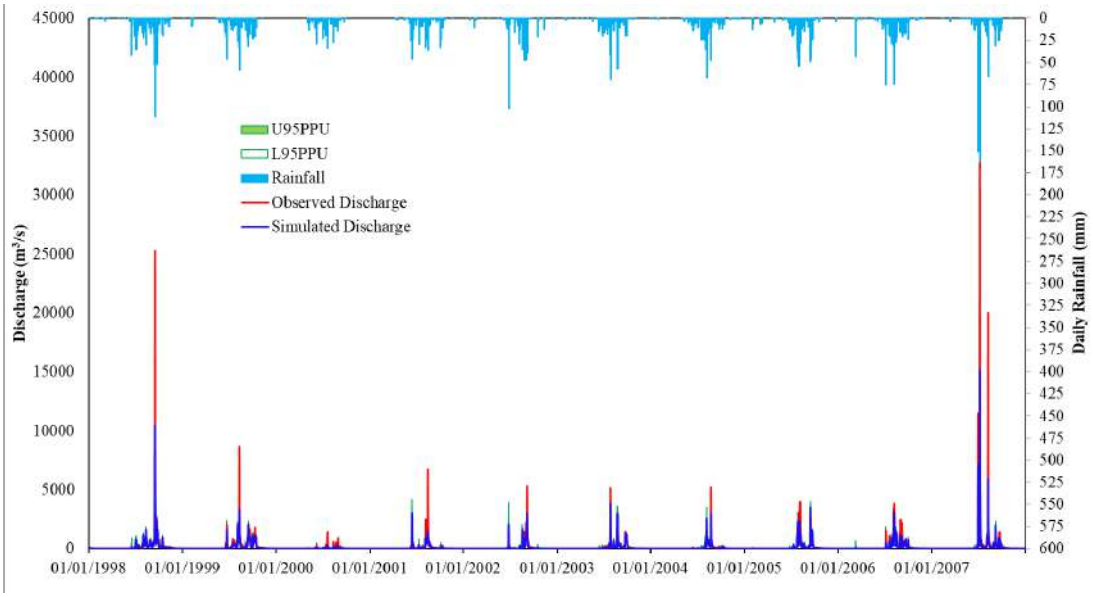

(b)

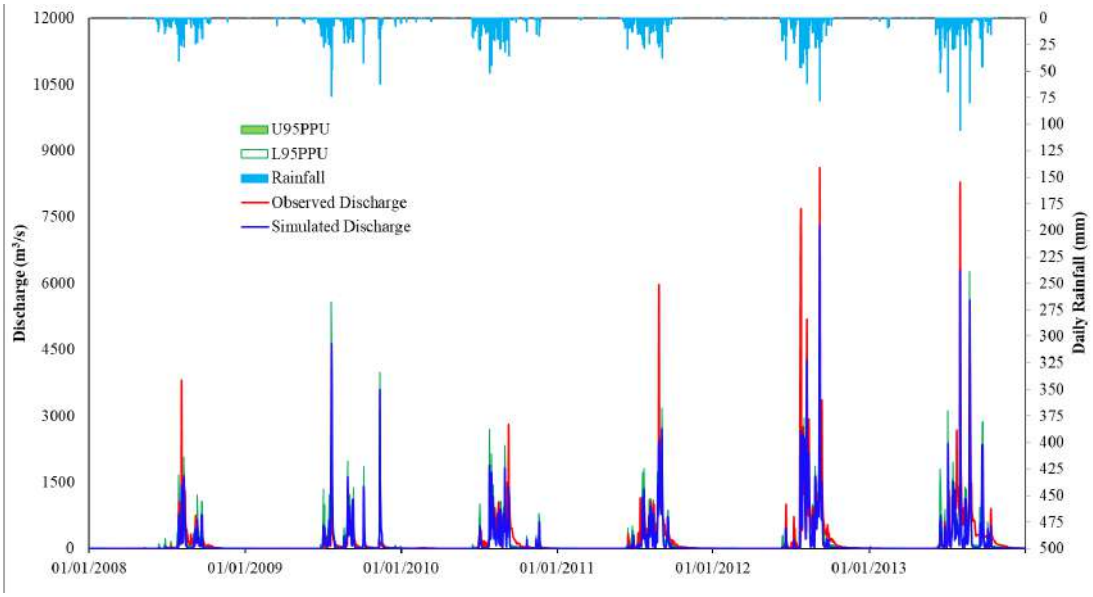

(c)

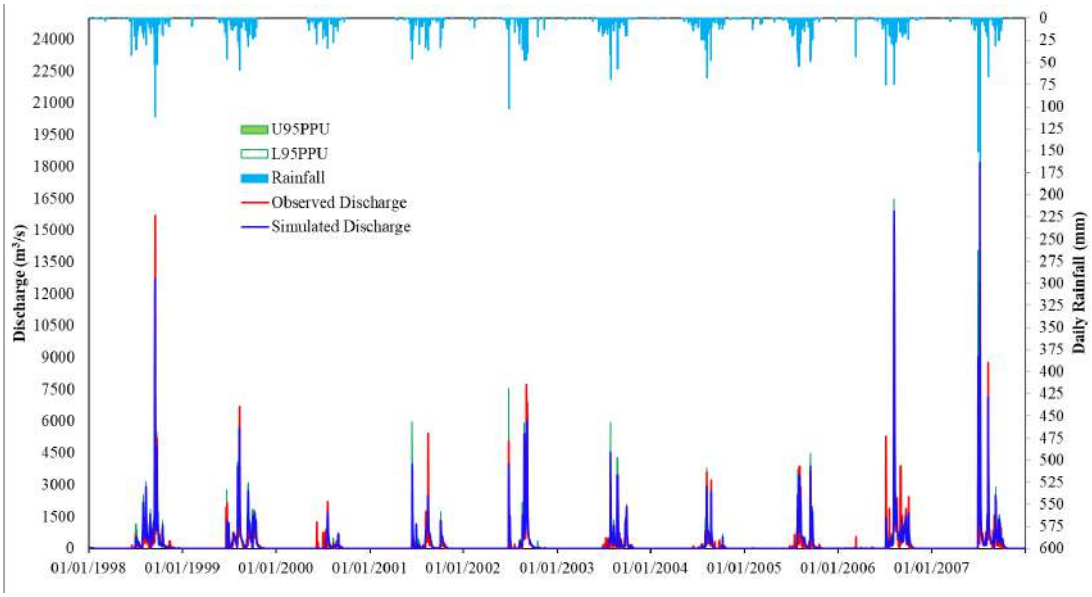
U95PPU
L95PPU
Rainfall
Observed Discharge
Simulated Discharge
Discharge (m³/s)
Daily Rainfall (mm)
01/01/1998
01/01/1999
01/01/2000
01/01/2001
01/01/2002
01/01/2003
01/01/2004
01/01/2005
01/01/2006
01/01/2007

(d)

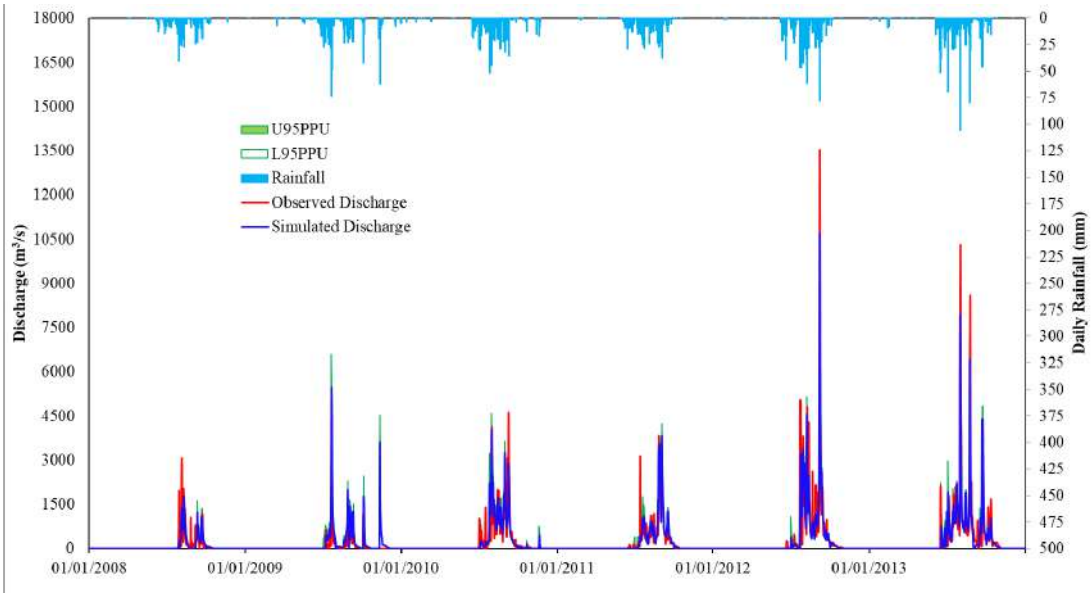
U95PPU
L95PPU
Rainfall
Observed Discharge
Simulated Discharge
Discharge (m³/s)
Daily Rainfall (mm)
01/01/2008
01/01/2009
01/01/2010
01/01/2011
01/01/2012
01/01/2013

(e)

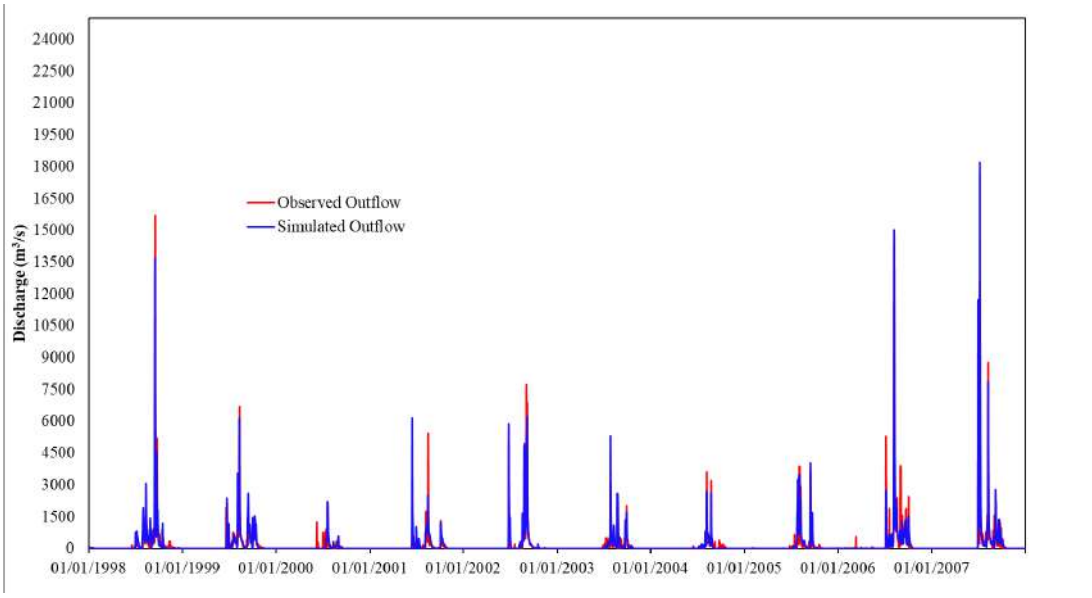
Observed Outflow
Simulated Outflow
Discharge (m³/s)
01/01/1998
01/01/1999
01/01/2000
01/01/2001
01/01/2002
01/01/2003
01/01/2004
01/01/2005
01/01/2006
01/01/2007

(f)

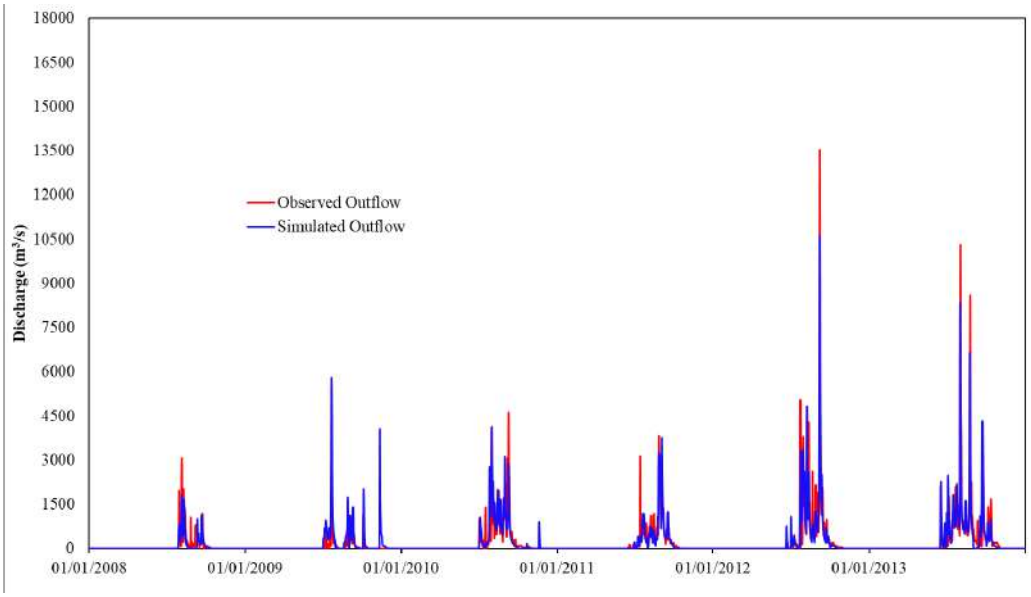

Fig. 5.7 Comparison of observed and simulated discharge at Burhanpur during (a) calibration, (b) validation period; inflow into Hatnur reservoir during (c) calibration and (d) validation period; and observed and simulated outflows from Hatnur reservoir during (e) calibration and (f) validation period

Table 5.9 Performance[$] evaluation of developed model at Burhanpur and Hatnur Reservoir

Period	Year	p-factor	r-factor	R^2	NSE	PBIAS (%)
Burhanpur sub-catchment						
Calibration	1998-2007	0.68	0.07	0.70	0.65	23.8
Validation	2008-2013	0.60	0.06	0.70	0.70	22.9
Inflow into Hatnur Reservoir						
Calibration	1998-2007	0.60	0.05	0.71	0.67	-8.7
Validation	2008-2013	0.70	0.06	0.72	0.71	-6.2
Outflow from Hatnur Reservoir						
Calibration	1998-2007	-	-	0.71	0.66	-8.6
Validation	2008-2013	-	-	0.70	0.68	-4.1

$The reference values of the performance indicators, as specified in Moriasi et al. (2007), are included in Table 2.1.

5.3 HYDROLOGICAL MODELING OF MIDDLE TAPI BASIN

The Middle Tapi Basin Starts from Hatnur Reservoir and extends up to Ukai Reservoir. Girna Reservoir is also one of the significant reservoirs which lies within watershed, which is constructed at one of the tributaries of Tapi River, namely Girna River. The total length of Tapi River from origin to outfall into the Arabian Sea is 724 km. The length of Middle Tapi River is 319.3 km covers an area of 32,927 km^2 under Middle Tapi basin. At Madhya Pradesh, the Tapi River flows for 282 km at the beginning, and it includes 54 km of flow at which the river shares boundary both with Madhya Pradesh and Maharashtra State. Before entering Gujarat, it flows for 228 km at Maharashtra, and at Gujarat, it flows for 214 km.

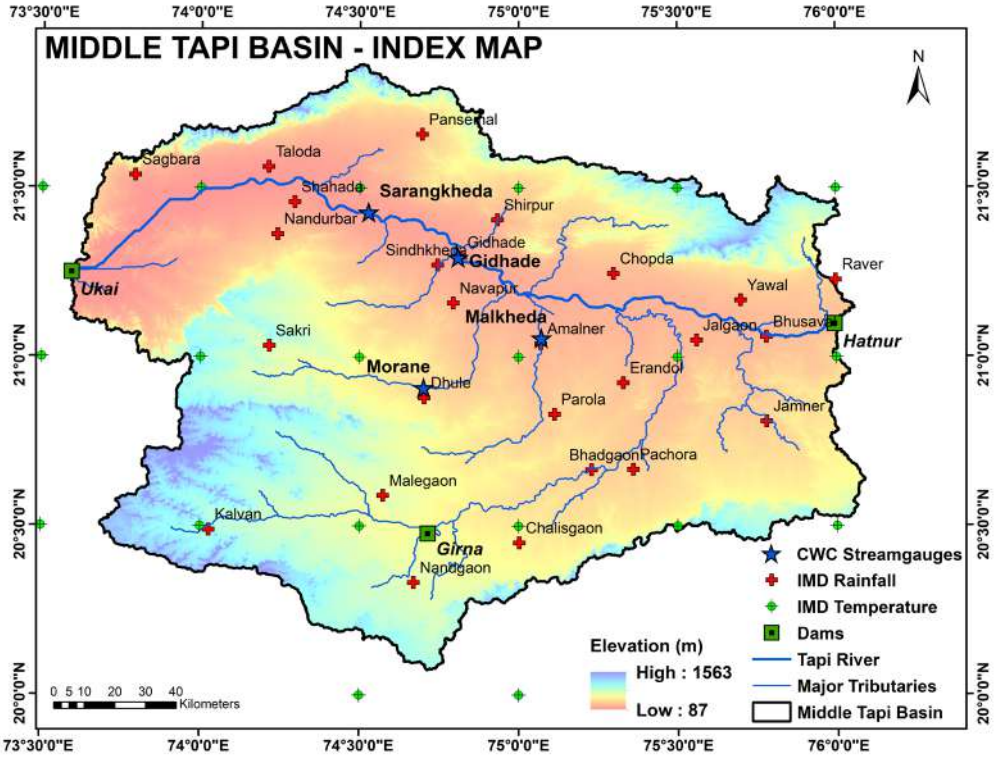

Fig. 5.8 Index map of Middle Tapi Basin

The index map showing DEM, location of rain gauge stations, stream gauging stations and tributaries of middle Tapi River are shown in Fig. 5.8. The main tributaries of MTB are River Girna, Bori, Panjhra, Amravati, Buna, and Anjali which join the main Tapi River from left and River Tori, Arunavati, Umri and Gomai join from Right. The Girna River is an important left-bank tributary covers the area 10,061 km^2, accounting nearly 31 % catchment area of the Middle Tapi River. The MTB bounded by Saputara Ranges from northern direction, Ajanta and Satmala Hills in the southern direction and the Western Ghats in west direction. The MTB covers a large area in the State of Maharashtra (89.4%) besides regions in the states of Madhya Pradesh (5.48%) and Gujarat (5.12%).

- **Data used and their sources**

The datasets used in this study for the generation of water balance parameters are Digital Elevation Model (DEM), Hydrological soil group map, Land use land cover (LULC) map, and datasets such as precipitation; temperature, other climatic data (Relative Humidity, Solar radiation, Wind Speed) and observed streamflow data. The details of the gauging stations of rainfall and streamflow are in Table 5.10.

Table 5.10 Characteristics of rain gauge stations and stream gauging stations

S. No.	Station	Latitude	Longitude	Elevation (m)	Data Availability
1	Amalner	21° 75' N	75° 4' E	184	1930-2016
2	Bhadgaon	20° 75' N	75° 14' E	261	1930-2016
3	Bhusaval	21° 75' N	75° 47' E	202	1942-2016
4	Chalisgaon	20° 75' N	75° 0' E	346	1930-2016
5	Chopda	21° 75' N	75° 18' E	202	1930-2016
6	Dhule	20° 74' N	74° 42' E	314	1942-2016
7	Erandol	20° 75' N	75° 20' E	217	1930-2016
8	Gidhade	21° 74' N	74° 49' E	148	1976-2016
9	Jalgaon	21° 75' N	75° 34' E	198	1991-2016
10	Jamner	20° 75' N	75° 47' E	256	1942-2016
11	Kalvan	20° 74' N	74° 2' E	604	1930-2016
12	Malegaon	20° 74' N	74° 34' E	467	1942-2016
13	Nandgaon	20° 74' N	74° 40' E	469	1930-2016
14	Nandurbar	21° 74' N	74° 14' E	216	1942-2016
15	Navapur	21° 74' N	74° 47' E	201	1942-2016
16	Pachora	20° 75' N	75° 22' E	263	1930-2016
17	Pansemal	21° 74' N	74° 42' E	243	1962-2011
18	Parola	20° 75' N	75° 7' E	251	1930-2016
19	Raver	21° 76' N	76° 0' E	250	1942-2016
20	Sagbara	21° 73' N	73° 47' E	175	1952-2013
21	Sakri	21° 74' N	74° 13' E	494	1942-2016
22	Shahada	21° 74' N	74° 17' E	140	1942-2016
23	Shirpur	21° 25' N	74° 56' E	190	1950-2013
24	Sindhkheda	21° 74' N	74° 45' E	163	1944-2016
25	Taloda	21° 74' N	74° 13' E	123	1930-2016
26	Yawal	21° 75' N	75° 42' E	246	1930-2016
		Temperature Grids			
IMD grids are used for the Middle Tapi Basin 0.5° X 0.5° resolution having data from 1951-2017					
		Stream Gauging Stations			
1	Sarangkheda	21°26'N	74°31'E	130	1977-2013
2	Ukai	21°15'N	73°35'E	72	1991-2013
3	Gidhade	21°17'N	74°49'E	188	1970-2013
4	Malkheda	21°3'N	75°4'E	98	1974-2004
5	Morane	20°55'N	74°42'E	277	1978-2004

- **SWAT model Setup**

To determine the collective impacts of water management, land management, and sediment yields in a vast area of the basin with continuously changing environmental variables for a period, the development of the swat model has been carried out (Arnold et al. 2012). It created several hydrologic response units (HRUs) systems using geographical data such as soil

characteristics, land use data, and slope data. The threshold value is necessary to identify the area required to form the stream origin to prepare the basins networks. According to Vilaysane et al. (2015), the threshold area decreases with the increase in the detailing of sub-basin networks and the number of HRUs (See Fig. 5.9a). The threshold limit for land use characteristics, soil characteristics, and slope class were used as 5, 5, and 5%, respectively (See Fig. 5.9b), considering the study's goal and paying attention to HRU characteristics as significant elements determining runoff. As a result, the Middle Tapi basin has a total of 1,118 HRUs. Sub-basin classification to HRUs improves accuracy, providing a more detailed physical description (Mtalo et al. 2012). HRU analysis identified and analysed spatial scale data such as land use/land cover, soil, and slope. The Arc SWAT maps were 100% overlapped; the prepared soil map, LULC map, slope map, and delineated watershed were overlapped entirely. After running the SWAT model simulation, the model input was completed, and consequently, the output from the model was produced and analysed. The LULC and slope classes for MTB are shown in Fig. 5.9c and 5.9d respectively.

- **Calibration and Validation**

The process of fine-tuning or changing model parameters and their values within suggested ranges to maximize the model output to fit the actual observed datasets is known as Calibration (Vilaysane et al. 2015). For calibration of the model using observed streamflow data, the Sequential Uncertainty Fitting-2 (SUFI-2) approach had been used in SWAT-CUP software. The process of estimating the degree to which a model accurately represents the observed datasets from the standpoint of the model's intended usage is known as validation. It is a method of comparing the outputs from the model with an observed dataset that does not require any further adjustments to the parameter values (Abraham et al. 2007). The method was repeated until the period for validation of the stream flows was simulated and ultimately finalised that the model performed adequately.

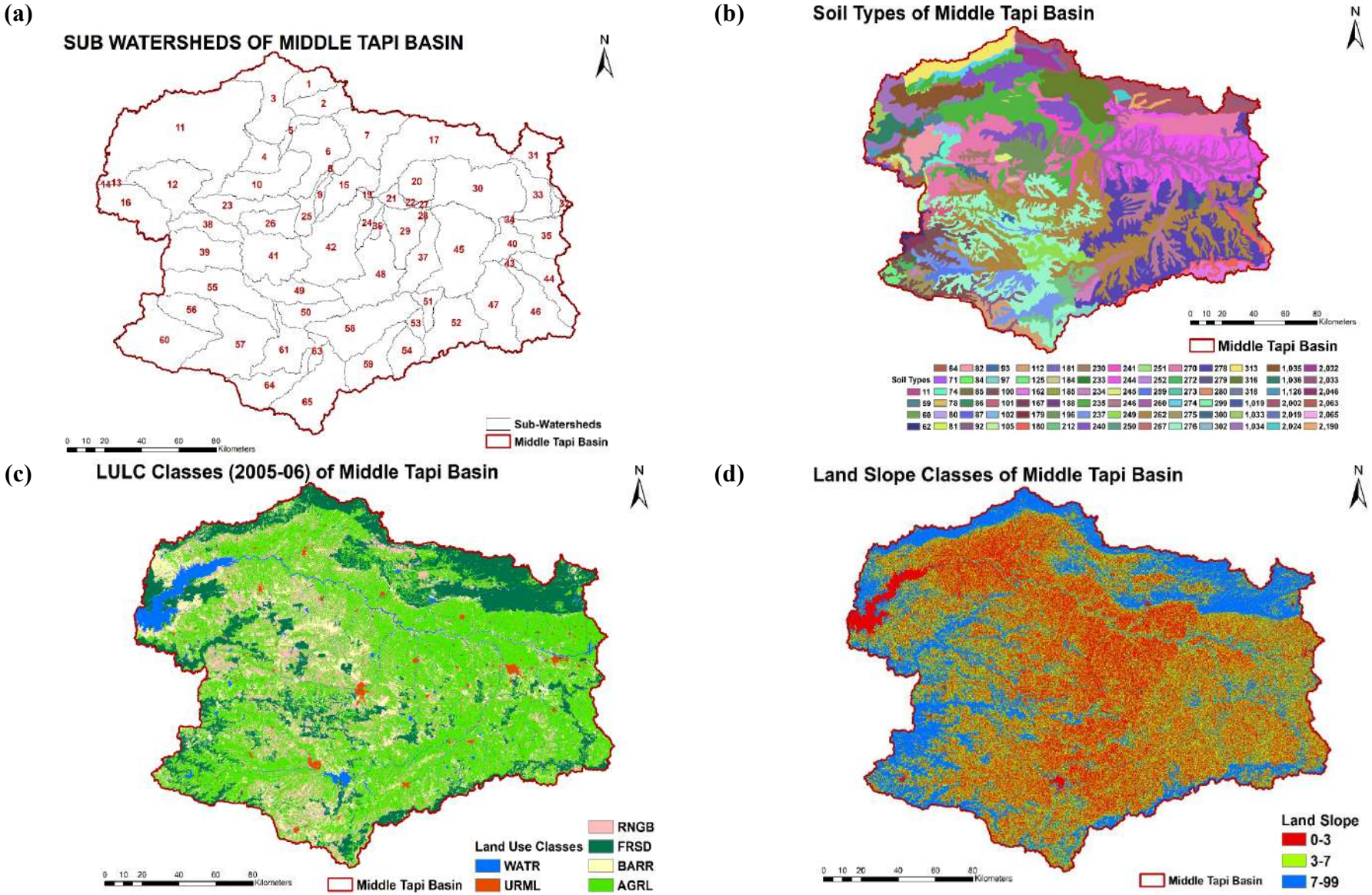

Fig. 5.9 (a) Sub-watersheds (b) NBSS&LUP soil polygons, (c) LULC classes, and (d) Slope classes, in Middle Tapi basin

As a result, calibration and validation were conducted out utilizing daily observed flow data for 20 years (1994–2013) in this work. Model warmup (1994–1997), calibration (1998–2007), and validation (2008–2013) phases were used to partition the data. A longer calibration time was employed to improve model parameterization and reduce the uncertainty of outputs from the model (Gashaw et al. 2018). The flow statistics during calibration and validation period at varius gauging stations are shown in Table 5.11.

Table 5.11 Daily stream flow statistics of Middle Tapi Basin during calibration and validation period

Statistical Parameter	**Calibration Period (1998 – 2007)**			**Validation Period (2008 – 2013)**		
(In m^3/s)	**Sarangkheda**	**Ukai**	**Gidhade**	**Sarangkheda**	**Ukai**	**Gidhade**
Average	263.24	297.21	246.06	224.79	248.14	219.21
Standard deviation	1,029.39	1,069.8	996.2	642.09	667.6	657.41
Peak discharge	23,400	22,400	23,130	9,163	7,520	9,644

Coefficient of determination (R^2) and Nash–Sutcliffe efficiency (NSE) are used to estimate the strength of correlation between simulated and measured data along with the prediction capability as per simulated data. Values of R^2 ranging from 0 to 1, where 0.5 is the acceptable value and higher value of R^2 higher would be the corelation between simulated and measured data (Santhi et al. 2001). NSE is a number that ranges from $-\infty$ to 1, with 1 being the highest value. Values between 0 and 1 are considered acceptable; however, values less than 0 indicate that the performance is unsatisfactory (Moriasi et al. 2007). Percent bias (PBIAS) has an optimum value of 0.0, and lesser the value of PBIAS, higher will be the accuracy of simulation. PBIAS measures the degree of over estimation or under estimation of the overall simulated data with respect to observed data.

- **Sensitivity Analysis and Performance Evaluation**

Sensitivity analysis is a process in which each parameter is changed within its absolute range while all other values remain constant. The process was conducted for 19 different parameters. With the change in the parameters used as input of the SWAT model, the output variables also change in magnitude. This process of finding out the rate of difference between those is known as Sensitivity Analysis (Moriasi et al. 2007). This is an essential step in calibrating the model to figure out critical parameters and parameter precision. To identify the most essential SWAT parameters for this study, 19 flow parameters (Table 5.12) from Absolute_SWAT_Value.txt on SWAT-CUP were initially chosen. In the SWAT-CUP, there are two methods to carry out

parameter sensitivity analysis: First is global sensitivity analysis, which enables you to change every parameter at once, and second is one-at-a-time sensitivity analysis, which allows you to change only a single parameter at once. SWAT-CUP 2012 used global sensitivity analysis to accomplish this. Sensitivity was measured and assessed using the t-stat and the p-value indices (Abbaspour et al. 2017); higher values of t-stat indicate better sensitivity, and a p-value tends to zero indicates greater signification (Chaibou Begou et al. 2016). The sources of uncertainty in distributed models are parameter uncertainty, model input uncertainty, response uncertainty, and structural uncertainty, according to Yang et al. 2008. It is critical that the model undergoes extensive calibration and uncertainty analysis to produce a good result and assist judgments on different management methods in the areas of climate change, LULC change pollution control, and water allocation. The SUFI-2 algorithm, which accounts for all uncertainty, was used to conduct the uncertainty analysis for this investigation.

Table 5.12 Selected Parameters with its maximum minimum and fitted values

S. No.	Parameter Name	Min value	Max value	Fitted Value	t-Stat	P-Value	Rank
1	*R__CN2.mgt*	-0.2	0.2	-0.0972	-11.27	0	1
2	*R__SOL_AWC(..).sol*	0	0.8	0.476	0.92	0.36	15
3	*V__ESCO.bsn*	0.4	0.9	0.7865	1.14	0.26	18
4	*V__GWQMN.gw*	4000	5000	4555	-0.12	0.9	7
5	*V__GW_REVAP.gw*	0.1	0.25	0.22435	1.37	0.17	19
6	*V__REVAPMN.gw*	50	150	53.9	0.81	0.42	14
7	*V__GW_DELAY.gw*	100	200	165.9	0.29	0.77	10
8	*V__ALPHA_BF.gw*	0	0.4	0.3004	-0.53	0.6	6
9	*R__SOL_K(..).sol*	-0.6	0.3	-0.5739	-1.3	0.19	4
10	*R__OV_N.hru*	0.3	0.9	0.5022	0.38	0.7	12
11	*R__SOL_BD(..).sol*	1.1	1.4	1.2773	-1.85	0.07	2
12	*V__HRU_SLP.hru*	0.001	0.008	0.001175	0.94	0.35	16
13	*V__SURLAG.bsn*	0.1	1.5	1.4202	0.35	0.73	11
14	*V__RCHRG_DP.gw*	0.003	0.01	0.009461	-1.39	0.16	3
15	*V__EPCO.bsn*	0.7	0.9	0.8118	-1.27	0.21	5
16	*R__SOL_ZMX.sol*	0.2	0.5	0.4235	0.02	0.98	9
17	*R__SOL_Z(..).sol*	0.3	0.7	0.69	1.04	0.3	17
18	*R__SLSUBBSN.hru*	0.2	0.4	0.2606	0	1	8
19	*R__SOL_ALB(..).sol*	-0.7	-0.5	-0.6998	0.51	0.61	13

The ranges of the 19 selected parameters given in Table 5.12 were changed to undertake a global sensitivity analysis. This analysis of the model parameters requires many simulations. In Table 5.12, the p-values, and t-stats for each of the parameters is arranged rank wise with the most sensitive parameter at top and least sensitive at bottom of the bar chart. The SCS

runoff curve number (CN2) is the most sensitive parameter, which highly affects the change in simulation. Other than that, Moist bulk density (SOL BD), Deep aquifer percolation fraction (RCHRG DP), and Saturated soil hydraulic conductivity (SOL K) were all highly sensitive with p-values less than 0.20, according to the global sensitivity analysis.

As shown in Table 5.12, After conducting simulations using SWAT CUP, the spatial parameter CN2 is coming out to be between -0.2 to 0.2 with fitted value of -0.097 having a mixed land-use situation throughout the middle basin. All the land-use classes were captured by the HRUs that were created during the delineation process. The soil layer's available water capacity for a range between 06% and 30%. The soil texture at MTB is mostly clay, loam at some portions, and sandy as least available with typical bulk density 1.0 to 1.4 g/cm^3 of in different soil types. Deep aquifer percolation fraction varies from a range of 0.003 to 0.01. For the channel, the average hydraulic conductivity was 18 mm/h. The period of the series of data, data frequency, conditions of climate, and basin type all may affect the hydrologic model's calibration. Based on the average and standard deviation of total annual precipitation. As a result, all three rainfall circumstances are included in the historical precipitation forcings analysed in this study. This was done to ensure that the SWAT model's calibration for various rainfall situations could perform optimally for future precipitation variations. As per the fitted values from every selected parameter, the SWAT model was calibrated on a daily scale at three different stations, Sarangkheda, Gidhade, and inflow at Ukai Dam for the years 1998-2007.

Since a long period of 10 years has been selected for the calibration, it included all the different types of rainfall conditions, including low, medium, and high rainfall, which resulted in different inflow conditions, including low, medium, and high. The initial ranges of all parameters were given as input to SWAT-CUP within the absolute range of every parameter. After this, SWAT-CUP suggests new parameters with a change in the number of iterations. Those parameters should also be within the absolute range. To acquire the suitable range of each parameter and an adequate mix of the selected parameters, this process continues until a convenient goal function is reached.

The calibration was carried out using this method. Table 5.12 shows the maximum, minimum, and final fitted values for the parameters used as input for the discharge at three different stations. The model, which was calibrated for the daily flows at Sarangkheda, Gidhade, and inflow into Ukai Dam, which was validated using the parameters range same as used in

calibration for six years (2008–2013), proving to be very much satisfactory model performance. Table 5.13 shows the results of the performance indicators collected for daily flows at Middle Tapi Basin, including both calibration and validation periods. The coefficient of correlation values during the calibration period (1998-2007) have been found to be 0.77 and 0.81 at Sarangkheda and Gidhade respectively and NSE values during the same period (1998-2007) have been found to be 0.76 and 0.77 at Sarangkheda and Gidhade respectively. The PBIAS values for calibration period were -5.6 and -19.9 for both the stations. In addition, in Fig. 5.10a-b, and Fig. 5.11a-b, the observed and simulated streamflow at Sarangkheda, Gidhade, and inflow into Ukai Dam during the calibration and validation periods are quantitatively compared. During both calibration and validation periods, the model's performance was judged to be between very good, according to Moriasi et al. (2007). To implement the developed SWAT model to be used to study future climate change effects, it requires to have good predictability. Using daily data of rainfall for 26 different IMD stations and daily gridded IMD temperature data, the calibrated model was used to predict the daily discharge data at Sarangkheda, Gidhade, and inflow into Ukai Dam for the Period 2008–2013. For the mentioned duration, the coefficient of correlation between the observed flow and simulated flows for 2 different CWC stations (Sarangkheda and Gidhade) were 0.77 and 0.76 (Table 5.13). NSE for both stations for same duration were 0.76 and 0.7. And PBIAS values are -6.4 and -24.7. For the Validation Period 2008–2013, the calibrated SWAT model appears to be working well. The SWAT model's performance indexes during calibration (1998–2007), validation (2008–2013) establish the model's performance for future applications.

Table 5.13: Performance Indicators for Sarangkheda, Gidhade and inflows to Ukai Dam

Performance Indicators[$]	**Calibration Period (1998 – 2007)**			**Validation Period (2008 – 2013)**		
	Sarangkheda	***Ukai***	***Gidhade***	***Sarangkheda***	***Ukai***	***Gidhade***
P-factor	0.23	0.37	0.16	0.11	0.35	0.07
R-factor	0.26	0.27	0.24	0.36	0.36	0.31
R^2	0.77	0.85	0.81	0.77	0.79	0.76
NSE	0.76	0.84	0.77	0.76	0.77	0.7
RSR	0.52	0.4	0.5	0.5	0.51	0.56
MNS	0.65	0.71	0.65	0.71	0.69	0.67
PBIAS (%)	-5.6	5.7	-19.9	-6.4	13.5	-24.7
bR^2	0.63	0.65	0.75	0.61	0.48	0.67

$The reference values of the performance indicators, as specified in Moriasi et al. (2007), are included in Table 2.1.

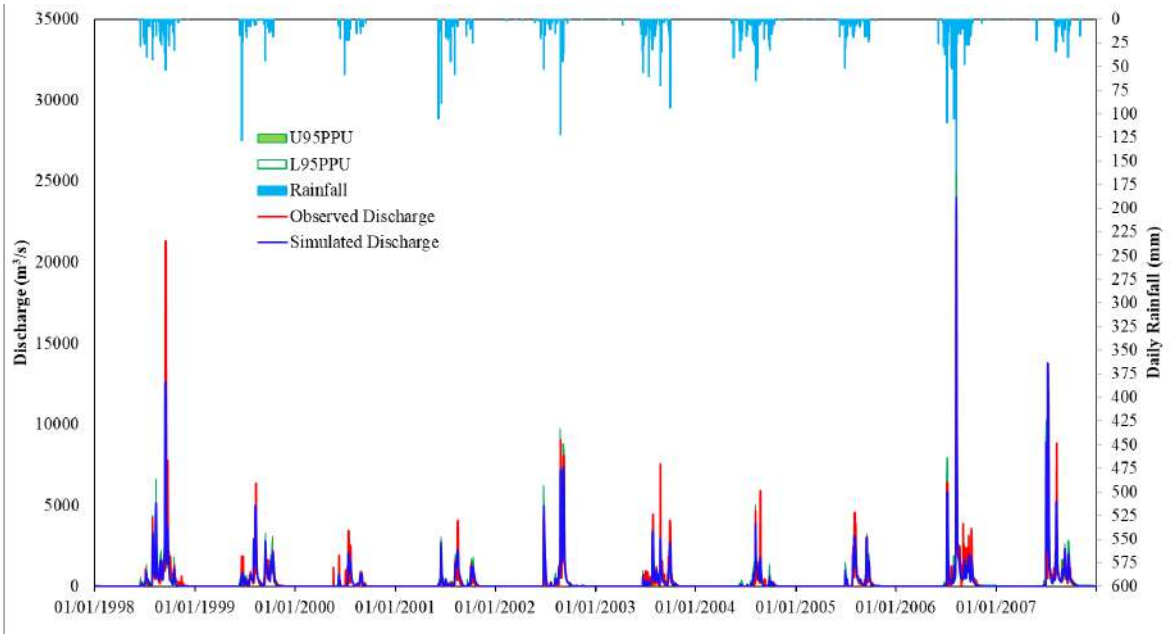

(a)

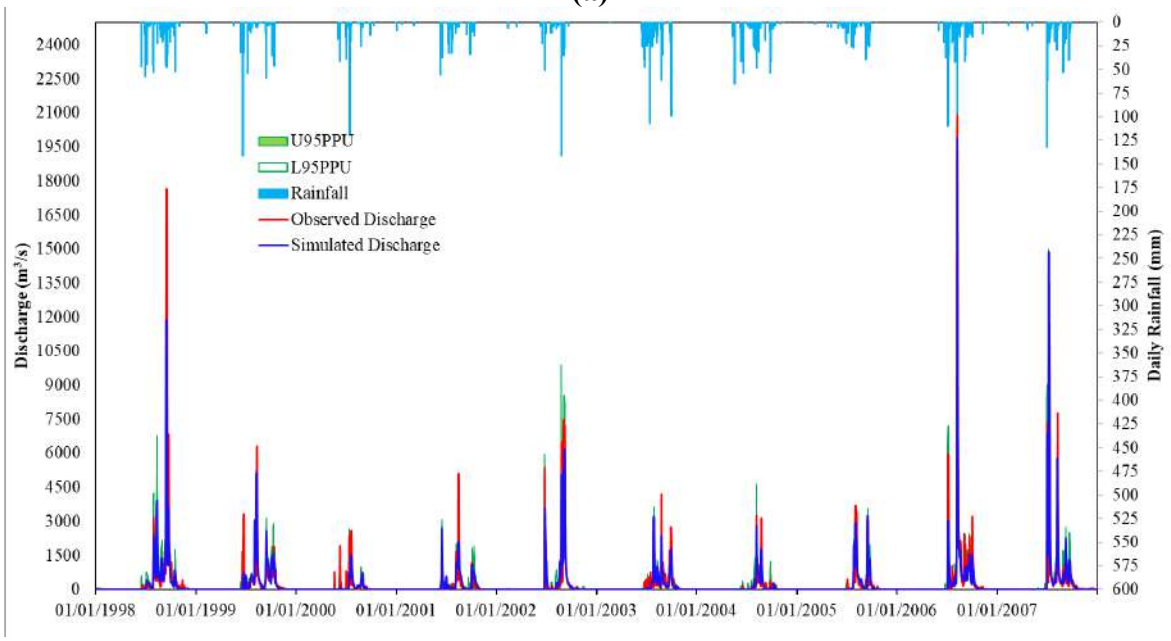

(b)

Fig. 5.10 Comparison of Observed and Simulated Flow for Calibration Period (1998-2007) (a) at Sarangkheda and (b) at Gidhade

- **Prediction of Inflows into Ukai Reservoir**

The flow of complete Upper and Middle Tapi Basin contribute for the inflow into Ukai reservoir and the performance indices mentioned above (R^2, NSE and PBIAS) were used to evaluate the performance of the simulated SWAT model. The performance of simulated model was evaluated at daily scale as shown in Fig. 5.12 (a) and 5.12 (b). The coefficient of correlation and NSE values during the calibration period (1998-2007) have been found to be 0.85, 0.84

and 0.79, 0.77 for validation period (2008-2013). The PBIAS values for calibration and validation are 5.7 and 13.5 respectively (Table 5.13).

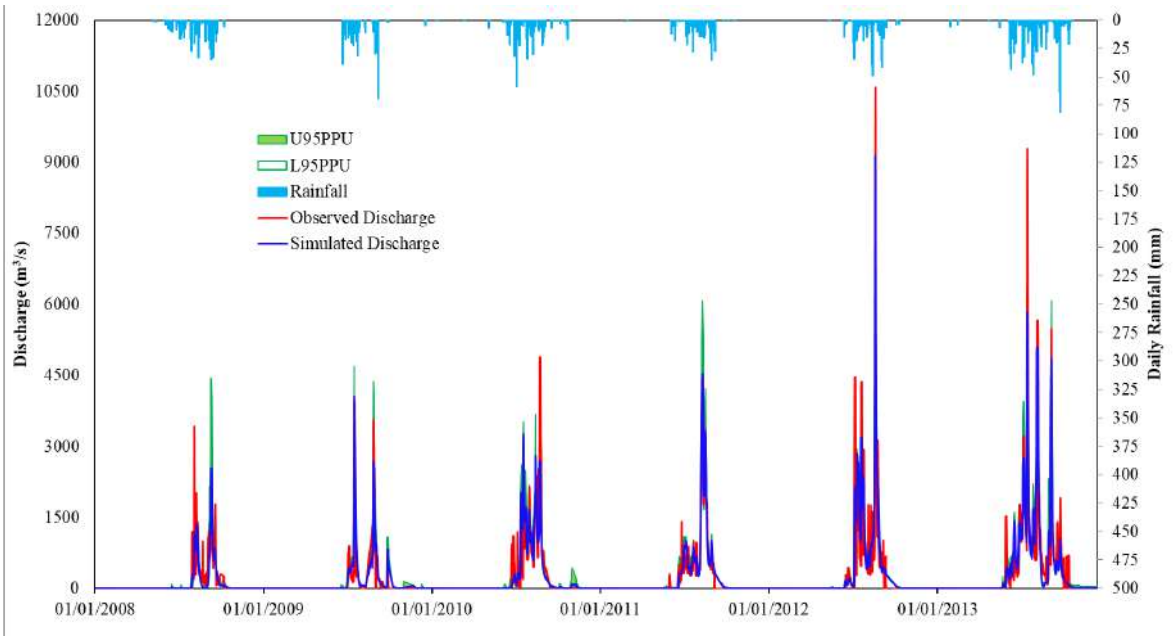

(a)

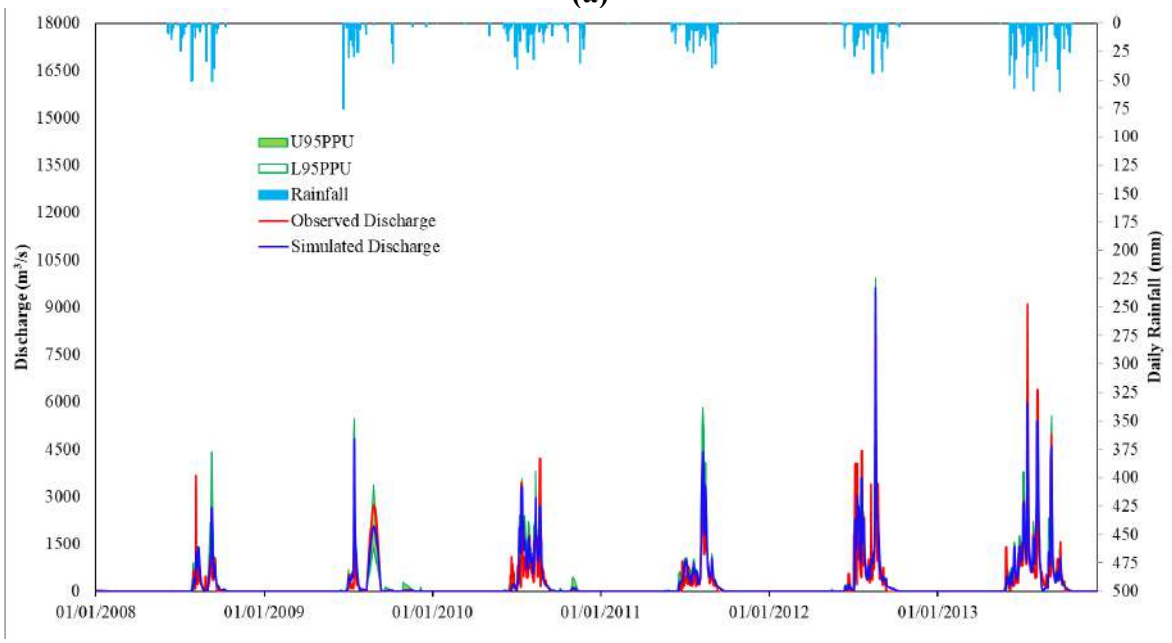

(b)

Fig. 5.11 Comparison of Observed and Simulated Flow for Validation Period (2008-2013) (a) at Sarangkheda and (b) at Gidhade

Through sensitivity analysis, model calibration, and validation, the SWAT model's performance and applicability were effectively assessed. The results revealed that surface and subsurface water model parameters are sensitive and have physical meaning, with the CN2, SOL BD, RCHRG DP, GW REVAP, and SOL K being the most sensitive parameters in the

Middle Tapi Basin in terms of stream flow prediction. The SWAT's performance in modeling stream flow at a daily scale at the MTB's outlet was satisfactory. The model has a high level of confidence and represents the water balance and outflow hydrographs at the MTB outlet well. As a result of the simulated model performance, the SWAT model can be applied to the Middle Tapi River Basin on a daily scale. The future scenarios of RCP 4.5 and 8.5 were simulated with all five GCMs using the calibrated parameters of the base model described above.

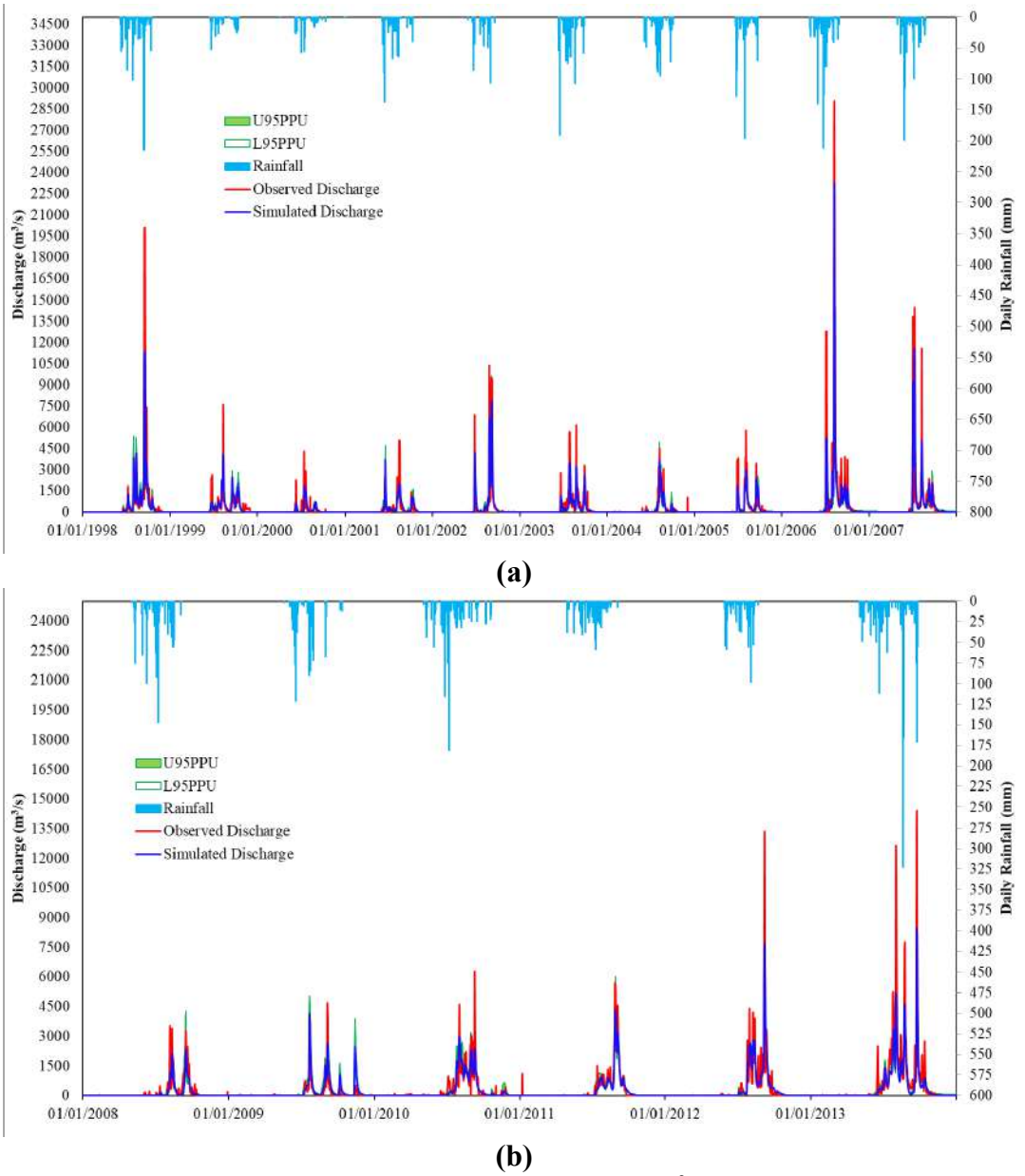

Fig. 5.12 Comparison of Observed and Simulated Flow (m^3/sec) at Ukai for (a) Calibration Period (1998-2007) and (b) Validation Period (2008-2013)

5.4 HYDROLOGICAL MODELING OF LOWER TAPI BASIN

The Lower Tapi basin (LTB) is a smaller part of the basin compared to UTB and MTB. The lower Tapi basin has an area of 2,790 km^2, with long-term streamflow availability at the Ghala stream gauging station operated by CWC. However, the streamflow measurements at Ghala are not available from June 2005. The Ukai dam is the largest multipurpose project in the Tapi basin, present at the upstream of LTB. The LTB has been frequently flooded in the past mostly due to release from Ukai Dam. (Gehlot et al. 2021) reported the increase in daily rainfall intensity with an increase in maximum 1-day and 5-day extreme rainfall (1944-2013) for the LTB. Such a significant rise in rainfall can generate a large amount of runoff volume. The large runoff in addition to riverine flow, could aggravate the flooding situation in LTB. Therefore, the development of an integrated rainfall-runoff and hydrodynamic models would be helpful in efficient water resource and flood management in LTB.

- **Prediction of Water Level using MIKE-SHE/MIKE 11 in Lower Tapi basin**

The MIKE SHE/MIKE 11 is a distributed physics-based integrated hydrological model, as explained in subsection 2.3.2. The developed model has been calibrated for continuous streamflow data at the Ghala stream gauging station over the period of 1991 to 1999 (nine years). The model has been validated for independent data of duration2000-2007 using the split sampling technique. The performance of the calibrated and validated model has also been evaluated using different statistical indices. Lastly, the total water balance of the Lower Tapi basin is estimated for simulated model parameters.

- **Development of MIKE SHE/MIKE 11 Model**

The physics-based distributed hydrological model has been developed with extensive data enlisted in Table 3.3. The detailed methodology adopted is shown in Fig. 4.3. The hydrological processes such as overland flow, evapotranspiration, and unsaturated flows are simulated in MIKE SHE whereas the river system is simulated using MIKE 11.

- **Topography**

The Topography of the study area is one of the major and important input in any hydrological model. Due to terrain variability across the LTB the DEM is developed from the contours (vector) collected from different sources considering their respective accuracy. The 20 m contours were digitized from the Survey of India (SOI) toposheet ranging from 360 m to 20 m

covering the hilly, rural, and agricultural areas from the upper and middle part of LTB. The physically surveyed 0.5 m contours for the Surat-Hazira twin city and 1 m interval contours for Lower Tapi River from Ukai dam to the Arabian Sea were collected from the SMC. The 10 m interval contours were generated from Shuttle Radar Topographic Mission (SRTM) for the remaining coastal part of LTB due to paucity of the physical survey data. The SRTM DEM has better vertical accuracy compared to other sources of DEM (Jain et al. 2018) in the low-elevation coastal zone within a 30-km area adjoining to coastline having elevation below 20 m. The contours (vector) for the LTB from different sources were combined and converted to raster by using the spatial interpolation tool 'Topo to Raster' in ArcGIS 10.6.1, as shown in Fig. 5.13. The generated DEM (30 m) was converted into .dfs2 file format by using the Grid2Mike tool in the Mike Zero toolbox. The computational time required for the model highly depends on the grid size, the grid size of 250 × 250 m spatial resolution is adopted in the current study.

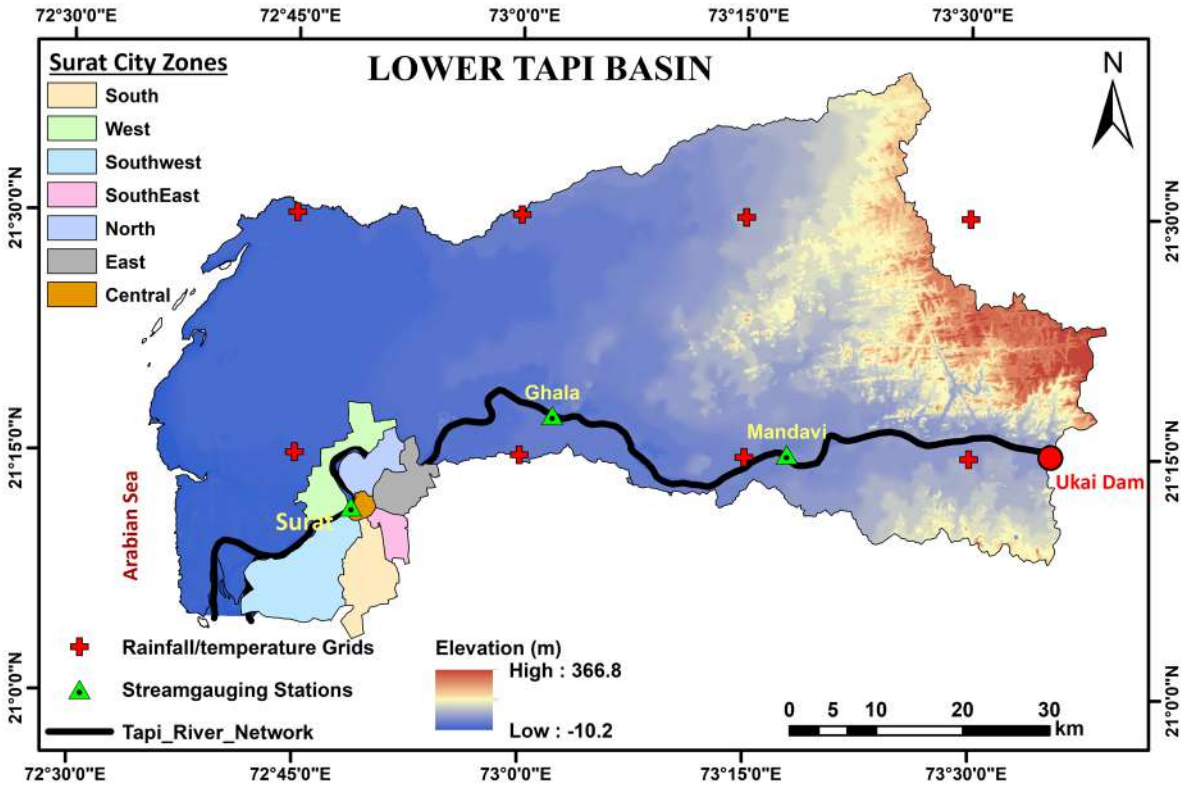

Fig. 5.13 Generated DEM with stream gauging station, rainfall/temperature grids in LTB

- **Meteorological data (Rainfall and Potential Evapotranspiration)**

The daily gridded rainfall data (0.25º×0.25º) (See Fig. 5.14a) over the lower Tapi Basin is used as input to simulate the runoff at the catchment outlet. The lumped type of Thiessen polygon method was used to obtain weighted mean precipitation across the grids using ArcGIS 10.6.1.

A similar approach has been adopted for the areal distribution of Potential Evapotranspiration (PET). The PET at each grid (0.25º×0.25º) were calculated by using temperature based Samini (2000) method explained in Eq. 2.36. The grid locations for rainfall and PET across LTB are shown in Fig. 5.14a.

- **Land use land cover classification (vegetation and surface roughness)**

The leaf area index (LAI) is a quantifiable measure of the density of vegetation, and root depth (RD) is a average Depth of root in unsaturated zone are the two crucial parameters required in the computation of actual evapotranspiration (AET). The vegetation across the lower Tapi basin was decided based on the existing land use land cover of year 2000 (See Fig. 5.14c). The LULC map was obtained from the supervised classification of the Landsat 7 satellite image shown in Fig. 5.14b. The LAI and RD values for each land class are given in Table 5.14. Also, the temporal variation of LAI, RD, and crop co-efficient for the crop and fallow land based on the cropping pattern of the basin shown in Fig. 5.15

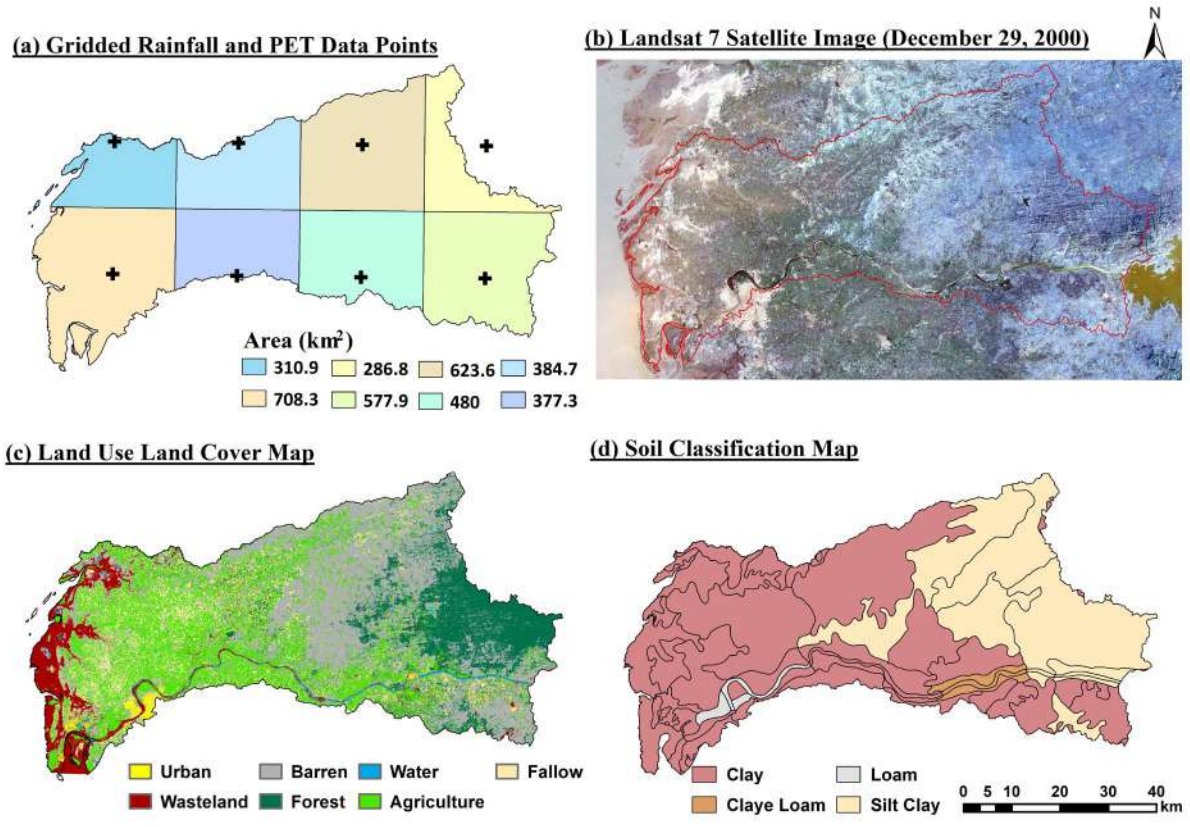

Fig. 5.14 Rainfall/PET distribution, LULC and soil classification across LTB

The roughness coefficient Manning's 'M' (inverse of manning's n) is responsible for the resistance to overland flow. The surface roughness affects the velocity of horizontal flow. The

roughness coefficient 'M' values are also based on the existing land use land cover of the area. The respective value of 'M' for each class is shown in Table 5.14. In the current study of Lower Tapi Basin, LAI, RD, and Manning's 'M' for the different land-use classes obtained from past literature (Chow et al. 1988; Loliyana and Patel 2018).

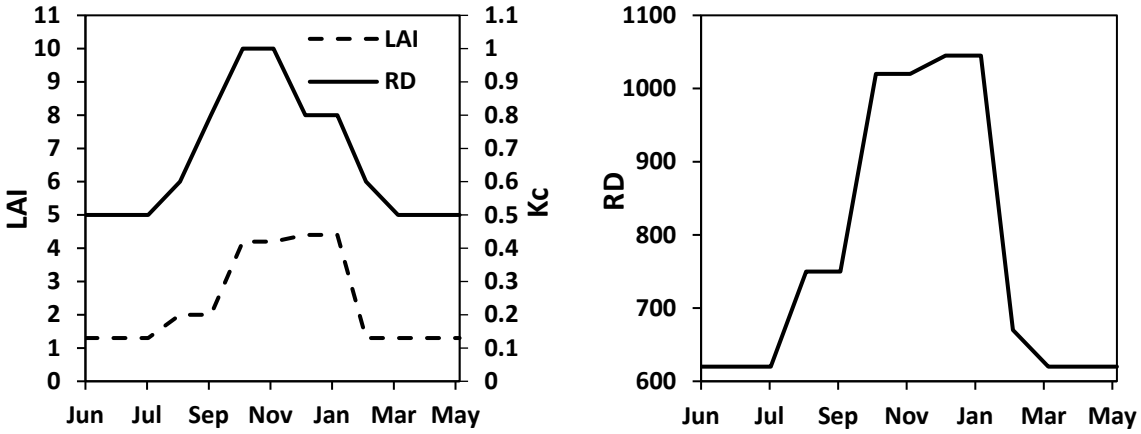

Fig. 5.15 Temporal distribution of LAI, RD and Crop Coefficient for agriculture and fallow land

- **Unsaturated zone modeling**

The soil maps obtained from the NBSS&LUP (1:2,50,000 scale) were digitised in vector format. The soil across the study domain broadly classified in four classes (See Fig. 5.14d) which was given input to the model. The 2-layer water balance method is used to model unsaturated flow in MIKE SHE. The MIKE SHE calculates the unsaturated flow only in vertical direction. The infiltration of rainfall in (downward movement) within unsaturated zone depends on the maximum water content at saturation (θ_s), water content at field capacity (θ_{fc}), water content at wilting point (θ_{wp}) and saturated hydraulic conductivity (K_s). These parameters of unsaturated flow needs to be calibrated from available data.

Table 5.14 LAI, RD, Kc and Manning's 'M' for Lower Tapi Basin

Land class	Area (%)	LAI	RD	Kc	Manning's n ($m^{-1/3}s$)	Manning's M ($m^{1/3}s$)
Agriculture	27.9	1-4.8	620-1045	0.5 - 1.0	0.035	28.57
Fallow	11.4	1-4.8	620-1045	0.5 – 1.0	0.040	25
Water	0.8	0	0	0	0.030	33.33
Forest	15.6	6	800	1	0.150	6.67
Urban	1.0	0	0	0	0.150	6.67
Barren	35.3	3	400	0	0.055	18.18
Wasteland	8.0	3	400	0	0.033	30.1
Total	**100**					

- **Channel flow model in MIKE 11**

The one-dimensional channel flow model from Ukai dam to the Arabian sea of total 125 km length developed in MIKE 11 using four editors as river network, cross sections, boundary condition and HD parameters. The river network generated from river centreline (x-y co-ordinates) in the AutoCAD file. The cross sections data at different important location were extracted from the AutoCAD file. The identical lowest point in all the cross sections were joined to form the thalweg line, whereas the left bank and right bank lines were also marked along the river. The daily outflow from the Ukai dam is taken as upstream boundary condition for the model, whereas the daily average tide at the mouth of the Arabian sea considered as downstream boundary condition. The daily tide levels were obtained by synchronising the observed tide (during December 6, 2009, to January 5, 2010) with the simulation period in both calibration and validation periods. The 1D HD model needs to be calibrated for the channel bed roughness. In the present investigation the value of channel bed roughness coefficient 'n' = 0.03 was taken from the past studies of Timbadiya et al. (2014a) and Vora et al. (2018) to simulate the channel flow in lower Tapi River of aforesaid stretch.

The channel flow model in MIKE 11 coupled with MIKE SHE to simulate the hydrological processes across Lower Tapi basin. The integrated physics based distributed hydrological model of LTB was simulated for overland flow, evapotranspiration, channel flow and unsaturated flow with distributed model parameters. The model is calibrated for total 19 parameters up to the subsurface zone and, finally, the water balance component was calculated for LTB. Due to unavailability of consistent data on underground soil strata (lithology wells), the saturated flow (ground water modeling) is not included in the current analysis.

- **Calibration and Validation of the Model (MIKE SHE/MIKE 11)**

The period of calibration (1991-1999) and validation (2000-2007) is chosen to include dry, average, and wet years. The long-term daily streamflow data is available at the Ghala stream gauging station along the Lower Tapi River, and the same has been used for the model calibration. The daily streamflow data at Ghala station from June 2005 to December 2007 is computed from observed water levels using the curve fitting approach (See Fig. 5.16). The 2-degree polynomial equation is fitted in MATLAB R2014b to get the relationship between observed water level and discharge (during 1991-2000). The equation with co-efficient (95 % confidence bound) is given in Eq. 5.1. In comparing observed vs. simulated streamflow at

Ghala station during the year 1991-2000, the equation resulted in R^2 = 0.99 and RMSE = 21.24 m^3/s.

$$f(x) = p1x^2 + p2x + p3 \quad (5.1)$$

p1 = 100.1 (99.24, 100.2); *p2* = -524.5 (-526.3, -522.6); and *p3* = 701.3 (696.6, 706)

The values in the bracket indicates the upper and lower 95 % prediction bound respectively.

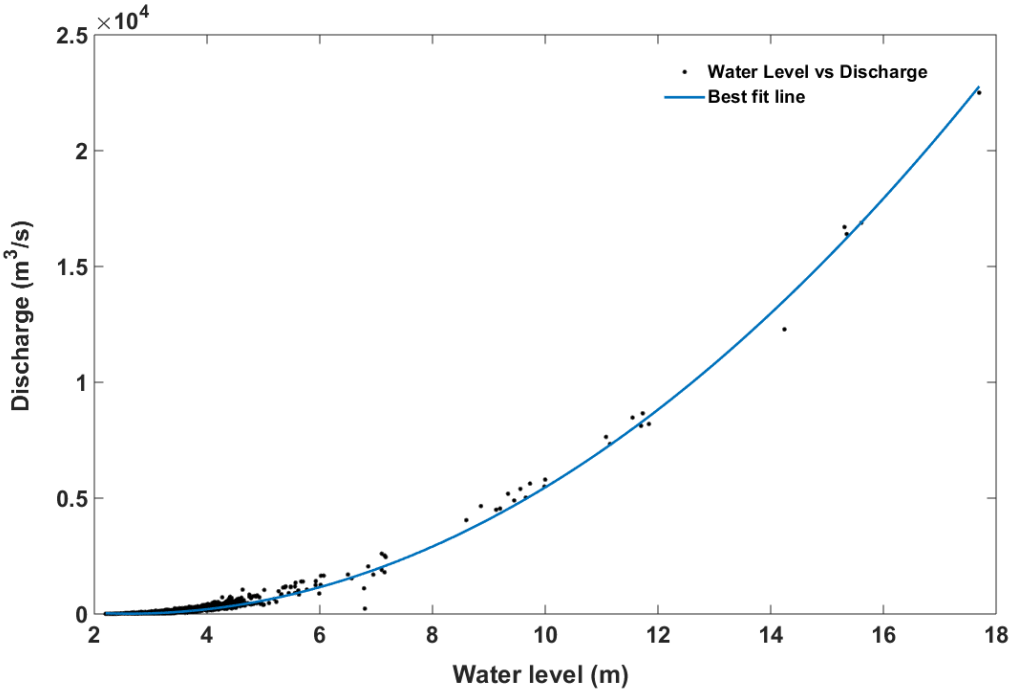

Fig. 5.16 Water level vs discharge relationship at Ghala stream gauging station

The model has been calibrated to obtain the optimal value of nineteen (19) model parameters (see Table 5.15) with the objective of overall agreement in the shape of discharge hydrograph at Ghala (minimizing RMSE) station. The initial values of the model parameters during the calibration process were chosen from the prevailing conditions of the study area, relevant literature, and modeling perception. The performance of the developed model under the calibration stage during 1991-1999 in terms of monthly and daily time scale, including the monsoon period of 1994 and 1998 (wet years) is shown in Fig. 5.17. The performance of the model for the calibrated parameter has also been evaluated using statistical indices such as co-efficient of determination (R^2) and Nash Sutcliff Efficiency (NSE) tabulated in Table 5.16. The RMSE (395.7 m^3/s), R^2 (0.86), and NSE (0.77) on the daily time scale show good agreement between observed and simulated discharge with underprediction of peak flow which further improved in the monthly time scale. The calibrated model parameters are validated with the help of independent data set at the Ghala stream gauging station for period 2000 to 2007. The

performance of the model under validation stage for observed and simulated monthly and daily flows is shown in Fig. 5.18. The statistical indices during the validation process are shown in Table 5.16. It is observed that the peak flows are invariably under predicted whereas the lean period flows are overpredicted during calibration as well as validation period. Such discrepancies in the prediction of stream flow are attributed to (a) giving rainfall as input with Thiessen polygon (semi-distributed) approach instead of gridded distributed rainfall, (b) one-dimensional flow model in unsaturated zone i.e., entire water recharges the groundwater and not generating any interflow to the stream (Loliyana et al. 2018).

Table 5.15 Calibration of MIKE SHE/MIKE 11 model parameters for daily streamflow data

Components	Parameters	Unit	Range	Initial Value	Calibrated Value
Surface Zone and Stream Channel					
Surface Roughness	Manning's M	$m^{1/3}s$	Table 5.14	-	-
Storage	Detention Storage (D_s)	mm	0.0-5.0	2	2.1
Channel Roughness	Manning's n	$m^{-1/3}s$	0.03	-	-
ET Zone					
Vegetation	Leaf Area Index (LAI)	-	Table 5.14	-	-
	Root Depth (RD)	mm	Table 5.14	-	-
	Co-efficient of interception (C_{Int})	mm	0.01-0.1	0.02	0.04
	ET surface Depth	m	0.1-2.0	1.5	1.0
Unsaturated Zone					
Clay Soil	Moisture content at saturation (θ_s)	-	0.3-0.6	0.4	0.51
	Moisture content at field capacity (θ_{fc})	-	0.2-0.45	0.2	0.43
	Moisture content at wilting point (θ_{wp})	-	0.1-0.25	0.1	0.28
	saturated hydraulic conductivity (K_s)	m/s	$1x10^{-8}$ - $1x10^{-5}$	$1.2x10^{-6}$	$6.9 x10^{-8}$
Clay Loam	θ_s	-	0.3-0.6	0.4	0.45
	θ_{fc}	-	0.2-0.45	0.2	0.35
	θ_{wp}	-	0.1-0.25	0.1	0.21
	K_s	m/s	$1x10^{-8}$ - $1x10^{-5}$	$1.2x10^{-6}$	$5.0 x10^{-7}$
Loam	θ_s	-	0.3-0.6	0.4	0.42
	θ_{fc}	-	0.2-0.45	0.2	0.29
	θ_{wp}	-	0.1-0.25	0.1	0.16
	K_s	m/s	$1x10^{-8}$ - $1x10^{-5}$	$1.2x10^{-6}$	$8.7 x10^{-5}$
Silt Clay	θ_s	-	0.3-0.6	0.4	0.46
	θ_{fc}	-	0.2-0.45	0.2	0.33
	θ_{wp}	-	0.1-0.25	0.1	0.19
	K_s	m/s	$1x10^{-8}$ - $1x10^{-5}$	$1.2x10^{-6}$	$5.7 x10^{-7}$

- **Water Balance Computation**

Water balance is an important part of model simulation, giving useful information on water availability for sustainable usage and planning within the basin shown in Fig. 5.19. The Table 5.17 shows the annual water balance for each component (in mm) for the entire lower Tapi basin during the calibration and validation period. Precipitation is the major inflow into the system (100 %), of which 50 % is lost due to actual evapotranspiration, 24.9 % generates runoff, and 36 % as a recharge to the saturated zone through the soil matrix during the calibration period. A similar proportion is observed during the validation period. The error in the water balance computation is less than 1 % in both the calibration and validation process.

Table 5.16 Performance of the developed model under calibration and validation period

Time scale	Calibration stage (1991-1999)			Validation stage (2000-2007)		
	RMSE (m^3/s)	R^2	NSE	RMSE (m^3/s)	R^2	NSE
Daily Flow	395.7	0.86	0.77	348.7	0.90	0.86
Monthly Flow	152.8	0.97	0.88	150.3	0.94	0.90

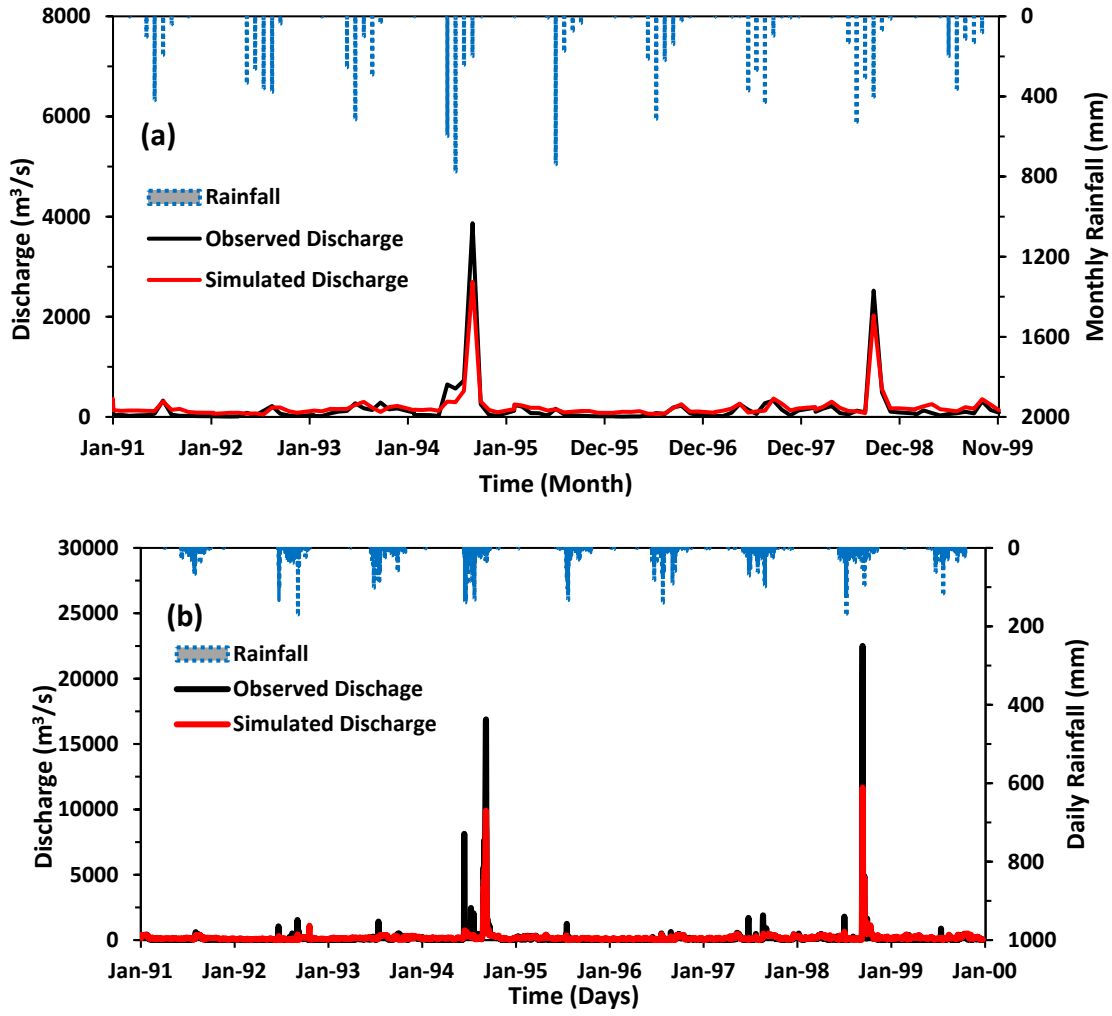

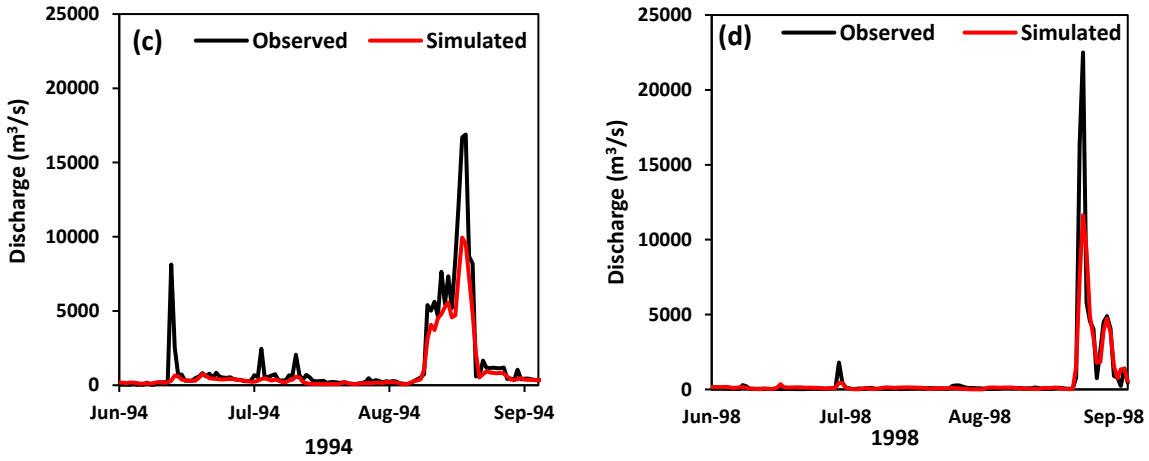

Fig. 5.17 Comparison of observed and simulated streamflow during calibration at Ghala station (a) monthly discharge (b) daily scale, monsoon period of (c) year 1994, and (d)1998

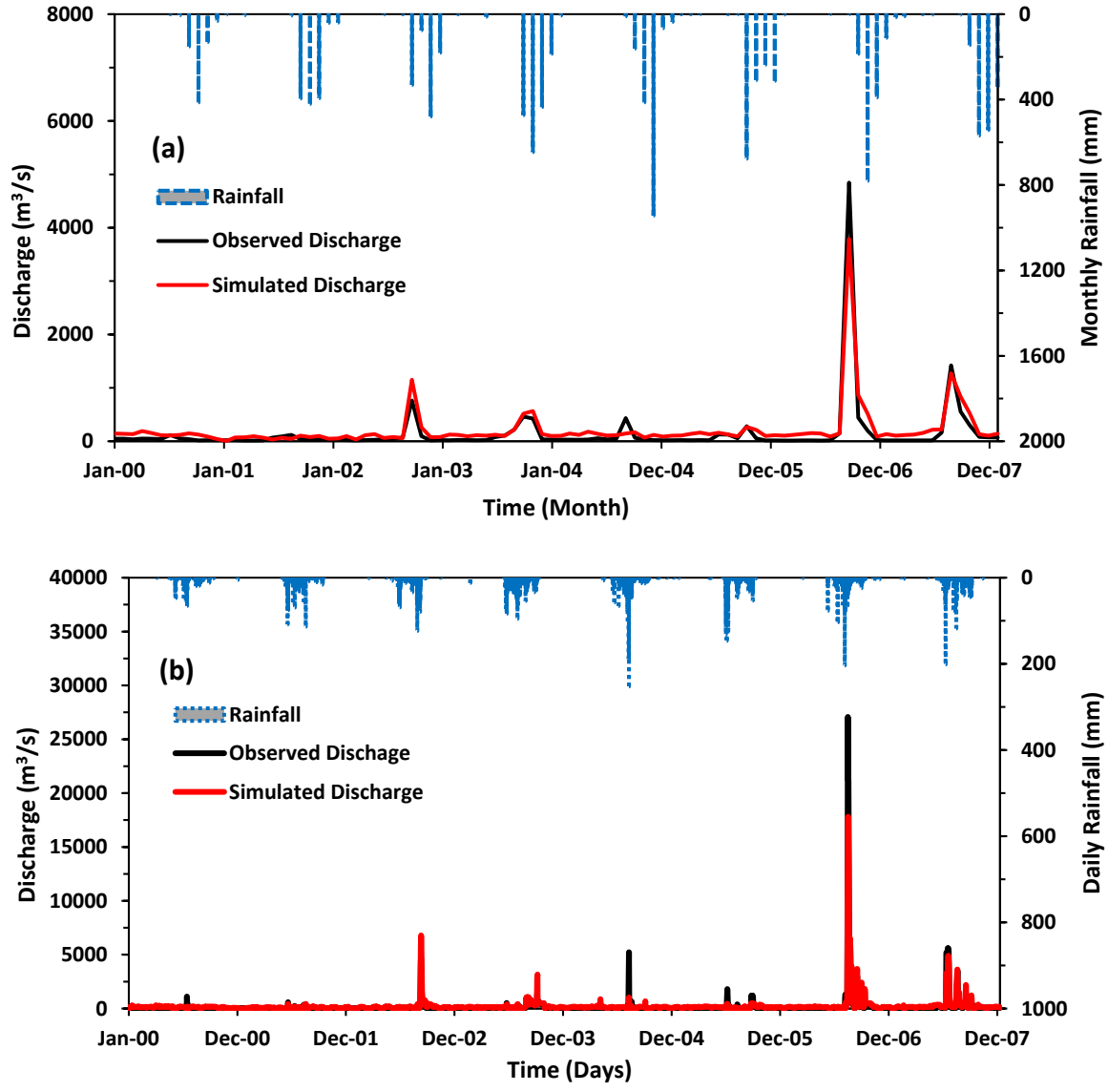

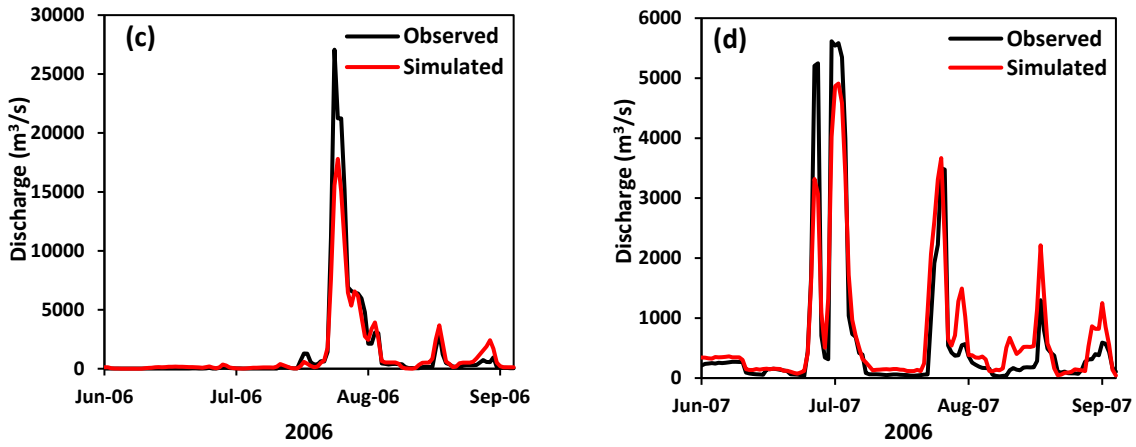

Fig. 5.18 Comparison of observed and simulated streamflow during validation at Ghala station (a) monthly discharge (b) daily scale, monsoon period of (c) year 2006, and (d)2007

5.5 HYDRAULIC MODELING OF LOWER TAPI BASIN

The Tapi River experiences large flood in year in 1727, 1776, 1782, 1829, 1837, 1872, 1944, 1959, 1968, 1970, 1994, 1998 and 2006. The flood of the year 1968, with a peak discharge of 42,500 m^3/s, was the largest flood recorded in the last century. The flooding situation in Lower Tapi, including Surat city, worsens when the dam releases coincide with the high tide condition in the Arabian sea. The flood of the year 2006 (peak discharge of 25,780 m^3/s) after the construction of the Ukai dam inundated almost 80% area of Surat city and incurred losses to the tune of Rs 21,000/- crores and 150 lives (Patel and Srivastava 2013). To deal with such a disastrous flood event and their management in the future, particularly in LTB, a hydrodynamic model is required. The hydrodynamic model results can be used to study the flood hazard and flood risk in LTB with densely populated Surat city.

- **Flood Inundation Mapping and Risk Assessment of Surat City**

The MIKE 21 flow model is used in flood inundation modeling. The MIKE 21 flow model is capable of simulating 2D free-surface flows using numerical solution approach based on depth-average Navier Stokes equations which describes the conservation of mass and momentum in two horizontal dimensions (DHI 2017b). The model has been developed and calibrated for the 2006 flood event that occurred in the Surat city by considering the outflow from Ukai as the upstream and tidal level at the Arabian Sea as a downstream boundary condition. The calibrated model results were used to develop the flood hazard maps for different return period floods. The socio-economic vulnerability for each ward of Surat city was computed from the census-

based indicators. Finally, the risk maps were developed with the integration of hazard and vulnerability for the coastal urban flood plain of Surat city.

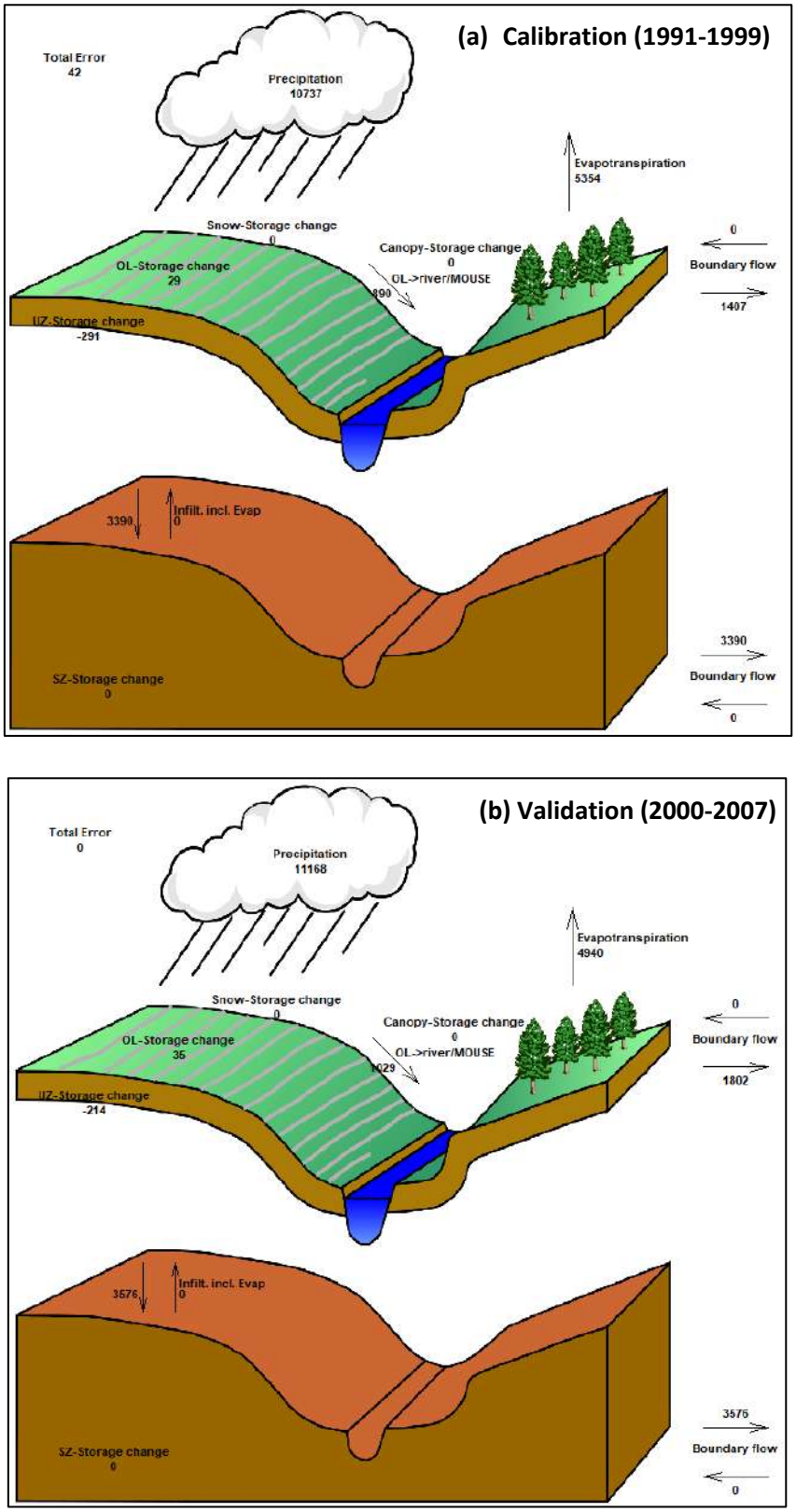

Fig. 5.19 Simulated water balance during (a) 1991-1999 and (b) 2000-2007 for Lower Tapi Basin

Table 5.17 Annual water balance components (in mm) of the simulation 1991–2007 for Lower Tapi Basin

	Inflow		Outflow									Storage				
	P	**C_i**	**EP**	**BOL**	**OLR**	**RUN**	**TRZ**	**ET**	**REC**	**UZD**	**Total outflow**	**ΔC**	**ΔOL**	**±ΔS**	**$(\pm\Delta S)_c$**	**Error**
	1	2	3	4	5	6 (4+5)	7	8 (2+3+7)	9	10	11 (6+8+9+10)	12	13	14 (12+13)	15 (1-11)	16 (14-15)
1991	753.8	52.3	69.8	57.6	17.3	74.8	574.8	696.9	306.4	-294.6	783.6	0.0	11.8	11.8	-29.8	41.6
1992	1355.0	70.9	107.1	219.3	129.8	349.1	359.9	538.0	439.5	14.8	1341.4	0.0	13.8	13.8	13.7	0.1
1993	1184.2	67.9	116.9	146.4	83.5	229.9	421.0	605.8	337.9	7.2	1180.8	0.0	3.3	3.3	3.4	-0.1
1994	1801.8	152.4	98.7	354.7	196.6	551.3	350.4	601.5	660.1	-12.8	1800.0	0.0	1.8	1.8	1.8	0.0
1995	1025.8	61.0	72.6	188.0	97.5	285.5	356.8	490.4	260.6	-9.2	1027.2	0.0	-1.6	-1.6	-1.4	-0.1
1996	1115.9	74.2	90.6	94.8	100.7	195.5	409.8	574.6	338.5	6.0	1114.6	0.0	1.3	1.3	1.3	0.0
1997	1172.8	65.4	115.7	82.5	95.8	178.3	406.1	587.2	388.4	18.0	1172.1	0.0	0.8	0.8	0.8	0.0
1998	1435.7	109.3	117.8	196.0	130.3	326.2	415.2	642.3	457.9	5.5	1431.9	0.0	3.7	3.7	3.8	-0.1
1999	892.2	64.3	90.4	67.8	38.9	106.6	462.3	617.0	200.2	-25.9	897.9	0.0	-5.6	-5.6	-5.7	0.1
Total	**10737.4**	**717.8**	**879.6**	**1407.1**	**890.3**	**2297.4**	**3756.2**	**5353.6**	**3389.5**	**290.9**	**10749.5**	**0.0**	**-29.4**	**-29.4**	**-12.2**	**41.6**
%	**100**					**21.4**		**49.9**	**31.56**							**0.003**
2000	742.3	56.6	58.4	52.7	25.6	78.2	628.9	744.0	144.5	-235.5	731.1	0.0	11.2	11.2	11.2	0.0
2001	1281.1	89.9	97.0	92.6	140.5	233.1	401.9	588.9	440.2	7.7	1269.8	0.0	11.3	11.3	11.3	0.0
2002	1102.6	63.9	86.5	115.2	100.5	215.7	395.0	545.4	350.3	-10.7	1100.6	0.0	2.0	2.0	2.0	0.0
2003	1796.0	160.4	101.7	251.2	188.2	439.4	355.5	617.5	711.6	19.2	1787.8	0.0	8.1	8.1	8.2	-0.1
2004	1631.6	100.1	84.8	375.8	172.1	547.8	429.4	614.4	469.0	1.2	1632.3	0.0	-0.5	-0.5	-0.7	0.2
2005	1524.7	104.9	89.0	350.8	149.4	500.2	399.8	593.6	434.4	-4.3	1523.8	0.0	0.8	0.8	0.9	-0.1
2006	1508.9	114.6	86.4	254.4	128.2	382.6	410.1	611.1	499.0	15.1	1507.9	0.0	1.0	1.0	1.1	-0.1
2007	1580.6	132.7	99.3	309.3	125.0	434.3	393.0	625.0	526.8	-6.4	1579.7	0.0	0.8	0.8	0.9	-0.1
Total	**11167.7**	**823.0**	**703.1**	**1801.9**	**1029.4**	**2831.3**	**3413.7**	**4939.8**	**3575.7**	**-213.8**	**11133.0**	**0.0**	**34.7**	**34.7**	**34.7**	**0**
%	**100**					**25.35**		**44.2**	**32.0**							**0.0**

Note- P = Rainfall, C_i = Canopy interception, EP = Evaporation from ponded water, BOL = Boundary outflow, OLR = Overland flow to river, RUN = Total runoff, TRZ = Transpiration from root zone, ET = Actual evapotranspiration, REC = Recharge in saturated zone through soil matrix, UZD = Unsaturated zone deficit (amount of air in profile), ΔC = Change in canopy interception, ΔOL = Change in overland storage, ±ΔS = Total storage, $(\pm\Delta S)_c$ = Change in storage

- **Model Development**

The detailed methodology adopted for developing a flood hazard, socio-economic vulnerability, and flood risk map for Surat city using the results 2D hydrodynamic model (MIKE 21) for the coastal urban flood plain of Surat city is shown in Fig. 4.5.

- **Creation of flood plain bathymetry**

The accurate representation of flood plain topography plays a major role in 2D flood plain model simulation. The DEM (raster) generated in the previous section was converted into .dfs2 file format using the Grd2Mike tool in MIKE ZERO (see Fig. 5.13). The cell size of the grid affects the accuracy and calculation time significantly (Begnudelli et al. 2008). However, Bates and De Roo (2000) reported that up to 50 m cell size provides the optimal efficiency in flood inundation studies. In the present study, 30 × 30 m grid resolution is used to represent the bathymetry of LTB. The land value is taken as 320 m so that cell values greater than 320 m will not be part of the calculation.

- **Flood plain roughness**

The classified LULC map of year 2006 (56 m spatial resolution) obtained from NRSE was further modified to a spatial resolution of 30 m and six major land cover classes, viz. agriculture, fallow, built-up, forest, water, and wasteland. Agricultural land is the dominant land class within the study area with 46.68 %. The Manning's roughness value '*n'* for the given land cover is given in Table. 5.18, adopted from the past studies (Chow 1988; Timbadiya et al. 2014b and Patel et al. 2017).

Table. 5.18 Manning's roughness value 'n' for respective land class

SR. No	Class	Area (km^2)	Area (%)	n ($m^{-1/3}s$)	M ($m^{1/3}s$)
1	Water	553.4	10.5	0.030	33.33
2	Agriculture	2451.3	46.7	0.035	28.57
3	Fallow	571.5	10.9	0.040	25
4	Wasteland	845.7	16.1	0.055	18.18
5	Forest	561.7	10.7	0.150	6.67
6	Built-up	267.0	5.0	0.150	6.67
	Total	**5250.528**	**100.0**		

- **Boundary Conditions**

For unsteady simulation, discharge hydrograph and water levels are perpetually considered upstream and downstream boundary conditions. Accordingly, hourly releases from the Ukai

dam during the year 2006 flood were used as the upstream boundary condition. In the 2D HD model, the upstream boundary condition was entered as a point source in the uppermost river section along the width of the river. The inflow hydrograph for each cell is computed by dividing the ordinates of discharge (see Fig. 5.20a) hydrograph (Ukai release) at zero chainage of the river by 16, as a total 16 nos. of cells (30m×30m) were identified along the river width. Along with the discharge hydrograph velocity and its direction for each cell is also needed in the upstream boundary condition for 2D floodplain modeling. The velocity at each cell is calculated by using Manning's equation, considering the uniform flow condition. The hourly variable tide at the Arabian Sea (see Fig. 5.20b), synchronized with the simulation period, has been used as downstream boundary condition.

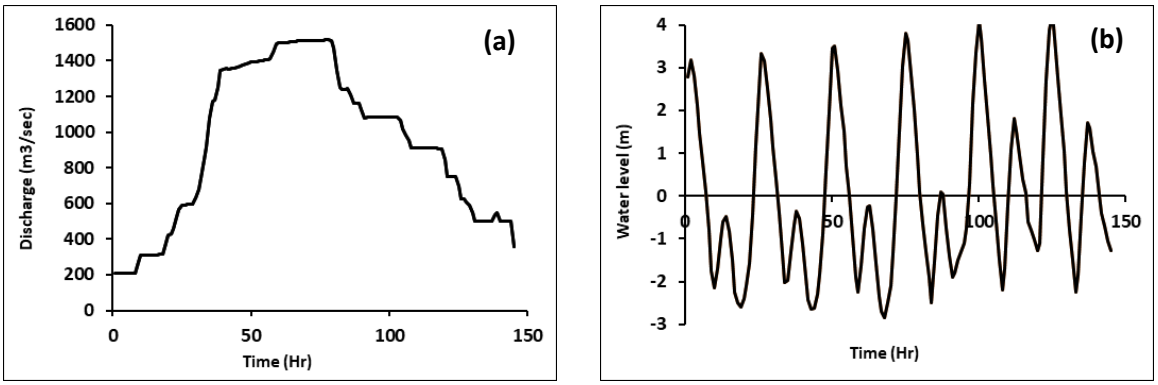

Fig. 5.20 (a) Hourly Discharge Hydrograph per cell from Ukai in 2006 (b) Tidal Levels at the Arabian Sea

- **Initial Conditions**

In the present study, the floodplain is considered dry, with 1 m water depth in the channel section as an initial condition. The value of time step Δt is taken as 2 sec.

- **Performance of 2D HD model**

The performance of the 2D HD model across the channel is evaluated by comparing the observed and simulated water levels at Nehru bridge in Surat city as shown in Fig. 5.21. The scatter plot of observed versus simulated water level shows that the model performs satisfactorily at Nehru Bridge Surat (R^2 = 0.9479) across the channel. Also, the performance of the model across the coastal urban flood plain of Surat city was evaluated for 325 observational points (all seven zones) by using the scatter plot of the highest water depth shown in Fig. 5.22 and 5.23. The zone-wise Root Mean Square Error (RMSE) is also calculated and shown in Table. 5.19.

The 2D HD model is performing better in the central zone, east zone, and west zone with RMSE of 0.58, 0.73, and 0.96 m, respectively. The model is performing moderately well in the north zone and south-west zone with an RMSE of 0.81 and 0.67 m respectively. The model is not performing well in the southeast and south zone where the comparison is made with fewer points. For total 325 points across all the zones (Surat city), models give the RMSE of 0.86 m which is better than the previous study carried out by Timbadiya et al. (2014b).

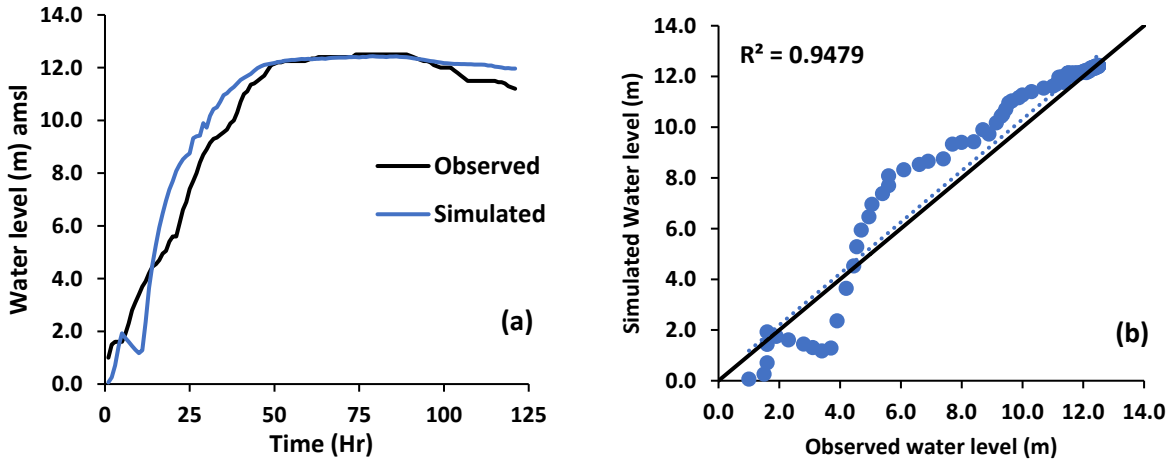

Fig. 5.21 (a) Comparison of observed and simulated water levels (b) Scatter plot of observed versus simulated water levels at Nehru Bridge Surat

- **Flood Hazard Maps for Surat City**

The calibrated flood model simulates the flood of the different return periods (See Fig. 4.7c). The flood inundation (maximum Depth) map for densely populated Surat city and its outskirt area are shown in Fig. 5.24. The flood inundation depth is categorized into five different classes. From Table 5.20, it is evident that, for a 5-year flood total 261.1 km^2 (29.3 %) area gets inundated with water depth more 1.5 m, which increases to 372.5 km^2 (41.9 %) and 396.2 km^2 (44.5 %) for 100- and 200-year, flood respectively. The west zone, nearby outskirt area, and north zone are the worst affected regions experiencing high flood depth on larger areas even in case of low magnitude flood. The area under high flood depth increases with an increase in flood magnitude.

Further, the flood model output i.e., flood depth and flow velocity (i.e., product of depth and velocity) were used to develop the flood hazard maps for different return period flood along with percentage of area under each hazard class are shown in Fig. 5.25. The area under each hazard class (km^2) is also given in Table. 5.21. It is observed that total 282.3 km^2 of Surat city

and its outskirt area is under the high to very high hazard category for a 100-year flood. The West and north zones are the worst affected regions with a larger area under the high to very-high hazard category. The characteristics of flood inundation maps are reflected in the flood hazard maps as the area under the high hazard category increases with an increase in the magnitude of the flood.

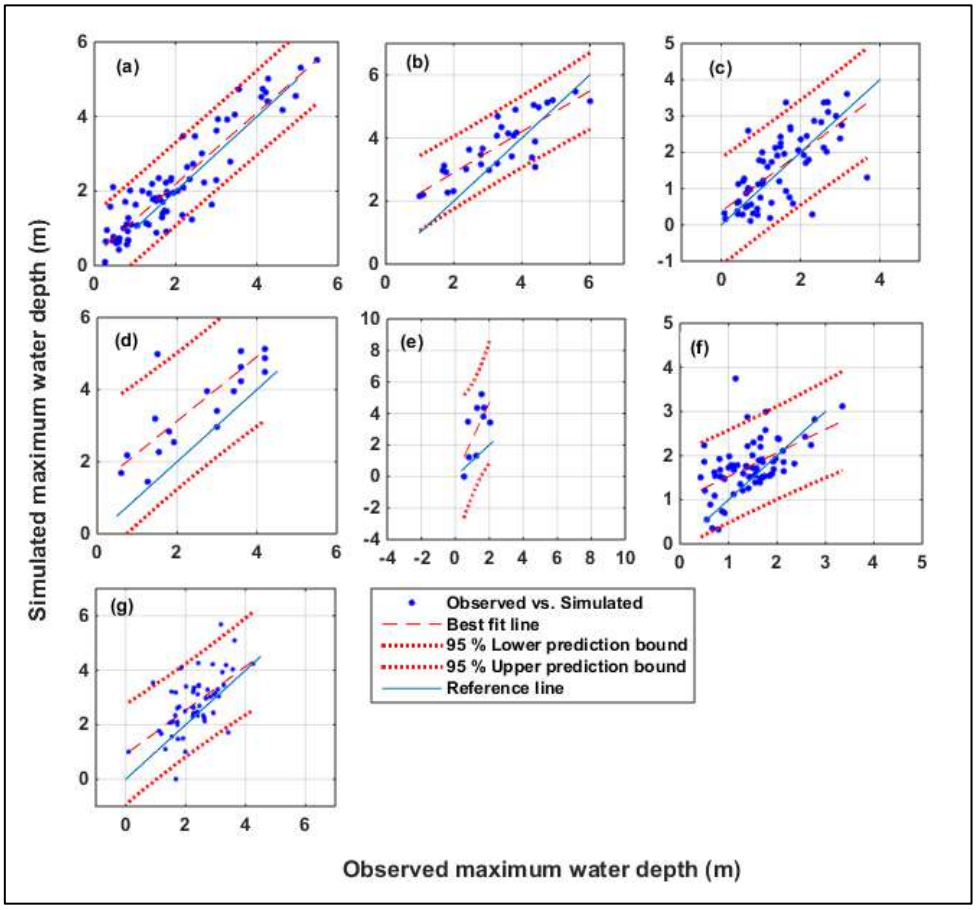

Fig. 5.22 Scatter plot of highest water depth for (a) central zone (b) north zone (c) east zone (d) south-east zone (e) south zone (f) south-west zone (g) west zone

Socio-economic Vulnerability of Surat city

The socio-economic vulnerability represents the capability of community or population to cope up with the coming hazard. The total 326.52 km^2 is under Surat Municipal Corporation (SMC) jurisdiction, having population of 44,66,826 (census 2011). At first, the socio-economic vulnerability for each ward of city is computed using simple averaging approach as shown in Fig. 5.26a. The 8 out of 89 wards (≈ 10 %) of the city was found to be under the high to very-high vulnerable class whereas, 28 (≈ 44.43 %) wards were under the medium to very high vulnerable category. The averaging is simple method yet not so accurate as it treats all the

indicators equally, which is not a practically correct approach. It can underestimate or overestimate any of the important or less important indicators with each other.

The PCA-DEA aggregation is a more accurate technique to overcome the limitation of simple averaging by optimizing each indicator to compute the discrete piecewise frontier estimation. The outcome of the PCA-DEA approach for Surat city as shown in Fig. 5.26b, led to 66 out of 89 wards (≈ 85 % of area) of the Surat city is under the medium to very-high vulnerable category. However 44 wards covering ≈ 66 % of the city falls under very-high vulnerable class. It is noted that, the highly vulnerable area of city has high population density.

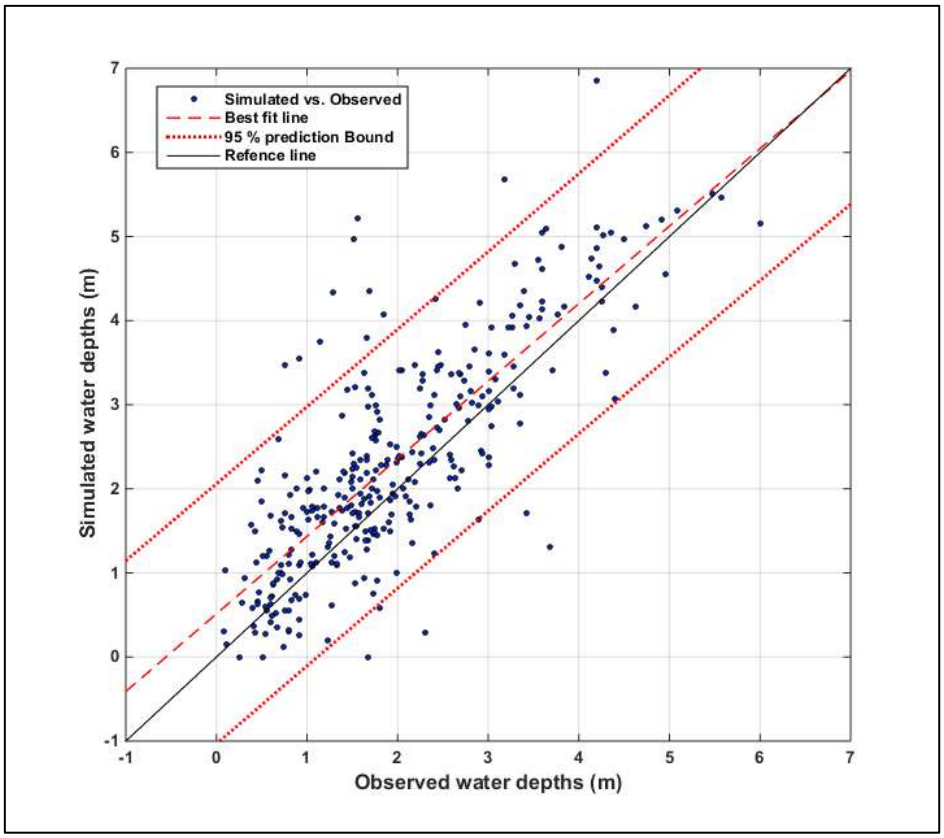

Fig. 5.23 Scatter plot of highest water depth across all seven zones of Surat city

Table. 5.19 Performance of the model across urban-coastal flood plain of Surat city

Sr. no.	Zones	RMSE (m)
1	Central	0.58
2	North zone	0.81
3	East zone	0.73
4	Southeast Zone	1.34
5	South Zone	2.21
6	Southwest zone	0.67
7	West Zone	0.96
8	**All zones**	**0.86**

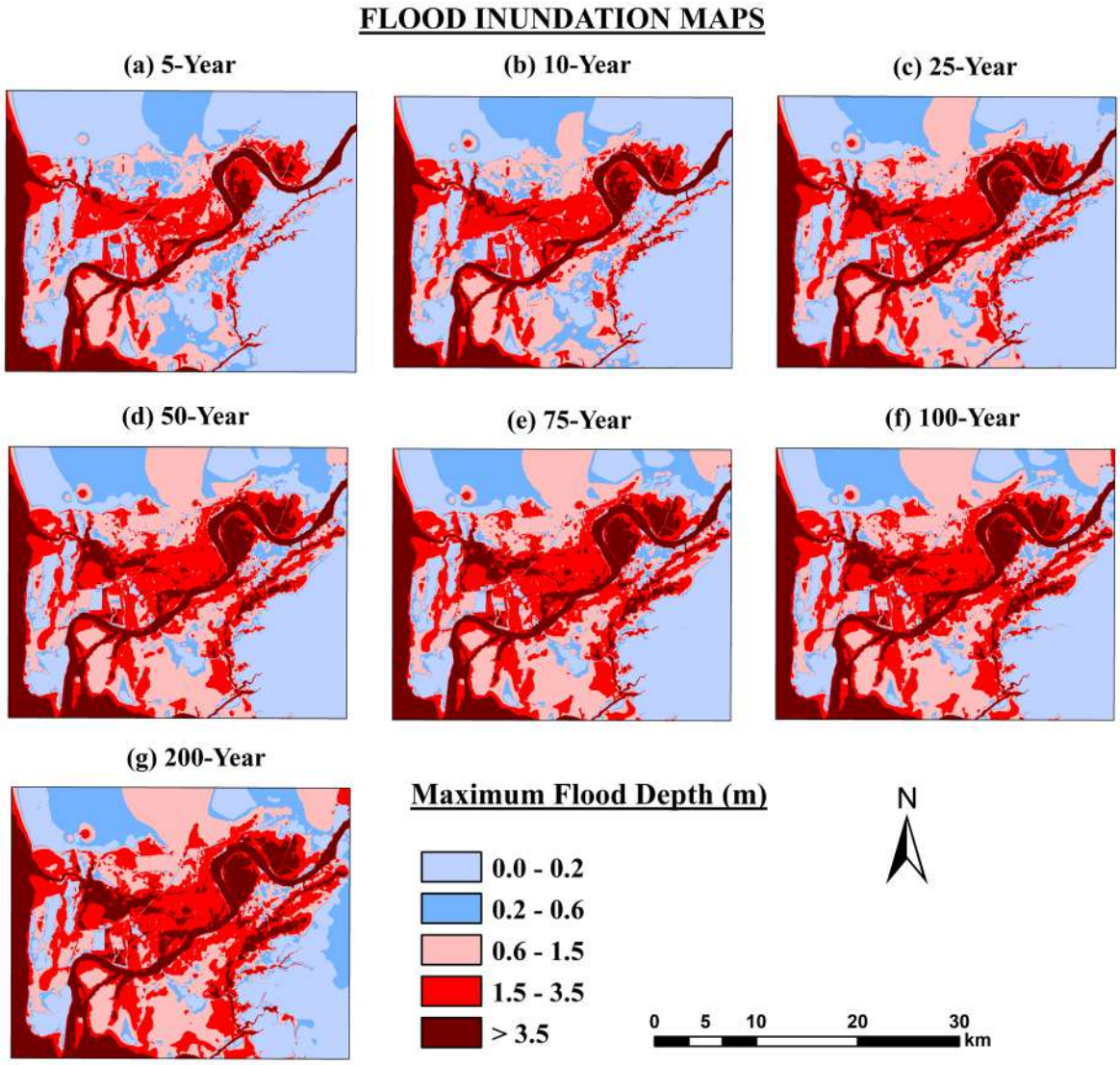

Fig. 5.24 Flood inundation maps for densely populated Surat city and its outskirt area for different return period

Table 5.20 Classification of inundated areas for different return period

Maximum Depth (m)	5-Year	10-Year	25-Year	50-Year	75-Year	100-Year	200-Year
0.0-0.2	384.2	327.2	276.8	234.0	220.6	212.7	173.2
0.2-0.6	101.8	106.8	90.5	101.6	95.4	91.1	106.6
0.6-1.5	142.6	167.5	197.5	205.8	211.2	213.4	213.7
1.5-3.5	141.9	159.6	181.9	195.8	205.0	211.4	227.0
>3.5	119.2	128.6	143.0	152.5	157.5	161.1	169.2
Total (km^2)				**889.7**			

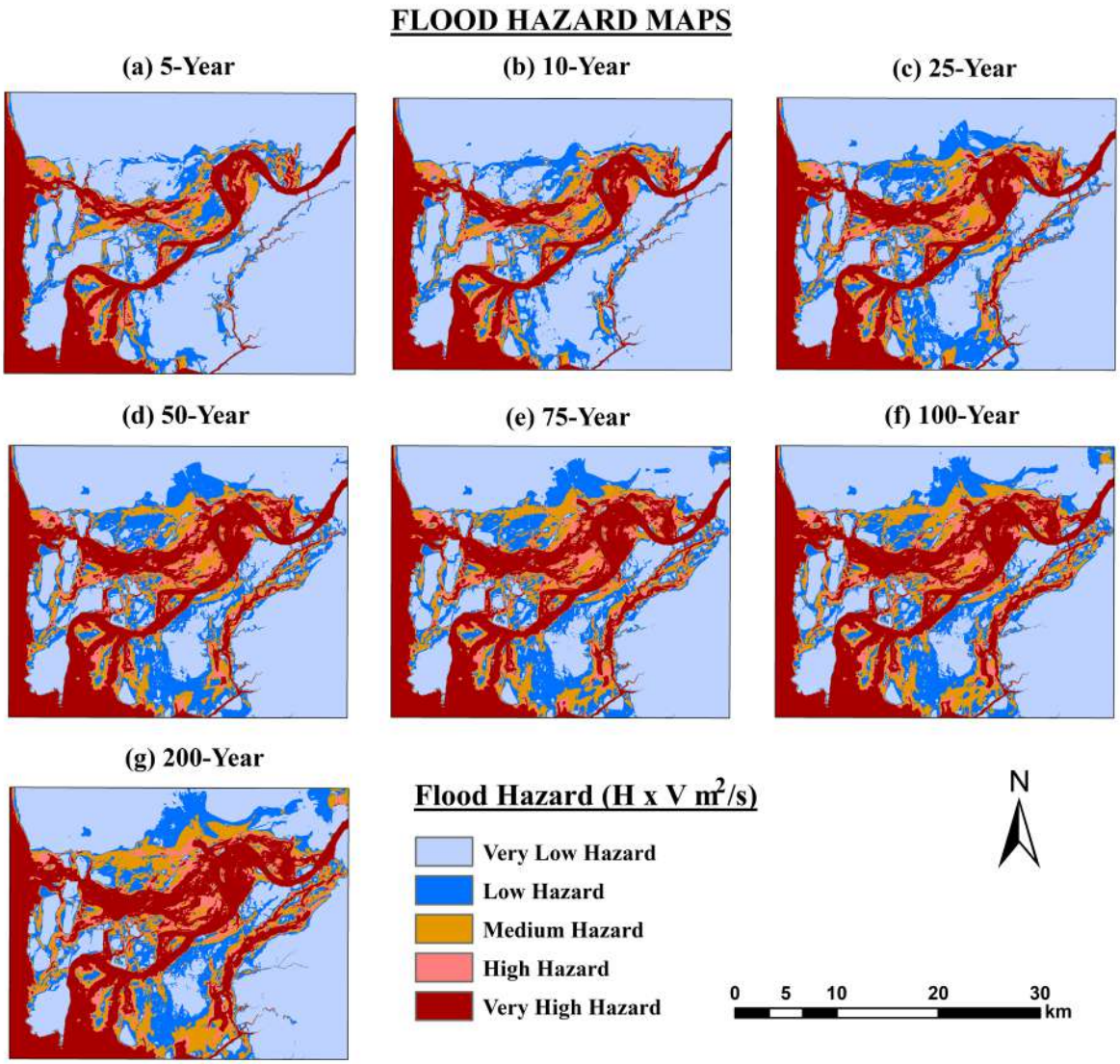

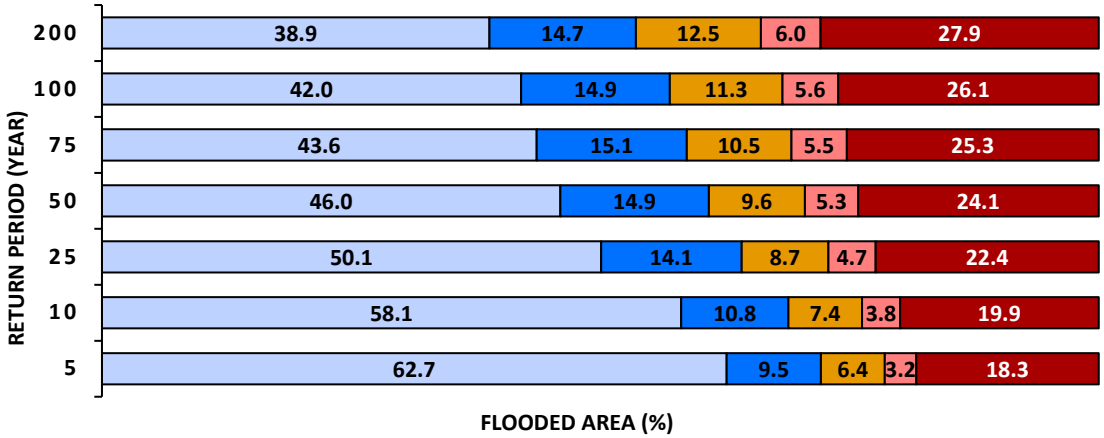

Fig. 5.25 Flood hazard maps for densely populated Surat city and its outskirt area for different return period

Table. 5.21 Classification of flood hazard areas for the different return periods

Hazard Class	5-Year	10-Year	25-Year	50-Year	75-Year	100-Year	200-Year
Very Low	557.5	517.1	445.6	409.2	388.0	374.1	345.9
Low	84.2	95.7	125.3	132.5	134.1	132.8	130.7
Medium	57.0	65.7	77.5	85.7	93.4	100.5	111.6
High	28.1	34.0	42.1	47.5	49.4	49.7	53.2
Very High	162.8	177.3	199.1	214.7	224.9	232.6	248.3
Total (km^2)				**889.7**			

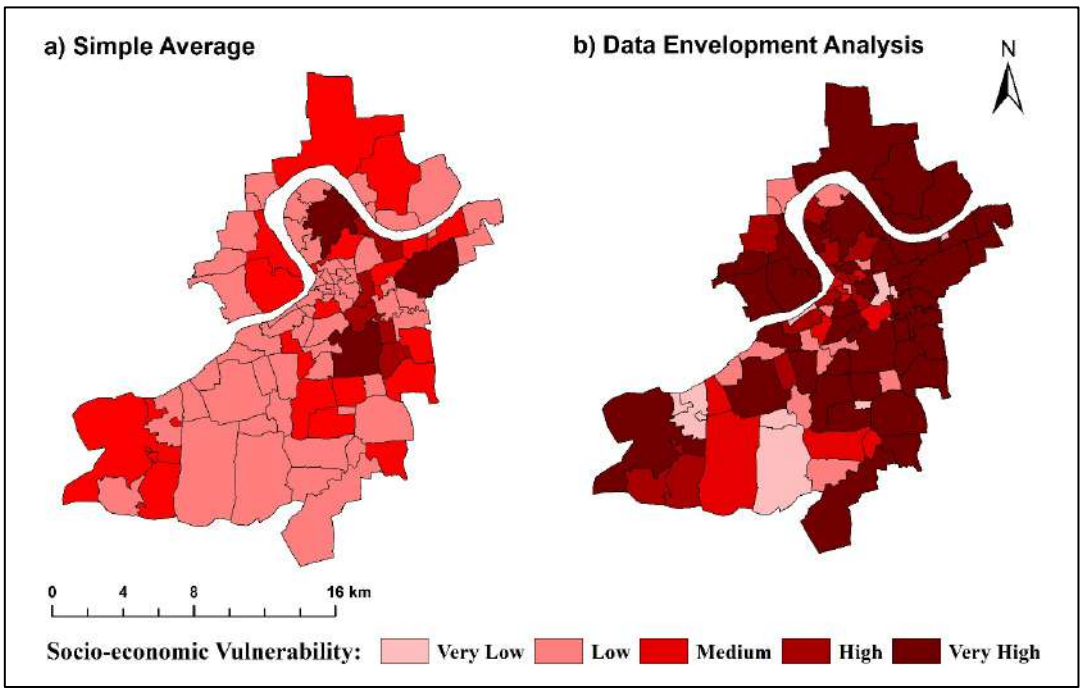

Fig. 5.26 Socio-economic vulnerability using **(a)** Simple averaging, **(b)** Data envelopment analysis for Surat city, India

Flood Risk assessment for Surat city

In the case of bivariate method, the flood risk is evaluated with the individual contribution of flood hazard and socio-economic vulnerability. The flood risk maps are developed for different return periods represented by 5 × 5 choropleth as shown in Fig. 5.27. The bar graph indicates the percentage of area under different risk class for Surat city. In case of 100-year flood, the risk in a maximum area of southeast and south zone is majorly due to socio-economic vulnerability. On the other hand, the risk in the tail portion of the southwest zone and part of the west zone is majorly due to high flood hazard. The risk in the North zone and the major portion of the west zone is due to equal contributions from contributed equally by socio-economic vulnerability and flood hazard.

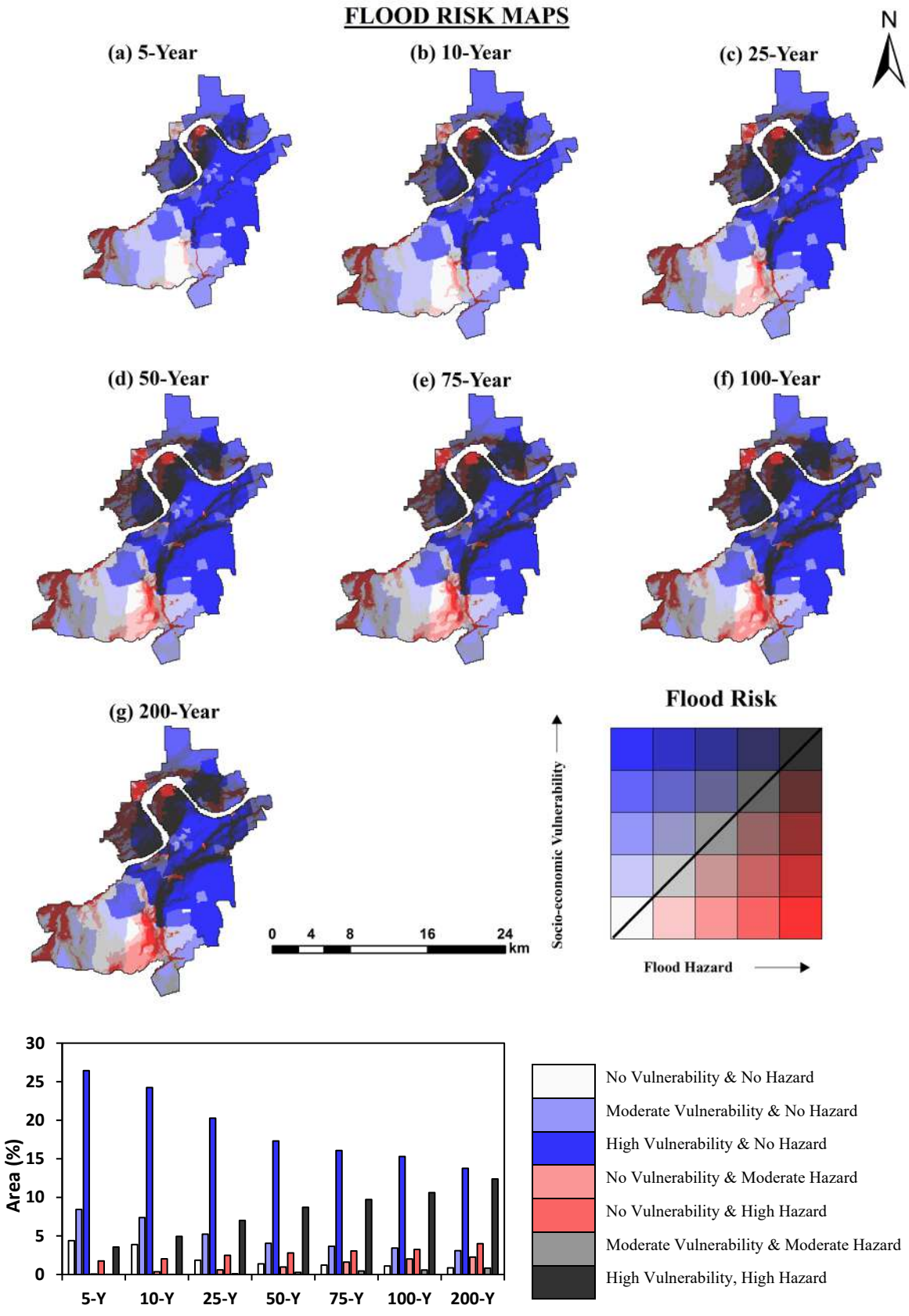

Fig. 5.27 Flood Risk maps for densely populated Surat city and its outskirt area for the different return period

As in the present case, vulnerability is kept constant; therefore, the contribution of vulnerability in the risk decreases with the increase in flood magnitude (See. Fig. 5.27). However, the percentage of areas under high risk with equal involvement of high vulnerability and risk is increasing for flood magnitude for the different return periods.

5.6 CLOSURE

Keeping in view the heterogeneous physiographic and hydro-climatic characteristics of the TRB, separate hydrological models are developed for the Upper, Middle, and Lower Tapi basin. In case of Purna sub-catchment during single site calibration (SSC), most of the sensitive parameters are related to the ground water flow whereas, in multisite calibration (MSC), the sensitive parameters are related to surface, subsurface and ground water flow. The statistical performance indices for the developed SWAT model are well within satisfactory range i.e., R^2 = 0.80 and *NSE* = 0.85 for Purna sub-catchment; R^2 = 0.71, and *NSE* = 0.67 for Burhanpur sub-catchment; and R^2 = 0.76, and *NSE* = 0.70 for Middle Tapi basin. The relative error in simulating water balance component for Purna sub-catchment, Burhanpur sub-catchment and middle Tapi basin is within ±5%. The statistical performance of the distributed MIKE SHE/MIKE 11 model for Lower Tapi basin shows R^2 = 0.86, and *NSE* = 0.77, whereas the error in water balance component is less than 1%. The flood assessment for the densely populated Surat city situated at the tale portion of Tapi River is also performed. The 44 out of 89 wards of the Surat city falls under high socio-economically vulnerable class. The north zone and west zone of the Surat city are the worst affected with high flood depth which is reflected in subsequent flood hazard and bivariate risk maps.

CHAPTER 6
CLIMATE CHANGE IMPACT ANALYSIS AND DISCUSSIONS

6.1 GENERAL

The methodology adopted for various aspects of the current study and development of the hydrologic and hydrodynamic models have been discussed in Chapter 4. This chapter includes the results obtained for spatio-temporal variability of hydroclimatic variables for baseline and various climate scenarios. The impacts of climate change on water availability, derived through hydrologic models, are discussed with the help of flow duration curves. The impacts on drought scenarios, crop water demands etc. under the future climate are also discussed. The impacts of climate change on the flooding situations in the Surat city are also described in conjunction with the baseline period for observed flood return levels. The chapter also discusses the likely implications of the change in climatic regime of the basin on human health, water availability, cropping pattern and ecosystem etc.

6.2 IMPACTS ON HYDROCLIMATIC VARIABILITY

The rainfall, temperature and streamflow indices discussed in Table 4.1 were analyzed for their temporal variability over the TRB and the obtained results are discussed below in following subsections.

6.2.1 Spatio-Temporal Assessment of Rainfall

- **Basic rainfall indices**

The magnitude, duration and intensity of total rainfall are represented by PRCPTOT, RD, and SDII indices, which constitute the basic rainfall indices. The statistical analyses of PRCPTOT (total annual rainfall on rainy days) reflects considerable rainfall variability (*Cv*) across Tapi basin, ranging from 25.7% to 47.1%, with the highest variability in LTB and lowest in UTB. The west coast of India exhibits high magnitude and variability observed in rainfall due to strong orographic influence of the Western Ghats (Goswami et al. 2006; Vittal et al. 2013). The temporal variation of PRCPTOT (1944 - 2013) across Tapi basin has been found to be 796.5 ± 165.1 mm, with its spatial average values across LTB, MTB and UTB for aforesaid period are reported to be 1253.9 mm, 719.6 mm, and 821.0 mm respectively. Further, the role of topographic variations can evidently be observed from the spatial values of PRCPTOT over Burhanpur (925.4 mm) and Purna (761.1 mm) sub-catchments of UTB. The spatial variation of PRCPTOT across the entire Tapi basin, (see Fig. 6.1a), ranges from 536.9 mm to 1656.4

mm, wherein 67.86% of the basin receives annual rainfall less than the basin average (i.e., 796.5 mm). This shows the asymmetric spatial distribution of rainfall in the basin. From the trend analyses, it has been found that 41.5% (56.6%) stations exhibit increasing (decreasing) trend in PRCPTOT, including 7.5% (9.4%) stations showing statistically significant trends. It is clear from Fig. 6.1a that LTB, generally experiences sub-humid climate and receives highest rainfall in the Tapi basin, exhibits coherent increasing trend in PRCPTOT, wherein, the Olpad and Surat stations depict significantly rising trends. On other hand, the mountainous regions of UTB, viz., Multai, Atner, Bhainsdehi and Dharni stations (except Chikhalda) have shown decreasing trend, in PRCPTOT, possibly due to significant deforestation in UTB (Sharma et al. 2018). The MTB overall exhibits decreasing trends in PRCPTOT, with Bhusaval, Raver and Pachora stations showing significant decrease.

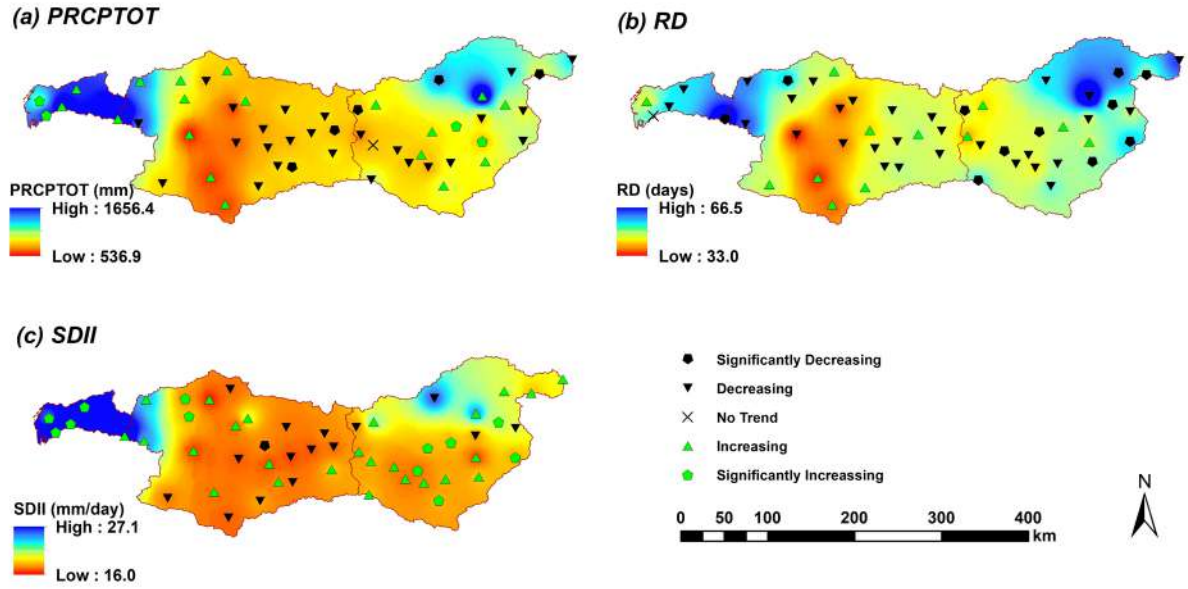

Fig. 6.1 Spatial pattern of time averaged values and trend in basic rainfall indices

The temporal variation in rainy days (RD) observed across the Tapi basin is 43 ± 7 days, with maximum and minimum values of RD reported over the entire basin as 58 days (in year 1955) and 30 days (in year 1972) respectively. From the spatial pattern of RD (Fig. 6.1b), stations in the proximity of the Gwaligarh hills in UTB and the Western Ghats (windward side) have the highest RD, while those in the rain shadow region of the Western Ghats (leeward side) have the least RD. The spatially averaged values of RD across LTB and Burhanpur sub-catchment of UTB are 49.4 days and 46.3 days respectively, while MTB and Purna sub-catchment of UTB have shown low RD values of 41.2 days and 43.4 days respectively. The analysed results showed that 75.5% of the stations exhibit decreasing trends in RD, out of which 27.5% are

statistically significant, majority of which are concentrated in Burhanpur and Purna sub-catchments in UTB. The analysis of simple daily intensity index (SDII) shows that the average intensity of annual rainfall in Tapi basin is 18 mm/day, with maximum (minimum) SDII of 27.1 (16.0) mm/day at Kamrej (Shahada) stations (see Fig. 6.1c). It is noticed that SDII is very high in LTB and Burhanpur sub-catchment of UTB, and their respective SDII values are found to be 24.8 mm/day and 19.2 mm/day. The SDII is relatively lower for MTB (17.3 mm/day) and Purna (17.2 mm/day) sub-catchment (in UTB) vis-à-vis LTB and Burhanpur sub-catchment (in UTB). Thus, headwater region of UTB and flood plains of LTB could be prone to flash floods due to higher values of SDII. The trend analyses of SDII over Tapi basin reveals that nearly 70% of the basin experiences rise in SDII (see Fig. 6.1c), out of which 32% are statistically significant. Further, two major urban centres, viz. Amaravati (in Purna sub-catchment) and Surat stations (in LTB) have experienced significant increasing trends in SDII.

- **Extreme rainfall indices**

The extreme rainfall indices, in present study, comprise of absolute indices (Rx1day and Rx5day), threshold-based indices (R95p and R99p) and a relative index (R5TOT). The aforesaid extreme rainfall indices have shown high correlation (at 1% significant level) amongst each other, except R5TOT. The one-day maximum rainfall, Rx1day, in Tapi basin varies from 75.1 mm (at Sakri in MTB with Cv = 40.9%) to 180.2 mm (at Songadh in LTB with Cv = 60.6%) (see Fig. 6.2a), wherein, the higher Cv values infer higher variability associated with Rx1day. The maximum spatially averaged Rx1day across Tapi basin was found to be 173.8 ± 73.9 mm during the year 2006, which corresponds to severe flood event in the basin. The Rx5day represents the maximum cumulative sum of 5-day rainfall in a year. The variation in Rx5day ranges from 132.0 mm at Sakri (Cv = 38.0%) to 397.1 mm at Songadh (Cv = 65.9%) (see Fig. 6.2b). From Fig. 6.2a-b, it is clearly seen that aforesaid extreme rainfall indices display higher magnitude over LTB and upper part of Burhanpur sub-catchment vis-à-vis MTB and Purna sub-catchment. The spatial average values of Rx1day and Rx5day over LTB are found to be 157.1 mm and 318.9 mm respectively, while the corresponding values for Burhanpur sub-catchment are 104.7 mm and 198.7 mm respectively. On other hand, the corresponding spatial average values over MTB and Purna sub-catchment region are 91.2 mm and 163.4 mm; 89.9 mm and 159.8 mm respectively. This clearly highlights the incoherent characteristics of extreme rainfall across the Tapi basin.

The trends in Rx1day and Rx5day are observed to increase across LTB and Purna sub-catchment, while decreasing trends are discerned over the MTB (see Fig. 6.2 a). Further, 47.2% (1.9%) stations show increasing (significant increasing) trends in Rx1day, whereas 52.8% (9.4%) stations show decreasing (significant decreasing) trends in Rx1day. On other hand, 47.2% (50.9%) of stations in the basin show decreasing (increasing) trends in Rx5day, wherein 5.7% are statistically significant. In LTB, particularly Surat city, has undergone increase in Rx1day and significant increase in Rx5day during 1944-2013. The Surat city is located on the coastal urban flood plains of the Tapi River. Due to its unique geographical setting in the basin, the Surat city is susceptible to multiple and compound flood hazards in near future.

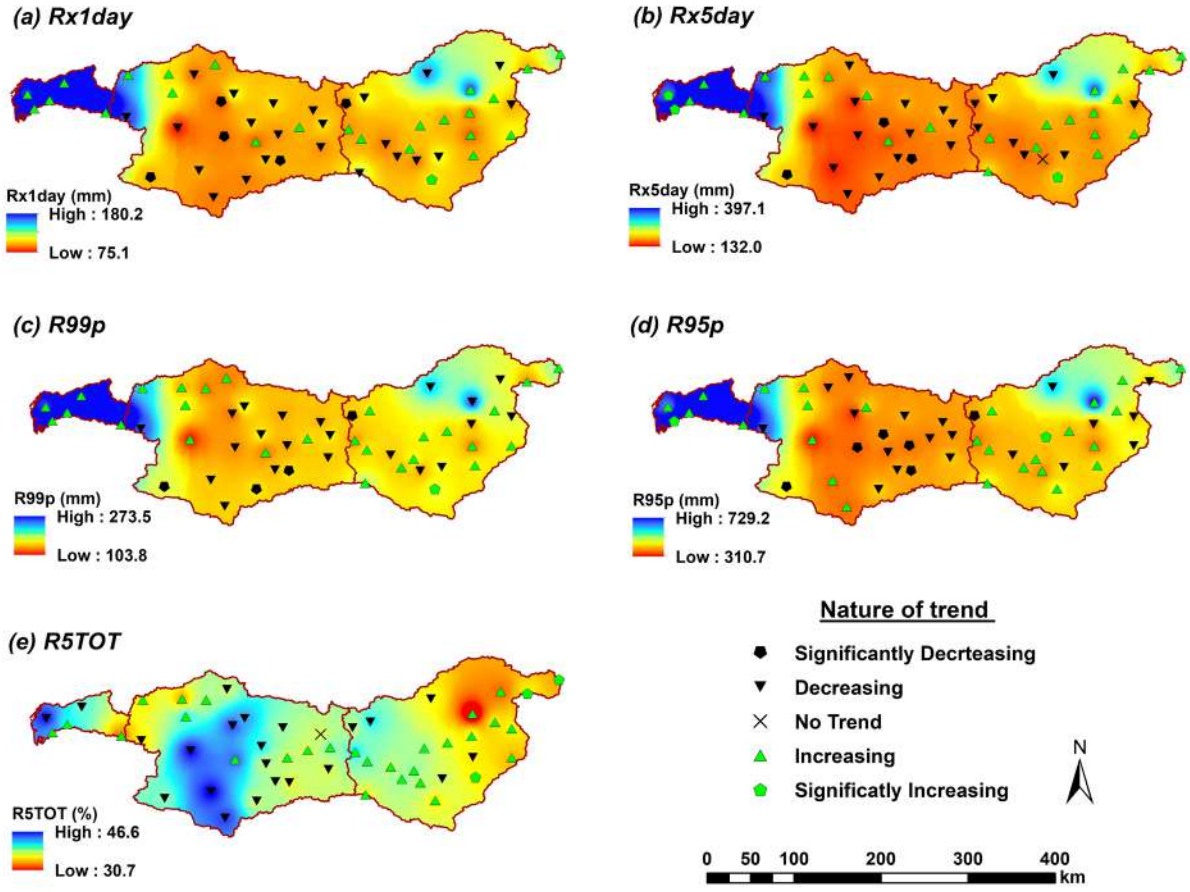

Fig. 6.2 Spatial pattern of time averaged values and trend in extreme rainfall indices

The R95p (R99p) represents the sum of rainfall received in a single rainy day with magnitude equal to or more than 95th (99th) percentile value of rainfall for the period 1944-2013. The daily rainfall data of monsoon season (as it records 90% of total annual rainfall in the basin) is considered for estimation of extreme rainfall thresholds, i.e., R95 and R99. The analysis revealed that nearly 46.7% and 15.3% of total annual rainfall occur with rainfall magnitudes

more than R95 and R99 respectively. The Tapi basin, on an average, had experienced R99 (R95) events at least once a year around 67.7% (99%) of time. It is worth mentioning that 48.9% (17.7%), 51.0% (18.2%), 45.2% (15.6%) and 48.8% (17.4%) of total rainfall are contributed by R95p (R99p) events across LTB, MTB, Burhanpur and Purna sub-catchment respectively, depicting highly spasmodic nature of rainfall over Tapi basin. The analysis of trends in R95p and R99p indicated that LTB and Purna sub-catchments have shown increasing trends, while MTB experienced decreasing trends during the period of analysis (see Fig. 6.2c-d). Overall, 47.2% (52.8%) stations in the basin show decreasing (increasing) trends in both the indices including 1.9% (7.5%) and 3.8% (11.3%) significantly increasing (decreasing) trends respectively in R99p and R95p.

The R5TOT, a relative index, representing the percentage contribution of top five rainfall events in a year, and reveals the degree of non-uniformity in temporal distribution of rainfall. It seems that around 40% of total annual rainfall across Tapi basin is received in top five rainfall events every year. The average R5TOT values over LTB, MTB, Burhanpur and Purna sub-catchments are 41.0%, 41.2%, 36.3% and 37.7% respectively. It is apparent from Fig. 6.2e that R5TOT varies from 46.6% (at Malegaon station in MTB) to 30.7% (at Chikhalda station in UTB) across the basin. The results of trend in R5TOT (see Fig. 6.2e) revealed that the rain shadow region of the Western Ghats and its nearby region have shown decreasing trends, while UTB reflected the increasing trend. From the analyses, it is also observed that 56.6% (41.5%) of the stations in Tapi basin shows increasing (decreasing) trends in R5TOT, of which 5.7% are significantly increasing. Overall, the trends in all the extremes indices have shown inconsistent and sporadic behaviour in significant trends across the basin.

- **Duration-based indices**

The duration or count-based indices used are moderate rainy days (Rmod), heavy rainy days (Rheavy), consecutive dry days (CDD) and consecutive wet days (CWD). Two of the indices, i.e., Rmod and Rheavy are count and threshold-based indices. The statistical analysis of Rmod and Rheavy indicated that their respective spatial average values are 28.3 days and 3.4 days for LTB; 23.6 days and 1.3 days for MTB; 28.3 days and 1.9 days for Burhanpur sub-catchment; and 25.4 days and 1.3 days for Purna sub-catchment. Therefore, moderate rainy days shows marginal deviation across the basin, whereas, the heavy rainy days are considerably high for LTB vis-à-vis other parts of Tapi basin. The results indicated further that LTB experiences rising trends in Rmod (except Mangrol and Songadh stations) and Rheavy indices. It is also

found that Rmod exhibit decreasing (increasing) trends at 64.2% (35.8%) stations including 7.5% stations with significant effect. On other hand, Rheavy days has been found to be increasing (decreasing) trends at 54.7% (45.3%) stations including 3.8% (7.5%) stations with statistical significance.

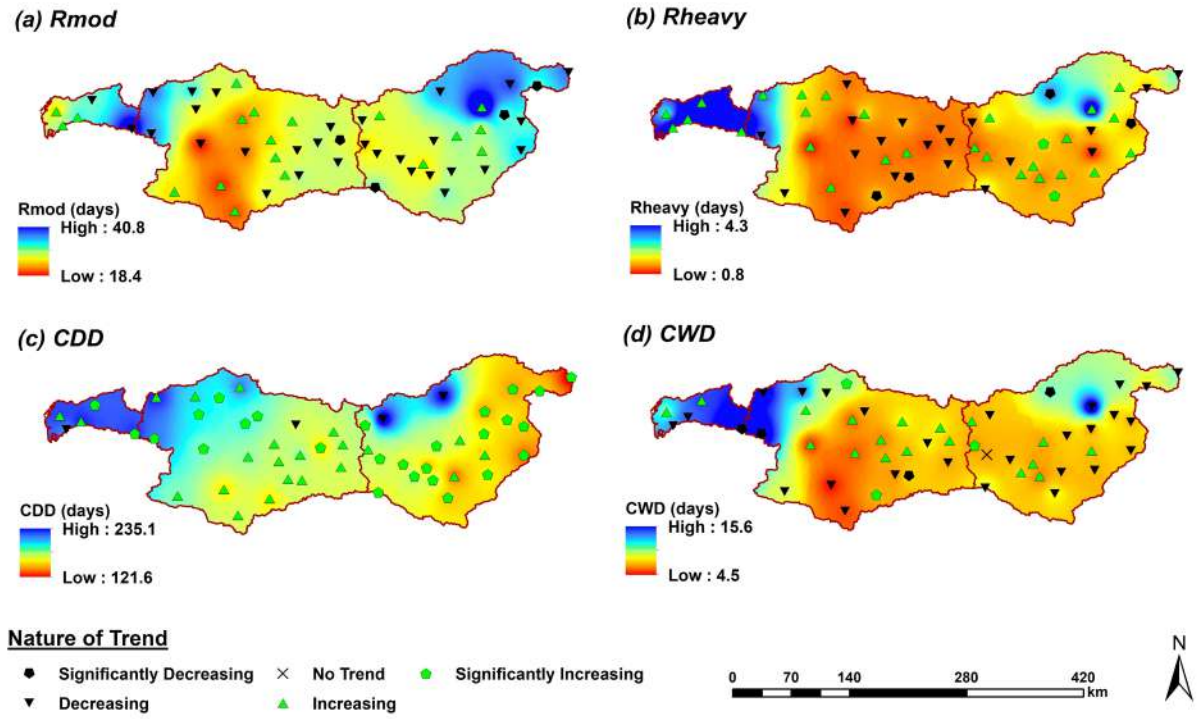

Fig. 6.3 Spatial pattern of time averaged values and trend in duration-based rainfall indices

The consecutive dry days (CDD) and consecutive wet days (CWD) are duration-based indices which describes the characteristic behaviour of dry and wet spells in a year. From Fig. 6.3c, it is evident that dry spells are consistently high over LTB and the region near the foothills of Satpura ranges. Furthermore, wet spells are higher for LTB as compared to rest of the basin (except Chikhalda, Navapur and Sagbara stations), while lower values are mapped over MTB and Purna sub-catchment (see Fig. 6.3d). The spatially averaged dry (wet) spells over LTB, MTB, Burhanpur and Purna sub-catchment are 212.6 (11.2) days, 176.3 (6.7) days, 179.2 (7.5) days and 152.6 (6.1) days respectively. This shows that LTB shows paradoxical behaviour in occurrence of dry and wet spells than other parts of the basin. Overall, 92.5% stations of the basin exhibit increasing trend in CDD, with 50.9% stations showing significant increasing trends. The analysis of trends in wet spells revealed that 58.5% (39.6%) stations of the basin showed decreasing (increasing) trends, wherein, 7.5% (5.7%) stations show significant nature of trend.

Keeping in view the rainfall patterns across the basin, it is justifiable in stating that LTB (MTB) are the wettest (rain scarce or driest) regions in the Tapi basin. Thus, it is expected that rise in total rainfall, in general, and rainfall extremes would make LTB vulnerable to flooding in near future. On other hand, the rainfall scarce regions of the basin (particularly MTB) might experience drought, if the decreasing trends in total rainfall and increasing dry spells may persist in near future. The severity and hazardous effect of such disasters largely depend upon the magnitude of change, socio-economic importance of the area and its resilience. The likely increase in large duration extreme rainfall for Surat city (located on coastal plains of LTB) would increase the vulnerability of urban flooding for prolonged period in near future. The situation may likely to aggravate further when the urban floods occur in concurrence with riverine floods in the Tapi River along with prevailing high tide conditions in the Arabian Sea. Similar conditions were encountered in Surat city during 2013 flood, which was a combination of urban and riverine floods, whereas 2006 flood was a combination of riverine and tidal floods. It worth stating here that the Surat city is the fourth fastest growing city in the world having population of around 4.5 million (www.citymayors.com accessed in April 2019). The increase in rainfall extremes and their intensity would lead to increase in erosion of top fertile belt of the agrarian dominated Purna sub-catchment, thereby, adversely impacting the crop production and yield. The entire MTB (except upstream of Ukai reservoir), characterised by water deficit conditions, is likely to experience severe water stress conditions. Further, it is not a good indicator, specifically, since the persistence of dry spells results in wilting of standing crops. Overall, a distinct heterogeneous response of changing climatic conditions is evident on the rainfall pattern across the basin, wherein, simultaneous dry and wet condition are prevalent in LTB and dry conditions are prevalent over MTB and remaining parts of the basin show mixed responses.

6.2.2 Spatio-Temporal Assessment of Temperature

- **Extreme temperature indices**

The UTB which includes major urban centres such as Amravati, Akola, Buldana, Burhanpur, Bhusaval shows uniform (spatially) significant increase in hottest days (TXx) (see Fig. 6.4a) with MMK Z ranges from 2.28 to 4.45, whereas the maximum value of median slope is found to be 0.02 ºC/year. On the other hand, LTB shows decreasing (insignificant) and MTB shows the inconsistent nature of trend. From Fig. 6.4b, the coldest days (TXn) are uniformly decreasing (insignificant) over the basin excepts some of the grids in PSC which shows the increasing (insignificant) trend. However, maximum rate of decrease in TXn is found to be -

0.0005 ºC/year (median slope) across the basin. The warmest nights (TNx) are decreasing over the UTB and MTB (See Fig. 6.4c) with statistically significant decline (max Z = -3.95) at grids concentrated over the region of MTB. On the other hand, the contrasting nature of trend is observed over the LTB i.e., TNx are increasing with statistically significant rise (max Z = 2.21) over the urban coastal region. The median slope for change in the TNx ranges from -0.014 to 0.008 ºC/year. The Fig. 6.4d clearly indicate the increasing trend in coldest nights over the entire study area, with statistically significant uniform upsurge (spatially) over the LTB (max Z= 4.36) and part of MTB (max Z = 3.71). The maximum and minimum value of median slope for increase in TNn is found to be 0.003 and 0.03 ºC/year respectively.

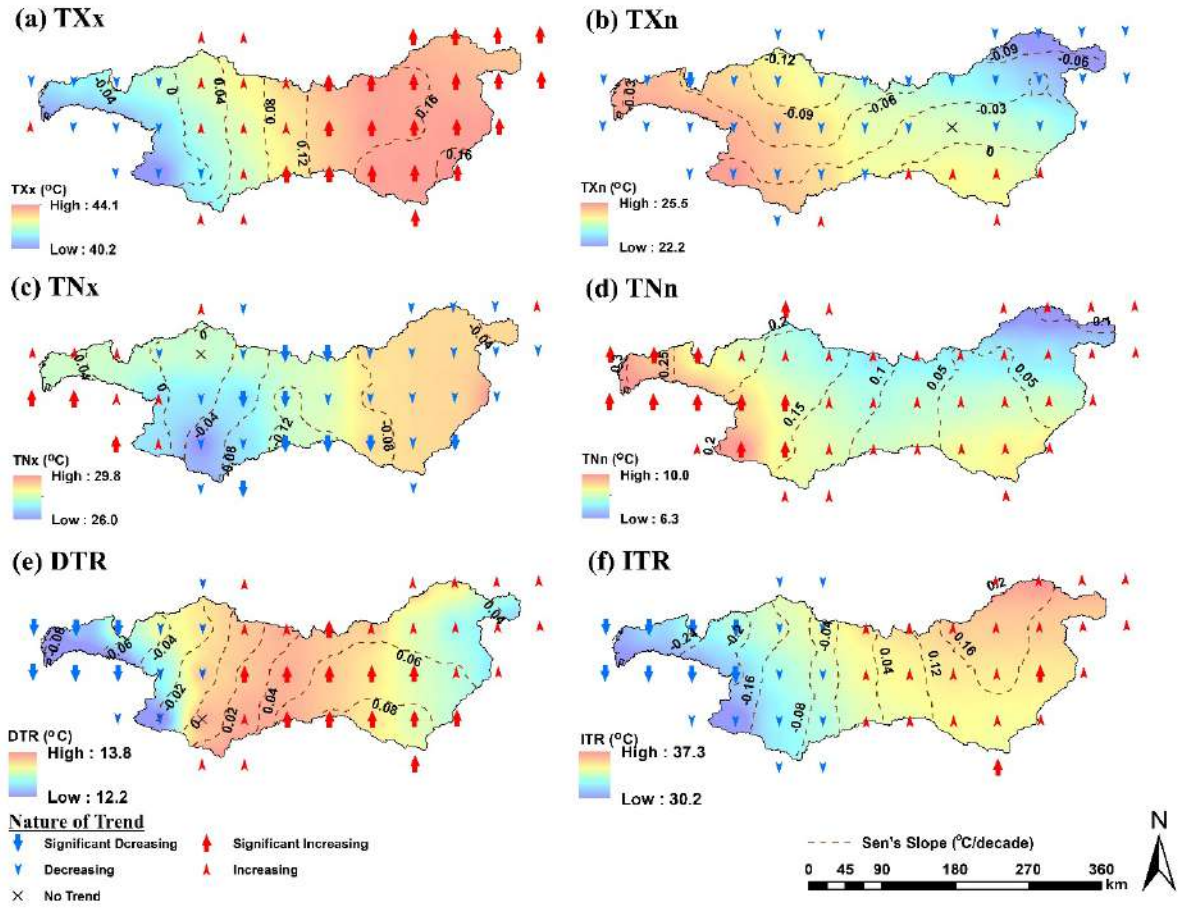

Fig. 6.4 Spatial pattern of time averaged values and trend in extreme temperature indices

The trend in diurnal temperature range (DTR) for the annual scale is shown in Fig. 6.4e, it is increasing over the entire part of UTB with statistically significant rise (max Z = 4.11) in part of PSC and MTB. Contrasting to the nature of trend in UTB, LTB shows uniform statically significant decline (max = -3.79) in DTR. The MTB shows the mix nature trend for the said period, the maximum value of Z for the significant upsurge is found to be 3.32. The median

slope of the changes in DTR over the MTB is ranges from -0.009 to 0.009 ºC/year. Like the DTR, Intra-annual Extreme Temperature Range (ITR) shows the increasing (insignificant) trend (see Fig. 6.4f) over the entire UTB, Mix trend over MTB and statistically significant decrease over the LTB (max Z= -2.68). The increasing trend in DTR and ITR is the clear indicator of increasing temperature variability across UTB, however the contrasting behaviour is observed in LTB.

- **Count and duration-based temperature indices**

The trend in hot spells (HSpC) are decreasing throughout the basin (see Fig. 6.5a) except urban coastal part of LTB and nearby area of Western Ghats with (increase) no significant changes, the median slope for the changes in hot spell count is ranges from -0.027 and 0.029 spells/year. On the contrary, longest (duration) hot spells (HSpMax) are increasing across the entire basin (See Fig. 6.5b) of which only four grids (spatially non uniform) show significant increase (max Z = 3.26). The cold spell counts (CSpC) are decreasing over the entire basin (See Fig. 6.5c) with statistically significant decrease at hilly portion of BSC (max Z = -4.82). From Fig 6.5d it is observed that, the longest cold spells show heterogeneous nature of trend across the study area, increasing (non-significant) over the UTB except hilly portion of BSC where it decreases. The longest duration of cold spells is decreasing over the LTB with significant changes near coastal part (Max Z= -2.84) on the other hand MTB exhibits the mix trend. From Fig. 6.5e, it is observed that the basin Tx37 is increasing uniformly over the entire basin with significant increase in the coastal part of LTB and south-west region of MTB (Max Z = 2.68). The minimum and maximum value of median slope of Tx37 is found to be 0.02 and 0.27 days/year. The increase in Tx37 likely to cause adverse impact on human health. With a high humidity a person can suffer from heat stress disorders even with the temperature at 37°C or 38°C.

6.2.3 Spatio-Temporal Assessment of Streamflow Indices

- **Detection and attribution of gradual changes in streamflow**

The gradual trends in annual runoff series have been investigated using Modified Mann-Kendall (MMK) and Spearman Rho (SR) tests. Further, the magnitude of trend in the time series is estimated from Sen's slope estimator test. The changes in streamflow trends are attributed to annual rainfall variability and the impact of anthropogenic changes such as changes in the land use pattern, streamflow regulation, etc., and necessary inferences were drawn, as described in following paragraphs. The streamflow analysis revealed decreasing trend in annual runoff across the Purna sub-catchment at Lakhpuri, Gopalkheda and Yerli

stream gauging stations (see Fig. 6.6). The decrease in magnitude of trend of annual runoff obtained from Sen's slope (β) are found to be -2.57, -1.05 and -29.36 Mm^3/year for Lakhpuri, Gopalkheda and Yerli stations respectively.

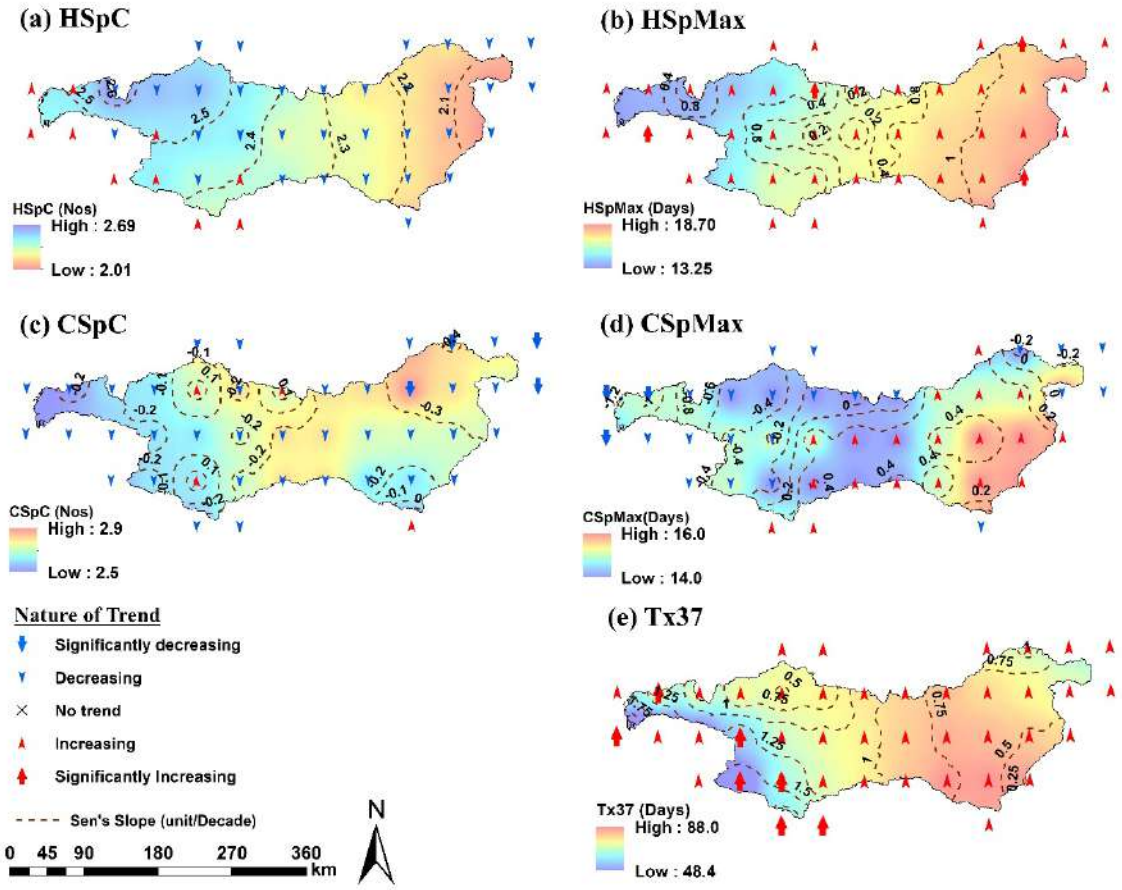

Fig. 6.5 Spatial pattern of time averaged values and trend in count & duration temperature indices

The LULC analyses for Purna sub-catchment show that post 1990, there has been a steady rise in the agricultural land owing to improvement in the irrigation facilities due to enhancement in minor and medium hydraulic structures (water bodies) in the sub-catchment. The streamflow analyses of Burhanpur sub-catchment revealed an increase in annual runoff at all the three stream gauging stations, see Fig. 6.6. The magnitude of such increasing trend, represented as Sen's slope β values, were 23.00, 5.22 and 44.36 Mm^3/year for Dedtalai, Burhanpur and Hatnur dam respectively. The rainfall exhibits inverse correlation with runoff at all the stations in this sub-catchment, wherein increase in annual runoff and corresponding decrease in annual rainfall are observed. However, such inverse correlation has been found to be very weak. The increase in annual runoff could possibly be due to significant deforestation in the Burhanpur sub-

catchment, wherein, the forest cover has been found to decrease by 18.07% during the period from 1980-2010.

The annual runoff exhibits decreasing trends for both Girna dam and Dapuri stream gauging stations, see Fig. 6.6. Compared to Girna dam (β = -3.65 Mm^3/year), a sharp decrease in annual runoff is observed for Dapuri (β = -11.50 Mm^3/year) stream gauging station. This is attributed to non-release of flows from Girna dam on regular basis, as the spillway is operated to pass the heavy floods very infrequently. A decreasing trend in annual rainfall across the Girna sub-catchment has been reported over the period of analysis. Thus, it can be summarized that decrease in runoff in the Girna sub-catchment is partially attributed to decrease in annual rainfall and partially due to anthropogenic changes in form of enhancement in agricultural land and streamflow regulation exercised by the Girna reservoir on Dapuri stream gauging station. The annual runoff reported decreasing trends for Bori and Panjhara sub-catchments, see Fig. 6.6. The slope of the trend magnitude (β) of annual runoff at Malkheda and Morane are found to be -1.38 and -1.14 Mm^3/year respectively. On the other hand, the annual rainfall exhibited increasing trends for Bori (β = 2.5 mm/year) and Panjhara (β = 2.4 mm/year) sub-catchments. Thus, the rainfall and runoff behave in a contrary manner, wherein, the annual runoff is found to decrease despite increase in the annual rainfall. Under such circumstances, the influence of possible anthropogenic changes becomes more evident and could be the primary reason for decrease in runoff.

The analysis of gradual trends in streamflows of Tapi River in the Middle Tapi sub-basin (excluding Girna, Bori and Panjhara sub-catchments) indicated consistent decrease in annual runoff at all the four stations (see Fig. 6.6). The MMK *Z*-values for annual runoff at Savkheda, Gidhade, Sarangkheda and Ukai dam are found to be -2.22, -2.21, -0.75 and -0.05 respectively. The annual rainfall exhibits decreasing trend at Savkheda, Gidhade and Ukai dam sub-catchments, while increasing trend has been observed at Sarangkheda sub-catchment. This decrease in annual rainfall is found in line with the decrease in annual runoff in the Middle Tapi sub-basin. Thus, the climatic variability is the major driving factor for declining streamflows in the main Tapi River in Middle Tapi sub-basin.

The streamflow analyses exhibited decreasing trends in annual runoff at Ghala stream gauging station during the period 1978-2004, see Fig. 6.6. A significant decrease in annual runoff has

been observed at Ghala station (β = -190.47 Mm^3/year) vis-à-vis Ukai dam (β = -6.83 Mm^3/year). This significant decrease in annual runoff at Ghala station is primarily due to decrease in annual rainfall in Upper and Middle Tapi sub-basins, which enforces reduction in the reservoir releases due to lesser availability of water in the Ukai reservoir.

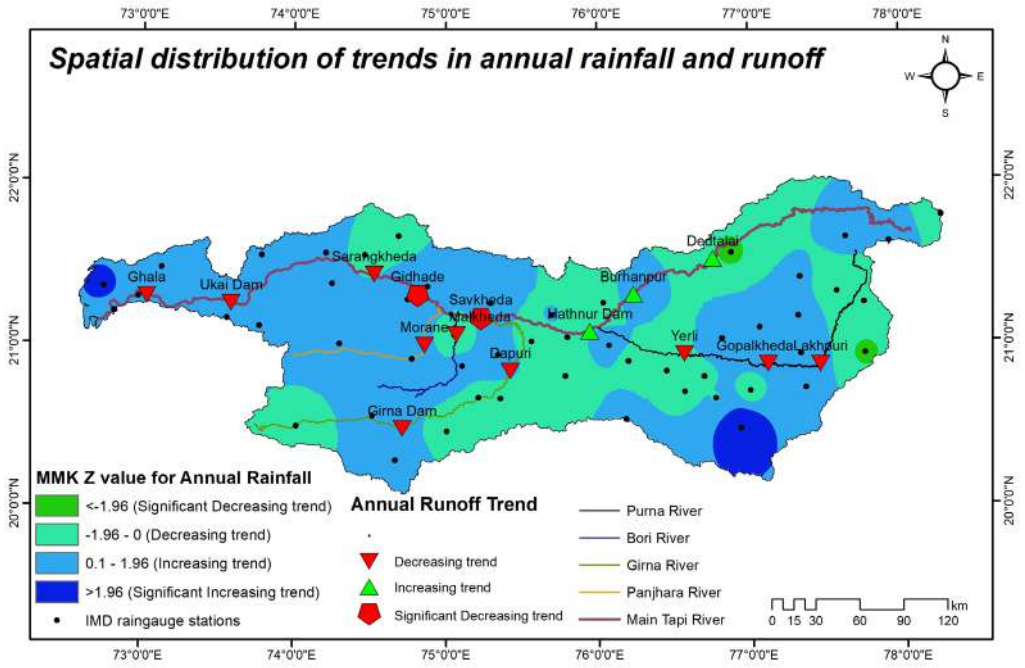

Fig. 6.6 Spatial distribution of trends in annual rainfall and runoff across Tapi basin

- **Trends in extreme rainfall and streamflow indices**

The trends in extreme rainfall and streamflow indices, mentioned in Table 3.3, are estimated using non-parametric Modified Mann-Kendall (MMK) and Sen's slope estimator tests. The spatial variation of trends in extreme rainfall indices considering the rain gauge stations in the Tapi basin are demonstrated using spatial analyst tool of ArcGIS® 10.6, see Fig. 6.7, whereas the station-wise nature of trends for extreme streamflow indices derived from MMK test are also represented on the same map as a point feature. From Fig. 6.7a, it is seen that the headwater region of Tapi River exhibits increasing trend in Rx1day which precipitates into increasing Qx1day in the stream gauging stations (viz., Dedtalai, Burhanpur and Hatnur dam) along the Tapi River in Upper Tapi sub-basin. Moreover, the headwater and downstream region of Purna River reflects decreasing trend in Rx1day, while increasing trend is observed in the mid latitudes of Purna River which has resulted into increasing trends in Qx1day for Lakhpuri and Gopalkheda stations and decreasing trend at Yerli station. Further, most parts of the Middle exhibit decreasing trends in Rx1day, whereas Lower Tapi basin exhibits increasing trend. The analysis of trends in Rx5day shows increasing trends across most parts of the basin. The trends

in Qx5day showed decreasing tendency across 9 out of 14 stream gauging stations, contrary to increasing trend in Rx5day, see Fig. 6.7b. Further, increasing trends in Qx5day were observed at Dedtalai, Malkheda and Morane stations, which are in line with the Rx5day trends.

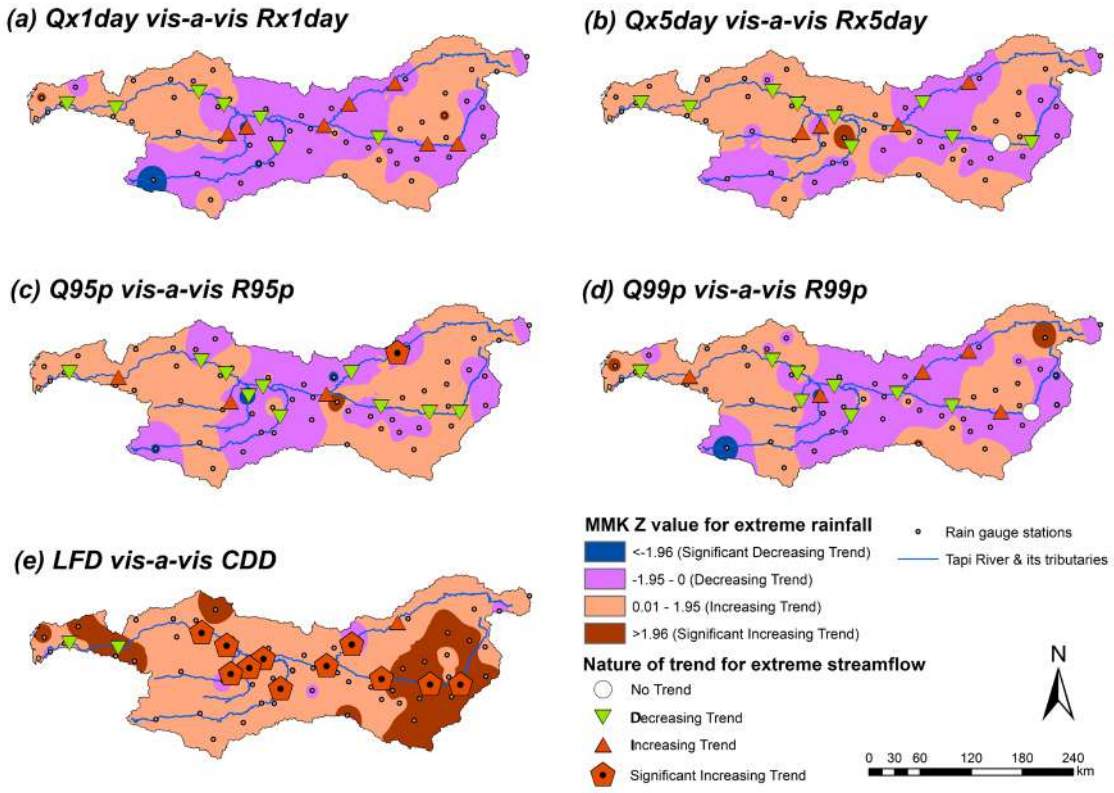

Fig. 6.7 Spatial distribution of trends in extreme rainfall and streamflow indices across Tapi basin

The trends in R95p and R99p exhibit heterogeneity across the basin, however, they exhibit similar spatial pattern as that of Rx1day trends. From Figs. 6.7c-d, it can be observed that the extreme rainfall shows decreasing trends over most parts of Middle Tapi basin and partially over the plains of Purna River. On other hand, the streamflow indices Q95p and Q99p exhibit decreasing trends across most stations, except for Ukai dam and Dedtalai for both indices. The maximum consecutive dry days (CDD) and low flow days (LFD) were estimated for the study period 1973-2013. From Fig. 6.7e, uniformly alarming increasing trends in CDD can be observed across the Tapi basin, with predominantly significant increasing trend in Lower Tapi basin and Purna sub-catchment. The increase in CDD would imply prolonged dry weather conditions which would result in rise in mean temperature across the basin. Further, the LFD were also found to be significantly increasing at all the stations except Ukai dam and Ghala stations.

6.2.4 Impact of Climate Change on hydro-climatology of Tapi River Basin

The hydroclimatic variability in precipitation and temperature for the period 2011-2100 under RCP 4.5 and RCP 8.5 scenarios have been ascertained for different sub-periods, i.e., near-, future (NF) 2011-2040, mid-future (MF) 2041-2070, and far-future (FF) 2071-2100. The rainfall and temperature indices, discussed in Table 4.1, are derived separately for five GCM models. The calculated indices are ensembled using REA (Giorgi and Mearns 2002), and then changes in mean and temporal variability were assessed for the three different sub-periods (Kumar et al. 2021). Keeping in view the physio-climatic heterogeneity of TRB, the mean values have been calculated for different sub-basins, i.e., Purna and Burhanpur sub-catchments in UTB, MTB, and LTB.

The total rainfall (PRCPTOT) values for the base line period (1951-2005), statistically downscaled from GCMs (ensembled average), are approximately 23.70% lower than corresponding IMD values for the same period over the TRB. The downscaled PRCPTOT values are invariably lower than their corresponding IMD values for base line period for Upper (UTB), middle (MTB) basins for near, mid, and far future. On the other hand, these downscaled values are higher for LTB for all future periods for RCP 4.5 and RCP 8.5 scenarios. Further it is noted that PRCPTOT values are continuously increasing from near future to far future for both RCP 4.5 and RCP 8.5 scenarios. The downscaled values of rainy days (RD) for the baseline period (1951-2005) are constantly higher than corresponding IMD values over the entire TRB for the same period. Also, the downscaled RD values are consistently increasing for Upper Tapi basin (Purna and Burhanpur sub-catchment) from near to far future under RCP 4.5 scenario. The simple daily intensity index (SDII) (See Fig. 6.8 - 6.9 and Table 6.1) the ratio of PRCPTOT to RD is underestimated by 35%, on average for TRB for GCM historical period (1951-2005) as compared to the corresponding IMD values for the same period. The SDII values estimated from downscaled precipitation has been found to be higher for LTB than UTB and MTB.

The consecutive dry days (CDD) values (See Fig. 6.8 - 6.9 and Table 6.1) estimated from the GCM downscaled data for the base line period is underestimated with reference to the corresponding IMD values of the same period. Further, the CDD values are consistently decreasing for UTB (Purna and Burhanpur sub-catchment) and MTB for near to far future for RCP 4.5 and 8.5 scenarios. However, such decreasing trends are not seen in the LTB. The consecutive wet days (CWD) values are estimated from downscaled data from the GCM are

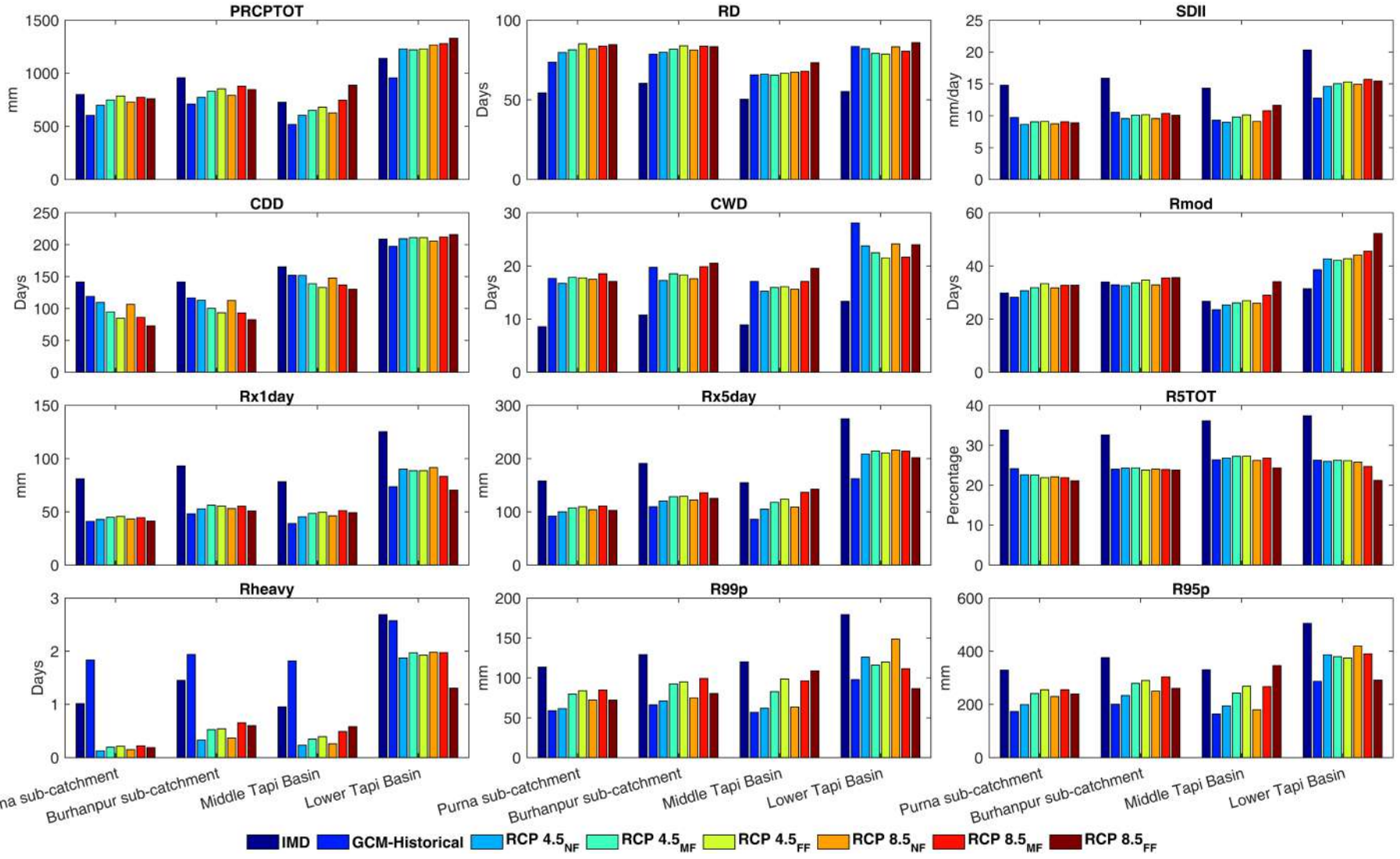

Fig. 6.8 Mean values of extreme rainfall indices over TRB during near-, mid-, and far-future under RCP 4.5 and RCP 8.5 scenarios

Table 6.1 Variation of mean rainfall indices over TRB for RCP 4.5 and RCP 8.5 scenarios during near-, mid-, and far-future

Emission Scenarios	Rainfall Indices	Purna sub-catchment			Burhanpur sub-catchment			Middle Tapi Basin			Lower Tapi Basin		
		NF	MF	FF	NF	MF	FF	NF	MF	FF	NF	MF	FF
RCP 4.5	PRCPTOT	697.5	748.3	785.6	772.5	830.7	852.8	604.3	649.9	680.7	1228.1	1220.3	1227.4
	RD	79.6	81.3	85.1	79.9	81.7	83.8	66.1	65.6	66.7	82.1	79.1	78.7
	SDII	8.6	9.0	9.1	9.5	10.1	10.2	9.0	9.8	10.1	14.6	15.0	15.3
	CDD	109.3	94.6	84.7	113.1	100.3	93.3	151.9	138.8	132.9	209.2	211.2	211.2
	CWD	16.7	17.8	17.8	17.3	18.5	18.3	15.2	15.9	16.1	23.8	22.5	21.5
	Rmod	30.7	31.8	33.3	32.6	33.7	34.6	25.3	26.1	27.0	42.6	42.1	42.7
	Rx1day	42.8	44.9	45.6	52.7	56.1	55.5	45.4	48.4	49.6	90.0	88.5	88.6
	Rx5day	100.2	107.3	109.6	120.4	128.5	129.2	104.7	117.9	123.9	208.5	214.1	210.8
	R5TOT	22.6	22.6	21.9	24.3	24.4	23.8	26.8	27.2	27.3	26.0	26.3	26.1
	Rheavy	0.1	0.2	0.2	0.3	0.5	0.5	0.2	0.3	0.4	1.9	2.0	1.9
	R99p	61.5	79.5	83.8	71.0	92.5	95.0	62.0	82.7	98.6	125.9	116.1	120.0
	R95p	199.4	241.2	255.1	233.8	279.0	290.0	194.5	242.9	268.7	386.7	379.5	374.8
RCP 8.5	PRCPTOT	729.7	772.8	759.2	790.8	876.9	845.9	626.4	745.6	887.5	1266.4	1278.2	1328.9
	RD	81.9	83.7	84.7	81.3	83.7	83.3	67.3	67.8	73.4	83.2	80.5	85.8
	SDII	8.7	9.0	8.9	9.6	10.4	10.1	9.1	10.8	11.6	14.9	15.7	15.5
	CDD	106.5	85.9	72.8	112.6	93.1	82.5	147.7	136.7	130.2	205.5	212.1	215.9
	CWD	17.5	18.5	17.1	17.6	19.9	20.5	15.6	17.1	19.5	24.2	21.7	24.0
	Rmod	31.8	32.7	32.7	32.9	35.5	35.6	26.0	28.9	34.1	44.1	45.6	52.2
	Rx1day	43.2	44.5	41.4	53.0	55.2	50.8	46.3	51.2	49.3	91.7	83.2	70.3
	Rx5day	103.8	110.7	102.6	122.3	135.8	125.2	108.9	136.9	142.6	216.0	213.9	202.0
	R5TOT	22.1	21.9	21.1	24.0	23.9	23.8	26.2	26.8	24.3	25.8	24.7	21.2
	Rheavy	0.2	0.2	0.2	0.4	0.7	0.6	0.3	0.5	0.6	2.0	2.0	1.3
	R99p	72.2	84.6	72.1	74.9	99.2	80.5	63.5	96.2	108.8	148.5	111.4	86.7
	R95p	229.7	255.6	239.7	250.4	303.8	260.4	179.8	267.3	346.1	419.7	390.4	291.6

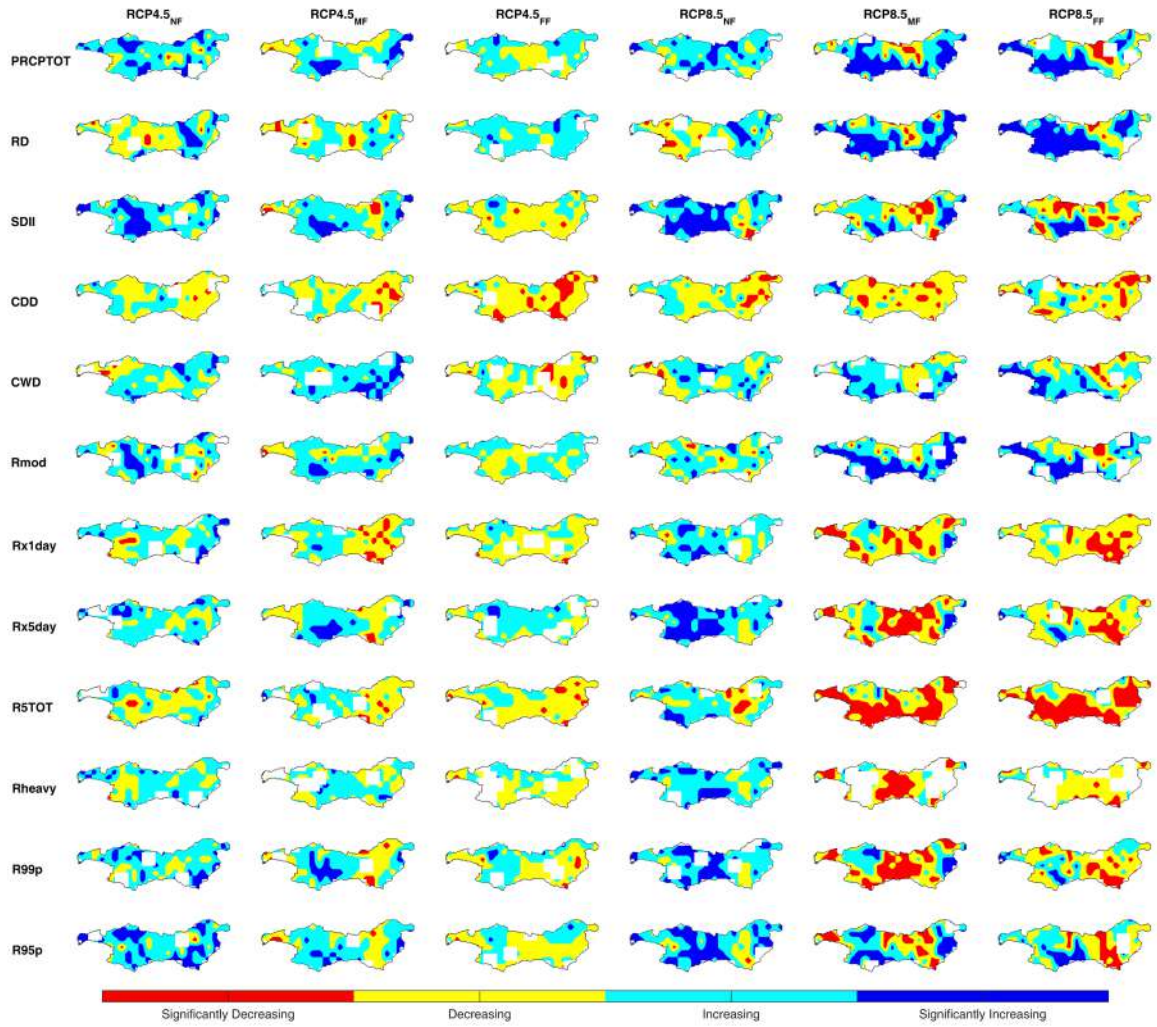

Fig. 6.9 Nature of trend in extreme rainfall indices over TRB during near-, mid-, and far-future under RCP 4.5 and RCP 8.5 scenarios

overestimated with reference to corresponding IMD values for the baseline period. The CWD area increasing from near future (NF) period to Mid future (MD) and then became constant for far future (FF) for the UTB and MTB for RCP 4.5 scenario. However, for RCP 8.5 scenario, the CWD values, may continuously increase from NF to FF for UTB and MTB sub basins.The number of moderate rainy days (Rmod) for UTB i.e., for both Purna and Burhanpur sub-catchment s area marginally higher for the future periods as compared to the baseline period. The Rmod for the base line period is higher than those estimated from the GCM model. Further, in future the Rmod is consistently increasing from NF-FF for both RCP 4.5 and RCP 8.5 (See Fig. 6.8 - 6.9 and Table 6.1).

The estimated annual maximum one-day rainfall (Rx1day) (See Fig. 6.8 - 6.9 and Table 6.1) amount, obtained from GCM downscaled precipitation is underestimated by 47.2% for TRB

for the base line period. The Rx1day amount is higher for Lower Tapi Basin for historical as well as future periods. Incidentally for RCP 8.5, the Rx1day is decreasing continuously from NF to FF in lower Tapi basin. The annual maximum five-day continuous rainfall (Rx5day) is very similar to Rx1day as described above. On the other hand, the proportion of annual rainfall from top 5 events in a year (R5TOT) for MTB and LTB are marginally higher than UTB for baseline as well as future periods. In RCP 8.5 scenario R5TOT is decreasing continuously from NF to FF periods for LTB. The number of days when rainfall ≥ 65.5 mm and < 124.5 mm (Rheavy) (see Fig. 6.8 and 6.9) estimated from downscaled GCM rainfall shows that, it is overestimated for UTB and MTB with reference to historically observed values. The Rheavy is likely to decrease significantly for NF, MF and FF periods for both RCP 4.5 and 8.5 scenarios. However, the Rheavy will have higher values for LTB in future compared to UTB and MTB. The extremely wet days (R99p) estimated for downscaled rainfall for historical periods indicates the underestimation for TRB with reference to observed period. However, the estimated values are increasing continuously from NF to FF for UTB and MTB. The similar characteristics are shown by very wet days (R95p) as those reflected R99p.

The variation of temperature-based indices, as shown in Table 4.1, were quantified for period 2011 to 2100 over the UTB (Purna and Burhanpur sub-catchments), MTB and LTB (See Fig. 6.10 - 6.11 and Table 6.2) with reference to their mean values during base line period (1951-2005). The indices TXm, TNm TXx, TXn, TNx and TNn are increasing continuously for near future from NF to FF for both RCP 4.5 and 8.5 with reference to their values for base-line period for all three sub-basins. As expected, the rise in more for RCP 8.5 and RCP 4.5 in the whole TRB. The variation of aforesaid temperature indices over the TRB for different sub-periods in future for RCP 8.5 and RCP4.5 scenarios shown in Fig. 6.11. The DTR is invariably overestimated for the GCM downscaled data vis-à-vis their historical values for all the sub-basins of TRB. The DTR is continuously decreasing from NF to FF (see Fig. 6.10 and Table 6.2) for RCP 4.5 and 8.5 scenarios. The longest duration of hot spell (HSpMax) estimated from GCM downscaled temperature data is overestimated as compared to the values of base-line period. For RCP 4.5 scenarios, the HSpMax is likely to increase from NF to MF period, however, it decreases from MF to FF for all the sub-basins of TRB. On the other hand, HSpMax is likely to continuously increase from NF to FF for RCP 8.5 scenario for all the subbasins of TRB. Similarly, the Hot spell count (HSpC) is significantly overestimated for base-line period via-a-vis corresponding values of HSpC for the base line period. The HSpC values are likely to increase continuously from NF to FF for both RCP 4.5 and 8.5 scenario in the TRB.

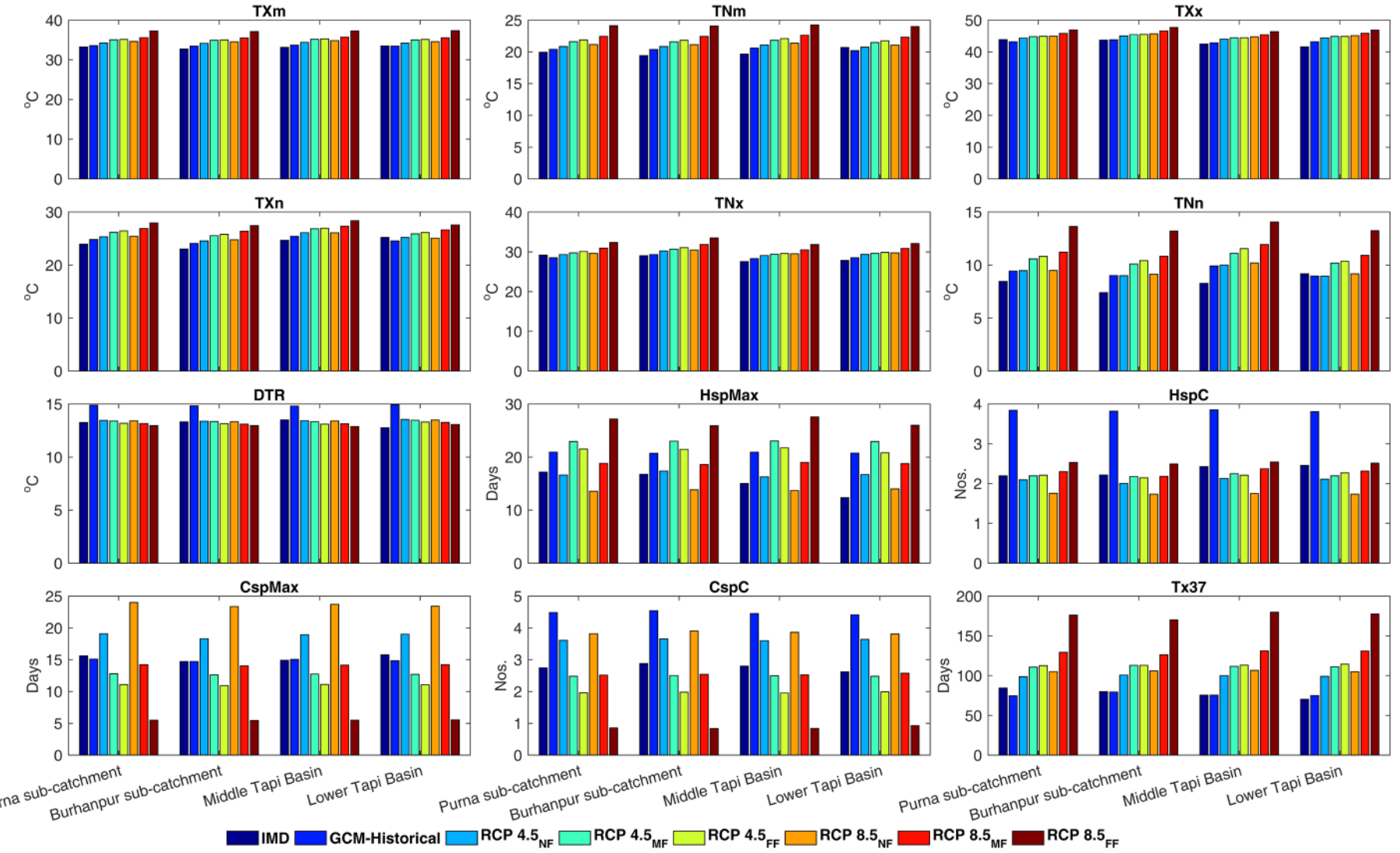

Fig. 6.10 Mean values of extreme temperature indices over TRB during near-, mid-, and far-future under RCP 4.5 and RCP 8.5 scenarios

Table 6.2 Variation of mean Temperature indices over TRB for RCP 4.5 and RCP 8.5 scenarios during near-, mid-, and far-future

Emission Scenarios	Temperature Indices	Purna sub-catchment			Burhanpur sub-catchment			Middle Tapi Basin			Lower Tapi Basin		
		NF	MF	FF	NF	MF	FF	NF	MF	FF	NF	MF	FF
RCP 4.5	TXm	34.2	35.0	35.1	34.1	34.9	35.0	34.4	35.1	35.2	34.2	35.0	35.1
	TNm	20.8	21.6	21.9	20.8	21.6	21.8	21.1	21.8	22.1	20.7	21.5	21.7
	TXx	44.3	44.8	44.9	45.0	45.5	45.5	44.0	44.4	44.4	44.4	44.8	44.8
	TXn	25.3	26.2	26.5	24.6	25.5	25.8	26.1	26.8	26.9	25.2	25.9	26.2
	TNx	29.3	29.7	30.1	30.2	30.6	31.0	29.1	29.4	29.6	29.3	29.6	29.9
	TNn	9.5	10.6	10.8	9.0	10.1	10.4	10.0	11.1	11.5	9.0	10.2	10.4
	DTR	13.5	13.4	13.2	13.4	13.4	13.2	13.4	13.3	13.1	13.5	13.5	13.3
	HspMax	16.6	22.9	21.5	17.4	23.0	21.4	16.3	23.0	21.7	16.7	22.9	20.8
	HspC	2.1	2.2	2.2	2.0	2.2	2.1	2.1	2.2	2.2	2.1	2.2	2.3
	CspMax	19.1	12.8	11.1	18.3	12.6	10.9	18.9	12.8	11.1	19.0	12.7	11.1
	CspC	3.6	2.5	2.0	3.7	2.5	2.0	3.6	2.5	2.0	3.6	2.5	2.0
	Tx37	98.7	110.6	112.5	100.7	113.0	112.9	100.0	111.6	113.1	99.1	111.0	114.4
RCP 8.5	TXm	34.6	35.6	37.3	34.5	35.5	37.1	34.8	35.7	37.3	34.6	35.5	37.3
	TNm	21.1	22.4	24.1	21.1	22.4	24.1	21.4	22.6	24.3	21.0	22.3	24.0
	TXx	45.0	45.9	46.9	45.7	46.6	47.7	44.7	45.4	46.4	45.1	45.9	46.9
	TXn	25.4	26.9	28.0	24.8	26.4	27.5	26.1	27.3	28.4	25.1	26.6	27.6
	TNx	29.6	30.9	32.4	30.4	31.8	33.5	29.5	30.5	31.8	29.7	30.8	32.1
	TNn	9.5	11.2	13.6	9.1	10.8	13.2	10.2	11.9	14.0	9.2	10.9	13.2
	DTR	13.4	13.2	13.0	13.3	13.1	13.0	13.4	13.1	12.9	13.5	13.3	13.1
	HspMax	13.6	18.8	27.2	13.8	18.6	25.9	13.7	19.0	27.6	14.0	18.8	26.0
	HspC	1.8	2.3	2.5	1.7	2.2	2.5	1.8	2.4	2.5	1.7	2.3	2.5
	CspMax	24.0	14.2	5.5	23.4	14.0	5.5	23.7	14.1	5.5	23.4	14.2	5.5
	CspC	3.8	2.5	0.9	3.9	2.5	0.8	3.9	2.5	0.8	3.8	2.6	0.9
	Tx37	105.0	129.3	176.2	106.0	126.1	170.1	106.6	131.1	179.7	104.9	130.8	177.6

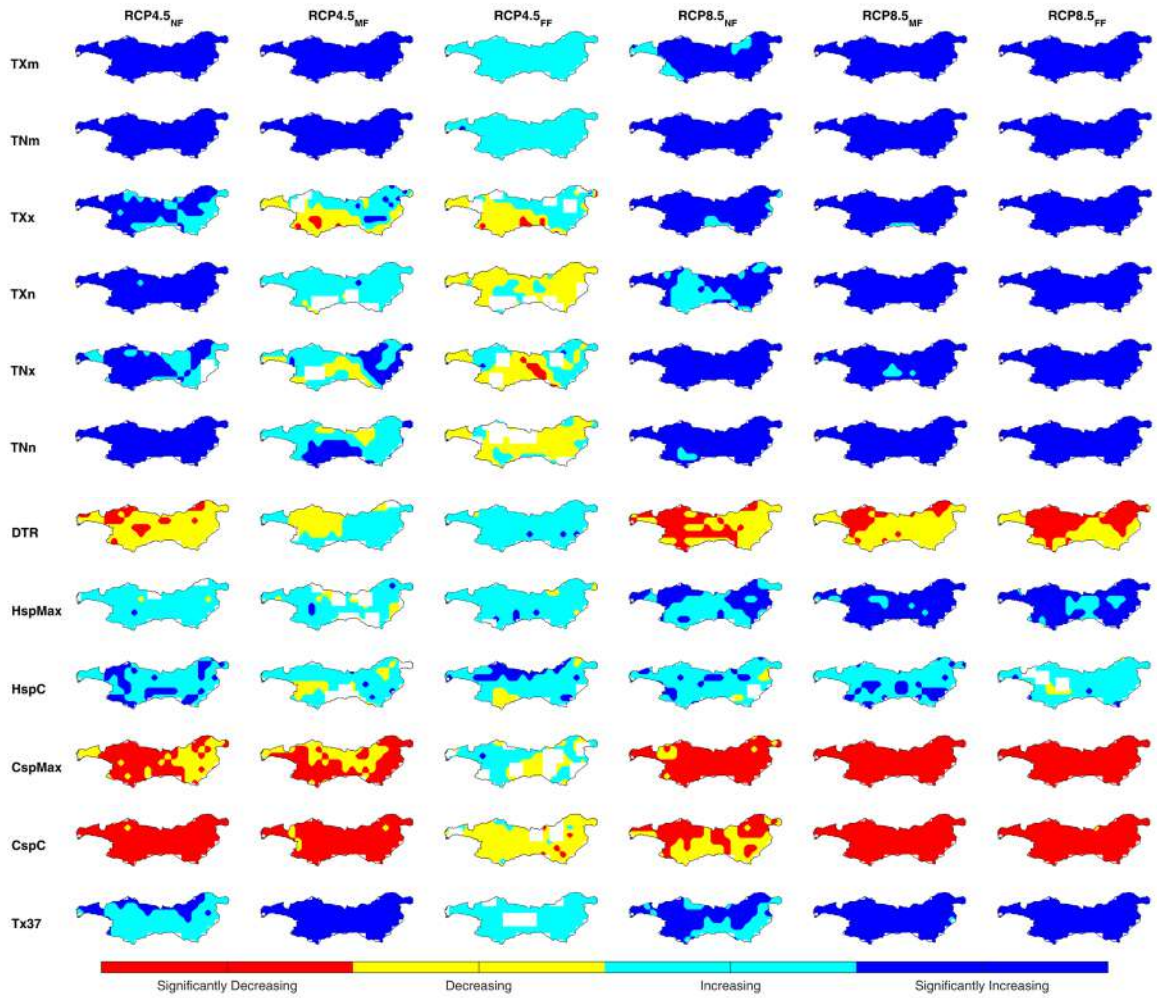

Fig. 6.11 Nature of trend in extreme temperature indices over TRB during near-, mid-, and far-future under RCP 4.5 and RCP 8.5 scenarios

The Longest duration of cold spell (CSpMax) is invariably having identical values which area derived from statistically downscaled temperature data and those obtained from the IMD data for the corresponding period. Further it is seen that CSpMax values are continuously decreasing from NF to FF for both RCP 4.5 and 8.5 scenarios. The decrease is at the steep rate for RCP 8.5 compared to RCP 4.5. The TX37 derived from statistically downscaled GCM data is having similar values as those obtained from IMD data for the baseline period. The Tx37 value are continuously increasing from NF-MF-FF periods for all subbasins of TRB. The increase is more vigorous for RCP4.5 vis-à-vis RCP 4.5 scenario.

6.3 IMPACTS ON WATER AVAILABILITY

The baseline hydrologic models developed using observed IMD data for the period 1994-2013 were used to estimate the water availability at various stream gauging sites in TRB for historical and future periods. The KRSD data of five GCM models have been used to simulate the

response of TRB sub-catchments under the changing climate. The change in long-term mean for historical, near-, mid-, and far-future periods are estimated for the corresponding period, i.e., 1981-2005, 2011-2040, 2041-2070, and 2071-2100. The estimated changes were then ensembled considering equal weights to all five GCMs, and assuming the changes to be Gaussian, the 95% confidence bounds were calculated (Giorgi and Mearns 2002). The respective changes in the percentage dependable flows during near-, mid-, and far-future are discussed with the help of the flow duration curve (FDC).

6.3.1 Purna sub-catchment

The long-term mean of rainfall, temperature (Tmax and Tmin), and streamflow in the Purna sub-catchment for RCP 4.5 and RCP 8.5 scenarios are calculated for different sub-periods and are reported in Annexure (see Fig. **A3 to A10, in Annexure**). The ensembled change in the mean (and their uncertainty band, i.e., 95% confidence band) are shown in Fig. 6.12. The simulated Tmax (Tmin) during the historical reference period varied within -6.0% to 6.1% (-3.7% to 9.2%) of the observed data, and their respective confidence bounds are 0.2ºC – 1.3ºC (0.2ºC – 1.0ºC). From Fig. 6.12, it is seen that June – August months would be getting lesser rainfall while September – May months may likely to get more rainfall in the future. Notedly, the non-monsoonal rainfall is overestimated by 7.1% to 170.7% during the future period for both RCP 4.5 and RCP 8.5 scenario. The maximum temperature (Tmax), invariably, is expected to be higher than historical mean in future with continuous rise from NF to FF, for both RCPs scenarios. The minimum temperature (Tmin) is increasing more vigorously in the basin as compared to Tmax for the future periods for both RCP 4.5 and 8.5 scenarios.

Apart from the mean changes discussed above, it is evident from Fig. 6.12 that the uncertainty in the future rainfall estimates is very high during monsoon and post-monsoon seasons. The increasing rainfall conditions over winter and pre-monsoon seasons with less uncertainty indicate the change is very likely. On the contrary, considerable uncertainties are involved in the change estimated in the monsoon and post-monsoon streamflows. Unlike rainfall and streamflow, the Tmax and Tmin indicate consistently rising temperature in the future under both the RCP scenarios; however, the uncertainty is also very high in both variables. The flow duration curve (FDC) at three gauging sites, i.e., Yerli, Gopalkheda, and Lakhpuri (see Fig. 6.13) for present and future periods, are also analysed. Also, the FDC at the outlet point of the Purna sub-catchment is analysed using the simulated outflow at the confluence point (see Fig. **A11, in Annexure**).

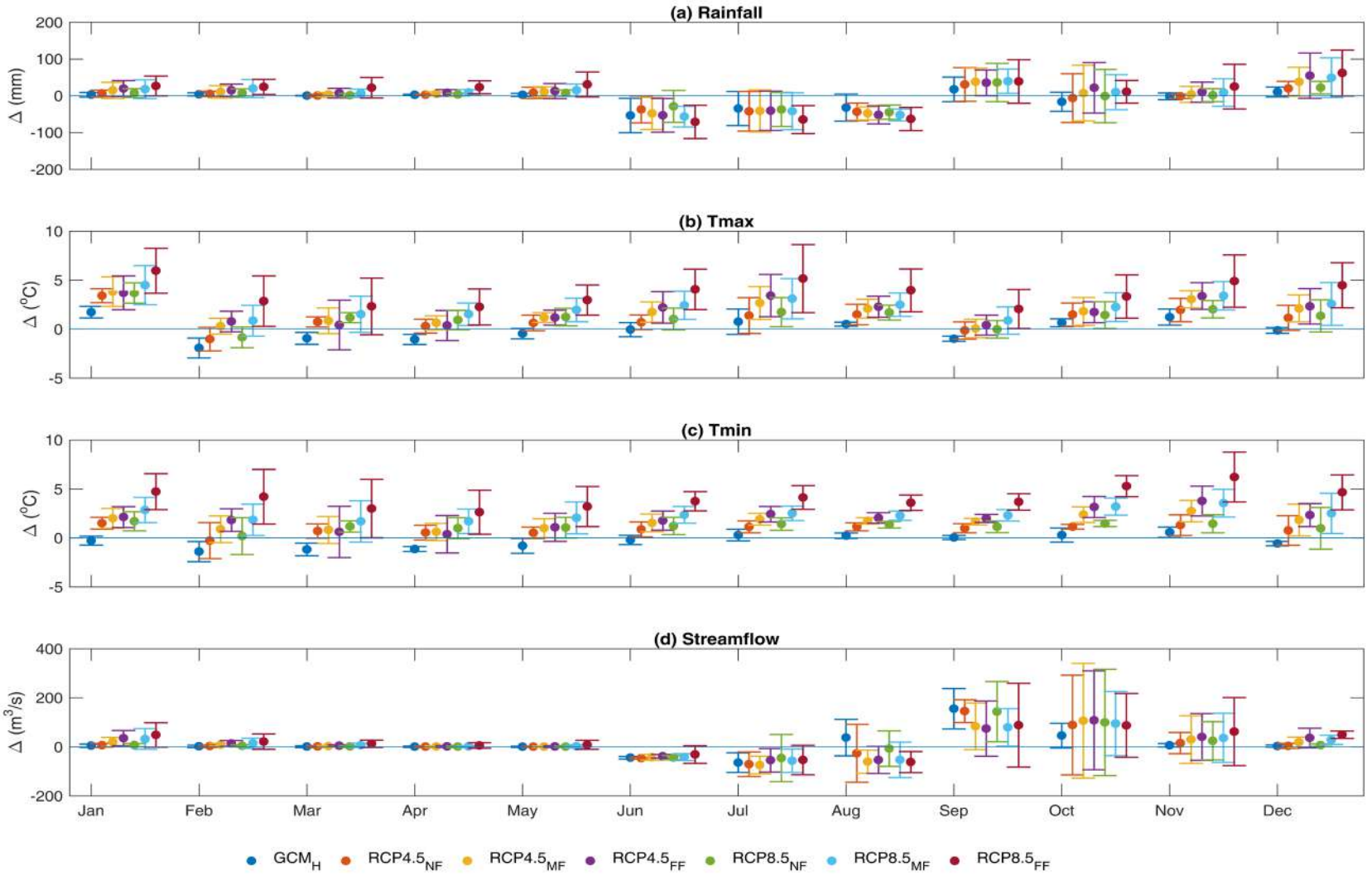

Fig. 6.12 Mean change in Rainfall, Tmax, Tmin, and Streamflow in Purna sub-catchment during near-, mid-, and far-future under RCP 4.5 and RCP 8.5 scenarios.

From Fig. 6.13, the FDC at Yerli, Gopalkheda and Lakhpuri stream gauging stations for different sub-periods under RCP 4.5 and 8.5 scenarios indicate the following:

- The 10% (Q_{10}) and 50% (Q_{50}) average monthly dependable flow, in m^3/s, (monthly yield, in MCM) at Yerli, Gopalkheda, and Lakhpuri gauging sites during the reference period are 195.7 (507.2), 100.0 (259.2), and 42.6 (110.4); and 5.3 (13.7), 3.8 (9.7), and 1.2 (3.0) respectively. The corresponding estimates at the outlet of the Purna sub-catchment are 215.5 (558.8) and 7.48 (19.4), respectively.
- The Q_{10} and Q_{50} monthly yield (in MCM) at the outlet point of Purna sub-catchment during near-, mid-, and far-future under RCP 4.5 (RCP 8.5) scenario would be 607.1 (738.7), 1096.3 (1036.9), and 1075.6 (953.0); and 21.1 (21.9), 29.3 (40.1), and 45.3 (85.7) respectively. The corresponding monthly yields at Yerli stream gauging station are 704.1 (736.0), 605.7 (635.6), and 636.4 (647.6); and 22.8 (24.1), 28.5 (35.8), and 39.8 (70.7) respectively; at Gopalkheda stream gauging station are 413.8 (440.2), 389.6 (412.6), and 396.4 (417.0); and 13.3 (13.5), 17.2 (21.6), and 24.5 (39.7) respectively; and at Lakhpuri stream gauging station are 157.5 (169.0), 141.8 (142.1) and 147.4 (116.8); and 4.9 (4.9), 5.6 (6.7), and 7.0 (10.2) respectively.

(a)

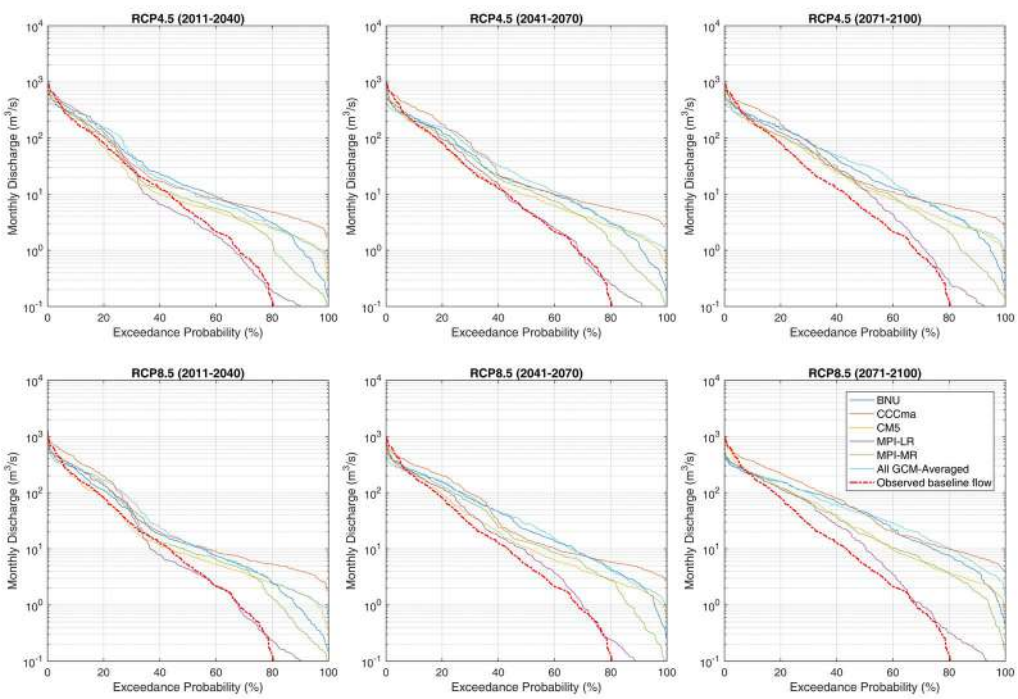

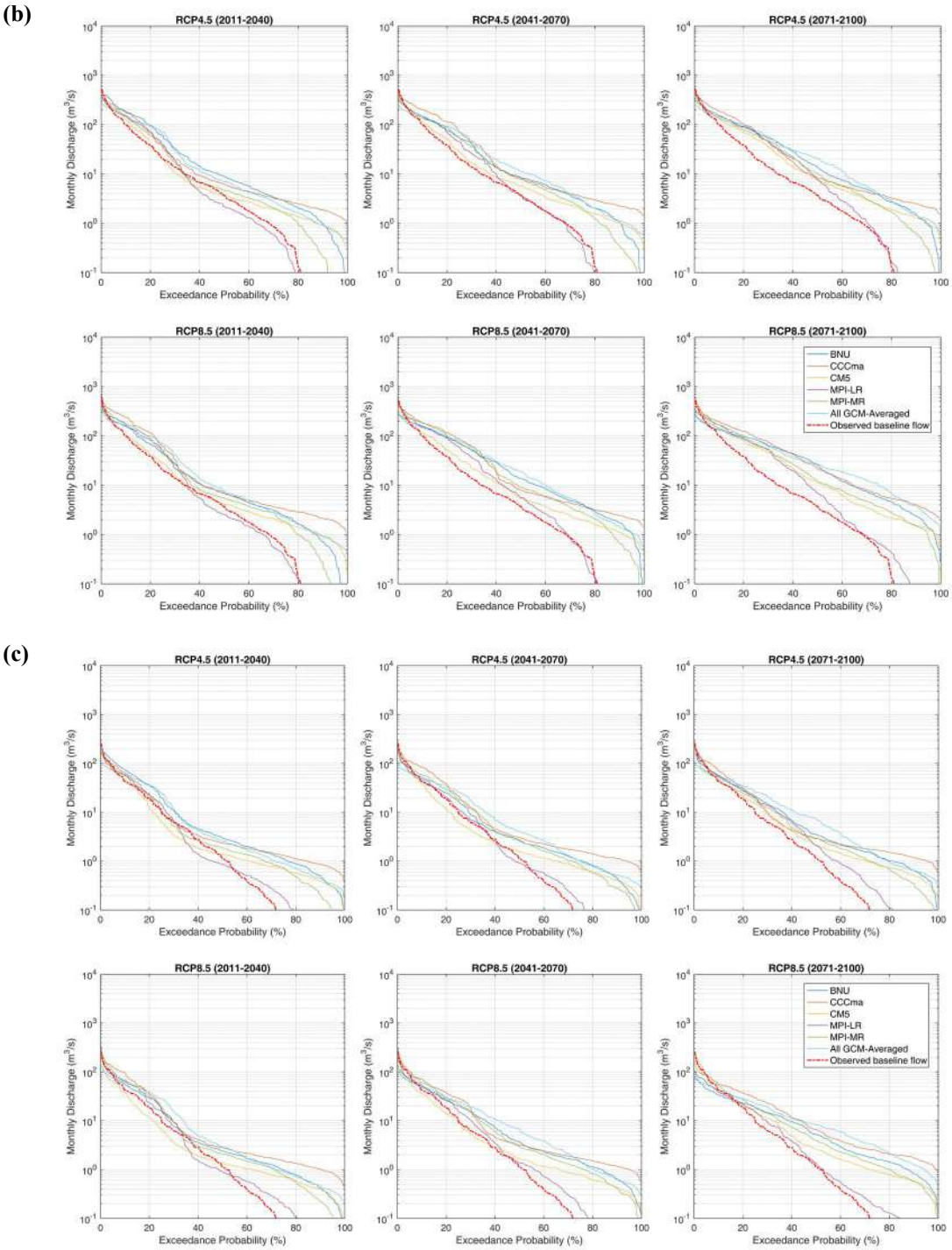

Fig. 6.13 Flow duration curves at the outlet of (a) Yerli, (b) Gopalkheda, and (c) Lakhpuri stream gauging stations under RCP 4.5 and RCP 8.5 scenarios.

- Invariably, the simulated streamflows with less dependability (low flows) are higher than corresponding observed flows during the baseline period. These results are in line with the trend of downscaled rainfall wherein the sub-catchment is likely to be in wet regime during the lean period.

- On the contrary, extreme stream flows (high flows) with less dependability are underpredicted while giving the future rainfall inputs to the SWAT model. This is also expected as per the downscaled results of rainfall for monsoon season wherein lesser rainfall is expected in future period vis-à-vis baseline period.
- The large deviations in the tail-end of the FDCs show considerable uncertainty in the simulated streamflows in the catchment during low flows. The extended tail of FDC at all three gauging sites and the Purna sub-catchment outlet indicates the increased dependable flow at the end of the century. Also, the dependable flows increase significantly under RCP 8.5 scenarios compared to RCP 4.5.

Therefore, by the end of the 21st century, the winter season may get a five-fold (six-fold) rise in the rainfall while streamflow may increase by five-fold (six-fold) under RCP 4.5 (8.5) scenarios. The other seasons, i.e., post-monsoon and pre-monsoon seasons, might also experience an increased rainfall condition. It is also interesting to note that the contribution of monsoon season rainfall and streamflow may reduce to 69.7% (62.0%) and 60.0% (57.3%), respectively, under the RCP 4.5 (8.5) scenario against the contribution of 86.8% and 83.8% respectively during the baseline period. The Q_{10} or higher flows are reducing while the flows at Q_{50} are increasing by the end of the 21st century under both the RCP scenarios with reference to baseline period flows. The present assessment of the Purna sub-catchment indicates that the rainfall conditions may no longer remain concentrated to monsoon season, i.e., a more uniform distribution of rainfall is expected in the future, and the same is reflected in terms of the extended tail of FDC, a likely indicator that river might become perennial in nature.

The major components of interest in a hydrological cycle are evapotranspiration and water yield. The evapotranspiration and water yield during the baseline period are found to be 48.1% and 15.1%, respectively, for the Purna sub-catchment. Apart from the evapotranspiration from the surface and vadose zone, the ground water extraction for irrigation also contributes to evapotranspiration. Due to non-availability of the data, the evapotranspiration is calculated using Hargreaves method and the irrigation components are not considered in the present study. The water balance components during the baseline period and future period are described in Table 6.3. Also, the pictorial variation of the precipitation, evapotranspiration and water yield during the future sub-periods are shown in Fig. 6.14. By the end of the 21st century, the rate of evapotranspiration is expected to increase with rising temperature and proportional to the daily temperature variability (see Fig. 6.14). Also, it is seen that the precipitation is likely to increase

by the end of the century; however, the overall water availability might get reduced, leading to water stress conditions in the basin area. It is important to note that the Purna sub-catchment is already experiencing absolute water scarcity (Sharma et al. 2019).

Table 6.3 Water balance components and relative error in model simulations for Purna sub-catchment for baseline and RCP scenarios

Period (Baseline/Future Scenario)	P (mm)	ET (mm)	SURQ (mm)	LATQ (mm)	PERC (mm)	ΔS (mm)	Relative Error
Baseline period (1998 – 2013)	809.6	389.5	77.3	1.1	370.2	3.2	-3.9%
RCP Scenarios of five GCM Model runs (2011 – 2100)							
BNU 4.5	775.1	327.8	17.5	0.8	437.6	-8.1	-0.1%
BNU 8.5	775.4	332.6	19.2	0.8	439.4	-1.0	-2.0%
CCCma 4.5	800.5	301.8	18.9	1.0	494.9	0.5	-2.1%
CCCma 8.5	845.3	324.4	25.0	1.1	511.8	-0.5	-1.9%
CM5 4.5	690.5	310.2	11.0	0.6	382.5	-0.4	-2.0%
CM5 8.5	694.5	306.9	11.3	0.6	389.4	1.6	-2.2%
MPI-LR 4.5	786.9	369.5	18.0	1.0	414.9	-1.5	-1.9%
MPI-LR 8.5	791.7	374.0	19.6	1.0	413.4	-3.9	-1.6%
MPI-MR 4.5	787.7	370.4	9.3	1.2	419.1	-2.8	-1.2%
MPI-MR 8.5	814.0	382.1	16.0	1.3	429.0	-2.9	-1.4%

P: Precipitation; ET: Evapotranspiration; SURQ: Surface Runoff; LATQ: Lateral Flow; PERC: Percolation in Soil; ΔS: Change in Storage.

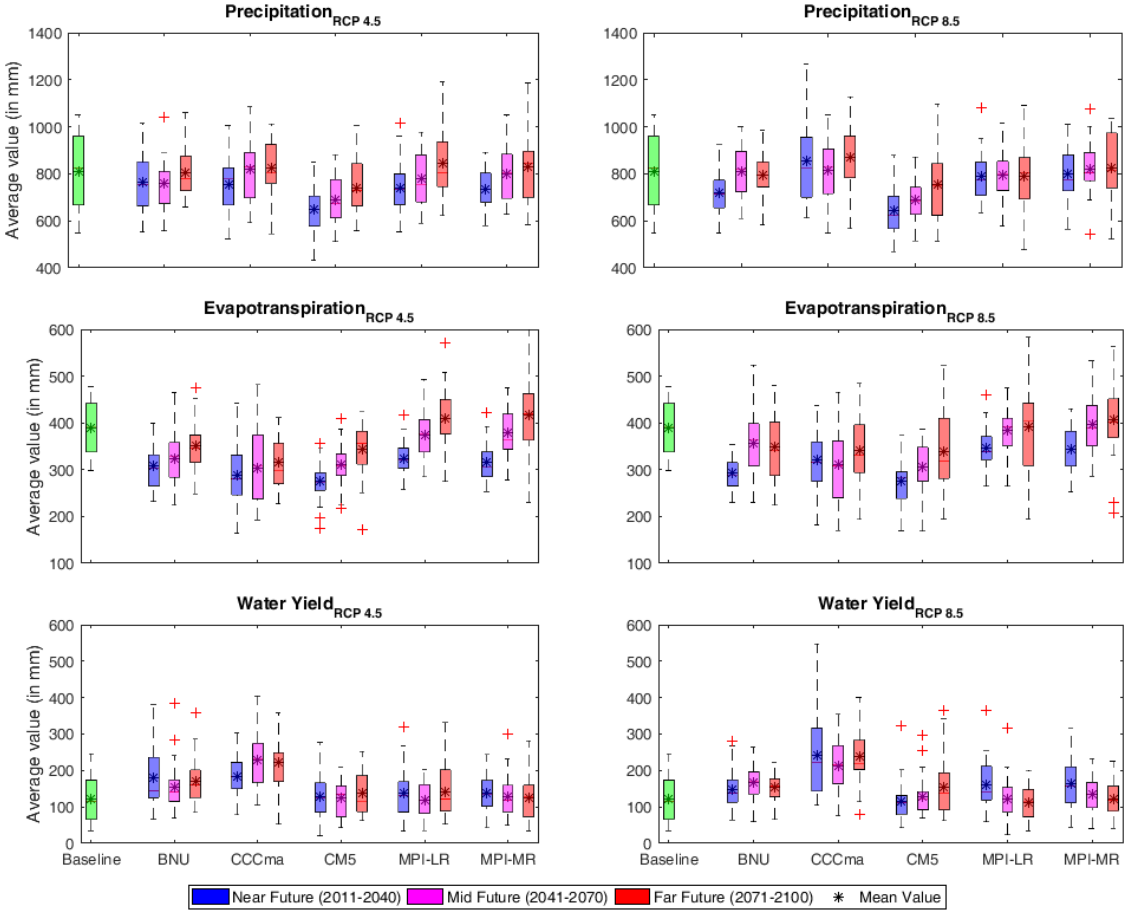

Fig. 6.14 Water balance components for Purna sub-catchment

6.3.2 Burhanpur sub-catchment

The monthly variations in rainfall, temperature, and stream flow of all the five GCMs selected in this study for the RCP 4.5 and RCP 8.5 scenarios along with IMD rainfall data which is termed as observed in all the subsequent figures (see Fig. **A12 to A19, in Annexure**). The GCMs historical and IMD observed data were taken from the year 1981 to 2005, and the future projected data of both the scenarios were taken from the year 2011 to 2100. Fig. 6.15 shows the ensembled change with respect to reference datasets and it was found that the GCMs rainfall in the winter months (December, January, and February) has increased from the observed rainfall in mid and far future while in the monsoon months specially in July and August months the GCMs rainfall has decreased from the observed rainfall in RCP 4.5 scenario. The BNU GCM shows decreasing trend in all the three-time series in both the months while CCCma model shows increased rainfall in mid and far future for July month and decreased rainfall in the month of August for all the three-time series. The CM5 model shows decreased values in mid and far future in June, July, and August months. The MPI-LR and MPI-MR shows increased values in the month of December, January, and February in all the three-time series of RCP 4.5 scenario. Similarly, the rainfall of BNU model in RCP 8.5 scenario shows increased values in the months of December, January, and February. Rainfall in the months of July and August decreases from the observed IMD rainfall in RCP 8.5 for all the five GCMs scenario as shown in Fig. 6.15a. Fig. 6.15 also show the variations of mean monthly maximum/minimum temperature for both the RCP scenarios for all the five GCMs selected for the study for Burhanpur Sub-Catchment. It can be seen that there is increment (1 to 2^{o}C) in the mean monthly minimum temperature from the observed IMD data in the RCP 4.5 scenario in the end of the century. While the RCP 8.5 scenario shows the increment of around 2 to 4^{o}C in the mean monthly minimum temperature for the study area. There is slight variations in maximum temperature for the RCP 4.5 scenario for all the five GCMs with IMD data but shows increasing trends from near future to far future. The RCP 8.5 scenario also shows the increasing trend in mean monthly maximum temperature for the three-time series for all the five GCMs (Fig. 6.15). The variation of stream flow for both the RCP scenarios for all the five GCMs have also been shown in Fig. 6.15. The stream flow variation is following the similar trends as the rainfall. For both the RCP scenarios stream flow for the months July, August and September have been decreased from the observed data. While in the months of November, December, and January the BNU, MPI-LR and MPI-MR model shows increasing trends in all the three-time series (Fig. 6.15).

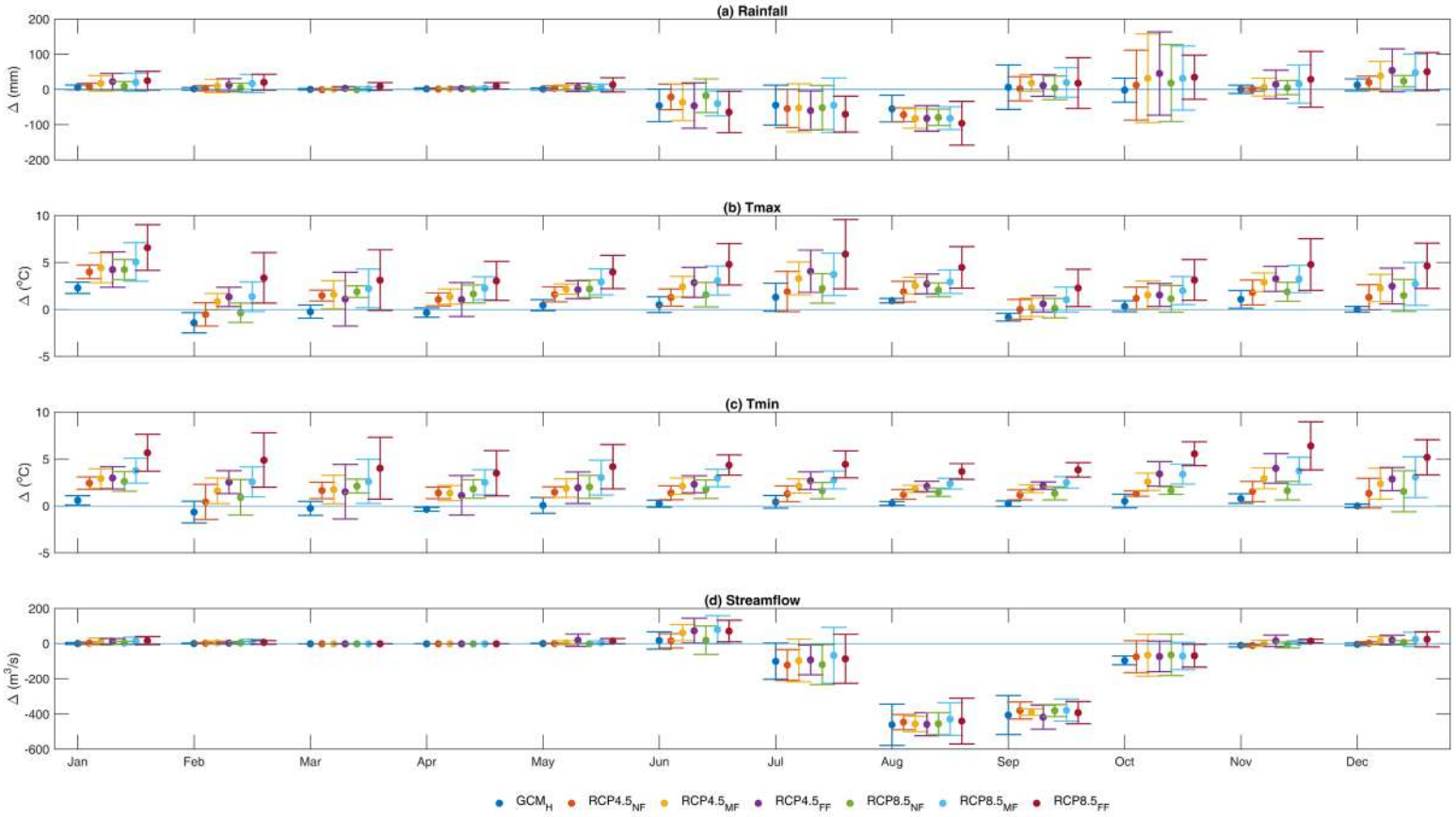

Fig. 6.15 Mean change in Rainfall, Tmax, Tmin and Streamflow in Burhanpur sub-catchment during near-, mid-, and far-future under RCP 4.5 and RCP 8.5 scenario

The daily flow duration curves at Burhanpur and Hatnur were plotted under different climate scenarios and are presented in Fig. 6.16a and 6.5b. The flow duration curve was found to be the most informative way of representing the complete range of river discharges for the selected period (Sahana and Timbadiya 2020).

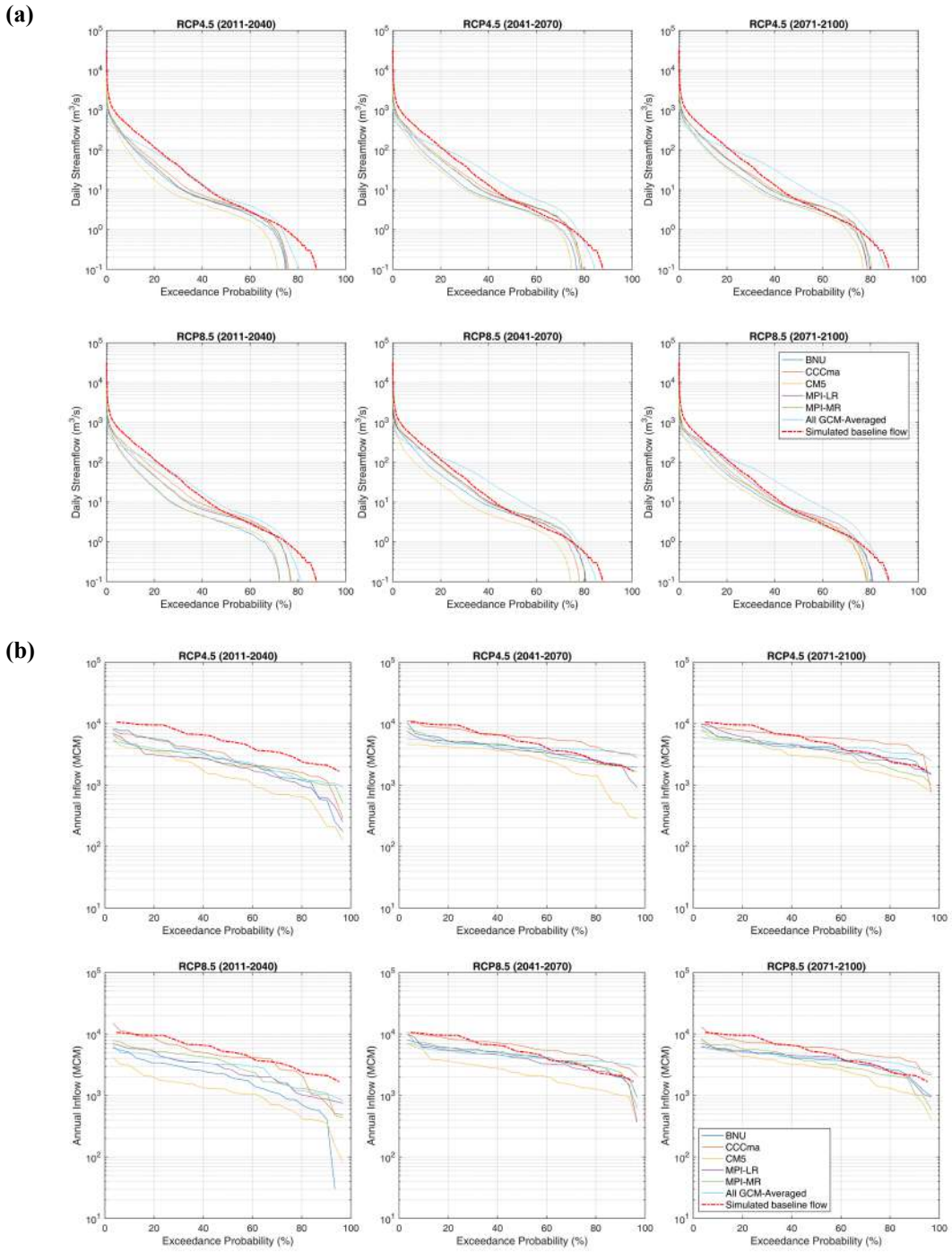

Fig. 6.16 Daily flow duration curve under different climate scenarios at (a) Burhanpur and (b) Hatnur

The peak flow was decreased with respect to the corresponding value in the historical period for all GCM climates for both RCP 4.5 and RCP 8.5 scenarios and for all three time durations at Burhanpur station (Fig. 6.16a) while the low flow shows the similar behaviour of GCMs in the near, mid and far future, as reflected in the closely spaced flow duration curves and very less variations in flow magnitude at Burhanpur gauge station (Fig. 6.16a). Similarly, it was observed from the inflow simulated by SWAT using all GCM rainfall at Hatnur, that for RCP4.5 and RCP8.5, high flows showed less variation for 10% of the total time considered, for all the three-time series for all flow magnitudes, between the climate scenarios. The flow duration curves from all GCMs were dispersed for all flow magnitudes at Hatnur (Fig. 6.16b), which may have been due to differences in projected rainfall for all GCMs. The low flow is decreased in near future and increased in mid and far future from historical stream flow for all GCMs at Hatnur. The BNU, CM5, MPI LR and MPI MR model shows the increased value of low flow in far future for both the RCP scenarios from the historical flow while the CCCma model shows the decreased value of low flow in far future for both the RCP scenarios (Fig. 6.16b).

To examine the potential effects of projected climate change on the water balance components of the Burhanpur sub-catchment, the soil and land-use properties were held constant, and the calibrated SWAT model was run for both the RCPs (4.5 and 8.5) of all five GCMs under three time slices i.e., Near future (2011-2040), Mid future (2041-2070) and Far future (2071-2100). The Table 6.4 shows the comparison of annual average basin values for baseline period and future scenarios. The relative error in the water balance components for baseline line period was found to be -0.15%. All the five GCMs shows the that the surfaces runoff, lateral flow and percolation have been decreased while the actual evapotranspiration has been increased in BSC for both the RCP scenarios. The relative error varies from 0.54% (CCCma 4.5) to 0.88% (CM5 8.5) in the water balance computation for all the five GCMs in both the RCP scenarios (Table 6.4). Fig. 6.17 shows the box plot of precipitation, evapotranspiration, and water yield for both the RCP scenarios in all the three-time series for BSC. The BNU, CCC-ma, CM5, MPI-LR and MPI-MR model shows decrement in rainfall of around 13.01%, 7.18%, 22.45%, 14% and 11.93% from the baseline period rainfall in near future for RCP 4.5 scenario. Similar decreasing trend were seen in rainfall for BNU, CM5, MPI-LR and MPI-MR model for mid and far future in RCP 4.5 scenario while CCCma model shows increment in rainfall of about 2.4% and 2.6% in mid and far future for RCP 4.5 scenario. For RCP 8.5 scenario the BNU, CM5, MPI-LR and MPI-MR models shows decreased values in rainfall of around 22.60%, 23.58%, 8.93% and

7.07% respectively in near future while the CCCma model shows increment of about 0.83% in rainfall in near future for RCP 8.5 scenario. The BNU and CM5 models shows decrement in rainfall in mid and far future while the CCCma and MPI-LR models shows the increased values in rainfall for mid and far future for RCP 8.5 scenario. The water yield of all the five GCMs have been decreased while the evapotranspiration has been increased in all the three-time series for both the RCP scenarios from the baseline period. All the five GCMs shows 52-59% decrement in water yield in near future for RCP 4.5 while for RCP 8.5 it varies from 41-65% in near future. The highest decrement in water yield was shown by the CM5 model in the near, mid, and far future for both the RCP scenarios (Fig. 6.17).

Table 6.4 Average Annual Basin Values of Future Scenarios of Burhanpur Sub-Catchment

Period (Baseline/Future Scenario)	P (mm)	SURQ (mm)	ET (mm)	LATQ (mm)	PERC (mm)	ΔS (mm)	Relative Error
Baseline	989.50	289.36	412.10	10.11	279.03	0.38	-0.15%
RCP Scenarios of GCM Models (2011-2021)							
BNU 4.5	848.10	133.20	537.00	8.06	171.23	-7.92	0.76%
BNU 8.5	842.30	139.37	534.00	8.08	162.28	-8.31	0.81%
CCCma 4.5	983.30	162.84	590.00	10.21	221.04	-6.11	0.54%
CCCma 8.5	1027.10	173.94	609.40	11.04	233.36	-6.65	0.58%
CM5 4.5	785.50	122.17	496.70	7.60	160.49	-7.79	0.80%
CM5 8.5	752.40	106.72	493.40	7.44	146.22	-8.00	0.88%
MPI-LR 4.5	915.90	153.52	559.60	9.14	194.84	-7.56	0.69%
MPI-LR 8.5	964.70	176.40	581.50	9.60	198.40	-7.88	0.69%
MPI-MR 4.5	913.80	153.80	557.40	9.08	194.85	-7.80	0.70%
MPI-MR 8.5	953.10	186.01	563.40	9.39	195.82	-8.22	0.70%

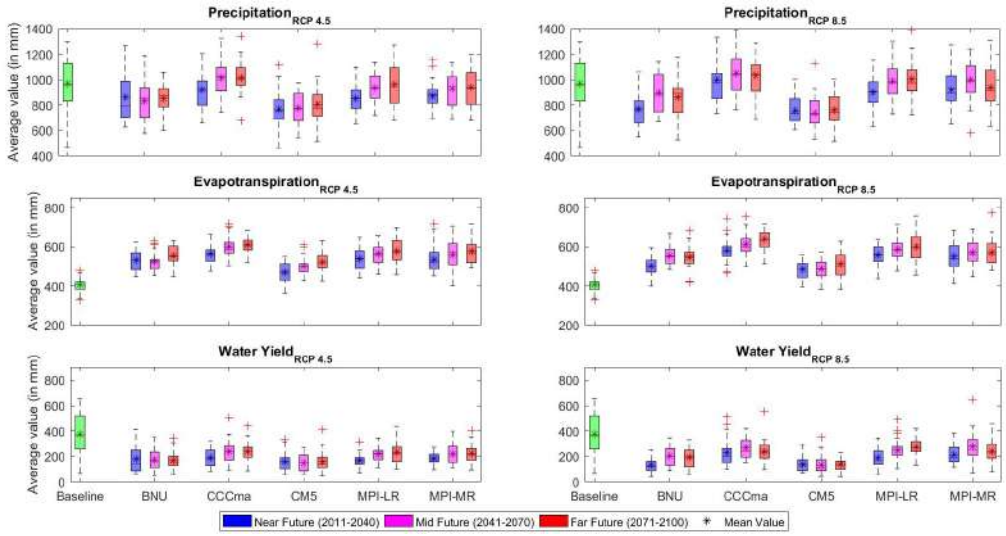

Fig. 6.17 Annual average simulated values for hydrologic variables for the BSC under different climate scenarios.

6.3.3 Middle Tapi Basin

The rainfall, temperature, and streamflow data for individual months for each of the five selected GCMs for both RCP4.5 and RCP8.5 scenarios have been displayed along with its comparison with the observed IMD rainfall and temperature data bar chart format (Fig. **A20 to A27, in Annexure**). For the historical period of different GCMs, a period of 1981-2005 has been selected. Similarly, for Observed data from IMD same period of 1981-2005 have been selected. For Future GCM data of both RCP scenarios a period of 2011-2100 was used in which the complete period of 90 years was divided into three separate periods of 30 years each, and are classified as near future (2011-2040), mid future (2041-2070) and far future (2071-2100).

For MTB the rainfall for GCMs for both RCP scenarios for the months of June, July, August, and September are lesser as compared to the observed IMD rainfall data which include the monsoon months too. However, for the winter season (December, January, and February), the GCM rainfall tends to increase slightly than the observed IMD rainfall data for both RCP scenarios (Figs. **A20-A21, in Annexure**).

In general, BNU GCM displays a decreasing trend for the monsoon months of July and August for both RCP scenarios. At the same time, CCCma GCM shows a sudden increase in the magnitude of rainfall for the month of October and a slight increase for November month. As a result, the annual rainfall for CCCma GCM increased compared to other GCMS. CNRM GCM also shows a decreasing trend for the months June and August. MPI LR and MPI MR show a decreasing trend for June, a mixed trend for July, and an increasing trend for the rest of the months.

The monthly average variation of maximum temperature for the RCP 4.5 scenario and RCP 8.5 scenario is displayed in Figs. **A22-A23** (**in Annexure**) for each of five GCMs employed for MTB. According to the graphs for RCP 4.5 for each of GCM model show an increase in monthly average temperature from near future to far future of about 1^{o}C to 2^{o}C. In contrast, the increase in monthly average temperature for all the GCMs from near future to far future is around 2^{o}C to 4^{o}C, which is significantly higher as compared to the RCP 4.5 scenario. On comparing these GCM models with the observed IMD monthly average temperature data, there is an increasing trend in each of the months for each model. As there is an increase in monthly average temperature from the near future to the far future for both the RCP scenarios, there is an apparent increase in the variation of the monthly average temperature of the GCM models with respect to the observed IMD monthly average temperature.

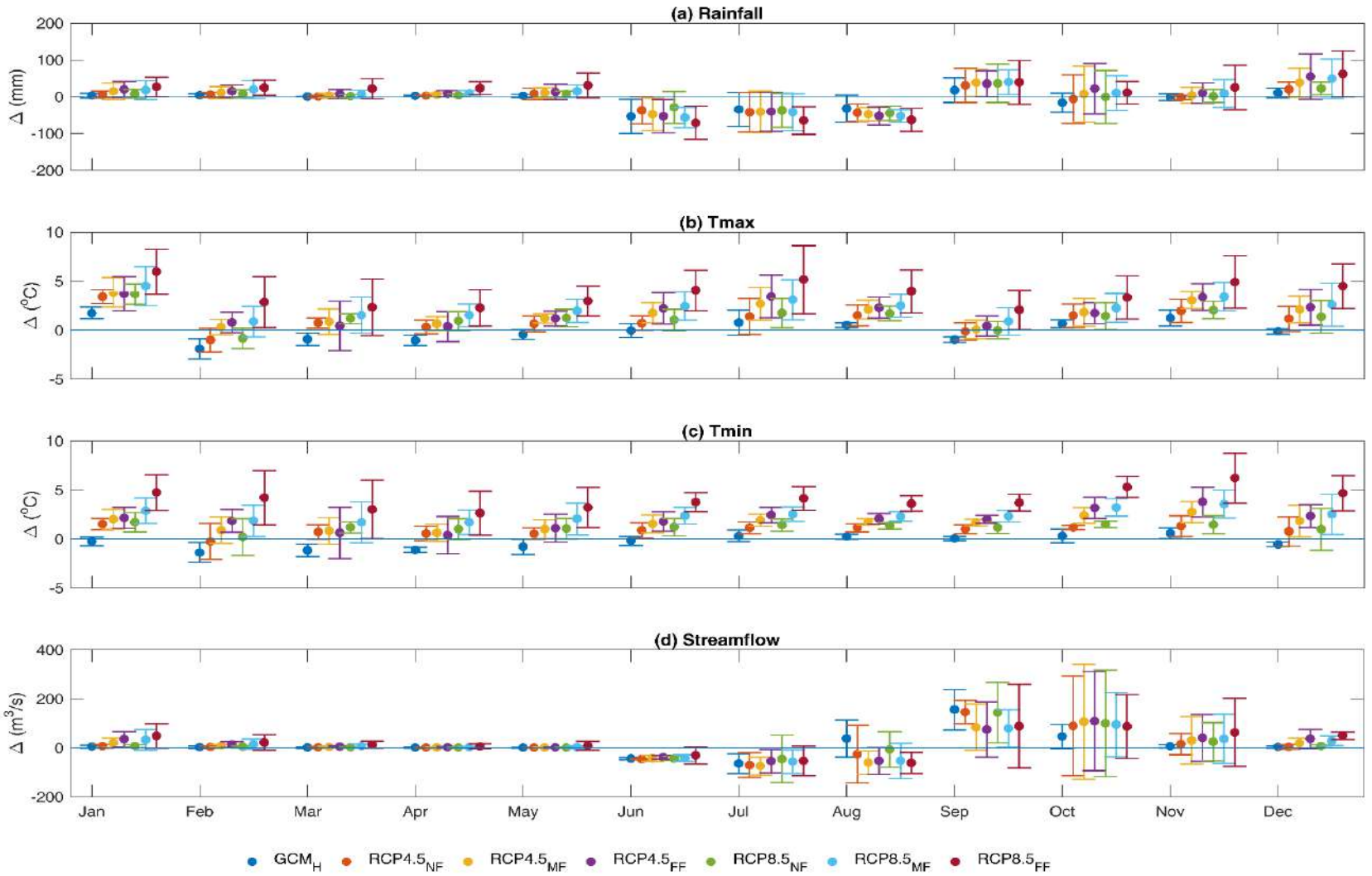

Fig. 6.18 Mean change in Rainfall, Tmax, Tmin and Streamflow in Middle Tapi Basin during near-, mid-, and far-future under RCP 4.5 and RCP 8.5 scenarios

In Fig. A26-A27 (**see Annexure**), the change of stream flow for both RCP scenarios for all five GCMs is also displayed. The variations in stream flow follow the same patterns as the variations in rainfall. Stream flow has been reduced in both RCP scenarios during the months of July, August, and September, compared to observed data. While the BNU, MPI-LR, and MPI-MR models show rising trends in all three-time series in November, December, and January. For the months of October, November, and December, the CCCma model shows a significant increase in streamflows. Besides the changes discussed above, Fig. 6.18 shows that throughout the monsoon and post-monsoon seasons, the uncertainty in future rainfall forecasts is quite high. With less uncertainty, rising rainfall circumstances throughout the months of June to December imply that a shift is extremely likely. Similarly, the predicted shift in streamflows is associated with substantial uncertainty for the months of June to December. Unlike rainfall and streamflow, Tmax and Tmin clearly imply rising temperatures in the future under both RCP scenarios, although both variables have a significant level of uncertainty

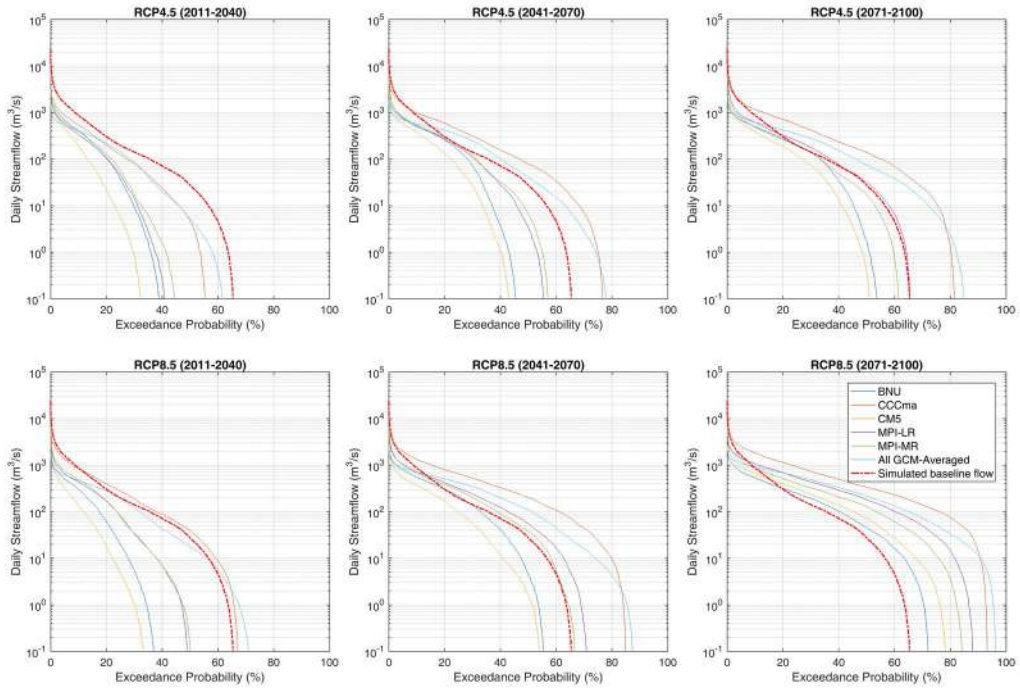

(a)

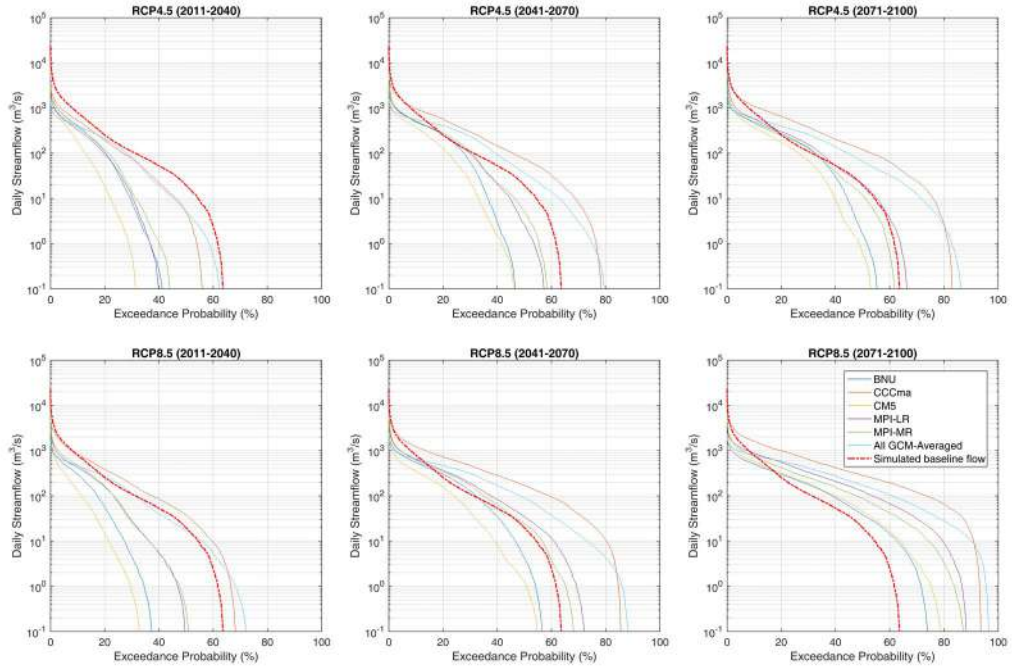

(b)

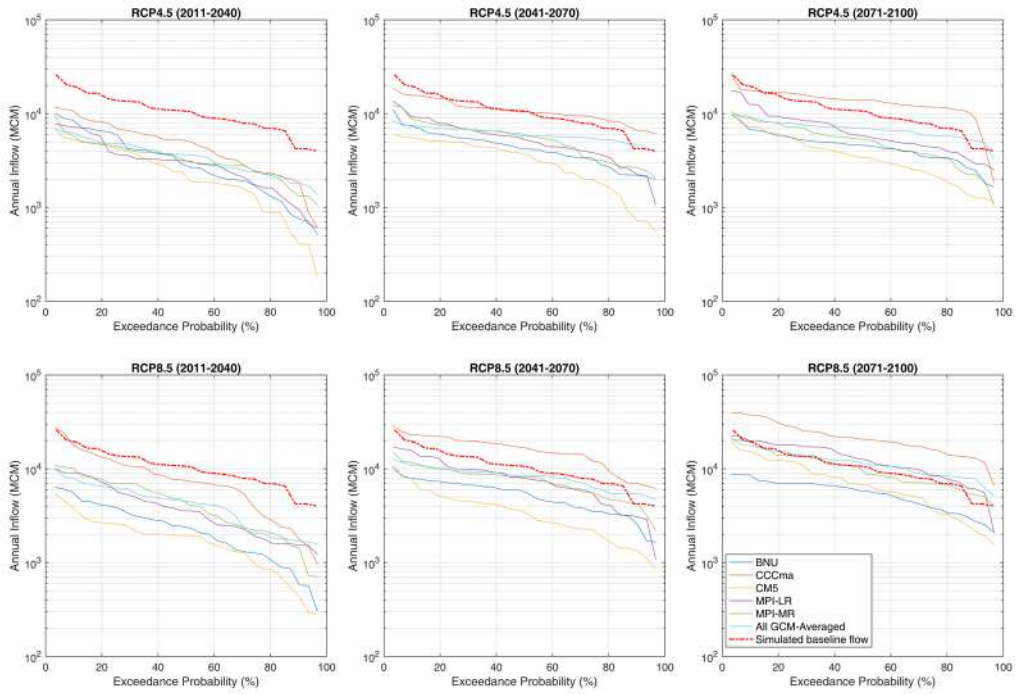

(c)

Fig 6.19 Flow duration curves at the outlet of (a) Sarangkheda, (b) Gidhade, and (c) Ukai stream gauging stations under RCP 4.5 and RCP 8.5 scenarios.

According to three different time slices for RCP4.5 and RCP8.5, flow duration curves were plotted on a daily scale for Sarangkheda, Ukai and Gidhade, stations and are presented in Fig. 6.19 (a), (b), and (c). Comparison of different components Water Balance for Middle Tapi

Basin is shown in Fig. 6.20. Flow duration curve is an innovative and explanatory method to depict a complete range of discharge for the given time frame. In all the cases, simulated flows for future GCM were being compared with the observed flow for the same station, same time slice, and same RCP scenario. As per the graphs, significant changes can be noted for every case. At Sarangkheda station (Fig. 6.19 (a)), the simulated discharges for RCP4.5 near future displayed lesser disparity for Q_{10} flow. Q_{10} is that discharge value that exceeds 10% of the completed time considered. For RCP4.5 mid-future and RCP8.5 near future, the discrepancy between all future GCMs increased for Q_{10}. Further, for RCP4.5 far-future and RCP8.5 mid-future, the variation of flow duration curves for all future GCMs for Q_{10} tends to increase even more than the earlier. For RCP8.5 far future, the highest dispersion was noted between the flow duration curves for all future GCMs for Q_{10}. It was also noted that the flow duration curves in all the mentioned cases are somewhat dispersed only; the primary reason for this can be the variation of precipitation data for all the future GCMs. Similar trends were noted for discharges Gidhade station and inflow at Ukai reservoir in Fig 6.8 (c). Comparison of different components Water Balance for Middle Tapi Basin, where the variation of flow duration curves for all future GCMs for Q_{10} increase with moving from near future to far future.

Comparing historically observed flows with all GCM averaged at Sarangkheda station, the median flow Q_{50} is observed to be around $5m^3/s$ for the near future, however, ranges from 40 m^3/s to $65m^3/s$ for mid future and far future, respectively, for RCP4.5. Similarly, for RCP8.5, median flow Q_{50} ranges from $20m^3/s$ to approximately $180m^3/s$ from near future to far future. Same trend for an increase in Q_{50} median flow has been observed at Gidhade and inflow at Ukai where median flow magnitudes increase from near to far future for all averaged GCMs with respect to historical observed. This signifies an increase in the availability of water in future. Considering these results, more barren land can be converted to agricultural land, and water can always be maintained above the optimum moisture content, which can increase crop productivity. However, if this increase in discharge is observed in a lesser duration, there may be chances of flooding scenarios.

The hydrological processes of the Middle Tapi Basin were simulated by SWAT model. The average annual basin values of the calibrated model developed at daily scale from 1985 to 2013 for MTB are shown in Table 6.5. The rainfall received by the MTB was 712.8 mm and surface runoff was 148.27 mm. The actual evapotranspiration was 346 mm, while the amount of water moving from Shallow Aquifer to plants was 161.34 mm and percolation out of soil was 235.15

mm. The water balance components of the MTB as simulated by the calibrated SWAT model showed a 20.8% surface runoff, 29.8% water yield and 48.5% actual evapotranspiration contribution out of the total 100% rainfall input into the MTB.

Total water goes into the watershed primarily from precipitation, converted into a surface runoff, baseflow, evapotranspiration, percolation into the soil, re-vaporisation, and other water balance components. According to the outcomes of the base period (1985-2013), 20.8% of the precipitation was converted into surface runoff, and the total water yield, including surface runoff was 29.85%. For the period (1990-2013), observed inflow into the Ukai Reservoir is 9878.6 MCM, which includes both the streamflow contribution from Middle Tapi Basin and the Upper Tapi Basin. The observed streamflow magnitudes are equivalent to the calibrated streamflow. Also, for the same base period (1985-2013) annual average evapotranspiration for MTB was 48.54% of the total precipitation. Using Penman Monteith method, the potential evapotranspiration (PET) was computed determined to be 1904.7 mm.

According to the land use land cover dataset was developed by NRSC (National Remote Sensing Centre) India for 2005-06, after its reclassification into six major land use classes, the agricultural land use was 49.14% for MTB. In the MTB, agricultural activities were directly linked to the majority of evapotranspiration components in the water balance. However, groundwater extraction for irrigation was not considered in this study, which may have resulted in a more significant amount of evapotranspiration.

For the baseline period of 29 years, the Average Annual Precipitation for Middle Tapi Basin was 712.8 mm. To analyse the possible effects of projected climate change on the Middle Tapi Basin's balance components, the soil and land-use properties were kept constant, and the calibrated SWAT model was run for both the RCPs (4.5 and 8.5) of all five GCMs over three time slices: near future (2011-2040), mid future (2041-2070), and far future (2041-2080). (2071-2100). The comparison of annual average basin values for the baseline period and future scenarios is shown in Table 6.5. For the baseline line scenario, the relative error in the water balance components was found to be -3.70 percent.

Table 6.5 Water balance components and relative error in model simulations for Middle Tapi Basin for Baseline and RCP scenarios

Period (Baseline and Future Scenario)	P (mm)	SURQ (mm)	ET (mm)	LATQ (mm)	Perc (mm)	ΔS (mm)	Relative Error
Baseline	712.80	148.27	346.00	0.24	235.15	9.54	-3.70
RCP Scenarios of GCM Models (2011-2100)							
BNU 4.5	575.83	19.84	386.83	0.12	186.35	-9.53	-1.35
BNU 8.5	603.43	31.15	385.00	0.12	205.27	-0.70	-2.88
CCCma 4.5	906.97	100.16	407.93	0.21	410.57	65.96	-8.59
CCCma 8.5	1161.03	170.44	423.77	0.28	575.33	97.94	-9.19
CM5 4.5	600.30	27.73	384.10	0.12	204.56	-6.12	-1.68
CM5 8.5	712.53	50.69	401.57	0.15	275.36	19.09	-4.82
MPI-LR 4.5	698.00	55.65	394.13	0.15	263.18	16.32	-4.50
MPI-LR 8.5	874.07	86.57	412.70	0.20	387.82	43.43	-6.48
MPI-MR 4.5	678.47	46.58	395.30	0.14	252.05	11.22	-3.95
MPI-MR 8.5	822.87	81.70	411.33	0.18	343.76	34.93	-5.96

P: Precipitation; SURQ: Surface Runoff; ET: Evapotranspiration; LATQ: Lateral Flow; PERC: Percolation in Soil; ΔS: Change in Storage

The precipitation, land use patterns, temperature, elevation, characteristics of soil, and inlet discharges from upper tapi are the critical data used as input for SWAT in this study. For future simulation period, the parameters from the historical SWAT model, for land elevation, soil characteristics, land use patterns, groundwater, channel network, etc. are considered to be constant during the future scenarios because the availability of climatic variables available to this study is limited (precipitation and temperature). Modeling for dynamic aspects of the hydrological system for the current case study is outside the project's scope, but it can be considered a future project. In addition, if the rate of change in the properties of the factors as mentioned earlier (elevation, land use, soil characteristics, channel networks, and ground water) is compared with the rate of change in climate properties, then change climatic properties are comparatively faster and impacts are significantly higher. As a result, studying the impacts of change in climate on a basin's hydrology is essential. According to Joseph et al. (2018), the uncertainty caused by hydrological parameters is trivial compared to climate model uncertainties for Indian settings. As a result, various climate forecasts are employed in the current study to provide a more accurate picture of potential hydrologic changes and aid in water management methods.

The study of impacts of climate change impact studies primarily aims at the average values of hydrological variables and their average variability with relation to past observed hydrological variables to aid in planning and adaptation measures. As a result, the average of more extensive

period of the simulated hydrologic variables from multiple periods was compared to historical observations in this study. These periods are classified as Near future (2011–2040), Mid Future (2041–2070), and Far Future (2071–2100) for both the RCP scenarios 4.5 and 8.5. To estimate the possible reaction of the water balance components of MTB due to the change in climate for RCP 4.5 and RCP 8.5, five CMIP5 GCMs were chosen. In Fig. 6.20, the box plot of different water balance components for both RCP scenarios was represented along with the mean of each GCM.

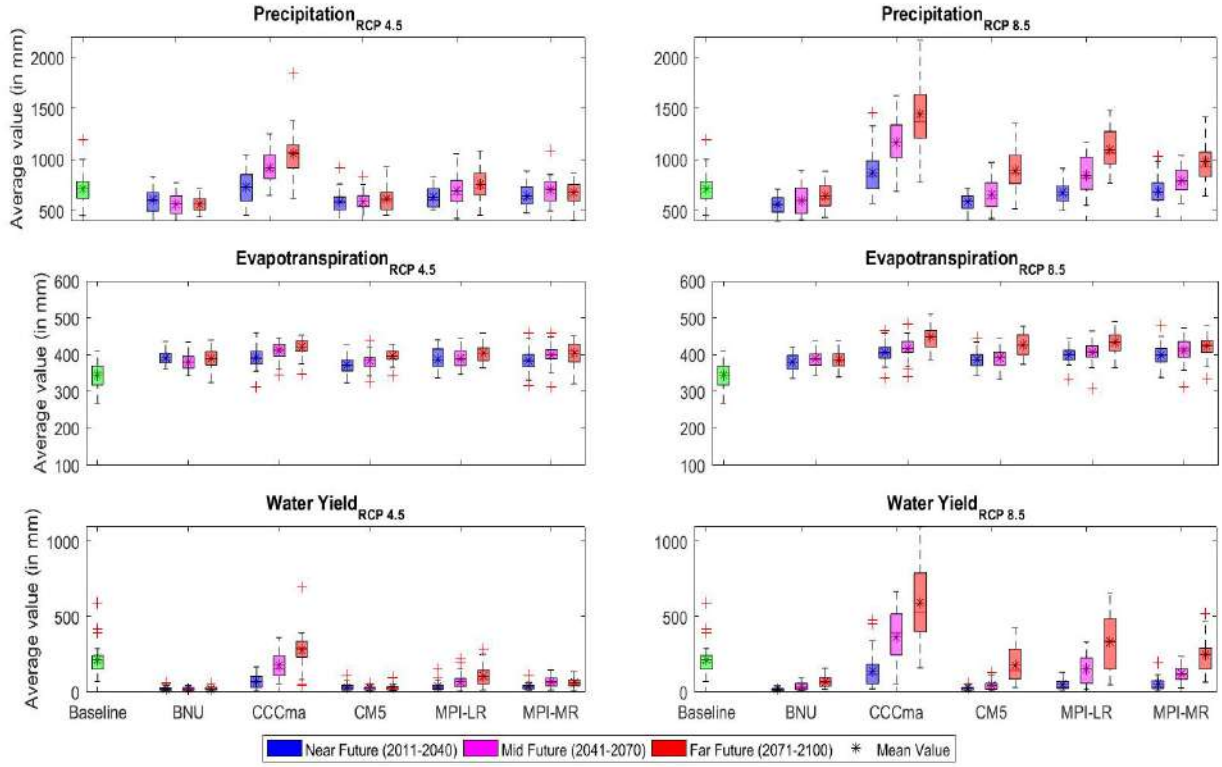

Fig. 6.20 Annual average simulated values for hydrologic variables for the Middle Tapi Basin under different climate scenarios.

The average annual components of water balance for MTB for the historical period were 712.8 mm of precipitation, 148.27 mm of surface runoff, 212.77 mm of water yield, and 346 mm of evapo-transpiration. Compared to the historical period, water balance components of future GCMs tend to vary in magnitude. For all future scenarios, the water balance components reported in CCCma are comparably greater and tend to increase significantly in the far future. In general, precipitation for different climatic models in the near future scenario was lower than previously observed. In contrast, precipitation in the mid-future is comparatively similar to RCP 4.5. However, it increased slightly for RCP 8.5, and precipitation in the far future was increased somewhat to RCP 4.5 but increased tremendously for RCP 8.5. Except for the distant

future scenario of RCP 8.5, where water yield is comparably higher than the historical period, all future scenarios show a more considerable decline in water yield at first, but it gradually increases with time. In the case of evapotranspiration, a smaller rise was detected in comparison to their historical counterparts, and all future scenarios are roughly identical. However, for the future GCM scenarios, there was no significant temperature change, even though evapotranspiration changes were determined to be higher due to changes in precipitation, affecting the water balance of MTB.

This section discusses the amount of average annual water balance components future GCMs and their changes over time compared to the water balance components of the historical period. The BNU ESM climatic variables provided the lowest values of water yield in RCP4.5, with a 90 % change for each variable. In contrast, the CCCma CanESM2 GCM yielded a 66 % change in water yield and a 66 % change in surface runoff, with minor alterations. For the mid-future era, the BNU ESM simulated climate variables had the most significant differences of 91 % in water yield and 88 % in surface runoff, while CCCma CanESM2 had the most minor variations of -16 % in water yield and -30 % in surface runoff, respectively. During the far-future scenario, surface runoff and water yield showed 5 % and 88%, differences.

BNU ESM climate, with 31 % and 2% changes in water yield and surface runoff in CCCma CanESM2, respectively. During the early future for the RCP8.5 scenario, the BNU ESM showed the most prominent changes (91%), while the CCCma CanESM2 showed minor changes (32%) for water yield. Furthermore, the most significant change in water yield (82%) and biggest change in surface runoff (78%) were recorded for BNU ESM during the mid-future simulations. In comparison, the increase in changes of water yield and surface runoff for CCCma CanESM2 were 71 % and 19 %, respectively. The BNU ESM showed the largest change in water yield and surface runoff of 85% and 86 %, respectively, and least change in water yield and surface runoff of 67 % and 70 %, respectively, during the far-future scenario. In contrast, other climate GCMs showed significantly higher increases in both the surface runoff and total water yield.

For all time slices, CCCma CanESM2 climate produced the highest rise in evapotranspiration for the most likely scenario RCP4.5, with 13 %, 18 %, and 21 % for the near, mid, and far future, respectively. The CNRM CM5 climate showed the lowest evapotranspiration rise, at 8% in the near future, whereas the BNU ESM climate had 10% and 12% values in the mid and far future scenario, respectively. For the historical period as modeled by SWAT, the average

annual base flow and lateral flow and combined was 64.5 mm. However, for the future scenarios, the average annual base flow and lateral flow combined ranged from 3 to 342 mm. the change in this component with respect to the historical period is from 95 % to 430 %.

6.3.4 Lower Tapi Basin

The calibrated and validated, physics based distributed hydrological model in MIKE SHE/MIKE 11 for LTB is further used to simulate the response of statistically downscaled future rainfall and temperature over the basin. The hydrological model is simulated using the output of five GCM models, viz. BNU, CCCma, CM5, MPI-LR and MPI-MR and two RCP scenarios i.e., RCP 4.5 and 8.5 respectively. The RCP 4.5 signifies the intermediate pathway scenario which shows good agreement with recent policy by global community for lower greenhouse emission whereas, RCP 8.5 signifies the highest impact of climate change. Therefore, considering the importance of RCP 4.5 and 8.5 both are used in the present investigation to identify the possible impact of climate change over LTB.

The water balance for RCP 4.5 and RCP 8.5 is calculated for LTB for all climate change scenarios given in Table 6.6 and Table 6.7. It is observed that, the amount of precipitation (input) is lost majorly due to actual evaporation loss which ranges from 39% to 50% and 41% to 52% in RCP 4.5 and RCP 8.5 respectively. Nearly 30% to 37% of water contributes to the recharge in both RCP 4.5 and 8.5. It is to be noted that, the error in computation of water balance is less than 1 % for all the scenarios. The comparison of different hydrological processes such as runoff, actual evapotranspiration, and recharge against the given input as observed precipitation, GCM historical and for future scenarios for both RCP 4.5 and RCP 8.5 are shown in Fig. 6.21 and Fig. 6.22 respectively. From Fig. 6.21 and 6.22 it is seen that, invariably, the actual evapotranspiration is increasing continuously from NF-MF-FF periods. The increase in actual evapotranspiration is more for RCP 8.5 vis-à-vis RCP 4.5 scenario. The computed water balance for different future scenario may be useful for sustainable usage, better practices, and planning management within the sub-catchment.

Table 6.6 Future projected (2011-2100) average water balance components (in mm) for RCP 4.5 for Lower Tapi Basin

	Inflow		**Outflow**									**Storage**				
	P	**C_i**	**EP**	**BOL**	**OLR**	**RUN**	**TRZ**	**ET**	**REC**	**UZD**	**Total outflow**	**ΔC**	**ΔOL**	**±ΔS**	**$(\pm\Delta S)_c$**	**Error**
	1	2	3	4	5	6 (4+5)	7	8 (2+3+7)	9	10	11 (6+8+9+10)	12	13	14 (12+13)	15 (1-11)	16 (14-15)
Observed (calibration-validation) Period																
1991-2007	**1210.7**	80.7	98.2	161.6	102.5	**264.0**	414.7	**593.5**	**387.0**	-32.7	1211.8	0.0	3.8	3.8	-1.1	4.9
BNU																
Near Future (2011-2040)	**1531.3**	136.5	126.3	209.4	109.9	**319.4**	399.5	**662.3**	**555.2**	-6.7	1530.2	0.0	1.2	1.2	1.2	0.0
Mid Future (2041-2070)	**1477.7**	137.2	128.3	193.8	99.4	**293.2**	392.3	**657.8**	**532.4**	-6.7	1476.7	0.0	1.1	1.1	1.1	0.0
Far Future (2071-2100)	**1509.0**	144.1	129.7	211.5	100.2	**311.7**	392.0	**665.8**	**537.3**	-7.0	1507.9	0.0	1.1	1.1	1.1	0.0
CCCma																
Near Future (2011-2040)	**1356.4**	115.2	109.1	176.8	88.6	**265.4**	417.1	**641.4**	**455.3**	-6.9	1355.3	0.0	1.0	1.0	1.1	0.0
Mid Future (2041-2070)	**1396.0**	122.1	117.6	190.8	80.3	**271.1**	419.9	**659.7**	**471.2**	-7.0	1395.0	0.0	1.0	1.0	1.0	0.0
Far Future (2071-2100)	**1353.7**	125.4	123.6	154.4	70.3	**224.8**	422.4	**671.5**	**463.5**	-7.0	1352.7	0.0	1.0	1.0	0.9	0.0
CM5																
Near Future (2011-2040)	**1366.1**	115.9	103.6	179.4	111.0	**290.4**	376.3	**595.8**	**486.0**	-7.2	1365.0	0.0	1.1	1.1	1.1	0.0
Mid Future (2041-2070)	**1529.0**	134.7	104.2	244.0	147.9	**391.9**	365.7	**604.6**	**538.0**	-6.6	1527.9	0.0	1.1	1.1	1.1	0.0
Far Future (2071-2100)	**1427.1**	128.3	106.9	212.5	117.6	**330.1**	381.7	**617.0**	**485.3**	-6.4	1425.9	0.0	1.1	1.1	1.1	0.0
MPI-LR																
Near Future (2011-2040)	**1315.7**	109.9	116.7	160.8	87.2	**248.0**	400.0	**626.6**	**447.0**	-7.0	1314.6	0.0	1.0	1.0	1.0	0.0
Mid Future (2041-2070)	**1265.8**	104.4	114.7	156.4	75.3	**231.7**	410.2	**629.3**	**410.6**	-6.7	1264.9	0.0	0.8	0.8	0.8	0.0
Far Future (2071-2100)	**1453.1**	125.8	120.3	220.6	103.7	**324.3**	400.6	**646.7**	**487.8**	-6.6	1452.2	0.0	1.0	1.0	1.0	0.0
MPI-MR																

Near Future (2011-2040)	**1604.1**	134.2	117.1	251.1	146.0	**397.1**	380.1	**631.4**	**581.4**	-7.0	1602.9	0.0	1.2	1.2	1.2	0.0
Mid Future (2041-2070)	**1469.3**	132.3	116.5	228.2	110.4	**338.6**	382.2	**631.1**	**505.2**	-6.8	1468.1	0.0	1.1	1.1	1.2	0.0
Far Future (2071-2100)	**1385.2**	123.1	119.8	188.6	97.3	**285.9**	397.1	**640.0**	**463.6**	-5.5	1383.9	0.0	1.3	1.3	1.3	0.0

Note- P = Rainfall, C_i = Canopy interception, EP = Evaporation from ponded water, BOL = Boundary outflow, OLR = Overland flow to river, RUN = Total runoff, TRZ = Transpiration from root zone, ET = Actual evapotranspiration, REC = Recharge in saturated zone through soil matrix, UZD = Unsaturated zone deficit (amount of air in profile), ΔC = Change in canopy interception, ΔOL = Change in overland storage, ±ΔS = Total storage, $(\pm\Delta S)_c$ = Change in storage

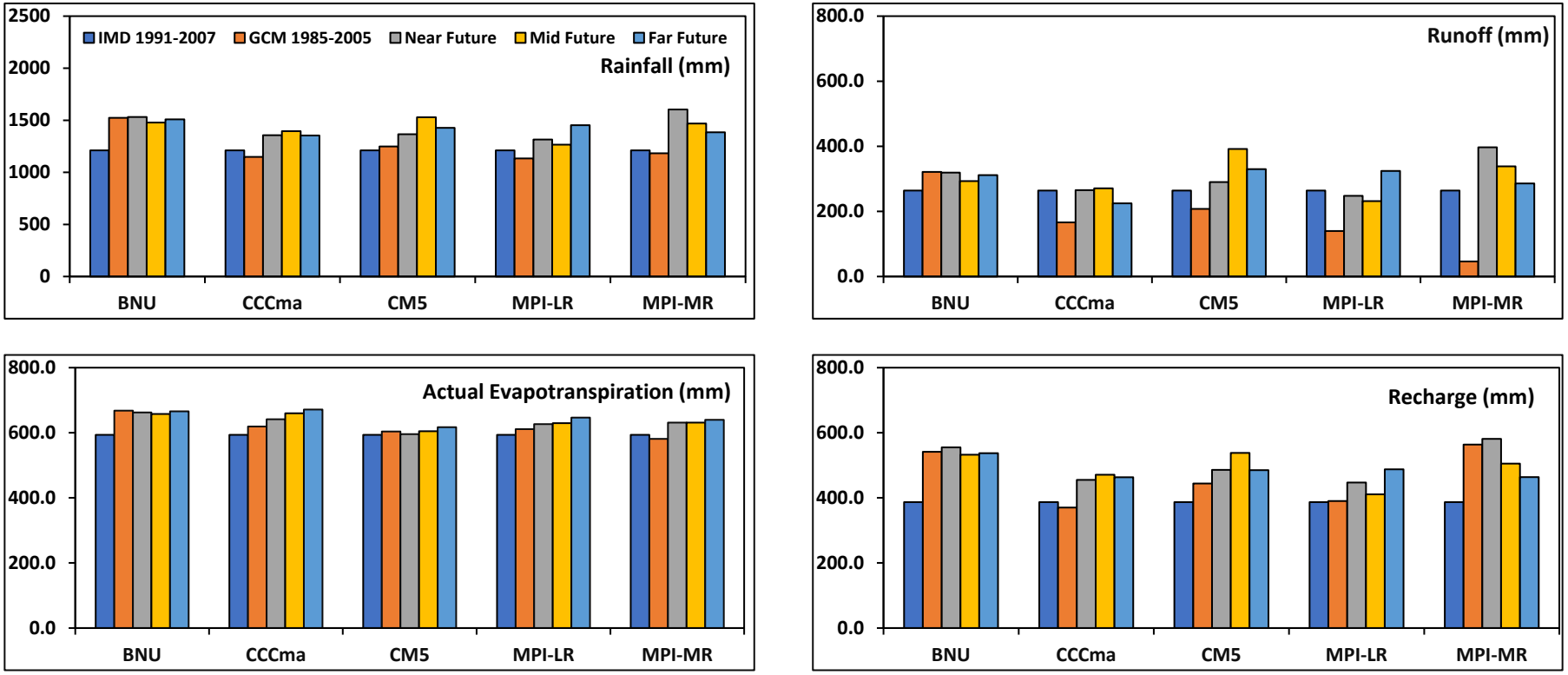

Fig. 6.21 Water balance contribution in major hydrological process for RCP 4.5 during 2011-2100

Table 6.7 Future projected (2011-2100) average water balance components (in mm) for RCP 8.5 for Lower Tapi Basin

	Inflow		**Outflow**									**Storage**				
	P	**C_i**	**EP**	**BOL**	**OLR**	**RUN**	**TRZ**	**ET**	**REC**	**UZD**	**Total outflow**	**ΔC**	**ΔOL**	**±ΔS**	**$(\pm\Delta S)_c$**	**Error**
	1	2	3	4	5	6 (4+5)	7	8 (2+3+7)	9	10	11 (6+8+9+10)	12	13	14 (12+13)	15 (1-11)	16 (14-15)
Observed (calibration-validation) Period																
1991-2007	**1210.7**	80.7	98.2	161.6	102.5	**264.0**	414.7	**593.5**	**387.0**	-32.7	1211.8	0.0	3.8	3.8	-1.1	4.9
BNU																
Near Future (2011-2040)	**1501.4**	132.3	123.1	217.5	109.7	**327.2**	400.1	**655.5**	**523.6**	-6.0	1500.3	0.0	1.2	1.2	1.2	0.0
Mid Future (2041-2070)	**1584.1**	155.0	125.8	242.6	118.6	**361.2**	381.1	**661.9**	**566.6**	-6.7	1583.1	0.0	1.1	1.1	1.1	0.0
Far Future (2071-2100)	**1319.3**	131.3	133.3	127.4	65.2	**192.7**	411.2	**675.8**	**456.0**	-6.1	1318.4	0.0	1.0	1.0	0.9	0.0
CCCma																
Near Future (2011-2040)	**1520.8**	139.2	113.4	228.6	102.7	**331.4**	401.9	**654.4**	**540.1**	-6.3	1519.6	0.0	1.2	1.2	1.2	0.0
Mid Future (2041-2070)	**1429.1**	142.1	121.6	172.2	78.6	**250.7**	413.7	**677.3**	**507.1**	-7.1	1428.1	0.0	1.0	1.0	1.0	0.0
Far Future (2071-2100)	**1541.0**	187.1	121.6	178.2	90.2	**268.5**	411.2	**719.9**	**456.0**	-6.1	1438.3	0.0	1.1	1.1	102.7	-101.6
CM5																
Near Future (2011-2040)	**1429.4**	123.3	110.5	193.6	121.5	**315.1**	382.5	**616.2**	**504.3**	-7.2	1428.4	0.0	1.0	1.0	1.0	0.0
Mid Future (2041-2070)	**1477.4**	127.2	110.3	239.6	131.5	**371.1**	385.3	**622.7**	**489.2**	-6.7	1476.3	0.0	1.1	1.1	1.1	0.0
Far Future (2071-2100)	**1357.2**	186.2	42.1	53.9	12.2	**260.0**	390.7	**618.9**	**484.4**	-6.4	1356.8	0.0	0.4	0.4	0.4	0.0
MPI-LR																
Near Future (2011-2040)	**1417.5**	118.7	120.8	196.6	98.4	**295.0**	403.2	**642.6**	**485.7**	-6.9	1416.4	0.0	1.1	1.1	1.1	0.0
Mid Future (2041-2070)	**1435.3**	132.4	131.6	190.9	83.3	**274.2**	407.7	**671.7**	**494.8**	-6.5	1434.1	0.0	1.1	1.1	1.1	0.0
Far Future (2071-2100)	**1514.5**	169.4	136.0	176.9	85.7	**262.5**	397.7	**703.1**	**554.1**	-6.4	1513.2	0.0	1.2	1.2	1.2	0.0
MPI-MR																

Near Future (2011-2040)	**1522.4**	131.4	119.1	230.2	121.8	**352.0**	394.6	**645.1**	**531.1**	-6.9	1521.2	0.0	1.2	1.2	1.2	0.0
Mid Future (2041-2070)	**1432.1**	132.7	127.6	200.2	89.2	**289.5**	403.0	**663.2**	**485.5**	-7.0	1431.1	0.0	1.0	1.0	1.0	0.0
Far Future (2071-2100)	**1578.9**	167.7	146.6	218.4	93.0	**311.4**	399.9	**714.2**	**558.9**	-6.7	1577.8	0.0	1.1	1.1	1.1	0.0

Note- P = Rainfall, C_i = Canopy interception, EP = Evaporation from ponded water, BOL = Boundary outflow, OLR = Overland flow to river, RUN = Total runoff, TRZ = Transpiration from root zone, ET = Actual evapotranspiration, REC = Recharge in saturated zone through soil matrix, UZD = Unsaturated zone deficit (amount of air in profile), ΔC = Change in canopy interception, ΔOL = Change in overland storage, ±ΔS = Total storage, $(\pm\Delta S)_c$ = Change in storage

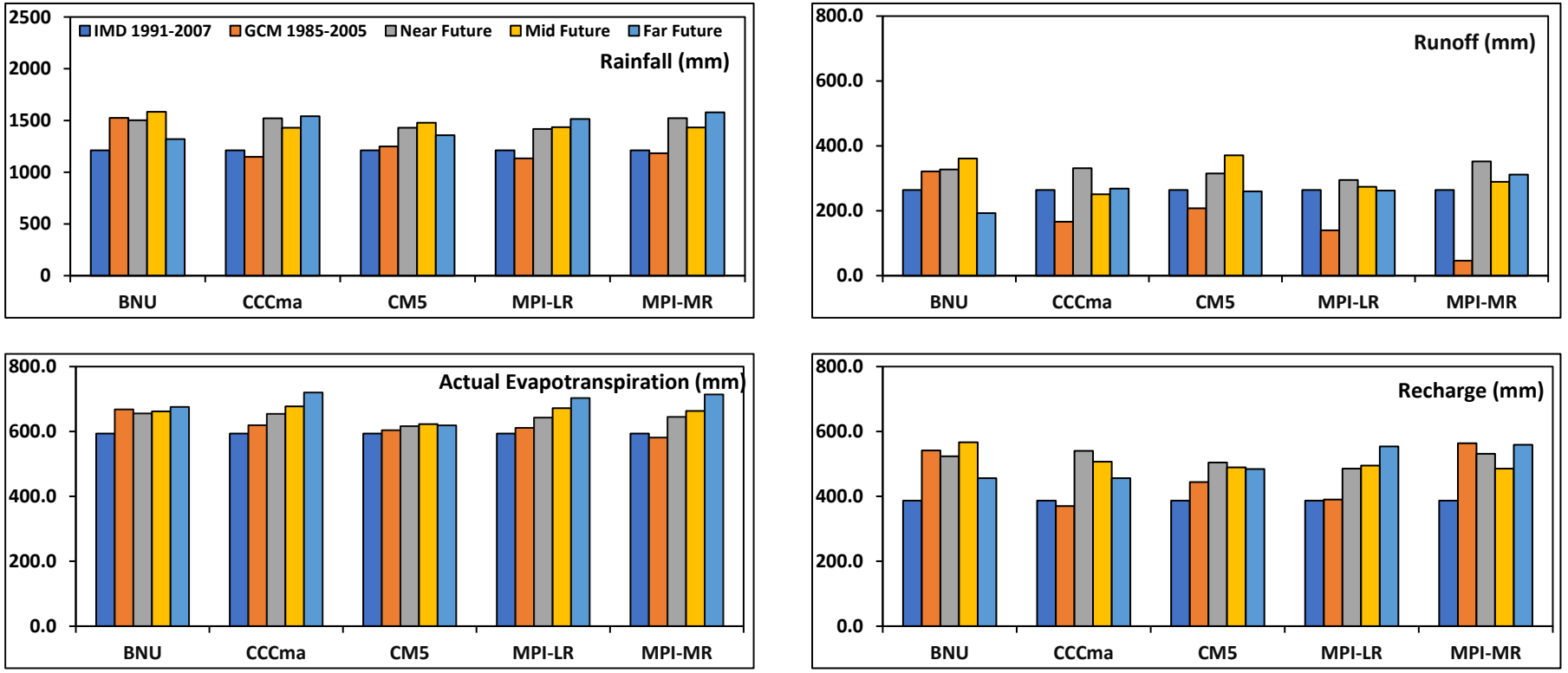

Fig. 6.22 Water balance contribution in major hydrological processes for RCP 8.5 scenario during 2011-2100

6.4 IMPACTS ON IRRIGATION WATER DEMAND

6.4.1 Impact on Irrigation Water Demand in Ukai-Kakrapar Command Area

The crop data including the major (Season wise) crop in the gross command area of Ukai-Kakrapar command area and its cropping pattern in the command area are available for the period (2010 to 2018). Crop data such as crop coefficient (Kc), crop seasons (kharif, rabi and hot) period (sowing to harvesting) are available for command area. The resolution of the gridded rainfall data available from IMD is 0.25º×0.25º while the gridded temperature data is available at 1.0º×1.0º resolution. For, consistency of the dataset, the temperature dataset was interpolated to 0.25º×0.25º using bilinear interpolation as temperature is a smooth hydroclimatic variable. The daily Tmax and Tmin data is used to estimate daily PET, temperature-based Hargreaves method (Samani 2000) is adopted for calculation of the potential evapotranspiration. The effective rainfall is estimated using soil conservation service (SCS) method (Ashofteh et al. 2013).

The absolute values of the long-term mean rainfall, reference evapotranspiration, crop water demand and gross irrigation water requirement in the Ukai-Kakrapar command area for RCP 4.5 and RCP 8.5 scenarios, using ensembled downscaled climatic variables for five GCMs, were estimated on monthly scales see Fig. 6.23. The values indicated in Fig. 6.23, shows the changes in the variables with reference to their respective values for observed IMD data for the base line period. From Fig. 6.23 (b), it is revealed that reference evapotranspiration (ET_o) values decrease for February month with reference to their corresponding value of IMD data for historical period. On the other hand, the value of the parameter increases during January, March, April, May, Jun, November, and December months. Such decrease/ increase in the ET_o values is due to monthly variations in ($T_{max} - T_{min}$) parameters in their respective months. The crop water requirement for different months, depending upon the stage of Kharif, Rabi and Hot seasonal crops, were estimated from the estimated reference crop evapotranspiration (ET_C). The net irrigation demands values were subsequently computed by subtracting the effective rainfall for each month and adding additional irrigation requirement such as leaching etc. Subsequently, from Net irrigation requirement, the field irrigation requirement and gross irrigation requirement are obtained by giving due consideration of water application efficiency and conveyance efficiency respectively. From Fig. 6.23(d), it is apparent that, the gross irrigation requirement (GIR) would increase (decrease) in future for January to May, and December months (August, October, and November months) with reference to the base line

period. This increase in GIR in December month is due to increase in ET_o in the same month (Fig. 6.23(b)). Similarly, the decrease in GIR in August, October and November months is due to increase in effective rainfall in future in such months (See Fig. 6.23(a)). In the remaining months, the GIR remains invariant with reference to the base line period in future.

6.4.2 Impact on Irrigation Water Demand in Girna Command Area of Middle Tapi Basin

The plots shown in the Fig. 6.24 shows the average change in actual magnitude (Δ) in each month with respect to IMD observed data for rainfall, ETo (reference evapotranspiration), CWD (crop water demand) and GIWR (gross irrigation water requirement). The zero line indicates the average IMD observed data line (as datum) and the negative or positive variations of all the parameters indicates the increase or decrease in values respectively. Ensemble method has been adopted and the results are analyzed for near-future, mid-future and far-future for RCP 4.5 and RCP 8.5 scenarios. It is also observed that the future temperature is increasing with respect to IMD observed data throughout the year.

The rainfall data variations of actual magnitude show insignificant change for December, January, February, March, April, and May month whereas, it shows a significant change (decrease) in the month of June, July, and August (monsoon period). There is a significant increase of rainfall in the month of October and November (post monsoon period). One can also observe that the maximum change in rainfall pattern is in the far-future for both RCP 4.5 and RCP 8.5 scenarios with the variation of 107.3 mm and 118.3 mm respectively in the month of October.

The ETo plot show that there are significant changes in the values throughout the year. There is an increasing in the ETo values for the month of January, May, June, July, August, and September (monsoon period). There is a decrease in the ETo values for the month of February, March, April, October, November, and December (pre and post monsoon). One can also observe that the maximum increase in variations as well as the decrease in variations are in the month of January and February respectively. One can also observe that the maximum increase in ETo is in the near-future for both RCP 4.5 and RCP 8.5 scenarios with the variation of 69.0 mm and 77.4 mm respectively in the month of January whereas the maximum decrease in ETo is in the near-future for both RCP 4.5 and RCP 8.5 scenarios with the variation of 70.4 mm and 70.0 mm respectively in the month of February.

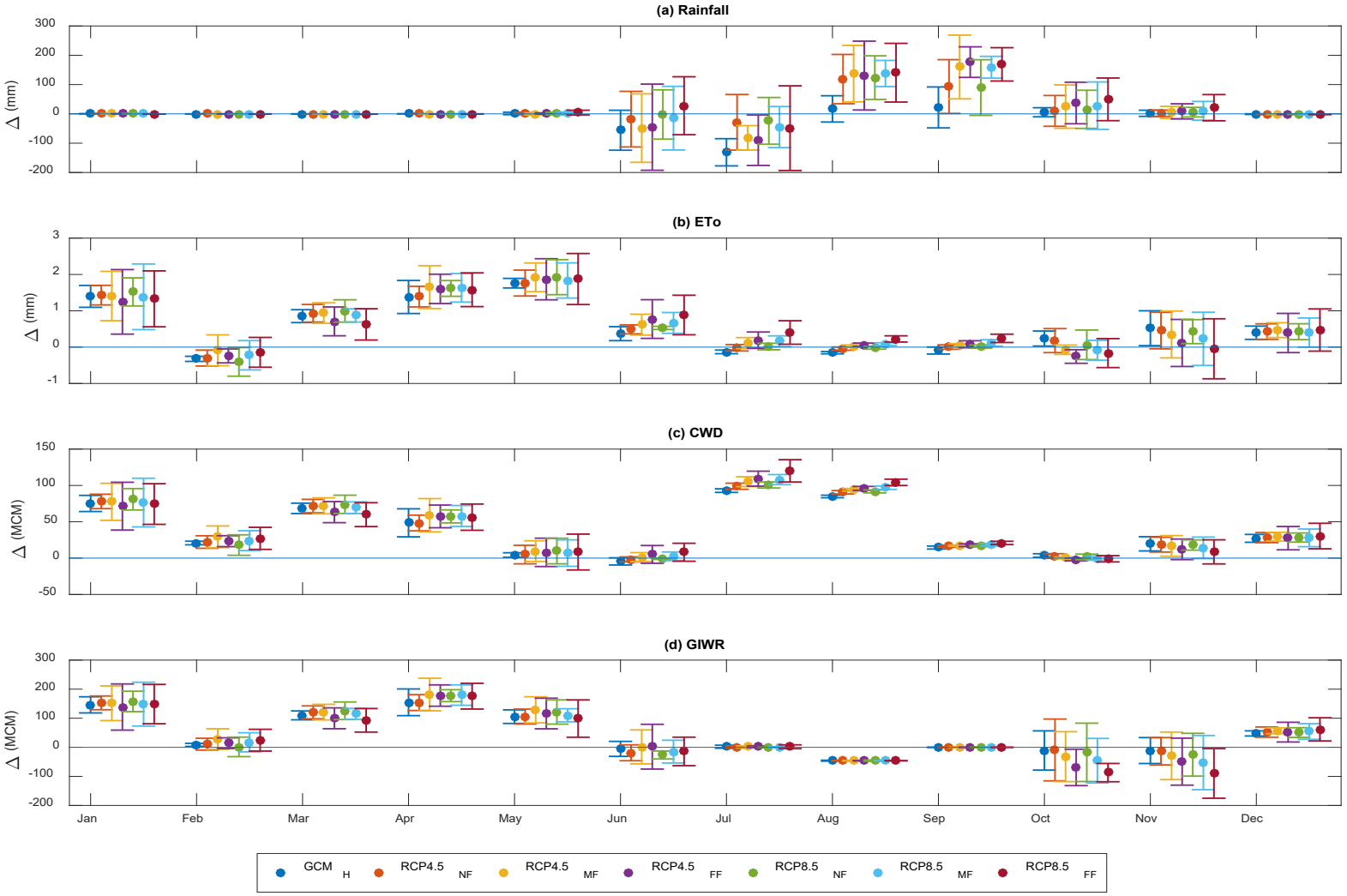

Fig. 6.23 Mean change in Rainfall, ETo, CWD and GIWR in Ukai-Kakrapar command area with reference to their respective values for base line period for near-, mid-, and far-future under RCP 4.5 and RCP 8.5 scenarios for ensembled output of GCM Models (in figure, Zero line corresponds to the values for reference (base line) period, Δ (mm), Δ (MCM) are the relative change of the parameters with reference to the base line period)

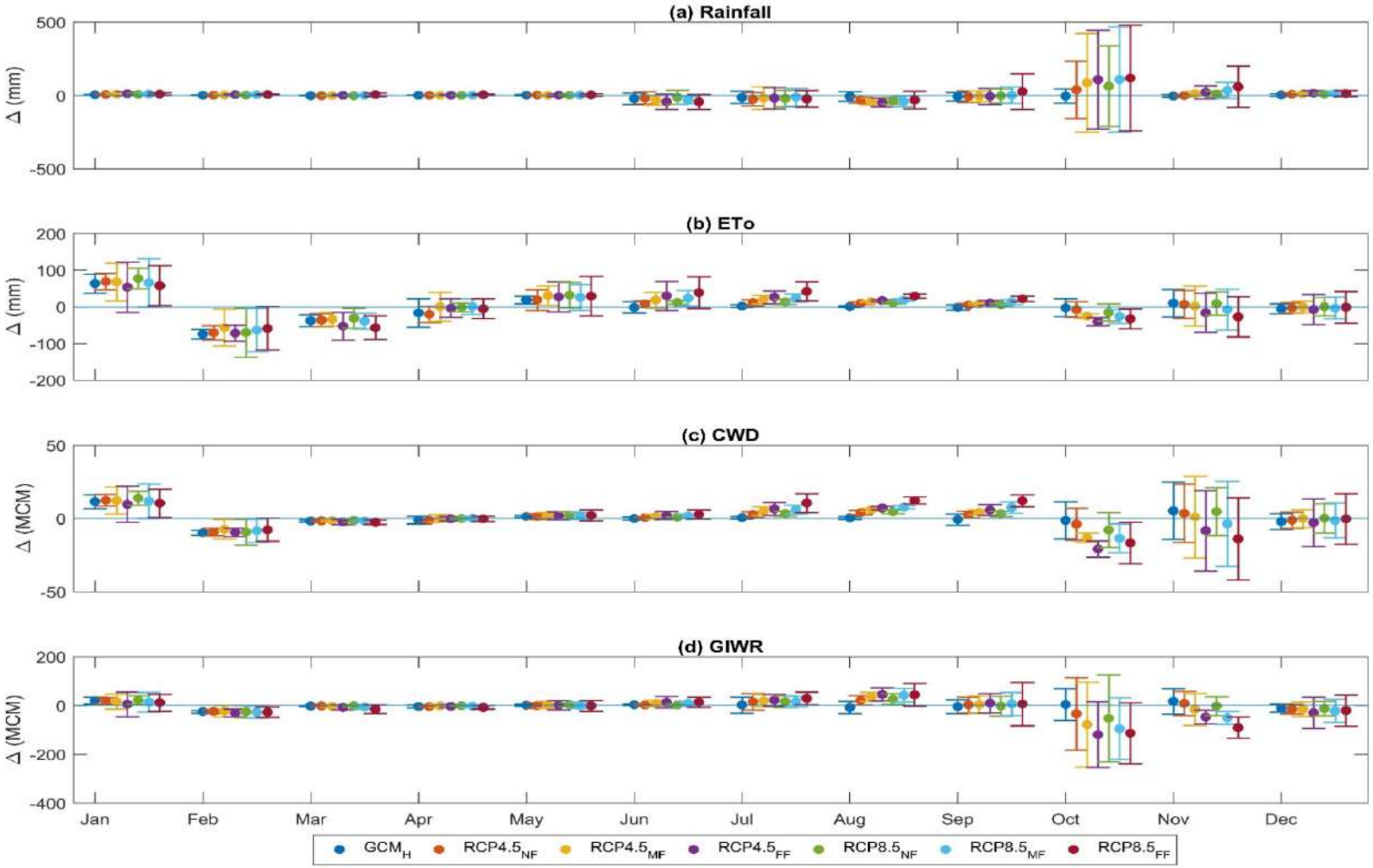

Fig. 6.24 Mean change in Rainfall, ETo, CWD and GIWR in Girna command area with reference to their respective values for baseline period during near-, mid-, and far-future under RCP 4.5 and RCP 8.5 scenarios for ensembled output of GCM Models (in figure, Zero line corresponds to the values for reference (base line) period, Δ (mm), Δ (MCM) are the relative change in the parameters with reference to the base line period)

The CWD (crop water demand) plot show that there are significant changes in the values throughout the year. There is an increasing in the CWD values for the month of January, May, June, July, August, and September (monsoon period). There is a decrease in the CWD values for the month of February, March, April, October, November, and December (pre and post monsoon). One can also observe that the maximum increase in variations as well as the decrease in variations are in the month of January and October respectively. One can also observe that the maximum increase in CWD is in the near-future for both RCP 4.5 and RCP 8.5 scenarios with the variation of 12.4 MCM and 13.9 MCM respectively in the month of January whereas the maximum decrease in CWD is in the far-future for both RCP 4.5 and RCP 8.5 scenarios with the variation of 20.9 MCM and 16.7 MCM respectively in the month of October.

The GIWR (gross irrigation water requirement) plot show that there are significant changes in the values throughout the year. There is an increasing in the GIWR values for the month of January, May, June, July, August, and September (monsoon period). There is a decrease in the GIWR values for the month of February, March, April, October, November, and December (pre and post monsoon). One can also observe that the maximum increase in variations as well as the decrease in variations are in the month of August and October respectively. One can also observe that the maximum increase in GIWR is in the far-future for both RCP 4.5 and RCP 8.5 scenarios with the variation of 45.5 MCM and 44.1 MCM respectively in the month of August whereas the maximum decrease in GIWR is in the far-future for both RCP 4.5 and RCP 8.5 scenarios with the variation of 119.3 MCM and 113.2 MCM respectively in the month of October.

6.5 IMPACTS ON DROUGHTS

The resolution of the gridded rainfall data available from IMD is 0.25º×0.25º while the gridded temperature data is available at 1.0º×1.0º resolution. For, consistency of the dataset, the temperature dataset was interpolated to 0.25º×0.25º using bilinear interpolation as temperature is a smooth hydroclimatic variable. The daily Tmax and Tmin data is used to estimate daily PET data for estimation of climatic water balance (CWB), difference of rainfall and PET. Due to non-availability of the other meteorological variables, temperature-based Hargreaves method (Samani 2000) is adopted for calculation of the potential evapotranspiration. The aggregated monthly rainfall and CWB is used for estimation of meteorological drought indices, i.e., SPI and SPEI. The multivariate standardize drought index (MSDI) is also computed using

the joint probability distribution of the rainfall and CWB for respective months during the period under consideration. The marginal probabilities for all the drought indices are calculated using empirical Gringorten plotting position formula. The drought indices are calculated at 3-, 6- and 12-month aggregation period to study the short-term, moderate, and long-term drought conditions in the basin. The estimated meteorological drought indices are then used for computation of annual drought parameters, i.e., annual drought duration (ADD), annual drought peak (ADP) and annual drought severity (ADS). The annual drought parameters were then harnesses for the temporal variability during reference period, using IMD data for 1951-2005, and future period, using KRSD data for near-, mid- and far-future. The analysis for future period was carried out using the ensembled outputs of the drought parameters. The temporal variability in drought parameters for individual GCM model are shown in Annexure Figs. A28-A30.

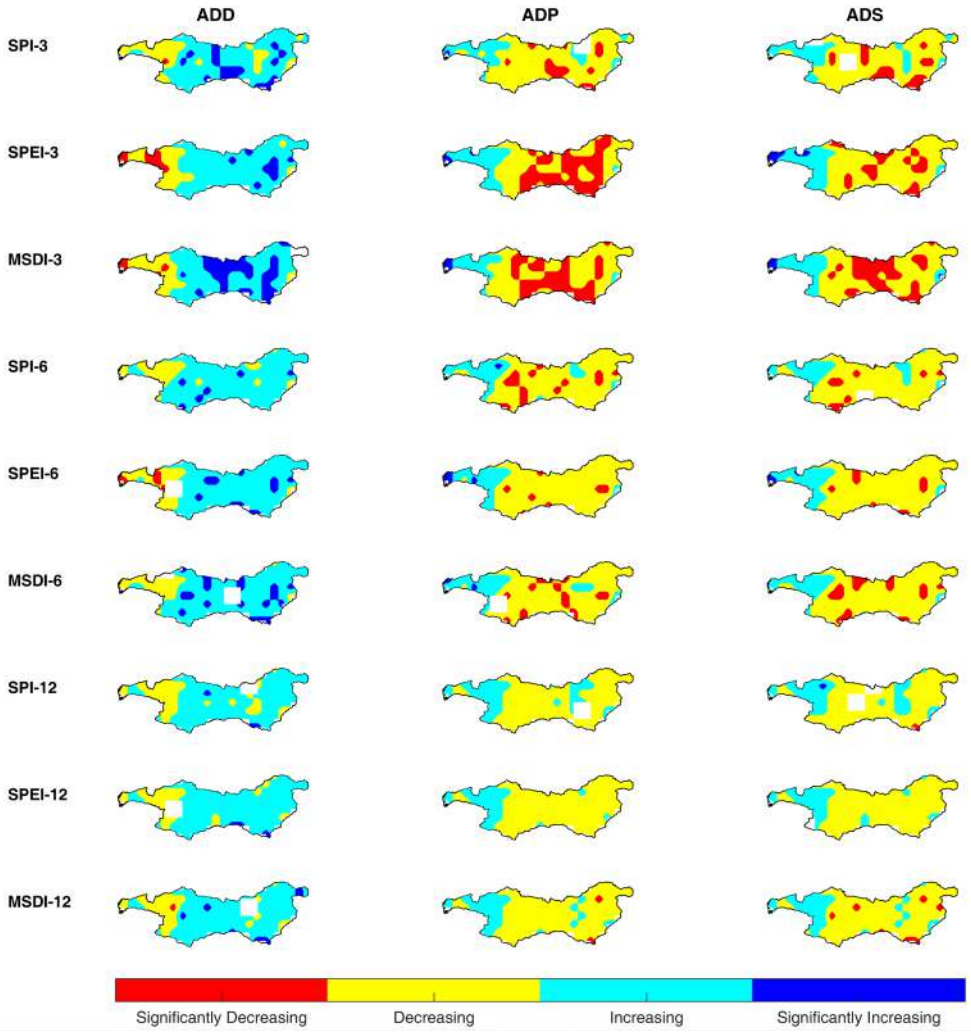

Fig. 6.25 Nature of trend in drought parameters for short-term, moderate and long-term meteorological drought indices for period 1951-2005. **(**The uncoloured region in the basin boundary shows the region of no trend.)

(a)

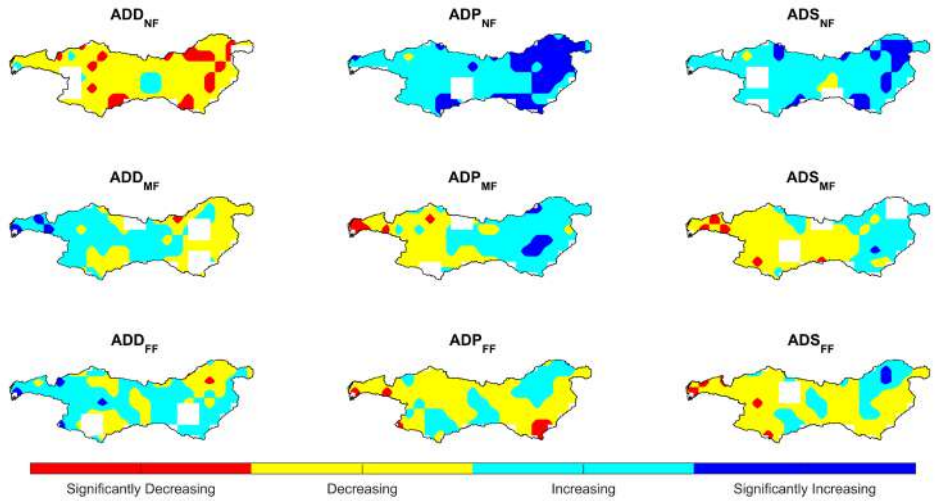

(b)

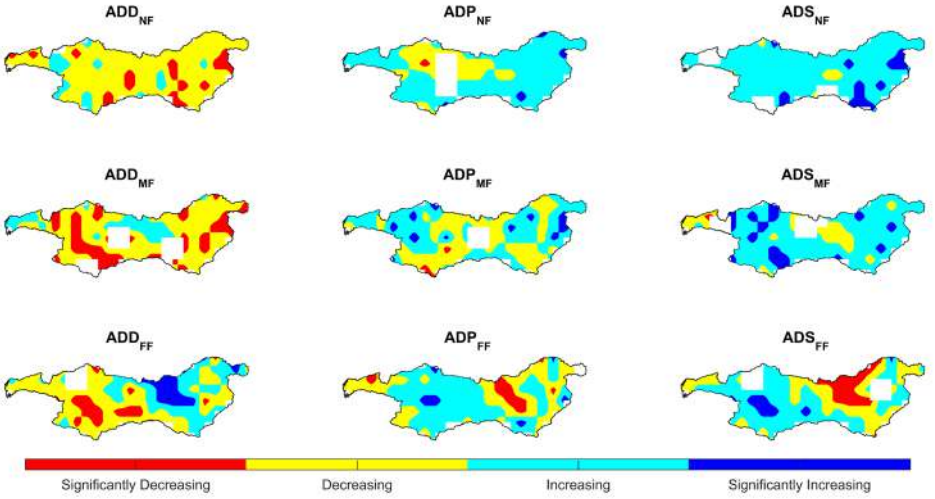

Fig. 6.26 Nature of trend in drought parameters for MSDI-3 for near-, mid-, and far-future, denoted by NF, MF, and FF respectively under (a) RCP 4.5 and (b) RCP 8.5 scenarios. **(**The uncoloured region in the basin boundary shows the region of no trend.)

The short-term, moderate, and long-term drought indices, i.e., SPI, SPEI and MSDI are calculated for the period 1951-2005 and analysed using the drought parameters estimated from the aforesaid drought indices. The increasing trend in ADD is a likely indicator for prolonged drought conditions in the recent period. On the other hand, the increasing trend in the ADS and ADP a likely indicator that the region is observing better or improved rainfall conditions. The spatial variation of the nature of trend in ADD, ADP and ADS calculated using short-term drought indices (SPI-3, SPEI-3, and MSDI-3), moderate term drought indices (SPI-6, SPEI-6, and MSDI-6), and long-term drought indices (SPI-12, SPEI-12 and MSDI-12) are shown in Fig. 6.25. From Fig. 6.25, it can be inferred that all the drought indices, i.e., SPI, SPEI and MSDI, at various temporal scale, i.e., 3-, 6-, and 12-month are similar with each other. The significantly increasing in ADD in conjunction with

significantly decreasing ADS and ADP in SPI-3, SPEI-3 and MSDI-3 shows that the region has been more prone to short term drought conditions. It is also evident that with increase in the aggregation period, the prevailing drought conditions are gradually reducing. Thus, it can be concluded that the short-term drought conditions in the basin are primarily due to the short and very heavy spells of the rainfall. The rising drought conditions need to be managed actively by developing the water retention structures so cater the drought like situations.

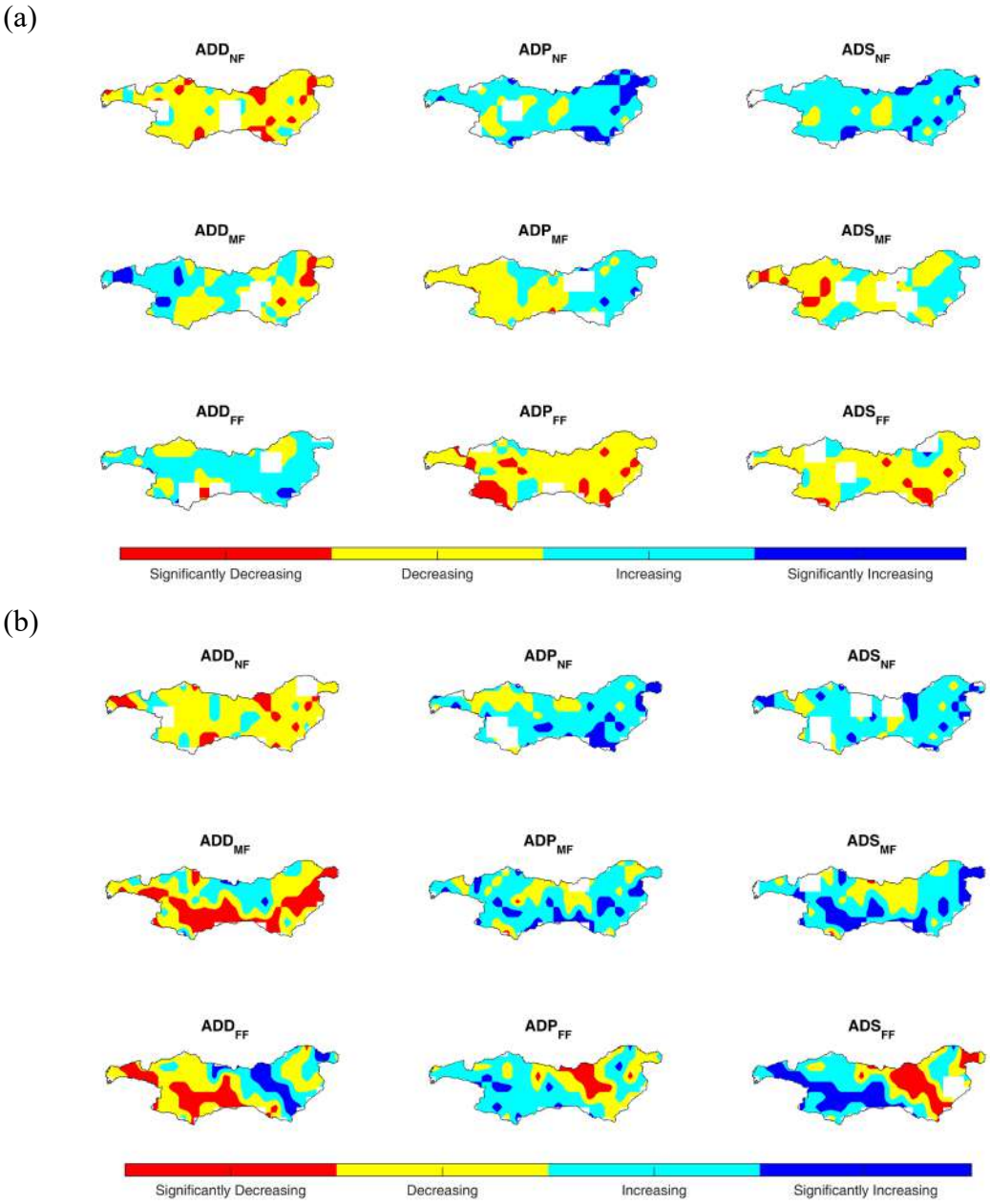

Fig. 6.27 Nature of trend in drought parameters for MSDI-6 for near-, mid-, and far-future, denoted by NF, MF, and FF respectively under (a) RCP 4.5 and (b) RCP 8.5 scenarios. **(**The uncoloured region in the basin boundary shows the region of no trend.)

(a)

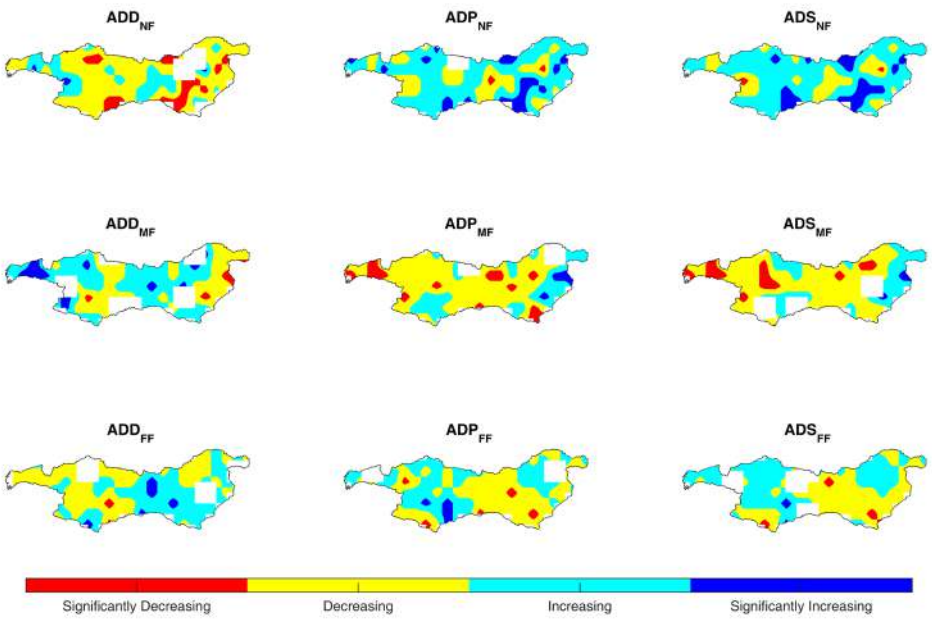

(b)

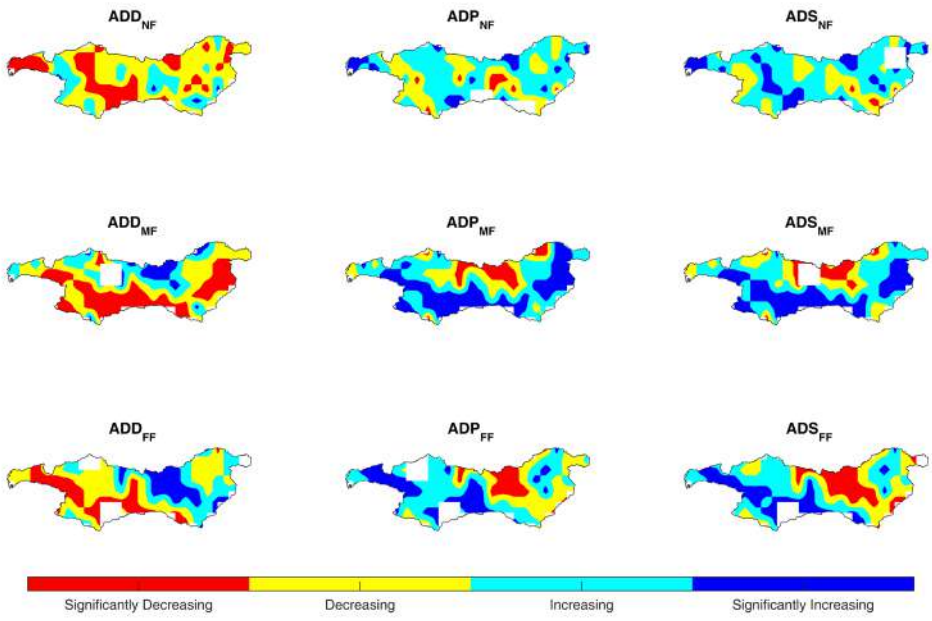

Fig. 6.28 Nature of trend in drought parameters for MSDI-12 for near-, mid-, and far-future, denoted by NF, MF, and FF respectively under (a) RCP 4.5 and (b) RCP 8.5 scenarios. **(**The uncoloured region in the basin boundary shows the region of no trend.)

The KRSD data of five GCM models was used to derive the drought parameters and they were ensembled before estimation of the temporal trend in the indices. The MSDI being bivariate drought index, it can account for drought events at lesser probabilities also. Thus, MSDI is used for calculations of the drought parameters. The aggregation period used for estimation of MSDI are 3-, 6-, and 12-month to consider short-, moderate, and long-term droughts respectively for RCP 4.5 and RCP 8.5 scenarios (see Fig. 6.26-6.28). The short-term drought seems to increase

over majority of the basin area, however, the temporal trend shown are not significant at 5% level of significance (see Fig. 6.26). A portion of the UTB, in the vicinity of the Hatnur reservoir shows the tendency of aggravating short-term drought conditions under RCP 8.5 scenario. The similar observation holds true for higher aggregation period, i.e., for moderate and long-term drought under RCP 4.5 scenario. However, with increase in the aggregation period, the LTB and a part of MTB shows a tendency towards wet regime while the part of UTB shows prevailing drought conditions for short-, moderate, and long-term drought conditions under RCP 8.5 scenarios (see Fig. 6.27-6.28). The possible reason behind increasing drought tendency under RCP 8.5 scenario can be due rapidly rising temperature leading to heavy downpour. Though it leads to good annual total rainfall at the cost of prolonged dry spells.

6.6 IMPACTS ON FLOODING IN SURAT CITY

The long-term inflow (2011-2100) into Ukai reservoir is obtained from the calibrated hydrological model (SWAT) developed for the MTB and UTB. The inflow series for each model and RCP scenario is further divided into three sub-periods near future (2011-2040), mid future (2041-2070) and far future (2071-2100). The annual maximum series is derived for each sub-period, model and RCP scenario (see Fig. 6.29) and fitted with with 2-parameter log-normal (LN), Gumbel distribution and 3-parameter generalize extreme value (GEV), generalize Pareto (GPA), log-normal III (LN-III) and log-Pearson type-III (LP-III) distributions to compute the design flood for different return periods. The parameter estimation and goodness of fit (GOF) were performed by using EasyFit 5.6 software. The fitted distribution and 100-year return level flood magnitude given in Table 6.8.

The 100-year return period inflow flood for Ukai reservoir was 34, 459.4 m^3/s (Fig. 4.6). However, the values corresponding to 100-year return period for NF, MF and FF periods for different GCM models range from 3030 m^3/s to 9499.1 m^3/s, 3515.8 m^3/s to 14168 m^3/s and 4056.5 m^3/s to 13472 m^3/s respectively for RCP 4.5 scenario. The corresponding values for RCP 8.5 scenario for NF, MF and FF ranges from 2953 m^3/s to 10950 m^3/s, 6762.2 m^3/s to 12898 m^3/s and 2272.2 m^3/s to 8980.2 m^3/s respectively. Such significantly low values for 100-year return period inflow into Ukai reservoir is due to inability of GCM models to capture the extreme precipitation in the TRB.

- **Flood Risk Maps for Future scenarios of RCP 4.5 and RCP 8.5**

The flood risk assessment is caried out for coastal urban flood plain of densely populated Surat city. The analysis is performed for 100-year flood in all five GCM model including RCP 4.5 and 8.5 scenarios. The flood inundation maps with percentage of area under each flood depth class using bar graphs for different models is given in shown in Fig. 6.30. It is observed that, during 2011-2040 MPI-LR and MPI-MR for RCP 8.5 inundate larger area compared to other scenarios. The similar maps are also developed for mid future 2041-2070 and far future 2071-2100 given in Fig.A31 and Fig. A32 (in Annexure) respectively.

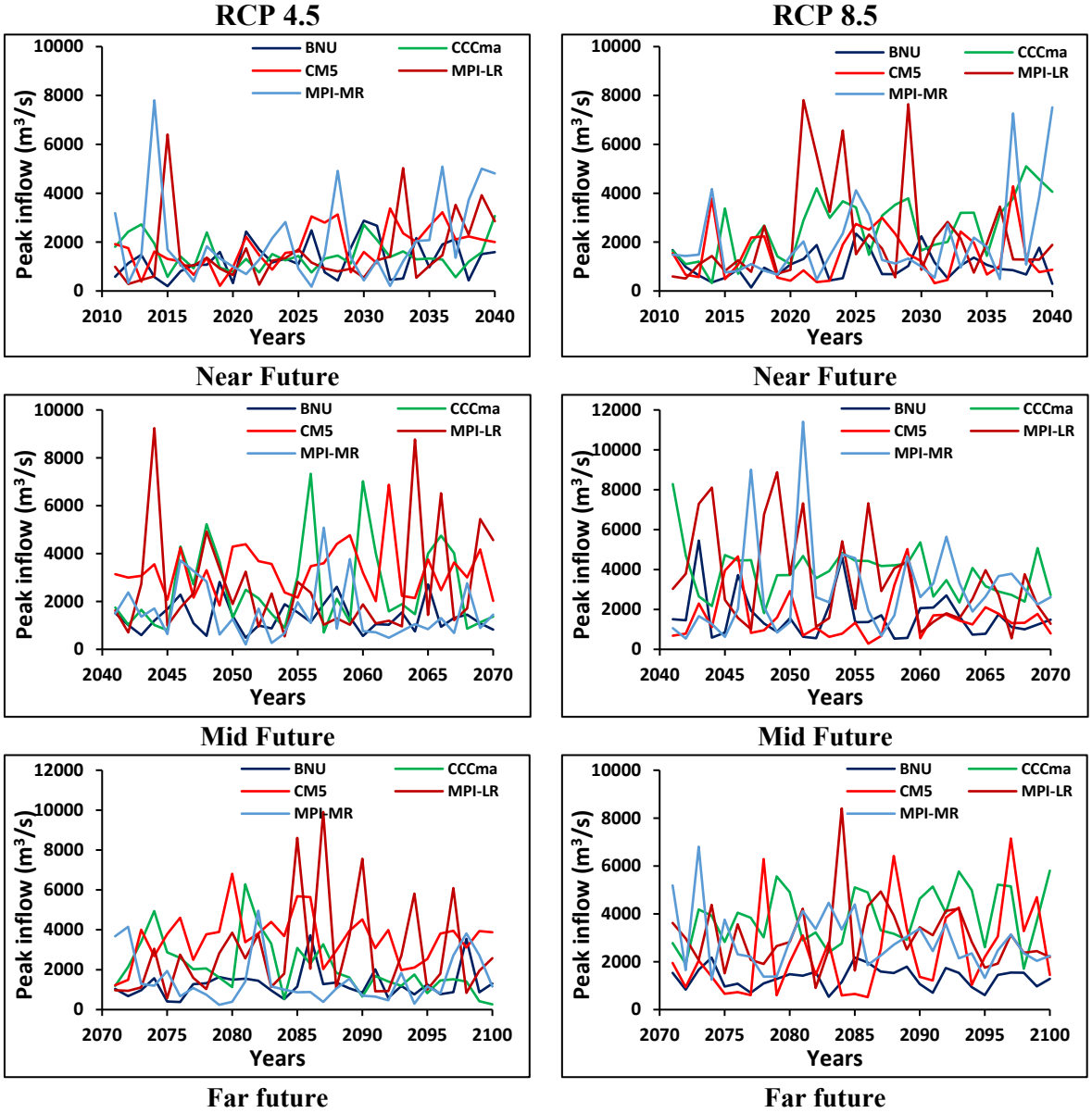

Fig. 6.29 Annual Maximum series derived from daily inflow into Ukai reservoir for RCP 4.5 and 8.5

The flood hazard maps are also developed based on the product of depth and velocity for all climate change scenarios. The flood hazard maps with area under different hazard class ranging from very low to very high hazard using bar graph for near future 2100-2040 are shown in Fig. 6.31. The hazard maps for remaining for periods 2041-2070 and 2071-2100 are given in Fig. **A33 and A34 (in Annexure)** respectively. In all the cases the area under high to very high hazard category ranges from 14 % to 22 %, which is very less compared to the results of hazard maps developed 100- year flood using observed inflow into Ukai reservoir. The results obtained for MPI-LR model during 2041-2070 and 2071-2100 for RCP 4.5 scenarios shows more dangerous situation where more than 20 % of the city specifically, west, and north zone is under high flood hazard.

Table 6.8 Climate model sub-periods with fitted distribution and respective 100-Year flood

RCP 4.5		**Fitted Distribution**	**100-Year Flood (m^3/sec)**
BNU	2011-2040	GPA	3030.0
	2041-2070	LP-III	3515.8
	2071-2100	GEV	4056.5
CCCma	2011-2040	Gumble	3534.4
	2041-2070	LN-III	14168.0
	2071-2100	LN-III	6847.0
CM5	2011-2040	LN-III	6518.5
	2041-2070	GEV	6490.7
	2071-2100	LN-III	6670.0
MPI-LR	2011-2040	GEV	8391.9
	2041-2070	LN-III	13685.0
	2071-2100	GPA	13472.0
MPI-MR	2011-2040	LP-III	9499.1
	2041-2070	Log-normal	6831
	2071-2100	LN-III	7342.3
RCP 8.5		**Fitted Distribution**	**100-Year Flood (m^3/sec)**
BNU	2011-2040	GEV	2953.0
	2041-2070	Log-normal	7870.6
	2071-2100	GEV	2272.2
CCCma	2011-2040	LN-III	5477.8
	2041-2070	GEV	7007.6
	2071-2100	GEV	6622.5
CM5	2011-2040	GEV	4878.8
	2041-2070	LP-III	6762.2
	2071-2100	GPA	8980.2
MPI-LR	2011-2040	LP-III	10950
	2041-2070	GEV	12898
	2071-2100	GEV	7273.4
MPI-MR	2011-2040	LP-III	10950.0
	2041-2070	GEV	12898
	2071-2100	GEV	7151

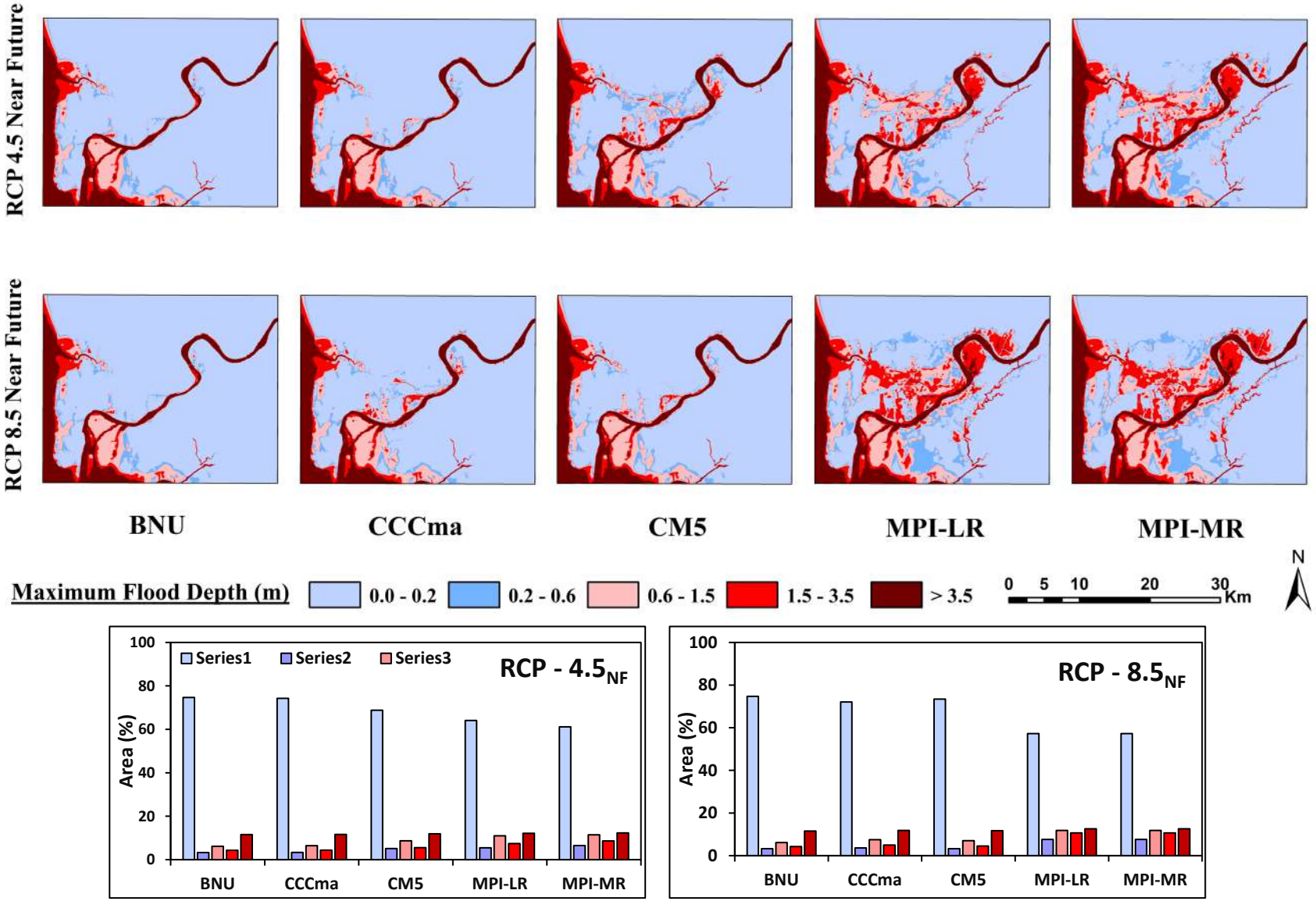

Fig. 6.30 Flood inundation maps for densely populated Surat city and its outskirt area for near future (2011-2040) and RCP 4.5 and 8.5

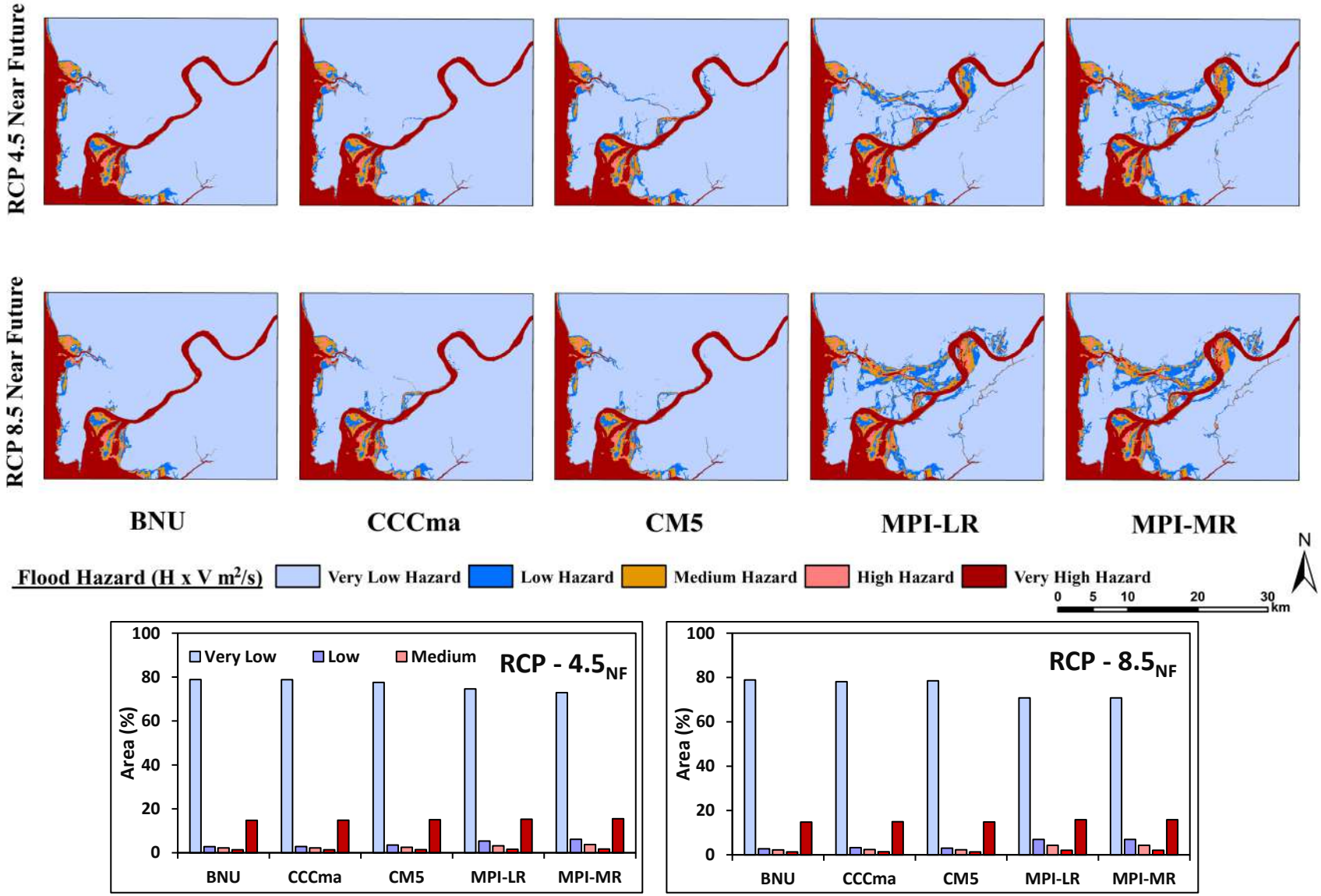

Fig. 6.31 Flood hazard maps for densely populated Surat city and its outskirt area for near future (2011-2040) and RCP 4.5 and 8.5

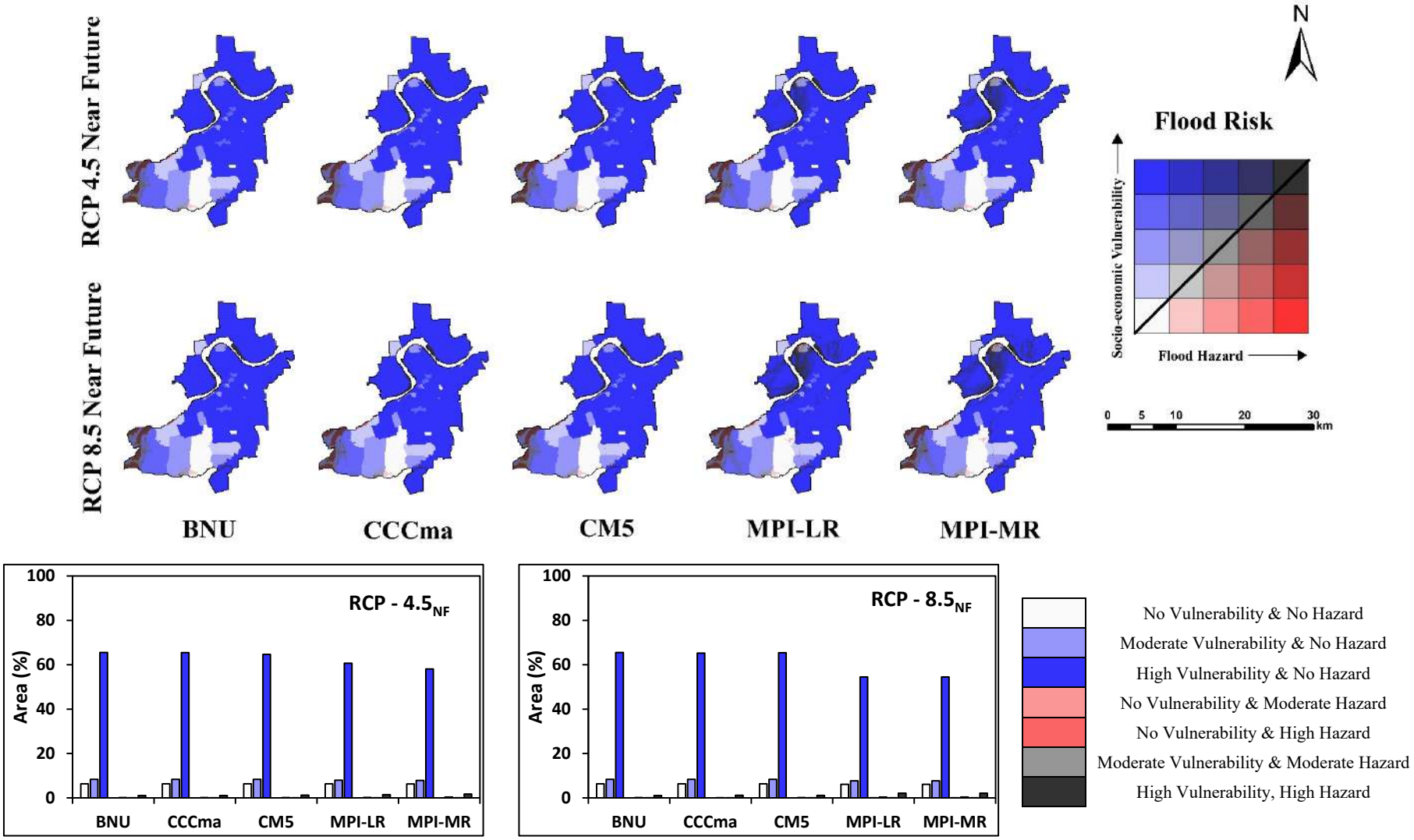

Fig. 6.32 Flood risk maps for densely populated Surat city and its outskirt area for near future (2011-2040) and RCP 4.5 and 8.5

Similar to flood inundation and hazard maps, the flood risk maps are also developed for area under jurisdiction of SMC. The socio-economic vulnerability is considered constant during 2011-2100. The flood risk maps for 2100-2040 are shown in Fig. 6.32 and for mid and far future periods are given in Fig. **A35 and A36** (in Annexure). In all the cases, larger area of the city except west and north zone, experiencing flood risk majorly due to socio-economic vulnerability. On the other hand, west zone and north zone are under high flood risk with equal contribution of flood hazard and vulnerability.

6.7 CLOSURE

The spatio-temporal variability of hydroclimatic variables viz. rainfall (1944-2013), temperature (1951-2016) and streamflow (1973-2013) considering the extreme indices are assessed for the baseline period using the non-parametric tests across the Tapi basin. The temperature indices would change uniformly across the TRB in future; however, the temperature indices derived from minimum temperature are more prone to significant rise than maximum temperature in the basin. Further, it is noted that PRCPTOT values are continuously increasing across TRB from NF to FF under both RCP scenarios.

The Purna sub-catchment has shown significant rise in SDII, CDD, TXx, DTR, HSpMax and CSpMax, whereas decrease in annual runoff has been reported during baseline period. Based on KRSD data analysis, Purna sub-catchment would get improved annual rainfall in both RCP 4.5 and 8.5 scenarios. The part of Purna sub-catchment is prone to short term drought in during baseline period and moderate to long term drought during far future under RCP 8.5 scenario. The Q_{10} or higher flows would reduce while the Q_{50} and lean period flows would increase by the end of the 21st century under both the RCP scenarios for Purna sub-catchment.

In case of Burhanpur sub-catchment, even though total rainfall is decreasing, the extreme rainfall events are increasing. The increase in annual runoff and temperature indices TXx, DTR and HSpMax is also reported. The part of Burhanpur sub-catchment is prone to short term drought during baseline period, and short-moderate- and long-term drought during far future under RCP 8.5 scenario. The water balance components simulated climate change scenario over 21st century indicated there would be decrease in contribution of surface runoff and water yields while evapotranspiration components would increase for the same period.

The MTB does not show significant temporal trend in rainfall indices, however, significant decrease in annual runoff at various stream gauging stations has been reported during the baseline period. The part of MTB is prone to short term drought during baseline period which changes to moderate drought condition during far future under RCP 4.5 scenario. The Q_{50} are

likely to increase from near-future to far-future compared to observed baseline data, whereas Q_{10} or higher flows would reduce under changing climate.

The LTB is characterized as wettest region with considerable rise in PRCPTOT, RD and SDII during bassline period. The LTB also experienced considerable rise in minimum temperature leading significant decrease in DTR and ITR during baseline period. Incidentally, for RCP 8.5, the Rx1day is decreasing continuously from NF to FF in LTB. The release from Ukai reservoir dominates the monsoonal flows, however, the decrease in annual runoff is observed in Lower Tapi River. The part of the LTB experienced decreasing drought conditions during the baseline period and small portion of the Lower Tapi basin can experience short-, moderate-, and long-term droughts in the mid-future under RCP 4.5. The actual evapotranspiration loss is increasing continuously from NF-MF-FF periods, and the increase in actual evapotranspirational losses is more in RCP 8.5 compared to RCP 4.5 scenario. During climate change scenarios, the area under high to very high flood hazard and flood risk category (100-year flood) is very less compared to corresponding flood based on observed inflow into Ukai reservoir.

CHAPTER 7
CONCLUSIONS & ADAPTATION MEASURES

7.1 GENERAL

A detailed description of the results of various project objectives is discussed in the previous chapters. The hydroclimatic variability in the rainfall, temperature, and streamflow for the entire Tapi River basin (TRB) has been studied using station/observed data of IMD and CWC for 1944-2013, 1951-2016, and 1973-2013 respectively. The gridded rainfall and temperature data ($0.25^o \times 0.25^o$) has been used to assess the meteorological droughts in the TRB from 1951-2005. Keeping in view the physio-climatological heterogeneity of TRB, the SWAT hydrological models have been developed separately for the Purna sub-catchment (by SVNIT-Surat), Burhanpur sub-catchment (by MNIT-Jaipur), and Middle Tapi basin (by MANIT-Bhopal) considering the baseline period as 1994-2013. The catchment hydrology of the Lower Tapi basin (by SVNIT-Surat) has been modeled using the MIKE-SHE model for the baseline period of 1991-2007. Considering the importance of Surat city and its history of riverine flooding, a 2D hydrodynamic flood model has also been prepared. Subsequently, the flood risk maps have been developed for different return levels of inflows into the Ukai reservoir. In addition, the irrigation water demands have also been calculated for the Ukai-Kakrapar and Girna command areas for baseline and future periods. The Kernel Regression-based statistically downscaled (KRSD) precipitation and bias corrected temperature data is used to assess the impacts of climate change on various aspects discussed above for future periods (NF: Near-Future, 2011-2040; MF: Mid-Future, 2041-2070 and FF: Far-Future, 2071-2100). The key findings from the above analyses are presented in this chapter. The adaptive measures are also recommended based on the inferences derived from the statistically downscaled climate data for future periods.

7.2 CONCLUSIONS

The key conclusion derived from the present assessment for different sub-catchments of TRB are as follows:

(a) Purna sub-catchment

- The trend analysis of data for period 1944-2013, indicated that there was a significant rise in daily rainfall intensity (SDII), with prolonged dry spells (CDD) over the Purna sub-catchment (*Subsection 6.2.1*). The sub-catchment exhibited a significant rise in the hottest day's temperature (TXx), daily temperature variability (DTR), and rising duration of the

hot and cold spells (HSpMax and CSpMax) (*Subsection 6.2.2*). Also, the annual runoff in the Purna sub-catchment has decreased during the period 1973-2013 (though insignificant), led to water stress conditions in the recent decade. The runoff analysis was reported for period 1973-2013 due to non-availability of streamflow data for the period 1944-1972 (*Subsection 6.2.3*).

- The KRSD data states that the Purna sub-catchment would get improved rainfall conditions in future with rising total annual rainfall, no. of rainy days, decreasing dry spells under RCP 4.5 scenario. Similar inferences are derived for the Burhanpur sub-catchment also. (*Subsection 6.2.4*)
- The temperature indices show uniform changes across the basin under different sub-periods and RCP scenarios. The temperature indices derived from minimum temperature are more prone to significant rise than maximum temperature under both RCP scenarios, thus, reducing the diurnal temperature range. The change in temperature indices would be negligible in mid-, and far-future periods under the RCP 4.5 scenario due to the projected curb on global greenhouse gas emissions post-2040. The only noteworthy observation in future data indicated that the no. of days exceeding 37 ºC would rise by 50% (and 130%) by the end of the 21st century under the RCP 4.5 (8.5) scenario (*Subsection 6.2.4*).
- The temporal trend in the annual drought indices showed that the part of the Purna sub-catchment is prone to short-term drought conditions compared to moderate-and long-term droughts during the baseline period. A small portion of the catchment can experience moderate- and long-term droughts in far-future under RCP 8.5.
- The top five sensitive parameters of SWAT model corresponding to the single-site calibration (SSC) over the Purna sub-catchment *GWQMN.gw*, *GW_REVAP.gw*, *CN2.mgt*, *RCHRG_DP.gw,* and *CNCOEF.bsn* while the sensitive parameters during multi-site calibration (MSC) are *GW_REVAP.gw*, *SOL_BD.sol*, *CN2.mgt*, *CNCOEF.bsn*, and *CH_N2.rte*. It can be observed that during SSC, most of the sensitive parameters are related to the ground water flow while the MSC results into the sensitive parameters which includes surface, subsurface and ground water flow.
- The performance indicators shows that the multi-site calibration has resulted into R^2 >0.80, bR^2 > 0.80, *NSE* >0.85, *MNS* > 0.65, and *RSR* <0.5 at most of the instances, except at Lakhpuri gauging station. Also, the relative error in the simulated water balance components is within ±5%. Thus, the developed model can reliably simulate the catchment's response to future climate scenarios for the Purna sub-catchment.

- The contribution of monsoon season rainfall and streamflow in the Purna sub-catchment reduces to 69.7% (62.0%) and 60.0% (57.3%) of annual rainfall and streamflow respectively by end of the 21st century under RCP 4.5 (8.5) scenario against the contribution of same parameters as 86.8% and 83.8%, respectively during the reference period. Also, the Q_{10} or higher flows would reduce while the Q_{50} and lean period flows would increase by the end of the 21st century under both the RCP scenarios.

(b) Burhanpur sub-catchment

- The trend analysis of rainfall data for baseline period (1944-2013), indicated that there was decrease in the total rainfall (PRCPTOT) in the Burhanpur sub-catchment while the extreme rainfall events were found to increase (*Subsection 6.2.1*). The area exhibited a significant rise in the hottest day's temperature (TXx), daily temperature variability (DTR), and rising duration of the hot spells (HSpMax) (*Subsection 6.2.2*). The Burhanpur and Hatnur are the only stream gauging stations in TRB with an increasing trend of annual runoff for the period 1973-2013 (*Subsection 6.2.3*).
- The temporal trend in the annual drought indices showed that the part of the Burhanpur sub-catchment is prone to short-term drought conditions compared to moderate-and long-term droughts during the baseline period. A small portion of the catchment can experience short-, moderate- and long-term droughts in far-future under RCP 8.5 (*Subsection 6.5*).
- The most sensitive parameters for the Burhanpur sub-catchment are *CN2*, *GWQMN*, *GW_REVAP*, *SOL_AWC*, *SLSOIL*, *SLSUBBSN,* and *ESCO* under single-site calibration of the SWAT model.
- The SWAT model under calibration period, on daily time scale, resulted into R^2 = 0.70, *NSE* = 0.65, and *PBIAS* = 23.8% for Burhanpur stream gauging station while the same statistical parameters for Hatnur stream gauging station were R^2 =0.71, *NSE* = 0.67, and *PBIAS* = -8.7%. On the other hand, the performance of the model for independent period during validation were R^2 = 0.7, *NSE* = 0.71, and *PBIAS* = 22.9% for Burhanpur stream gauging station while the same parameters for Hatnur stream gauging station are R^2 = 0.72, *NSE* = 0.71, and *PBIAS* = -6.2%.
- The water balance components of the Burhanpur sub-catchment as simulated by the calibrated SWAT model showed surface runoff as 29%, water yield as 39%, and evapotranspiration as 42%, out of the total 100% rainfall input into the system. The water balance components as simulated for future time periods indicated there would be decrease

in contribution of surface runoff and water yields while evapotranspiration components would increase for the same period (*Subsection 6.3.2*).

(c) Middle Tapi basin (MTB)

- The MTB does not show significant temporal trends in most instances; however, the MTB had indicated the minimal annual rainfall (PRCPTOT of 719 mm) in the entire TRB. Also, the MTB has been observed to have persistent dry spells (CDD) in the basin. The rainfall extremes have been found to decrease, but not significantly (*Subsection 6.2.1*). A mixed trend pattern is observed in temperature indices with a significantly increasing (and decreasing) trend in the diurnal temperature range (and warmest night) (*Subsection 6.2.2*). Also, significant reduction has been noted in the annual runoff at various stream gaging stations in the MTB (*Subsection 6.2.3*).
- Contrary to the trend of rainfall during the baseline period, the total annual rainfall magnitude, rainy days, magnitude and intensity of rainfall extremes are likely to increase under RCP 4.5 for near-future to far-future. These observations are likely to be more intensified under the RCP 8.5 scenario (*Subsection 6.2.4*).
- The temporal trend in the annual drought indices showed that the part of the Middle Tapi basin is prone to short-term drought conditions compared to moderate-and long-term droughts during the baseline period. A small portion of the Middle Tapi basin can experience moderate droughts condition in the far-future under RCP 4.5.
- The SCS runoff curve number (*CN2*) has been found to the most sensitive parameter. Moist bulk density (*SOL_BD*), Deep aquifer percolation fraction (*RCHRG_DP*), and Saturated soil hydraulic conductivity (*SOL_K*) were also found to be the sensitive parameters in the SWAT modeling of MTB under multi-site calibration.
- The performance indicators showed that the model resulted in R^2 >0.76, *NSE* >0.7, *MNS* > 0.65, and *RSR* <0.56 at Gidhade, Sarangkheda stations, and Ukai reservoir. Also, the relative error in the simulated water balance components has been found to be within ±5%. Thus, the developed model can reliably simulate the response of the catchment to future climate scenarios in the Middle Tapi basin.
- The simulated ensembled GCM output for streamflows indicated that median flows (Q_{50}) are likely to increase from near-future to far-future compared to observed flows for the baseline period (1981-2005). On the other hand, the high flows (Q_{10}) are likely to decrease in the future compared to the baseline period (*Subsection 6.3.3*).

(d) Lower Tapi basin (LTB)

- The LTB is characterized as the wettest region with a considerable rise in total annual rainfall, daily rainfall intensity, frequency and magnitude of extremes. Along with a significant rise in rainfall extremes, the LTB also has experienced a considerable rise in minimum temperature extremes, leading to a substantial down surge in daily (DTR) and intra-annual temperature (ITR) variability (*Subsection 6.2.1-6.2.2*). The releases from the Ukai reservoir dominate the monsoonal flows in the LTB; however, annual run off has been found to decrease in the basin (*Subsection 6.2.3*).
- It is noted that PRCPTOT values are continuously increasing across TRB from NF to FF under both RCP scenarios. Incidentally, for RCP 8.5, the Rx1day is decreasing continuously from NF to FF in LTB (*Subsection 6.2.4*).
- The temporal trend in the annual drought indices showed that the part of the Lower Tapi basin experienced decreasing drought conditions during the baseline period. However, a small portion of the Lower Tapi basin can experience short-, moderate-, and long-term droughts in the mid-future under RCP 4.5.
- The performance of the MIKE SHE/MIKE 11 model under the calibration period showed that *RMSE* = 395.7 m^3/s and *NSE* = 0.875 at the Ghala stream gauging station. The validation of the model with independent data set (at Ghala) resulted in *RMSE* = 348.7 m^3/s and *NSE* = 0.77 at a daily time scale specifying the acceptable performance of the model.
- The simulated streamflows indicated that error in water balance computation is less than 1%. The water balance computation for the Lower Tapi basin resulted in 50 % and 45 % water loss due to actual evapotranspiration during the calibration and validation periods, respectively. In case of future climate change scenarios, the loss of water budget due to actual evapotranspiration ranges from 39% to 50% and 41% to 52% in RCP 4.5 and 8.5 respectively.
- The 2D HD model has been developed for the Lower Tapi basin with distributed floodplain roughness co-efficient based on existing land use land cover classification. The performance of the model has been evaluated for predicting the maximum water level at Nehru bridge in Surat (R^2 = 0.947) as well as maximum water depth in all seven zones of Surat city (*RMSE* = 0.86 m) and found satisfactory.
- The flood hazard maps are developed for coastal urban flood plain and densely populated Surat city for different return period flood obtained from flood frequency analyse. For 100-Year flood, 329 km^2 area of Surat city and its outskirt area has been found be under high to

very high hazard category. The north zone and west zone are the worst affected areas of the city.

- The census-based socio-economic vulnerability of Surat city has been computed by using PCA-DEA aggregation technique. The 44 out of 89 wards covering ≈ 66 % of the area is under very high-vulnerable category which mostly concentrated over densely populated area.
- The bivariate approach been used to develop the flood risk maps with distinct contribution of flood hazard and socio-economic vulnerability. For 100-Year flood, the north zone and larger area of west zone is under high flood risk which is due to equal contribution of flood hazard and socio-economic vulnerability. The area under high to very hazard and high risk is increasing with increase in magnitude of flood for higher return period.
- For 100- year return period flood, the MPI-LR, and MPI-MR for RCP 8.5 in near future (2011-2040), inundate the larger area compared to other scenarios. For all the climate change scenarios, the area under the high to very high flood hazard category ranges from 14% to 22%. The larger area of the north and west zones of the Surat city is under high flood risk with equal contribution of flood hazard and socio-economic vulnerability.
- The gross irrigation water requirements (GIWR) are likely to increase (decrease), particularly for January, March, April, May, and December months (August, October, and November months) months with reference to the baseline period in the Ukai-Kakrapar command area. On the other hand, in Girna command area, the GIWR are likely to increase (decrease), particularly for January, July, and August months (February, September, October, and November months) months.

7.3 ADAPTATION MEASURES

- The rainfall during the monsoon period is likely to decrease in the future. On the other hand, the rainfall would increase during the lean period. Similar results are observed in simulated streamflows for both monsoonal and lean period flows. Due to such changing pattern of the rainfall/streamflow may affect the cropping pattern in the command area.
- The estimation of gross irrigation water requirement (GIWR) for the future period indicates that there would be an increase in GIWR during the Rabi and Hot weather crops for the Ukai-Kakrapar command area. Accordingly, the available water resources are to be augmented, and drip irrigation system may be adopted in the future to cope with likely increase in GIR in the command area. It is also emphasized to use more water retaining

structures like lakes, ponds, check dams, etc. to recharge the groundwater system in the command area.

- The future inflows into the Ukai reservoir have not been captured well while using downscaled GCM rainfall for baseline period and future period. However, the flood risk map, prepared based on flood hazard and vulnerability map for Surat city, showed that the Surat city is under high risk to flooding. Thus, suitable early warning system must be adopted for reducing the flooding conditions and risk in the Surat city.
- Invariably, the maximum and minimum temperature increases in the TRB with a pronounced increase in Tmin. This would likely to have a negative impact on crops, particularly paddy yield over the TRB. The suitable cropping pattern can be adopted to cope up with rising T_{min} temperature.
- Also, in TRB, it is found that temperature would likely to go more than 37ºC for 110 days (170 days) under RCP 4.5 (RCP 8.5) scenarios by the end of the 21st century. The notable increase in temperature beyond 37ºC would like to have heat stress on the people in the basin. This may reduce the work performance of the people in the basin.
- The simulated water balance using hydrological models indicated that there would be water-stress conditions in the basin in future. Also, the spatiotemporal trend of streamflow in TRB for baseline period showed that there is significant decrease in water availability in the basin. It is suggested that water conservation measures like, rainwater harvesting, lining of canal, charging the farmers for water based on volumetric method, prevention of leakage in water distribution system, efficient recycling of treated waste water in the municipality etc. must be adopted in the basin.

REFERENCES

Abbaspour, K. C. (2011). SWAT-CUP: SWAT calibration and uncertainty programs—a user manual. *Eawag: Dübendorf, Switzerland*, 1-103.

Abbaspour, K. C., Vaghefi, S. A., and Srinivasan, R. (2017). A guideline for successful calibration and uncertainty analysis for soil and water assessment: a review of papers from the 2016 international SWAT conference. *Water*, 10(1), 6.

Abbaspour, K.C., Rouholahnejad, E., Vaghefi, S., Srinivasan, R., Yang, H., and Kløve, B., (2015). A continental-scale hydrology and water quality model for Europe: Calibration and uncertainty of a high-resolution large-scale SWAT model. *Journal of Hydrology* 524,733–752.

Abbaspour, K.C., Yang, J., Maximov, I., Siber, R., Bonger, K., Mieleitner, J., Zobrist, J., and Srinivasan, R. (2007). Modelling hydrology and water quality in the pre-alpine Thur watershed using SWAT. *Journal of Hydrology* 333 (2), 413-430.

Abbott, M. B., and Ionescu, F. (1967). On the numerical computation of nearly horizontal flows. *Journal of Hydraulic Research*, 5(2), 97-117.

Abeysingha, N. S., Singh, M., Sehgal, V. K., Khanna, M., and Pathak, H. (2016). Analysis of trends in streamflow and its linkages with rainfall and anthropogenic factors in Gomti River basin of North India. *Theoretical and Applied Climatology*, 123(3), 785-799.

Abraham, L. Z., Roehrig, J., and Chekol, D. A. (2007, October). Calibration and validation of SWAT hydrologic model for Meki watershed, Ethiopia. In *Conference on International Agricultural Research for Development, University of Kassel-Witzenhausen and University of Gottingen* (Vol. 5).

Alexandersson, H. (1986). A homogeneity test applied to precipitation data. *Journal of Climatology*, 6(6), 661-675.

Alfonso, L., Mukolwe, M. M., and Di Baldassarre, G. (2016). Probabilistic flood maps to support decision-making: Mapping the value of information. *Water Resources Research*, 52(2), 1026-1043.

Arnold, J. G., Moriasi, D. N., Gassman, P. W., Abbaspour, K. C., White, M. J., Srinivasan, R., Santhi C., Harmel R. D., Van Griensven A., Van Liew M. W., Kannan N. and Jha, M. K. (2012). SWAT: Model use, calibration, and validation. *Transactions of the ASABE*, *55*(4), 1491-1508.

Arnold, J. G., Srinivasan, R., Muttiah, R. S., and Williams, J. R. (1998). Large area hydrologic modeling and assessment part I: model development 1. *JAWRA Journal of the American Water Resources Association*, 34(1), 73-89.

Ashofteh, P. S., Bozorg Haddad, O., and Mariño, M. A. (2013). Scenario assessment of streamflow simulation and its transition probability in future periods under climate change. *Water Resources Management*, *27*(1), 255-274.

Begnudelli, L., Sanders, B. F., and Bradford, S. F. (2008). Adaptive Godunov-based model for flood simulation. *Journal of Hydraulic Engineering*, 134(6), 714-725.

Bisht, D. S., Chatterjee, C., Raghuwanshi, N. S., and Sridhar, V. (2018). Spatio-temporal trends of rainfall across Indian river basins. *Theoretical and Applied Climatology*, 132(1), 419-436.

Buishand, T. A. (1982). Some methods for testing the homogeneity of rainfall records. *Journal of Hydrology*, 58(1-2), 11-27.

Canadell, J. G., Le Quéré, C., Raupach, M. R., Field, C. B., Buitenhuis, E. T., Ciais, P., Conway, T. J., Gillett, N. P., Houghton, R. A., and Marland, G. (2007). Contributions to accelerating atmospheric CO2 growth from economic activity, carbon intensity, and efficiency of natural sinks. *Proceedings of the National Academy of Sciences*, 104(47), 18866-18870.

Central Water and Power Commission (CWPC). (1952). *Hydrological data of river basins of India: The Tapi Basin*, A Government of India Publication, New Delhi

Central Water Commission (CWC). (2014). *Tapi Basin*. Ministry of Water Resources, River Development and Ganga Rejuvenation, New Delhi.

Chaibou Begou, J., Jomaa, S., Benabdallah, S., Bazie, P., Afouda, A., and Rode, M. (2016). Multi-site validation of the SWAT model on the Bani catchment: Model performance and predictive uncertainty. *Water*, *8*(5), 178.

Chandra, P., Patel, P. L., and Porey, P. D. (2016). Prediction of sediment erosion pattern in Upper Tapi Basin, India. *Current Science* (00113891), 110(6).

Chandra, P., Patel, P. L., Porey, P. D., and Gupta, I. D. (2014). Estimation of sediment yield using SWAT model for Upper Tapi basin. *ISH Journal of Hydraulic Engineering*, 20(3), 291-300.

Chen, F. W., and Liu, C. W. (2012). Estimation of the spatial rainfall distribution using inverse distance weighting (IDW) in the middle of Taiwan. *Paddy and Water Environment*, 10(3), 209-222.

Chow, V. T., Maidment, D. R., and Mays, L. W. (1988). *Applied Hydrology*, Mcgraw Hill, New York.

CRED and UNDRR (2021). 2020: The Non-COVID Year in Disaster. Brussels: CRED

Das, B., Jain, S. K., Thakur, P. K., and Singh, S. (2021). Assessment of climate change impact on the Gomti River basin in India under different RCP scenarios. *Arabian Journal of Geosciences*, 14(2), 1-16.

Dash, S., and Maity, R. (2019). Temporal evolution of precipitation-based climate change indices across India: contrast between pre-and post-1975 features. *Theoretical and Applied Climatology*, 138(3), 1667-1678.

Deshpande, N. R., Kothawale, D. R., and Kulkarni, A. (2016). Changes in climate extremes over major river basins of India. *International Journal of Climatology*, 36(14), 4548-4559.

DHI (Danish Hydraulic Institute) (2017a) User guide and reference manual to MIKE SHE: An Integrated hydrological modeling framework. *Software Manual,* DHI, Denmark.

DHI (Danish Hydraulic Institute) (2017b) User guide and reference manual to MIKE 11: Modeling system for the rivers and channels. *Software Manual*, DHI, Denmark.

DHI (Danish Hydraulic Institute) (2017c). *User guide and reference manual to MIKE 21:* Costal and sea hydrodynamic modeling. *Software Manual*, DHI, Denmark.

Domeneghetti, A., Vorogushyn, S., Castellarin, A., Merz, B., and Brath, A. (2013). Probabilistic flood hazard mapping: effects of uncertain boundary conditions. *Hydrology and Earth System Sciences*, 17(8), 3127-3140.

Duhan, D., and Pandey, A. (2013). Statistical analysis of long term spatial and temporal trends of precipitation during 1901–2002 at Madhya Pradesh, India. *Atmospheric Research*, 122, 136-149.

Eini, M., Kaboli, H. S., Rashidian, M., and Hedayat, H. (2020). Hazard and vulnerability in urban flood risk mapping: Machine learning techniques and considering the role of urban districts. *International Journal of Disaster Risk Reduction*, 50, 101687.

Fan, M., and Shibata, H. (2015). Simulation of watershed hydrology and stream water quality under land use and climate change scenarios in Teshio River watershed, northern Japan. *Ecological Indicators*, 50, 79-89.

FAO. Soils resources, management and conservation service. (1983). *Guidelines: land evaluation for rainfed agriculture*. FAO.

Farahmand, A., and AghaKouchak, A. (2015). A generalized framework for deriving nonparametric standardized drought indicators. *Advances in Water Resources*, 76, 140-145.

Faramarzi, M., Abbaspour, K. C., Vaghefi, S. A., Farzaneh, M. R., Zehnder, A. J., Srinivasan, R., and Yang, H. (2013). Modeling impacts of climate change on freshwater availability in Africa. *Journal of Hydrology*, 480, 85-101.

Farooq, M., Shafique, M., and Khattak, M. S. (2019). Flood hazard assessment and mapping of River Swat using HEC-RAS 2D model and high-resolution 12-m TanDEM-X DEM (WorldDEM). *Natural Hazards*, 97(2), 477-492.

Foster, S. B., and Allen, D. M. (2015). Groundwater—surface water interactions in a mountain-to-coast watershed: effects of climate change and human stressors. *Advances in Meteorology*, 2015.

Garg, S. K. (2005). *Irrigation Engineering and Hydraulic Structures* (9 ed.). Delhi: Khanna Publishers.

Gashaw, T., Tulu, T., Argaw, M., and Worqlul, A. W. (2018). Modeling the hydrological impacts of land use/land cover changes in the Andassa watershed, Blue Nile Basin, Ethiopia. *Science of the Total Environment*, 619, 1394-1408.

Gassman, P. W., Reyes, M. R., Green, C. H., and Arnold, J. G. (2007). The soil and water assessment tool: historical development, applications, and future research directions. *Transactions of the ASABE*, 50(4), 1211-1250.

Gehlot, L. K., Jibhakate, S. M., Sharma, P. J., Patel, P. L., and Timbadiya, P. V. (2021). Spatio-temporal variability of rainfall indices and their teleconnections with El Niño-Southern oscillation for Tapi Basin, India. *Asia-Pacific Journal of Atmospheric Sciences*, 57(1), 99-118.

General, U. S. (1994). United Nations convention to combat drought and desertification in countries experiencing serious droughts and/or desertification, particularly in Africa. *Particularly in Africa*.

Ghaffari, G., Keesstra, S., Ghodousi, J., and Ahmadi, H. (2010). SWAT-simulated hydrological impact of land-use changes in the Zanjanrood basin, Northwest Iran. *Hydrological Processes: An International Journal*, 24(7), 892-903.

Ghosh, M., Mohanty, M. P., Kishore, P., and Karmakar, S. (2021). Performance evaluation of potential inland flood management options through a three-way linked hydrodynamic modelling framework for a coastal urban watershed. *Hydrology Research*, 52(1), 61-77.

Ghosh, S., Vittal, H., Sharma, T., Karmakar, S., Kasiviswanathan, K. S., Dhanesh, Y., Sudheer, K. P., and Gunthe, S. S. (2016). Indian summer monsoon rainfall: implications of contrasting trends in the spatial variability of means and extremes. *PloS one*, 11(7), e0158670.

Giorgi, F., and Mearns, L. O. (2002). Calculation of average, uncertainty range, and reliability of regional climate changes from AOGCM simulations via the "reliability ensemble averaging" (REA) method. *Journal of climate*, *15*(10), 1141-1158.

Gong, Y., Shen, Z., Liu, R., Wang, X., and Chen, T. (2010). Effect of watershed subdivision on SWAT modeling with consideration of parameter uncertainty. *Journal of Hydrologic Engineering*, 15(12), 1070-1074.

Gosain, A. K., Rao, S., and Arora, A. (2011). Climate change impact assessment of water resources of India. *Current Science*, 356-371.

Guhathakurta, P., Pai, D. S., and Rajeevan, M. N. (2017). Variability and Trends of Extreme Rainfall and Rainstorms. In *Observed Climate Variability and Change over the Indian Region* (pp. 37-49). Springer, Singapore.

Gusain, A., Mohanty, M. P., Ghosh, S., Chatterjee, C., and Karmakar, S. (2020). Capturing transformation of flood hazard over a large River Basin under changing climate using a top-down approach. *Science of the Total Environment*, 726, 138600.

Hamed, K. H., and Rao, A. R. (1998). A modified Mann-Kendall trend test for autocorrelated data. *Journal of Hydrology*, 204(1-4), 182-196.

Han, J. C., Huang, G. H., Zhang, H., Li, Z., and Li, Y. P. (2014). Heterogeneous precipitation and streamflow trends in the Xiangxi River watershed, 1961–2010. *Journal of Hydrologic Engineering*, 19(6), 1247-1258.

Hao, Z., and AghaKouchak, A. (2013). Multivariate standardized drought index: a parametric multi-index model. *Advances in Water Resources*, 57, 12-18.

Hao, Z., and AghaKouchak, A. (2014). A nonparametric multivariate multi-index drought monitoring framework. *Journal of Hydrometeorology*, 15(1), 89-101.

Hao, Z., and Singh, V. P. (2015). Drought characterization from a multivariate perspective: A review. *Journal of Hydrology*, 527, 668-678.

Hargreaves, G. H., and Samani, Z. A. (1985). Reference crop evapotranspiration from temperature. *Applied Engineering in Agriculture*, 1(2), 96-99.

Hirsch, R. M., Slack, J. R., and Smith, R. A. (1982). Techniques of trend analysis for monthly water quality data. *Water Resources Research*, 18(1), 107-121.

Huang, Y., Chen, X., Li, Y., Willems, P., and Liu, T. (2010). Integrated modeling system for water resources management of Tarim River Basin. *Environmental Engineering Science*, 27(3), 255-269.

Jain, A. O., Thaker, T., Chaurasia, A., Patel, P., and Singh, A. K. (2018). Vertical accuracy evaluation of SRTM-GL1, GDEM-V2, AW3D30 and CartoDEM-V3. 1 of 30-m resolution with dual frequency GNSS for lower Tapi Basin India. *Geocarto International*, *33*(11), 1237-1256.

Jain, S. K., Agarwal, P. K., and Singh, V. P. (2007). *Hydrology and water resources of India* (Vol. 57). Springer Science and Business Media.

Jha, R. K., and Gundimeda, H. (2019). An integrated assessment of vulnerability to floods using composite index–A district level analysis for Bihar, India. *International Journal of Disaster Risk Reduction*, 35, 101074.

Joseph, J., Ghosh, S., Pathak, A., and Sahai, A. K. (2018). Hydrologic impacts of climate change: Comparisons between hydrological parameter uncertainty and climate model uncertainty. *Journal of Hydrology*, 566, 1-22.

Joshi, N., Gupta, D., Suryavanshi, S., Adamowski, J., and Madramootoo, C. A. (2016). Analysis of trends and dominant periodicities in drought variables in India: a wavelet transform based approach. *Atmospheric Research*, 182, 200-220.

Kamali, B., Abbaspour, K. C., and Yang, H. (2017). Assessing the uncertainty of multiple input datasets in the prediction of water resource components. *Water*, 9(9), 709.

Kannan, S., and Ghosh, S. (2011). Prediction of daily rainfall state in a river basin using statistical downscaling from GCM output. *Stochastic Environmental Research and Risk Assessment*, 25(4), 457-474.

Kannan, S., and Ghosh, S. (2013). A nonparametric kernel regression model for downscaling multisite daily precipitation in the Mahanadi basin. *Water Resources Research*, 49(3), 1360-1385.

Kao, S. C., and Govindaraju, R. S. (2010). A copula-based joint deficit index for droughts. *Journal of Hydrology*, 380(1-2), 121-134.

Karmakar, S., Simonovic, S. P., Peck, A., and Black, J. (2010). An information system for risk-vulnerability assessment to flood. *Journal of Geographic Information System*, 2(03), 129.

Kendall, M. G. (1955). Rank Correlation Methods*: By Maurice G. Kendall*. Hafner.

Khalid, K., Ali, M. F., Abd Rahman, N. F., Mispan, M. R., Haron, S. H., Othman, Z., and Bachok, M. F. (2016). Sensitivity analysis in watershed model using SUFI-2 algorithm. *Procedia Engineering*, 162, 441-447.

Kumar, N., Goyal, M. K., Gupta, A. K., Jha, S., Das, J., and Madramootoo, C. A. (2021). Joint behaviour of climate extremes across India: Past and future. *Journal of Hydrology*, *597*, 126185.

Kumar, N., Jaswal, A. K., Mohapatra, M., and Kore, P. A. (2017). Spatial and temporal variation in daily temperature indices in summer and winter seasons over India (1969–2012). *Theoretical and Applied Climatology*, 129(3), 1227-1239.

Kumar, S., Chanda, K., and Pasupuleti, S. (2020). Spatiotemporal analysis of extreme indices derived from daily precipitation and temperature for climate change detection over India. *Theoretical and Applied Climatology*, 140(1), 343-357.

Kundzewicz, Z. W. (2008). Climate change impacts on the hydrological cycle. *Ecohydrology and Hydrobiology*, 8(2-4), 195-203. https://doi.org/10.2478/v10104-009-0015-y

Lacombe, G., and McCartney, M. (2014). Uncovering consistencies in Indian rainfall trends observed over the last half century. *Climatic Change*, 123(2), 287-299.

Lobell, D. B., Schlenker, W., and Costa-Roberts, J. (2011). Climate trends and global crop production since 1980. *Science*, 333(6042), 616-620.

Loliyana, V. D., and Patel, P. L. (2018). Performance evaluation and parameters sensitivity of a distributed hydrological model for a semi-arid catchment in India. *Journal of Earth System Science,* 127(8), 117.

Loliyana, V. D., and Patel, P. L. (2019). Evaluation of soil moisture prediction for Gopalkheda sub-catchment, India. *ISH Journal of Hydraulic Engineering*, 1-10.

Loliyana, V. D., and Patel, P. L. (2020). A physics based distributed integrated hydrological model in prediction of water balance of a semi-arid catchment in India. *Environmental Modelling and Software*, 127, 104677.

Mango, L. M., Melesse, A. M., McClain, M. E., Gann, D., and Setegn, S. G. (2011). Land use and climate change impacts on the hydrology of the upper Mara River Basin, Kenya: results of a modeling study to support better resource management. *Hydrology and Earth System Sciences*, 15(7), 2245-2258.

Mani, P., Chatterjee, C., and Kumar, R. (2014). Flood hazard assessment with multiparameter approach derived from coupled 1D and 2D hydrodynamic flow model. *Natural Hazards*, 70(2), 1553-1574.

Mann, H. B. (1945). Nonparametric tests against trend. *Econometrica: Journal of the Econometric Society*, 245-259.

McKee, T. B., Doesken, N. J., and Kleist, J. (1993). The relationship of drought frequency and duration to time scales. In *Proceedings of the 8th Conference on Applied Climatology* 17(22), 179-183.

Mishra, A. K., and Singh, V. P. (2010). A review of drought concepts. *Journal of hydrology*, 391(1-2), 202-216.

Mishra, V., Tiwari, A. D., Aadhar, S., Shah, R., Xiao, M., Pai, D. S., and Lettenmaier, D. (2019). Drought and famine in India, 1870–2016. *Geophysical Research Letters*, 46(4), 2075-2083.

Moazami Goudarzi, F., Sarraf, A., and Ahmadi, H. (2020). Prediction of runoff within Maharlu basin for future 60 years using RCP scenarios. *Arabian Journal of Geosciences*, 13(14), 1-17.

Mohanty, M. P., Mudgil, S., and Karmakar, S. (2020). Flood management in India: a focussed review on the current status and future challenges. *International Journal of Disaster Risk Reduction*, 49, 101660.

Mohanty, M. P., Vittal, H., Yadav, V., Ghosh, S., Rao, G. S., and Karmakar, S. (2020). A new bivariate risk classifier for flood management considering hazard and socio-economic dimensions. *Journal of Environmental Management*, 255, 109733.

Mondal, A., and Mujumdar, P. P. (2015a). Modeling non-stationarity in intensity, duration and frequency of extreme rainfall over India. *Journal of Hydrology*, 521, 217-231.

Mondal, A., and Mujumdar, P. P. (2015b). Regional hydrological impacts of climate change: implications for water management in India. *Proceedings of the International Association of Hydrological Sciences*, 366, 34-43.

Moriasi, D. N., Arnold, J. G., Van Liew, M. W., Bingner, R. L., Harmel, R. D., and Veith, T. L. (2007). Model evaluation guidelines for systematic quantification of accuracy in watershed simulations. *Transactions of the ASABE*, 50(3), 885-900.

Moriasi, D. N., Gitau, M. W., Pai, N., and Daggupati, P. (2015). Hydrologic and water quality models: Performance measures and evaluation criteria. *Transactions of the ASABE*, 58(6), 1763-1785.

Mtalo, F. W., Mkhandi, S. H., Jeremiah, J., and Nobert, J. (2012). Hydrological Response of Watershed Systems to Land Use/Cover Change: a Case of Wami River Basin.

Munoth, P., and Goyal, R. (2019). Effects of DEM source, spatial resolution and drainage area threshold values on hydrological modeling. *Water Resources Management*, 33(9), 3303-3319.

Narsimlu, B., Gosain, A. K., and Chahar, B. R. (2018). Hydrological Modeling to Evaluate Future Climate Change Impacts in Sind River Basin, India. *International Journal of Environmental Science and Development*, 9(3), 1-6.

Neitsch, S. L., Arnold, J. G., Kiniry, J. R., and Williams, J. R. (2011). *Soil and water assessment tool theoretical documentation version* 2009. Texas Water Resources Institute.

Nilawar, A. P., and Waikar, M. L. (2019). Impacts of climate change on streamflow and sediment concentration under RCP 4.5 and 8.5: A case study in Purna river basin, India. *Science of the total Environment*, 650, 2685-2696.

Nkhonjera, G. K., Dinka, M. O., and Woyessa, Y. E. (2021). Assessment of localized seasonal precipitation variability in the upper middle catchment of the Olifants River basin. *Journal of Water and Climate Change*, 12(1), 250-264.

Palmer, W. C. (1965). *Meteorological drought* (Vol. 30). US Department of Commerce, Weather Bureau.

Panda, D. K., Mishra, A., Kumar, A., Mandal, K. G., Thakur, A. K., and Srivastava, R. C. (2014). Spatiotemporal patterns in the mean and extreme temperature indices of India, 1971–2005. *International Journal of Climatology*, 34(13), 3585-3603.

Panda, D. K., Panigrahi, P., Mohanty, S., Mohanty, R. K., and Sethi, R. R. (2016). The 20th century transitions in basic and extreme monsoon rainfall indices in India: Comparison of the ETCCDI indices. *Atmospheric Research*, 181, 220-235.

Pasquier, U., He, Y., Hooton, S., Goulden, M., and Hiscock, K. M. (2019). An integrated 1D–2D hydraulic modelling approach to assess the sensitivity of a coastal region to compound flooding hazard under climate change. *Natural Hazards*, 98(3), 915-937.

Patel, D. P., and Srivastava, P. K. (2013). Flood hazards mitigation analysis using remote sensing and GIS: correspondence with town planning scheme. *Water Resources Management*, 27(7), 2353-2368.

Patel, D. P., Ramirez, J. A., Srivastava, P. K., Bray, M., and Han, D. (2017). Assessment of flood inundation mapping of Surat city by coupled 1D/2D hydrodynamic modeling: a case application of the new HEC-RAS 5. *Natural Hazards*, 89(1), 93-130.

Pettitt, A. N. (1979). A non-parametric approach to the change-point problem. *Journal of the Royal Statistical Society: Series C (Applied Statistics)*, 28(2), 126-135.

Pingale, S. M., Khare, D., Jat, M. K., and Adamowski, J. (2014). Spatial and temporal trends of mean and extreme rainfall and temperature for the 33 urban centers of the arid and semi-arid state of Rajasthan, India. *Atmospheric Research*, 138, 73-90.

Ramteke, G., Singh, R., and Chatterjee, C. (2020). Assessing impacts of conservation measures on watershed hydrology using MIKE SHE model in the face of climate change. *Water Resources Management,* 34(13), 4233-4252.

Rani, S., and Sreekesh, S. (2020). Flow regime changes under future climate and land cover scenarios in the Upper Beas basin of Himalaya using SWAT model. *International Journal of Environmental Studies*, 1-16.

Refsgaard, J. C. (1997). Parameterisation, calibration and validation of distributed hydrological models. *Journal of Hydrology*, 198(1-4), 69-97.

Riha, S. J., Wilks, D. S., and Simoens, P. (1996). Impact of temperature and precipitation variability on crop model predictions. *Climatic Change*, 32(3), 293-311.

Russo, B., Gómez, M., and Macchione, F. (2013). Pedestrian hazard criteria for flooded urban areas. *Natural Hazards*, 69(1), 251-265.

Sahana, V., and Timbadiya, P. V. (2020). Spatiotemporal Variation of Water Availability under Changing Climate: Case Study of the Upper Girna Basin, India. *Journal of Hydrologic Engineering*, 25(5), 05020004.

Sahana, V., Mondal, A., and Sreekumar, P. (2021). Drought vulnerability and risk assessment in India: Sensitivity analysis and comparison of aggregation techniques. *Journal of Environmental Management*, 299, 113689.

Sahoo, B., and Bhaskaran, P. K. (2018). Multi-hazard risk assessment of coastal vulnerability from tropical cyclones–A GIS based approach for the Odisha coast. *Journal of Environmental Management*, 206, 1166-1178.

Sahoo, S. N., and Sreeja, P. (2015). Development of flood inundation maps and quantification of flood risk in an urban catchment of Brahmaputra River. *ASCE-ASME Journal of Risk and Uncertainty in Engineering Systems, Part A: Civil Engineering*, 3(1), A4015001.

Salvi, K., S. Kannan and Ghosh, S. (2013). High-resolution multisite daily rainfall projections in India with statistical downscaling for climate change impacts assessment. *Journal of Geophysical Research: Atmospheres*, 118(9), 3557-3578.

Samani, Z. (2000). Estimating solar radiation and evapotranspiration using minimum climatological data. *Journal of Irrigation and Drainage Engineering*, 126(4), 265-267.

Sandu, M. A., and Virsta, A. (2015). Applicability of MIKE SHE to simulate hydrology in Argesel River Catchment. *Agriculture and Agricultural Science Procedia*, 6, 517-524.

Santhi, C., Arnold, J. G., Williams, J. R., Dugas, W. A., Srinivasan, R., and Hauck, L. M. (2001). Validation of the SWAT model on a large rwer basin with point and nonpoint sources 1. *JAWRA Journal of the American Water Resources Association*, *37*(5), 1169-1188.

Schneider, S. H. (1996). *Encyclopedia of Climate and Weather* (Vol. 2). Oxford University Press, USA.

Shah, D., and Mishra, V. (2020). Integrated Drought Index (IDI) for drought monitoring and assessment in India. *Water Resources Research*, 56(2), e2019WR026284.

Sharma, A., and Goyal, M. K. (2020). Assessment of drought trend and variability in India using wavelet transform. *Hydrological Sciences Journal*, 65(9), 1539-1554.

Sharma, P. J. (2021). *Integrated Assessment of Hydroclimatic Variability including Streamflow Modelling of a Climatically Heterogeneous Basin in India*. Sardar Vallabhbhai National Institute of Technology, Surat.

Sharma, P. J., Loliyana, V. D., SR, R., Timbadiya, P. V., and Patel, P. L. (2018). Spatiotemporal trends in extreme rainfall and temperature indices over Upper Tapi Basin, India. *Theoretical and Applied Climatology*, 134(3), 1329-1354.

Sharma, P. J., Patel, P. L., and Jothiprakash, V. (2019). Impact of rainfall variability and anthropogenic activities on streamflow changes and water stress conditions across Tapi Basin in India. *Science of the Total Environment*, *687*, 885-897.

Sherly, M. A., Karmakar, S., Parthasarathy, D., Chan, T., and Rau, C. (2015). Disaster vulnerability mapping for a densely populated coastal urban area: an application to Mumbai, India. *Annals of the Association of American Geographers*, 105(6), 1198-1220.

Shu, Y., Li, H., and Lei, Y. (2018). Modelling groundwater flow with MIKE SHE using conventional climate data and satellite data as model forcing in Haihe plain, China. *Water,* 10(10), 1295.

Shu, Y., Villholth, K. G., Jensen, K. H., Stisen, S., and Lei, Y. (2012). Integrated hydrological modeling of the North China Plain: Options for sustainable groundwater use in the alluvial plain of Mt. Taihang. *Journal of Hydrology,* 464, 79-93.

Singh, G. R., Dhanya, C. T., and Chakravorty, A. (2021). A Robust Drought Index Accounting Changing Precipitation Characteristics. *Water Resources Research*, 57(7), e2020WR029496.

Singh, S., Kannan, S., and Timbadiya, P. V. (2016). Statistical downscaling of multisite daily precipitation for Tapi basin using kernel regression model. *Current Science*, 1468-1484.

Sinha, R. K., Eldho, T. I., and Subimal, G. (2020). Assessing the impacts of historical and future land use and climate change on the streamflow and sediment yield of a tropical mountainous river basin in South India. *Environmental Monitoring and Assessment*, 192(11), 1-21.

Sonali, P., and Kumar, D. N. (2013). Review of trend detection methods and their application to detect temperature changes in India. *Journal of Hydrology*, 476, 212-227.

Stisen, S., Jensen, K. H., Sandholt, I., and Grimes, D. I. (2008). A remote sensing driven distributed hydrological model of the Senegal River basin. *Journal of Hydrology*, 354(1-4), 131-148.

Stocker, T. F., Qin, D., Plattner, G. K., Tignor, M. M. B., Allen, S. K., Boschung, J., Nauels, A., Xia, Y., Bex, V., Midgley, P. M., Alexander, L. V., Allen, S. K., Bindoff, N. L., Breon, F. M., Church, J. A., Cubasch, U., Emori, S., Forster, P., Friedlingstein, P., Gillett, N., Gregory, J. M., Hartmann, D. L., Jansen, E., Kirtman, B., Knutti, R., Kumar Kanikicharla, K., Lemke, P., Marotzke, J., Masson-Delmotte, V., Meehl, G. A., Mokhov, I. I., Piao, S., Plattner, G. K., Dahe, Q., Ramaswamy, V., Randall, D., Rhein, M., Rojas, M., Sabine, C., Shindell, D., Talley, L. D., Vaughan, D. G., Xie, S. P., Allen, M. R., Boucher, O., Chambers, D., Hesselbjerg C., Jens, C., Philippe, C., Peter U., Collins, M., Comiso, J. C., Vasconcellos M., Viviane, F., Richard A., Fichefet, T., Fiore, A. M., Flato, G., Fuglestvedt, J., Hegerl, G., Hezel, P. J., Johnson, G. C., Kaser, G., Kattsov, V., Kennedy, J., Klein T., Albert M.G., Le Q., Corinne, M., Gunnar, O., Timothy, P., Antony J., Perlwitz, J., Power, S., Prather, M., Rintoul, S. R., Rogelj, J., Rusticucci, M., Schulz, M., Sedlacek, J., Stott, P. A., Sutton, R., Thorne, P. W., and Wuebbles, D. Climate Change 2013. The Physical Science Basis. Working Group I Contribution to the Fifth Assessment Report of the Intergovernmental Panel on Climate Change - Abstract for decision-makers; Changements climatiques 2013. Les elements scientifiques. Contribution du groupe de travail I au cinquieme rapport d'evaluation du groupe d'experts intergouvernemental sur l'evolution du CLIMAT - Resume a l'intention des decideurs. France.

Subramanya, K. (2013). *Engineering Hydrology, 4e*. Tata McGraw-Hill Education.

Sunil, A., Deepthi, B., Mirajkar, A. B., and Adarsh, S. (2021). Modeling future irrigation water demands in the context of climate change: a case study of Jayakwadi command area, India. *Modeling Earth Systems and Environment*, 7(3), 1963-1977.

Tan, M. L., Gassman, P., Yang, X., and Haywood, J. (2020). A review of SWAT applications, performance and future needs for simulation of hydro-climatic extremes. *Advances in Water Resources*, 103662.

Tansar, H., Babur, M., and Karnchanapaiboon, S. L. (2020). Flood inundation modeling and hazard assessment in Lower Ping River Basin using MIKE FLOOD. *Arabian Journal of Geosciences*, 13(18), 1-16.

Thomas, T., Ghosh, N. C., and Sudheer, K. P. (2021). Optimal reservoir operation–A climate change adaptation strategy for Narmada basin in central India. *Journal of Hydrology*, *598*, 126238.

Timbadiya, P. V., Mirajkar, A. B., Patel, P. L., and Porey, P. D. (2013). Identification of trend and probability distribution for time series of annual peak flow in Tapi Basin, India. *ISH Journal of Hydraulic Engineering*, 19(1), 11-20.

Timbadiya, P. V., Patel, P. L., and Porey, P. D. (2014a). One-dimensional hydrodynamic modelling of flooding and stage hydrographs in the lower Tapi River in India. *Current Science*, 708-716.

Timbadiya, P. V., Patel, P. L., and Porey, P. D. (2014b). A 1D–2D coupled hydrodynamic model for river flood prediction in a coastal urban floodplain. *Journal of Hydrologic Engineering*, 20(2), 05014017.

Trenberth, K. E. (2011). Changes in precipitation with climate change. *Climate Research*, 47(1-2), 123-138.

Triana, J. S. A., Chu, M. L., Guzman, J. A., Moriasi, D. N., and Steiner, J. L. (2019). Beyond model metrics: The perils of calibrating hydrologic models. *Journal of Hydrology*, 578, 124032.

Tukimat, N. N. A., Harun, S., and Shahid, S. (2017). Modeling irrigation water demand in a tropical paddy cultivated area in the context of climate change. *Journal of Water Resources Planning and Management*, 143(7), 05017003.

USDA, S. (1972). *National Engineering Handbook, Hydrology, Section 4*. United States Department of Agriculture, Soil Conservation Service (Chapters 4–10).

Vicente-Serrano, S. M., Beguería, S., and López-Moreno, J. I. (2010). A multiscalar drought index sensitive to global warming: the standardized precipitation evapotranspiration index. *Journal of Climate*, 23(7), 1696-1718.

Vicente-Serrano, S. M., López-Moreno, J. I., Beguería, S., Lorenzo-Lacruz, J., Azorin-Molina, C., and Morán-Tejeda, E. (2012). Accurate computation of a streamflow drought index. *Journal of Hydrologic Engineering*, 17(2), 318-332.

Vilaysane, B., Takara, K., Luo, P., Akkharath, I., and Duan, W. (2015). Hydrological stream flow modelling for calibration and uncertainty analysis using SWAT model in the Xedone river basin, Lao PDR. *Procedia Environmental Sciences*, 28, 380-390.

Vinnarasi, R., Dhanya, C. T., Chakravorty, A., and Aghakouchak, A. (2017). Unravelling diurnal asymmetry of surface temperature in different climate zones. *Scientific Reports*, 7(1), 1-8.

Vittal, H., Karmakar, S., and Ghosh, S. (2013). Diametric changes in trends and patterns of extreme rainfall over India from pre-1950 to post-1950. *Geophysical Research Letters*, 40(12), 3253-3258.

Vittal, H., Karmakar, S., Ghosh, S., and Murtugudde, R. (2020). A comprehensive India-wide social vulnerability analysis: highlighting its influence on hydro-climatic risk. *Environmental Research Letters*, 15(1), 014005.

von Neumann, J. (1941). Distribution of the ratio of the mean square successive difference to the variance. *The Annals of Mathematical Statistics*, 12(4), 367-395.

Vora, A., Sharma, P. J., Loliyana, V. D., Patel, P. L., and Timbadiya, P. V. (2018). Assessment and prioritization of flood protection levees along the lower Tapi River, India. *Natural Hazards Review*, 19(4), 05018009.

Wang, Q., Xu, Y., Xu, Y., Wu, L., Wang, Y., and Han, L. (2018). Spatial hydrological responses to land use and land cover changes in a typical catchment of the Yangtze River Delta region. *Catena*, 170, 305-315.

Williams, J. R. (1969). Flood routing with variable travel time or variable storage coefficients. *Transactions of the ASAE*, 12(1), 100-0103.

Williams, J. R., and Berndt, H. D. (1977). Sediment yield prediction based on watershed hydrology. *Transactions of the ASAE*, 20(6), 1100-1104.

Worku, T., Khare, D., and Tripathi, S. K. (2017). Modeling runoff–sediment response to land use/land cover changes using integrated GIS and SWAT model in the Beressa watershed. *Environmental Earth Sciences*, 76(16), 550.

World Meteorological Organization (WMO). (1986). Report on drought and countries affected by drought during 1974–1985. *WMO, Geneva*, 118.

WRD (2015). Standard operating procedure for flood control in Tapi basin at Hatnur dam. Water Resources Department, Government of Maharashtra, Jalgaon, India.

Yadeta, D., Kebede, A., and Tessema, N. (2020). Potential evapotranspiration models evaluation, modelling, and projection under climate scenarios, Kesem sub-basin, Awash River basin, Ethiopia. *Modeling Earth Systems and Environment*, 6(4), 2165-2176.

Yan, J., and Smith, K. R. (1994). Simulation of Integrated Surface Water and Ground Water Systems-Model Formulation 1. *JAWRA Journal of the American Water Resources Association*, 30(5), 879-890.

Yang, J., Reichert, P., Abbaspour, K. C., Xia, J., and Yang, H. (2008). Comparing uncertainty analysis techniques for a SWAT application to the Chaohe Basin in China. *Journal of Hydrology*, 358(1-2), 1-23.

Yirga, S. A. (2019). Modelling reference evapotranspiration for Megecha catchment by multiple linear regression. *Modeling Earth Systems and Environment*, 5(2), 471-477.

Yuan, J., Xu, Y., Wu, L., Wang, J., Wang, Y., Xu, Y., and Dai, X. (2019). Variability of precipitation extremes over the Yangtze River Delta, eastern China, during 1960–2016. *Theoretical and Applied Climatology*, 138(1), 305-319.

Zachos, L. G., Swann, C. T., Altinakar, M. S., McGrath, M. Z., and Thomas, D. (2016). Flood vulnerability indices and emergency management planning in the Yazoo Basin, Mississippi. *International Journal of Disaster Risk Reduction*, 18, 89-99.

Zhang, A., Zhang, C., Fu, G., Wang, B., Bao, Z., and Zheng, H. (2012). Assessments of impacts of climate change and human activities on runoff with SWAT for the Huifa River Basin, Northeast China. *Water Resources Management*, 26(8), 2199-2217.

Zhang, S., Liu, Y., and Wang, T. (2014). How land use change contributes to reducing soil erosion in the Jialing River Basin, China. *Agricultural Water Management*, 133, 65-73.

Zhu, X., and Troy, T. J. (2018). Agriculturally relevant climate extremes and their trends in the world's major growing regions. *Earth's Future*, 6(4), 656-672.

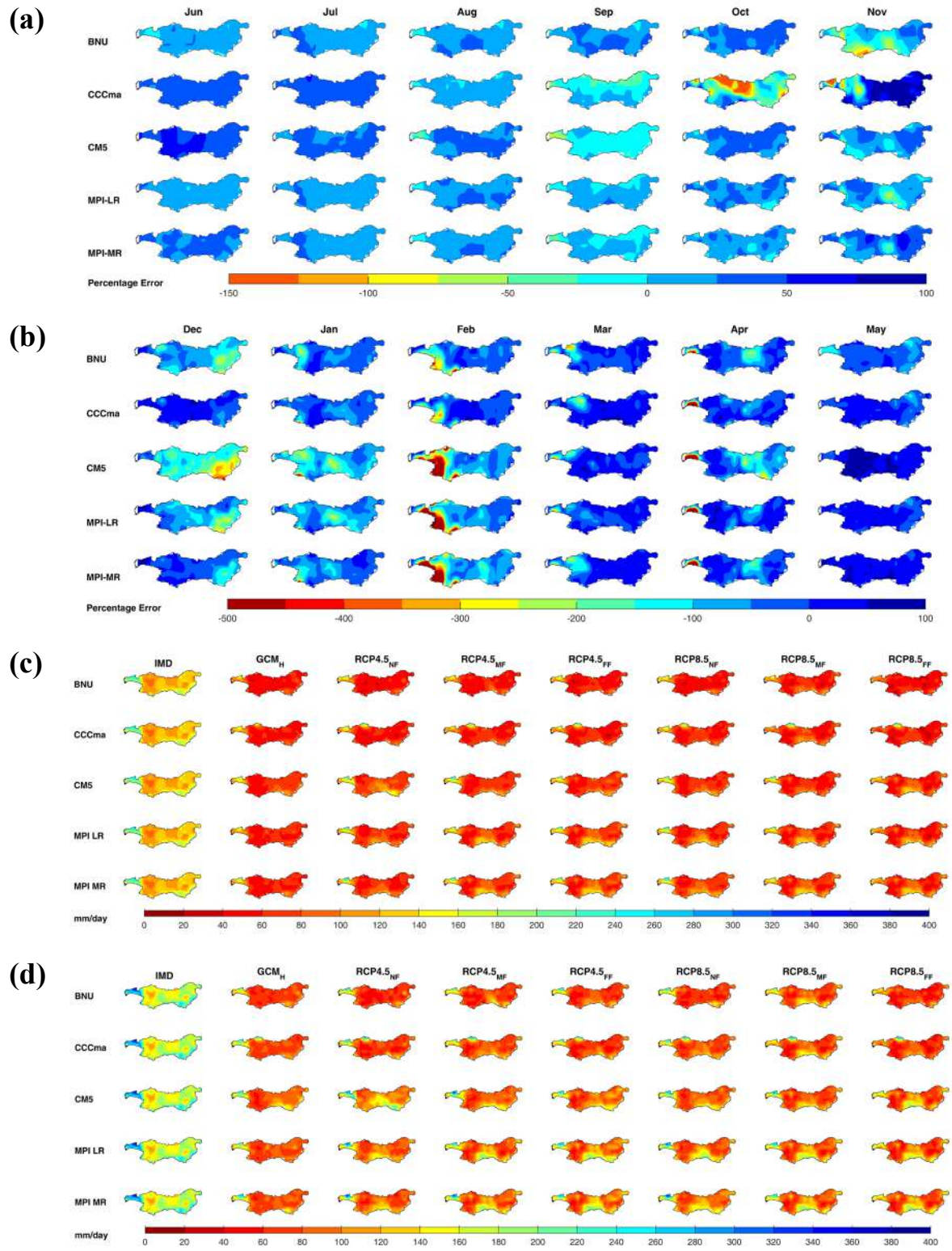

Fig. A1 Percentage error in PRCPTOT derived from KRSD-Historical period rainfall for (a) June-November months, and (b) December-May months; and Return levels of annual maximum rainfall for (c) 10- and (d) 50-year return periods

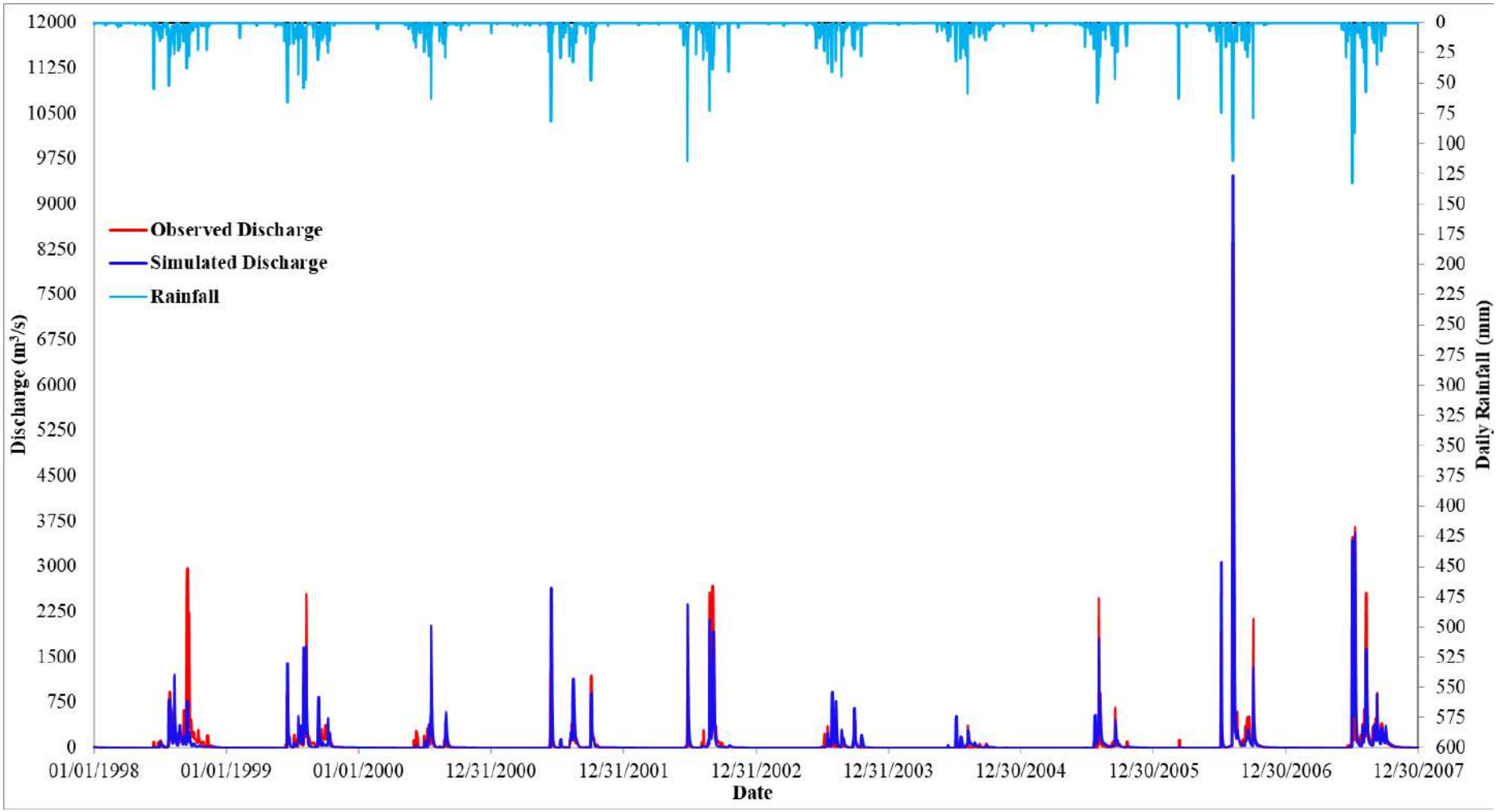
Observed Discharge
Simulated Discharge
Rainfall
Discharge (m³/s)
Daily Rainfall (mm)
Date
12000
11250
10500
9750
9000
8250
7500
6750
6000
5250
4500
3750
3000
2250
1500
750
0
0
25
50
75
100
125
150
175
200
225
250
275
300
325
350
375
400
425
450
475
500
525
550
575
600
01/01/1998
01/01/1999
01/01/2000
12/31/2000
12/31/2001
12/31/2002
12/31/2003
12/30/2004
12/30/2005
12/30/2006
12/30/2007

(a)

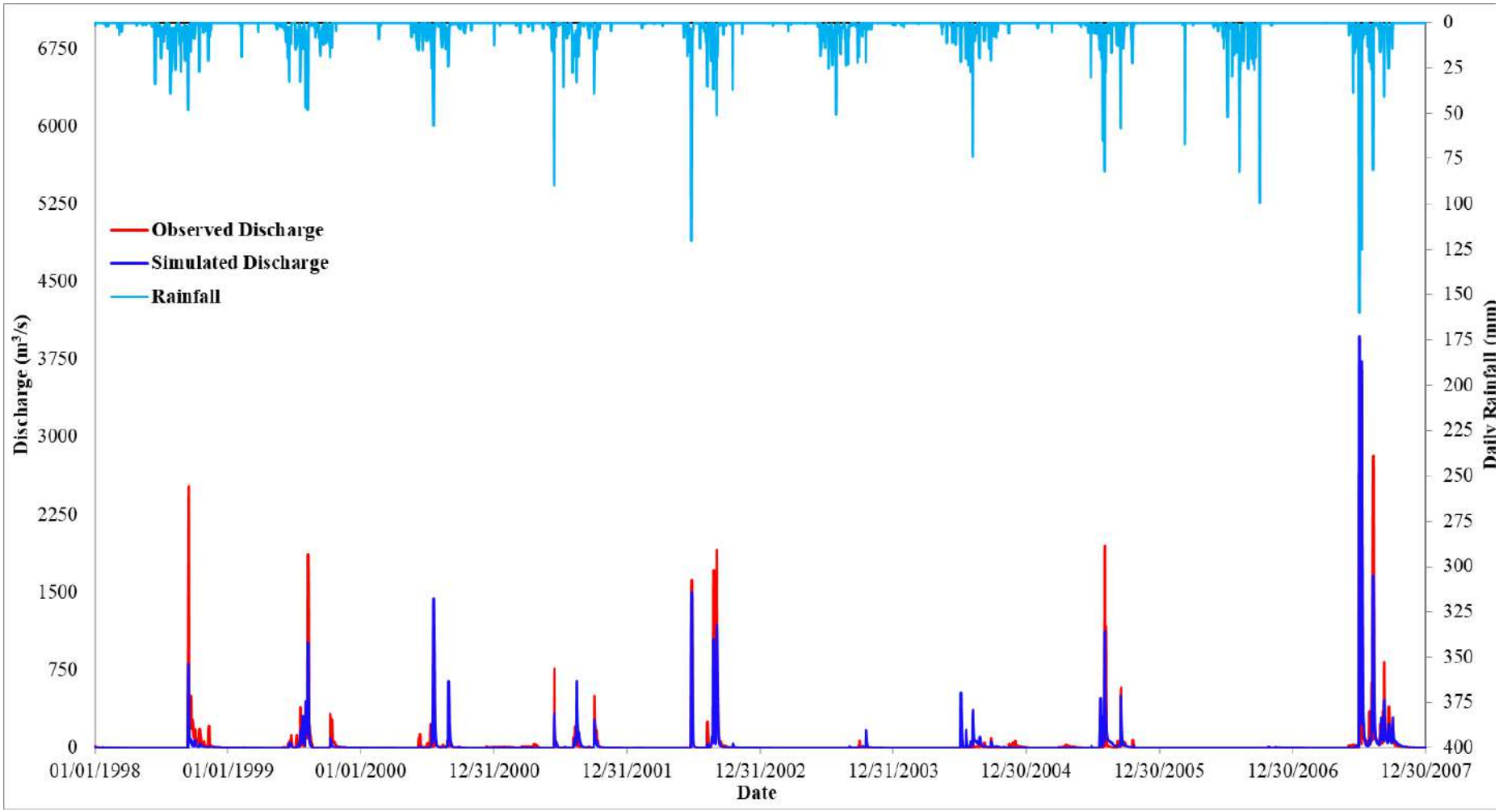
Observed Discharge
Simulated Discharge
Rainfall
Discharge (m³/s)
Daily Rainfall (mm)
Date
6750
6000
5250
4500
3750
3000
2250
1500
750
0
0
25
50
75
100
125
150
175
200
225
250
275
300
325
350
375
400
01/01/1998
01/01/1999
01/01/2000
12/31/2000
12/31/2001
12/31/2002
12/31/2003
12/30/2004
12/30/2005
12/30/2006
12/30/2007

(b)

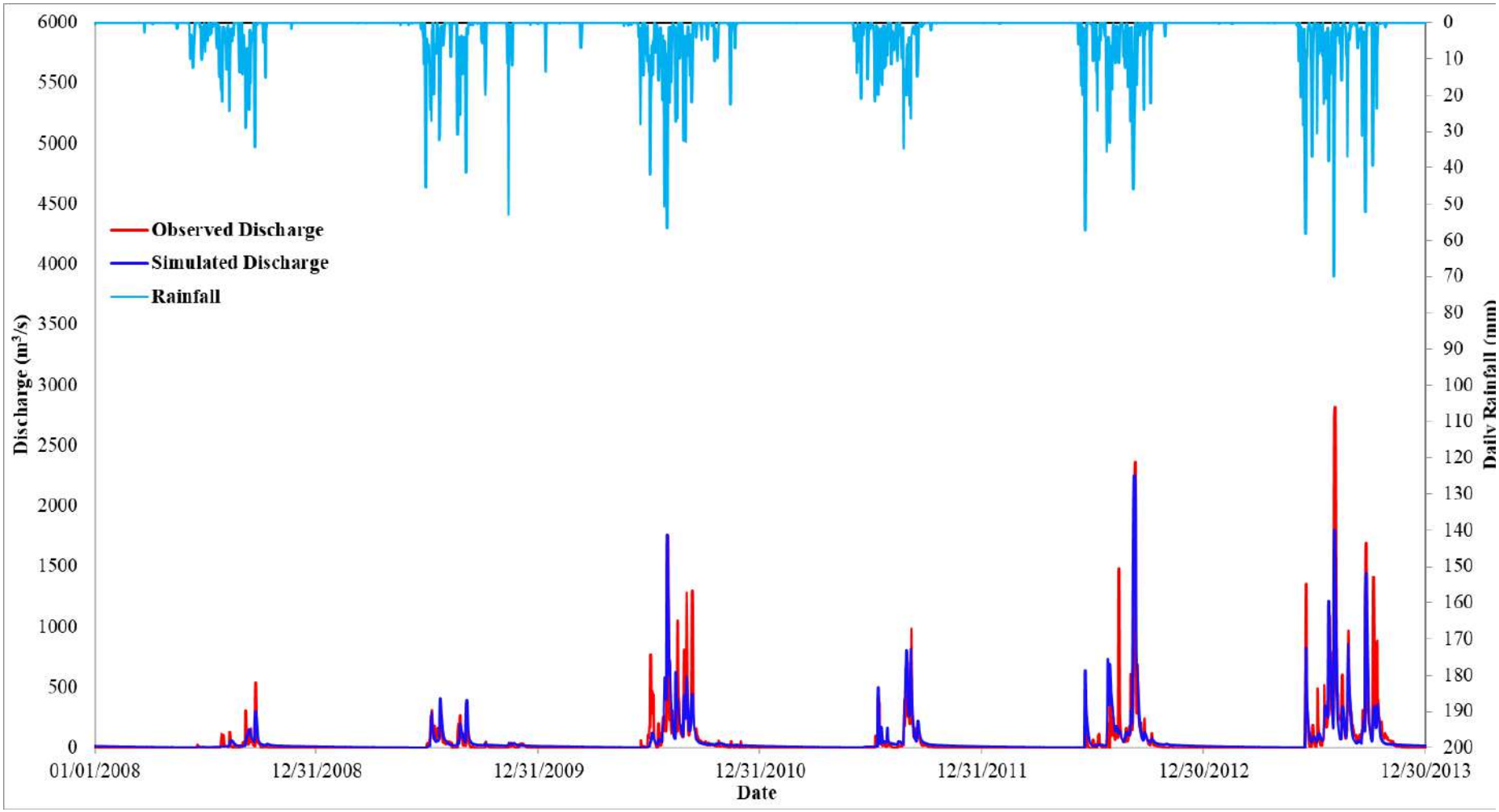
Observed Discharge
Simulated Discharge
Rainfall
Discharge (m³/s)
Daily Rainfall (mm)
Date
6000
5500
5000
4500
4000
3500
3000
2500
2000
1500
1000
500
0
0
10
20
30
40
50
60
70
80
90
100
110
120
130
140
150
160
170
180
190
200
01/01/2008
12/31/2008
12/31/2009
12/31/2010
12/31/2011
12/30/2012
12/30/2013

(c)

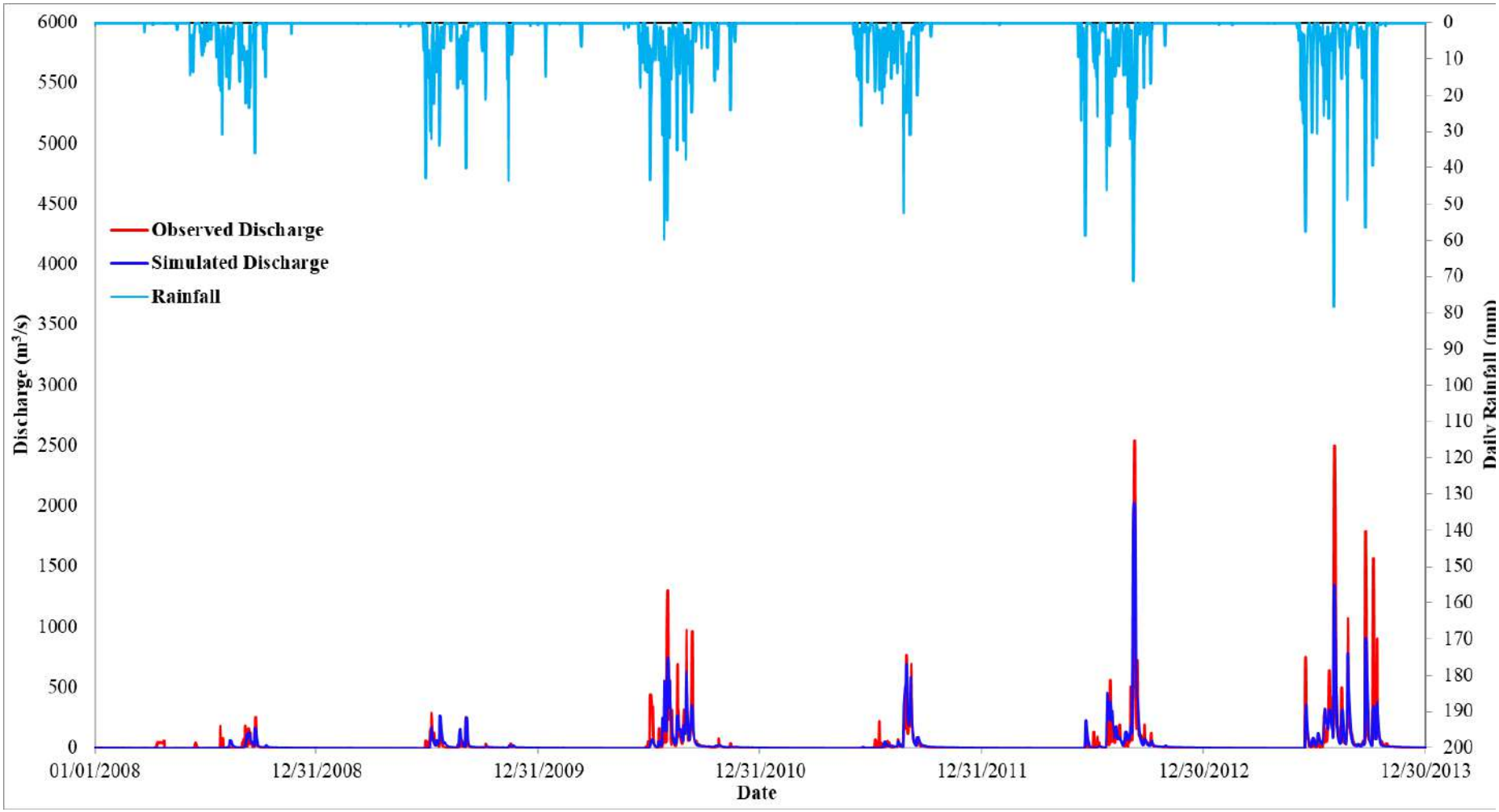

(d)

Fig. A2 Time series of daily observed and simulated discharge for MSC at Yerli stream gauging station during (a) calibration, (b) validation periods and Gopalkheda stream gauging station during (c) calibration, (d) validation periods

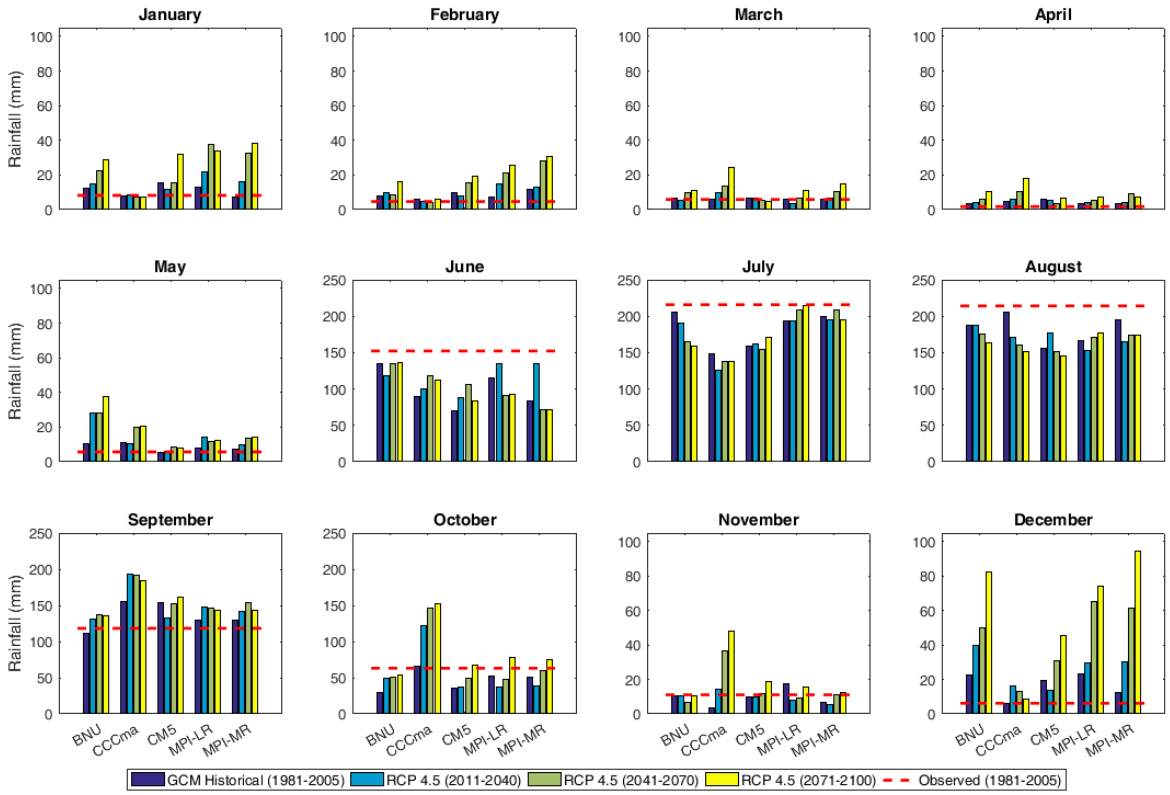

Fig. A3 Mean Rainfall over Purna sub-catchemnt for RCP 4.5 scenario

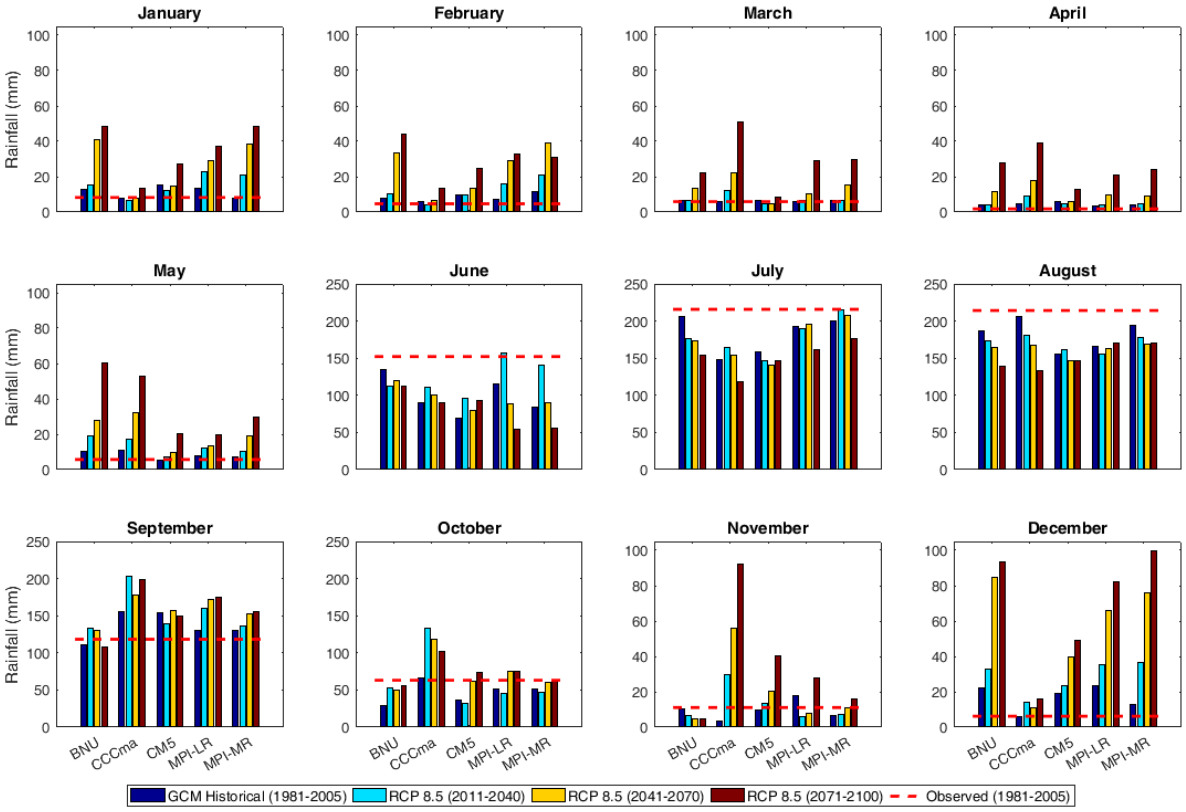

Fig. A4 Mean Rainfall over Purna sub-catchemnt for RCP 8.5 scenario

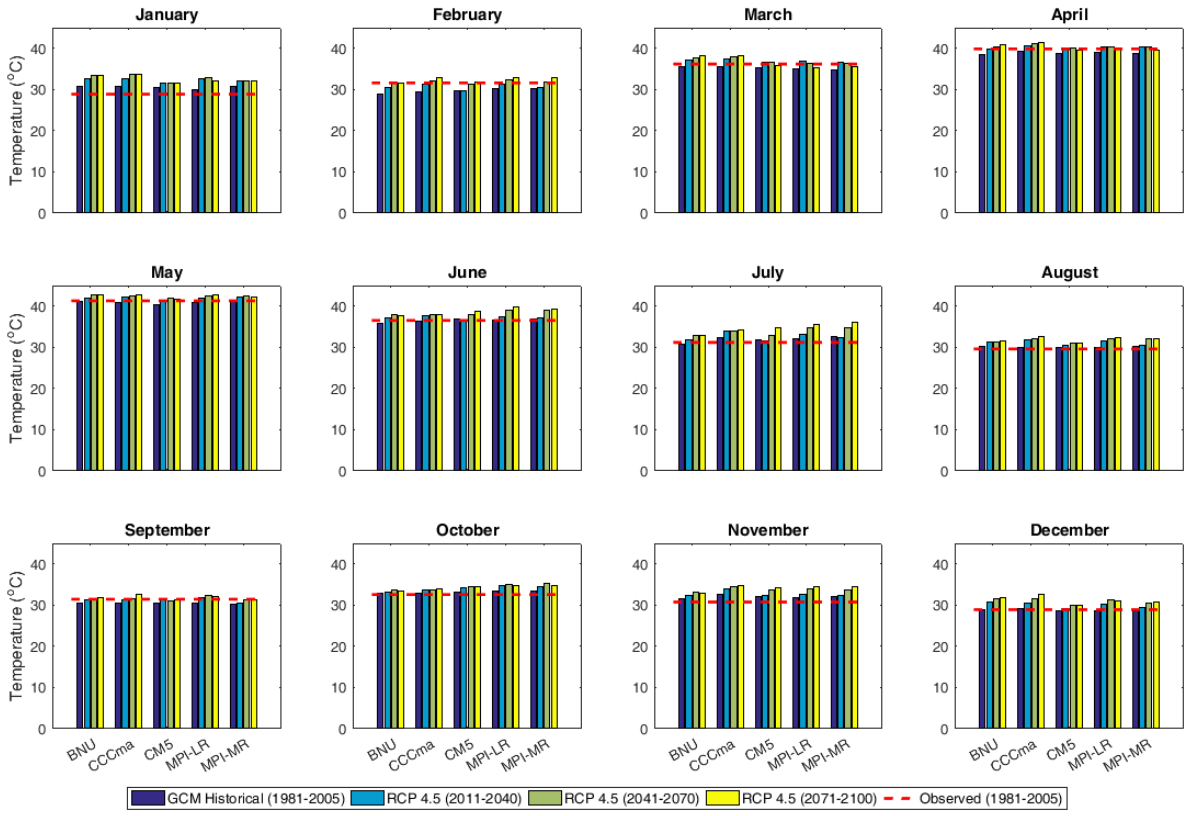

Fig. A5 Maximum Temperature over Purna sub-catchemnt for RCP 4.5 scenario

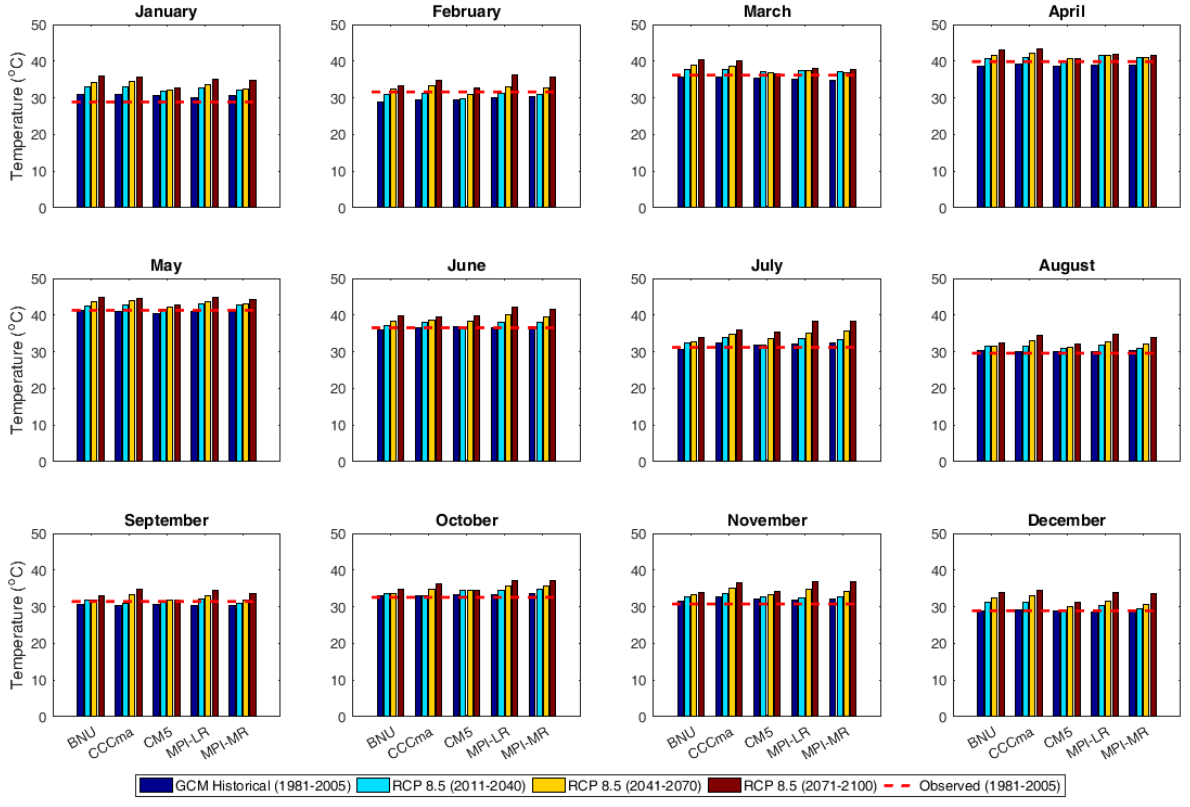

Fig. A6 Maximum Temperature over Purna sub-catchemnt for RCP 8.5 scenario

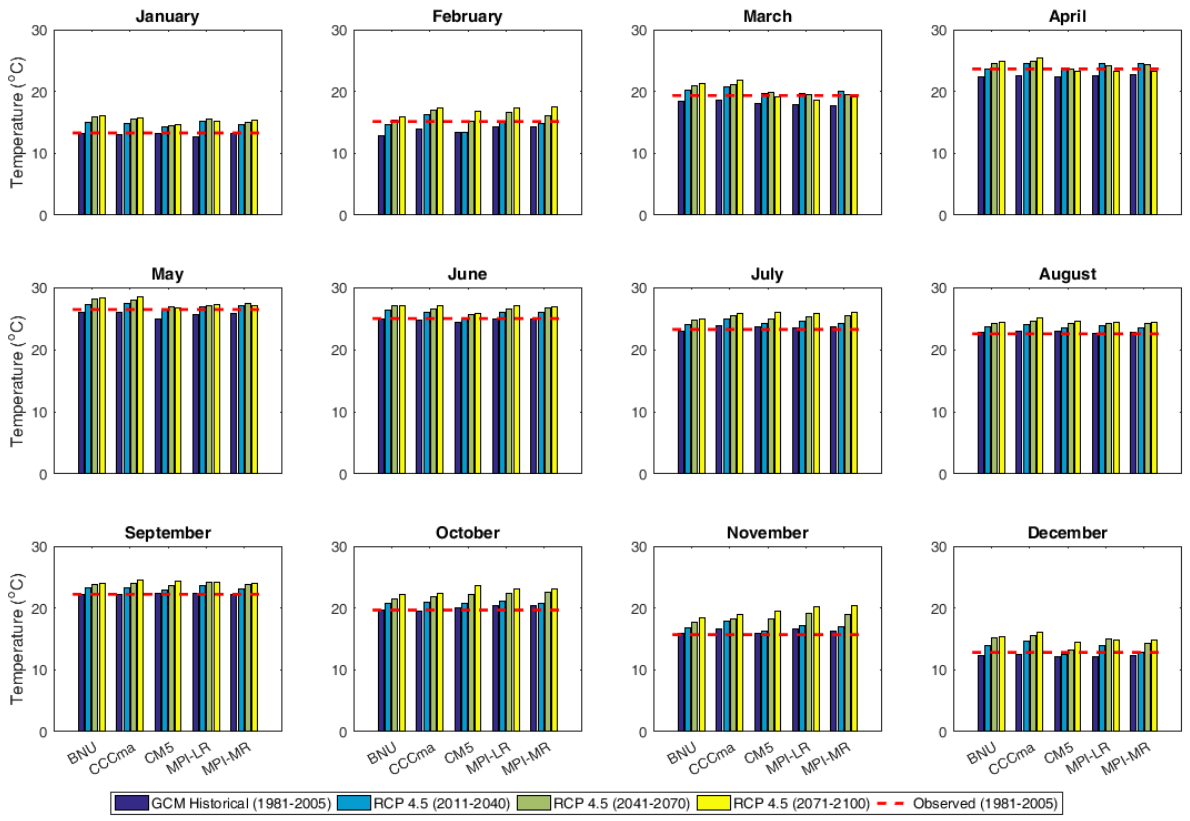

Fig. A7 Minimum Temperature over Purna sub-catchemnt for RCP 4.5 scenario

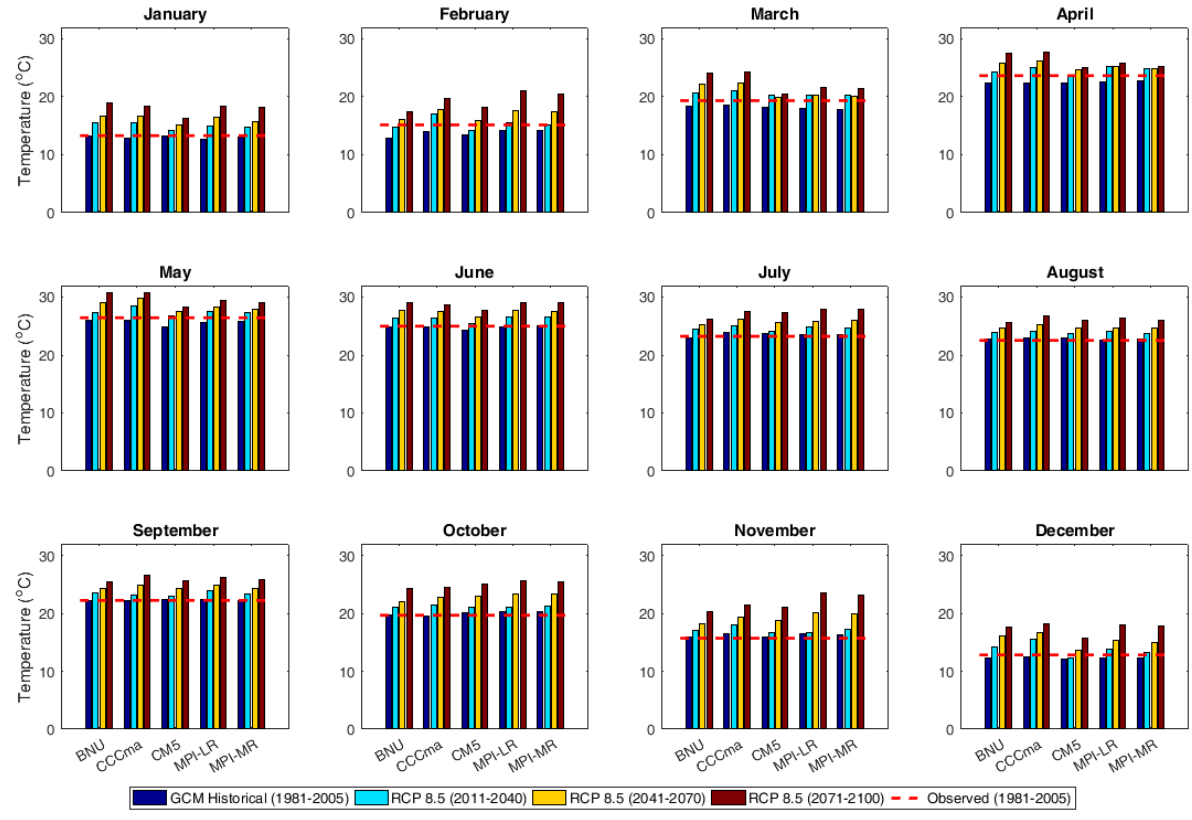

Fig. A8 Minimum Temperature over Purna sub-catchemnt for RCP 8.5 scenario

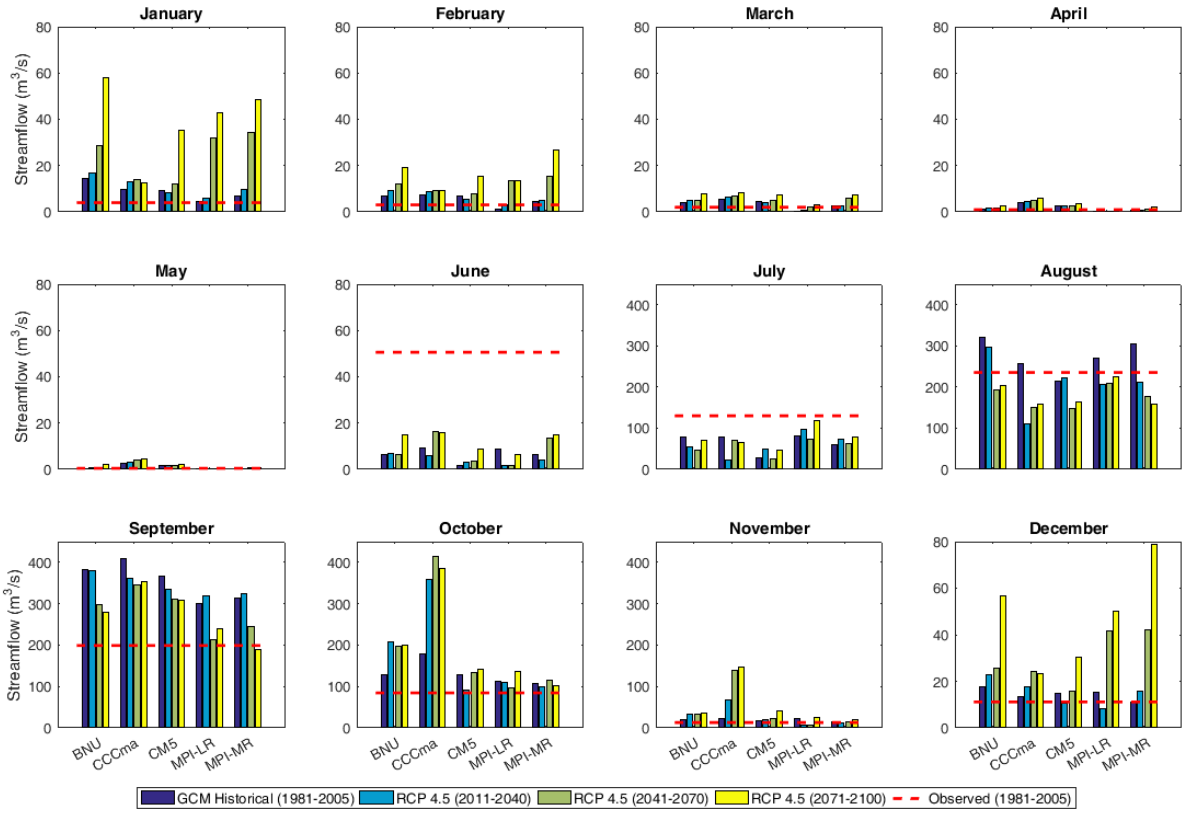

Fig. A9 Mean Streamflows at Yerli sub-catchemnt for RCP 4.5 scenario

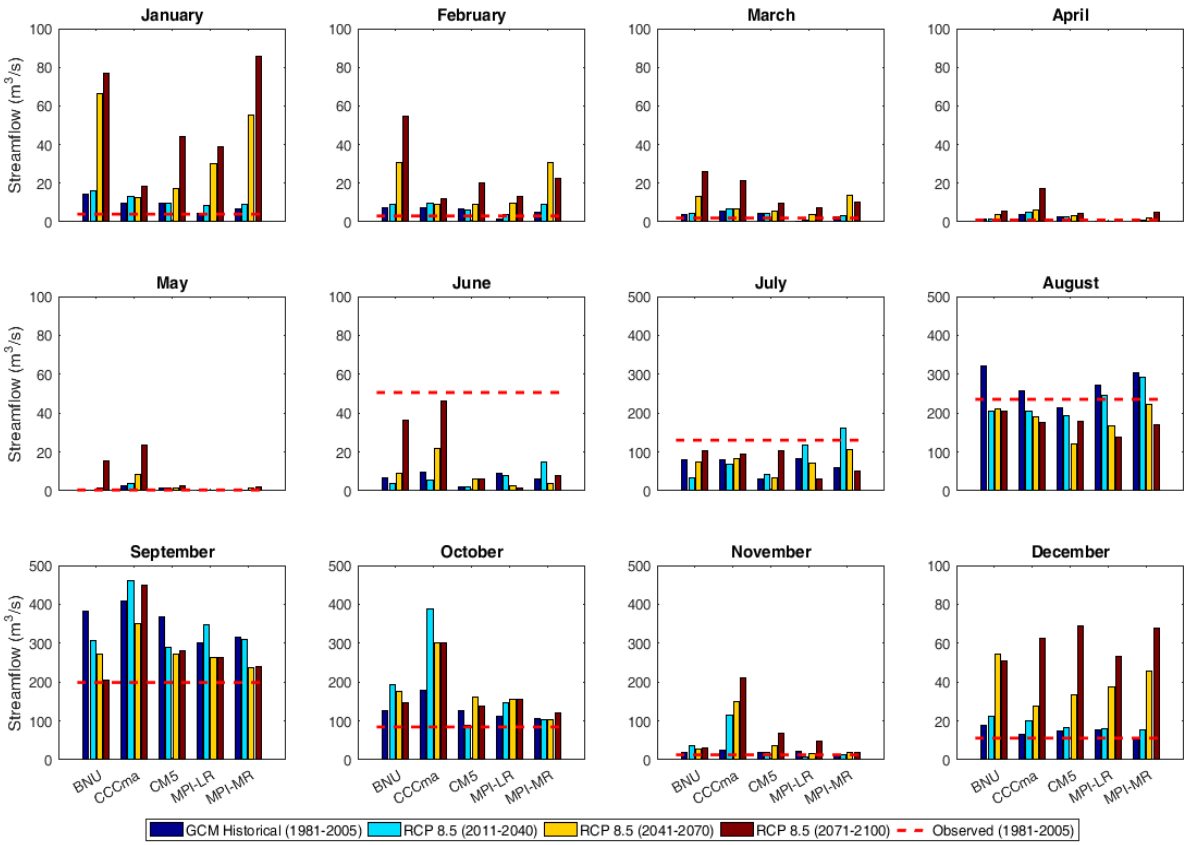

Fig. A10 Mean Streamflows at Yerli sub-catchemnt for RCP 8.5 scenario

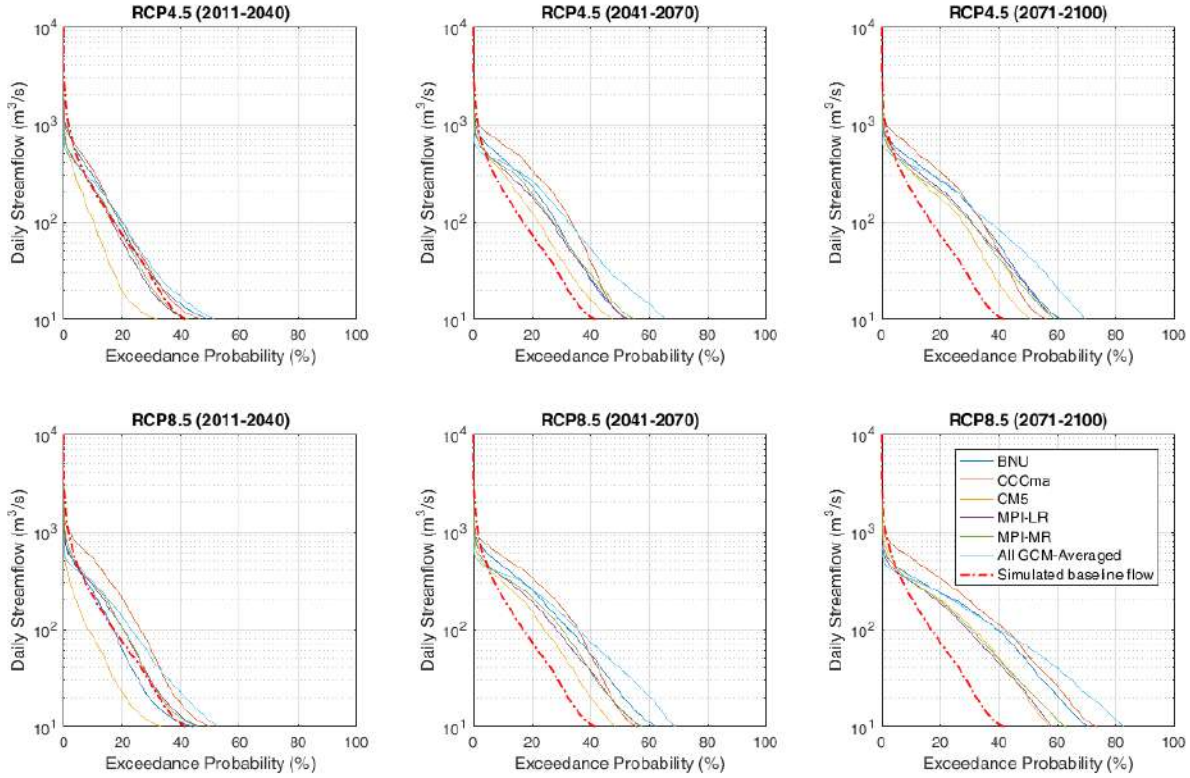

Fig. A11 Flow duration curves at the outlet of Purna sub-catchemnt under RCP 4.5 and RCP 8.5 scenarios.

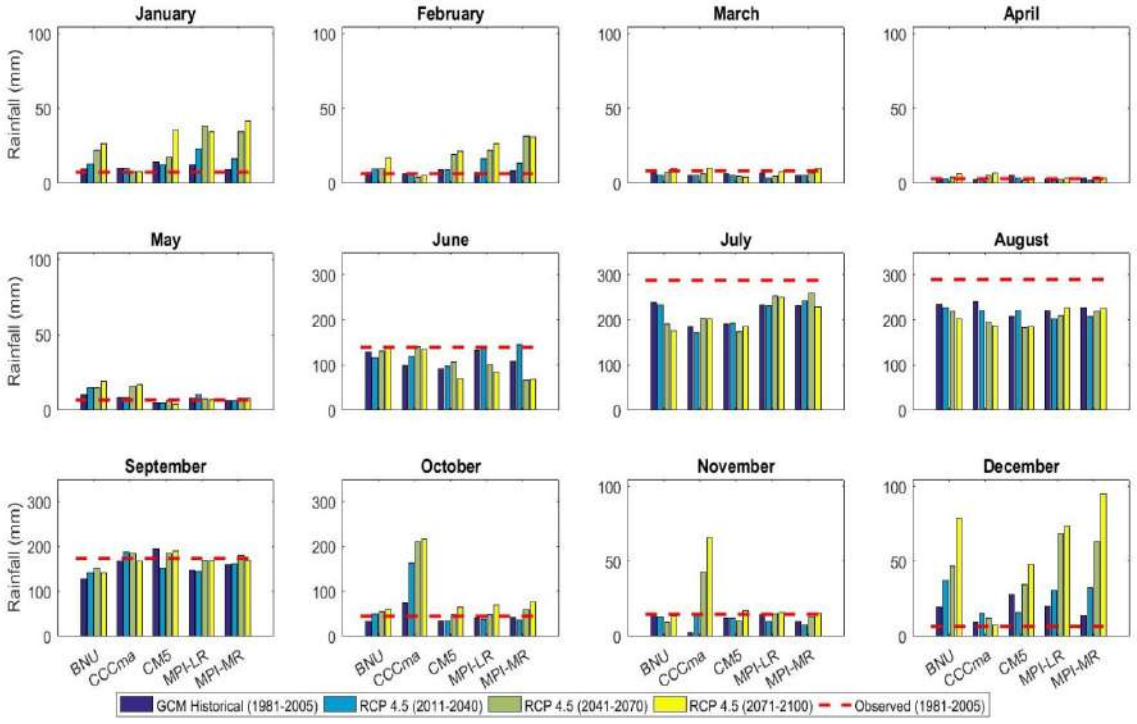

Fig. A12 Mean Rainfall over Burhanpur sub-catchemnt for RCP 4.5 scenario

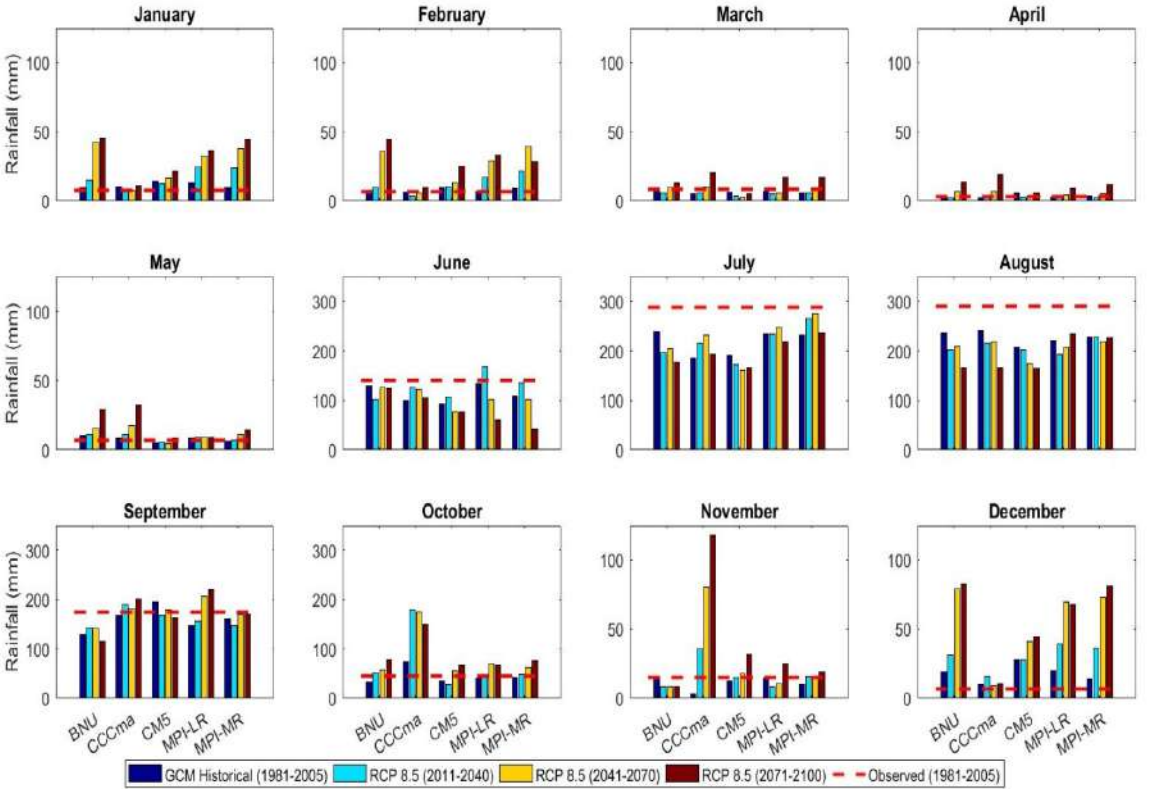

Fig. A13 Mean Rainfall over Burhanpur sub-catchemnt for RCP 8.5 scenario

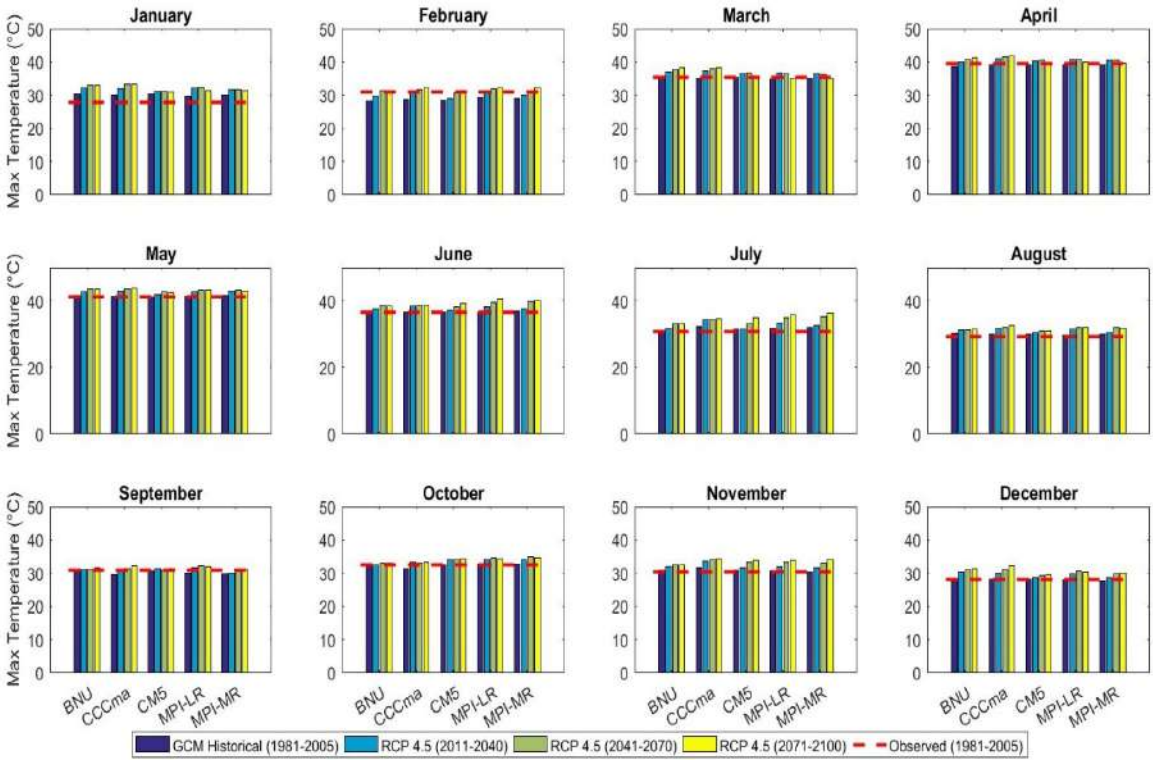

Fig. A14 Maximum Temperature over Burhanpur sub-catchemnt for RCP 4.5 scenario

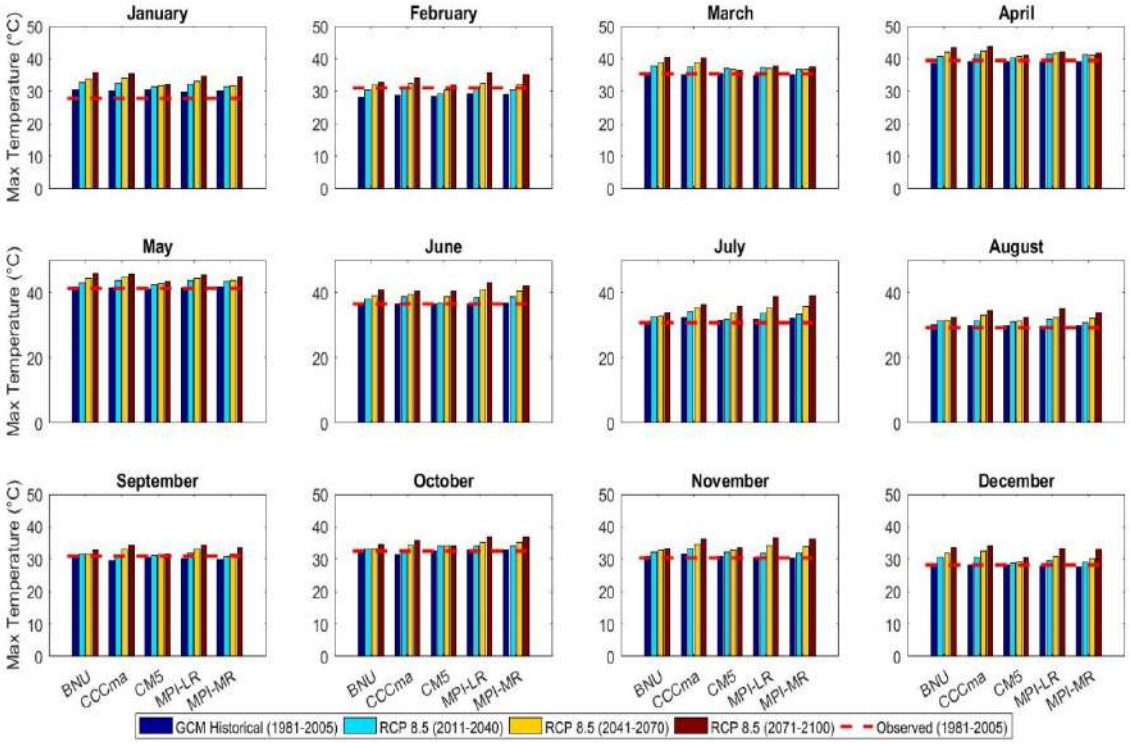

Fig. A15 Maximum Temperature over Burhanpur sub-catchemnt for RCP 8.5 scenario

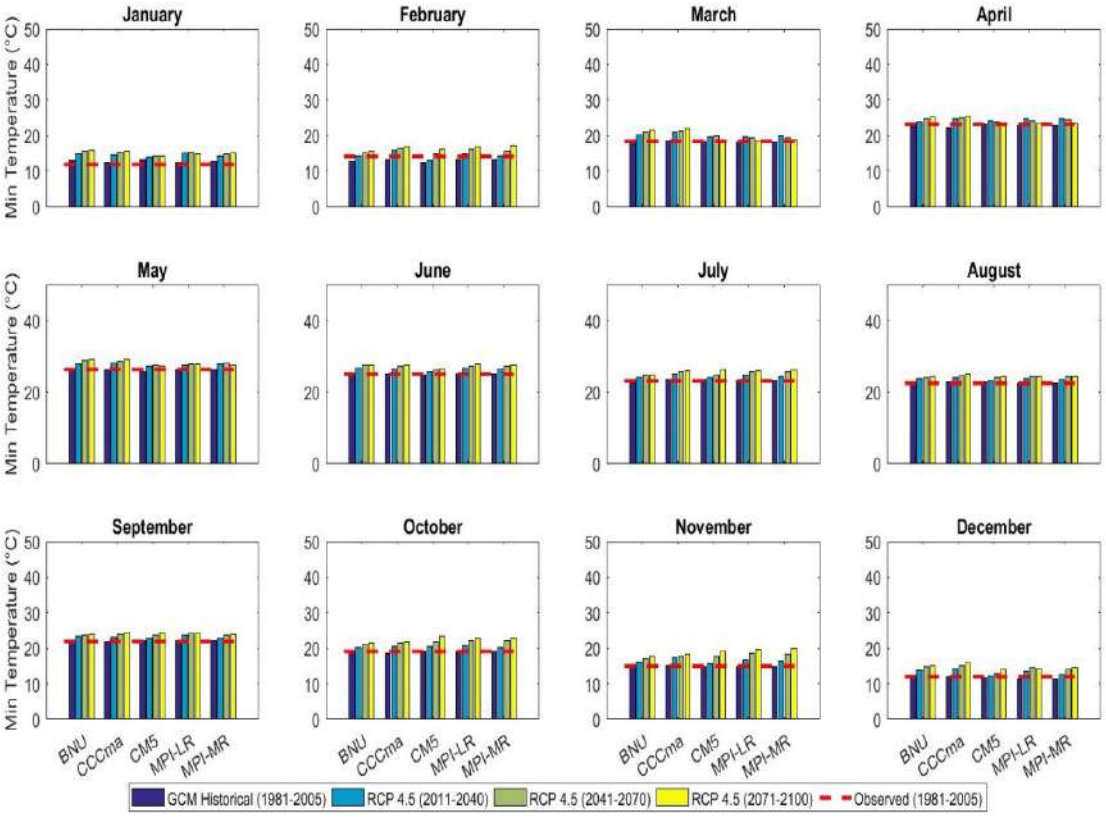

Fig. A16 Minimum Temperature over Burhanpur sub-catchemnt for RCP 4.5 scenario

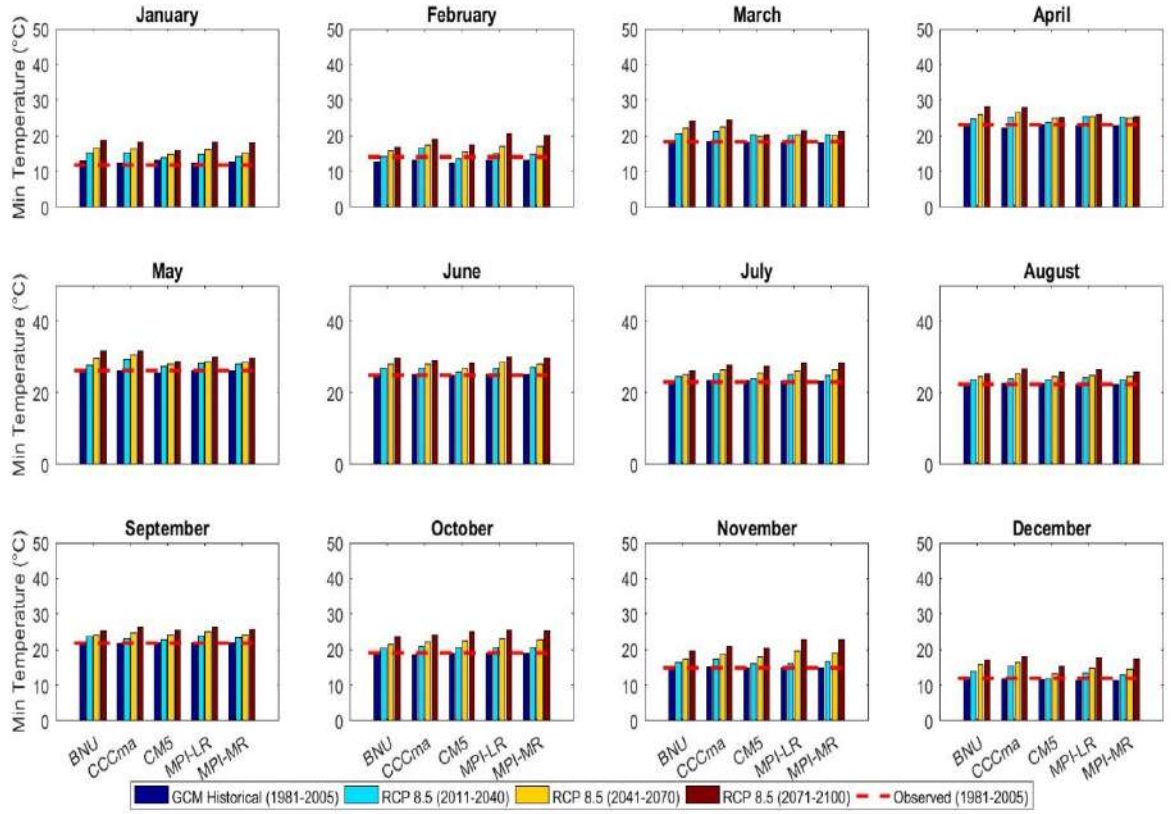

Fig. A17 Minimum Temperature over Burhanpur sub-catchemnt for RCP 8.5 scenario

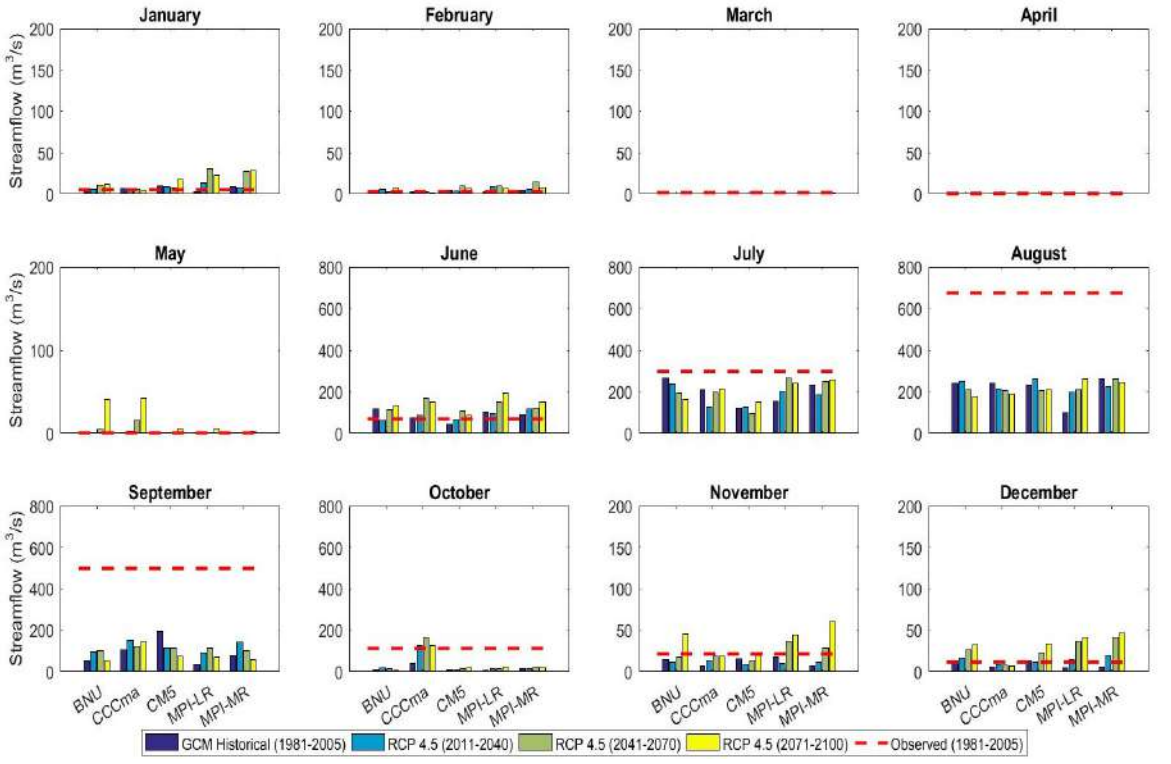

Fig. A18 Mean Streamflows at Burhanpur for RCP 4.5 scenario

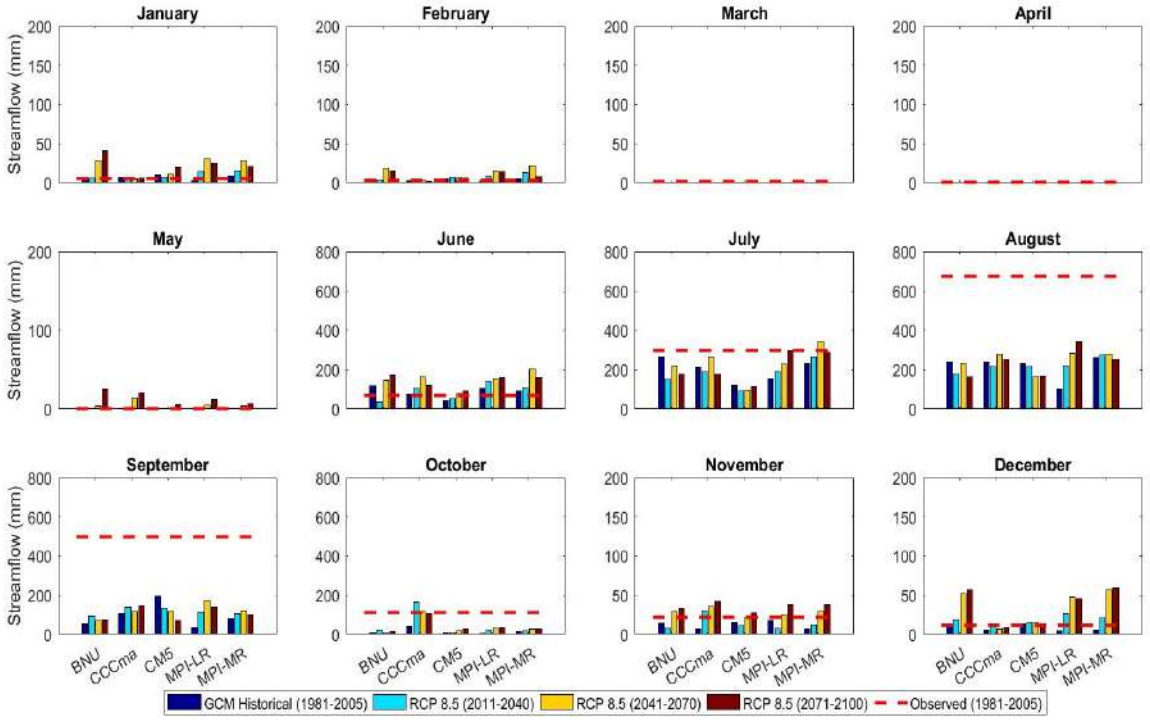

Fig. A19 Mean Streamflows at Burhanpur for RCP 8.5 scenario

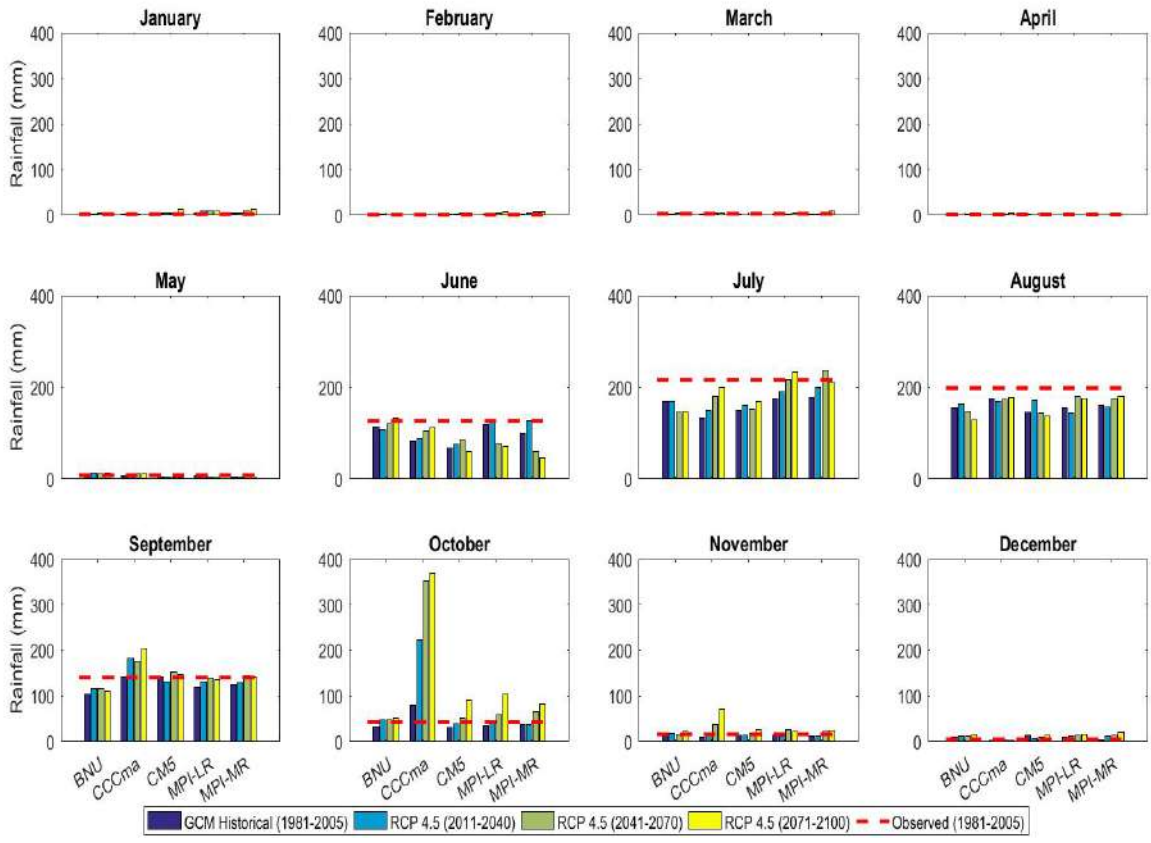

Fig. A20 Mean Rainfall over Middle Tapi Basin for RCP 4.5

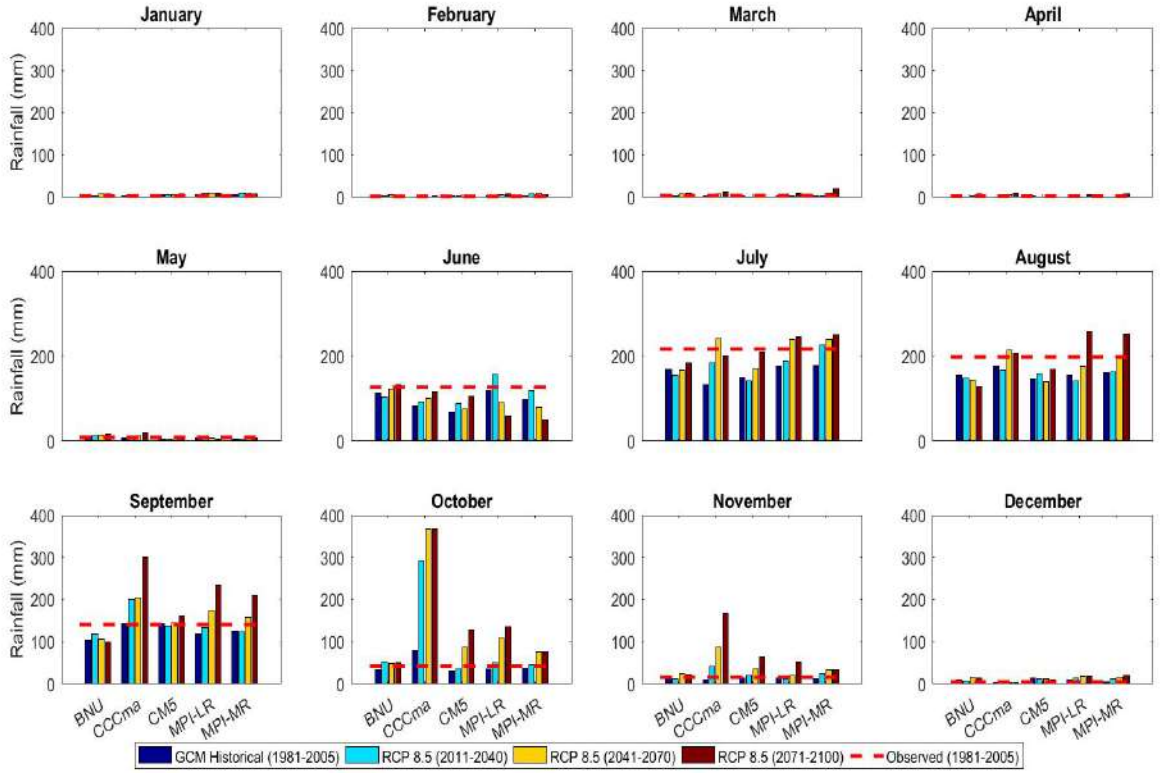

Fig. A21 Mean Rainfall over Middle Tapi Basin for RCP 8.5

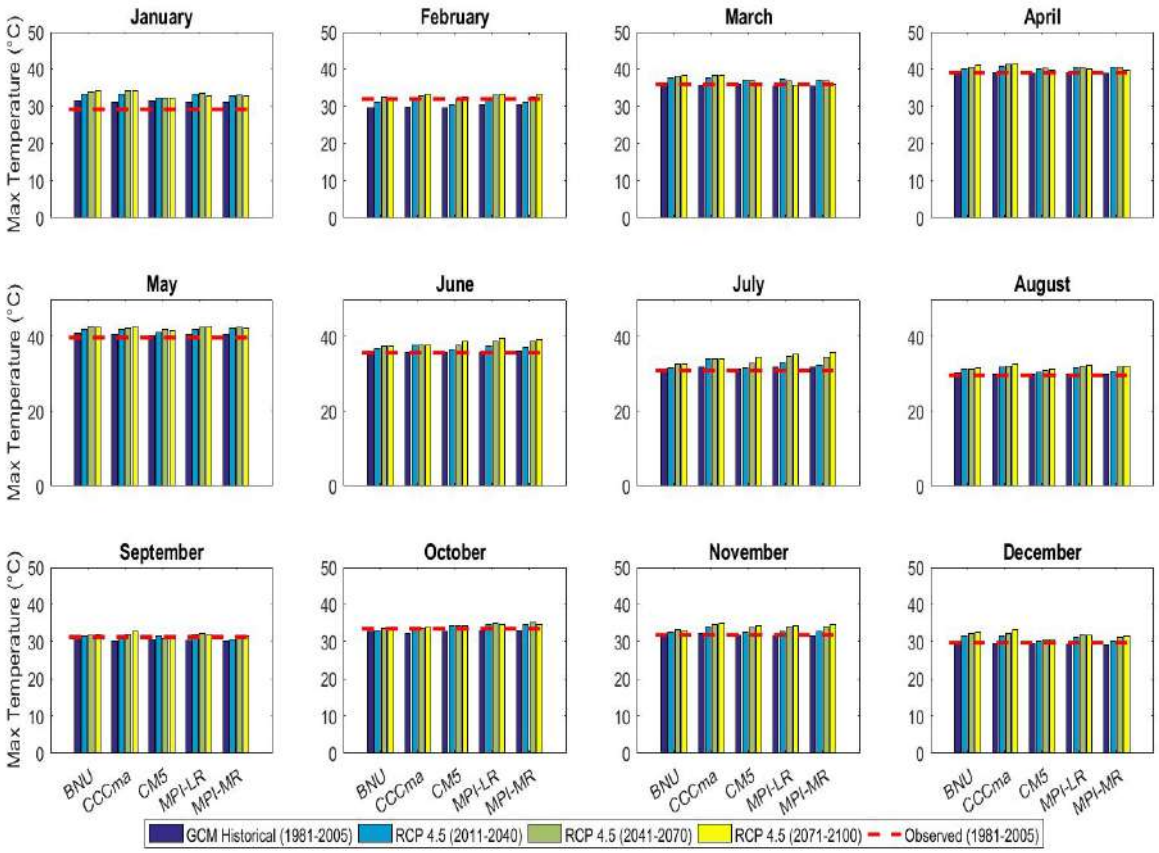

Fig. A22 Maximum Temperature over Middle Tapi Basin for RCP 4.5 scenario

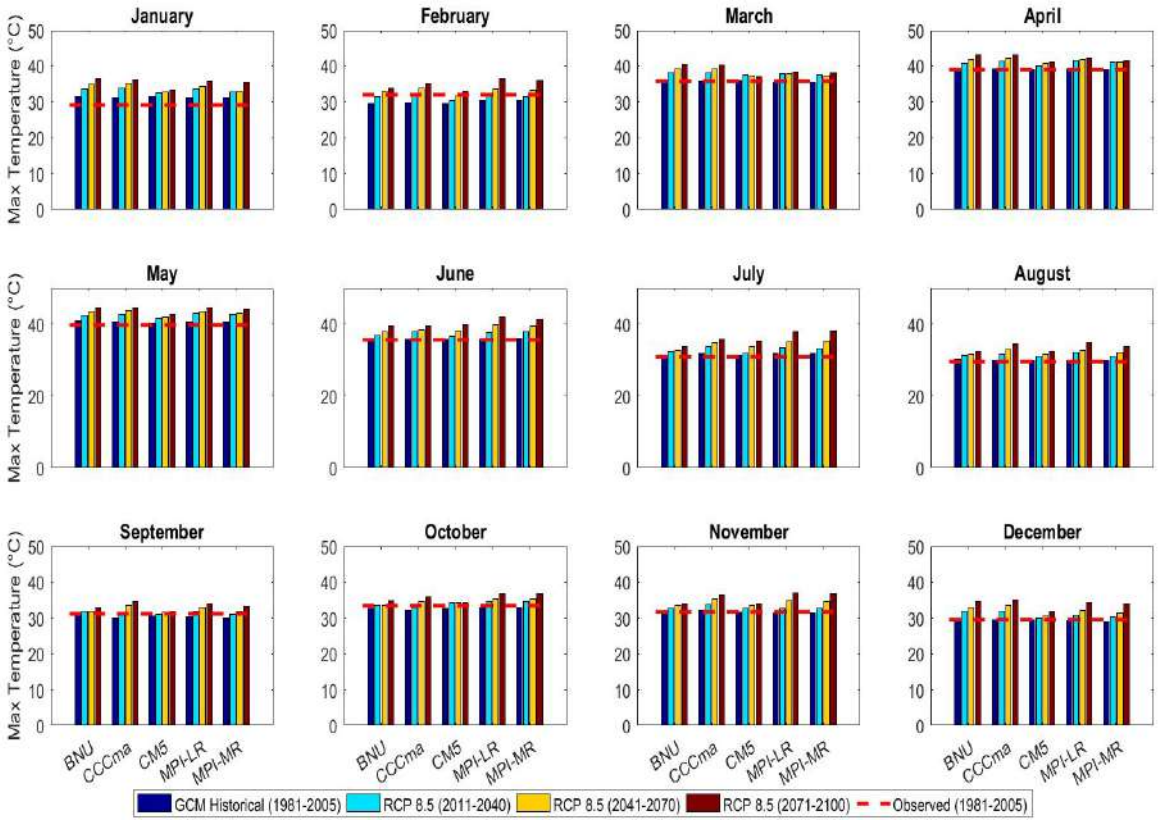

Fig. A23 Maximum Temperature over Middle Tapi Basin for RCP 8.5 scenario

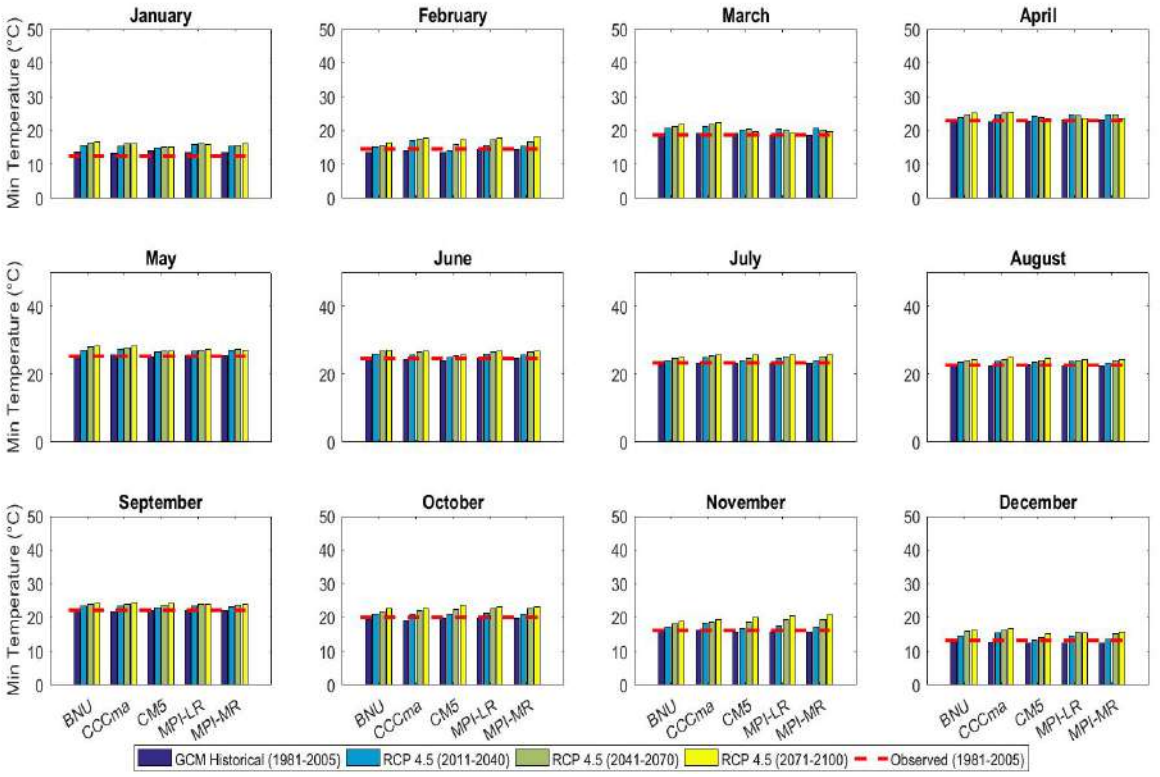

Fig. A24 Minimum Temperature over Middle Tapi Basin for RCP 4.5 scenario

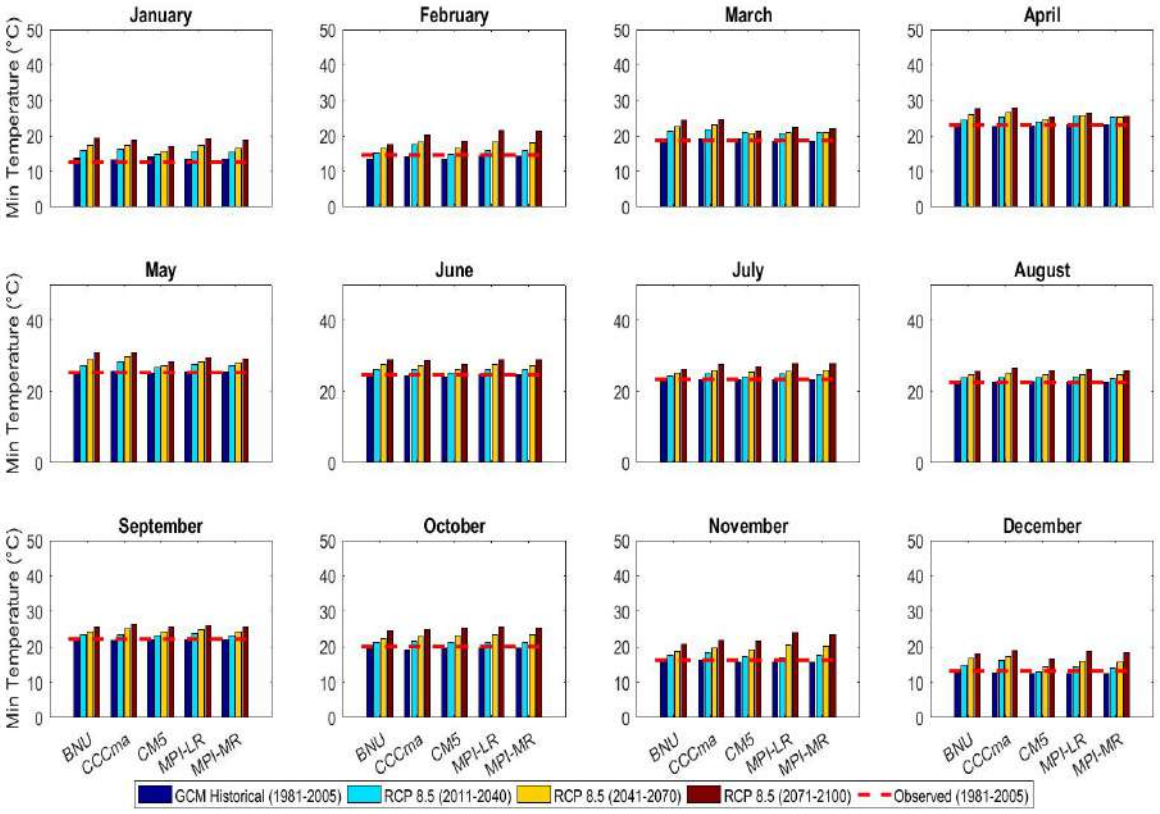

Fig. A25 Minimum Temperature over Middle Tapi Basin for RCP 8.5 scenario

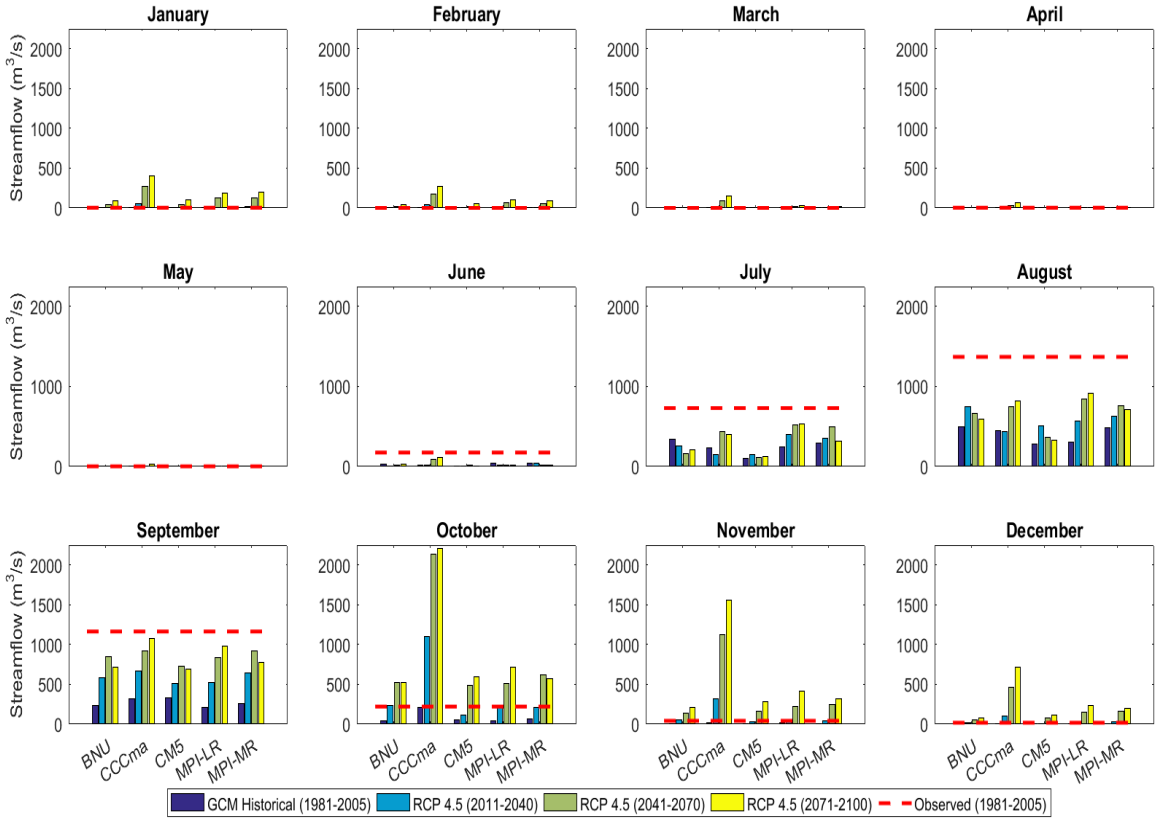

Fig. A26 Mean Streamflows at Ukai, outlet of Middle Tapi Basin for RCP 4.5 scenario

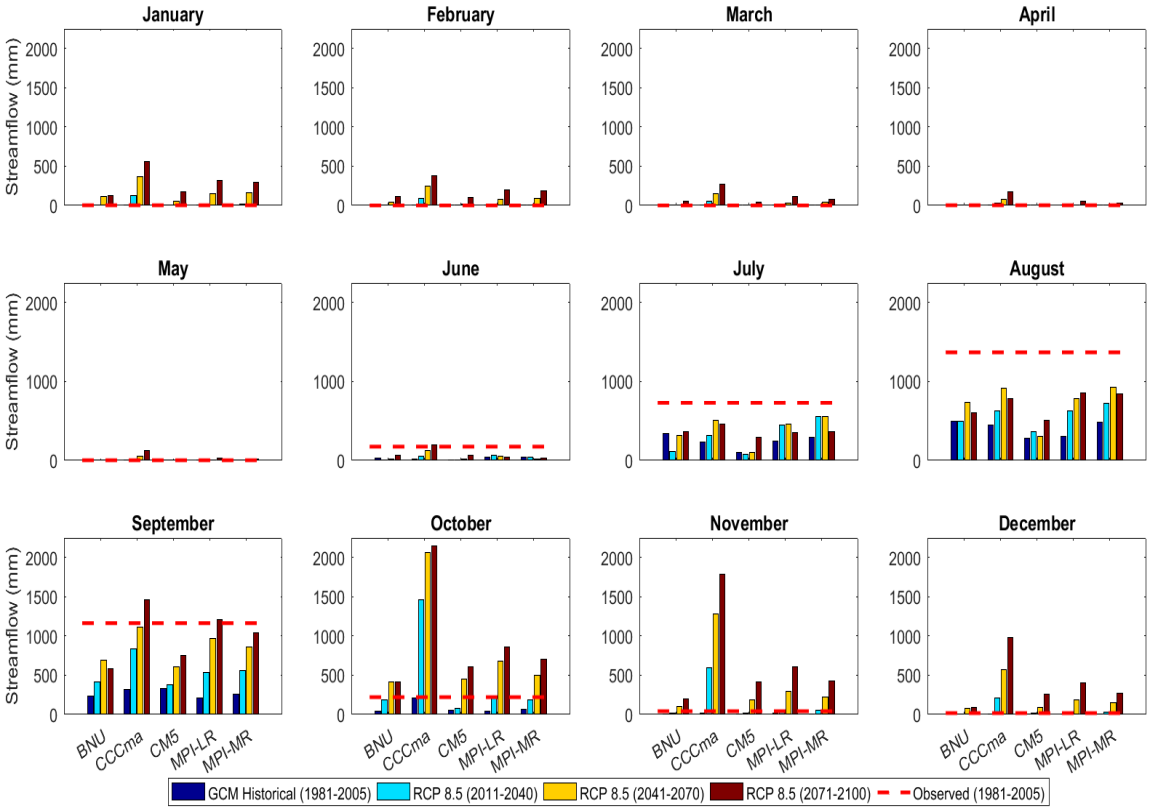

Fig. A27 Mean Streamflows at Ukai, outlet of Middle Tapi Basin for RCP 8.5 scenario

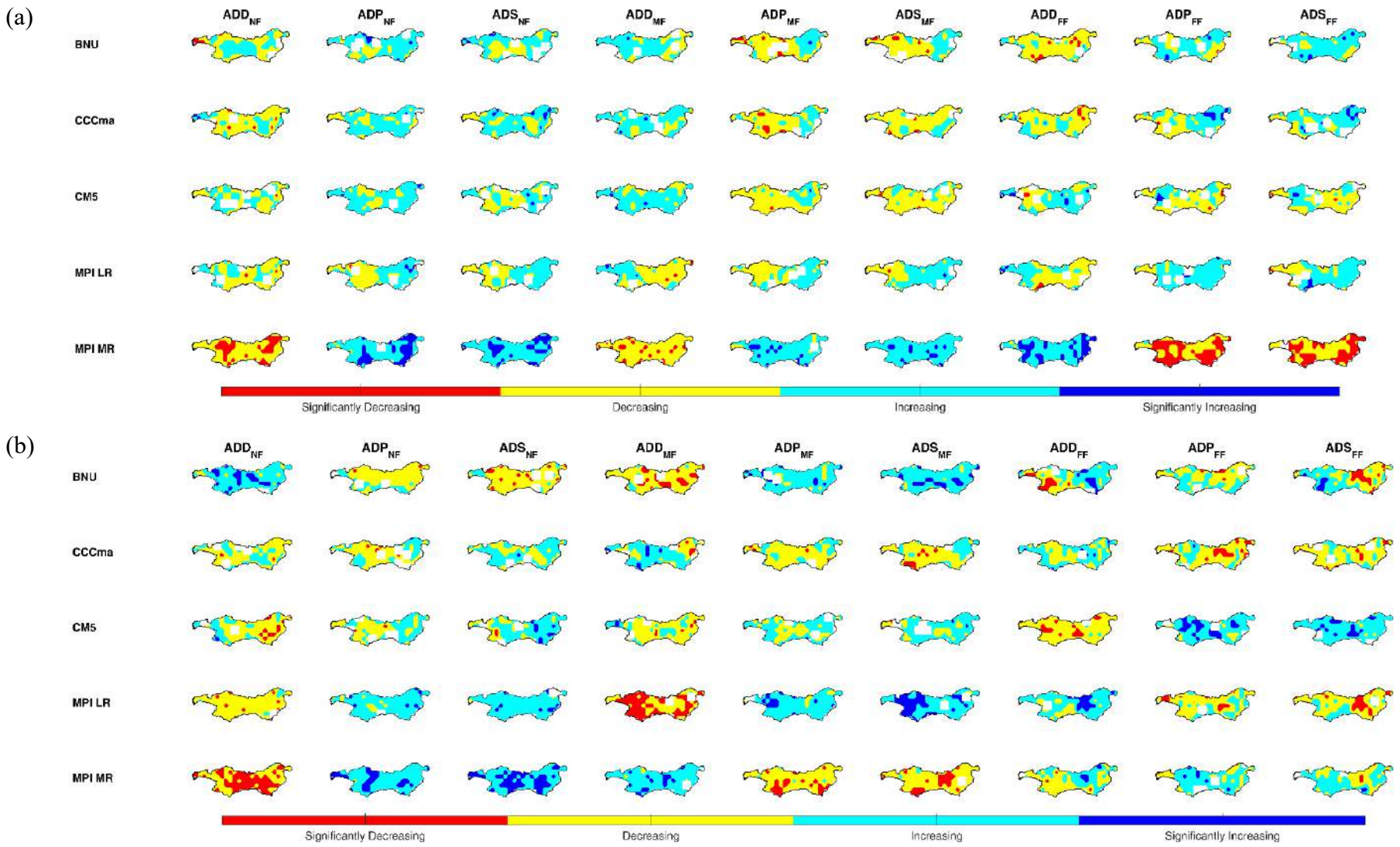

Fig A28 Nature of trend in drought parameters calculated using MSDI-3 for (a) RCP 4.5 and (b) RCP 8.5 scenarios of five GCM models for near-, mid-, and far-future, denoted by NF, MF, and FF respectively. The uncoloured region in the basin boundary shows the region of no trend.

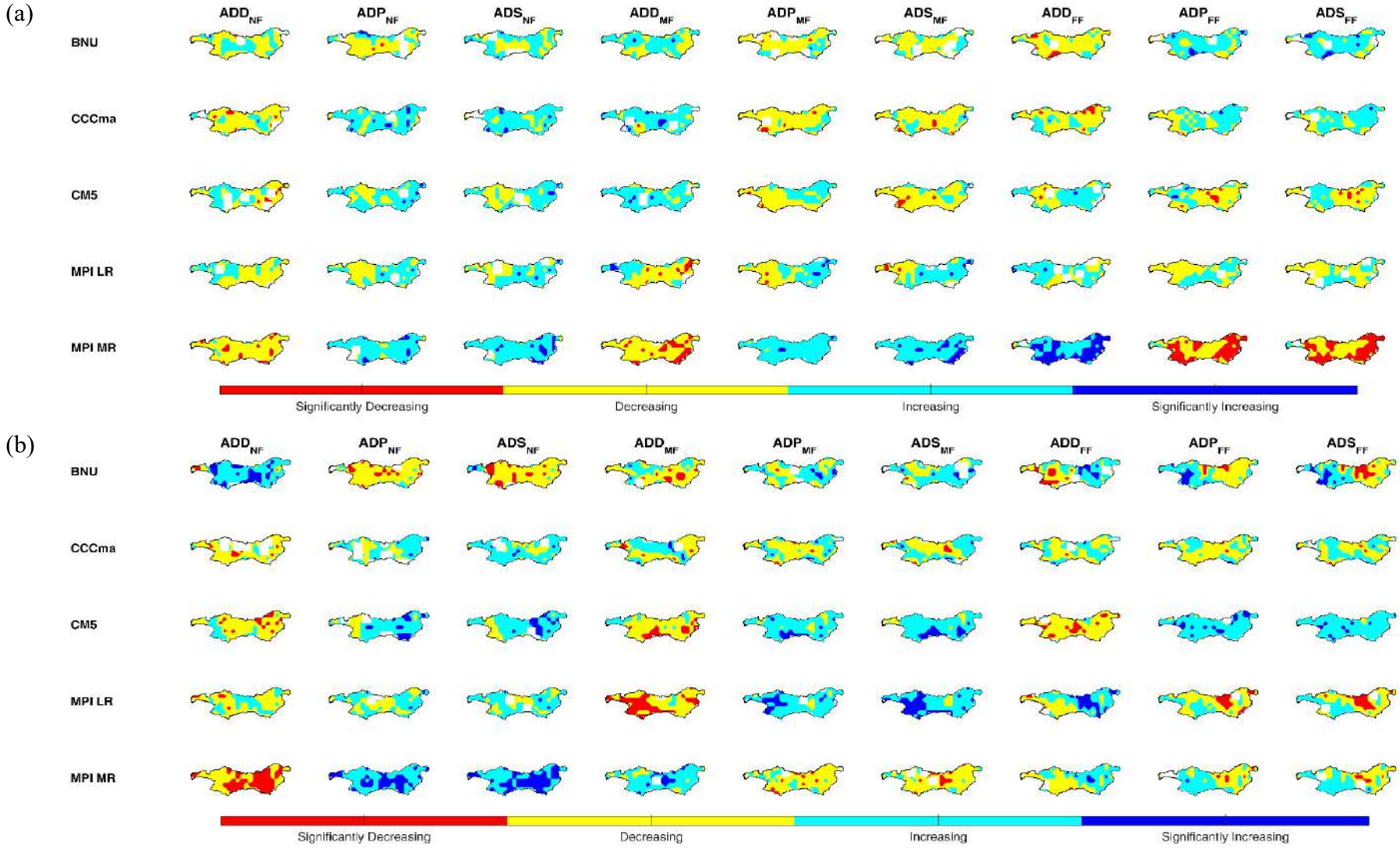

Fig A29 Nature of trend in drought parameters calculated using MSDI-6 for (a) RCP 4.5 and (b) RCP 8.5 scenarios of five GCM models for near-, mid-, and far-future, denoted by NF, MF, and FF respectively. The uncoloured region in the basin boundary shows the region of no trend.

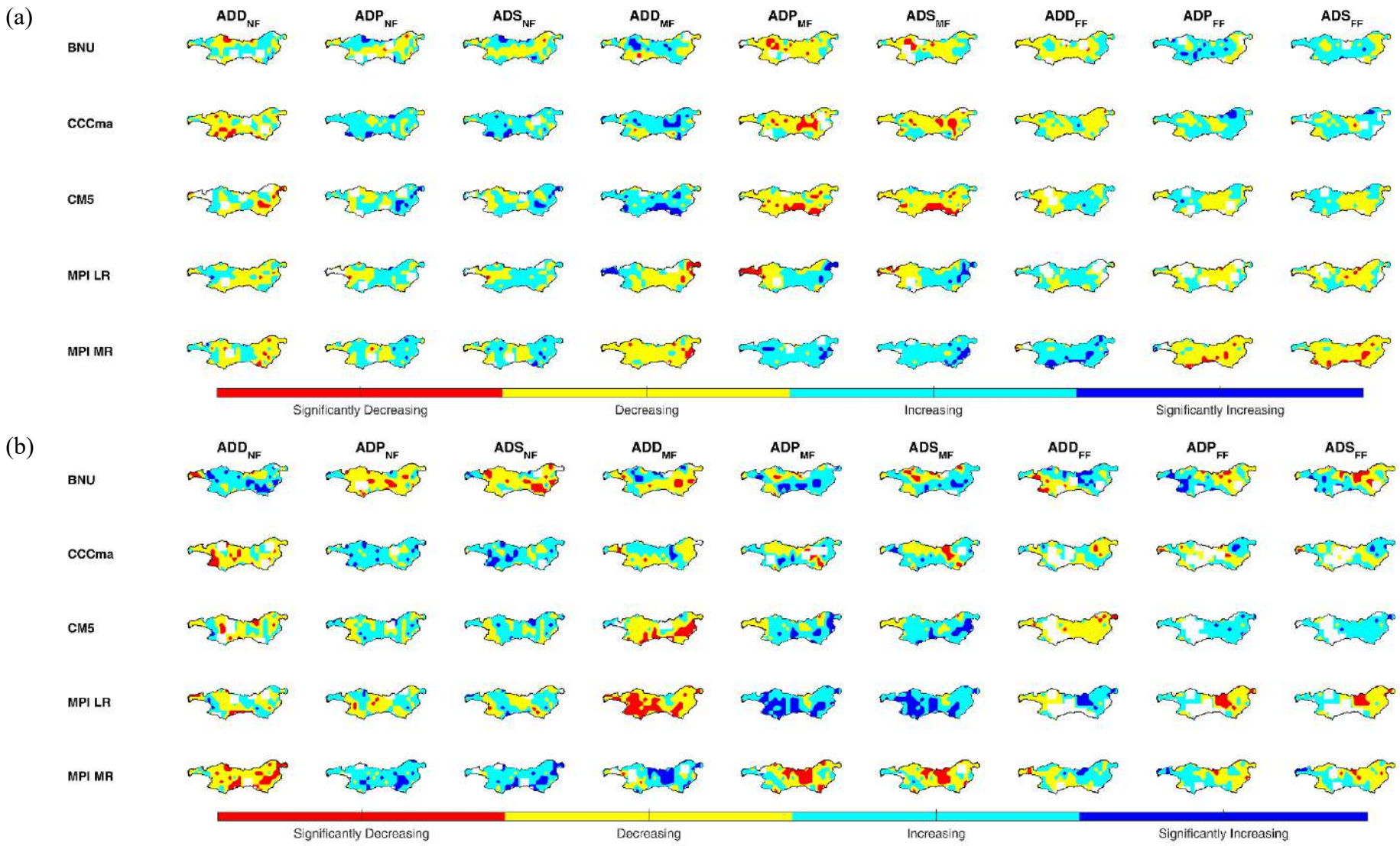

Fig A30 Nature of trend in drought parameters calculated using MSDI-12 for (a) RCP 4.5 and (b) RCP 8.5 scenarios of five GCM models for near-, mid-, and far-future, denoted by NF, MF, and FF respectively. The uncoloured region in the basin boundary shows the region of no trend.

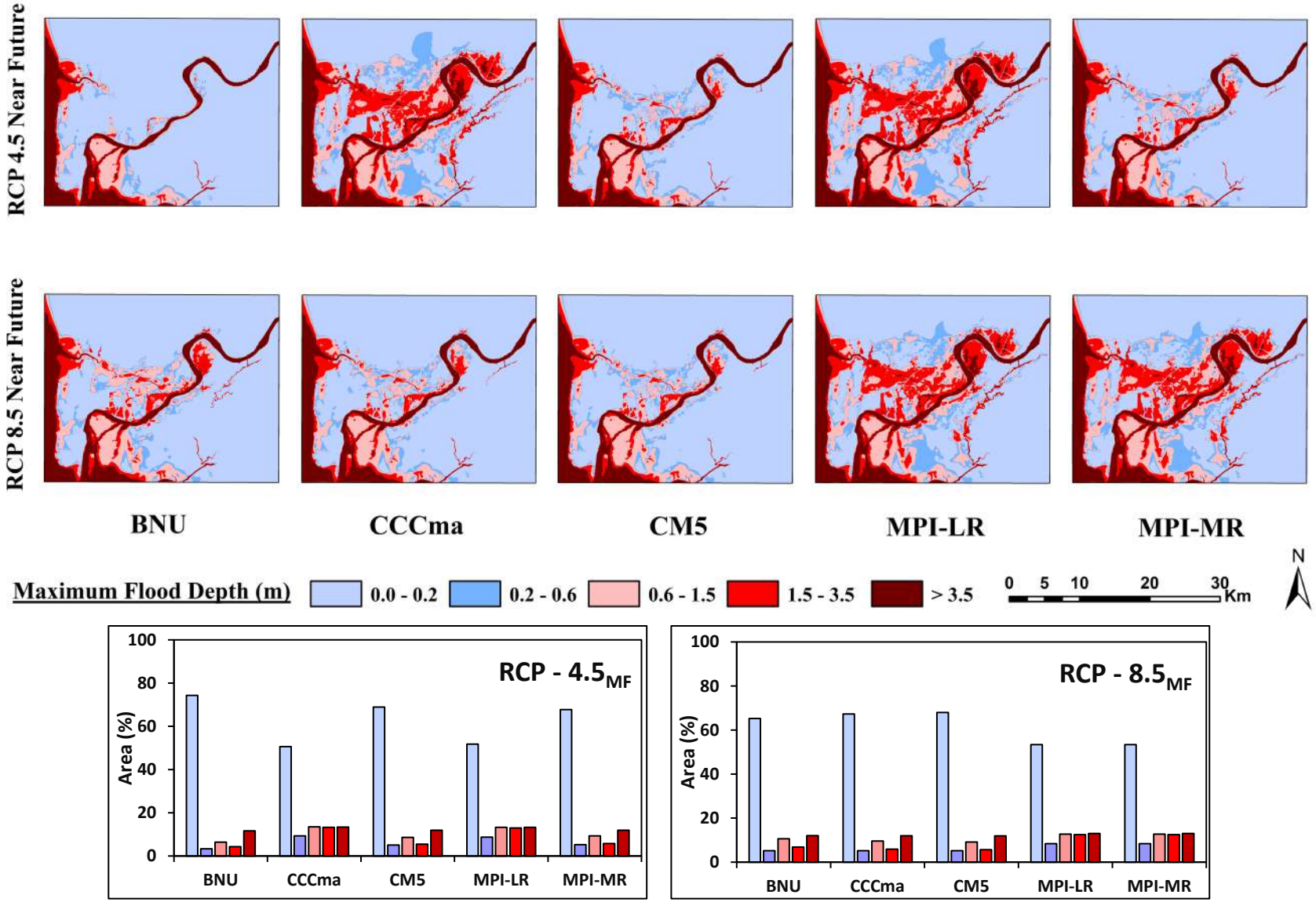

Fig. A31 Flood inundation maps for densely populated Surat city and its outskirt area for mid future (2041-2070) and RCP 4.5 and 8.5

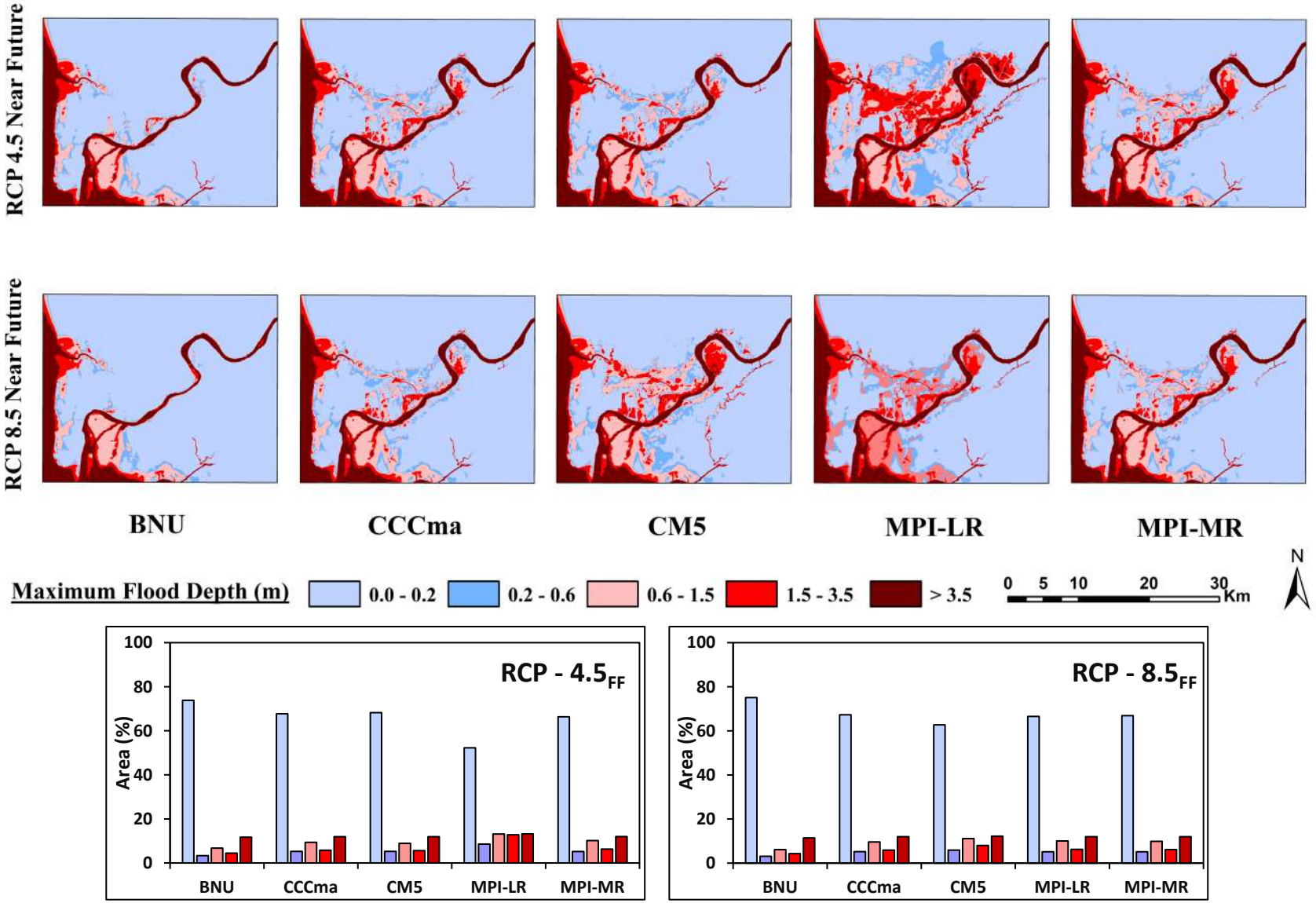

Fig. A32 Flood inundation maps for densely populated Surat city and its outskirt area for far future (2071-2100) and RCP 4.5 and 8.5

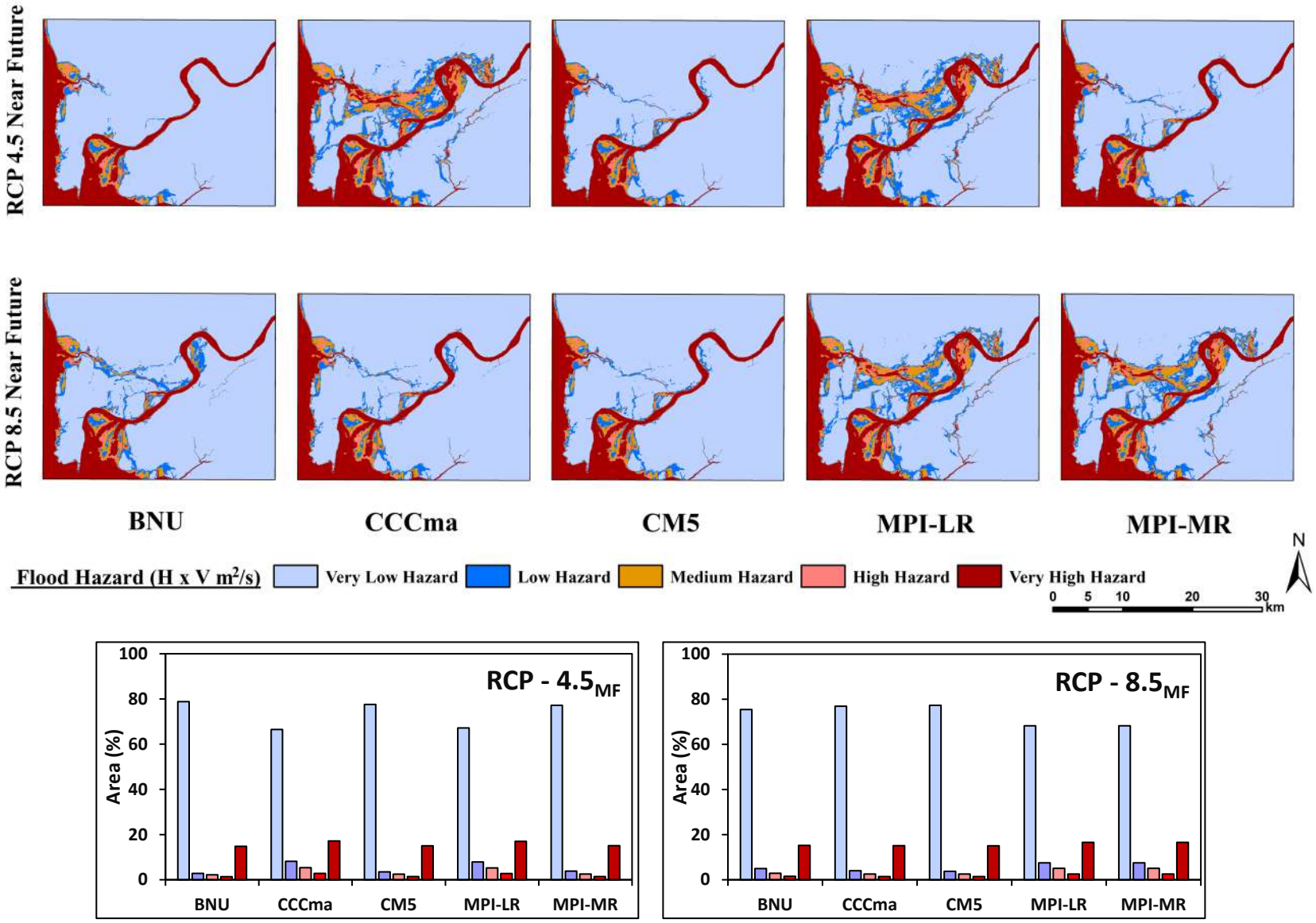

Fig. A33 Flood hazard maps for densely populated Surat city and its outskirt area for mid future (2041-2070) and RCP 4.5 and 8.5

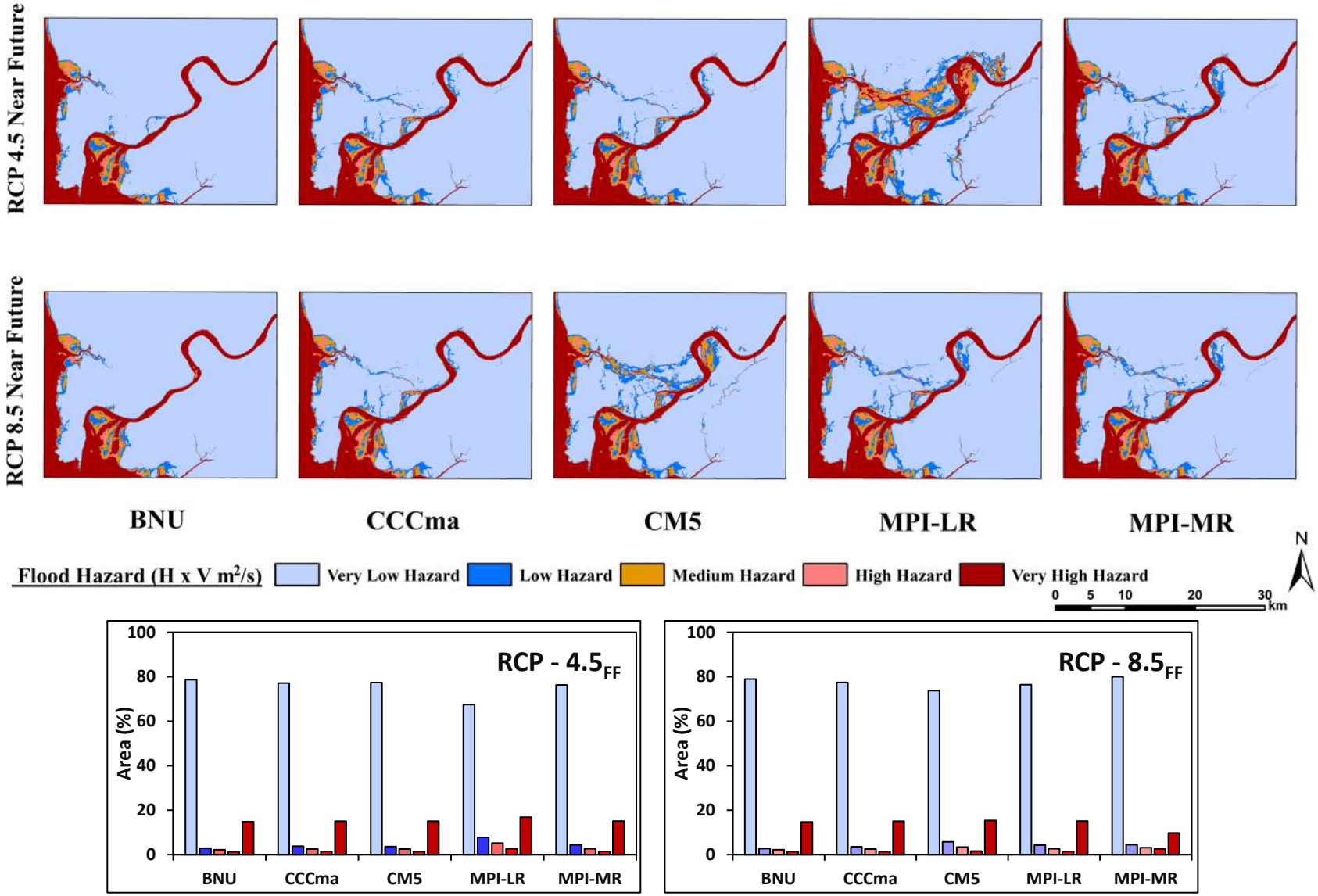

Fig. A34 Flood hazard maps for densely populated Surat city and its outskirt area for far future (2071-2100) and RCP 4.5 and 8.5

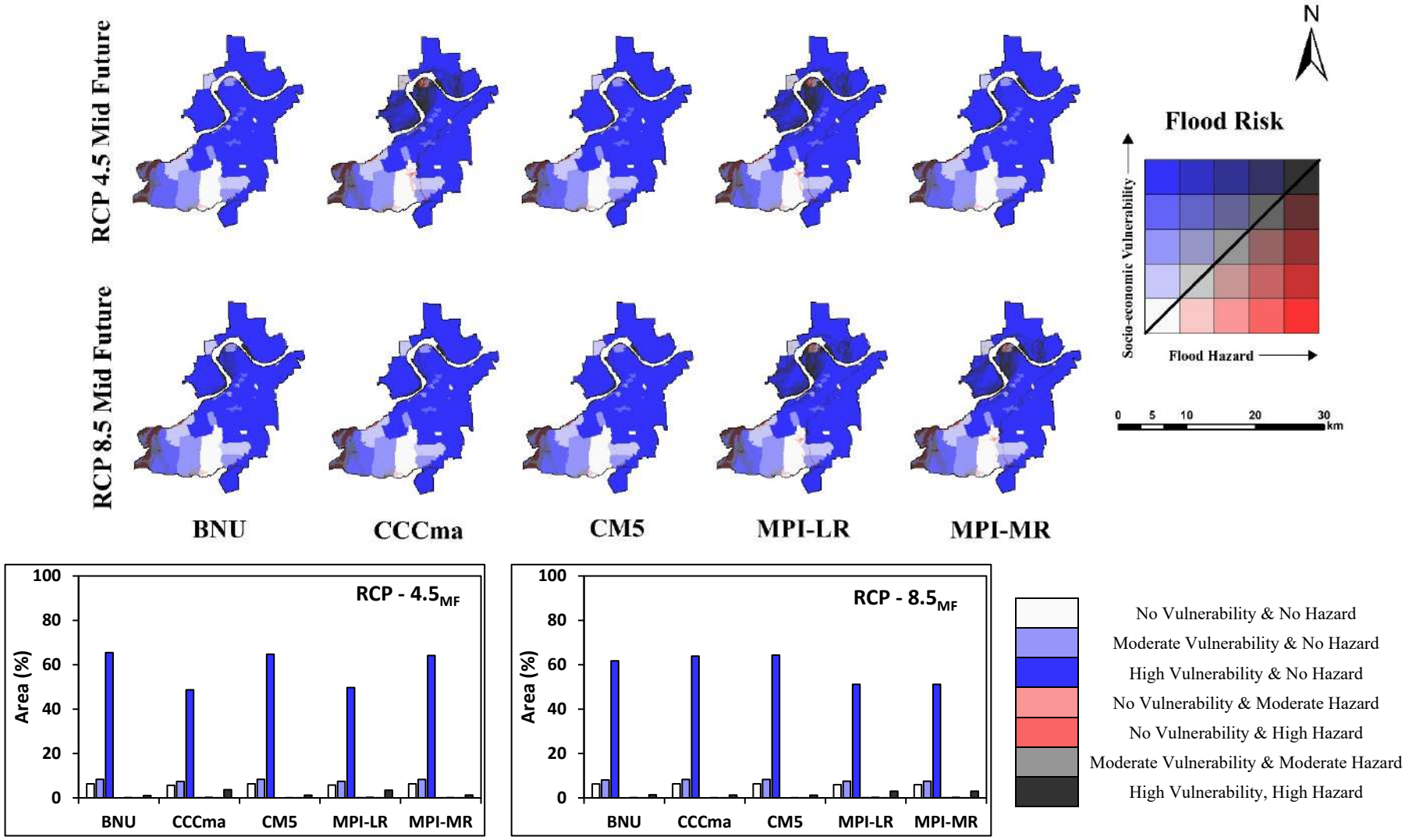

Fig. A35 Flood risk maps for densely populated Surat city and its outskirt area for mid future (2041-2070) and RCP 4.5 and 8.5

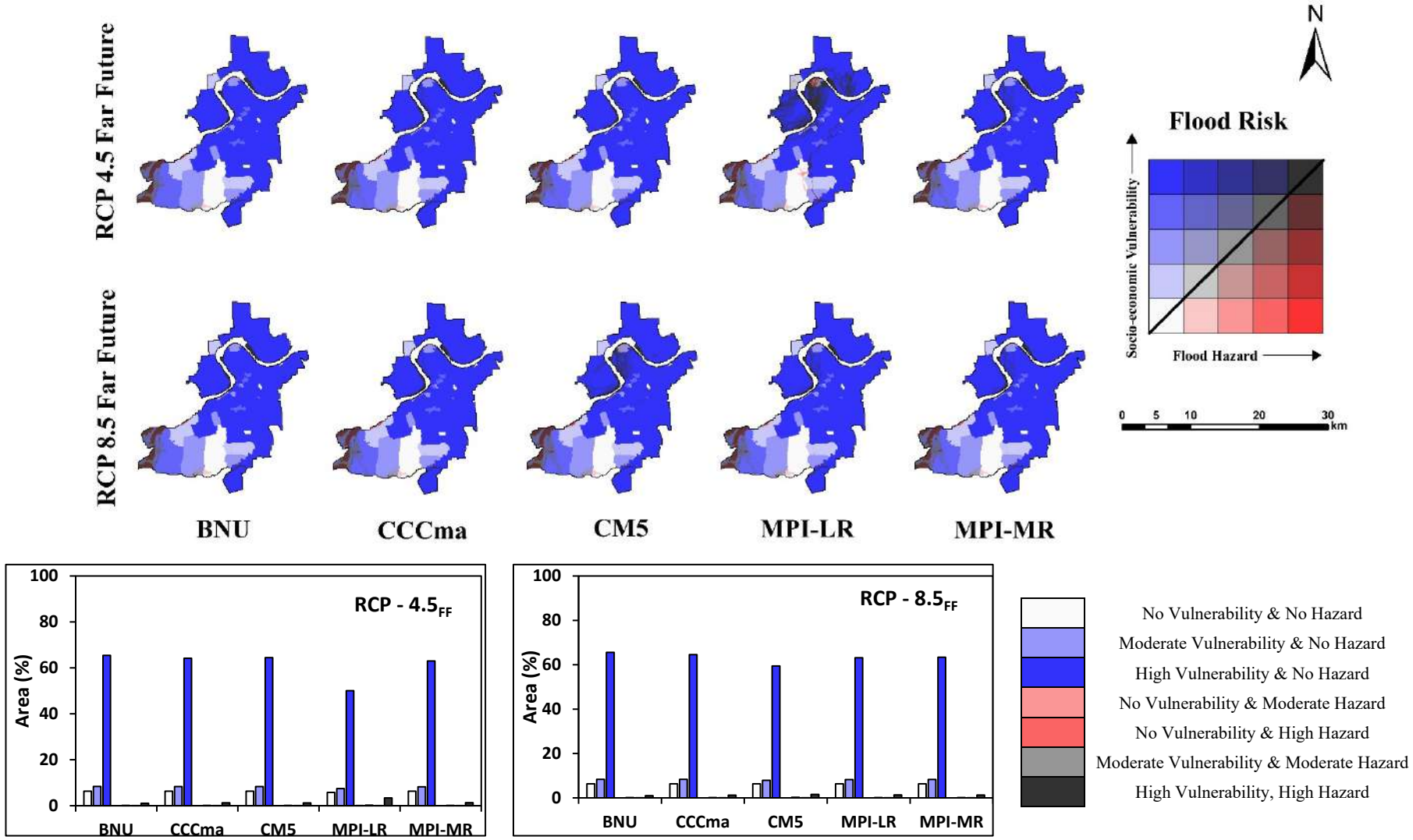

Fig. A36 Flood risk maps for densely populated Surat city and its outskirt area for far future (2071-2100) and RCP 4.5 and 8.5

Table A1: Cropping patterns for calculation of irrigation water demand

Sr.No.	Name of Division	Year	Season	Crops										
				Sugarcane	Plantain	Other Pere.	Ground Nut.	Paddy	Cotton	Vegetable	Wheat	Juwar/ bajri	Others	Total
1	2	3	4	5	6	7	8	9	10	11	12	13	14	15
1	Surat Canal Dn., surat.	2009-10	Kharif	19206	121	168	0	5445	30	333	0	0	7540	32843
			Rabi	20908	81	177	0	590	30	258	47	0	6994	29085
			Hot	18438	65	156	4	788	0	285	0	0	6285	26021
			Total	**58552**	**267**	**501**	**4**	**6823**	**60**	**876**	**47**	**0**	**20819**	**87949**
2	Ambica Dn., Navasri.		Kharif	5350	6	1222	0	6630	0	182	0	1170	10068	24628
			Rabi	7217	33	1813	0	193	0	239	15	1142	5348	16000
			Hot	6199	30	1460	0	193	0	177	0	825	5449	14333
			Total	**18766**	**69**	**4495**	**0**	**7016**	**0**	**598**	**15**	**3137**	**20865**	**54961**
3	K.R.B.C. Dn., Surat.		Kharif	18582	23	152	0	9013	83	571	0	74	5302	33800
			Rabi	23609	21	238	10	2391	88	843	2076	414	5761	35451
			Hot	19250	19	245	102	2551	8	954	0	415	3782	27326
			Total	**61441**	**63**	**635**	**112**	**13955**	**179**	**2368**	**2076**	**903**	**14845**	**96577**
4	K.R.B.C. Dn., Surat (0 To 35 Km.)		Kharif	4436	30	21	0	725	0	3	0	0	1129	6344
			Rabi	5543	31	23	0	61	0	16	0	55	1064	6877
			Hot	4956	15	26	2	164	0	11	0	152	793	6119
			Total	**14935**	**76**	**70**	**2**	**950**	**0**	**30**	**0**	**207**	**2986**	**19340**
5	U.R.B.C. Dn., Ank.		Kharif	10347	100	182	0	2649	337	141	0	0	781	14537
			Rabi	13709	54	229	0	594	790	222	913	11	1672	18194
			Hot	11113	59	273	0	723	7	200	0	0	1231	13606
			Total	**35169**	**213**	**684**	**0**	**3966**	**1134**	**563**	**3136**	**11**	**3684**	**46337**
6	ULBC Dn., Valod		Kharif	9312	15	128	0	2411	0	0	0	0	0	11866
			Rabi	13156	23	93	536	467	0	362	121	128	5751	20553
			Hot	12596	10	101	662	614	0	360	0	149	4958	19450
			Total	**35064**	**48**	**322**	**1198**	**3492**	**0**	**722**	**121**	**277**	**10709**	**51869**

Sr.No.	Name of Division	Year	Season	Crops										
				Sugarcane	Plantain	Other Pere.	Ground Nut.	Paddy	Cotton	Vegetable	Wheat	Juwar/ bajri	Others	Total
1	2	3	4	5	6	7	8	9	10	11	12	13	14	15
1	Surat Canal Dn., surat.	2010--11	Kharif	19405	58	94	0	1856	30	282	0	0	8023	29748
			Rabi	21710	54	123	0	2784	30	326	59	0	9089	34175
			Hot	17603	51	140	2	2313	0	547	0	0	8076	28732
			Total	**58718**	**163**	**357**	**2**	**6953**	**60**	**1155**	**59**	**0**	**25188**	**92655**
2	Ambica Dn., Navasri.		Kharif	5451	7	1370	0	4551	0	177	0	1379	2456	15391
			Rabi	7170	8	1630	0	4147	0	257	0	1383	10304	24899
			Hot	6911	8	1748	0	4179	0	237	0	2736	9006	24825
			Total	**19532**	**23**	**4748**	**0**	**12877**	**0**	**671**	**0**	**5498**	**21766**	**65115**
3	K.R.B.C. Dn., Surat.		Kharif	20421	10	84	0	7323	22	369	0	21	3020	31270
			Rabi	24986	4	235	97	3079	31	812	1862	258	6826	38190
			Hot	19072	4	251	101	3075	0	987	0	222	4792	28504
			Total	**64479**	**18**	**570**	**198**	**13477**	**53**	**2168**	**1862**	**501**	**14638**	**97964**
4	K.R.B.C. Dn., Surat (0 To 35 Km.)		Kharif	4707	19	16	0	245	0	1	0	0	286	5274
			Rabi	5898	19	16	0	120	0	19	63	0	1208	7343
			Hot	4696	10	18	0	133	0	21	0	4	1053	5935
			Total	**15301**	**48**	**50**	**0**	**498**	**0**	**41**	**63**	**4**	**2547**	**18552**
5	U.R.B.C. Dn., Ank.		Kharif	9725	60	135	0	1076	73	67	0	0	100	11236
			Rabi	14362	57	268	0	822	771	195	909	32	1597	19013
			Hot	11554	35	265	5	1346	48	215	0	12	1494	14974
			Total	**35641**	**152**	**668**	**5**	**3244**	**892**	**477**	**909**	**44**	**3191**	**45223**
6	ULBC Dn., Valod		Kharif	10833	36	545	0	779	0	0	0	0	0	12193
			Rabi	15821	48	157	2238	1380	0	372	32	252	5557	25857
			Hot	14693	0	130	2443	1618	0	575	0	563	4093	24115
			Total	**41347**	**84**	**832**	**4681**	**3777**	**0**	**947**	**32**	**815**	**9650**	**62165**

Sr.No.	Name of Division	Year	Season	Crops										
				Sugarcane	Plantain	Other Pere.	Ground Nut.	Paddy	Cotton	Vegetable	Wheat	Juwar/ bajri	Others	Total
1	2	3	4	5	6	7	8	9	10	11	12	13	14	15
1	Surat Canal Dn., surat.	2011--12	Kharif	19908	51	97	0	3046	32	421	0	0	8487	32042
			Rabi	22682	46	116	0	2940	32	1201	27	16	6973	34033
			Hot	19539	78	160	0	3025	0	1420	0	248	5292	29762
			Total	**62129**	**175**	**373**	**0**	**9011**	**64**	**3042**	**27**	**264**	**20752**	**95837**
2	Ambica Dn., Navasri.		Kharif	5622	7	1336	0	4794	0	179	0	1035	4977	17950
			Rabi	7060	9	1628	0	4384	0	211	0	2290	8970	24552
			Hot	6926	9	1814	0	4512	0	259	0	3769	6638	23927
			Total	**19608**	**25**	**4778**	**0**	**13690**	**0**	**649**	**0**	**7094**	**20585**	**66429**
3	K.R.B.C. Dn., Surat.		Kharif	19693	8	77	0	7991	19	363	0	60	918	29129
			Rabi	23937	4	221	20	3650	42	729	1856	344	6887	37690
			Hot	17653	7	239	80	4485	2	1081	0	249	5123	28919
			Total	**61283**	**19**	**537**	**100**	**16126**	**63**	**2173**	**1856**	**653**	**12928**	**95738**
4	K.R.B.C. Dn., Surat (0 To 35 Km.)		Kharif	4581	10	22	0	297	0	4	0	0	310	5224
			Rabi	5872	10	25	3	170	0	11	66	1	959	7117
			Hot	4720	10	29	0	255	0	16	0	0	1076	6106
			Total	**15173**	**30**	**76**	**3**	**722**	**0**	**31**	**66**	**1**	**2345**	**18447**
5	U.R.B.C. Dn., Ank.		Kharif	9701	50	158	0	960	73	52	0	0	1902	12896
			Rabi	14474	45	188	0	1384	753	243	934	69	1946	20036
			Hot	10976	47	262	0	1512	16	296	0	61	2531	15701
			Total	**35151**	**142**	**608**	**0**	**3856**	**842**	**591**	**3136**	**130**	**6379**	**48633**
6	ULBC Dn., Valod		Kharif	5371	0	55	0	222	0	1	0	0	60	5709
			Rabi	14821	0	183	2761	2116	0	444	51	298	6105	26779
			Hot	14066	0	142	2786	1698	0	680	0	622	4566	24560
			Total	**34258**	**0**	**380**	**5547**	**4036**	**0**	**1125**	**-2151**	**920**	**10731**	**57048**

Sr.No.	Name of Division	Year	Season	Crops										
				Sugarcane	Plantain	Other Pere.	Ground Nut.	Paddy	Cotton	Vegetable	Wheat	Juwar/ bajri	Others	Total
1	2	3	4	5	6	7	8	9	10	11	12	13	14	15
1	Surat Canal Dn., surat.	2012-13	Kharif	21856	87	104	0	3655	29	2183	0	0	4099	32013
			Rabi	22686	83	120	6	3331	29	1658	21	0	7471	35405
			Hot	20098	69	151	0	2819	0	1502	0	0	5429	30068
			Total	**64640**	**239**	**375**	**6**	**9805**	**58**	**5343**	**21**	**0**	**16999**	**97486**
2	Ambica Dn., Navasri.		Kharif	5440	9	1359	0	5555	0	1096	0	3619	5438	22516
			Rabi	6565	10	1561	0	4373	0	1237	0	4559	6331	24636
			Hot	6327	8	1541	0	4385	0	946	0	4346	6170	23723
			Total	**18332**	**27**	**4461**	**0**	**14313**	**0**	**3279**	**0**	**12524**	**17939**	**70875**
3	K.R.B.C. Dn., Surat.		Kharif	19042	9	174	0	8002	85	544	0	91	1374	29321
			Rabi	22456	5	258	55	4828	61	872	1644	601	6943	37723
			Hot	16434	4	242	39	4725	5	816	0	432	4514	27211
			Total	**57932**	**18**	**674**	**94**	**17555**	**151**	**2232**	**1644**	**1124**	**12831**	**94255**
4	K.R.B.C. Dn., Surat (0 To 35 Km.)		Kharif	4390	12	17	0	402	0	12	0	0	333	5166
			Rabi	5880	9	35	3	133	6	75	59	0	1000	7200
			Hot	4726	8	21	0	132	0	19	0	0	894	5800
			Total	**14996**	**29**	**73**	**3**	**667**	**6**	**106**	**59**	**0**	**2227**	**18166**
5	U.R.B.C. Dn., Ank.		Kharif	10423	49	164	0	1830	96	116	0	0	841	13519
			Rabi	14610	36	200	0	1487	741	225	690	20	2527	20536
			Hot	10716	37	234	0	1007	15	188	0	0	2634	14831
			Total	**35749**	**122**	**598**	**0**	**4324**	**852**	**529**	**690**	**20**	**6002**	**48886**
6	ULBC Dn., Valod		Kharif	4354	0	0	0	2147	0	0	0	0	268	6769
			Rabi	14338	0	138	2756	1893	0	361	77	346	7649	27558
			Hot	13301	0	142	2426	2105	0	385	0	359	6630	25348
			Total	**31993**	**0**	**280**	**5182**	**6145**	**0**	**746**	**77**	**705**	**14547**	**59675**

Sr.No.	Name of Division	Year	Season	Crops										
				Sugarcane	Plantain	Other Pere.	Ground Nut.	Paddy	Cotton	Vegetable	Wheat	Juwar/ bajri	Others	Total
1	2	3	4	5	6	7	8	9	10	11	12	13	14	15
1	Surat Canal Dn., surat.	2013-14	Kharif	19357	74	110	0	2097	26	1425	0	0	6558	29647
			Rabi	22213	57	139	1	3152	26	1891	22	183	7724	35408
			Hot	18729	64	156	1	3027	0	1824	70	0	7131	31002
			Total	**60299**	**195**	**405**	**2**	**8276**	**52**	**5140**	**92**	**183**	**21413**	**96057**
2	Ambica Dn., Navasri.		Kharif	4580	5	1288	0	3079	0	313	0	1741	5864	16870
			Rabi	5956	8	1534	0	4308	0	510	0	3921	8244	24481
			Hot	5737	10	1923	0	4341	0	514	0	5388	5496	23409
			Total	**16273**	**23**	**4745**	**0**	**11728**	**0**	**1337**	**0**	**11050**	**19604**	**64760**
3	K.R.B.C. Dn., Surat.		Kharif	17871	4	100	0	6849	61	258	0	60	1428	26631
			Rabi	16586	4	197	22	3898	9	595	194	350	2356	24211
			Hot	14870	3	259	29	3986	8	1060	0	265	3637	24117
			Total	**49327**	**11**	**556**	**51**	**14733**	**78**	**1913**	**194**	**675**	**7421**	**74959**
4	K.R.B.C. Dn., Surat (0 To 35 Km.)		Kharif	4683	6	17	0	88	0	2	0	0	276	5072
			Rabi	4619	6	16	0	33	0	5	8	0	246	4933
			Hot	3847	6	26	0	74	0	13	0	38	604	4608
			Total	**13149**	**18**	**59**	**0**	**195**	**0**	**20**	**8**	**38**	**1126**	**14613**
5	U.R.B.C. Dn., Ank.		Kharif	10117	36	125	0	485	107	116	0	0	787	11773
			Rabi	12254	18	181	0	608	263	240	72	37	1928	15601
			Hot	9846	19	227	0	715	100	361	0	95	2504	13867
			Total	**32217**	**73**	**533**	**0**	**1808**	**470**	**717**	**3136**	**132**	**5219**	**41241**
6	ULBC Dn., Valod		Kharif	0	0	0	0	0	0	0	0	0	0	0
			Rabi	14117	0	168	2645	2048	0	416	67	220	9036	28717
			Hot	12944	0	165	2596	2218	0	633	0	333	7415	26304
			Total	**27061**	**0**	**333**	**5241**	**4266**	**0**	**1049**	**67**	**553**	**16451**	**55021**

Sr.No.	Name of Division	Year	Season	Crops										
				Sugarcane	Plantain	Other Pere.	Ground Nut.	Paddy	Cotton	Vegetable	Wheat	Juwar/ bajri	Others	Total
1	2	3	4	5	6	7	8	9	10	11	12	13	14	15
1	Surat Canal Dn., surat.	2014-15	Kharif	20689	60	162	0	3187	25	1700	0	0	7077	32900
			Rabi	21482	41	122	0	2909	25	1991	10	0	8870	35450
			Hot	17983	27	196	0	2737	0	1654	0	0	7703	30300
			Total	**60154**	**128**	**480**	**0**	**8833**	**50**	**5345**	**10**	**0**	**23650**	**98650**
2	Ambica Dn., Navasri.		Kharif	5120	7	1554	0	4344	0	590	0	5641	4623	21879
			Rabi	5785	8	1561	0	4124	0	1212	0	6925	5194	24809
			Hot	5408	11	1600	0	4161	0	945	0	5819	5092	23036
			Total	**16313**	**26**	**4715**	**0**	**12629**	**0**	**2747**	**0**	**18385**	**14909**	**69724**
3	K.R.B.C. Dn., Surat.		Kharif	19367	8	224	0	8215	113	598	0	287	2826	31638
			Rabi	20980	10	291	6	5224	102	790	1212	287	6481	35383
			Hot	16422	6	372	36	5793	0	851	0	435	3884	27799
			Total	**56769**	**24**	**887**	**42**	**19232**	**215**	**2239**	**1212**	**1009**	**13191**	**94820**
4	K.R.B.C. Dn., Surat (0 To 35 Km.)		Kharif	4967	0	18	0	130	0	6	0	0	769	5890
			Rabi	5799	6	21	0	47	0	9	29	0	1096	7007
			Hot	4715	7	21	0	74	0	13	0	0	1161	5991
			Total	**15481**	**13**	**60**	**0**	**251**	**0**	**28**	**29**	**0**	**3026**	**18888**
5	U.R.B.C. Dn., Ank.		Kharif	11234	20	97	0	827	292	190	0	2	1420	14082
			Rabi	13950	2	169	0	1088	503	402	351	83	3953	20501
			Hot	10490	23	282	0	1161	25	448	0	32	2162	14623
			Total	**35674**	**45**	**548**	**0**	**3076**	**820**	**1040**	**3136**	**117**	**7535**	**49206**
6	ULBC Dn., Valod		Kharif	5110	0	0	0	370	0	0	0	0	118	5598
			Rabi	13506	0	130	2148	2096	0	636	157	283	9624	28580
			Hot	12963	157	0	2052	2112	0	533	0	377	8419	26613
			Total	**31579**	**157**	**130**	**4200**	**4578**	**0**	**1169**	**-2628**	**660**	**18161**	**60791**

Sr.No.	Name of Division	Year	Season	Crops										
				Sugarcane	Plantain	Other Pere.	Ground Nut.	Paddy	Cotton	Vegetable	Wheat	Juwar/ bajri	Others	Total
1	2	3	4	5	6	7	8	9	10	11	12	13	14	15
1	Surat Canal Dn., surat.	2015-16	Kharif	19845	26	147	0	2950	27	2312	0	264	8235	33806
			Rabi	21186	42	325	0	3087	26	2253	11	0	8278	35208
			Hot	18139	22	271	0	2921	0	1425	0	0	7828	30606
			Total	**59170**	**90**	**743**	**0**	**8958**	**53**	**5990**	**11**	**264**	**24341**	**99620**
2	Ambica Dn., Navasri.		Kharif	4529	6	1294	0	4209	0	687	0	5685	4989	21399
			Rabi	5342	6	1589	0	3995	0	1014	0	6406	5801	24153
			Hot	5028	6	1618	0	4056	0	657	0	5616	6026	23007
			Total	**14899**	**18**	**4501**	**0**	**12260**	**0**	**2358**	**0**	**17707**	**16816**	**68559**
3	K.R.B.C. Dn., Surat.		Kharif	18911	18	401	4	8582	63	707	0	322	2856	31864
			Rabi	18822	26	509	9	6740	40	905	1073	244	4140	32508
			Hot	15448	26	531	9	7000	1	815	0	341	4008	28179
			Total	**53181**	**70**	**1441**	**22**	**22322**	**104**	**2427**	**1073**	**907**	**11004**	**92551**
4	K.R.B.C. Dn., Surat (0 To 35 Km.)		Kharif	4721	9	17	0	124	0	5	0	0	324	5200
			Rabi	4855	9	19	0	70	0	13	20	0	714	5700
			Hot	4590	10	21	1	102	0	21	1	0	907	5653
			Total	**14166**	**28**	**57**	**1**	**296**	**0**	**39**	**21**	**0**	**1945**	**16553**
5	U.R.B.C. Dn., Ank.		Kharif	10885	23	202	0	938	232	190	0	0	1607	14077
			Rabi	14103	2	266	0	1122	503	380	2591	0	1213	20180
			Hot	11078	2	366	50	1202	10	411	0	40	2985	16144
			Total	**36066**	**27**	**834**	**50**	**3262**	**745**	**981**	**2591**	**40**	**5805**	**50401**
6	ULBC Dn., Valod		Kharif	9643	20	98	0	3480	0	223	0	0	7536	21000
			Rabi	12116	30	99	2627	2465	0	362	2	293	11506	29500
			Hot	11995	20	131	1845	1991	0	328	0	310	9798	26418
			Total	**33739**	**70**	**343**	**4422**	**7946**	**0**	**888**	**0**	**604**	**28769**	**76918**

Sr.No.	Name of Division	Year	Season	Crops										
				Sugarcane	Plantain	Other Pere.	Ground Nut.	Paddy	Cotton	Vegetable	Wheat	Juwar/ bajri	Others	Total
1	2	3	4	5	6	7	8	9	10	11	12	13	14	15
1	Surat Canal Dn., surat.	2016-17	Kharif	19981	25	152	0	2933	27	2193	0	0	8844	34155
			Rabi	19698	25	309	0	2306	27	2215	0	0	9007	33587
			Hot	18098	25	276	0	2897	0	1515	0	0	7892	30703
			Total	**57777**	**75**	**737**	**0**	**8136**	**54**	**5923**	**0**	**0**	**25743**	**98445**
2	Ambica Dn., Navasri.		Kharif	4047	6	1445	0	4123	0	655	0	3902	6025	20203
			Rabi	4530	6	1547	0	3666	0	904	0	4643	6554	21850
			Hot	4454	6	1568	0	3679	0	844	0	5393	5738	21682
			Total	**13031**	**18**	**4560**	**0**	**11468**	**0**	**2403**	**0**	**13938**	**18317**	**63735**
3	K.R.B.C. Dn., Surat.		Kharif	16790	40	518	0	9329	45	679	0	106	4027	31534
			Rabi	16691	35	538	0	8098	48	934	841	362	5823	33370
			Hot	13883	31	536	5	8849	0	977	0	309	4235	28825
			Total	**47364**	**106**	**1592**	**5**	**26276**	**93**	**2590**	**841**	**777**	**14085**	**93729**
4	K.R.B.C. Dn., Surat (0 To 35 Km.)		Kharif	4392	10	25	0	150	0	21	0	0	660	5258
			Rabi	4458	7	23	0	120	0	18	10	0	822	5458
			Hot	4331	11	28	0	170	0	13	0	0	1202	5755
			Total	**13181**	**28**	**76**	**0**	**440**	**0**	**52**	**10**	**0**	**2684**	**16471**
5	U.R.B.C. Dn., Ank.		Kharif	10561	30	285	0	1109	5	315	0	10	2062	14377
			Rabi	13347	4	260	21	1433	227	342	0	70	3573	19277
			Hot	9639	7	246	1	1569	20	400	0	60	2843	14785
			Total	**33547**	**41**	**791**	**22**	**4111**	**252**	**1057**	**0**	**140**	**8478**	**48439**
6	ULBC Dn., Valod		Kharif	380	0	0	0	910	0	0	0	0	1789	1500
			Rabi	10251	30	123	805	512	0	171	1828	318	11271	23481
			Hot	12179	37	131	1528	2890	0	809	0	341	10210	26450
			Total	**22810**	**67**	**254**	**2333**	**4312**	**0**	**980**	**1828**	**659**	**23270**	**51431**

Sr.No.	Name of Division	Year	Season	Crops										
				Sugarcane	Plantain	Other Pere.	Ground Nut.	Paddy	Cotton	Vegetable	Wheat	Juwar/ bajri	Others	Total
1	2	3	4	5	6	7	8	9	10	11	12	13	14	15
1	Surat Canal Dn., surat.	2017-18	Kharif	20012	20	134	0	3321	26	1833	0	0	7556	32902
			Rabi	19957	19	293	0	1762	26	2559	0	3	8402	33021
			Hot	18377	19	266	0	2172	10	1409	0	5	8698	30956
			Total	**58346**	**58**	**693**	**0**	**7255**	**62**	**5801**	**0**	**8**	**24656**	**96879**
2	Ambica Dn., Navasri.		Kharif	4002	4	1398	0	4138	0	690	0	4671	5006	19909
			Rabi	4288	4	1393	0	180	0	237	0	4636	7067	17805
			Hot	4179	4	1423	0	189	0	498	0	4512	6520	17325
			Total	**12469**	**12**	**4214**	**0**	**4507**	**0**	**1425**	**0**	**13819**	**18593**	**55039**
3	K.R.B.C. Dn., Surat.		Kharif	15939	32	488	0	10323	72	743	0	270	3432	31299
			Rabi	17123	28	551	0	3658	62	926	817	195	5629	28989
			Hot	15523	32	543	3	4466	0	767	0	392	5241	26967
			Total	**48585**	**92**	**1582**	**3**	**18447**	**134**	**2436**	**817**	**857**	**14302**	**87255**
4	K.R.B.C. Dn., Surat (0 To 35 Km.)		Kharif	4140	6	15	0	172	0	11	0	0	472	4816
			Rabi	4202	10	20	0	21	0	5	2	0	305	4565
			Hot	4109	7	30	0	76	0	16	0	0	708	4946
			Total	**12451**	**23**	**65**	**0**	**269**	**0**	**32**	**2**	**0**	**1485**	**14327**
5	U.R.B.C. Dn., Ank.		Kharif	10020	12	288	0	1081	120	375	0	0	2443	14339
			Rabi	13183	15	369	0	1096	291	416	0	215	2930	18515
			Hot	10079	5	316	0	1056	30	457	0	275	1857	14075
			Total	**33282**	**32**	**973**	**0**	**3233**	**441**	**1248**	**0**	**490**	**7230**	**46929**
6	ULBC Dn., Valod		Kharif	1200	0	0	0	800	0	0	0	0	1872	2000
			Rabi	13882	95	465	2113	172	0	1514	2064	926	12809	32000
			Hot	12710	95	410	2405	1428	0	1490	1272	989	9773	29300
			Total	**27792**	**190**	**875**	**4518**	**2400**	**0**	**3004**	**3336**	**1915**	**24454**	**63300**

Sr.No.	Name of Division	Year	Season	Crops										
				Sugarcane	Plantain	Other Pere.	Ground Nut.	Paddy	Cotton	Vegetable	Wheat	Juwar/ bajri	Others	Total
1	2	3	4	5	6	7	8	9	10	11	12	13	14	15
1	Surat Canal Dn., surat.	2018-19	Kharif	19855	16	142	0	1813	30	2099	0	0	7013	30968
			Rabi	17800	20	273	0	124	30	2076	0	0	6535	26858
			Hot	16227	6	174	0	539	0	1099	0	0	6370	24415
			Total	**53882**	**42**	**589**	**0**	**2476**	**60**	**5274**	**0**	**0**	**19918**	**82241**
2	Ambica Dn., Navasri.		Kharif	3748	4	1417	0	3057	0	490	0	3880	5234	17830
			Rabi	3847	0	1366	0	53	0	252	0	4633	5461	15612
			Hot	3575	0	1350	0	53	0	267	0	4180	5576	15001
			Total	**11170**	**4**	**4133**	**0**	**3163**	**0**	**1009**	**0**	**12693**	**16271**	**48443**
3	K.R.B.C. Dn., Surat.		Kharif	15842	38	505	0	9443	51	837	0	69	4169	30954
			Rabi	14363	40	553	0	394	43	1016	1036	156	5067	22668
			Hot	11822	35	548	0	778	0	1017	0	415	5627	20242
			Total	**42027**	**113**	**1606**	**0**	**10615**	**94**	**2870**	**1036**	**640**	**14863**	**73864**
4	K.R.B.C. Dn., Surat (0 To 35 Km.)		Kharif	4800	0	9	0	75	0	13	0	0	431	5328
			Rabi	3990	18	13	0	0	0	7	11	0	269	4308
			Hot	2600	5	20	0	23	0	8	0	0	300	2956
			Total	**11390**	**23**	**42**	**0**	**98**	**0**	**28**	**11**	**0**	**1000**	**12592**
5	U.R.B.C. Dn., Ank.		Kharif	10700	1	294	0	692	140	310	0	0	665	12802
			Rabi	10870	5	323	0	60	165	330	110	30	2323	14216
			Hot	9027	23	358	0	167	30	480	0	0	1369	11454
			Total	**30597**	**29**	**975**	**0**	**919**	**335**	**1120**	**110**	**30**	**4357**	**38472**
6	ULBC Dn., Valod		Kharif	1230	0	0	0	411	0	0	247	4	108	2000
			Rabi	11309	30	229	90	442	0	401	0	448	9501	22450
			Hot	10740	15	186	205	83	0	621	0	326	10837	23013
			Total	**23279**	**45**	**415**	**295**	**936**	**0**	**1022**	**247**	**778**	**20446**	**47463**

Table A2 Daily scale performance evaluation of multisite calibration and validation in Purna sub-catchment

Performance Indicators	Calibration Period (1998 – 2007)		Validation Period (2008 – 2013)	
	Yerli	***Gopalkheda***	***Yerli***	***Gopalkheda***
P-factor	0.54	0.54	0.32	0.38
R-factor	0.58	0.46	0.63	0.45
R^2	0.75	0.68	0.71	0.72
NSE	0.72	0.65	0.71	0.71
RSR	0.53	0.59	0.54	0.53
MNS	0.52	0.48	0.60	0.56
PBIAS (%)	-8.3	-3.4	-7.2	-11.1
bR^2	0.68	0.55	0.55	0.52

Table A3 Input variables for Reservoir module in SWAT

Variable Name	Definition	Min Value	Max Value
MORES	Month the reservoir became operational	0	12
IYRES	Year the reservoir become operational	0	9999
RES_ESA	Reservoir Surface area when the reservoir is filled to the emergency spillway (ha)	1	3000
RES_EVOL	Volume of water needed to fill the reservoir to the emergency spillway (10^4 m^3)	15	3000
RES_PSA	Reservoir Surface area when the reservoir is filled to the principal spillway (ha)	1	1000
RES_PVOL	Volume of water needed to fill the reservoir to the principal spillway (10^4 m^3)	10	100
RES_VOL	Initial reservoir volume (10^4 m^3)	10	100
RES_K	Hydraulic conductivity of the reservoir bottom (mm/hr)	0	1
IRESCO	Outflow Simulation options	0	3
RES_RR	Average principal spillway release rate (m^3/sec)	0	1000
STARG	Target Reservoir Volume specified for a given month (m^3)	0	100000
IFLODR1	Beginning month of non-flood season	1	12
IFLODR2	Ending month of non-flood season	1	12
NDTARGR	Number of Days to reach target storage from current reservoir storage	0	200
OFLOWMX	Maximum daily outflow data for the month (m^3/sec)	0	2000
OFLOWMN	Minimum daily outflow data for the month (m^3/sec)	0	1000

ANNEXURE-B: Minutes of One-day Workshop

Minutes of the one-day workshop on 'Impact of Climate Change on Water Resources of Tapi Basin' held on May 21, 2022

1. The area under chronic water shortage within Tapi basin is increased from 34.0% in 1981 to 63.2% in 2011. The aggravating chronic water shortage in the basin is a matter of concern about water availability in future within the Tapi basin.
2. The increasing trend in simple daily intensity index (SDII) is observed over Lower Tapi basin (LTB) and Purna sub-catchment, whereas, decreasing trend is observed over the middle Tapi basin (MTB) for the baseline period. The increase in frequency and magnitude of extremes over the LTB makes it susceptible to the urban and flash floods (short and long-duration), while MTB is more susceptible to prolonged dry conditions and might lead to short-term drought conditions in the subbasin.
3. The increase in average temperature indicates the shifting of the basin toward warmer phase. The hottest days, coldest nights temperatures are increasing significantly over Upper Tapi basin (UTB) and LTB respectively. The increase in diurnal temperature range (DTR) over Purna sub-catchment and MTB can intensify cardiovascular and respiratory diseases in elderly persons and children in the basin. The consistent increase in the number of days with a maximum temperature exceeding 37°C would increase the chances of heat stress across the entire basin. Dr. R P Pandey, Member Secretary, INCCC recommended the use of station-based records for hydrometeorological assessments of extremes.
4. The downscaled annual rainfall from GCM is underestimated, with reference to the observed rainfall in the baseline period (1951-2005), by 21.7 - 28.4%. The MPI ESM LR model has been found to be performing better compared to other GCM models. All the GCM models underpredict the extremes (maximum rainfall) within the Tapi River basin. Prof. Nagesh Kumar recommended to quantify the changes in the monthly rainfalls/temperatures in future in terms of the percentage changes to the baseline period. Prof. V Jothiprakash emphasized in calculating the % area of the basin with the corresponding % rise/fall in the rainfall.
5. The total annual rainfall, magnitude and intensity of rainfall extremes are likely to increase under RCP 4.5 for near (2011-2040) to mid (2041-2070) and far future (2071-2100) periods as compared to the corresponding downscaled parameters for baseline period (1951-2005). These changes are further intensified under RCP 8.5 scenario. The number of days with

tempearature more than 37°C will be increased by 50% under RCP 4.5 and 130% under RCP 8.5 scenario by the end of 21st century.

6. The hydrological model for Purna sub-catchment, calibrated based on multisite observations, reveals that monsoonal streamflows would decrease to 60% for 69.7% decrease in the rainfall for the same season at the end of 21st century for RCP 4.5 scenario. The streamflows would further reduce to 57.3% for a 62% decrease in rainfall under RCP 8.5 scenario for the same sub-catchment. The flow duration curves at various gauging sites in the sub-catchment indicate the large-scale variability/uncertainity in the future streamflows. The reduction in future monsoonal streamflows and subsequent increase in non-monsoonal flows indicates the transition of Purna river from intermittent to perennial characteristics. Prof. V Jothiprakash stated that the sharp drops in the flow duration curves can be an indicator of high losses in the Purna sub-catchment. He also recommended the use of annual flows for flow duration curves to estimate dependable flow calculations for the reservoirs. Dr. R P Pandey, Member Secretary, INCCC, pointed out that the presented flow duration curves can be extended up to the minimum discharge of 0.1 m^3/s. It was also suggested that flow duration curves for all the stream gauging stations be prepared for baseline and future periods and transitions of the river(s) from ephemeral to intermittent and perennial or otherwise be quantified.
7. The calibrated hydrological model for Burhanpur sub-catchment revealed the reduction in the surface runoff and water yield for future periods. On the contrary, an increase in evapotranspiration is reported for both RCP scenarios.
8. The calibrated hydrological model for Middle Tapi indicates the increase in the magnitude of Q_{50} (median) flows at Sarankheda, Gidhade, and inflow into Ukai for all averaged GCMs in future. The flow duration curves indicate the increase in water availability in the Middle Tapi Basin for Near, Mid, and Far Future with reference to the simulated stream flows for the baseline period (1981-2005) using the downscaled rainfall for the same period.
9. The simulated flow duration curves for future period, at different stream gauging stations, indicate that peak flows (Q_{10}) are underpredicted while low flows are overpredicted with reference to the corresponding values for the baseline period.
10. The calibrated distributed hydrological model for Lower Tapi basin reveals increase evapotranspirational losses for all five GCM models during all three sub-periods of the 21st century.
11. With reference to the baseline period, gross irrigation requirements are likely to increase (decrease) in the months of December, January, February, March, April, and May (August,

October, and November) months. Prof. V. Jothiprakash suggested that the impact of climate change on irrigation water demand be calculated for the command areas of both Hatnur and Girna reservoirs.

12. Dr. R P Pandey, Member Secretary, INCCC has given the suggestion to include the difference in magnitude of gross irrigation demand (GIR) of future and the GIR of baseline period (in MCM) for the Ukai-Kakrapar command area. Also, it was suggested to recommend a drip irrigation system in the future to cope with likely increase in GIR in the command area. It is also emphasized to use more water retaining structures like lakes, ponds, check dams, etc. to recharge the groundwater system in the command area.
13. The flood hazard maps developed for the coastal urban flood plain of densely populated Surat city for different return period flood, indicated that the north zone and west zone are the worst affected areas of the city. The census-based socio-economic vulnerability of Surat city using the PCA-DEA approach resulted in 66% of the area under a very high vulnerable category. Finally, the bivariate flood risk assessment of urban-coastal flood plain of Surat city, reveals that the north zone and larger area of west zone are under high flood risk which is due to equal contribution of flood hazard and socio-economic vulnerability for the baseline period for the same zones. The use of more than three observed flood hydrographs is advisable in the computation of non-dimensional flood hydrograph for Ukai reservoir.
14. The significant increase in Annual Drought Duration (ADD), subsequent reduction in annual drought severity (ADS), and annual drought peak (ADP) in SPI-3, SPEI-3 and MSDI-3 indicates that the Tapi River Basin is more prone to short-term drought conditions. A small fraction of the UTB (MTB & LTB) can experience short-, moderate- and long-term droughts in far-future under RCP 8.5 (RCP 4.5).
15. The rainfall during the monsoon period is likely to decrease in the future. On the other hand, the rainfall would increase during the lean period. Similar results are observed in simulated streamflows for both monsoonal and lean period flows. Due to such changing pattern of the rainfall/streamflow, suitable cropping pattern has to be adopted accordingly in the command areas.
16. The estimation of gross irrigation water requirement (GIWR) for the future period indicates that there would be an increase in GIWR during the Rabi and Hot weather crops for the Ukai-Kakrapar command area. Accordingly, the available water resources are to be augmented, and rainwater harvesting measures have to be adopted in the Ukai-Kakrapar command area to meet the future GIWR in the command area.

17. The simulated streamflows indicated that extreme flows (flood) are decreasing in the basin. Hence, the flooding condition would likely to reduce in the future. The simulated flood for 100 years returns period flood in the Surat city is less severe than the corresponding flood for the baseline period. However, the changing land use-land cover pattern in the Surat city in the future is likely to be kept in mind, which may cause further reduction in the flood-carrying capacity of the Tapi River in Surat city.
18. Invariably, the maximum and minimum temperature increases in the TRB with a pronounced increase in Tmin. This would be likely to have a negative impact on crops, particularly paddy yield over the TRB. The suitable cropping pattern can be adopted to cope up with rising T_{min} temperature.
19. Also, in TRB, it is found that temperature would likely go more than 37ºC for 110 days (170 days) under RCP 4.5 (RCP 8.5) scenarios by the end of the 21st century. The notable increase in temperature beyond 37ºC would like to cause heat stress to the people residing in the basin. This may reduce the work performance of the people in the basin.
20. The analyzed data indicated that annual temperature would likely increase over the TRB. This would increase the evapotranspirational requirement, increasing the water demand for the farming in the basin. Thus, rainwater harvest measures are recommended to be adopted in the basin to cope with the increasing water demand in the future.

ANNEXURE-C: List of Publications

List of Publications in International Journals:

- Gehlot, L. K., Jibhakate, S. M., Sharma, P. J., Patel, P. L., and Timbadiya, P. V. (2021). Spatio-temporal variability of rainfall indices and their teleconnections with El Niño-Southern oscillation for Tapi Basin, India. Asia-Pacific Journal of Atmospheric Sciences, 57(1), 99-118. https://doi.org/10.1007/s13143-020-00179-1
- Munoth, P., and Goyal, R. (2020). Hydromorphological analysis of Upper Tapi River Sub-basin, India, using QSWAT model. Model. Earth Syst. Environ, Springer. Volume 6, Issue 4, pp 2111–2127. https://doi.org/10.1007/s40808-020-00821-x.
- Sharma, P. J., Patel, P. L., and Jothiprakash, V. (2019). Hydroclimatic teleconnections of large-scale oceanic-atmospheric circulations on hydrometeorological extremes of Tapi basin, India. Atmospheric Research. [Published online: 26 November 2019]
- Sharma, P. J., Patel, P. L., and Jothiprakash, V. (2019). Impact of Rainfall Variability and Anthropogenic Activities on Streamflow Changes and Water Stress Conditions across Tapi Basin in India. Science of the Total Environment, 687, 885-897.
- Munoth, P. and Goyal, R. (2019). Effects of area threshold values and stream burn-in process on runoff and sediment yield using QSWAT model. ISH Journal of Hydraulic Engineering, Taylor and Francis. https://doi.org/10.1080/09715010.2019.1670107.
- Munoth, P. and Goyal, R. (2019). Effects of DEM Source, Spatial Resolution and Drainage Area Threshold Values on Hydrological Modeling. Water Resources Management, Springer. Volume 33, Issue 9, pp 3303–3319.
- Munoth, P. and Goyal, R. (2019). Impacts of Land Use Land Cover Change on Runoff and Sediment Yield of Upper Tapi River Sub Basin, India. Int. J. of River Basin Management, Taylor and Francis. Volume 18, Issue 2, pp 177–189.

List of Publications in International Conferences:

- Gehlot, L. K., Patel, P. L., & Timbadiya, P. V (2021). Assessment of Kernel Regression Based Statistically Downscaled Rainfall over Tapi River Basin, India. Oral presentation in 26th International Conference on Hydraulics, Water Resources and Coastal Engineering (HYDRO 2021).
- Baladaniya K., Patel, P. L. and Timbadiya, P. V. (2021). Investigation of Crop Evapotranspiration and Irrigation Water Requirement in the Ukai-Kakrapar Command Area, India. Oral presentation in 26th International Conference on Hydraulics, Water Resources and Coastal Engineering (HYDRO 2021).
- Jibhakate, S. M., Timbadiya, P. V., and Patel, P. L. (2021). Computation of Socio-economic Vulnerability for Densely Populated Surat City, India. Oral presentation in 26th International Conference on Hydraulics, Water Resources and Coastal Engineering (HYDRO 2021).
- Jibhakate, S. M., Timbadiya, P. V., and Patel, P. L. (2021). Dam Break Flood Analysis from Ukai Dam in Lower Tapi River, India. Proceedings of ICOLD Symposium on Sustainable Development of Dams and River Basins (ICOLD 2021), February 2021, New Delhi, India.
- Jibhakate, S. M., Timbadiya, P. V., and Patel, P. L. (2021). Flood Hazard Assessment of Coastal Urban Flood Plain. Proceedings of International Conference on Sustainable Water Resources Development and Management (SWARDAM-2021) at Aurangabad (MH), India during Mar. 08-09, 2021.
- Gehlot, L. K., Patel, P. L., and Timbadiya, P. V. (2021). Uncertainty in Streamflow Simulation Due to Rainfall Inputs in Swat Model of Gopalkheda Sub-Catchment in Tapi Basin, India. Proceedings

of International Conference on Sustainable Water Resources Development and Management (SWARDAM-2021) at Aurangabad (MH), India during Mar. 08-09, 2021.

- Dwivedi P., Gehlot, L. K., and Patel, P. L. (2021). Correlation Assessment of Water Balance Parameters using Swat Model for Upper Girna Sub-Catchment in Tapi Basin, India. Proceedings of International Conference on Sustainable Water Resources Development and Management (SWARDAM-2021) at Aurangabad (MH), India during Mar. 08-09, 2021.
- Baladaniya K., Patel, P. L. and Timbadiya, P. V. (2021). Hydrodynamic Modelling of Middle Tapi River Using MIKE 11. Accepted for Oral Presentation in 25th International Conference on Hydraulics, Water Resources and Coastal Engineering (HYDRO 2020).
- Gehlot, L. K., Patel, P. L., and Timbadiya, P. V. (2021). Identification of Hydraulically Efficient Regions in Semi-Arid Yerli Sub-Catchment of Upper Tapi Basin, India. Accepted for Oral Presentation in 25th International Conference on Hydraulics, Water Resources and Coastal Engineering (HYDRO 2020).
- Jibhakate, S. M., Timbadiya, P. V., and Patel, P. L. Prediction of Water Level/Runoff Using Physics Based Hydrological Model in Lower Tapi Basin, India. Accepted for Oral Presentation in 25th International Conference on Hydraulics, Water Resources and Coastal Engineering (HYDRO 2020).
- Gehlot, L. K., Patel, P. L., and Timbadiya, P. V. (2019). Investigation on characteristics and trend of rainfall over Middle Tapi basin, India. Proceedings of 24th International Conference on Hydraulics, Water Resources and Coastal Engineering (HYDRO 2019) at Hyderabad, India during Dec. 18-20, 2019.
- Jibhakate, S. M., Timbadiya, P. V., and Patel, P. L. (2019). Assessment of recent changes in extreme rainfall variability over Lower Tapi Basin, India. Proceedings of 24th International Conference on Hydraulics, Water Resources and Coastal Engineering (HYDRO 2019) at Hyderabad, India during Dec. 18-20, 2019.
- Goyal, R. and Munoth, P. (2019). Identification of Relationships among Morphometric Parameters and QSWAT Model Output. International SWAT Conference, Vienna, Austria, BOKU, 17-19 July 2019.
- Munoth, P. and Goyal, R. (2018). "Hydrological Modeling of Upper Tapi River Sub Basin India using QSWAT Model and SUFI-2 Algorithm". International SWAT conference, India, IIT Madras, January 10-12, 2018.
- Munoth, P. and Goyal, R. (2017). "Morphometric analysis of Upper Tapi River Basin: a GIS approach". International Conference on Emerging Trends in Water Resources and Environmental Engineering, MVGR College of Engineering, Vizianagaram, AP, India. March 30th – April 1st 2017.